Novel Chemical Modifications in "Non-Genetic" Nucleic Acids for Selective Targeting of DNA or RNA

Thesis Submitted to
The University of Pune for the degree of

Doctor of Philosophy
in
Chemistry

BY

NAMRATA ERANDE

Research Supervisor
Dr. Vaijayanti A. Kumar

Division Of Organic Chemistry
National Chemical Laboratory
Pune-411008

September, 2013

CERTIFICATE

This is to certify that the work presented in the thesis entitled "**Novel Chemical Modifications in "Non-Genetic" Nucleic Acids for Selective Targeting of DNA or RNA**" submitted by Namrata Erande, was carried out by the candidate at the National Chemical Laboratory Pune, under my supervision. Such materials as obtained from other sources have been duly acknowledged in the thesis.

Dr. Vaijayanti A. Kumar **September, 2013**

(Research Supervisor)

Division of Organic Chemistry

National Chemical Laboratory

Pune 411008

CANDIDATE'S DECLARATION

I hereby declare that the thesis entitled "**Novel Chemical Modifications in "Non-Genetic" Nucleic Acids for Selective Targeting of DNA or RNA"** submitted for the award of degree of ***Doctor of Philosophy*** in Chemistry to the University of Pune has not been submitted by me to any other university or institution. This work was carried out by me at the National Chemical Laboratory, Pune, India. Such materials as obtained from other sources have been duly acknowledged in the thesis.

Namrata Erande **September, 2013**

National Chemical Laboratory
Pune- 411 008

Dedicated to
my Parents

Acknowledgement

Foremost, I would like to express my deep and sincere gratitude to my research guide Dr. (Mrs.) Vaijayanti A. Kumar who gave me the golden opportunity to do this wonderful work. I am thankful to her for her patience, motivation, advoice and the continuous support, during the every stage of this work. Her guidance helped me in all the time of research and writing of this thesis. I could not have imagined having a better advisor and mentor for my Ph.D study.

Furthermore I would also like to express my deepest appreciation to Dr. (Mrs.) Moneesha and Mrs. Anita Gunjal. Their encouragement, understanding and suggestions were invaluable during my stay in the lab and went a long way towards the completion of this thesis.

My sincere thanks also goes to Dr. Anil Kumar, Dr. (Mrs.) V. S. Pore, Dr. Kalkote, Dr R. A. Joshi, Dr. (Mrs.) R. R. Joshi, Dr. Ramana, and Prof. D. D. Dhavale for their advice, various kinds of help and encouragement during the course of this work. I am also thankful to Mrs. M. V. Mane for HPLC analysis, and also special thanks to Dr. Mahesh Kulkarni and Mrs Shanta Kumari for the MALDI-TOF and LC-MS experiments. The kind support from NMR group is greatly acknowledged and I am specially thankful to Dr.Rajmohanan, Shrikant, Snehal, Mayur and Roshan. Thanks to Dr. Rajesh Gonade, Shridhar and Ekta for the X-ray analysis.

I admire the co-operation of my seniors and colleagues who have taught me many things. I thank Dr.Ravi, Dr.Kishore, Dr.Rahul Dr Raman, Dr.Nilkantha, Dr Amit, Dr.Sathe, Dr.Shengte, Dr. Shridhar, Pradnya, Dr.Ashwani, Dr.Mahesh, Dr.Gitali, Dr.Roopa, Dr.Manaswini, Deepak, Nitin, Tanprit, Satish.

I thank my labmates Dr. Khirud Gogoi, Dr. Madhuri, Dr. Sachin,, Dr. Seema, Parameshwar, Harshal, Harshit, Kiran, Venu, Manoj, Anjan, Tanaya, Govind, Amit, Harsha, and Ragini for their support, help, and for all the fun we have had in the last six years. Thanks you all, for making my last period of work fun, enjoyable and sometimes unforgettable. I thank Bhumkar for the laboratory assistance.

I also thank my beloved friends Jyoti, Dr. Seema, Sarika, Vaishli, Anusuya, Madhuri, manisha, Arvind, and Sunil, for their individual support and encouragement during my carrier.

I would like to thank my father, Mr. Diliprao Erande and mother Mrs Rajani Erande for giving me unconditional love, without their, continuous support and encouragement I never would have been able to achieve my goals. I would also like to thank my brother Mr. Rohan Erande for his love in all the way. I would also like to thank my husband Mr. Atul Waghmare for love, kindness and support he has shown during the past five years it has taken me to finalize this thesis. I thank my all family members and In-laws for their constant support and encouragement. Without the support of all family members, my ambition can hardly be realized.

My greatest regards to the Almighty for bestowing upon me the courage to face the complexities of life and complete this dissertation successfully and for inculcating in me the dedication and discipline to do whatever I undertake well.

I offer my sincere regards to people who have inspired me directly or indirectly in research and life during my doctoral study.

I am grateful to UGC, New Delhi, for awarding the senior research fellowship and Dr. Sourav Pal, present Director, and Dr. Shivram, former director, National Chemical Laboratory to carry out my research works, extending all infrastructural facilities and to submit this work in the form of a thesis for the award of Ph. D degree.

Namrata Erande

Contents

Publication /Symposia i
Abbreviations ii
Abstract v

Chapter 1

1 Antisense technologies: Improvement through novel chemical modifications in genetic and nongenetic nucleic acids

1.1 Introduction ……..... 1
1.2 Nucleic acids……..... 1
1.2.1 Genetic and nongenetic nucleic acids: Structural overview…..... 1
1.2.2 DNA Conformations……..... 4
1.2.3 Stereoelectronic effects in sugar conformation of nucleosides…..... 6
1.2.4 Helical structure of nucleic acids..... 9
1.3 Antisense technology..... 10
1.4 Antisense oligonucleotides: Improvement through novel chemical modifications……..... 12
1.5 2′-5′ Linked oligonucleotide: nongenetic nucleic acids (ngDNA/ngRNA)……..... 14
1.5.1 Structural features of nongenetic nucleic acids (ngDNA/ngRNA)….. 15
1.5.2 Chemical modifications in nongenetic nucleic acids (ngDNA/ngRNA)..... 18
1.5.2a Backbone modifications……..... 18
1.5.2b Sugar modifications……..... 21
1.6 Spectroscopic technique……..... 23
1.6.1 Ultraviolet spectroscopy……..... 23
1.6.2 Circular dichroism (CD) spectroscopy……..... 25
1.6.3 Mass spectroscopy:MALDI-TOF……..... 26
1.7 Present work……..... 27
1.8 References……..... 29

Chapter 2

2 Synthesis of 3′-deoxy-3′-fluoro ribo/xylouridine nucleosides ($^{R}U^{F}$ and $^{X}U^{F}$) their incorporation into ngDNA, and effect on binding properties to target sequences

2.1 Introduction…….. 38
2.2 Rationale, design and objectives of the present work..... 42

2.3 Present work, results and discussion..... 45
2.3.1 Synthesis of $^{X}U^{F}$,and $^{R}U^{F}$ phosphoramidite monomers …..... 45
2.3.1a Synthesis of $^{X}U^{F}$ phosphoramidite monomer..... 46
2.3.1b Synthesis of $^{R}U^{F}$ phosphoramidite monomer……..... 48
2.3.2 Preliminary study of sugar pucker using ^{1}H NMR $J_{1',2'}$ coupling constant……..... 51
2.3.3 Synthesis of oligonucleotides containing modified units their purification and characterization……..... 52
2.3.3a Solid phase synthesis of control and complementary 3′-5′-linked oligonucleotides..... 52
2.3.3b Solid phase synthesis of modified and control ngDNA oligomers..... 53
2.3.3c Purification and MALDI-TOF characterization of ngDNA oligomers……. 55
2.3.4 Duplex stability and CD studies of the derived oligomers…….. 56
2.3.4a Thermal stabilities of duplex formed by $^{X}U^{F}$ -and $^{R}U^{F}$-modified ngDNA..... 56
2.3.4b Synthesis and thermal stability study of $^{X}U^{F}$- modified 3′-5′-linked oligonucleotide..... 61
2.3.4c CD study of $^{X}U^{F}$- and $^{R}U^{F}$- modified ngDNA..... 63
2.4 Summary and conclusion..... 65
2.5 Experimental..... 66
2.5.1 Synthesis of compounds/monomers..... 66
2.5.2 Synthesis of buffers..... 81
2.5.3 Synthesis of oligonucleotides..... 81
2.5.4 Purification and characterization..... 82
2.5.5 Biophysical techniques……..... 83
2.6 Appendix A..... 84
2.7 References..... 113

Chapter 3

3 Synthesis of 3′-deoxy-3′-fluoro ribo/xylo thyminyl nucleosides ($^{R}T^{F}$, $^{X}T^{F}$), 3′-deoxy-3′-fluoro ribo/xylo and S-type locked adenine-containing nucleosides ($^{R}A^{F}$, $^{X}A^{F}$ and $^{L}A^{S}$) and arabino-uridine (^{ara}U), their incorporation into ngDNA, and effect on binding properties to target sequences and nuclease resistance property

Section A

3.1 Synthesis and biophysical study of $^{X}T^{F}$, $^{X}A^{F}$, $^{R}T^{F}$, $^{R}A^{F}$, and $^{L}A^{S}$ monomers
3.1.1 Introduction..... 118
3.1.2 Rationale, design and objectives of the present work..... 119
3.1.3 Present work, result and discussion..... 121

3.1.3.1 Synthesis of $^{R}T^{F}$, $^{X}T^{F}$, $^{R}A^{F}$, $^{X}A^{F}$ and $^{L}A^{F}$ phosphoramidite monomers..... 121
3.1.3.1a Synthesis of $^{X}T^{F}$ nucleoside and $^{X}A^{F}$ phosphoramidite monomer..... 121
3.1.3.1b Synthesis of $^{R}T^{F}$ and $^{R}A^{F}$ phosphoramidite monomers..... 122
3.1.3.1c Synthesis of S-type locked adenosine ($^{L}A^{F}$) phosphoramidite monomer..... 123
3.1.3.2 Preliminary study of sugar pucker using ^{1}H NMR $J_{1',2'}$ coupling constant..... 125
3.1.3.3 Synthesis of oligonucleotides containing modified units their purification and characterization…… 126
3.1.3.3a Purification and MALDI-TOF characterization of ngDNA oligomers..... 126
3.1.3.4 Duplex stability and CD studies of the derived oligomers. 127
3.1.3.4a Thermal stabilities of duplex formed by $^{R}T^{F}$-, $^{R}A^{F}$-, $^{X}A^{F}$- and $^{L}A^{F}$- modified ngDNA..... 128
3.1.3.4b CD study of $^{R}T^{F}$- and $^{R}A^{F}$- modified ngDNA.. 132

Section B

3.2 Synthesis and rationale for designing arabino-uridine (^{ara}U) monomer its incorporation into ngDNA and binding study
3.2.1 Introduction..... 133
3.2.2 Rationale, design and objectives of the present work..... 134
3.2.3 Present work, result and discussion..... 135
3.2.3.1 Synthesis of arabino-uridine (^{ara}U) phosphoramidite monomer..... 135
3.2.3.2 Preliminary study of sugar pucker using ^{1}H NMR $J_{1',2'}$ coupling constant..... 136
3.2.3.3 Synthesis of oligonucleotides containing modified units their purification and characterization..... 136
3.2.3.3a Purification and MALDI-TOF characterization of modified ngDNA..... 136
3.2.3.4 Duplex stability studies of arabino-uridine (^{ara}U) modified oligomers..... 137

Section C

3.3 Stability of oligonucleotide to SVPD
3.3.1 Introduction..... 139
3.3.2 Present work, result and discussion..... 141
3.4 Summary and conclusion..... 146
3.5 Experimental..... 147
3.5.1 Synthesis of compounds/monomers..... 147
3.5.2 Synthesis of buffers..... 167

3.5.3 Synthesis of oligonucleotides, purification and charecterization..... 167
3.5.4 Biophysical techniques..... 167
3.6 Appendix B..... 168
3.7 References..... 202

Chapter 4

4 Conformational studies of $^{R}U^{F}$, $^{R}A^{F}$, $^{X}U^{F}$, $^{X}A^{F}$, $^{L}A^{S}$, and ^{ara}U nucleoside using NMR, X-ray crystal structure and Matlab Pseudorotation GUI program
4.1 Introduction..... 208
4.1.1 Conformational analysis of the furanose ring..... 210
4.1.2 Matlab Pseudorotation GUI program..... 211
4.2 Rationale and objectives of the present work..... 216
4.3 Present work, result and discussion..... 217
4.3.1 Assignments and coupling constant from ^{1}H NMR spectra of modified nucleoside analogue..... 218
4.3.2 Matlab Pseudorotation GUI results..... 223
4.3.3 NOE experiments for modified nucleoside analogue..... 230
4.3.4 X-ray crystal structure of modified nucleoside analogue..... 234
4.4 Comparative results..... 237
4.5 Summary and conclusion..... 238
4.6 Supporting information..... 239
4.6.1 Matlab Pseudorotation textual output..... 239
4.6.2 Crystal data..... 247
4.7 Appendix C..... 249
4.8 References..... 253

List of Research Publications:

1. " Probing the furanose conformation in the 2′-5′ strand of *iso*DNA:RNA duplexes by freezing the nucleoside conformations." **Namrata Erande**, Anita D. Gunjal, Moneesha Fernandes and Vaijayanti A. Kumar* ***Chem. Commun***., 2011, 47, 4007–4009.

2. "Synthesis and structural studies of S-type/N-type locked/frozen nucleoside analogues and their incorporation in RNA-selective, nuclease resistant 2′-5′ linked oligonucleotides." **Namrata Erande**, Anita D. Gunjal, Moneesha Fernandes, Rajesh Gonnade and Vaijayanti A. Kumar* ***Org. Biomol. Chem***. 2013, 11, 746.

3. "Introduction of S/N-type frozen 3′-fluorinated nucleoside in to nongenetic nucleic acid enhance the duplex stability as well as resistance to exonuclease" **Namrata Erande**, Anita D. Gunjal, Moneesha Fernandes and Vaijayanti A. Kumar* manuscript under preparation

Symposia Attended/Poster/Oral Presentations:

1. Attended 4th INSA-KOSEF Symposium in Organic Chemistry. Contemporary Organic chemistry and its future directions. National Chemical Laboratory, Pune India, January 12-13, 2009.

2. Attended 11th CRSI National Symposium in Chemistry. National Chemical Laboratory, Pune India, February 5-8, 2009.

3. Attended National Seminar on Biocatalysis and Biomimetic Catalysis in Organic Chemistry. Dr. Babasaheb Ambedkar Marathwada University, Aurangabad India, March 20-21, 2009.

4. National Science Day, NCL Research Foundation, National chemical Laboratory, Pune. February 28, 2010; Poster Presentation on "Preferred S-type sugarconformation in 2′-5′-isoDNA:RNA duplexes" Namrata erande, Anita Gunjal, Moneesha D'Costa and Vaijayanti A. Kumar.*

5. Attended 6th Cambridge Symposium on nucleic acids chemistry and biology 4th to 7th September 2011. At Queens College, Cambridge, UK. Poster presentation on "Conformational preferences of *iso*DNA strand of *iso*DNA:RNA duplexes" Namrata Erande, and Vaijayanti A. Kumar.*

6. National Science Day, NCL Research Foundation, National chemical Laboratory, Pune. February 24-25, 2013; Poster Presentation on "Comparative Conformational Analysis of Nucleosides by NMR, X-ray, and MATLAB Pseudorotation GUI Program" **Namrata Erande**, Anita D. Gunjal, Moneesha Fernandes, Rajesh Gonnade and Vaijayanti A. Kumar.*

7. Attended International Meeting on Chemical Biology (IMCB-2013) Indian Institute of Science Education and Research, Pune, May 26-28, 2013

Abbreviations

A	Adenine
A	Absorbance
Å	Angstrom
Ac_2O	Acetic anhydride
ACN	Acetonitrile
AcOH	Acetic acid
ADA	Allose-diacetonide
aq.	Aqueous
AS-ONs	Antisense oligonucleotide
Bn	Benzyl
BNA	Bridged Nucleic Acid
Bz	Benzoyl
C	Cytosine
Calc.	calulated
Cat.	Catalytic/catalyst
CD	Circular Dichroism
Conc.	Concentrated
CPG	Controlled Pore Glass
COSY	Correlation Spectroscopy
DEPT	Distortionless Enhancement by Polarization Transfer
DCA	Dichloroacetic acid
DCM	Dichloromethane
DAST	Diethylammonium sulphur trifluoride
DMTr-Cloride	4, 4′-dimethoxytrityl chloride
DIPEA/DIEA	Diisopropylethylamine
DMAP	4',4'-Dimethylaminopyridine
DMF	*N*,*N*-dimethylformamide
DMSO	*N*,*N*-Dimethyl sulfoxide
DNA	2'-deoxyribonucleic acid
ds	Double stranded
DI	Deionized
1D	One Dimensional
2D	Two Dimensional
EDTA	Ethylenediaminetetraacetic acid

EtOH	Ethanol
EtOAc	Ethyl acetate
g	gram
G	Guanine
GUI	Graphical User Interface
GDA	Glucose-diacetonide
h	Hours
HIV	Human Immuno Difficiency Virus
HPLC	High Performance Liquid Chromatography
Hz	Hertz
HRMS	High Resolution Mass Spectrometry
IR	Infra red
L	liter
LCMS	LiquidChromatography-Mass Spectrometry
LNA	Locked Nucleic Acids
MALDI-TOF	Matrix Assisted Laser Desorption-Time-Of-Flight Ionisation-Time of Flight
MeOH	Methanol
MF	Molecular formula
ma	Major anomer
mg	milligram
MHz	Megahertz
min	minutes
M	Mole
µL	Microliter
µM	Micromolar
mL	milliliter
mM	millimolar
mmol	millimoles
m.p	melting point
MS	Mass spectrometry
MW	Molecular weight
N	Normal
N-type	North type
ng	nongenetic

nm	Nanometer
NMR	Nuclear Magnetic Resonance
NOESY/NOE	Nuclear Overhauser Effect Spectroscopy
Obsd.	Observed
ONs	Oligonucleotides
ORTEP	Oak Ridge Thermal Ellipsoid Plot Program (molecular modeling)
ppm	Parts per million
PO-oligo	Phosphodiester-oligomer
PS-oligo	Phosphorothioate-oligoer
Py	Pyridine
PNA	Peptide Nucleic Acid
Pet-ether	Petrolium ether
PCC	Pyridinium chlorochromate
RNA	Ribose Nucleic Acid
R_f	Retention factor
RNase H	Ribonuclease H
RNase L	Ribonuclease L
RP	Reversed Phase
rt	Room temperature
RP-HPLC	Reversed Phase-HPLC
ss	Single stranded
s	Second
SVPD	Snake Venom Phosphodiesters
T	Thymine
TEAA	Triethyl ammonium acetate
TEA/Et_3N	Triethylamine
TFA	Trifluoroacetic acid
THAP	2', 4', 6'-trihydroxyacetophenone
THF	Tetrahydrofuran
TLC	Thin layer chromatography
TMSOTf	Trimethylsilyltrifluoromethanesulfonate
T_m	Melting temperature
U	Uracil
UV-Vis	Ultraviolet-Visible

Abstract

The Thesis entitled ‘‘**Novel Chemical Modifications in “Non-Genetic” Nucleic Acids for Selective Targeting of DNA or RNA”** has been divided into four chapters.

Chapter 1: Antisense technologies: Improvement through novel chemical modifications in genetic and nongenetic nucleic acids

Chapter 2: Synthesis of 3′-deoxy-3'-fluoro ribo/xylouridine nucleosides ($^{R}U^{F}$ and $^{X}U^{F}$), their incorporation into ngDNA, and effect on binding properties to target sequences

Chapter 3: Synthesis of 3′-deoxy-3′-fluoro ribo/xylo thyminyl nucleosides ($^{R}T^{F}$, $^{X}T^{F}$), 3′-deoxy-3′-fluoro ribo/xylo and S-type locked adenine-containing nucleosides ($^{R}A^{F}$, $^{X}A^{F}$ and $^{L}A^{S}$) and arabino-uridine (^{ara}U), their incorporation into ngDNA, and effect on binding properties to target sequences and nuclease resistance property

Section 3.1: Synthesis and biophysical study of $^{X}T^{F}$, $^{X}A^{F}$, $^{R}T^{F}$, $^{R}A^{F}$, and $^{L}A^{S}$ monomers

Section 3.2: Synthesis and rationale for designing arabino-uridine (^{ara}U) monomer its incorporation into ngDNA and binding study

Section 3.3: Stability of oligonucleotide to SVPD

Chapter 4: Conformational studies of $^{R}U^{F}$, $^{R}A^{F}$, $^{X}U^{F}$, $^{X}A^{F}$, $^{L}A^{S}$, and ^{ara}U nucleoside using NMR, X-ray crystal structure and Matlab Pseudorotation GUI program

Chapter 1. Antisense technologies: Improvement through novel chemical modifications in genetic and nongenetic nucleic acids

The potential of modified oligonucleotides to act as antisense agents to inhibit the expression of the target genes in sequence-specific manner may be used for therapeutic and other biological applications. Besides having a specific binding affinity to a complementary target oligonucleotide sequence, antisense oligonucleotides (AS-ON) should meet the requirements for therapeutic purposes, e.g., specificity, nuclease stability, bioavailability, low toxicity and low cost. Several modifications have been developed over the last two decades to enhance the effectiveness of AS-ONs. The sites of the modifications include

sugar, base and phosphate groups of nucleotide. Modifications in the phosphodiester linkage include phosphorothioate, phosphoramidates and methyl phosphonates called as the first generation AS-ONs. Modifications of sugar units to conformationally lock or freeze into 3′-*endo* geometries include 2′-OMe and LNA and are called as the 2nd generation AS-ONs. The third generation modifications include examples where the sugar phosphate backbone has been completely replaced, like in peptide nucleic acids (PNA) morpholino NA and there analogues. The ONs having 'nongenetic' 2′-5′ phosphodiester linkages (ngDNA) were also being explored as candidates for antisense application due to their RNA selective hybridization properties and enzymatic stability. This chapter reviews the literature that is focused on ngDNA/ngRNA, their structural feature, and modifications.

Chapter 2. Synthesis of 3′-deoxy-3'-fluoro ribo/xylouridine nucleosides ($^{R}U^{F}$ and $^{X}U^{F}$), their incorporation into ngDNA, and effect on binding properties to target sequences

In addition to the predominant 3′-5′ internucleotide linkage, a less abundant 2′-5′ internucleotide linkage called as nongenetic nucleic acids (ngDNA/ngRNA) could also be prone to new chemical modifications to improve their therapeutic value (Figure 1). These nongenetic nucleic acids associate to form Watson-Crick base-paired duplex structures with complementary ssRNA but their binding is relatively weak. These ngDNA/ngRNA are also known to be comparatively stable to nucleases. These properties make them to be explored as the right lead candidates for their development as AS-ONs. The mixed backbone ONs (MBOs) containing 2′-5′ and 3′-5′ DNA/RNA, with phosphodiester as well as phosphorothioate backbone have been evaluated earlier without much success. Some chemical modifications with 2′-5′-linkages reported in the literature were incorporated only in the native 3′-5′ DNA and not in ngDNA. These MBOs formed duplexes with both cDNA as well as RNA which showed large destabilization. Much less attention is given for modifying homogeneous 2′-5′-linked ONs. Chemical modifications of the sugar moiety, as in the case of earlier reported 3′-5′linked genetic DNA, were envisaged to be useful to improve the binding strength of these ngONs to the target mRNA.

The modeling studies have suggested that the expected furanose ring pucker in the ngDNA strand in the ngDNA:RNA duplexes would be S-type as against the preferred N-

type geometry in DNA:RNA duplexes. The structural requirements of the ngRNA/ngDNA:RNA duplexes (S-type) do not match with the sugar conformations at the single stranded 2′-5′ oligomer level (N-type).

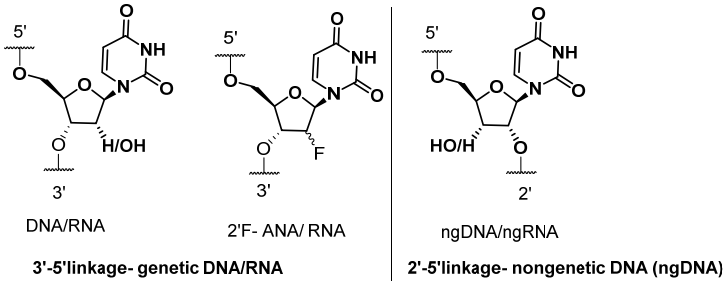

Figure 1. Structures of DNA/RNA and 2'F-ANA/RNa and proposed nucleic acids

Considering these predictions, it was thought to study the effects of incorporation of monomers bearing either locked or frozen S-type/N-type sugar conformations into 2′-5′-linked ONs. We envisaged that applying such structural restrictions on the ngDNA strand would allow us to understand the structural preferences of the sugars in the isomerically-linked strand of the hybrid duplexes and thereby provide an experimental proof for the proposed structural preferences based on modeling studies. Fluorine substitutions in furanose ring show a strong influence on the conformational properties of the nucleic acids. It is known that the replacement of 2′-OH of RNA by either 2′-ribo/arabino-fluoro group have large impact on the thermal stability of the 3′-5′ linked 2′F-RNA:RNA and 2′F-ANA:RNAduplexes. We initially chose 3′-fluoro substitution of the furanose ring of nucleosides (uridine). The xylo- and ribo- configuration of fluorine would restrict the sugar geometry in N-type and S-type conformations respectively due to strong favourable O_4'-C4′-C3′-F_3′ gauche effect. In this Chapter, we describe the synthesis of the 3′-deoxy-3′-fluoro ribo/xylouridine ($^{R}U^{F}$ and $^{X}U^{F}$) and their incorporation in ngDNA to study their effect on duplex stability and CD studies.

Synthesis of $^{X}U^{F}$, $^{R}U^{F}$ phosphoramidite monomers:

The fluorinated nucleosides are shown in Figure 2

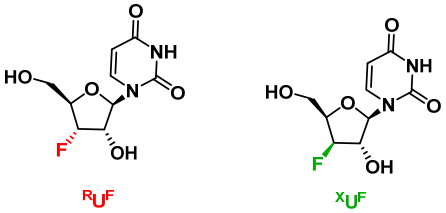

Figure 2. 3′-deoxy-3'-fluoro ribo/xylouridine ($^{R}U^{F}$ and $^{X}U^{F}$)

Synthesis of $^{X}U^{F}$ phosphoramidite monomer: 3′-deoxy-3′-fluoro-β-D-xylouridine monomer was synthesized using D-glucose as a starting material (Scheme 1).

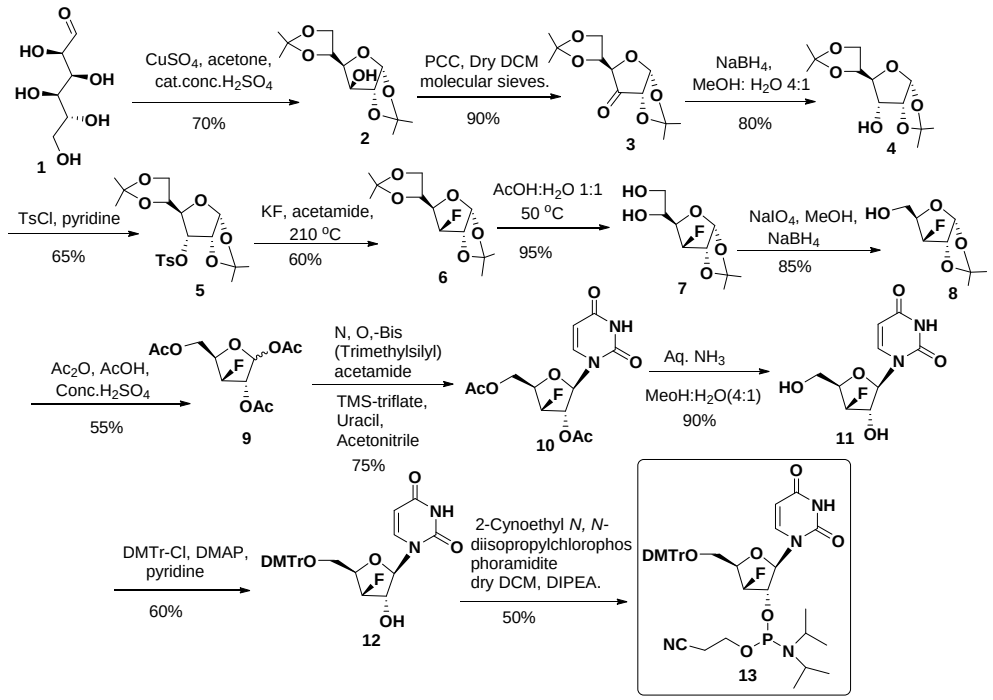

Scheme 1. Synthesis of $^{X}U^{F}$ phosphoramidite monomer

Synthesis of $^{R}U^{F}$ phosphoramidite monomer: 3′-deoxy-3′-fluoro-β-D-ribouridine monomer was synthesized using D-Xylose as a starting material (Scheme 2).

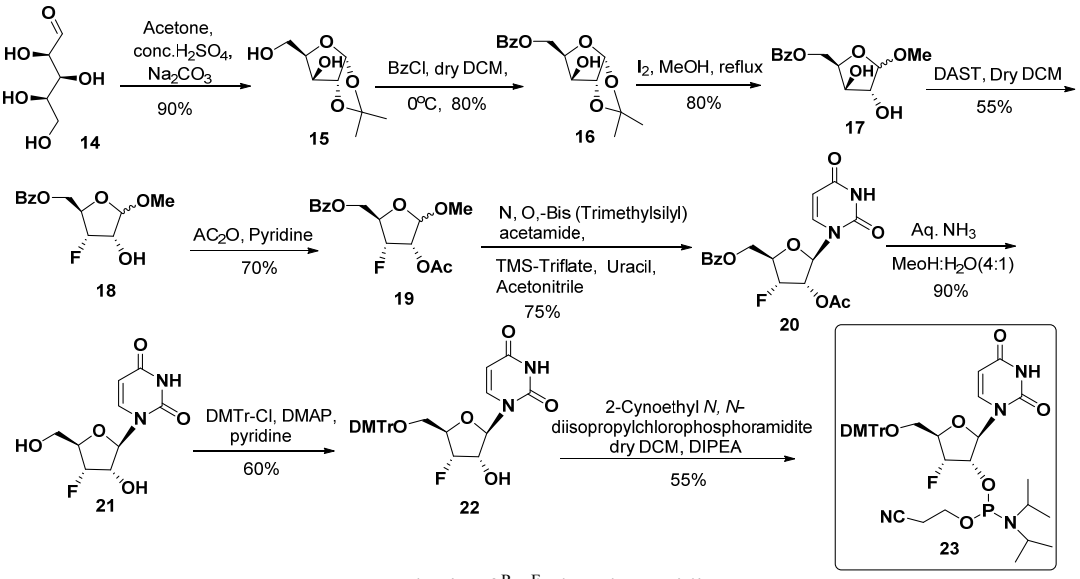

Scheme 2. Synthesis of $^{R}U^{F}$ phosphoramidite monomer

Preliminary study of sugar pucker using ^{1}H NMR $J_{1',2'}$ coupling constant

The %S character for sugar ring was calculated by ^{1}H NMR using empirical formula **%S = 100 X ($J_{1',2'}$-1)/6.9.** The %S for 3′-deoxy-3′-fluoro ribouridine **11** and 3′-deoxy-3′-fluoro xylouridine **21,** were found to be 97.23% and 0.29% respectively.

Synthesis of ngDNA containing $^{X}U^{F}$ and $^{R}U^{F}$ modified units their purification, characterization, duplex stability and CD studies

Nucleoside derivatives $^{X}U^{F}$ and $^{R}U^{F}$ were incorporated into ngDNA1 and ngDNA2 using the automated DNA synthesizer. These modified oligomers were purified by RP- HPLC and characterized by MALDI-TOF mass spectrometry. UV-*T*m studies were carried out to investigate the binding efficiency of the modified ONs to complementary DNA and RNA (Table 1).

Table 1: Synthesized ngDNA oligomers, MALDI-TOF values and UV-*T*m

Entry No	Sequence code	Sequence (5′ → 2′)	Expt./ Obsd.	T_m °C cDNA1	T_m °C RNA1	ΔT_m (°C)
1	ngDNA1	CACCATTGTCACACTCCA	5364/5362	NB	50.5	0.0
2	ngDNA1-1	CACCATTGTCACAC^{X}U^{F}CCA	5368/5365	NB	45.7	-4.8
3	ngDNA1-2	CACCATTG^{X}U^{F}CACAC^{X}U^{F}CCA	5372/5374	NB	44.5	-6.0
4	ngDNA1-3	CACCATTGTCACAC^{R}U^{F}CCA	5368/5366	NB	50.5	0.0
5	ngDNA1-4	CACCATTG^{R}U^{F}CACAC^{R}U^{F}CCA	5372/5372	NB	51.7	+1.2
6	ngDNA1-5	CACCA^{R}U^{FR}U^{F}GTCACACTCCA	5372/5373	NB	49.2	-1.3
7	ngDNA2	CCTCTTACCTCAGTTACA	5369/5368	NB	46.0	0.0
8	ngDNA2-1	CCTCTTACCTCAGT^{R}U^{F}ACA	5373/5376	NB	48.3	+2.3
9	ngDNA2-2	CCTCTTACC^{R}U^{F}CAGT^{R}U^{F}ACA	5377/5379	NB	49.4	+3.4

Similar to the ngRNA sequences reported by Damha *et al.,* all modified ngDNA sequences studied were also found to bind only to complementary RNA and not to cDNA. Oligomers bearing $^{R}U^{F}$**,** *i. e.* S-type frozen monomers units, formed more stable complexes with RNA compared to the unmodified complex, while the complexes formed by oligomers containing $^{X}U^{F}$ N-type frozen monomer with complementary RNA were considerably destabilized compared to unmodified complex. In this case, the consecutive modification by $^{R}U^{F}$ S-type frozen monomers units were not able to cause additive stabilization, in fact,

the duplex formed was marginally destabilized. In another sequence, ngDNA2, $^{R}U^{F}$ derived sequences stabilized the duplex much better. In the sequence context, the difference is that one of the modified units is flanked by a purine instead of pyrimidine at the 2′-end.

Synthesis and thermal stability study of $^{X}U^{F}$ modified 3′-5′-linked oligonucleotide

It is known that the N-type locked or frozen modified nucleosides like LNA/BNA and 2′F-RNA increases the thermal stability of 3′-5′-linked DNA:RNA duplexes. We have studied here the effect of N-type sugar geometry of $^{X}U^{F}$ (2′-5′ monomer unit) on the stability of native 3′-5′-linked DNA:DNA or DNA:RNA duplexes. Two modified ONs **DNA1-1** and **DNA1-2** containing one and two $^{X}U^{F}$ monomer unit were synthesized (Table 2). In this case these modification leads to large destabilization of duplexes with complementary DNA as well as RNA with relatively same Δ*T*m.

Table 2: 3′-5′-linked ONs, MALDI-TOF values and UV-*T*m

No	Seq. code	Sequence (5′ → 3′)	Mass Expt./Obs.	T_m °C cDNA1	ΔT_m (°C)	T_m °C RNA1	ΔT_m (°C)
1	**DNA1**	CACCATTGTCACACTCCA	5364/5364	59.7	0.0	60.0	0.0
2	**DNA1-1**	CACCATTGTCACAC^{X}U^{F}CCA	5368/5368	46.0	-13.7	46.0	-14.0
3	**DNA1-2**	CACCATTG^{X}U^{F}CACAC^{X}U^{F}CCA	5372/5372	49.5	-10.2	49.4	-10.6

CD study of $^{X}U^{F}$ and $^{R}U^{F}$ modified ngDNA

It was observed that the CD spectra were similar for all the complexes studied (Figure 3) and resemble A-type DNA1:RNA1 duplex CD spectra.

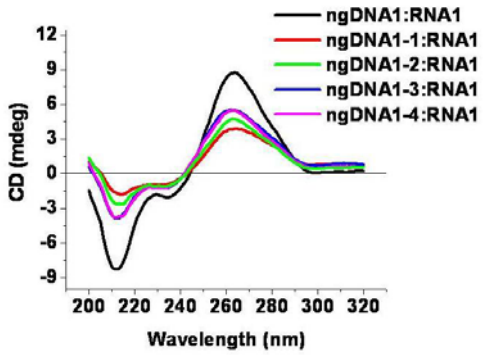

Figure 3. Duplex CD spectra of modified ngDNA1 complexes

Summary and Conclusion

Stabilization of ngDNA:RNA by S-type-frozen monomer and destabilization of the same by N-frozen monomers provides a proof, for the first time, for the prediction that in ngDNA:RNA duplexes, the ngDNA strand would necessarily assume S-type geometry.

Chapter 3. Synthesis of 3′-deoxy-3′-fluoro ribo/xylo thyminyl nucleosides ($^{R}T^{F}$, $^{X}T^{F}$), 3′-deoxy-3′-fluoro ribo/xylo and S-type locked adenine-containing nucleosides ($^{R}A^{F}$, $^{X}A^{F}$ and $^{L}A^{S}$) and arabino-uridine (^{ara}U), their incorporation into ngDNA, and effect on binding properties to target sequences and nuclease resistance property

The uracil containing 3′-deoxy-3′-fluoro ribo/xylo nucleoside ($^{R}U^{F}$ and $^{X}U^{F}$) frozen in S and N-type conformation when incorporated in ngDNA exhibited increase or decrease in binding strength while binding with complementary RNA as compared with the unmodified ngDNA (Chapter 2). Natural DNA exhibits higher binding affinities to complementary RNA compared to $^{R}U^{F}$ modified ngDNA:RNA, which indicate need of further improvement. As it is known that C-5 substitution (methyl, propynyl) of pyrimidines generally results in an improvement in duplex stability due to increase in the hydrogen bonding and base stacking interactions. We synthesized 3′-deoxy-3′-fluoro ribo/xylo thyminyl nucleosides ($^{R}T^{F}$ and $^{X}T^{F}$), and studied their effect on the binding properties of ONs. In addition, the stability of the ONs to 3′-exonucleases (SVPD) was also investigated, where we found that the stability of 2′ end adenosine is very less compared to other nucleosides. We again synthesized the modified 3′-deoxy-3′-fluoro ribo/xylo adenine containing nucleoside $^{R}A^{F}$, $^{X}A^{F}$ and S-type locked adenine $^{L}A^{S}$ monomer and incorporated them to 2′ end of the ngDNA to study their effect on enzymatic stability. In this chapter, we further present the synthesis and binding properties of oligomers containing compact arabino-uridine (^{ara}U).

Section 3.1: Synthesis and biophysical study of $^{X}T^{F}$, $^{X}A^{F}$, $^{R}T^{F}$, $^{R}A^{F}$, and $^{L}A^{S}$ monomers

Synthesis of $^{X}T^{F}$ nucleoside and $^{X}A^{F}$ phosphoramidite monomer: Synthesis of the $^{X}T^{F}$, $^{X}A^{F}$ nucleoside and its conversion to phosphoramidite derivative was achieved as described in Scheme 3.

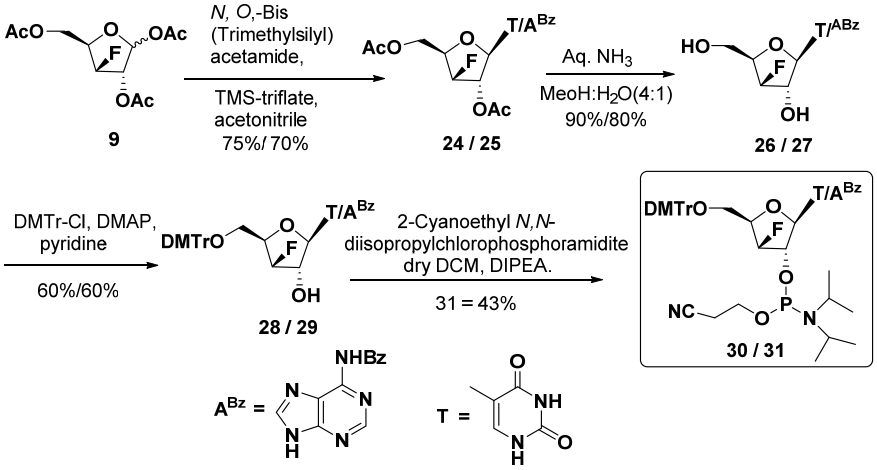

Scheme 3: Synthesis of $^{X}T^{F}$ nucleoside and $^{X}A^{F}$ phosphoramidite monomer

Synthesis of $^{R}T^{F}$ and $^{R}A^{F}$ phosphoramidite monomers:

Synthesis of the $^{R}T^{F}$, $^{R}A^{F}$ nucleoside and its conversion to phosphoramidite derivative was achieved as described in Scheme 4

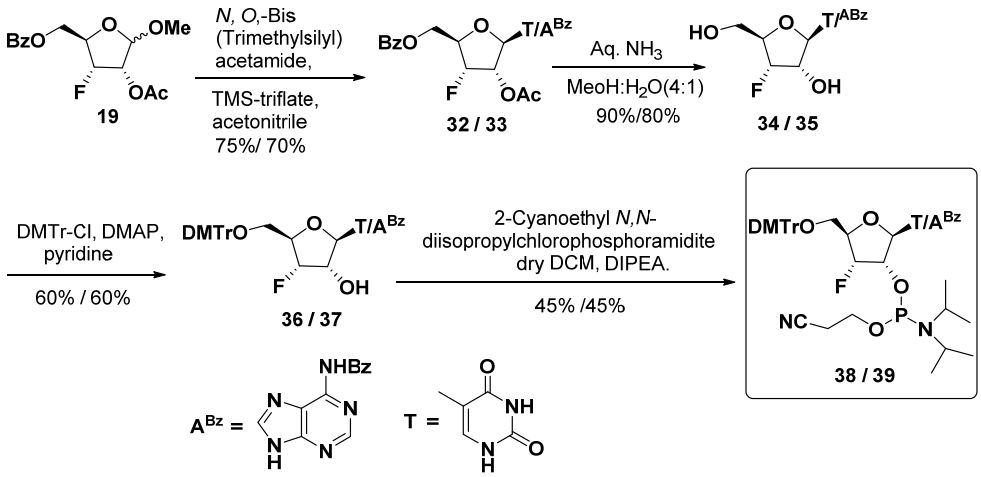

Scheme 4: Synthesis of $^{R}T^{F}$ and $^{R}A^{F}$ phosphoramidite monomers

Synthesis of S-type locked adenosine ($^{L}A^{F}$) phosphoramidite monomer

Synthesis of the $^{L}A^{F}$ nucleoside and its conversion to phosphoramidite derivative was achieved as described in Scheme 5.

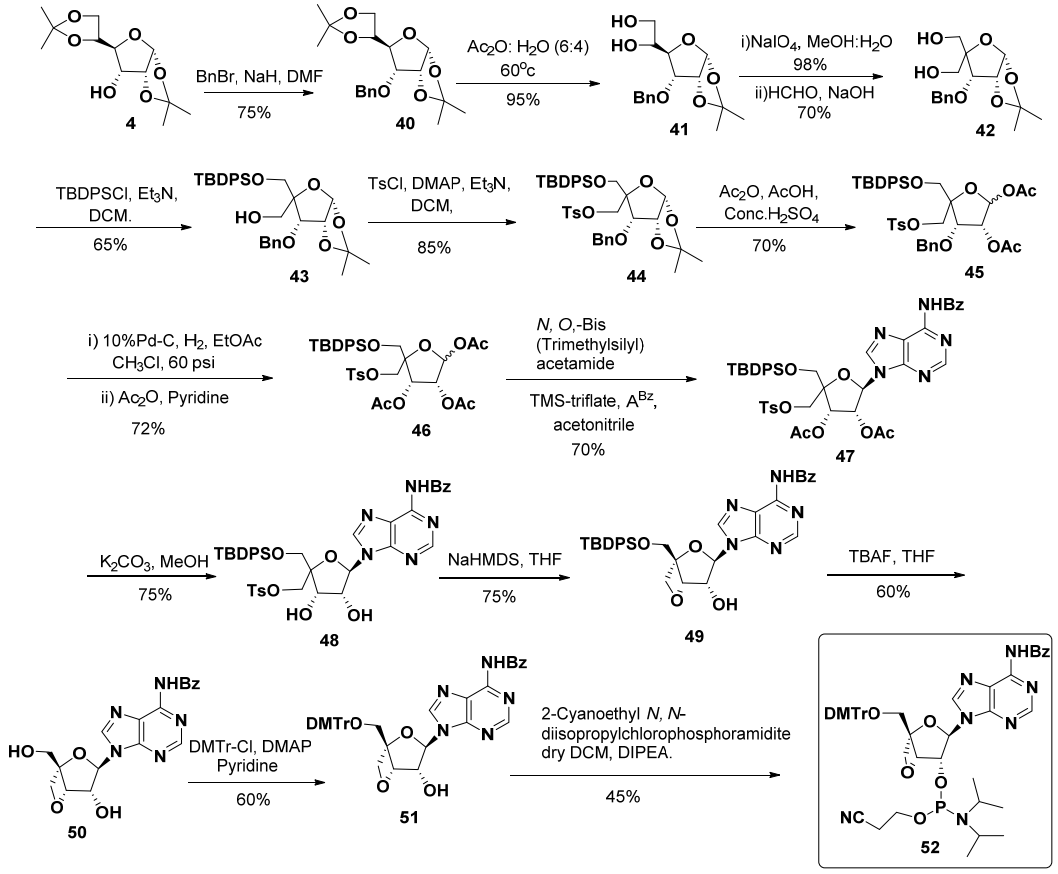

Scheme 5: Synthesis of $^{L}A^{S}$ phosphoramidite monomer

Preliminary study of sugar pucker using ^{1}H NMR $J_{1'2'}$ coupling constant

We calculated the %S for $^{R}A^{F}$ and $^{X}A^{F}$ nucleoside unit from the H1′-H2′ NMR coupling constants using formula **%S = 100 X ($J_{1'2'}$-1)/6.9.** The %S for monomeric conformations of $^{X}T^{F}$ nucleoside **26,** $^{X}A^{F}$ nucleoside **27**, $^{R}T^{F}$ nucleoside **34,** $^{R}A^{F}$ nucleoside **35**, and S-type locked $^{L}A^{S}$ nucleoside **51** were found to be 2.17%, 3.76%, 97.23%, 100% and 79.71% respectively.

Synthesis of oligonucleotides containing modified units their purification, characterization and duplex stability studies

Observed MALDI-TOF value and the UV-T_m, of the complexes containing the $^{X}A^{F}$, $^{R}T^{F}$, $^{R}A^{F}$, and $^{L}A^{S}$ units are summarized in Table 3. The complexes formed by oligomers containing increasing number of $^{R}T^{F}$ S-type frozen monomer with complementary RNA were found to be stabilizing the duplex as compared to the control ngDNA2:RNA2 sequence but the stability is less compared to $^{R}U^{F}$ containing complexes. This is in contrast to the general phenomenon in 3′-5′-linked DNA oligomers where substitution of T for U increases stability of duplex. The S-type frozen $^{R}A^{F}$ units stabilized the duplex and the stability increased with increase in the number of modified units. In fact the oligomer containing two $^{R}A^{F}$ units is found to be more stable compare to two $^{R}U^{F}$ and $^{R}T^{F}$ units. We again modified ngDNA2 with the combination of both $^{R}T^{F}$ and $^{R}A^{F}$ monomer unit spaced by two unmodified units. The stability further increased in such oligomer. The end modification either S-type frozen/locked $^{R}A^{F}$, $^{L}A^{S}$ or N-type frozen $^{X}A^{F}$ did not affect on the duplex stability and the T_m values were nearly same as the control. As expected, the sequence ngDNA1-9 where a single N-type frozen $^{X}A^{F}$ incorporated at middle of the sequence destabilized the duplex.

Table 3: Synthesized ngDNA oligomers their MALDI -TOF values and UV-*T*m

Entry No	Sequence code	Sequence (5' → 2')	Exp./Obs	T_m °C cDNA2	T_m °C RNA2	ΔT_m (°C)
1	ngDNA2	CCTCTTACCTCAGTTACA	5369/5368	NB	46.0	0.0
2	ngDNA2-3	CCTCTTACCTCAGT$^{R}T^{F}$ACA	5387/5386	NB	47.3	+1.3
3	ngDNA2-4	CCTCTTACC$^{R}T^{F}$CAGT$^{R}T^{F}$ACA	5405/5410	NB	48.8	+2.8
4	ngDNA2-5	CCTCTTACCTCAGTT$^{R}A^{F}$CA	5387/5388	NB	46.6	+0.6
5	ngDNA2-6	CCTCTTACCTC$^{R}A^{F}$GTT$^{R}A^{F}$CA	5405/5410	NB	49.8	+3.8
6	ngDNA2-7	CCTCTTACCTC$^{R}A^{F}$G$^{R}T^{F}$TACA	5405/5409	NB	49.8	+3.8
7	ngDNA2-8	CCTCTT$^{R}A^{F}$CCTC$^{R}A^{F}$GT$^{R}T^{F}$ACA	54235426	NB	50.4	+4.4
8	ngDNA1	CACCATTGTCACACTCCA	5364/5362	NB	50.5	0.0
9	ngDNA1-6	CACCATTGTCACACTCC$^{X}A^{F}$	5382/5381	NB	50.4	-0.1
10	ngDNA1-7	CACCATTGTCACACTCC$^{R}A^{F}$	5382/5383	NB	50.6	+0.1
11	ngDNA1-8	CACCATTGTCACACTCC$^{L}A^{S}$	5392/5395	NB	50.5	0.0
12	ngDNA1-9	CACCATTGTCAC$^{X}A^{F}$CTCCA	5382/5381	NB	47.1	-3.4

Section 3.2: Synthesis and rationale for designing arabino-uridine (^{ara}U) monomer its incorporation into ngDNA and binding study.

Arabinonucleosides are stereoisomers of ribonucleosides, differing only in the configuration at the 2′-position of the sugar ring. But such small change in configuration of 2′-hydroxy group from bottom face in ribonucleoside to the top face in arabinonucleoside produces some unique properties in 3′-5′-linked arabinonucleic acids (ANA).

As presented in the work so far the improved hybridization results were obtained by S-type frozen nucleosides with compact geometry using uracil, thymine and adenine compared to control ngDNA:RNA duplex. However, to achieve thermal stabilities comparable to or higher than those of unmodified natural 3′-5′-linked duplexes, a more favourable modification would be warranted for 2′-5′ -linked oligomers. Arabinonucleoside with 2′-5′ linkages is proposed for this study. In arabinonucleoside, sugar ring is in equilibrium between S and N-type. In this case 2′-hydroxy group is above the plane therefore P-P distance will be less and the nucleotide will be with the compact geometry in either S-type or N-type sugar conformation.

Synthesis of arabino-uridine (^{ara}U) phosphoramidite monomer: Synthesis of the ^{ara}U nucleoside and its conversion to phosphoramidite derivative was achieved as described in Scheme 6.

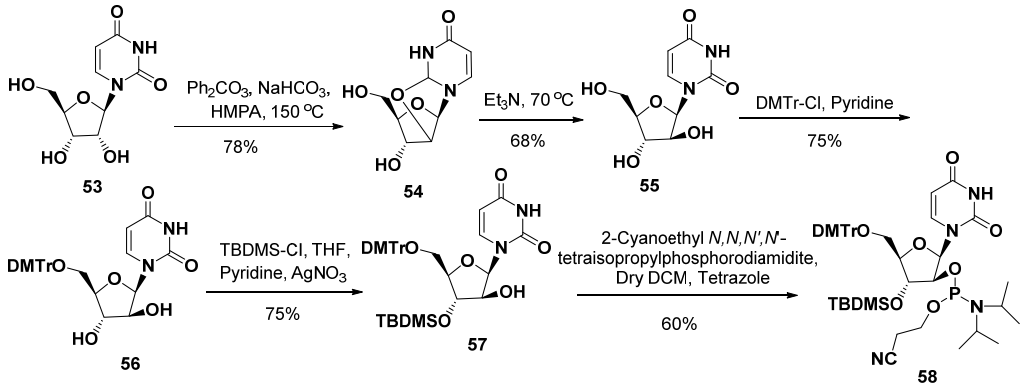

Scheme 6: Synthesis of ^{ara}U phosphoramidite monomer

Preliminary study of sugar pucker using ^{1}H NMR $J_{1',2'}$ coupling constant

We calculated the %S for compound **55** using formula **%S = 100 X ($J_{1',2'}$-1)/6.9** and H1′-H2′ NMR coupling constants as earlier reported and was found to be 47.8%.

Synthesis of oligonucleotides containing modified units their purification, characterization and duplex stability studies

ONs containing one and two modified ^{ara}U building blocks were synthesized. The MALDI-TOF values and UV-T_m of the duplexes with complimentary DNA and RNA are listed in Table 4. Both the modified ngDNA sequences bind only to complementary RNA. Introduction of a single monomeric unit towards the 2′ end in 18mer caused a destabilization with complementary RNA2. A cumulative effect was observed in destabilization when two ^{ara}U monomer units were incorporated.

Table 4. Synthesized ngDNA oligomers their MALDI -TOF values and UV-*T*m

Entry No	Sequence Code	Sequence (5′ → 2′)	Mass	UV-T_m ^oC		
			Expt./Obs.	cDNA2	RNA2	ΔT_m ^oC
1	ngDNA2	CCTCTTACCTCAGTTACA	5369/ 5368	NB	46.0	0.0
2	ngDNA2-9	CCTCTTACCTCAGT^{ara}UACA	5385/5383	NB	45.3	-0.7
3	ngDNA2-10	CCTCTTACC^{ara}UCAGT^{ara}UACA	5401/5392	NB	43.2	-2.3

Section 3.3: Stability of oligonucleotides to SVPD

Considering nuclease resistance as an important factor, we examined the 3′-exonuclease sensitivity of the unmodified and modified ngDNA using snake venom phosphodiesterase (SVPD) and compared them with natural DNA. The 18mer unmodified ngDNA1 and modified ngDNA1-2 and ngDNA1-4 containing two $^{R}U^{F}$ and $^{X}U^{F}$ unit respectively were chosen for the experiment (Table 5).

Table 5. ONs used for 3′-exonuclease degradation study

Entry No.	Scequence code	Sequences
1	DNA1	**5′** CACCATTGTCACACTCC**A 3′**
2	ngDNA1	**5′** CACCATTGTCACACTCC**A 2′**
3	ngDNA1-2	**5′** CACCATTG$^{X}U^{F}$CACAC$^{X}U^{F}$CC**A 2′**
4	ngDNA1-4	**5′** CACCATTG$^{R}U^{F}$CACAC$^{R}U^{F}$CC**A 2′**
5	ngDNA3	**5'**GAAGGGCTTCTTCCTTA**T 2'**

The natural 3′-5′ linked single strand DNA1 did not show any 3′-exonuclease resistance and was completely degraded in 20min. In the case of modified and unmodified ngDNA, the last nucleotide A18 was removed quickly within 20min to give 17mer ONs.

Once the A18 was cleaved, the 17mer of the unmodified as well as modified ngDNA were found to be considerably stable under these conditions. In Figure 4, total percentages of intact 17mer were plotted against time points to give SVPD digestion curves for each ONs.

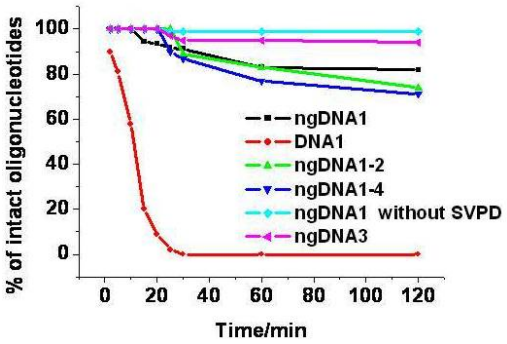

Figure 4: Stability assay of the 17mer (after A18Cleavage) ONs to degradation by SVPD

The above experiment indicated that the stability of 2′ end adenosine is very less compared to other nucleosides. In order to understand the relative nuclease resistance of oligomer having 2′end modification by $^{R}A^{F}$, $^{X}A^{F}$ and $^{L}A^{S}$ units, we conducted nuclease resistance experiment for sequences showed in Table 6. The results suggest that the incorporation of S-type frozen/locked adenosine gave greater nuclease resistance. The ngDNA1-6 with N-type frozen $^{X}A^{F}$ also showed higher stability than the unmodified ngDNA1 (Figure 5).

Table 6. 2′end adenosine modified ($^{R}A^{F}$, $^{X}A^{F}$ and $^{L}A^{S}$) ONs

Entry No	Sequence code	Sequence
1	ngDNA1	**5**‘CACCATTGTCACACTCC**A 2′**
2	ngDNA1-6	**5**‘CACCATTGTCACACTCC^{X}**A**^{F} **2′**
3	ngDNA1-7	**5**‘CACCATTGTCACACTCC^{R}**A**^{F} **2′**
4	ngDNA1-8	**5**‘CACCATTGTCACACTCC^{L}**A**^{S} **2′**

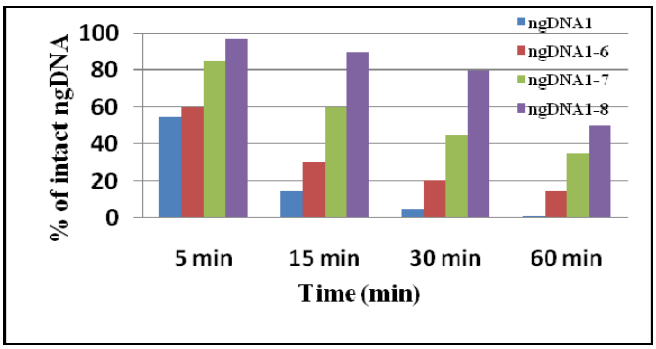

Figure 5: Stability assay of the ONs to degradation by SVPD

Summary and Conclusion

The duplex stabilization caused by the S-type frozen monomer ($^{R}T^{F}$ and $^{R}A^{F}$) and destabilization by N-type frozen $^{X}A^{F}$ and by the compact arabino uridine (^{ara}U) is shown again in accordance with the prediction of S-type conformation for the ngDNA strand in an ngDNA:RNA duplex. Thymine did not improve stability over uracil in 2′-5′ linked ngDNA which is in contrast to the natural DNA. This could be due to pseudoequatorial base in S-type geometry where stacking and hydrogen bonding is not strong. Nuclease resistance studies of all the 2′end modified ngDNA were stable for SVPD digestion over unmodified ngDNA and the stability order was $^{L}A^{S}$ ngDNA>> $^{R}A^{F}$ ngDNA> $^{X}A^{F}$ ngDNA > ngDNA. S-type frozen/locked $^{R}A^{F}$ and $^{L}A^{S}$ show high stability to SVPD, while the N-type frozen $^{X}A^{F}$ lead to successful modulation of the nuclease resistance.

Chapter 4: Conformational studies of $^{R}U^{F}$, $^{R}A^{F}$, $^{X}U^{F}$, $^{X}A^{F}$, $^{L}A^{S}$, and ^{ara}U nucleoside using NMR, X-ray crystal structure and Matlab Pseudorotation GUI program

We have discussed in Chapter 1 that the sugar puckering of natural ribo- and deoxyribonucleosides are known to exist in dynamic equilibrium between two major conformers: the North (N) and the South (S) types. In the solid state, one conformation is prevalent in relation to the other. In solution, the North/South interconversion is rapid, depending upon the energy barrier (Figure 6). The conformational behavior of natural or modified nucleosides was defined by the four structural parameters i.e. glycosidic torsion angle χ,, torsion angle γ, phase angle of pseudorotation *P* and the puckering amplitude ν_{max}, which ultimately gives S-type and N-type population for each monomer in solid state as well as in solution state.

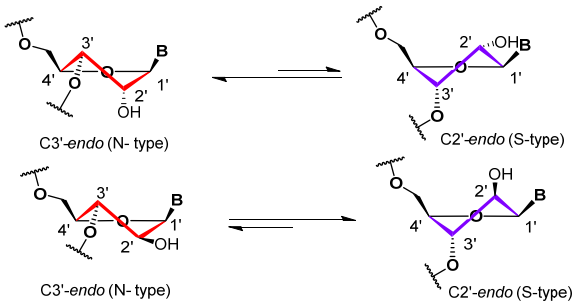

Figure 6. Sugar conformations in two-state *North*↔*South* equilibrium

Conformational analysis of the furanose ring

The origin for all the studies of nucleoside and nucleotide conformation is provided by the X-ray structural analysis, which provides accurate bond angles, bond lengths, and the torsional angles and thus accurately determines the conformations present in the solid state. However, most modified nucleosides show conformational equilibrium in aqueous solution. It is for this reason that NMR spectroscopy can be a valuable complement to X-ray crystallographic studies. The vicinal proton-proton ($^3J_{HH}$) couplings constant can be used to calculate mole fraction of N and S conformers as well as their geometry expressed by their phase angle of pseudorotation P_N and P_S and puckering amplitude ν_N and ν_S. Two different software's are available for such analysis one is PSEUROT program developed by Altona *et. al* and other is Matlab Pseudorotation GUI (Graphical User Interphase) program developed by Pieter MS *et.al*.

In this chapter, we present the results of our studies to understand the furanose ring conformation of $^{R}U^{F}$, $^{R}A^{F}$, $^{X}U^{F}$, $^{X}A^{F}$, $^{L}A^{S}$, and ^{ara}U nucleoside, in solution as well as solid state. We report an integrated ^{1}H NMR (400MHz) and X-ray crystallographic study on the conformation of the sugar rings of these synthesized nucleoside analogues. We analyzed vicinal scalar *J*-coupling constants $J_{1'2'}$, $J_{1'2''}$, $J_{2'3'}$ and $J_{3'4'}$ at different temperature and were used as an input for the pseudorotation analysis of the sugar using the Matlab GUI Pseudoroatation program. We also studied the nuclear Overhauser effects to reveal important information about the dynamic conformations in solution.

Comparative Results

Comparative result obtained from Sum rule, X-ray crystallography and Matlab GUI Pseurot calculation are shown in Table 7. The conformational properties of nucleoside $^{X}U^{F}$, $^{R}U^{F}$ and $^{X}A^{F}$ in solution and in the crystalline state were found to quite consistent picture. However in ^{ara}U nucleoside the X-ray crystallography results indicate S-type conformation of sugar ring in solid state while both sum rule calculation as well as Matlab Pseurotational calculations showed that it is in ~ 60 % N-type in solution state. The N-type conformation of ^{ara}U was also observed by NOE study. $^{R}A^{F}$ and $^{L}A^{S}$ show S-type conformation in solution.

Table 7: Comparative result from Sum rule, X-ray crystallography and Matlab GUI Pseurot

Nucleoside analogue	**%S= 100X(*J*1'2'-1)/6.9**	**Matlab Pseudorotation GUI** (285K)		**X-ray crstal structure**
$^{X}U^{F}$	% N=99.71 % S= 0.29	Conformer 1 P = 45.11 ν_{max} = 55.03 %N= 72.4	Conformer 2 P = 288.5 ν_{max} = 41* %S= 38.6	P = 0.88 ν_{max} =37.59 N-Type
$^{R}U^{F}$	% N=02.76 % S= 97.24	Conformer 1 P = 69.27 ν_{max} = 60 %N= 2.6	Conformer 2 P = 172.31 ν_{max} = 36.52 %S= 97.4	P = 171.2 ν_{max} =38.60 S-Type
$^{X}A^{F}$	% N=96.24 % S= 3.76	Conformer 1 P = 9.43 ν_{max} = 43.29 %N= 84.6	Conformer 2 P = 92.38 ν_{max} = 39.0* %S= 15.4	P = 14.64 ν_{m} =36.69 N-Type
$^{R}A^{F}$	% N=0 % S= 100	Conformer 1 P = -91.08 ν_{max} = 42.0* %N= 0.0	Conformer 2 P = 168.04 ν_{max} = 39.58 %S= 100	-----
^{ara}U	% N=52.2 % S= 47.8	Conformer 1 P = -44.9 ν_{max} = 40.8 %N= 59.8	Conformer 2 P = 84.29 ν_{max} = 38.5* %S= 40.2	P = 153.93 ν_{max} =37.85 S-Type
$^{L}A^{S}$	% N=20.29 % S= 79.71	Conformer 1 P = -10.10 ν_{max} = 51.92 %N= 23.2	Conformer 2 P = 146.54 ν_{max} = 48.0 %S= 76.8	-----

Summary and Conclusions

1. All the experimental results show that the sugar rings of $^{R}U^{F}$ and $^{R}A^{F}$ nucleosides are frozen in S-type conformation while the sugar rings of $^{X}U^{F}$ and $^{X}A^{F}$ nucleoside frozen in N-type conformation.
2. The conformation of sugar ring is locked in S-type in $^{L}A^{S}$ nucleoside.
3. In the case of ^{ara}U the sugar ring is in S-type in solid state while it is 60% N-type in solution state.

Thus, the configuration of fluorine at 3′ position of furanose ring in nucleoside affects the furanose ring conformation. The 3′ ribofluoro and 3′ xylofluoro substituents are responsible for frozen S-type and frozen N-type conformations of furanose ring respectively in solid as well as solution state.

Chapter 1

Antisense technologies: Improvement through novel chemical modifications in genetic and nongenetic nucleic acids

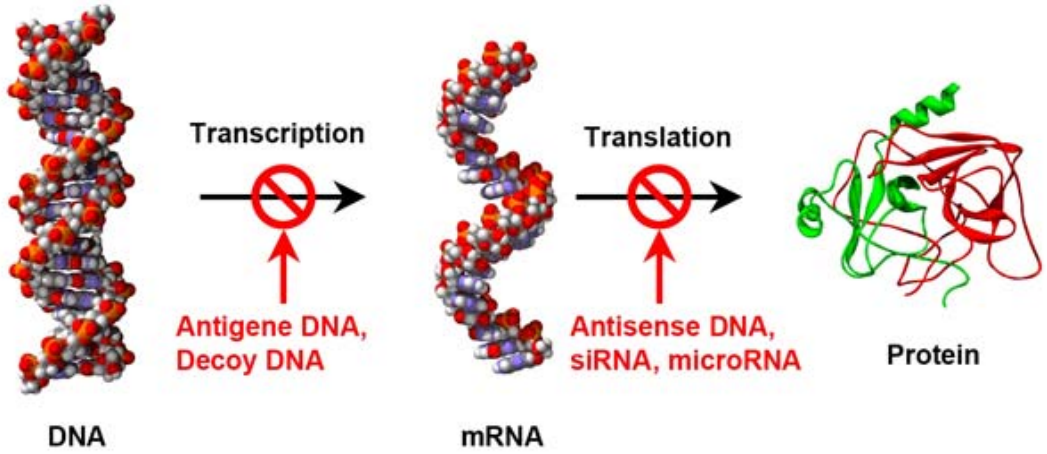

This chapter presents a brief review about the advancements in nucleic acid therapeutics with respect to different aspects of antisense oligonucleotides for selective inhibition of gene expression. The oligonucleotide therapeutic agents such as antisense DNA, ribozymes, siRNA, and miRNA, act on target mRNA and arrest the protein synthesis. The over production or abnormal production of proteins is implicated or associated with many diseases. Antisense technology prevents the production of disease causing protein which results in a therapeutic benefit to patients. This chapter also describes the relevant literature pertaining to the useful chemical modifications of DNA/RNA with a particular emphasis on genetic 3′-5′ and nongenetic 2′-5′ linked nucleic acids and their structural features.

1.1 Introduction

Antisense agents are valuable tools for inhibiting the expression of target genes in a sequence-specific manner, and have potential in therapeutics. The antisense oligonucleotides (AS-ONs) exhibit either corrective or disruptive activity through strong and specific interaction with target mRNA sequences. The disruptive antisense ONs down-regulate the synthesis of disease-causing functional proteins *via* various mechanisms like steric blocking of ribosomal machinery, RNase H susceptibility, ribozyme activation and/or RNA interference induced by short double stranded RNA molecules like siRNA/miRNA. In the case of corrective antisense ONs, restoration of the viable protein synthesis is effected by acting at pre-mRNA level *via* splice corrections. The research activity in this area is directed towards improving practical difficulties encountered by AS-ONs such as cellular delivery, intracellular stability, ability to hybridize with the target sequences, susceptibility to RNase H cleavage, ease of synthesis and safety.

To overcome these challenges several chemical modifications of DNA/RNA have been developed. The ONs having 'nongenetic' 2′-5′ phosphodiester linkages (ngDNA) were also considered as candidates for antisense applications due to their RNA selective hybridization properties and enzymatic stability.

In this chapter we describe the literature pertaining to the different antisense strategies, AS-ONs and chemical modifications, structural features, binding preferences and recent developments in the area of DNA and ngDNA.

1.2 Nucleic acids

1.2.1 Genetic and non genetic nucleic acids: Structural overview

DNA and RNA as genetic material is polymer of nucleotide units, and each nucleotide is a micromolecular component comprising of a heterocyclic nitrogenous base, a β−D-pentafuranose sugar moiety and a phosphodiester linkage (Figure 1). The heterocyclic bases are purines adenine (A) and guanine (G) and pyrimidines cytosine (C), thymine (T) and uracil (U). The difference in DNA and RNA is whether the pentose is 2′-deoxyribose (DNA) or ribose (RNA) and the thymine (T) is replaced by uracil (U) in RNA (Figure 1). The heterocyclic base is covalently linked (at *N*-1 of pyrimidines and *N*-9 of purines) via a

N-*β*-glycosyl bond to the 1′ carbon of the pentose. The phosphate forms a diester linkage between the 3′ and 5′–hydroxy groups of the adjacent sugars forming the biopolymer. In the natural DNA and RNA, the D-sugar enantiomer and *β*-glycosyl linkages are present over the L- and *α*-counterparts.

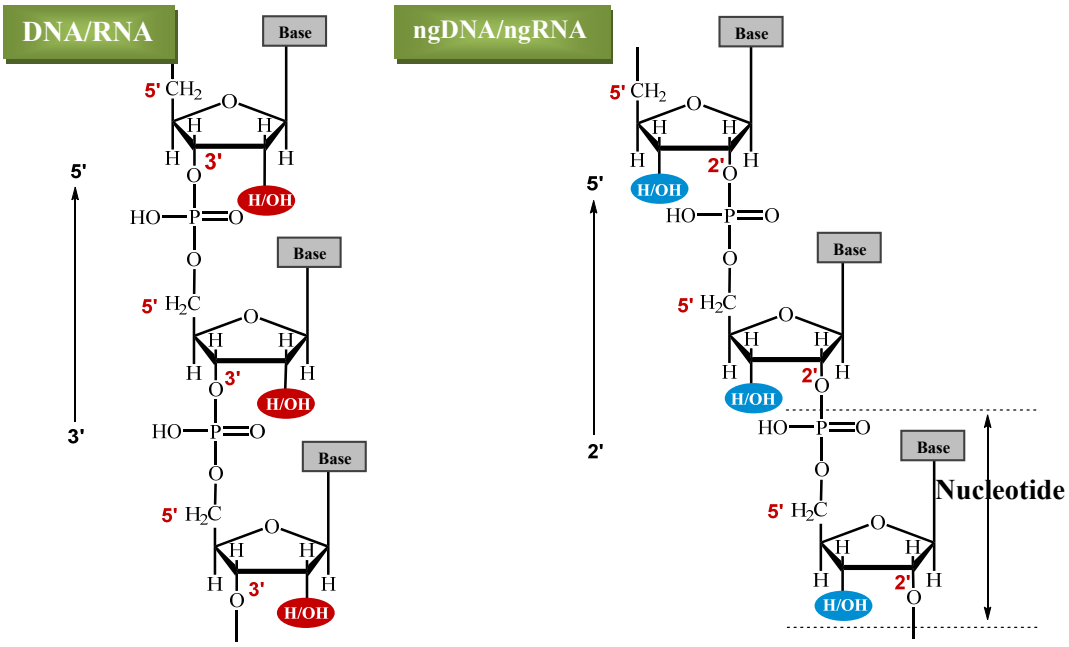

Figure 1. Genetic and non genetic nucleic acids

Natural nucleic acids with 3′-5′ phosphodiester linkages (Figure 1) function in encoding, transmitting and expressing genetic information, therefore are referred to as genetic nucleic acids. In most cases DNA carries the hereditary information from generation to generation and RNA functions as messenger to convert the genetic information into amino acid sequences which form functional proteins.

The nucleic acids with 2′-5′ phosphodiester linkages are also found in nature but they are not used to encode genetic information and hence are called as nongenetic nucleic acids (ngDNA, ngRNA) (Figure 1).

In 1953, J. D. Watson and F. H. Crick discovered the double stranded structure[1] of DNA (excluding viruses) (Figure 2a).[2] The nitrogenous base pairs in DNA (A–T and C–G) are formed *via* hydrogen bonds within the antiparallel double-stranded (ds) structure for DNA. The N-H groups of the bases are the hydrogen donors, while the sp^2- hybridized electron pairs on the oxygen's of the base C=O groups and the ring nitrogen's are hydrogen

bond acceptors, which are engaged in the formation of specific (Watson–Crick) A-T and G-C base pairs (Figure 2b).[2] A–T pairs form two hydrogen bonds while C–G pairs form three. RNA usually exists in the single-stranded (ss) form but may fold into secondary and tertiary structures through the formation of specific base pairings (A-U and C-G).

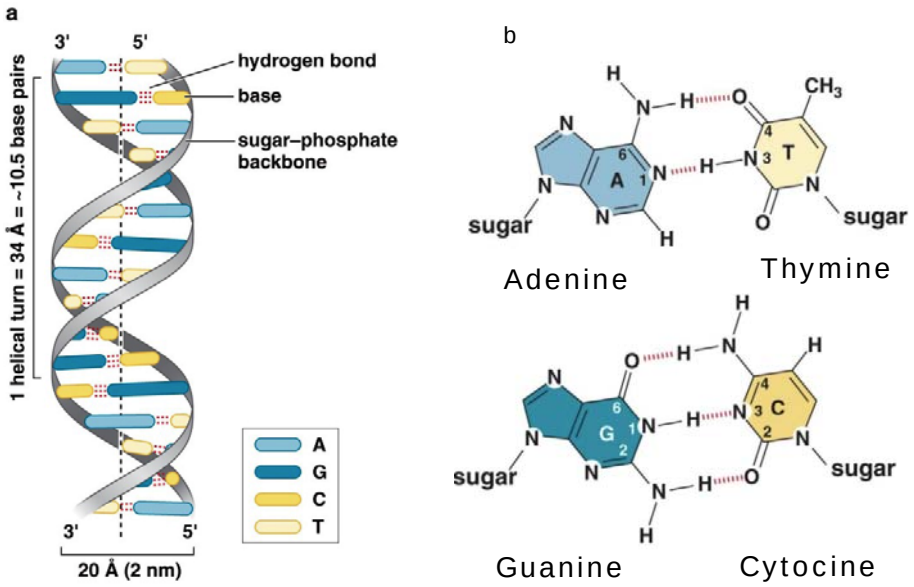

Figure 2. (a) Structure of Double-stranded DNA (B-DNA) (b) Watson and Crick hydrogen- bonding scheme for A: T and G: C base pair

Other significant base pairing are the Hoogsteen[3a] and Wobble[3b] base pairs. In Hoogsteen base pairing, the purine rotates 180° with respect to the helix axis and adopts *syn* conformation. Hoogsteen base pairs utilize the C6-N7 face of the purine for hydrogen bonding with Watson-Crick (N3-C4) face of the pyrimidine (Figure 3, a and b). This base pairing permits the formation of triple helix DNA also called triplex or H-DNA. In Wobble base pairing, a single purine is able to recognize a non complementary pyrimidine (e.g. IU and GU, where I= Inosine, U=Uracil) (Figure 3**,** c and d) and these have importance in the interaction of messenger RNA (mRNA) with transfer RNA (tRNA) on the ribosome during protein synthesis (codon-anticodon interactions). In ONs, the base pairs stack over each other (π-π interaction) further stabilizing the secondary structure.

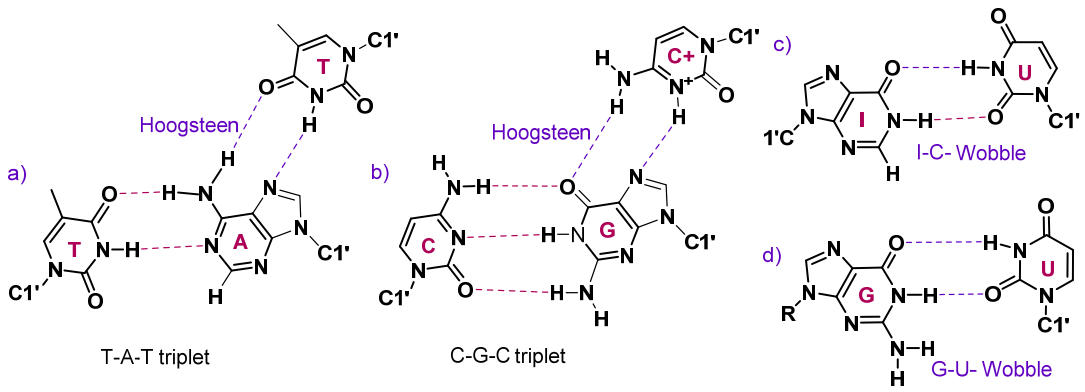

Figure 3. Hoogsteen (a,b) and Wobble (c,d) hydrogen-bonding

1.2.2 DNA Conformations

The conformations of nucleic acids are dynamic and are stabilized by several forces. Besides base pairing, the conformational features are constrained by *pseudo*-torsional angles for rotation around each bond. The details of the conformational structure of nucleotides are accurately defined by the torsional angles α, β, γ, δ, ε and ζ in the phosphate backbone, ν_0 to ν_4, in the furanose ring, and χ for the glycosidic bond (Figure 4).[4]

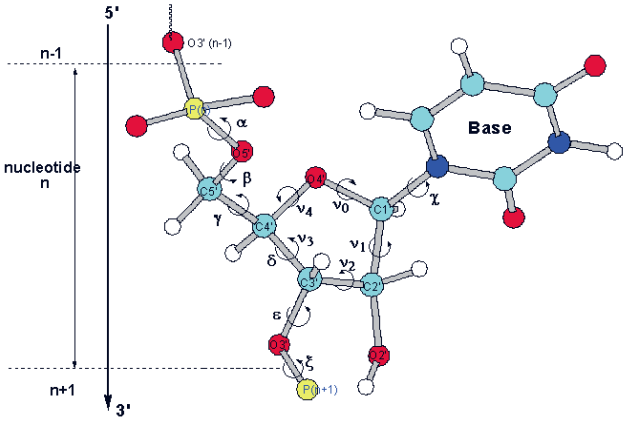

Figure 4. Torsional angle notations for one nucleotide

The six sugar phosphate backbone torsion angles [α, β, γ, δ, ε and ζ] are often roughly described as being in a conformational hyperspace such as *cis* (*c*) = 0 ± 30º, + *gauche* (*g*+) = 60 ± 30º, + *anticlinal* (*a*+) = 120 ± 30º, *trans* (*t*) = 180 ± 30º, - *anticlinal* (a-) = 240 ± 30º, - *gauche* (*g*-) = 300 ± 30º.

The base is attached to sugar by a glycosidic bond. The torsion angle about this bond is defined χ [O4′-C1′-N9-C4] for purines and [O4'-C1'-N1-C2] for pyrimidines. Torsion χ can adopt two main conformation called *syn* (-90º ≤ χ ≤ 90º) and *anti* (90º ≤ χ ≤ 180º). *Anti* orientation is more favorable compared to *syn* orientation because in the *anti* conformation there is no particular steric hindrance between sugar and nucleobase. However, the angle of χ can be tuned by the sugar pucker as well as the base type (purine or pyrimidine) and substituent on the base (adenosine is in *anti* conformation but 8-bromoadenosine is in *syn* conformation).

A planar conformation is energetically unfavorable for the pentafuranose sugar moiety of nucleotide because in this arrangement, all the substituents attached to carbon atoms are fully eclipsed. The system reduces its energy by puckering. The ring puckering arises from the effect of nonbonded interactions between substituents at the four ring carbon atoms-the energetically most stable conformation for the ring has all substituents as far apart as possible. This '*puckering*' is described by identifying the major displacement of the carbons *C*2′ and *C*3′ from the median plane of *C*1′-*O*4′-*C*4′. Thus, if the *endo*-displacement of *C*-2′ is greater than the *exo*-displacement of C3′, the conformation is called *C*2′-*endo* and so on for other atoms of the ring.[5] The *endo*-face of the furanose is on the same side as *C*5′ and the base; the *exo*-face is on the opposite face to the base (Figure 5).

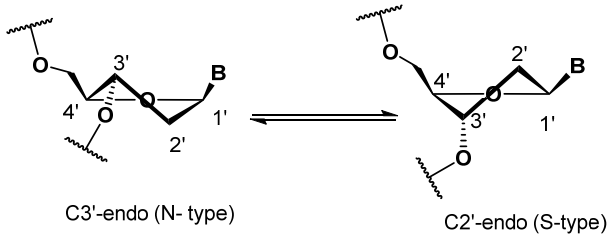

Figure 5. N-type and S-type sugar puckering

The concept of pseudorotation has been introduced to describe the conformation of ribose and deoxyribose rings in nucleotides with two variable parameters, the pseudorotation phase angle *P* and the puckering amplitude ν_{max}.[6] The both parameters P ($P = (\nu_4+\nu_{1)}-(\nu_3+\nu_0)/2\nu_2$ (sin36+sin72)) and ν_{max} ($\nu_{max} = \nu 2/\cos P$) is depends upon the furanose ring torsion angle ν_0 to ν_4. Under physiological conditions, the deoxyribofuranosyl sugars in DNA adopt preferentially 3′-*exo*, 2′-*endo* twist form (often referred to as *South* or S-type conformation), whereas ribofuranosyl sugars in RNA are in 3′-*endo*, 2′-*exo* twist form

(often referred to as *North* or N-type conformation). Interestingly the conformation predominantly adopted by a nucleoside/nucleotide is not always present in a oligonucleotide double helix. In solution, N-type and S-type conformations are in rapid equilibrium and are separated by a low energy barrier (Figure 5). The pseudorotation cycle of sugar part of nucleoside is shown in Figure 6.[7]

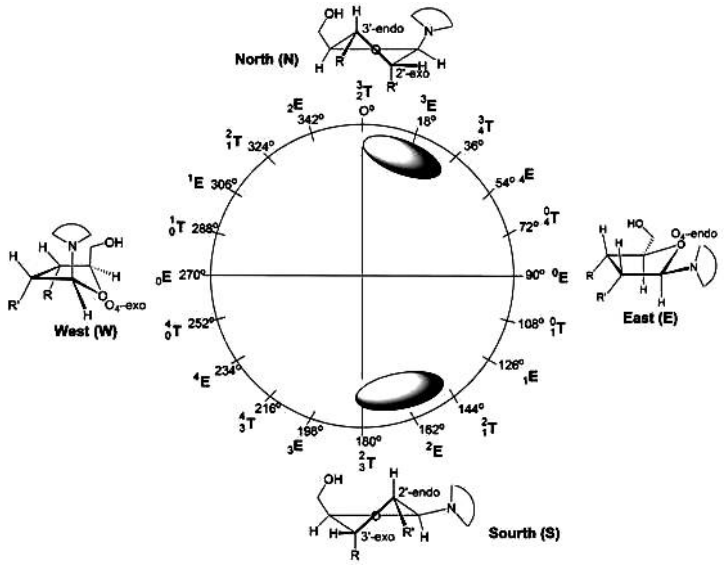

Figure 6. Pseudorotation cycle of the furanose ring in nucleosides. E = envelope; T = twist. The North type ($1^{o} \leq P \leq 34^{o}$) and South type ($137^{o} \leq P \leq 194^{o}$) pseudorotamers commonly populated in β-D-oligonucleotides are shaded.

1.2.3 Stereoelectronic effects in sugar conformation of nucleosides

The conformation of the pentofuranose sugars are not static in solution and are involved in two-state *North*↔*South* equilibrium (Figure 5). The dynamic nature of this equilibrium was evidenced by Chattopadhyaya's group[8,9] by temperature-dependent NMR studies, which showed that conformation adopted by a sugar depends upon a number of factors, such as the *anomeric* effect, *gauche* effect and steric interactions.

In terms of steric effect alone, for β-D-nucleosides, S-type pseudorotamers are energetically favored in comparison with N-type counterparts, since the pseudoequatorial oriented nucleobase in the former exerts less steric repulsions with the other substituents on the pentofuranose moiety than when it is pseudoaxial in the latter (Figure 7). But the energetics of N↔S conformational equilibrium is known to be determined by the relative strengths of *anomeric* and *gauche* effects.

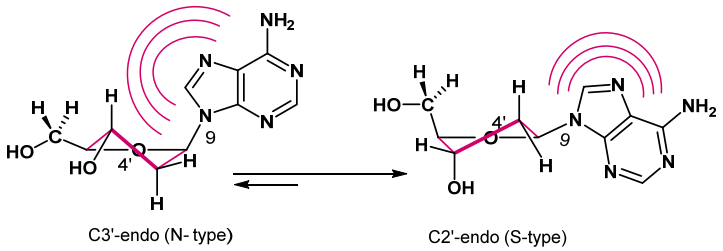

Figure 7. The drive of the two-state N ↔S equilibrium toward S- over N-type pseudorotamers by the steric effect of the nucleobase in DNA.

The O4'-C1'-N1/9 *anomeric* effect or Edward-Lemieux effect received its name from the term used to designate the C-1 carbon of a pyranose/furanose, the *anomeric* carbon. It is a stereoelectronic effect that describes the tendency of heteroatomic substituents adjacent to a heteroatom within a cyclohexane/cyclopentane ring to prefer the *axial* orientation instead of the less hindered *equatorial* orientation that would be expected from steric considerations. This is due to the stabilizing interaction (hyperconjugation) between the unshared electron pair on the one heteroatom (the endocyclic one in a sugar ring) and the σ* orbital for the axial (exocyclic) C–X bond (Figure 8).

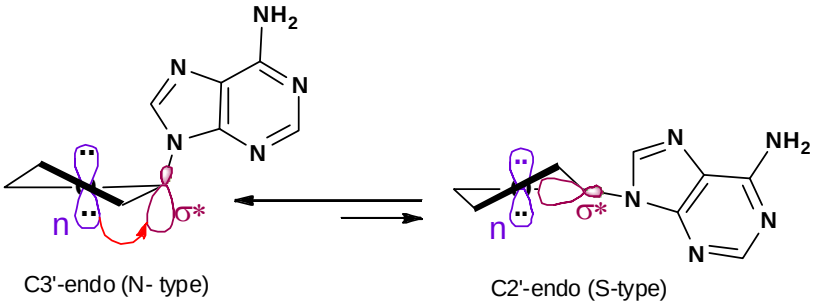

Figure 8. O4'-C1'- N1/9 anomeric effect in nucleos(t)ides in terms of molecular orbital overlap and hyperconjugation

The heterocyclic bases are involved in the *anomeric* effect by orbital mixing of one of the nonbonded lone pairs to the σ* orbital of the glycosyl bond (n (O4′) → σ* C-N) to drive the two-state N↔S pseudorotational equilibrium of the constituent *β*-D-pentofuranosyl moieties. The *anomeric* effect in nucleosides is optimal in O4′-*exo* (W) conformation with the pseudoaxial aglycone, but this optimal conformation is unacceptable for steric reasons. The N-type conformation is energetically favored over S-type in terms of the anomeric effect alone, and its strength is closely related to the electronic nature of the aglycone. The protonation of the nucleobase facilitates the n (O4′) →σ* C-N interactions, thereby resulting in the increased population of N-type conformers.

The term "*gauche*" refers to conformational isomers (conformers) where two vicinal groups are separated by a 60° torsion angle and hinder bond rotation. *Gauche* rotamer are more stable than the *anti* rotamer due to hyperconjugation.

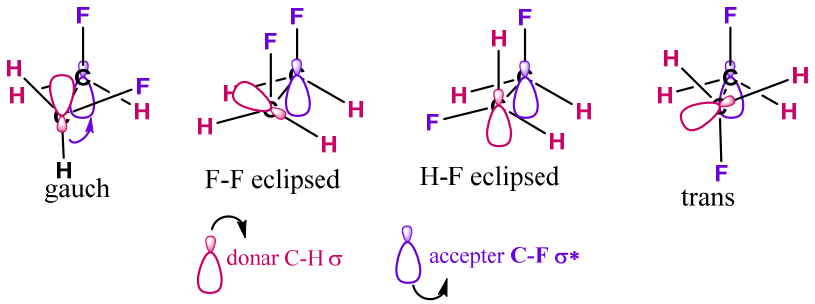

Figure 9. 1, 2-difluoroethane conformars

For example this effect is present in 1,2-difluoroethane (H_2FCCFH_2), where in the hyperconjugation model, the donation of electron density from the C–H σ bonding orbital to the C–F σ^*antibonding orbital is considered the source of stabilization in the *gauche* isomer. Due to the greater electronegativity of fluorine, the C–H σ orbital is a better electron donor than the C–F σ orbital, while the C–F σ^*orbital is a better electron acceptor than the C–H σ^*orbital. Only the *gauche* conformation allows good overlap between the better donor and the better acceptor (Figure 9).

The 3′-OH or 3′-OPO_3H groups in 2′-deoxynucleosides, and 2′-deoxynucleotides respectively in DNA drive the N↔S equilibrium toward S-type conformation through the tendency to adopt a *gauche* orientation of the [O_4′-C4′- C3′-O_3′] torsion angle. The 2′-OH in the ribonucleosides and ribonucleotides in RNA is involved in three gauche interactions which compete for the drive of N↔S equilibrium: (i) [O_4′- C1′-C2′-O_2′] drives toward N, (ii) [N1/9-C1′-C2′-O_2′] drives toward S, and (iii) [O_3′-C3′-C2′-O_2′] adopts gauche orientation in both N- and S-type sugar conformations (Figure 10).

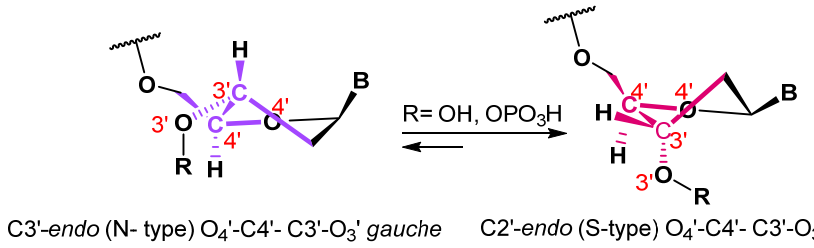

Figure 10. The 3′-OH or 3′- OPO_3 H- groups in DNA drive the N↔S equilibrium toward S-type conformation through *gauche* effect

1.2.4 Helical structure of nucleic acids

Under physiological conditions, DNA:DNA duplex exists in the B-form while DNA:RNA and RNA:RNA duplexes predominantly adopt the A-form. Both the A- and B-form exist as an anti-parallel right handed helix (Figure 11).[2,10]

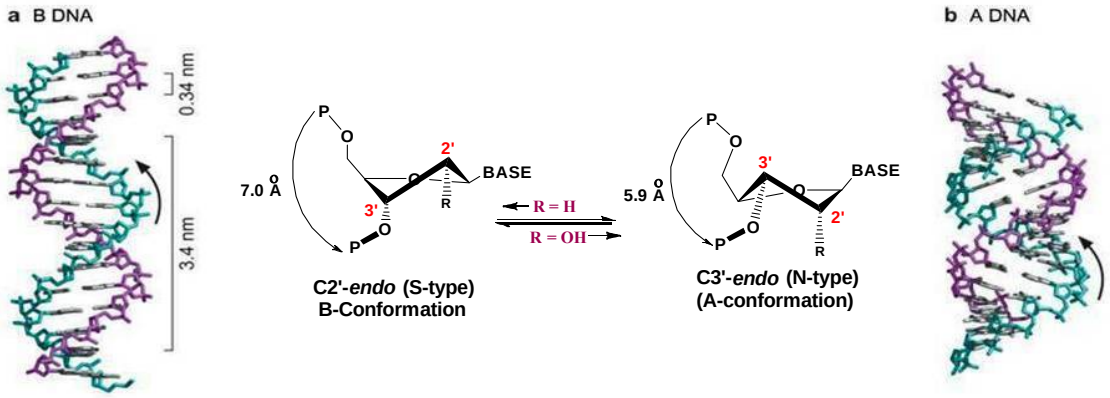

Figure 11. Double helical structure of B-forms DNA:DNA and A-form DNA:RNA/RNA:RNA. Sugar conformations in two-state *North*↔*South* equilibrium

An extremely important difference lies in the sugar conformation of the two forms of DNA, in the A-form the sugars adopt the *C3′-endo* conformation whereas in the B-form the conformation is C2'–*endo* (Figure 6). In A-DNA, the 2′-OH group in RNA single strand allows sugar puckers to be predominantly N-type because of *anomeric* and *gauche* effects as this structurally rigid RNA strand brings about the preferential N-type sugar conformations for the sugar in DNA strand of DNA:RNA duplex.. Some other differences include the number of base pairs per helical turn (10 versus 11 in B and A forms, respectively), the bases being perpendicular to the helical axis in B form and slightly tilted in the A form. Also distinctly visible in the different forms are two grooves, which can act as possible hydrogen bond acceptors and donors. The major groove of A-DNA is narrow and deep, while in B-DNA, it is wide and deeper. The minor groove of A-DNA is broad and shallow, whereas in B-DNA, it is deep and narrow.

1.3 Antisense technology

Genetic information flows from DNA to RNA in a process called transcription, and is then used to synthesize proteins by a process called translation. RNA synthesis is initiated by transcription which first synthesizes precursor-mRNA. The pre-mRNA is composed of exons and introns (intervening sequences). However, introns are not translated into the amino-acid chain of a protein. In order to produce a functional protein these introns are removed from the pre-mRNA by splicing and the coding sequences (exons, carrying the genetic information) are fused together and form mature mRNA. The mRNA is then transported to the cytoplasm where it undergoes 'translation' with the help of other RNA like tRNA (transfer RNA) and rRNA (ribosomal RNA) to produce proteins.

Conventional drugs bind to proteins related to the disease and thereby modulate their function to curb the diseased state. An alternative treatment is known as ‘antisense therapyy’. The antisense therapy involves inhibition of mRNA translation to proteins by using ssONs (DNA or RNA) having sequence complementary to their target mRNA. The term 'antisense' was coined to describe ONs that bind to the 'sense' mRNA in an anti-parallel, sequence specific manner *via* Watson-Crick hydrogen bonding. Antisense drugs could be selective and they have the potential to be more effective and less toxic than conventional drugs. The potential of ONs to act as antisense agents that inhibit viral replication in cell culture was discovered by Zamecnik and Stephenson in 1978.[11] Antisense technology has rapidly developed and been widely applied for investigating gene function and regulation, modulation of gene expression, and validation of new drug targets.[12] The first antisense drug, Vitravene, has been approved for the treatment of patients with cytomegalovirus- induced retinitis.[13] Several AS-ONs have entered phase I–III clinical trials as anticancer agents administered alone or in combination with conventional chemotherapy.

The AS-ONs exhibit either corrective or disruptive activity through strong and specific interaction with target mRNA sequences. The disruptive AS-ONs down-regulates the synthesis of disease-causing functional proteins by 'translational arrest' via steric blocking of ribosomal machinery, degradation of the mRNA by activation of RNA cleaving

enzymes such as RNase H or RNase L, ribozyme activation and/or RNA interference induced by small interfering RNA molecules like siRNA/miRNA (Figure 12).[14]

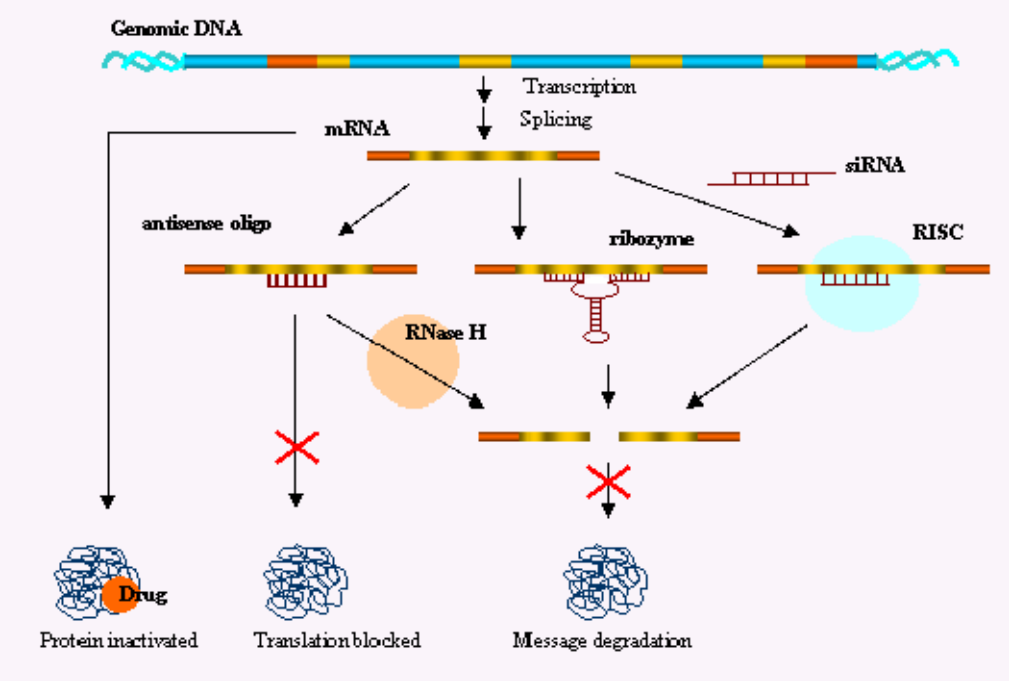

Figure 12. Various antisense mechanisms for inhibition/controlling of gene expression

In the former mode of action, AS-ONs strongly associate to the untranslated region of the mRNA and prevent translation. It has been shown that AS-ONs acting via 'translational arrest' are readily unwound by the ribosome and do not block mRNA translation when targeted within the coding region. Nevertheless a high affinity AS-ONs can overcome the unwinding activity of the initiation complex when targeted upstream to the coding region.

An alternative mode of action is by activation of RNA cleaving enzymes, such as RNase H and RNase L. RNase H is an ubiquitous enzyme that cleaves the RNA strand of a RNA:DNA hybrid duplex if the AS-ONs is structurally similar to DNA or the AS-ON:RNA duplex adopts a structure that resembles the DNA:RNA duplex. A second class of enzyme activating AS-ONs are the 2'-5'-linked adenylate-antisense chimera, that lead to mRNA degradation, by activation of a cellular enzyme called RNase L. The 2'-5'-A-antisense chimeras consists of a 2'-5' linked tetra-adenylate $(2'\text{-}5'A)_4$ linked to an AS-ONs *via* a flexible alkyl linker. The antisense oligonucleotide sequence binds to the mRNA

selectively and the 2'-5' adenylate portion activates RNase L leading to the localized RNA degradation of the RNA:AS-ONs duplex.

RNA interference (RNAi) also called post transcriptional gene silencing (PTGS), is a biological process in which small interfering double-stranded RNA (siRNA) molecules inhibit gene expression, typically by causing the destruction of specific mRNA molecules. In the siRNA pathway, the endonuclease enzyme DICER, binds to siRNA and helps it to load into RISC (RNA induced silencing complex) by forming RISC loading complex (RLC). During the activation of the RISC, the passenger strand (or sense) strand is cleaved, while guide strand (or antisense) strand, remains in the RISC.[15] The actual effector of the RNAi is the ribonucleoprotein complex RISC, which is guided by the siRNA to the complementary target RNA. As a result, the target RNA is cleaved at a specific site by catalytic protein Argonaut 2 (Ago2).[16] The cleaved mRNA is rapidly degraded by RNases and the coded protein can no longer be synthesized.

In the case of corrective antisense strategy, restoration of the viable protein synthesis is effected by acting at pre-mRNA levels for splice corrections (Figure 13).[17]

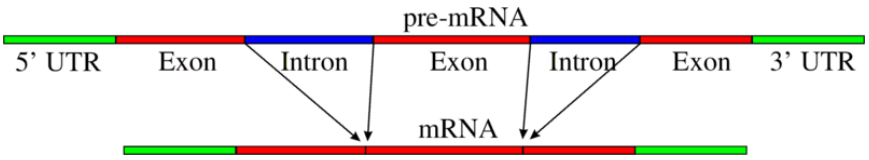

Figure 13. Simple illustration of exons and introns in pre-mRNA.The mature mRNA is formed by splicing. (UTR: Untranslated region)

1.4 Antisense oligonucleotides: Improvement through novel chemical modifications

The, AS-ONs requires strong and specific interactions with target mRNA sequences for their corrective as well as disruptive antisense activity. The platform where this interaction occurs may be either cytoplasm or nucleus and AS-ONs may have to compete with isosequential DNA for complex formation. Thus, ONs that would bind sequence specifically to RNA backbone assume importance.

Unmodified AS-ONs are rapidly attacked by nucleases in a biological system and being negatively charged their penetration through the cell membrane is not very effective. Several chemical modifications have been developed to enhance the nuclease resistance,

increase affinity and potency, of these AS-ONs. The general sites of modification are deoxyribo- or ribo- sugars, phosphate backbones, heterocyclic bases or complete replacement of the sugar phosphate backbone (Figure 14a). A vast number of chemically modified nucleotides have been used in antisense experiments most of which have been described in the recent review articles.[18]

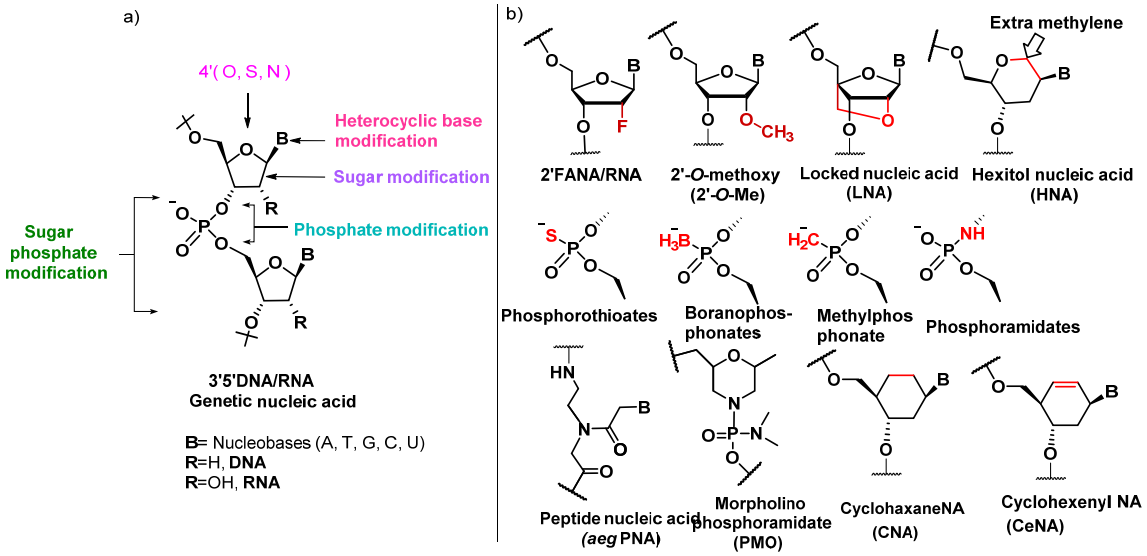

Figure 14: a) Modifications sites on an oligonucleotide dimer unit b) Different chemical modifications in genetic nucleic acids

The backbone modified ONs called 'first generation' antisense ONs, in which the phosphodiester linkage has been replaced with an alternate moiety. Examples of these include phosphorothioates,[19] boranophosphates,[20] phosphorodithioates, phosphoramidates[21] and methylphosphonates,[22] etc. Among these only first three are able to activate RNase H based degradation of RNA. These modifications enhance the stability towards nucleolytic hydrolysis, but decreases the stability of duplexes formed with complementary DNA or RNA than the natural phosphodiester linkage. The phosphorothioates were the first modified ONs resulting in a FDA approved drug named Vitravene.

The modification in heterocyclic bases is found to be very less in order to prevent any possible negative impact upon their hydrogen bonding and base stacking ability, both of which are important for recognition and duplex formation. It has been observed that *C-5* substitution (methyl) in pyrimidines generally results in an improvement of the desired properties. [6a,23]

The second generation of antisense ONs involve the modifications of sugar. Sugar modifications that favour a *C*3'-*endo* or *north* (N) conformation, typically found in RNA, tend to form the most stable duplexes. In DNA the *gauche* effect between O_3' and O_4' results in a *C*2'–*endo* or *south* (S) sugar conformation. By modifying the sugar with electronegative substituents at the *C*2′ and *C*3′ position the overall conformation of the sugar can be locked or frozen to yield ONs that bind with high affinity. Examples of sugar modified ONs are the 2′-*O*-methoxy (2′-*O*-Me),[24] arabinofuranosyl (ANA)[25] and 2'–fluoroarabinofuranosyl (2′F-ANA),[26] 2'-fluororibofuranosyl (2′F-RNA) etc.[27]

Locked nucleic acids (LNA/BNA) [28,29] are a class of high-affinity RNA analogs in which the ribose ring is "locked" in 3′-*endo* (N-type) conformation by 2′-*O*,-4′-C-methylene bridge. In addition, these sugar modifications at the 2′-position of RNA exhibit increased nuclease resistance, chemical stability against depurination and alter the lipophilicity, all of which contribute to improved pharmacokinetic properties. Some other examples of sugar modifications are hexitol nucleic acid (HNA),[30] cyclohexane nucleic acid (CNA), cyclohexenyl nucleic acid (CeNA),[31] and their several analogues. The third generation modification examples are where the sugar phosphate moiety has been completely replaced, like in peptide nucleic acids (PNA)[32] morpholino NA[33] and their analogues (Figure 14b).[34]

We focus our attention on the ONs having 'nongenetic' 2′-5′ phosphodiester linkages (ngDNA/ngRNA) and their modification due to their RNA selective hybridization properties and enzymatic stability.

1.5 2′-5′ Linked oligonucleotides: Nongenetic nucleic acids (ngRNA/ngDNA)

The 2′-5′ linked constitutional isomer supports Watson–Crick base pair association but with distinct properties and are not used for biological information storage and transfer thus called nongenetic nucleic acids.[35]

Almost all naturally occurring nucleic acids have 3'-5' phosphodiester linkages but studies suggest 2'-5' linkages were easier to form in the prebiotic world.[36] They are formed during intron splicing and also in interferon treated cells.[37] During nonenzymatic ONs synthesis, 2′-5′ linkages are formed more easily than 3′-5′ linkage.[38] It has been suggested

that 3'-5' linkages were selected during evolution because they hydrolyze slower than 2'-5' linkages,[39] and/or the duplex structures formed by 2'-5' oligomers are less stable than those formed by 3'-5' oligomers. The 2′-5′ linked ONs (ngDNA/ngRNA) offer high resistance to nuclease digestion[40] and also exhibit remarkable selectivity for complexation with complementary single stranded RNA but not to DNA.[41] This raises the possibility of the utility of 2′-5′-linked ONs in potential antisense and diagnostic applications.[42]

2′-5′-linked oligoadenylates (2′-5′-A_n) were detected in a variety of cells and tissues, including L1210 cells and human lymphocytes.[43] These oligoadenylates vary in length from 2 to 15 residues. The di-, tri- and tetra-adenylates are the most abundant products formed in the reaction and the amounts of larger oligoadenylate units diminish with increasing chain length.[44] 2′-5′-A_n are responsible for antiviral mechanism of interferon (Interferons play a critical role in host immune responses against viral infections) and are also involved in cell growth regulation and differentiation.[45] The biological action of the 2′-5′-A_n system is mediated by RNase L. The 2′-5′-A_n activate a ubiquitous endoribonuclease (RNase L), by binding to it and converting it from an inactive monomer to its catalytically active dimer which is then responsible for cleavage of RNA.[46] RNase L is an enzyme found in many eukaryotic cells sometimes known as 2′-5′A_n dependent ribonuclease, is an interferon induced ribonuclease which, upon activation, destroys all RNA within the cell (both cellular and viral). For this reason, the 2′-5′A_n molecule is a potent inhibitor of translation, blocking cell-free protein synthesis at nanomolar concentrations.

Additionally, these 2′-5′-A_n are also reported to inhibit the activities of HIV-1 reverse transcriptase and DNA topoisomerase-I in HIV-1-infected cells.[47] After a conjugation with an antisense 3′-5′ linked phosphodiester ONs, the 2′-5′-A_n portion of the chimeric ONs can also direct antisense cleavage of target mRNA, presumably through activation of RNase L in cell culture.

1.5.1 Structural features of nongenetic nucleic acids (ngDNA/ngRNA)

In 1991, Damha *et al*. synthesized the 2′-5′-linked RNA (ngRNA Figure 1) that was found to exhibit self-pairing as well as pairing with RNA but its complexation with complementary DNA was not observed.[41] The duplexes of ngRNA with complementary RNA (ngRNA:RNA) showed very similar CD patterns as the natural 3′-5′ DNA:RNA

duplexes, from which it was deduced that the overall structures of these complexes would be comparable i.e., compact A-form duplex structure.[48] NMR studies in solution for self-pairing ngRNA duplexes suggested a similar structure in which the ribose sugars assumed C2′-*endo* (S-type) puckering for the ngRNA strands.[49,42b] From the similarity found in the CD spectra of ngRNA:RNA and the self-pairing ngRNA duplexes, along with the NMR studies for the latter duplex, it was deduced that the ngRNA strand in the ngRNA:RNA duplex might also assume the structural features of a natural DNA strand and the sugar residues would adopt C2′-*endo* (S-type) conformations (Figure 15).

Very similar results were found independently by Breslow [50] and Switzer[51] for the 2′-5′-linked 3′-deoxyribonucleic acids (ngDNA) as well. CD spectroscopy, and modeling studies[52] predicted that the sugar conformations in the ngDNA strand of ngDNA:RNA duplexes would have predominantly S-type sugar conformations. Contrary to this, the NMR studies on single-stranded ngRNA[53a] and 2′-5′-d(G_4C_4)[53b] implied an extended structure in which the sugar conformations were N-type. The C3′-*endo* or N-type sugar pucker has also been observed for single-stranded ngRNA in crystal structures.[54]

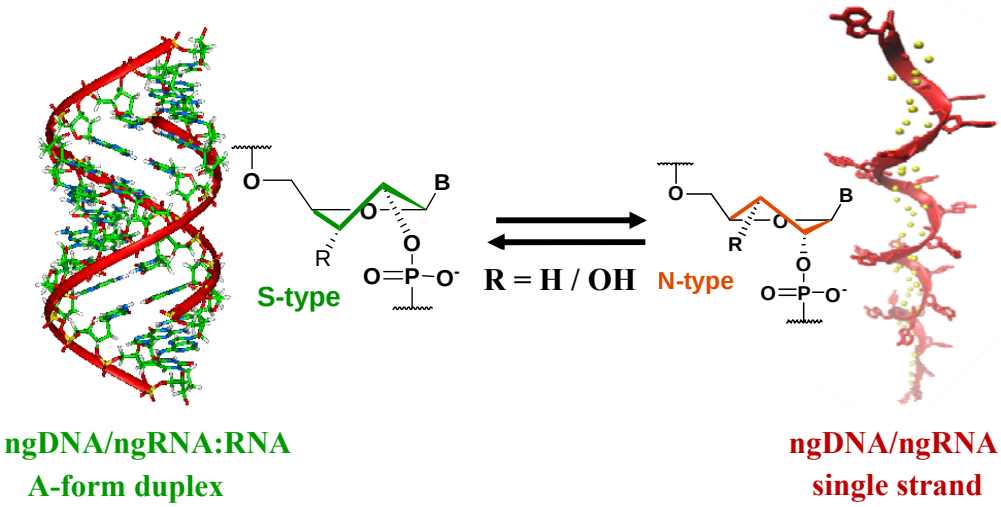

Figure 15: Sugar conformation of ngDNA nucleotide in single-stranded ngDNA/ngRNA and double stranded ngDNA/ngRNA:RNA A-form duplex

Molecular modeling studies reported by Yathindra *et al*.[52] also have suggested that to arrive at the compact A-type overall structure of the ngRNA:RNA duplex, the S-type or C2′-*endo* geometry of repeating nucleotides is stereochemically favoured in the ngRNA strand of the duplex.

Thus, the structural requirements of the ngRNA/ngDNA:RNA duplexes (predominant S-type geometry of the 2′-5′ strand in ngRNA/ngDNA:RNA duplex) do not match with the sugar conformations at the single stranded 2′-5′ oligomer level. In contrast to DNA in the single-stranded 2′-5′ oligomer, the stereoelectronic (*gauche* and *anomeric*) effects of the 2′-hydroxy group, would accentuate the preference for C3′-*endo* (N-type) sugar conformations. The N-type sugar pucker in 2′-5′oligomer leads to extended structure. While modelling the ngDNA:RNA duplex, it was therefore assumed that the RNA strand would impose its structure on the ngDNA strand, and the individual nucleosides in the isomeric DNA strand would be required to assume C2′-*endo* (S-type) conformation to give rise to a stable duplex. Thus, it was suggested that the 2′-5′-linked DNA would be under conformational and topological constraints when it forms duplex with complementary RNA.

Thus, it is postulated that geometry of 2′-5′ and 3′-5′ linkages are in an inverse relationship (Figure 16).[52,42b] A 2′-5′ linkage with a C2′-*endo* sugar would produce a compact geometry favorable for RNA binding while the C3′-*endo* sugar would produce extended nucleotide geometry. In the case of 3′-5′ linked oligomer the C2′-*endo* sugar would be in extended oligomer form, less suitable for RNA binding.

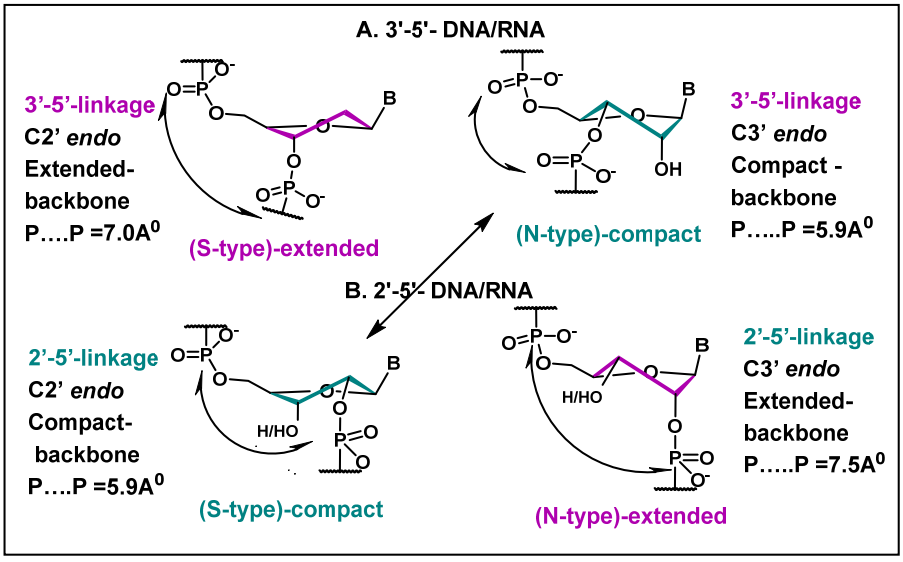

Figure 16: 3′-5′-DNA/RNA and 2′-5′-ngDNA/ngRNA in compact and extended conformations showing inverse relationship.

1.5.2 Chemical modifications in nongenetic nucleic acids (ngRNA/ngDNA)

In, ngDNA/ngRNA the linkage changes from C3' (as seen in DNA and RNA) to C2'. This leads to an increase in the number of bonds between O5' and phosphorus from six to seven. The experimental results suggest that an antiparallel duplex is formed by the ngDNA/ngRNA; however the overall stability is less than that of corresponding 3′-5′ duplexes. The order of the thermal stability was found to be RNA:RNA > DNA:DNA ≈ RNA:DNA ≈ DNA:RNA > ngRNA:RNA ≈ ngDNA:RNA > ngRNA:ngRNA >> DNA:ngRNA.[48] In addition, the ngDNA/ngRNA exhibit binding selectivity for 3′-5′ RNA over 3′-5′ DNA, and confer greater resistance to nucleolytic degradation as compared with the natural 3′-5′ DNA/RNA. The diminished strength of RNA:ngRNA or RNA:ngDNA complexes as compared to DNA:RNA or RNA:RNA complexes and also the fact that ngRNA:RNA or ngDNA:RNA duplexes are not substrates of the enzyme RNase H could be the possible reason that these have not yet been exploited in therapeutic applications. In order to improve the binding strength, and RNA specificity, some efforts towards the modification in the 2′-5′ nucleotides and their incorporation in mixed backbone oligonucleotide (MBO) containing ngDNA/RNA and 3′-5′ DNA/RNA are found in literature.[40] Very few chemical modifications in homogeneous ngDNA/ngRNA have been studied so far.

1.5.2a Backbone modifications

Backbone modifications in mixed 2′-5′ and 3′-5′ linked oligonucleotide

Mixed backbone oligonucleotide (MBOs)[40] containing 2′-5′-ribonucleotides and 3′-5′-deoxyribonucleotides bind to both DNA and RNA target strands. The affinity of the MBOs for the DNA complementary strand decreases with increasing 2′-5′-ribonucleotide linkages. MBOs having ngRNA linkages at both end and 3′-5′ DNA linkages at middle part of the sequence show lower thermal stability than control DNA and also show less nuclease resistance. The use of 3′-5′ linkages with phosphorothioate backbone in the same sequence increased nuclease resistance but decreased thermal stability.[55] 2′-5′/3′-5′ DNA phosphate chimeras have been used to inhibit 5α reductase expression in cell culture.[42] The single stranded DNA/ngRNA chimeras and ngDNA show less non-specific binding to plasma and cellular protein in comparison with 3′-5′ PS-ONs hence produce fewer side effects *in vivo*.[42]

The achiral uncharged phosphodiester replacement of 2′-5′ connection was explored by using 2′-5′ formacetal and thioformacetal linkages (Figure 17a).[56] The TT dimer for 2′-5′ formacetal and thioformacetal were incorporated into a ONs of the sequence 5′-TC*TC*TC*TC*TC*T^TT^TT-3′ where C*= 5-methyl-2′-deoxycytidine and T^T=2′-5′ modified thymidine dimers. The poor hybridization property of 2′-5′-linkages with DNA is confirmed in this study showing Δ*T*m of -8°C for only two 2′-5′ phosphodiester linkages which is only -2 °C for complementary RNA. The thioformacetal series shows a similar trend to the phosphodiester with the 2′-5′ connection resulting in particularly poor hybridization properties with a single strand DNA target (-7.5°C) and resulted in only a modest destabilization with RNA (-2.5°C). The 2′-5′ formacetal ONs results in comparable hybridization properties with DNA and RNA. The DNA binding properties show only modest (-2°C) destabilization relative to 3′-5′ phosphodiester and the RNA binding properties are nearly comparable to the 3′-5′ phosphodiester control for the 2′-5′ for formacetal (-l.0°C). Molecular modeling studies revealed reduced steric space for 2′-5′ phosphodiester linkage and the shorter non-bulky linkage between 2′ and 5′ positions was expected to be favored for both A and B conformations.[56] The 2′-5′ thioformacetal derivative resulted in substantial destabilization of duplex formation with ssRNA and ssDNA. The 2′-5′ formacetal ONs resulted in only modest destabilization with ssDNA and ssRNA as compared to the control 3′-5′ phosphodiester ONs.

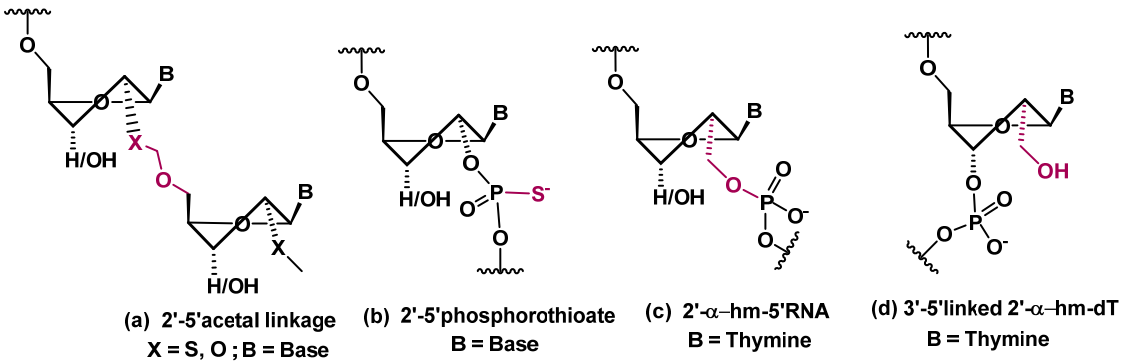

Figure17. Backbone modified ngDNA/RNA

Backbone modifications in homogeneous 2′-5′ linked oligonucleotide (ngDNA/ngRNA)

A phosphorothioate backbone modified homogeneous ngDNA sequence (Figure 17b)[42] again like phosphodiester backbone binds specifically to RNA but do not hybridize to complementary DNA. PS-ngDNA results in little destabilization compare to its PO-ngDNA, but this destabilization is relatively less as compared to the destabilization into the PS-DNA than PO-DNA. Thus, it is clear that phosphorothioate substitution in ngDNA is less destabilizing in comparison with genetic DNA when hybridized to complementary RNA. Like PO-ngDNA, PS-ngDNA also does not activate RNase H. However, incorporation of seven 3′-5′ linked phosphorothioates in the center of PS-ngDNA generates a chimeric oligonucleotide that can support RNase H activity. The 2′-5′-linked PS-ONs show less non-specific binding with cellular proteins and thrombin in comparison with the 3′-5′-linked PS-ONs. A reduction in these non-sequence specific protein interactions with the 2′-5′-linked phosphorothioate motif may produce fewer of these side effects *in vivo*.

In the A-type compact helices of ngRNA:RNA duplexes were shown to have smaller interstrand phosphate-phosphate distances and could have been the cause of destabilization. This point was considered by Peng and Damha,[57] when they introduced an extra carbon atom in 2′-hydroxymethyl(hm)-2′-5′ RNA oligomers (Figure 17c**,** 2′-α-hm-5′RNA), in order to lengthen the backbone and reduce the interstrand P-P repulsion, still keeping compact geometry. This modification in homogeneous ngRNA sequence unfortunately destabilized the complex with RNA. Both ngRNA:RNA and ngRNA:ngRNA duplexes with a single modification with 1-(2-deoxy-2-α-C-hydroxymethyl-β-D-ribofuranosyl)thymine (2′-α-hm-dT) show a small loss in respective stability (ΔTm ~ -0.8-0.9°C). When the number of modification units of 2′-α-hm-dT is increased to three the depression in Tm is only -0.3 °C/modification, suggesting a stabilizing effect by the nearly continuous 2′-α-hm-dT residues. 2′-α-hm-dT monomer was also incorporated in 3′-5′-linked RNA sequence, but here the destabilization effect of 2′-α-hm-dT unit is greater (ΔTm >-1 °C/modification) regardless of whether the target is complementary RNA or ngRNA. The 3′-5′ linked 2′-α-hm-dT monomer (Figure 17d) incorporated in homogeneous ngRNA but this also leads to reduced duplex stability with an equal destabilization with both complementary RNA and ngRNA.

1.5.2b Sugar modifications

Sugar modifications in mixed 2′-5′ and 3′-5′ linked oligonucleotide

The MBOs having five modifications in 3′-methoxy 2′-5′ -linked ONs (Figure 18-I)[55] units at the both ends of the 20mer 3′-5′ DNA sequence show unique properties such as higher affinity for RNA, adoption of A-conformation and resistance to RNase H and nuclease S1 than unmodified sequence (five 2′-5′ -linked ONs at the both end of the 20 mer 3′-5′ DNA sequence). But the stability is still less compared to natural 3′-5′ linked ONs. While a slight decrease in T_m value for fully modified 3′-methoxy 2′-5′-linked ONs was observed and which also shows weaker resistance towards SVPD can be improved upon by introducing few phosphorothioate linkages at the 3′ end of the oligonucleotide.

3'-*O*-methoxyethyl-RNA (MOE-RNA) is another modification in 2′-5′ -linked ONs (Figure 18-II). The NMR studies revealed that the substitution of 3′-OH group in 2′-5′-linked ONs by 3′-methoxyethoxy (3′-MOE) group resulted in C3′-*endo* (N-type) conformation.[53a]

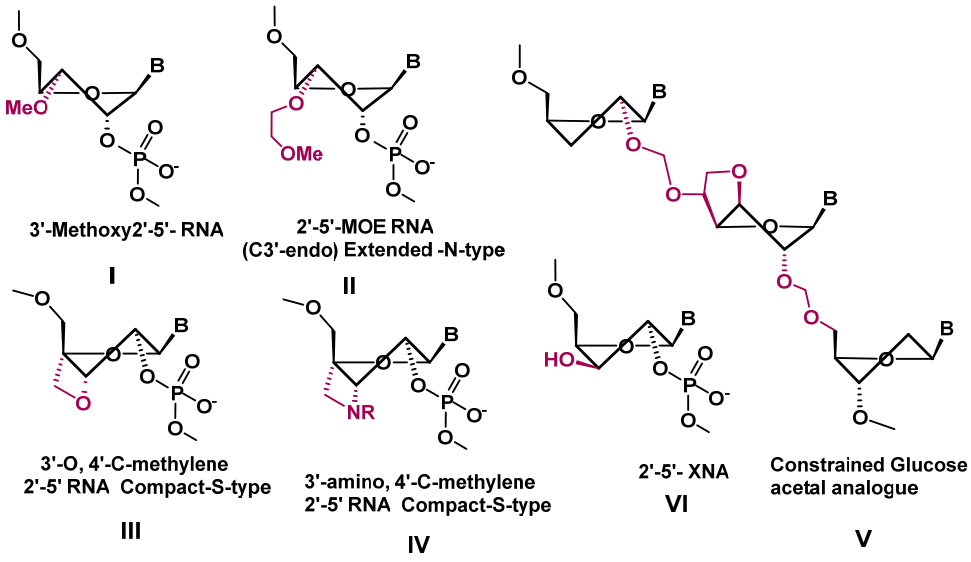

Figure 18: Sugar modified analogues of ngDNA/RNA

Conformational constraint was introduced in 2′-5′-linked ONs in the form of a bicyclic 3′-*O*, 4′-C methylene ribonucleoside, (Figure 18-III) and 3′-amino-3′-4′-BNA (Figure 18-IV) in which predominant S-type conformation was predicted by NMR and PM3 calculation.[58] One to six 2′-5′-linked modified monomer units were incorporated in

natural 3′-5′ ONs to check their binding affinity to the complementary DNA or RNA. The melting temperature (*T*m) for the modified ONs shows marginal change (increase or decrease) in *T*m towards complementary RNA as compared with the unmodified oligonucleotide, while moderate depression in *T*m were observed towards complementary ssDNA. This indicates that the modified ONs with the conformationally restricted bicyclic 2′-5′ nucleoside analogues have significant selectivity for RNA over ssDNA. Incorporation of these analogues at the 3′-end of the ONs was shown to enhance the nuclease resistance.

The conformationally restricted 5, 5 bicyclic ribose 2′-5′ formacetal was identified as a candidate to pre-order a nucleoside to resemble the bound duplex A-type conformation.[59] Trinucleoside bearing a two 2′-5′ formacetal linkages and a locked 3′, 6′-anhydro-glucose monomer (t^t_L^c^m) (Figure 18-V) was incorporated into an ONs sequence 5'-C^MTTC^MATTTT t^t_L^c^m -3′, where C^M = 5-methyl-2′-deoxycytidine. The *T*m for this sequence was compared with two control sequences, one is 5′-C^MTTC^MATTTTt^t^c^m-3′ which has t^t^c^m the non-conformationally restricted 2′-5′ formacetal-linked trimer and the remaining are 3′-5′ PO-linkages. The second sequence is 5′-C^MTTC^MATTTTTTC^M-3′ having all 3′-5′ PO-linkages. The *T*m of the ONs bearing two 2′-5′ formacetal linkages was 2.5 °C lower than that of corresponding with 3′-5′ phosphate and further modification by locked 5, 5 bicyclic ribose 2′-5′ formacetal moieties resulted in destabilization of the duplex with the target ssRNA compared to the 2′-5′ formacetal control. The rigid conformational restriction on the parent ribose ring and loss of flexibility to adopt a conformation suitable for duplex formation might have been the cause of this destabilization.

Thus from the current literature it appears that compact A-type conformation in 2′-5′ linked RNA could be C2′-*endo* and would favor the stabilization of the 2′-5′ isomeric DNA:RNA structures. Further changes/modifications need to be done that involve uniformity in the backbone, sequence variability etc. to clearly understand desired structural parameters for preferential RNA binding of 2′-5′ linked ONs.

Sugar modifications in homogeneous 2′-5′ linked oligonucleotide (ngDNA/ngRNA)

The inversion of configuration at 3′-OH in ngRNA, led to the synthesis of 2′-5′ xylose nucleic acids (ngXNA), (Figure 18-VI). The sugars of ngXNA adopt C3′-*endo* conformation due to two *gauche* effects along the O_3′-C3′-C4′-O_4′ and O_2′-C2′-C1′-O_4′, and

may therefore adopt an extended (DNA-like) conformation. The pre-organized extended conformation of ngXNA bound very weakly to the compact RNA target. The conformational incompatibility or spatial mismatching of two strands was thought to be the reason why extended XNA bound poorly to compact RNA.[60]

1.6 Spectroscopic techniques

Ultraviolet absorption (UV) and circular dichroism (CD) which looks into electronic properties of the bases and is highly useful and general tools for biophysical study of nucleic acids. MALDI TOF spectrometry is used as mass analysis technique.

1.6.1 Ultraviolet spectroscopy

The absorbance of polynucleotide depends on the sum of the absorbance of the nucleotide plus the effect of the interaction among the nucleotides. The interaction cause a single strand to absorb less than the sum of its nucleotides and a double strand absorbs less than its two component single strand. The effect is called hypochromicity which results from the coupling of the transition dipoles between neighbouring stacked bases and is larger in amplitude for A-U and A-T pairs.[61] In converse term, hyperchromicity refers to the increase in absorption when a double standed nucleic acid is dissociated into single strands. The UV absorption of a DNA duplex increases typically by 20-30 % when it is denatured. This transition from a stacked, hydrogen bonded double helix to an unstacked, strand-separated coil has a strong entropic component and is temperature dependent. The mid-point of this thermal transition is known as the **melting temperature** (T_m). Such a thermal dissociation of nucleic acid helices in solution to give single stranded DNA/RNA is a function of base composition, sequence, chain length as well as of temperature, salt concentration, and pH of the solvent (buffer). In particular, early observations of the relationship between T_m and base composition for different DNAs showed that A-T pairs are less stable than G-C pairs, a fact which is now expressed in a linear correlation between T_m and the gross composition of a DNA oligomer by the equation:

$$T_m = X + 0.41\ (\%\ C+ G)\ ^oC$$

The constant X is dependent on salt concentration and pH and has a value of 69.3ºC for 0.3M sodium ions at pH 7.[61]

A second consequence is that the steepness of the transition curve also depends on base sequence. Thus, melting curves for homooligomers have much sharper transitions than those for random-sequence oligomers. This is because A-T rich regions melt first to give unpaired regions which then extend gradually with rising temperature until; finally, even the pure G-C regions have melted. Short homooligomers melt at lower temperatures and with broader transitions than longer homooligomers. For example for poly (rA)n-poly (rU)n, the octamer melts at 9ºC, and the decamer at 20ºC, and long oligomers at 49ºC in the same sodium cacodylate buffer at pH 6.9. Consequently, in the design of synthetic self complementary duplexes for crystallization and X-ray structure determination, G-C pairs are often placed at the ends of hexamers and octamers to stop them 'fraying'. The converse of melting is the renaturation of two separated complementary strands to form a correctly paired duplex.

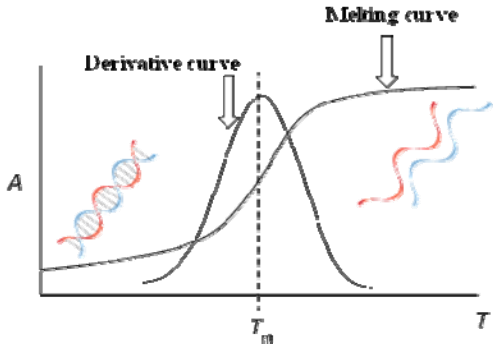

Figure 19: An oligonucleotide duplex melting curve and derivative curve

Duplex melting: According to the 'all or none model'[62], the UV absorbance value at any given temperature is an average of the absorbance of duplex and single strands. A plot of absorbance against temperature gives a sigmoidal curve in case of duplexes and the midpoint of the sigmoidal curve (Figure 19) called as the 'melting temperature' (T_m) (equilibrium point) at which the duplex and the single strands exist in equal proportions.

Triplex melting: In the case of triplexes, the first dissociation leads to melting of triplex generating the duplex (WC duplex) and third strand (Hoogsteen strand), followed by the duplex dissociation to form two single strands. The DNA triplex melting shows characteristic double sigmoidal transition and UV melting temperature for each transition is

obtained from the first derivative plots. The lower melting temperature (T_m1) corresponds to triplex to duplex transition while the second higher melting temperature (T_m2) corresponds to the transition of duplex to single strands.[63]

1.6.2 Circular dichroism (CD) spectroscopy

Circular dichroism (CD) spectroscopy measures differences in the absorption of left-handed polarized light versus right-handed polarized light which arise due to structural asymmetry. The absence of regular structure results in zero CD intensity, while an ordered structure results in a spectrum which can contain both positive and negative signals. CD is particularly useful for studying chiral molecules and has very special significance in the characterization of biomolecules (including the secondary structure of proteins and the handedness of DNA). The commonly used units in current literature are the mean residue ellipticity (degree cm^2 $dmol^{-1}$) and the difference in molar extinction coefficients called as molar circular dichroism or $\Delta\varepsilon$ (liter $mol^{-1}cm^{-1}$). The molar ellipticity [θ] is related to the difference in molar extinction coefficients by [θ] = 3298 ($\Delta\varepsilon$). In the nucleic acid, the heterocyclic bases that are principal chromophores. As these bases are planar, they don't have any intrinsic CD. CD arises from the asymmetry induced by linked sugar group. CD spectra from the dinucleotide exhibit hyperchromicity, being more intense by roughly an order of magnitude than those from monomers. It is when the bases are linked together in polynucleotide's, giving rise to many degenerate interactions and they gain additional characteristic associated with the asymmetric feature of secondary structure such as in proteins and nucleic acids.[64]

The simplest application of CD to DNA structure determination is for identification of polymorph present in the sample.[65] The CD signature of the B-form DNA as read from longer to shorter wavelength is a positive band centered at 275nm, a negative band at 240nm, with cross over around 258nm. These two bands arise not from a simple degenerate exciton coupling, but as a result of superimposition of all coupling transitions from all the bases. A-DNA is characterized by a positive CD band centered at 260nm that is larger than the corresponding B-DNA band, a fairly intense negative band at 210nm and a very intense positive band at 190nm (Figure 20). The 250-230nm region is also usually fairly flat though not necessarily zero. Naturally occurring RNAs adopt the A-form if they are duplex.

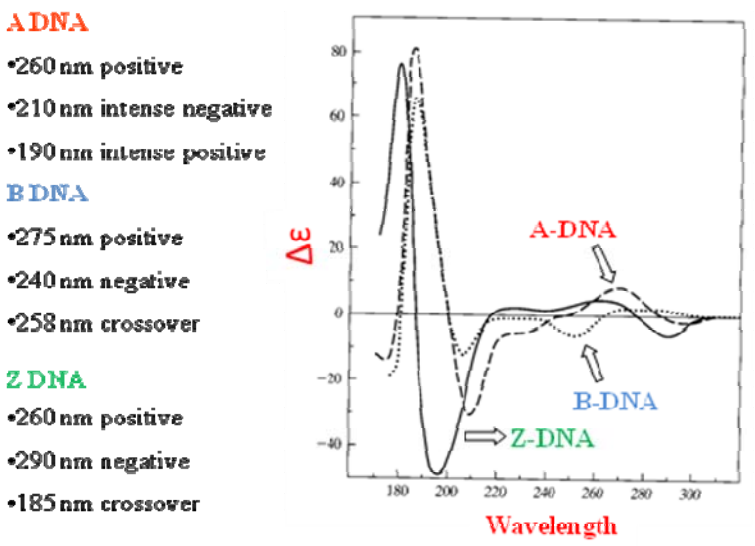

Figure 20: CD spectra of DNA secondary structure

CD denaturation (melting) and CD-Job's plots are equally important as they give T_m and binding stoichiometry of DNA/RNA complexes respectively.

Stoichiometry: The binding *stoichiometry* of ONs to target DNA/RNA by UV-titration (mixing): This is derived from Job's plot.[66] The two components of the complex are mixed in different molar ratios, so that the total concentration of each mixture should be constant, i.e., as the concentration of one strand decreases, concentration of the second strand increases and the UV-absorbance of each mixture is recorded. The absorbance decreases in the beginning to a minimum and then again increases. The molar ratio of the two strands at which absorbance reached minimum indicates the stoichiometry of complexation.

1.6.3 Mass spectroscopy: MALDI-TOF

Matrix-assisted laser desorption/ionization time-of-flight (MALDI TOF) is a soft ionization technique[67] used in the analysis of biomolecules (biopolymers such as DNA,[68] proteins, peptides and sugars) and large organic molecules (such as polymers, dendrimers and other macromolecules), where these large ions obtain in gas phase producing many fewer multiply charged ions. MALDI is a two step process. First, desorption is triggered by a UV laser (nitrogen lasers 337nm) beam. Matrix material heavily absorbs UV laser light, leading to the ablation of upper layer (~micron) of the matrix material. The hot plume produced during ablation contains many species: neutral and ionized matrix molecules,

protonated and deprotonated matrix molecules, matrix clusters and nanodroplets. Second, the analyte molecules are ionized (more accurately protonated or deprotonated) in the hot plume. The time-of-flight (TOF) analyzer uses an electric field to accelerate the ions through the same potential, and then measures the time they take to reach the detector. If the particles all have the same charge, the kinetic energies will be identical, and their velocities will depend only on their masses. Lighter ions will reach the detector first. Their time-of-flight is proportional to their $(MW)^{1/2}$.

The matrix is the crystallized, low molecular weight compound with several conjugated double bonds. The some basic properties of matrices is like they should not evaporate during standing in specrometer, often acidic for acting as a proton source to encourage ionization of the analyte molecules, strong optical absorption in either the UV or IR range. Most commonly used matrices are 3,5-dimethoxy-4-hydroxycinnamic acid (sinapinic acid, SA), α-cyano-4-hydroxycinnamic acid (alpha-cyano or alpha-matrix, CHCA) and 2, 5-dihydroxybenzoic acid (DHB). 2′,4′,6′ trihydroxy acetophenone (THAP). A solution of one of these molecules is made, often in a mixture of highly purified water and an organic solvent (normally acetonitrile (ACN) or ethanol). trifluoroacetic acid (TFA) or ammonium citrate may also be added.

1.7 Present work

Oligoribonucleotides comprising of 2'-5'-linked internucleotide linkages are known to bind selectively to RNA over DNA. The ability to bind to RNA renders them suitable as probes for 'antisense technology'. Experiments to study the effect of sugar conformation on the binding properties of 2'-5'-linked ONs are not very well studied in the current literature. To get insight into the role of sugar conformations, 2′-5′-linked ONs modified at the C3'-position of the furanose ring were synthesized and their binding to complementary single stranded DNA and RNA was studied. Their nuclease resistance ability was also evaluated.

As we have seen that 2′-ribo and 2′-arabino-fluoro group has large but opposite impact on the sugar conformations. The increased thermal stability of the 3′-5′ linked 2′F-RNA:RNA and 2′F-ANA:RNA duplexes is because of the favorable influence of the 2′-fluoro group on conformational restriction of the sugar pucker. The 3′-fluoro substitution of the furanose ring of nucleosides was therefore envisaged.

The thesis describes synthesis and conformational analysis of S-type or N-type-conformationally frozen uracil/thymine/adenine containing 2′-5′ nucleosides and S-type conformationally locked adenine 2′-5′ nucleoside. The incorporation of these modified units in RNA-selective, nuclease resistant 2′-5′-linked nongenetic deoxyribonucleic acid oligomers (ngDNA) and biophysical studies of these modified oligomers with target DNA/RNA sequences is discussed. Synthesis of compact arabino-uridine nucleoside, its incorporation in ngDNA and biophysical studies are presented briefly.

***Chapter 2*:** The synthesis of S/N-type- conformationally frozen, 3′-deoxy-3′-ribofluoro uridine ($^{R}U^{F}$) and 3′-deoxy-3′-xylofluoro ($^{X}U^{F}$) uridine nucleosides is described in this chapter. Synthesis of ngDNA containing these modified units and biophysical experiments to study the effects of these modifications on the stability of duplexes with target DNA/RNA are presented.

***Chapter 3*:** This chapter is divided into 3 sections.

Section A: This section describes the synthesis of S/N-type-frozen 3′-deoxy-3′-ribo/xylofluoro thyminyl nucleosides ($^{R}T^{F}$ and $^{X}T^{F}$) and S-type locked ($^{L}A^{S}$) and S/N-type frozen 3′-deoxy-3′-fluoro ribo/xyloadenine nucleoside analogues ($^{R}A^{F}$, $^{X}A^{F}$) for their incorporation in ngDNA. Synthesis of ngDNA containing these modified units and biophysical experiments to study the effects of these modifications on the stability of duplexes with target DNA/RNA are presented.

Section B: This section describes the rationale for designing arabino-uridine (^{ara}U), its synthesis and incorporation into ngDNA oligomers. The effect of such modification on binding with target DNA and RNA is studied using temperature dependent UV-*T*m experiments.

Section C: In this section we describe the nuclease resistance ability of the modified ngDNA oligomers in comparison with unmodified DNA and ngDNA by exposure to snake venom phosphodiesterase (SVPD).

***Chapter 4*:** This chapter describes the conformational studies of $^{R}U^{F}$, $^{R}A^{F}$, $^{X}U^{F}$, $^{X}A^{F}$, $^{L}A^{S}$, and ^{ara}U monomers using NMR, X-ray crystal structure and Matlab pseudorotation GUI program.

1.8 References

1. Watson, J. D.; Crick, F. H. C., Molecualar structure of nucleic acids-A structure for deoxyribose nucleic acid *Nature* **1953,** 171, (4356), 737-738.
2. Watson, J.D.; Baker, T.A.; Bell, S.P.; Gann, A.; Levine, M.; Losick, R., Molecular Biology of the Gene, Fifth Edition, CSHL Press, NY **2004**, Chapter 6.
3. Hoogsteen, K., Crystal and molecular structure of a hydrogen-bonded complex between 1-methylthymine and 9-methyladenine. *Acta Crystallographica* **1963,** 16, (9), 907-+. (b) Crick, F. H. C., Codon-anticodon pairing wobble hypothesis. *Journal of Molecular Biology* **1966,** 19, (2), 548-&.
4. IUPAC-IUB. Abbreviations and Symbols for the Description of Conformations of Polynucleotide Chains. *European Journal of Biochemistry* **1983**, 131, 9-15.
5. Sundaralingam, M. J., Stereochemistry of nucleic acids and their constituents. IV. Allowed and preferred conformations of nucleosides, nucleoside mono-, di-, tri-, tetraphosphates, nucleic acids and polynucleotides. *Biopolymers* **1969**, 7, (6), 821-860.
6. (a) Saenger W.; Principles of Nucleic Acid Structure, Springer- Verlag; New York,. **1984**. (b) Lescrinier, E.; Froeyen, M.; Herdewijn, P., Difference in conformational diversity between nucleic acids with a six-membered 'sugar' unit and natural 'furanose' nucleic acids. *Nucleic Acids Research* **2003,** 31, (12), 2975-2989.
7. Altona, C.; Sundaralingam, M. J., Conformational Analysis of the Sugar Ring in Nucleosides and Nucleotides. **A** New Description Using the Concept of Pseudorotation' *Journal of the American chemical Society* **1972,** 94, 8205-1822.
8. Plavec, J.; Thibaudeau, C.; Chattopadhyaya, J., How does the 2'-hydroxy group drive the pseudorotational equilibrium in nucleoside and nucleotide by the tuning of the 3'-gauche effect. *Journal of the American Chemical Society* **1994,** 116, (15), 6558-6560.
9. Plavec, J.; Tong, W. M.; Chattopadhyaya, J., How do the gauche and anomeric effects drive the pseudorotational equilibrium of the pentofuranose moiety of nucleosides. *Journal of the American Chemical Society* **1993,** 115, (21), 9734-9746.

10. (a) Richmond, T. J.; Davey, C. A., The structure of DNA in the nucleosome core. *Nature* **2003,** 423, (6936), 145-150. (b) Leslie, A. G. W.; Arnott, S.; Chandrasekaran, R.; Ratliff, R. L., Polymorphism of DNA double helices. *Journal of Molecular Biology* **1980,** 143, (1), 49-72. (c) Wahl, M. C.; Sundaralingam, M., Crystal structures of A-DNA duplexes. *Biopolymers* **1997,** 44, (1), 45-63. (d) Ghosh, A.; Bansal, M., A glossary of DNA structures from A to Z. *Acta Crystallographica Section D-Biological Crystallography* **2003,** 59, 620-626.(e) Herbert, A.; Rich, A., Left-handed Z-DNA: structure and function. *Genetica* **1999,** 106, (1-2), 37-47.
11. Zamecnik, P. C., Stephenson,M .L., Inhibition of Rous sarcoma virus replication and cell transformation by a specific oligodeoxynucleotide. *Proceedings of the National Academy of Sciences* USA **1978,** 75, (1), 280–284.
12. Crooke, S. T., Antisense Drug Technology, Principles, Strategies, and Applications. Marcel Dekker, New York **2001**.
13. Agrawal, S.; Zhao, Q. Y., Antisense therapeutics. *Current Opinion in Chemical Biology* **1998,** 2, (4), 519-528.
14. (a)Kurreck, J., Antisense technologies-Improvement through novel chemical modifications. *European Journal of Biochemistry* **2003,** 270, (8), 1628-1644.(b) Turner, J. J.; Fabani, M.; Arzumanov, A. A.; Ivanova, G.; Gait, M. J., Targeting the HIV-1 RNA leader sequence with synthetic oligonucleotides and siRNA: Chemistry and cell delivery. *Biochimica et Biophysica Acta-Biomembranes* **2006,** 1758, (3), 290-300.
15. Matranga, C.; Tomari, Y.; Shin, C.; Bartel, D. P.; Zamore, P. D., Passenger-strand cleavage facilitates assembly of siRNA into Ago2-containing RNAi enzyme complexes. *Cell* **2005,** 123, (4), 607-620.
16. Liu, J. D.; Carmell, M. A.; Rivas, F. V.; Marsden, C. G.; Thomson, J. M.; Song, J. J.; Hammond, S. M.; Joshua-Tor, L.; Hannon, G. J., Argonaute2 is the catalytic engine of mammalian RNAi. *Science* **2004,** 305, (5689), 1437-1441.

17. Dominski, Z.; Kole, R., Restoration of correct splicing in thalassemic premessenger R by antisense oligonucleotides. *Proceedings of the National Academy of Sciences of the United States of America* **1993,** 90, (18), 8673-8677.
18. (a) Kole, R.; Krainer, A. R.; Altman, S. RNA therapeutics: beyond RNA interference and antisense oligonucleotides. *Nature. Reviews. Drug. Discovery*. **2011**, 11, 125; (b) Prakash T, P. An overview of sugar-modified oligonucleotides for antisense therapeutics. *Chemistry and. Biodiversity*. **2011,** 8*,* 1616; (c) Bennett, C. F and Swayze, E, E RNA Targeting therapeutics: molecular mechanisms of antisense oligonucleotides as a therapeutic platform, *Annual. Review of. Pharmacology and. Toxicology*. **2010**, 50, 259; (d) Shukla, S.; Sumaria, C.S and Pradeepkumar, P.I. Exploring chemical modifications for siRNA therapeutics: A structural and functional outlook. *ChemMedChem* **2010**, 5, 328; (e) Kumar, V. A.; Ganesh, K. N., Structure-Editing of Nucleic Acids for Selective Targeting of RNA. *Current. Topics. In Medicinal Chemistry*. **2007**, 7, 715.
19. [19]Eckstein, F. Phosphorothioate oligonucleotides: What is their origin and what is unique about them? *Antisense Nucleic Acids Drug Development*. **2000**, 10, 117-121.
20. Li, H.; Huang, F.; Shaw, B. R. Conformational studies of dithymidine boranomonophosphate diastereoisomers. *Bioorganic &. Medicinal. Chemistry*. **1997**, 5, 787.
21. Froehler, B.; Ng, P.; Matteucci, M. Phosphoramidate analogs of DNA: Synthesis and thermal stabilities of heteroduplexes. *Nucleic Acid Research*. **1988**, 16, 4831.
22. Millar, P. S. Non-ionic antisense oligonucleotides. In Cohen, J. S. (ed.): Oligodeoxynucleotides-Antisense Inhibitors of Gene Expression. London: Macmillan Press, **1989**, 79.
23. Felsenfe.G; Miles, H. T., Physical and chemical properties of nucleic acids. *Annual Review of Biochemistry* **1967,** 36, 407.
24. Inoue, H.; Hayase, Y.; Imura, A.; Iwai, S.; Miura, K.; Ohtsuka, E., Synthesis and hybridization studies on 2 complementary nona(2'-*O*-methyl)ribonucleotides. *Nucleic Acids Research* **1987,** 15, (15), 6131-6148.

25. Damha, M. J.; Wilds, C. J.; Noronha, A.; Brukner, I.; Borkow, G.; Arion, D.; Parniak, M. A., Hybrids of RNA and arabinonucleic acids (ANA and 2' F-ANA) are substrates of ribonuclease h. *Journal of the American Chemical Society* **1998,** 120, (49), 12976-12977.
26. Watts, J. K.; Martin-Pintado, N.; Gomez-Pinto, I.; Schwartzentruber, J.; Portella, G.; Orozco, M.; Gonzalez, C.; Damha, M. J., Differential stability of 2'F-ANA:RNA and ANA:RNA hybrid duplexes: roles of structure, pseudohydrogen bonding, hydration, ion uptake and flexibility. *Nucleic Acids Research* **2012**, 38, (7), 2498-2511.
27. Viazovkina, E.; Mangos, M.M.; Elzagheid, M.I.; and Damha, M.J., Curr Protoc Nucleic Acid Chem, Chapter 4, unit 415. **2002**.
28. (a) Obika, S.; Nanbu, D.; Hari, Y.; Morio, K.; In, Y.; Ishida, T.; Imanishi, T., Synthesis of 2'-*O*,4'-C-methyleneuridine and -cytidine. Novel bicyclic nucleosides having a fixed C-3,-endo sugar puckering. *Tetrahedron Letters* **1997,** 38, (50), 8735-8738. (b) Obika, S.; Nanbu, D.; Hari, Y.; Andoh, J.; Morio, K.; Doi, T.; Imanishi, T., Stability and structural features of the duplexes containing nucleoside analogues with a fixed N-type conformation, 2'-*O*,4'-C-methyleneribonucleosides. *Tetrahedron Letters* **1998,** 39, (30), 5401-5404.
29. (a) Koshkin, A. A.; Singh, S. K.; Nielsen, P.; Rajwanshi, V. K.; Kumar, R.; Meldgaard, M.; Olsen, C. E.; Wengel, J., LNA (Locked Nucleic Acids): Synthesis of the adenine, cytosine, guanine, 5-methylcytosine, thymine and uracil bicyclonucleoside monomers, oligomerisation, and unprecedented nucleic acid recognition. *Tetrahedron* **1998,** 54, (14), 3607-3630.(b) Singh, S. K.; Nielsen, P.; Koshkin, A. A.; Wengel, J., LNA (locked nucleic acids): synthesis and high-affinity nucleic acid recognition. *Chemical Communications* **1998**, (4), 455-456. (c) Wengel, J., Synthesis of 3'-C- and 4'-C-branched oligodeoxynucleotides and the development of locked nucleic acid (LNA). *Accounts of Chemical Research* **1999,** 32, (4), 301-310.

30. Maier, T.; Przylas, I.; Strater, N.; Herdewijn, P.; Saenger, W., Reinforced HNA backbone hydration in the crystal structure of a decameric HNA/RNA hybrid. *Journal of the American Chemical Society* **2005,** 127, (9), 2937-2943.
31. Wang, J.; Verbeure, B.; Luyten, I.; Lescrinier, E.; Froeyen, M.; Hendrix, C.; Rosemeyer, H.; Seela, F.; Van Aerschot, A.; Herdewijn, P., Cyclohexene nucleic acids (CeNA): Serum stable oligonucleotides that activate RNase H and increase duplex stability with complementary RNA. *Journal of the American Chemical Society* **2000,** 122, (36), 8595-8602.
32. Nielsen, P. E.; Egholm. M.; Berg, R. H.; Buchardt, O., Sequence-selective recognition of DNA by strand displacement with a thymine-substituted polyamide. *Science* **1991**, 254, 1497-1500.
33. Summerton, J., Morpholino antisense oligomers: The case for an RNase Hindependent structural type. *Biochimica et. Biophysica. Acta* **1999**, 1489, 141–158.
34. Ganesh, K. N. and Nielsen, P. E. Peptide nucleic acids: Analogs and derivatives. *Current. Organic. Chemistry*. **2000**, 4, 931; (b) Kumar, V. A. Structural pre-organization of peptide nucleic acids: chiral cationic analogues with five- or six-membered ring structures. *European Journal of Organic Chemistry* **2002**, 2021; (c) Kumar, V. A.; Ganesh K. N. Conformationally Constrained PNA Analogues: Structural Evolution toward DNA/RNA Binding Selectivity. *Accounts of Chemical Research* **2005**, 38, 404; (d) Uhlmann, E.; Breipohl, G.; Will, D. PNA: Synthetic polyamide nucleic acids with unusual binding properties. *Angewandte Chemie International Edition* (*English*). **1998**, 37, 2796.
35. Dougherty, J. P.; Rizzo, C. J.; Breslow, R., Oligodeoxynucleotides that contain 2'-5' linkages-synthesis and hybridization properties. *Journal of the American Chemical Society* **1992,** 114, (15), 6254-6255.
36. Orgel, L. E. and. Lohrmann, R., Prebiotic chemistry and nucleic acid replication. *Accounts of Chemical Research* **1974,** 7, (11), 368-377.

37. Lesiak, K.; Imai, J.; Floydsmith, G.; Torrence, P. F., Biological-activities of phosphodiester linkage isomers of 2-5A. *Journal of Biological Chemistry* **1983,** 258, (21), 3082-3088.
38. Lohrmann, R.; Orgel, L. E., Preferential formation of (2'-5')-linked internucleotide bonds in non-enzymatic reactions. *Tetrahedron* **1978,** 34, (7), 853-855.
39. Dhingra, M. M.; Sarma, R. H., Why do nucleic-acids have 3'-5' phosphodiester bonds. *Nature* **1978,** 272, (5656), 798-801.
40. Kandimalla, E. R.; Manning, A.; Zhao, Q. Y.; Shaw, D. R.; Byrn, R. A.; Sasisekharan, V.; Agrawal, S., Mixed backbone antisense oligonucleotides: Design, biochemical and biological properties of oligonucleotides containing 2'-5'-ribo- and 3'-5'-deoxyribonucleotide segments. *Nucleic Acids Research* **1997,** 25, (2), 370-378
41. Giannaris, P. A.; Damha, M. J., Oligoribonucleotides containing 2′,5′-phosphodiester linkages exhibit binding selectivity for 3′,5′-RNA over 3′,5′-ssDNA. *Nucleic Acids Research* **1993,** 21, (20), 4742-4749.
42. (a) Bhan, P.; Bhan, A.; Hong, M. K.; Hartwell, J. G.; Saunders, J. M.; Hoke, G. D., 2',5'-linked oligo-3'-deoxyribonucleoside phosphorothioate chimeras: thermal stability and antisense inhibition of gene expression. *Nucleic Acids Research* **1997,** 25, (16), 3310-3317. (b) Lalitha, V.; Yathindra, N., Even nucleic-acids with 2',5'-linkages facilitate duplexes and structural polymorphism-prospects of 2',5'-oligonucleotides as antigene antisense tool in gene-regulation. *Current Science* **1995,** 68, (1), 68-75.
43. Cailla, H.; LeBorne De Kaouel, C.; Roux, D., Delage,M. and Marti,J., Monoclonal antibodies to 5'-triphospho-(2'-5')adenyladenosine oligonucleotides. *Proceeding of the National. Academy of Sciences* USA, **1982,** 79, 4742–4746.
44. Samanta, H.; Dougherty, J. P.; Lengyel, P., Synthesis of (2'-5')(A)N from ATP - characteristics of the reaction catalyzed by (2'-5')(A)N synthetase purified from mouse ehrlich ascites tumor-cells treated with interferon. *Journal of Biological Chemistry* **1980,** 255, (20), 9807-9813.
45. Johnston, M. I.; Torrence, P. F., In Friedman, R.M. (Ed.), Interferon: Mechanisms of Production and Action. 3Elsevier, Amsterdam, New York **1984,** 3, 189–298.

46. Kariko, K.; Sobol, R. W.; Suhadolnik, L.; Li, S. W.; Reichenbach, N. L.; Suhadolnik, R. J.; Charubala, R.; Pfleiderer, W., Phosphorothioate analogs of 2',5'-oligoadenylate enzymatically synthesized 2',5'-phosphorothioate dimer and trimer - unequivocal structural assignment and activation of 2',5'-oligoadenylate-dependent endoribonuclease. *Biochemistry* **1987,** 26, (22), 7127-7135.
47. Sobol, R. W.; Fisher, W. L.; Reichenbach, N. L.; Kumar, A.; Beard, W. A.; Wilson, S. H.; Charubala, R.; Pfleiderer, W.; Suhadolnik, R. J., Hiv-1 reverse-transcriptase - inhibition by 2',5'-oligoadenylates. *Biochemistry* **1993,** 32, (45), 12112-12118.
48. Wasner, M.; Arion, D.; Borkow, G.; Noronha, A.; Uddin, A. H.; Parniak, M. A.; Damha, M. J., Physicochemical and biochemical properties of 2',5'-linked RNA and 2',5'-RNA : 3',5'-RNA "hybrid" duplexes. *Biochemistry* **1998,** 37, (20), 7478-7486.
49. (a) Premraj, B. J.; Patel, P. K.; Kandimalla, E. R.; Agrawal, S.; Hosur, R. V.; Yathindra, N., NMR structure of a 2',5' RNA favors A type duplex with compact C2' endo nucleotide repeat. *Biochemical and Biophysical Research Communications* **2001,** 283, (3), 537-543.
50. Sheppard, T. L.; Breslow, R. C., Selective binding of RNA, but not DNA, by complementary 2',5'-linked DNA. *Journal of the American Chemical Society* **1996,** 118, (40), 9810-9811.
51. Prakash, T. P.; Jung, K. E.; Switzer, C., RNA recognition by the 2'-structural isomer of DNA. *Chemical Communications* **1996**, (15), 1793-1794.
52. Premraj, B. J.; Raja, S.; Yathindra, N., Structural basis for the unusual properties of 2'-5' nucleic acids and their complexes with RNA and DNA. *Biophysical Chemistry* **2002,** 95, (3), 253-272.
53. (a) Polak, M.; Manoharan, M.; Inamati, G. B.; Plavec, J., Tuning of conformational preorganization in model 2',5'- and 3',5'-linked oligonucleotides by 3'- and 2'-*O*-methoxyethyl modification. *Nucleic Acids Research* **2003,** 31, (8), 2066-2076. (b) Premraj, B. J.; Raja, S.; Bhavesh, N. S.; Shi, K.; Hosur, R. V.; Sundaralingam, M.; Yathindra, N., Solution structure of 2',5' d(G(4)C(4))-Relevance to topological restrictions and nature's choice of phosphodiester links. *European Journal of Biochemistry* **2004,** 271, (14), 2956-2966.

54. Wodak, S. Y.; Liu, M. Y.; Wyckoff, H. W., Structure of cytidilyl (2',5') adenosine when bound to pancreatic ribonuclease S. *Journal of Molecular Biology* **1977,** 116, (4), 855-875.
55. Kumar, P.; Takaku, H., Properties of mixed backbone oligonucleotides containing 3'-*O*-methyl ribonucleosides. *Bioorganic & Medicinal Chemistry Letters* **1999,** 9, (17), 2515-2520.
56. Pudlo, J. S.; Cao, X. D.; Swaminathan, S.; Matteucci, M. D., Deoxyoligonucleotides containing 2',5' acetal linkages - synthesis and hybridization properties. *Tetrahedron Letters* **1994,** 35, (50), 9315-9318.
57. Peng, C. G.; Damha, M. J., Synthesis and hybridization studies of oligonucleotides containing 1-(2-deoxy-2-alpha-C-hydroxymethyl-beta-D-ribofuranosyl) thymine (2'-alpha-hm-dT). *Nucleic Acids Research* **2005,** 33, (22), 7019-7028.
58. (a) Obika, S.; Morio, K.; Hari, Y.; Imanishi, T., Preparation and properties of 2',5'-linked oligonucleotide analogues containing 3'-*O*,4'-C-methyleneribonucleosides. *Bioorganic & Medicinal Chemistry Letters* **1999,** 9, (4), 515-518. (b) Obika, S.; Andoh, J.; Onoda, M.; Nakagawa, O.; Hiroto, A.; Sugimoto, T.; Imanishi, T., Synthesis of a novel bridged nucleoside bearing a fused-azetidine ring, 3'-amino-3',4'-BNA monomer. *Tetrahedron Letters* **2003,** 44, (28), 5267-5270.
59. Zou, R. M.; Matteucci, M. D., Synthesis and hybridization properties of an oligonucleotide analog containing a glucose-derived conformation-restricted ribose moiety and 2', 5' formacetal linkages. *Tetrahedron Letters* **1996,** 37, (7), 941-944.
60. Agha, K. A.; Damha, M. J., Synthesis and binding properties of a homopyrimidine 2',5'-linked xylose nucleic acid (2',5'-XNA). *Nucleosides Nucleotides & Nucleic Acids* **2003,** 22, (5-8), 1175-1178.
61. Blackburn, G. M.; Gait, M. J.; Loakes, D.; Williams, D. M., Nucleic acids in chemistry and biology. RSC publishing 3rd edition.
62. Cantor, C. R.; Schimmel, P. R. (Eds), Biophysical Chemistry part III *W. H. Freeman and Company* **1971,** New Yok.
63. Plum, G. E.; Park, Y.-H.; Singleton, S. F.; Dervan, P. B.; Breslauer, K. J., Thermodynamic characterization of the stability and the melting behavior of a DNA

triplex: A spectroscopic and calorimetric study. *Proceeding of the National. Academy of Sciences* USA **1990,** 87, 9436.

64. Vanholde, K. E.; Brahms, J.; Michelso.Am, Base interactions of nucleotide polymers in aqueous solutions *Journal of Molecular Biology* **1965,** 12, (3), 726.
65. (a) Stryer, L., Biochemistry, 3rd ed.; New York: W. H. freeman and Company. **1988**. (b) Egli, M.; Williams, L. D.; Gao, Q.; Rich, A., Structure of the pure-spermine form of Z-DNA (magnesium free) at 1-A resolution. *Biochemistry* **1991,** 30, (48), 11388-11402. (c) Calladine, C. R.; Drew, H. R., Understanding DNA, The molecule and how it works; *Cambridge: Academic Press LTd*. **1992**. (d) Beveridge, D. L.; Jorgensen, W. L., Computer Simulation of chemical and biomolecular systems. *Annals of the New York Academy of Sciences* **1986**, 482. (e) Gessner, R. V.; Frederick, C. A.; Quigley, G. J.; Rich, A.; Wang, A. H. J., The molecular-structure of the left-handed Z-DNA double helix at 10-A atomic resolution - geometry, conformation, and ionic interactions of d(CGCGCG). *Journal of Biological Chemistry* **1989,** 264, (14), 7921-7935.
66. (a) Job, P. Formation and stability of inorganic complexes in solution *Annali di Chimica Applicata* **1928,** 9, 113-203. (b) Huang, C. Y., Determination of binding stoichiometry by the continuous variation method-the job plot. *Methods in Enzymology* **1982,** 87, 509-525.
67. Little, D. P.; Cornish, T. J.; Odonnell, M. J.; Braun, A.; Cotter, R. J.; Koster, H., MALDI on a chip: Analysis of arrays of low femtomole to subfemtomole quantities of synthetic oligonucleotides and DNA diagnostic products dispensed by a piezoelectric pipet. *Analytical Chemistry* **1997,** 69, (22), 4540-4546.
68. Crain, P. F.; McCloskey, J. A., Applications of mass spectrometry to the characterization of oligonucleotides and nucleic acids. *Current Opinion in Biotechnology* **1998,** 9, (1), 25-34.

Chapter 2

Synthesis of 3′-deoxy-3'-fluoro ribo/xylouridine nucleosides ($^{R}U^{F}$ and $^{X}U^{F}$), their incorporation into ngDNA, and effect on binding properties to target sequences

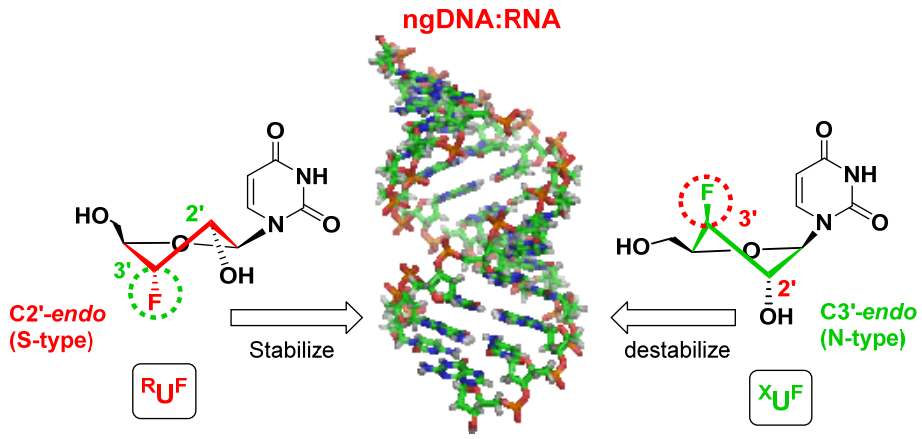

The ngDNA/ngRNA are potential candidates for antisense application due to their RNA selective hybridization properties. In spite of the fact that the overall stability of ngDNA:RNA duplexes is less than that of corresponding DNA:RNA, their enzymatic stability would improve their potency in biological system which is a highly desirable attribute for therapeutic applications. Conformationally constrained C3′-*endo* (N-type) modifications in genetic nucleic acids have been found to improve the thermal stability with very high degree, e.g. LNA or 2′F-ANA/RNA. Fluorine substitution has a strong influence on the conformational preferences of furanose ring of the nucleic acid. In this chapter we discuss the synthesis of 3′-deoxy-3′-fluoro ribo/xylouridine ($^{R}U^{F}$ and $^{X}U^{F}$), which are S/N-type-conformationally frozen nucleoside analogues. The synthesized nucleosides were incorporated into ngDNA and biophysical experiments were carried out to study the structural implications of these modified ngDNA oligomers on the stability of duplexes with target DNA/RNA.

2.1 Introduction

Antisense technology is based on a simple concept of binding complementary synthetic oligonucleotides (ONs) to specific mRNAs to inhibit the transfer of genetic information from mRNA to protein. Rapid degradation of natural phosphodiester backbone of oligonucleotides by cellular nucleases necessitated chemical modification of the ONs. In Chapter 1, we have discussed about these modifications. Among this multitude of chemical modifications, ONs containing conformationally restricted nucleotides in which the sugar moieties are locked/ frozen in defined sugar puckering are important in terms of both of binding properties with target nucleic acids as well as their nuclease resistance. The modified 2′,4′-bridged nucleic acid (BNA/LNA)[1,2] analogues lock the sugar pucker in 3′-*endo* conformation and improve AS-ONs affinity for its biological target (i.e., mRNA). Fluorine substitutions in furanose ring also show a strong influence on the conformational properties of the nucleic acids. The presence of arabino-D-sugar, the 2′-stereoisomer of ribose in the oligomers (ANA) allowed complex formation with both RNA and DNA, but with reduced stability.[3] While replacement of 2′-OH of arabino nucleic acid (ANA) by either 2′-ribo/arabino-fluoro group is known to have large impact on the thermal stability of the 3′-5′ linked 2′-fluoro DNA:RNA (2′F-RNA :RNA and 2′F-ANA:RNA)[4-5] duplexes because of the favorable influence of the 2′-fluoro group on conformational preference on the sugar pucker (Figure 1).

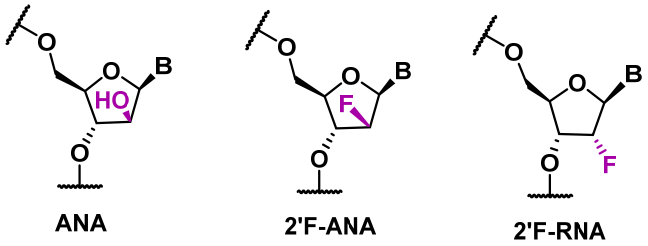

Figure 1. Arabinose and 2′-deoxy-2′-fluororibo/arabino nucleic acid (ANA, 2′F-RNA and 2′F-ANA)

The 2′F-ANA adopts a more DNA-like B-type helix conformation, not through the typical C2'-*endo* conformation but, rather, through an unusual O4′-*endo* (east) pucker. However, the presence of the electronegative fluorine leads to significant increase (ΔTm 1.2°C/mod) in melting temperature per modification. This stability was further attributed due to other factors, such as favourable inter-residue pseudo-hydrogen bond (2′F···purine

H8) that contrasts with unfavourable inter 2′-OH·· nucleobase steric interaction in the case of ANA:RNA hybrid duplexes.[6] Interactions between the 2′-substituent and the base may help to preorganize the single strand into an appropriate conformation for duplex formation with RNA in the case of 2′F-ANA, while disfavoring that conformation in the case of ANA (Figure 1). Both ANA and 2′F-ANA containing hybrids are structurally similar to DNA:RNA hybrid duplexes. The ANA strand is limited to more southern conformations (C2′-*endo* locked) due to an internal H-bonding with C5′-oxygen, while the lack of such interaction in 2′F-ANA allowed increased variability and sugar pucker shift towards east (O4′-*endo*), a conformation which is more compatible with the fixed northern (C3′-*endo*) conformation of the RNA strand. Thus DNA-like conformation of 2′F-ANA also allows the prefer RNase H activity for therapeutic applications. The change in stereochemistry of fluorine substitution from top face in 2′F-ANA to bottom face in 2′F-RNA increased the thermal stability of 2′F-RNA:RNA hybrid. The electronegative fluorine in 2′F-RNA causes the sugar to adopt the C3′-*endo* configuration, normally observed in RNA, which leads to an increase in duplex stability.

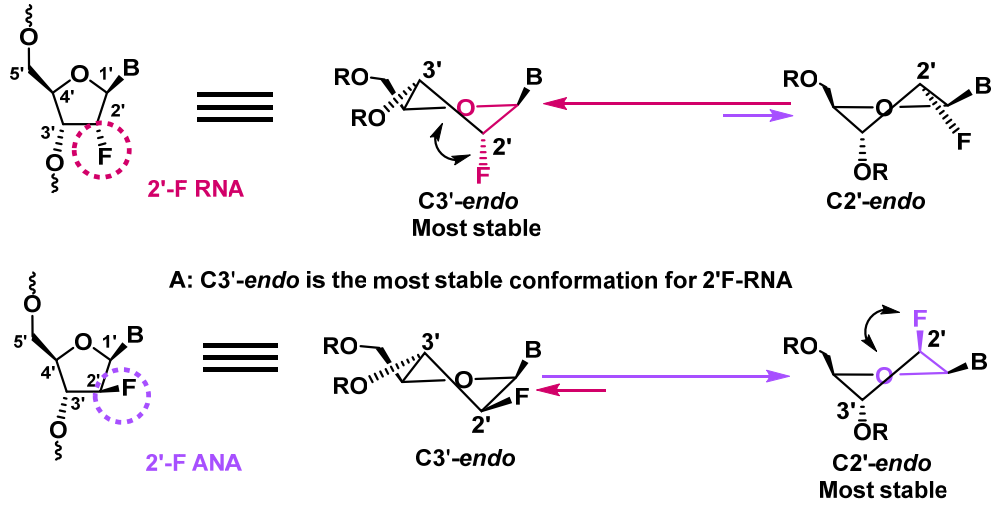

Figure 2. Sugar puckering equilibrium for 2′F- RNA and 2′F-ANA

The stronger *gauche* effect of the fluorine substituent due to its high electronegativity has a profound stereoelectronic effect on the stereochemical orientation of the neighbouring groups; thereby the fluorine substituent governs the overall conformation

of the sugar ring. In 2′-deoxy-2′-fluoro nucleic acid in the *ara* configuration (2′F-ANA) takes up the south-type or east conformation, whereas 2′-deoxy-2′-fluoro-nucleic acid in the *ribo* configuration (2′F-RNA) puckers preferentially in the north-type conformation due to O_4'-C1′-C2′-F_2′ *gauche* effect (Figure 2). This means that the strength of the fluorine-induced *gauche* effect which determines the overall conformation of the sugar ring is configuration-dependent. In addition, antisense drugs incorporating 2′F-ANA/RNA nucleotides exhibit enhanced metabolic stability, and improved pharmacokinetic and toxicological properties. Several AS-ONs drug candidates containing conformationally restricted nucleotides have entered clinical trials and continue to make progress for a variety of therapeutic indications.

There are some other examples of fluorine modified nucleic acids that give favorable properties to the ONs such as hexitol nucleic acids (HNA)[7] and cyclohexenyl nucleic acid (CeNA)[8] (Figure 3).

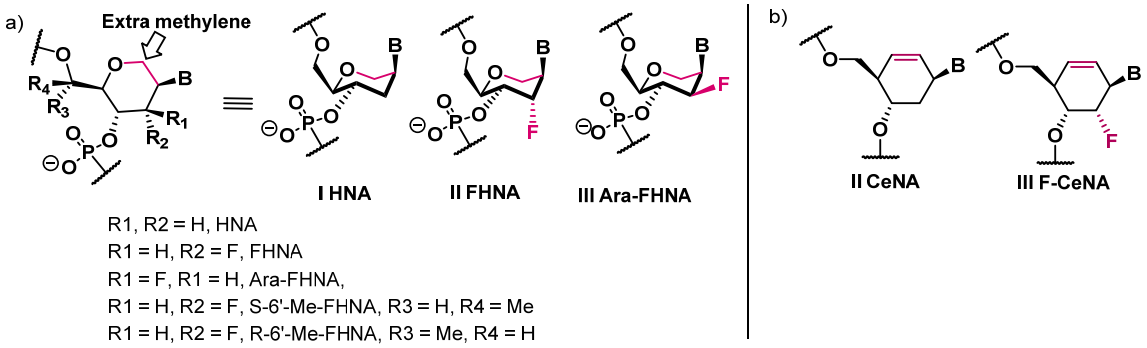

Figure 3. Fluorinated analogues of HNA and CeNA

In the hexitol series, the furanose ring is replaced with a six-membered pyranose ring and the position of the nucleobase is moved from the anomeric carbon to the 2′-position (Figure 3a). ^{1}H NMR analysis of a HNA dimer confirmed the axial orientation of the base moiety with respect to the hexitol ring, and this mimics the N-type sugar pucker of furanose nucleosides. In the 3′-fluoro hexitol nucleic acid (FHNA and Ara-FHNA)[7] modified ONs axial 3′-fluoro substitution (Figure 3a II, FHNA) boosts the RNA affinity of HNA, whereas fluorine in equatorial orientation (Figure 3a III, Ara-FHNA) results in a significant destabilization relative to HNA and DNA. Crystal structure at high resolution revealed that the equatorial 3′-fluorine substituent in Ara-FHNA pushes away the 3′-

flanking nucleotide thus disrupting stacking of nucleobases. It is also found that the S- and R-6′-methyl backbone modifications of 3′-fluoro hexitol nucleic acid (FHNA) show opposite effect on RNA affinity. The S-6′-Me-FHNA-T enhances duplex thermal stability like FHNA-T. On the other hand, incorporation of R-6′-Me-FHNA-T has a destabilizing effect, amounting to ~4°C relative to FHNA-T (Figure 3a).[9]

Cyclohexenyl nucleic acids (CeNAs), in which oxygen of furanose ring is replaced by ethylene group are characterized by a high degree of conformational rigidity of the oligomers. Recently 2′-fluoro modification was reported in cyclohexenyl nucleic acid (Figure 3b, F-CeNA).[8] F-CeNA modified ONs show equivalent duplex stabilizing properties relative to FRNA and CeNA, but slightly lower with complementary RNA as compared to that of more rigid 3′-fluoro hexitol nucleic acid (FHNA). However, F-CeNA modified ONs were significantly more stable against digestion by snake venom phosphodiesterase as compared to unmodified DNA, 2′-fluoro RNA, 2′-*O*-MOE and FHNA modified ONs. The crystal structural data demonstrate that the presence of fluorine at the 3′-position of CeNA does not fundamentally alter the conformational flexibility of the cyclohexenyl moiety. Paired with RNA, F-CeNA-modifications within a DNA can be expected to increase the stability relative to the corresponding CeNA-DNA chimeric strand by pseudo H-bonding or by locking the cyclohexenyl ring in a C3′-*endo* mimicking conformation.

We also discussed in Chapter 1 that in addition to the predominant 3′-5′ internucleotide linkage, a less abundant 2′-5′ internucleotide linkage called as nongenetic nucleic acids (ngDNA/ngRNA) could also be subjected to new chemical modifications to improve their therapeutic value. These nongenetic nucleic acids associate to form Watson-Crick base-paired duplex structures with complementary single-stranded RNA but their binding is weak. This ngDNA/ngRNA are also known to be stable to nucleases. These properties make them to be the right candidates as leads for development as antisense ONs, if the binding strength of these ngONs to the target mRNA could be improved.

The mixed backbone ONs (MBOs)[10] containing 2′-5′ and 3′-5′ RNA, or 2′-5′RNA and 3′-5′DNA segments, with phosphodiester as well as phosphorothioate backbone have been evaluated earlier without much success. Some chemical modifications with 2′-5′-linkages have been reported in the literature, such as 3′-methoxy 2′-5′-linked RNA,[11] 3′-*O*-

4′-C-methylene nucleoside, 3′-amino-3′ 4′-BNA[12] and 5, 5 bicyclic ribose 2′-5′ formacetal[13] (Chapter 1). These were incorporated only in the native 3′-5′ DNA and not in ngDNA. This lead to large destabilization of duplexes with cDNA and RNA. Much less attention is given for modifing homogeneous 2′-5′-linked ONs. Backbone modified PS-ngDNA sequences,[14] the 2′-α-hm-dT and 3′-α-hm-dT modification in ngRNA,[15] are the few examples, but were found to further destabilize the ngDNA/ngRNA:RNA duplex. The 2′-5′ xylose nucleic acid (ngXNA) is the example where the homogeneous ngXNA strand was synthesized. The ngXNA adopted C3′-*endo* conformation with extended geometry and bound very weakly to the compact RNA target.[16]

2.2 Rationale, design and objectives of the present work

The modeling studies have suggested that the expected furanose ring pucker in the ngDNA strand in the ngDNA:RNA duplexes would be S-type as against the preferred N-type geometry in DNA:RNA duplexes. The structural requirements of the ngRNA/ngDNA:RNA duplexes (predominant S-type geometry of the 2′-5′ strand in ngRNA/ngDNA:RNA duplex) do not match with the sugar conformations at the single strand 2′-5′ oligomer level.[17] In the single-stranded 3′-deoxy 2′-5′ oligomer, the stereoelectronic (*gauche* and anomeric) effects of the 2′-hydroxy group, would accentuate the preference for 3′-*endo* (N-type) sugar conformations. In the modeling studies of the ngDNA:RNA duplex, it was therefore assumed that the RNA strand would impose its structure on the ngDNA strand, and the individual nucleosides in the ngDNA strand would be required to assume S-type i.e., C2′-*endo* conformation to give rise to a stable duplex. Thus, it was suggested that the ngDNA would be under conformational and topological constraints while forming the duplex with complementary RNA.

Considering these predictions, it was thought to study the effects of incorporation of monomers bearing either locked or frozen S-type/N-type sugar conformations into 2′-5′-linked ONs. We envisaged here that applying such structural locks on the ngDNA strand should allow us to understand the structural preferences of the sugars in the isomerically-linked strand of the hybrid duplexes and thereby provide an experimental proof for the proposed structural preferences based on modeling studies. The specific RNA binding of

ngDNA, supplemented by favoured geometrical features for complex formation, would have potential applications in antisense therapeutics.

We chose 3′-fluoro substitution of the furanose ring of nucleosides (uridine) for the following reasons (Figure 4). The highly electronegative nature of the fluorine substitution in different orientation would impart very different electronic effects that could in turn influence the sugar ring conformations. These conformational restrictions due to fluorine substitutions may cause either improvement in binding strength of duplex or may be detrimental for duplex stability. This would be analogous to the highly improved binding strength of DNA:RNA duplexes with the frozen N-type sugar ring geometry in 2′F-RNA compare to the relatively less binding strength because of duplexes with O4′-*endo* (east) conformation in 2′F-ANA derived nucleic acids.

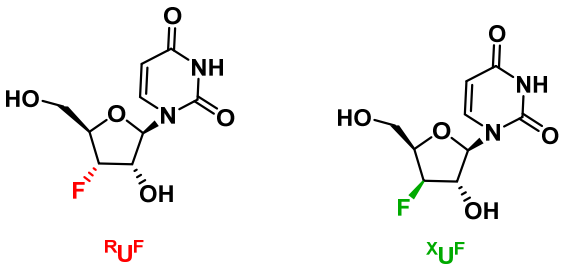

Figure 4. 3′-deoxy-3′-fluoro ribo/xylouridine ($^{R}U^{F}$ and $^{X}U^{F}$)

The 3′-deoxy-3′-fluoro xylouridine due to the favourable O_4'-C4′-C3′-F_3′ *gauche* effect restrict to C2′-*exo* conformation showing N-type sugar geometry, and the 3′-deoxy-3′-fluoro ribouridine preferred C2′-*endo* conformation showing S-type sugar pucker again due to dominating *O*$_4$′-C4′-C3′-F$_3$′ *gauche* effect (Figure 5).

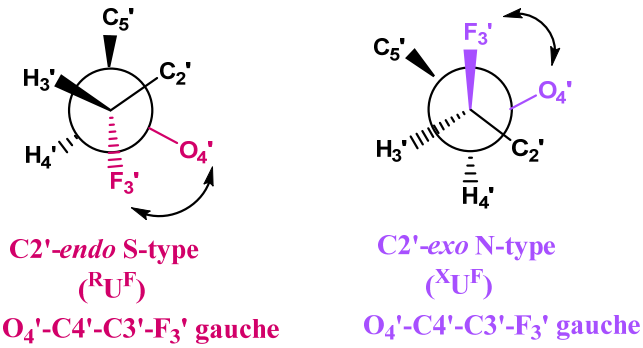

Figure 5. Fluorine-induced gauche effect is configuration-dependent

This again shows that opposite configuration of fluorine (ribo/xylo) at 3′ carbon freezes the sugar in opposite conformation. The sugar puckering equilibrium for $^{R}U^{F}$ and $^{X}U^{F}$ nucleoside is shown in Figure 6.

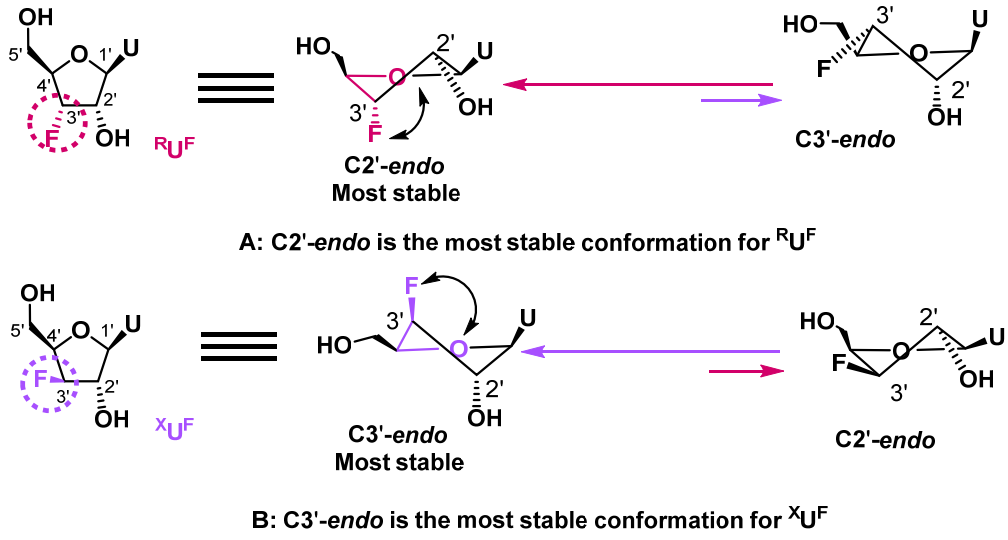

Figure 6. Sugar puckering equilibrium for $^{R}U^{F}$ and $^{X}U^{F}$

The present work describes the synthesis of S/N-type conformationally frozen, 3′-deoxy-3′-fluoro ribo/xylouridine nucleosides ($^{R}U^{F}$ and $^{X}U^{F}$). Synthesized nucleosides were incorporated into ngDNA sequences at predefined positions and biophysical experiments were carried out to study the structural preferences of these oligomers and their effect on the stability of duplexes with target DNA/RNA.

Objectives of the present work

1. Synthesis of 3′-deoxy-3′-fluoro ribouridine ($^{R}U^{F}$) and 3′-deoxy-3'-fluoro ($^{X}U^{F}$) xylouridine nucleosides (Figure 4).
2. Preliminary study of sugar puckering using ^{1}H NMR $J_{1'2'}$ coupling constant.
3. Synthesis of oligonucleotides containing these modified units their purification and characterization.
4. Duplex stability and CD studies of the derived oligomers.

2.3 Present work, results and discussion

2.3.1 Synthesis of $^{X}U^{F}$, $^{R}U^{F}$ phosphoramidite monomers

The 3′-deoxy-3′-fluoro-xylouridine **11** and 3′-deoxy-3′-fluoro-ribouridine **21** were synthesized from D-glucose[18] and D-xylose[19] as starting material respectively following reported procedures. Potassium fluoride (KF) and DAST (Et_2NSF_3, Diethylammonium sulphur trifluoride) is used as fluorinating reagent in the synthesis of **11** and **21** respectively. Nucleobase substitution was achieved by using most common Vorbrüggen glycosylation reaction condition.[20] Vorbrüggen glycosylation employs coupling of a nucleophilic silylated heterocyclic base and electrophilic sugar derivative in the presence of a Lewis acid at reflux temperature. The general mechanism of the reaction is as shown in Figure **7.**

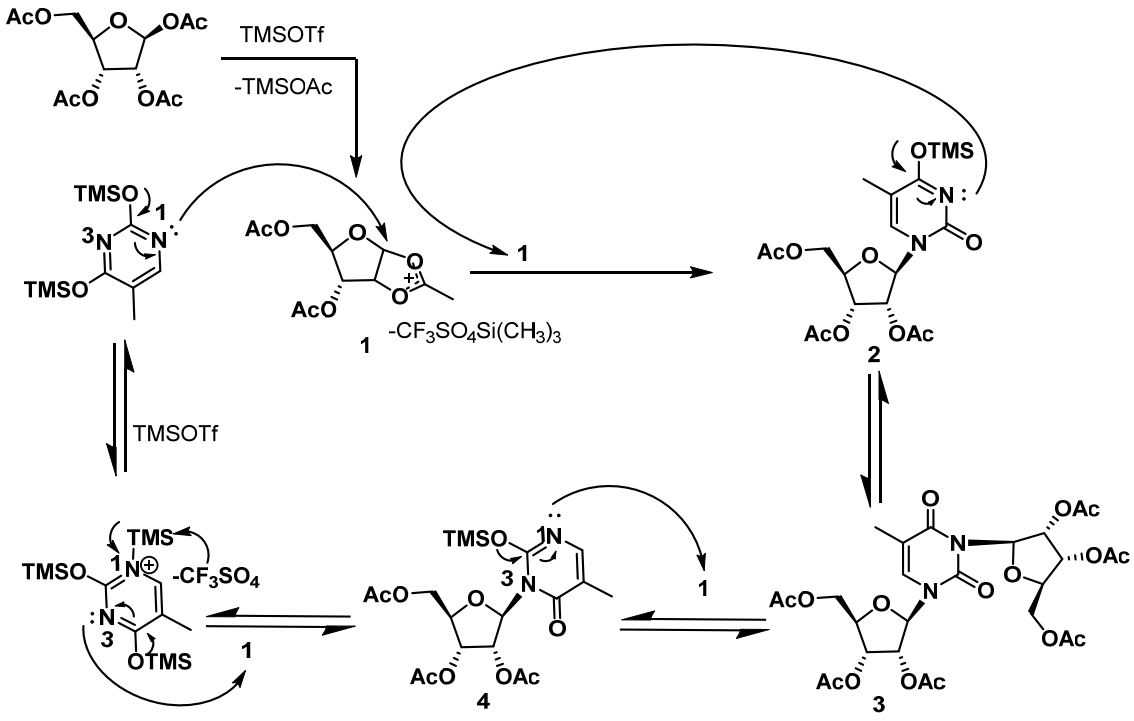

Figure 7. General mechanism of Vorbrüggen glycosylation reaction

In the presence of Lewis acid, the formation of the key cyclic cation **1**, is followed by nucleophilic attack at the anomeric position by the most nucleophilic nitrogen (N1 in pyrimidine or N9 in purine) yielding the desired β-nucleoside **2**. A second reaction of this

nucleoside with **1** generates bis(riboside) **3**. Depending on the nature of the Lewis acid used, coordination of the nucleophile to the Lewis acid may be significant. Reaction of this "blocked" nucleophile with **1** results in undesired constitutional isomer **4**, which may undergo further reaction to give **3**. Generally the use of Lewis acid like trimethylsilyl trifluoromethanesulfonate (TMS-triflate) does not create a coordination problem. The continuous and prolonged heating for 3-4h gives a 70-80 % of desired thermodynamically preferred product **2** avoiding the formation of kinetic product like bis(riboside) or other isomers (N3 for pyrimidine and N7/N1/N3 for purine).

2.3.1a Synthesis of $^{X}U^{F}$ phosphoramidite monomer

Robins *et al.* reported that opening of a purine ribonucleoside 2′-3′-α-epoxide gave 3'-fluoro xylonucleosides[21] but these transformations in the pyrimidine series have not been reported. D-glucose or D-xylose sugar is found to be an efficient precursor for the large scale preparation of the 3′- fluoro- xylonucleosides. Webber *et al.*[22] have shown that a C3-*O*-tosyloxy group of 1,2:5,6-di-*O*-isopropylidene-α-D-allofuranose (ADA) can be displaced by fluoride derived from tetrabutylammonium fluoride (TBAF). Analogously, Fox *et al* [23] have carried out the displacement using KF in acetamide at -210^{o}C. This was improved upon by Tewson *et al* [24] who demonstrated that reaction of the same non-tosylated sugar with DAST followed by vacuum distillation avoided an extra step of tosylation of C3-hydroxyl. Komiotis *et. al*[18] in 2007 reported an efficient synthesis starting from glucose diacetonide (GDA) where KF is used for fluorination and Vorbrüggen glycosylation for base attachment. We decided to follow the synthetic route described by Komiotis *et. al* with some modifications. All the synthesized compounds were purified by column chromatography and appropriately characterized using ^{1}H, ^{13}C, ^{31}P NMR and mass spectrometric analysis.

Synthesis of 3-deoxy-3-fluoro-1,2,5-tri-*O*-acetyl-D-xylofuranose

D-glucose **1** was used as starting material for the synthesis of the 3′-deoxy-3′-fluoro-xylouridine monomer (Scheme 1), which was first converted to 1,2:5,6-di-*O*-isopropylidene-α-D-glucofuranose (GDA) **2** with 70% yield by using acetone in presence of conc. H_2SO_4 and anhydrous $CuSO_4$. Oxidation of the glucose diacetonide (GDA) **2** with

pyridinium chlorochromate (PCC) in dry DCM, followed by stereoselective reduction with sodium borohydride ($NaBH_4$) in MeOH:H_2O gives allose diacetonide (ADA) **4** (80%). Tosylation of **4** with *p*-toluenesulfonyl chloride (TsCl) in pyridine gave the corresponding 1,2:5,6-di-*O*-isopropylidene-3-*O*-toluenesulfonyl-α-D-allofuranose **5** with 65% yield. S_N2 displacement of the tosyloxy group at C-3 by a fluorine atom was effected by reacting **5** with KF in acetamide at ~210°C (internal temperature) to obtain **6** (60%). Selective removal of the 5,6-*O*-isopropylidene group using 1:1 AcOH:H_2O mixture at 50°C for 1h afforded the 3-deoxy-3-fluoro-1,2-*O*-isopropylidene-α-D-glucofuranose **7** (95%), which upon periodate oxidation, followed by borohydride reduction of the resulting aldehyde (one pot), gave 3-deoxy-3-fluoro-1,2-*O*-isopropylidene-α-D-xylofuranose **8** (85%). The 1,2-acetonide group in **8** was deprotected and the compound was converted to the anomeric mixture of triacetates, 3-deoxy-3-fluoro-1,2,5-tri-*O*-acetyl-D-xylofuranose **9** in 55% yield by treatment with AcOH and Ac_2O in the presence of a catalytic amount of concentrated H_2SO_4.

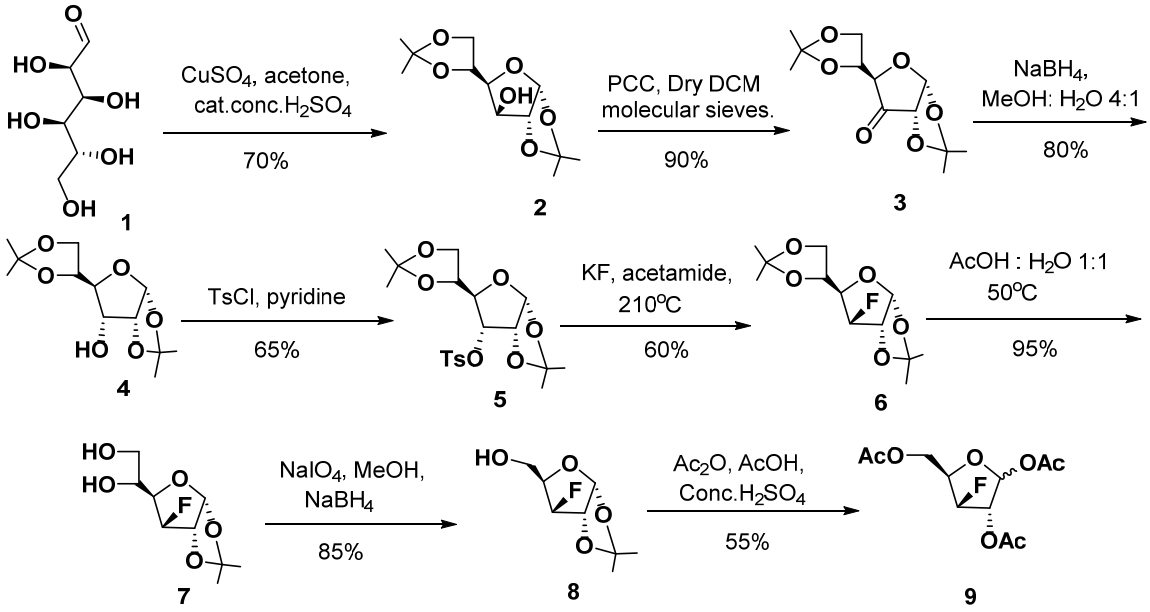

Scheme 1: Synthesis of 3-deoxy-3-fluoro-1,2,5-tri-*O*-acetyl-D-xylofuranose

Synthesis of 3′-deoxy-3′-xylofluoro uridine monomer ($^{X}U^{F}$)

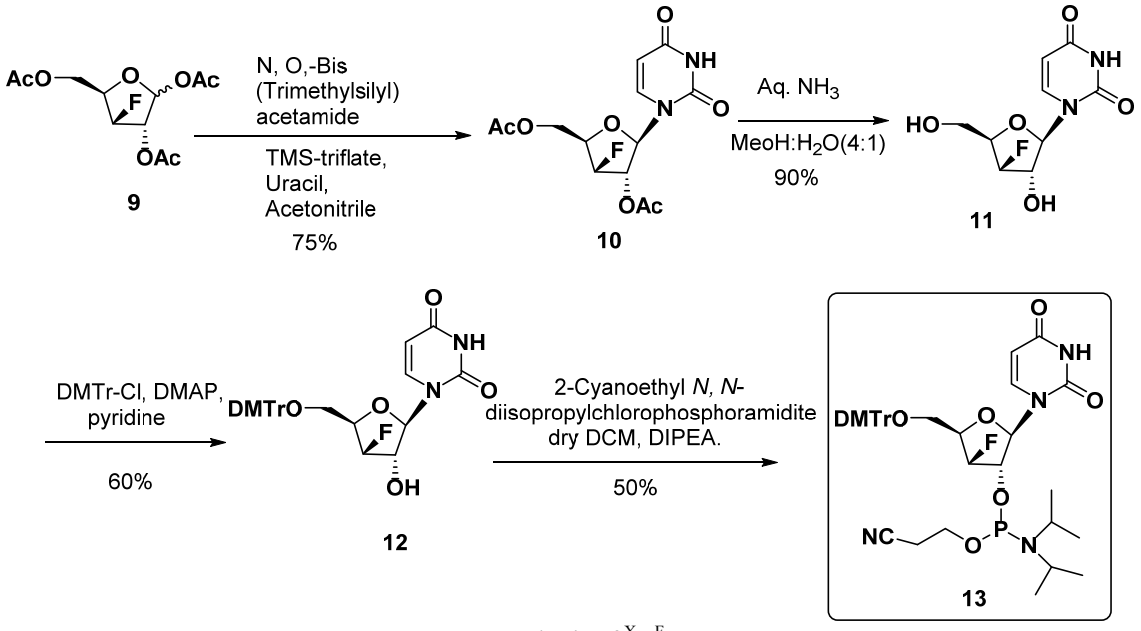

Scheme 2: Synthesis of $^{X}U^{F}$ monomer

The Vorbrüggen glycosylation coupling of a bis(trimethylsilyl)uracil (U·2TMS) with an anomeric mixture of 3-deoxy-3-fluoro-1,2,5-tri-*O*-acetyl-D-xylofuranose in the presence of TMS-triflate in dry ACN at reflux condition afforded β-nucleoside as the only isomer **10** (Scheme 2) with 75% yield. Where neighboring group participation of 2-*O*-acetyl groups allows exclusive formation of β-nucleoside. Compound **10** was then subjected to ammonolysis to give 3′-deoxy-3′-fluoro xylouridine **11** (90%). The free primary hydroxyl group in **11** was protected as its 4, 4′-dimethoxytrityl (DMTr) group using DMTr-chloride and a catalytic amount of 4,4′-Dimethylaminopyridine (DMAP) in dry pyridine to get **12** (60%). Compound **12** was phosphitylated at the 2′-hydroxy group with 2-Cyanoethyl *N,N*-diisopropylchlorophosphoramidite in dry DCM using *N,N*-diisopropylethylamine (DIPEA) base afforded the desired phosphoramidite building block **13** (50%) as 3′-deoxy-3′-fluoro xylouridine ($^{X}U^{F}$) monomer.

2.3.1b Synthesis of $^{R}U^{F}$ phosphoramidite monomer

Taylor *et al* [25] used Potassium bifluoride and sodium fluoride (KHF_2/NaF) in 1,2-ethylene glyco1 as fluorinating agent for the opening of epoxide of methyl 2, 3-anhydro-D-lyxofuranoside to get 3-deoxy-3-fluoro-1-*O*-methyl-D-ribofuranose. Mikhailopulo *et al* [26]

in 1991 reported the synthesis of 3'-deoxy-3'-fluoro-ribonucleosides for all the nucleobases, where the condensation of the silylated bases with 3-deoxy-3-fluoro-1-*O*-methyl-D-ribofuranose in the presence of Friedel-Crafts catalysts $SnCl_2$ or Lewis acid TMS-triflate was the key step for synthesis of nucleosides. Same group in 1999[19] again reported the novel route for the synthesis of 3'-deoxy-3'-fluoro-ribonucleosides where they used DAST for fluorination. DAST seems to be the most versatile reagent for fluorination in carbohydrate chemistry for a one-step exchange of a hydroxyl group by fluorine. We followed the same synthetic route what Mikhailopulo *et al* reported in 1999, to synthesize the ribofluoro uridine nucleoside. All the synthesized compounds were purified by column chromatography and appropriately characterized using ^{1}H, ^{13}C & ^{31}P NMR and mass spectrometric analysis.

Synthesis of 3-deoxy-3-fluoro-1-*O*-methyl-5-*O*-benzoyl-2-acetyl-D-ribofuranose

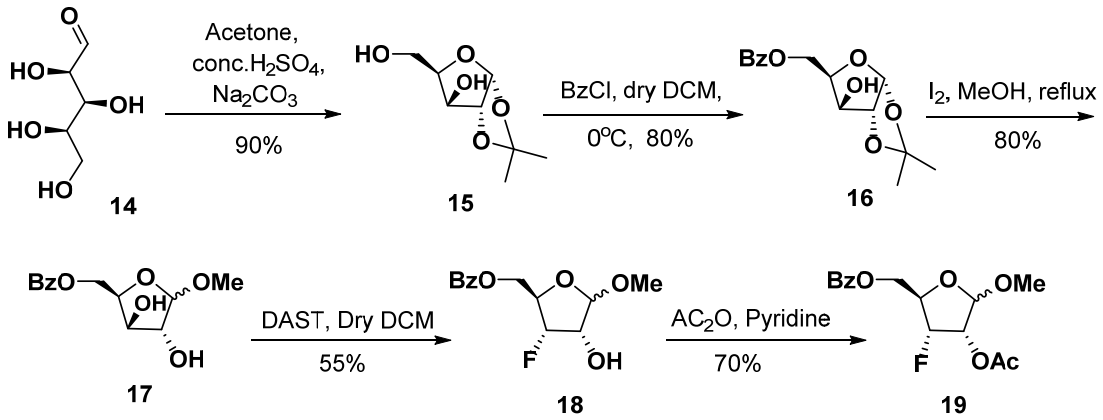

Scheme 3: 3-deoxy-3-fluoro-1-*O*-methyl-5-*O*-benzoyl-2-*O*-acetyl-D-ribofuranose

D-xylose **14** was used as starting material for the synthesis of 3-deoxy-3-fluoro-1-*O*-methyl-5-*O*-benzoyl-2-*O*-acetyl ribofuranose **19** (Scheme 3). D-xylose **14** was transformed to 1,2-*O*-isopropylidene-α-D-xylofuranose **15** (90%) using acetone, conc.H_2SO_4 and Na_2CO_3 in one pot reaction. Careful benzoylation of **15** in dichloromethane in the presence of triethylamine (Et_3N) gave the 5-*O*-benzoyl derivative **16** (80%), which was treated with Iodine (I_2) in methanol under reflux for 4h to afford a mixture of the desired β-D- and α-D-xylosides **17** in 80% yield. Treatment of anomeric mixture of methyl 5-*O*-benzoyl-D-xylofuranoside **17** with DAST in a molar ratio of 1:6 in dry DCM at room temperature for 19h, afforded the mixture of compounds 3′-fluoro α and β-D-riboside **18** (55%) with the

ribo-epoxide and arabino-difluoride as side product. In this case the C3-O-SF_2NEt_2 derivative undergoes intermolecular attack by an F-anion to give the desired major product. In this particular case two side product formed one is epoxide formed due to intramolecular nucleophilic attack by –OH group at C2 and other is the difluoride formed because of the reaction with an excess of DAST (Figure 8). Finally acylation of free secondary 2′-hydroxy group of **18** using acetic unhydride offerded 3-deoxy-3-fluoro-1-*O*-methyl-5-*O*-benzoyl-2-acetyl-D-ribofuranose **19** (70%).

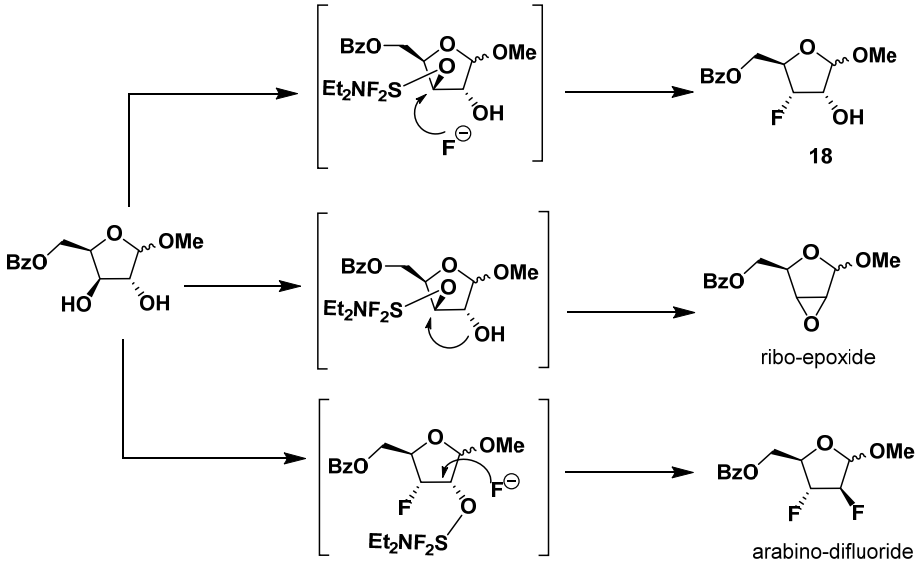

Figure 8. Mechanism of fluorination by DAST

Synthesis of 3′-deoxy-3′-ribofluoro uridine monomer ($^{R}U^{F}$)

Coupling of bis(trimethylsilyl)uracil (U·2TMS) with 3-deoxy-3-fluoro-1-*O*-methyl-5-*O*-benzoyl-2-*O*-acetyl-D-ribofuranose **19**, under Vorbrüggen condition gave only the uracil β-nucleoside derivative **20** (75%) selectively (Scheme 4). Here the neighboring group participation of 2-*O*-acetyl group helps for β- selectivity of uracil. Compound **20** was then subjected to ammonolysis to give 3′-deoxy-3′-fluoro ribouridine **21** (90%). The free primary hydroxyl group in **21** was protected as its 4, 4′-dimethoxytrityl (DMTr) group using DMTr-chloride and a catalytic amount of DMAP in dry pyridine to get **22** (60%). Compound **22** was then phosphitylated at the 2′-hydroxy group with 2-Cyanoethyl *N, N*-diisopropylchlorophosphoramidite to afford the desired phosphoramidite building block **23** (55%) as 3′-deoxy-3′-fluoro ribouridine ($^{R}U^{F}$) monomer.

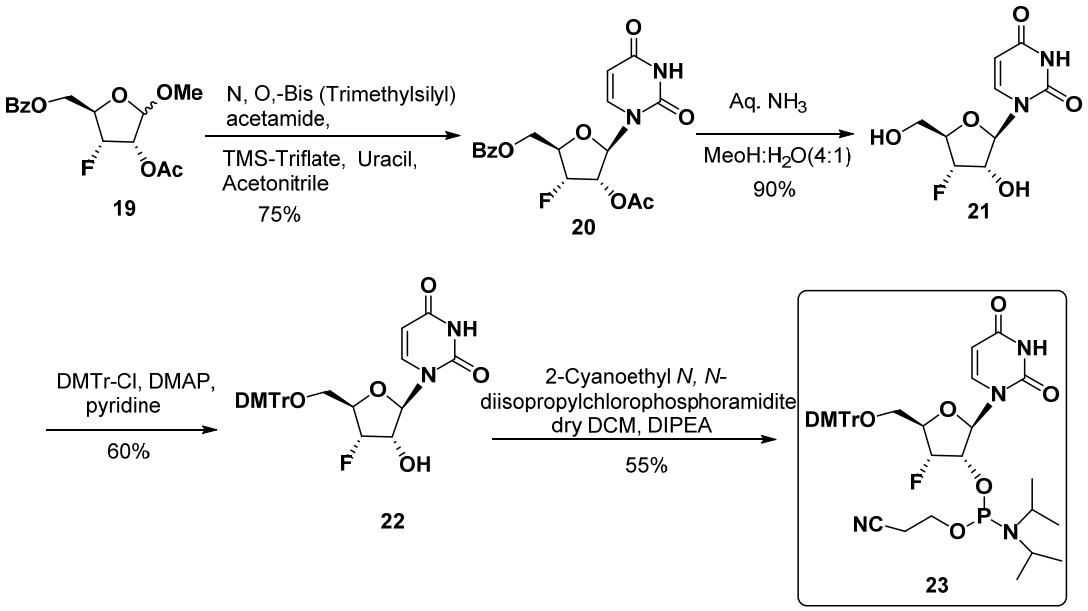

Scheme 4: Synthesis of $^{R}U^{F}$ monomer

2.3.2 Preliminary study of sugar puck using ^{1}H NMR $J_{1',2'}$ coupling constant

The homonuclear $^{3}J_{H1'-H2'}$ coupling constants are very sensitive to the dihedral angle and therefore directly reflect the sugar pucker in five-membered ribonucleosides. %S conformation for 3′-deoxy-3′-fluoro ribo/xylo nucleosides unit was calculated from the H1′–H2′ NMR coupling using formula **%S = 100 X ($J_{1',2'}$-1)/6.9** as earlier reported.[12a,27] A smaller *J* value of 0–3 Hz is typical of N-type sugar whereas the *J* value between 6–9 Hz is indicative of S-type sugar pucker. The %S for 3′-deoxy-3′-fluoro ribouridine **11** and 3′-deoxy-3′-fluoro xylouridine **21,** were found to be 97.23% and 0.29% respectively. This indicates that **11** and **21** are almost frozen in S-type and N-type conformations respectively. We have thoroughly analyzed the conformation of **11** and **21** using NMR, X-ray crystal structure and Matlab pseudorotation GUI program which we have discussed in chapter 4. We calculated all the four structural parameters i.e. glycosidic torsion angle χ,, torsion angle γ, phase angle of pseudorotation *P* and the puckering amplitude ν_{max}, which ultimately gives S-type and N-type population for each monomer in solid as well as in solution state. In Chapter 4 we also discuss the NOESY NMR study to analyze the *syn/anti* conformation of nucleobase.

2.3.3 Synthesis of oligonucleotides containing modified units their purification and characterization.

2.3.3a Solid phase synthesis of control and complementary 3′-5′-linked oligonucleotides

The two sequences chosen of the current study are of biological relevance: **DNA1** is used for miRNA down-regulation[28] and **DNA2** is used in the splice-correction assay developed by Kole *et al*.[29] The **DNA1** and **DNA2** are the control while **cDNA1** and **cDNA2** are the complementary oligonucleotides. All the four DNA ONs (Table 1) were synthesized on a Bioautomation MM4 DNA synthesizer using standard *β*-cyanoethyl phophoramidite chemistry.[30] General strategy for the solid phase synthesis is given in Figure 9. The natural DNA/RNA was synthesized in the 3′ to 5′ direction (reverse of the biological polymerization reaction), on a polystyrene solid support (CPG) with the required 3'-end nucleoside (A, T, C, G) attached to it via a linker. The oligonucleotides were cleaved from solid support by ammonia treatment, and desalted by gel filtration; their purity ascertained by RP-HPLC on a C18 column was found to be more than 95% and these were used without further purification in the biophysical studies of modified sequences. The RNA ONs **RNA1** and **RNA2** were obtained commercially.

Table 1: DNA/RNA oligonucleotide used in present work

Entry No	Sequence code	Sequence (5′ → 3′)
1	**DNA1**	CACCATTGTCACACTCCA
2	**DNA2**	CCTCTTACCTCAGTTACA
3	**cDNA1**	TGGAGTGTGACAATGGTG
4	**cDNA2**	TGTAACTGAGGTAAGAGG
5	**RNA1**	UGGAGUGUGACAAUGGUG
6	**RNA2**	UGUAACUGAGGUAAGAGG

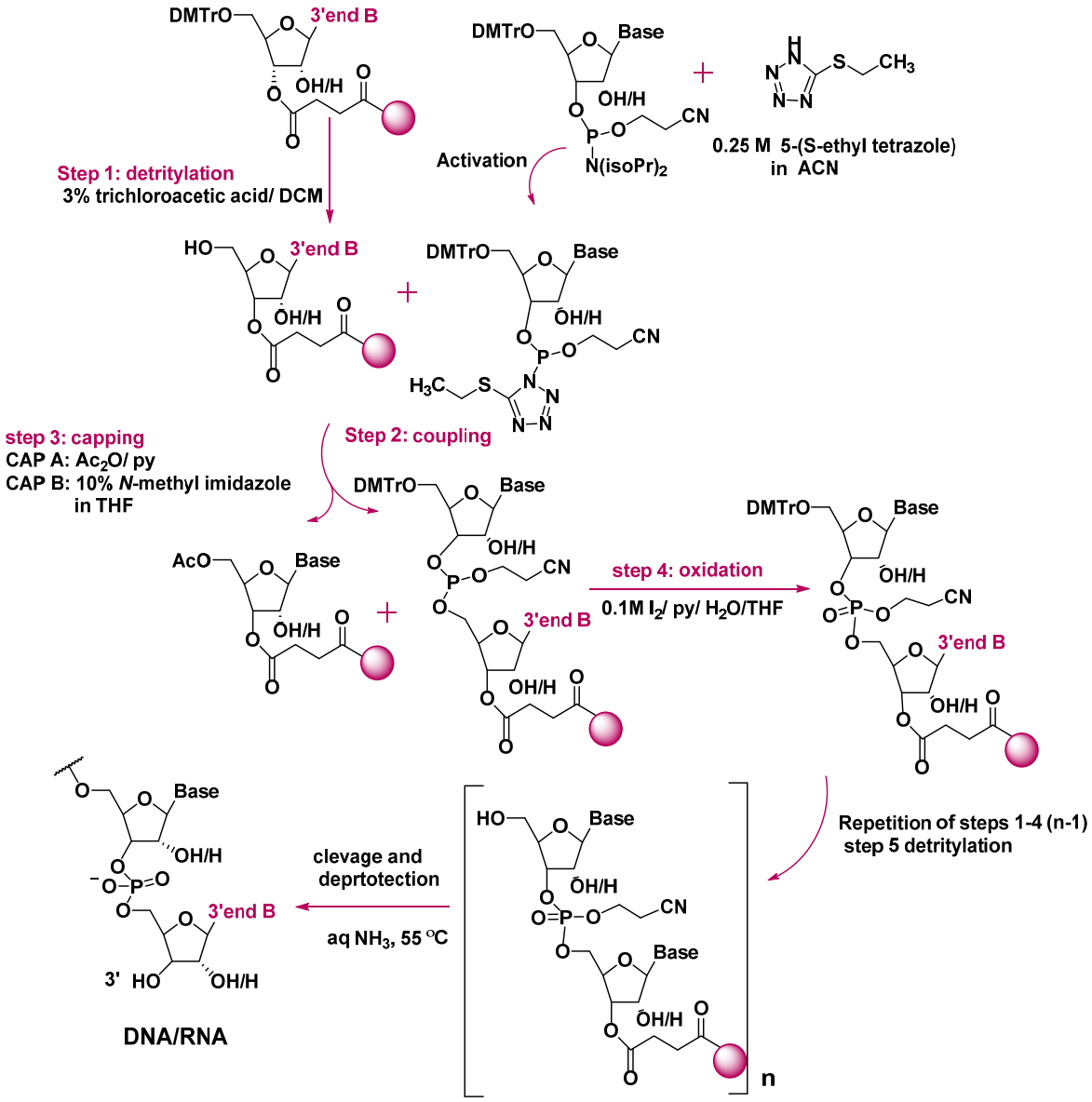

Figure 9. Solid phase synthesis of DNA

2.3.3b Solid phase synthesis of modified and control ngDNA oligomers

The modified and control ngDNA oligomers were also synthesized on an automated Bioautomation DNA synthesizer using commercially available 5′-*O*-DMT-3′-deoxy-2′-phosphoramidites. The ngDNA/ngRNA was synthesized in the 2′ to 5′ direction on a universal solid support. A universal support have the 3′-nucleoside without the nucleobase, which is added in the first cycle, giving an undesired phosphate linkage that gets removed during the cleavage/deprotection steps (Figure 10).

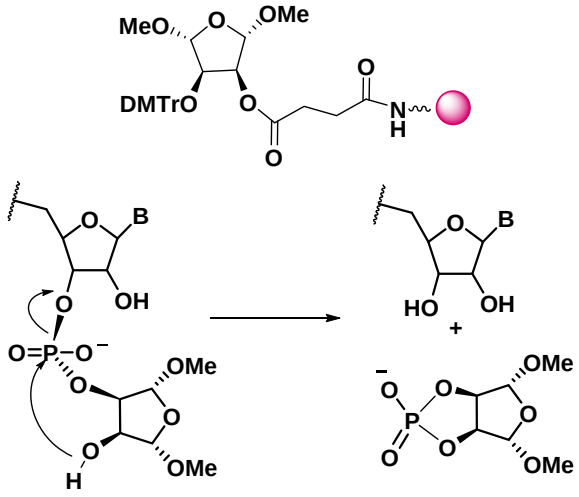

Figure 10. Universal solid support and cleavage mechanism

The ngDNA1 and ngDNA2 are the unmodified sequences. The two modified units **13** and **23** abbrivated as $^{X}\mathbf{U}^{F}$ and $^{R}\mathbf{U}^{F}$ (Figure 11) were incorporated at pre-determined positions using an extended coupling time to yield the modified oligomers efficiently (Table 2) using the same synthetic cycle shown in Figure 9, using 2'-amidites instead of 3'-amidites and using the universal solid support (Figure 10). The site of the modified units in the sequences was chosen so that these were either separated by 4-5 nucleosides or were consecutive. Also, the 3′-end neighbour could be a purine or pyrimidine. To obtain the desired oligonucleotide, the building blocks were sequentially coupled to the growing oligonucleotide chain in the order required by the sequence of the product. Upon completion of the chain assembly, the product was released from the solid phase to solution, deprotected, and collected.

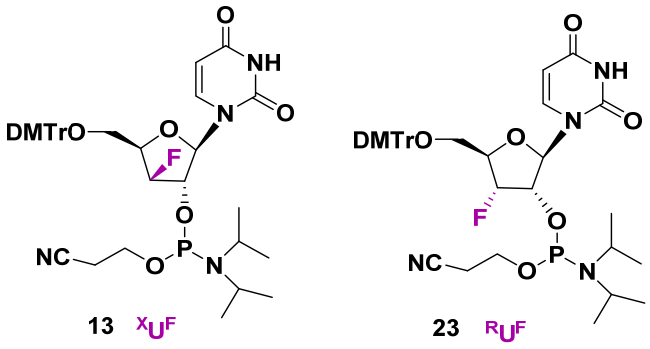

Figure 11. Modified phosphoramidite building blocks

2.3.3c Purification and MALDI-TOF characterization of ngDNA oligomers

The synthesized ONs were cleaved from the solid support with conc. NH_4OH at 55°C, lyophilized and desalted to get the crude oligonucleotides. The purity of the oligomers listed in Table 2 was checked by analytical RP-HPLC (C18 column, 0.1N TEAA buffer of pH 7.0- acetonitrile) which showed more than 75-80% purity. These oligomers were subsequently purified by RP-HPLC on a C18 column. The purity of the oligomers was again ascertained by analytical RP-HPLC and found to be > 95%. Their integrity was confirmed by MALDI-TOF (matrix assisted laser desorption ionization time-of-flight) mass spectrometric analysis. THAP (2,4,6-trihydroxy acetophenone) matrix with diammonium citrate as additive was used for MALDI-TOF mass analysis of oligomers. HPLC retention time and observed values of mass in MALDI-TOF spectrometry are listed in Table 2**.**

Table 2: ngDNA oligomers, their HPLC retention time and characterization using MALDI-TOF mass analysis

Entry No	Sequence code	Sequence (5′ → 2′)	HPLC t_R (min)	Mass	
				Expected	Observed
1	ngDNA1	CACCATTGTCACACTCCA	5.7	5364	5362
2	ngDNA1-1	CACCATTGTCACAC$^{X}U^{F}$CCA	6.6	5368	5365
3	ngDNA1-2	CACCATTG$^{X}U^{F}$CACAC$^{X}U^{F}$CCA	7.0	5372	5374
4	ngDNA1-3	CACCATTGTCACAC$^{R}U^{F}$CCA	7.0	5368	5366
5	ngDNA1-4	CACCATTG$^{R}U^{F}$CACAC$^{R}U^{F}$CCA	7.3	5372	5372
6	ngDNA1-5	CACCA$^{R}U^{FR}U^{F}$GTCACACTCCA	10.4	5372	5373
7	ngDNA2	CCTCTTACCTCAGTTACA	12.7	5369	5368
8	ngDNA2-1	CCTCTTACCTCAGT$^{R}U^{F}$ACA	10.6	5373	5376
9	ngDNA2-2	CCTCTTACC$^{R}U^{F}$CAGT$^{R}U^{F}$ACA	10.8	5377	5379

2.3.4 Duplex stability and CD studies of the derived oligomers

The presence of fluorine on the sugar moiety could have two possible effects; as mentioned previously, depending upon the stereochemistry at C3′-fluorine substitution, and

induced conformational bias due to fluorine on sugar ring. The desired conformation would lead to stabilization of the complex and vice versa. The thermal stability of the ngDNA duplex with complementary DNA/RNA was evaluated by UV-melting studies. The ngDNA oligonucleotides were individually hybridized with the complementary DNA and RNA using 1μM concentration of each of the two complementary strands to obtain duplexes. The T_m experiments of duplexes were carried out in 10mM sodium phosphate buffer (pH 7.4), containing 150mM sodium chloride. Melting temperatures (T_m) were obtained from the maxima of the first derivatives of the melting curves (A_{260nm} *versus* temperature) and each experiment was repeated at least thrice and the values are accurate to ± 0.5°C.

2.3.4a Thermal stabilities of duplex formed by $^{X}U^{F}$- and $^{R}U^{F}$- modified ngDNA

The melting temperature, T_ms, of the complexes containing the modified $^{R}U^{F}$ & $^{X}U^{F}$ units were determined and compared with the unmodified duplexes formed using ngDNA1. The results are summarized in Table 3 where $\Delta T_m = T_m - T_{m(control)}$.

Similar to the ngRNA sequences reported by Damha *et al.*[31] all the ngDNA sequences studied here (Table 3, entry 1-6) were also found to bind only to complementary RNA and not to complementary DNA. Sharp, well-defined sigmoid-shaped melting curves were observed for the complexes with complementary RNA with a 10-20% hyperchromicity at 260nm, while, for the complexes with complementary DNA, there was no sigmoid transition, indicating no complexation in the latter case (Figure 12).

The complexes formed by **ngDNA1-1** and **ngDNA1-2** containing increasing number of $^{X}\mathbf{U}^{F}$ N-type frozen monomer (Table 3, entry 2 & 3) with complementary RNA were considerably destabilized compared to the control 2′-5′-sequence **ngDNA1** (Figure 13, $\Delta T_m \approx$ -4.8 to -6.0°C). In contrast, the oligomers **ngDNA1-3** and **ngDNA1-4** containing one or two $^{R}\mathbf{U}^{F}$ S-type frozen monomers (Table 3 entry 4 & 5) showed similar or slightly more melting temperature compared to unmodified duplex (Figure 14, $\Delta T_m \approx$0.0 to + 1.0°C). Oligomers bearing $^{R}\mathbf{U}^{F}$ S-type frozen monomers units thus formed more stable complexes with RNA compared to the unmodified complex. Apparently, the S-type frozen conformation at the modified site would be in compliance with the predicted S-type conformations of the ngDNA strand in the ngDNA:RNA duplex and therefore could stabilize the duplex.

Table 3: UV-T_m (^oC) values of 18mer ngDNA1-1 to 5: DNA/RNA duplexes

Entry No	Sequence code	Sequence (5' → 2')	T_m°C cDNA1	T_m°C RNA1	ΔT_m (°C)
1	ngDNA1	CACCATTGTCACACTCCA	NB	50.5	0.0
2	ngDNA1-1	CACCATTGTCACAC$^{X}U^{F}$CCA	NB	45.7	-4.8
3	ngDNA1-2	CACCATTG$^{X}U^{F}$CACAC$^{X}U^{F}$CCA	NB	44.5	-6.0
4	ngDNA1-3	CACCATTGTCACAC$^{R}U^{F}$CCA	NB	50.5	0.0
5	ngDNA1-4	CACCATTG$^{R}U^{F}$CACAC$^{R}U^{F}$CCA	NB	51.7	+1.2
6	ngDNA1-5	CACCA$^{R}U^{FR}U^{F}$GTCACACTCCA	NB	49.2	-1.3

Melting temperatures (T_ms) were obtained from the maxima of the first derivatives of the melting curves (A260 nm versus temperature), measured in buffer containing 10mM sodium phosphate, 150mM sodium chloride, pH 7.4, using 1μM concentration of each of the two complementary strands. Each experiment was repeated at least thrice and the values are accurate to ±0.5°C. RNA1 = 5′-UGGAGUGUGACAAUGGUG-3′. cDNA1=5′-TGGAGTGTGACAATGGTG-3′. *T*m of DNA1:cDNA1 = 59.0°C. $\Delta T_m = T_m - T_m$(control).

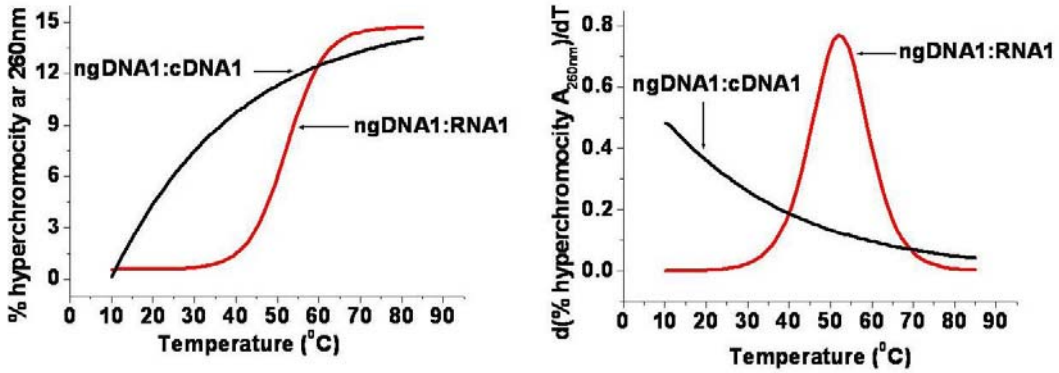

Figure 12. UV-melting plots of complexes of ngDNA1 with complementary RNA1 and complementary cDNA1 and corresponding first derivative curve

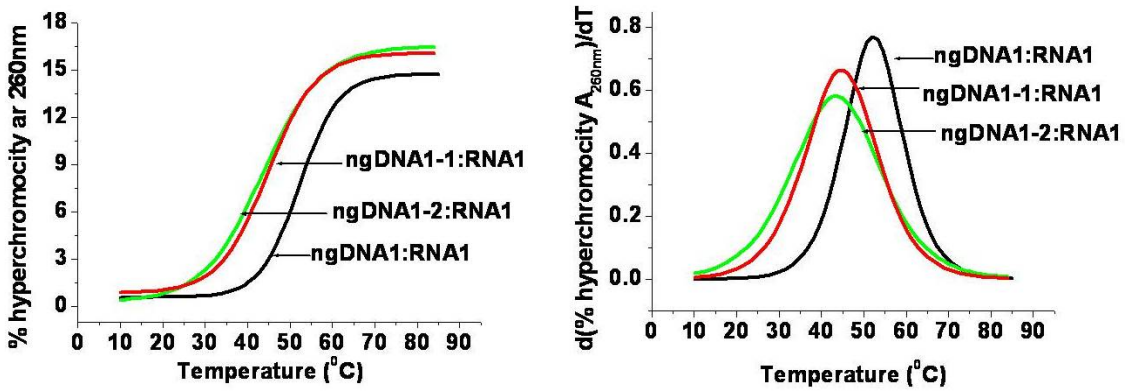

Figure 13. UV-melting plots of complexes of ngDNA1, ngDNA1-1, ngDNA1-2, with complementary RNA1 and corresponding first derivative curve

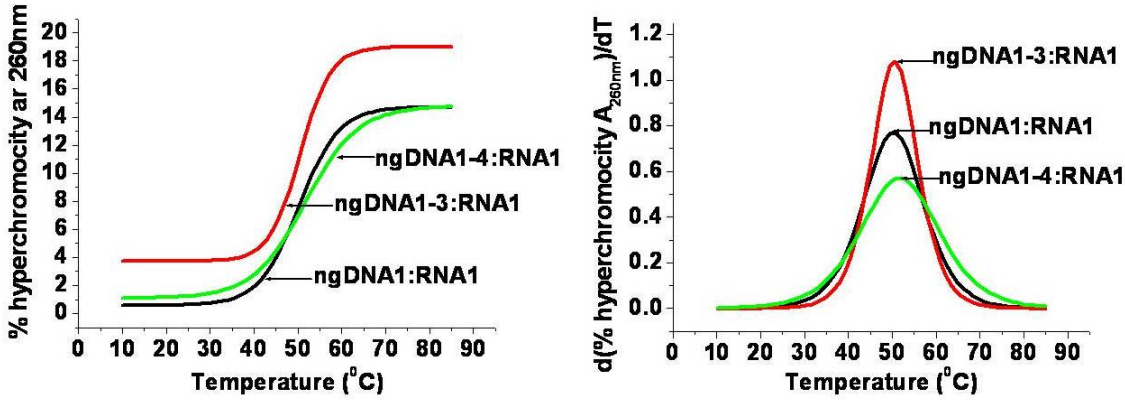

Figure 14. UV-melting plots of complexes of ngDNA1, ngDNA1-3 and ngDNA1-4 with complementary RNA1 and corresponding first derivative curve

The imparted stability due to pre-organization in this geometry was not found to be as large as in the case of 2′F-RNA:RNA duplexes ($\Delta T_m \approx +2$°C/mod).[3,4] This could be because the S-type conformations would bring the nucleobases in pseudoequatorial position in which, the stacking and hydrogen bonding interactions are not as strong as in the N-type sugar geometry, where the nucleobase assumes pseudoaxial orientation, as in 2′F-RNA:RNA duplexes. The significant destabilization of the ngDNA:RNA complex by freezing the sugar conformation in N-type geometry was also in compliance with the predicted geometry of the ngDNA:RNA duplex. These results indicate that N-type to S-type conformational change that the 3′-deoxyuridine presumably undergoes while in duplex state is to some extent resisted by 3′-deoxy-3′-fluoro xyloside ($^{X}U^{F}$ N-type frozen monomer) due to the favourable *O*4'-C4′-C3′-F3′ *gauche* effect in N-type sugar geometry,

considering comparable steric interactions between fluorine and hydrogen atoms. For the 3′-deoxy-3′-fluoro riboside ($^{R}U^{F}$ S-type frozen monomers) the preferred sugar pucker would be S-type again due to dominating *O*4′-C4′-C3′-F3′ *gauche* effect.

To study the additive stabilization effect of the conformational constraint $^{R}\mathbf{U}^{F}$, we modified consecutive sites in ngDNA1 as in **ngDNA1-5** (Table 3, entry 6,). In this case, the consecutive modified sites were not able to cause additive stabilization. In fact, the duplexes formed were marginally destabilized (Figure 15, $\Delta T_m \approx$ -1.5°C). This result is also in contrast to the 2′F-RNA:RNA duplexes where consecutive modified units show much better stabilization due to increased base-stacking interactions when the nucleobases are axially oriented.[3, 4]

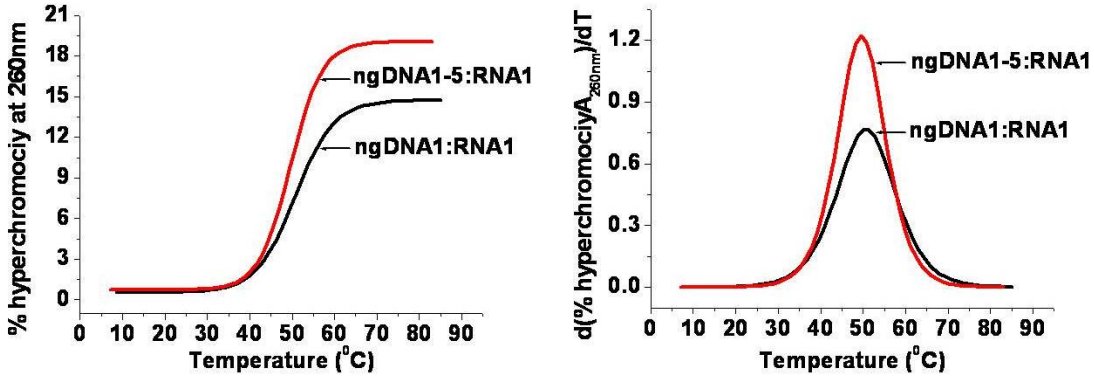

Figure 15. UV-melting plots of complexes of ngDNA1 and ngDNA1-5 with complementary RNA1 and corresponding first derivative curve

To further study the effect of modifications in the sequence context and the site of modifications, we synthesized another sequence **ngDNA2** (Table 4). The oligomers **ngDNA2-1** and **ngDNA2-2** having one and two S-type frozen $^{R}\mathbf{U}^{F}$ monomeric units (Table 4, entry 2 & 3) were synthesized and their stability of the duplexes with **RNA2** were compared in terms of T_m studies with the unmodified control duplex (ngDNA2:RNA2). The two modified units were spaced by four unmodified units. The results were qualitatively similar to those observed for **ngDNA1**. In fact, the 3′-deoxy-3′-ribofluorouridine $^{R}\mathbf{U}^{F}$ derived sequences stabilized the duplex much better (Figure 16, $\Delta T_m \sim$ +2°C/modification). In the sequence context, the difference is that one of the modified units is flanked by a purine instead of pyrimidine at the 2′-end.

Table 4: UV-T_m (°C) values of 18mer ngDNA2-1 & 2:DNA/RNA duplexes

Entry No	Sequence code	Sequence (5' → 2')	T_m°C cDNA2	T_m°C RNA2	ΔT_m (°C)
1	ngDNA2	CCTCTTACCTCAGTTACA	NB	46.0	0.0
2	ngDNA2-1	CCTCTTACCTCAGT$^{R}U^{F}$ACA	NB	48.3	+2.3
3	ngDNA2-2	CCTCTTACC$^{R}U^{F}$CAGT$^{R}U^{F}$ACA	NB	49.4	+3.4

Melting temperatures (T_ms) were obtained from the maxima of the first derivatives of the melting curves (A260 nm versus temperature), measured in buffer containing 10mM sodium phosphate, 150 mM sodium chloride, pH 7.4, using 1μM concentration of each of the two complementary strands. Each experiment was repeated at least thrice and the values are accurate to ±0.5°C. RNA2 = 5′-UGUAACUGAGGUAAGAGG-3′ cDNA2 = 5′-TGTAACTGAGGTAAGAGG-3′ *T*m of DNA2:cDNA2 = 54.0°C. $\Delta T_m = T_m - T_m$(control).

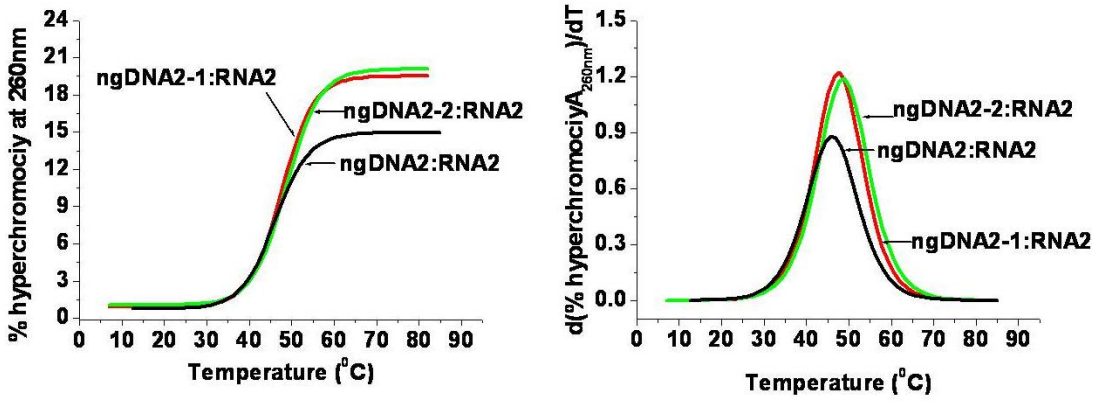

Figure 16. UV-melting plots of complexes of ngDNA2, ngDNA2-1and ngDNA2-2 with complementary RNA2 and corresponding firstderivative curve

The result presented here thus confirms that in ngDNA:RNA duplexes, the DNA strand would prefer to assume S-type geometry that is complemented by S-type frozen nucleoside units and the stability would be improved further depending on the flanking base sequence.

2.3.4b Synthesis and thermal stability study of $^{X}U^{F}$ modified 3′-5′-linked oligonucleotides

We have discussed in Chapter 1 that the N-type locked or frozen modified nucleoside like LNA/BNA and 2′F-RNA increases the thermal stability of 3′-5′-linked DNA:RNA duplexes. Among our two modified monomer unit $^{X}\mathbf{U}^{F}$ and $^{R}\mathbf{U}^{F}$ the 3′-deoxy-3′-fluoro xylouridine ($^{X}\mathbf{U}^{F}$) showed N-type sugar geometry due to the favorable O_4'-C4′-C3′-F_3′ *gauche* effect. Hence it became very interesting to study the effect of N-type sugar geometry of this 2′-5′ monomer unit on the stability of native 3′-5′-linked DNA:DNA or DNA:RNA duplexes. The control ON **DNA1** and two modified ONs **DNA1-1** and **DNA1-2** containing single and double $^{X}\mathbf{U}^{F}$ monomer units were synthesized. All three sequences were purified with HPLC and characterized by MALDI-TOF mass analysis. Their HPLC retention time and expected and observed mass are shown in table 5.

Table 5: Modified ONs with 3′-5′-linkages, their HPLC retention time and characterization using MALDI-TOF mass analysis

Entry No	Sequence code	Sequence (5′ → 3′)	HPLC t_R (min)	Mass	
				Expected	Observed
1	DNA1	CACCATTGTCACACTCCA	5.7	5364	5364
2	DNA1-1	CACCATTGTCACAC^{X}U^{F}CCA	6.6	5368	5368
3	DNA1-2	CACCATTG^{X}U^{F}CACAC^{X}U^{F}CCA	7.0	5372	5372

The thermal stability of modified **DNA1-1** and **DNA1-2** was compared with unmodified **DNA1:cDNA1** and **DNA1:RNA1** duplexes (Table 6, entries 2, 3). In this case these modification lead to large destabilization of duplexes with complementary DNA as well as RNA and ΔT_m is comparatively same with both DNA and RNA (Figure 17, 18 ΔT_m ~ -13°C for single and -10°C for double modification)**.** This is again in contrast to the stabilization of 2′F-RNA: RNA duplexes. Here the 2′-5′-linkage of the modified monomer unit may be the main cause of destabilization. The intermittent change to 2′-5′ linkage in continuous 3′-5′ backbone at one or two positions destabilized the duplexes.

Table 6: UV-T_m (^oC) values of 18mer DNA1-1 & 2 :DNA/RNA duplexes

Entry No	Sequence code	Sequence (5' → 3')	T_m°C cDNA1	ΔT_m (°C)	T_m°C RNA1	ΔT_m (°C)
1	DNA1	CACCATTGTCACACTCCA	59.7	0.0	60.0	0.0
2	DNA1-1	CACCATTGTCACAC$^{X}U^{F}$CCA	46.0	-13.7	46.0	-14.0
3	DNA1-2	CACCATTG$^{X}U^{F}$CACAC$^{X}U^{F}$CCA	49.5	-10.2	49.4	-10.6

Melting temperatures (T_ms) were obtained from the maxima of the first derivatives of the melting curves (A260nm versus temperature), measured in buffer containing 10mM sodium phosphate, 150mM sodium chloride, pH 7.4, using 1μM concentration of each of the two complementary strands. Each experiment was repeated at least thrice and the values are accurate to ±0.5°C. RNA1 = 5′-UGGAGUGUGACAAUGGUG-3′. cDNA1 = 5′-TGGAGTGTGACAATGGTG-3′. $\Delta T_m = T_m - T_m$(control).

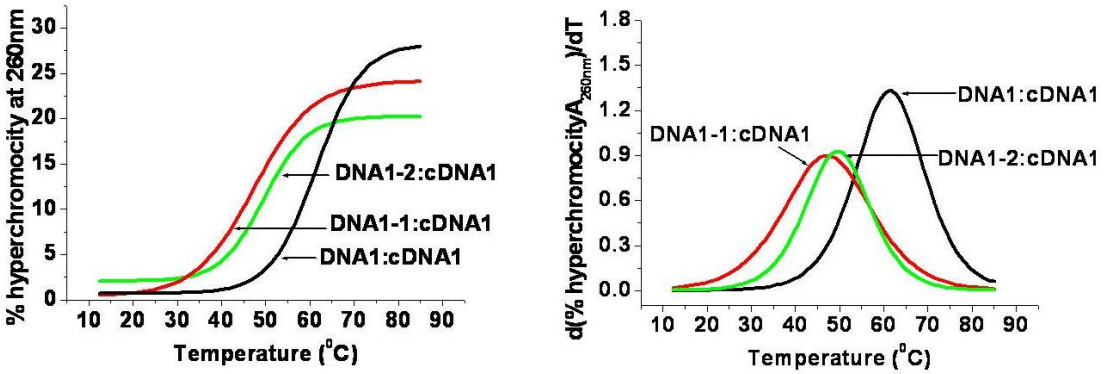

Figure 17. UV-melting plots of complexes of DNA1, DNA1-1and DNA1-2 with complementary DNA1 and corresponding first derivative curve

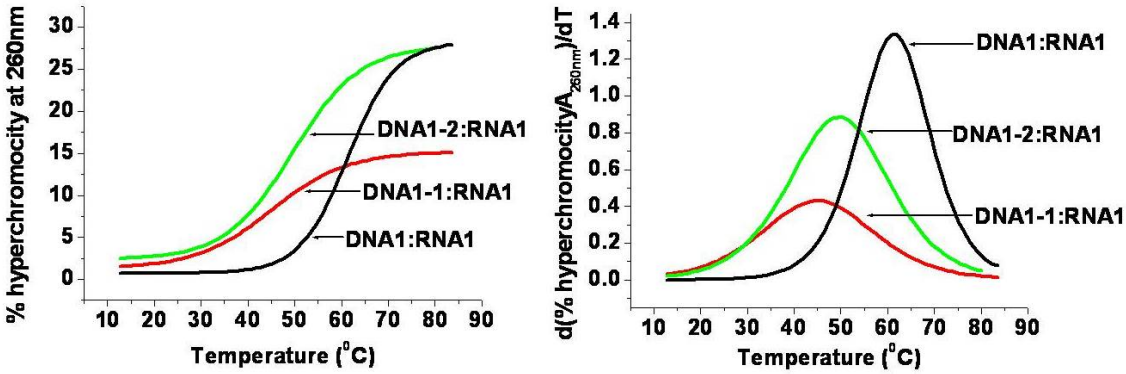

Figure 18. UV-melting plots of complexes of DNA1, DNA1-1and DNA1-2 with complementary RNA1 and corresponding first derivative curve

2.3.4c CD study of $^{X}U^{F}$- and $^{R}U^{F}$- modified ngDNA

The CD spectra of various single stranded 18mer ONs are shown in Figure 19. The CD spectra of the single stranded genetic DNA1 show a positive λ_{max} around 262nm, a cross over at 241nm, and a negative λ_{max} at 238nm. The corresponding band for RNA1 is slightly red shifted. The same single stranded DNA1 sequence with 2′-5′-linkages (ngDNA1) show similar CD pattern with slightly red shift with respect to both genetic DNA1 and RNA1. This ngDNA1 show positive λ_{max} around 278nm, a cross over at 250nm and a negative λ_{max} at 240nm. ngDNA1-1 and ngDNA1-2 sequences having single $^{X}U^{F}$ and $^{R}U^{F}$ modification show the very similar CD spectra with unmodified ngDNA1 indicating modification does not alter CD pattern.

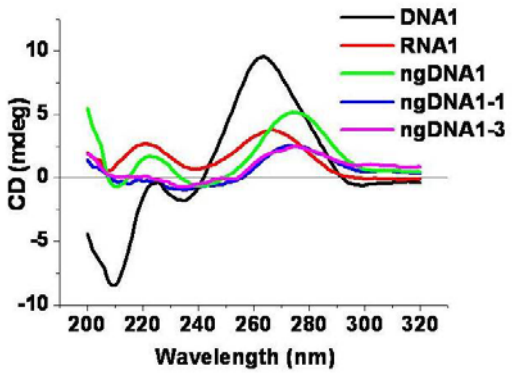

Figure 19. CD spectra of various single stranded 18mer oligonucleotides

The CD spectra of various duplexes in which the complementary strand is cDNA1 and RNA1 are shown in Figure 20. The unmodified ngDNA1:RNA1 and modified ngDNA1-4:RNA1 duplexes are similar and resemble with the DNA1:RNA1 duplex than to the DNA1:cDNA1 duplex giving a proof for the formation of A-type duplex.

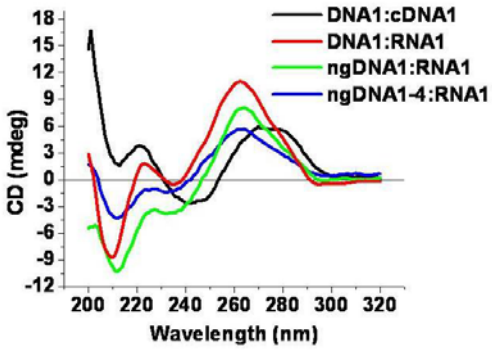

Figure 20. CD spectra for various duplexes

As an additional support for duplex formation in all the modifications used in the present studies, CD spectroscopic studies of complexes of all the modified oligomers with RNA1 (Table 3, entries 1, 2, 3, 4 and 5,) were also carried out. In all these cases, it was observed that the duplex CD spectra were similar for all the complexes studied (Figure 21) and resemble A-type DNA1:RNA1 duplex CD spectra.

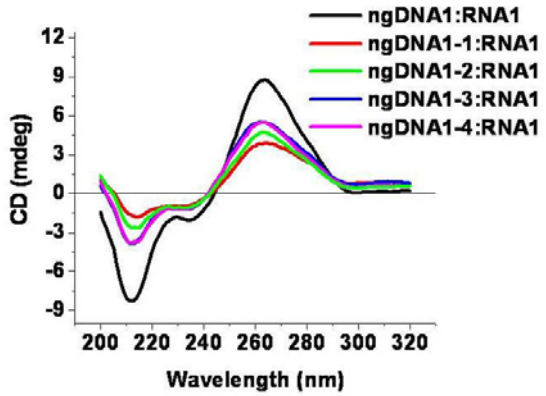

Figure 21. Duplex CD spectra of modified ngDNA1 complexes

CD spectra for duplex of ngDNA1:RNA1 and the summation of separate strand ngDNA1+RNA1 are shown in Figure 22. The additive CD spectrum of two strands is different than that for the duplex. This is another proof for complex formation by ngDNA: RNA strand.

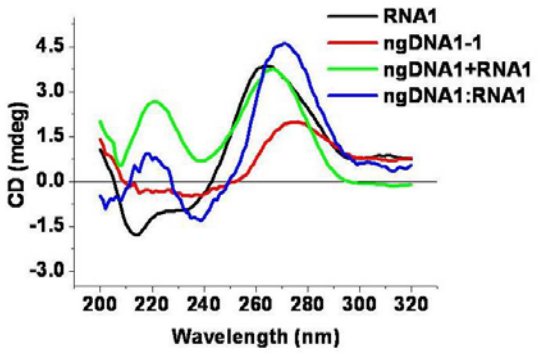

Figure 22. CD spectra for duplex of complementary strands and the summation of separate spectra for single-strands.

Duplex CD spectra of modified and unmodified ngDNA2 complexes are shown in figure 23. DNA2 is another sequence which we choose to study the effect of modifications in the sequence context and the site of modifications. The CD spectra for all modified

(ngDNA2-1:RNA, and ngDNA2-2:RNA) and unmodified (ngDNA2:RNA2) complexes for this sequence are similar and showing A-type duplex. The difference in the duplex CD spectrum of both the sequences is that the positive band for all the ngDNA1:RNA1 complexes are sharp and show λ_{max} around 265nm while it is broad in all the ngDNA2:RNA2 duplexes showing λ_{max} around 265-280nm.

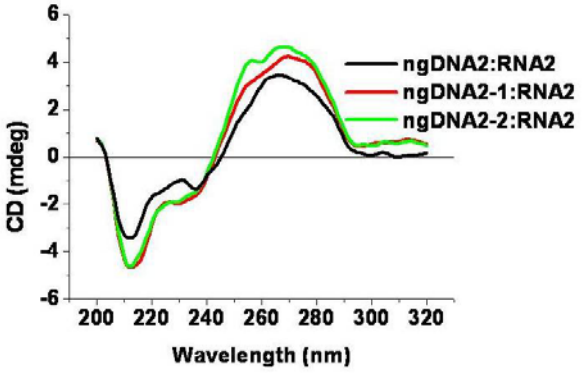

Figure 23. Duplex CD spectra of modified ngDNA2 complexes

2.4 Summary and conclusion

1. Synthesis of the 3′-deoxy-3′-fluoro xylo/ribo uridine monomers ($^{R}U^{F}$ and $^{X}U^{F}$) were done and these monomers were successfully incorporated into ngDNA oligomers.
2. Preliminary NMR study showed that $^{R}U^{F}$ and $^{X}U^{F}$ were frozen in to S and N-type sugar respectively.
3. The UV-T_m data shows that $^{R}U^{F}$ S-type frozen monomer modified ngDNA stabilizes the *ng*DNA:RNA duplexes, while the $^{X}U^{F}$ N-type frozen monomer destabilized the corresponding duplexes.
4. CD studies showed that all the modified and unmodified ngDNA:RNA duplexes show the similar CD signal and is matches the A-type DNA.

Conclusion

Stabilization of ngDNA:RNA by S-frozen monomer and destabilization of the same by N-frozen monomers provides a proof, for the first time, for the prediction that in ngDNA:RNA duplexes, the ngDNA strand would necessarily assume S-type geometry.

2.5 Experimental

2.5.1 Synthesis of compounds/monomers

General remarks: All the reagents were purchased from Sigma-Aldrich and used without purification. DMF, ACN, were dried over P_2O_5 and CaH_2 respectively and stored by adding 4 Å molecular sieves. Pyridine, TEA were dried over KOH and stored on KOH. THF was passed over basic alumina and dried by distillation over sodium. Reactions were monitored by TLC. TLCs were carried out on pre-coated silica gel GF254 sheets (Merck 5554). TLCs were run in either Pet-ether with appropriate quantity of EtOAc or DCM with an appropriate quantity of MeOH for most of the compounds. TLCs were visualized with UV light and iodine spray and/or by spraying perchloric acid solution and heating. Usual reaction work up involved sequential washing of the organic extract with water and brine followed by drying over anhydrous sodium sulfate (Na_2SO_4) and evaporation of the solvent under vacuum. Column chromatographic separations were performed using silica gel 60-120 mesh (Merck) and 200-400 mesh (Merck) and using the solvent systems EtOAc/Pet ether and MeOH/DCM.

^{1}H and ^{13}C NMR spectra were obtained using Bruker AC-200, AC-400 and AC-500 NMR spectrometers. The chemical shifts (δ/ppm) are referred to internal TMS/DMSO-d_6 for ^{1}H and chloroform-*d*/DMSO-d_6 for ^{13}C NMR. ^{1}H NMR data are reported in the order of chemical shift, multiplicity (s, singlet;d, doublet;t, triplet;br, broad;br s, broad singlet;m, multiplet and/ or multiple resonance), number of protons. Mass spectra were recorded on APQSTAR spectrometer, LC-MS on a Finnigan-Matt instrument. DNA oligomers were synthesized on CPG solid support using Bioautomation Mer-Made 4 synthesizer. The RNA oligonucleotides were obtained commercially (Sigma-Aldrich). RP-HPLC was carried out on a C18 column using either a Varian system (Analytical semi-preparative system consisting of Varian Prostar 210 binary solvent delivery system and Dynamax UV-D2 variable wavelength detector and Star chromatography software) or a Waters system (Waters Delta 600e quaternary solvent delivery system and 2998 photodiode array detector and Empower2 chromatography software). MALDI-TOF spectra were recorded on a Voyager-De-STR (Applied Biosystems) MALDI-TOF instrument or AB Sciex TOF/TOF^{TM} Series Explorer^{TM} 72085 instrument and the matrix used for analysis was

THAP (2', 4', 6'-trihydroxyacetophenone). UV experiments were performed on a Varian Cary 300 UV-VIS spectrophotometer fitted with a Peltier-controlled temperature programmer. CD spectra were recorded on a Jasco J-715 Spectropolarimeter, with a ThermoHaake K20 programmable water circulator for temperature control of the sample.

Experimental procedures and spectral data

1,2:5,6-Di-*O*-isopropylidene-*α*-D-glucofuranose (2)

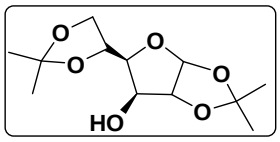

Under N_2 atmosphere mixture of D-glucose (5g, 27.75mmol) and absolutely anhydrous $CuSO_4$ (9g, 56.64mmol) was added to dry acetone (65mL) and cooled it to 0°C in ice bath. After stirring for few minute at ice cold temperature, catalytic amount of conc. H_2SO_4 (0.3mL) was added slowly with glass pipette. Then reaction mixture was brought to rt and stirred for 48h. After which the reaction mixture was neutralized with saturated aqueous solution of K_2CO_3 and filtered using whatman filter paper. The filtrate was Concentrated under reduced pressure and obtained solid compound was recrstalized using pet-ether which gave the compound **2** as white crystal. Yield 5g, 70%.

Mol. Formula	**:**	$C_{12}H_{20}O_6$
Mol. Weight	**:**	260.29
ESI-Ms m/z	**:**	283.2916 ($M+Na^+$)
^{1}H NMR (200MHz, $CDCl_3$)	**:**	δ_H (ppm) 1.32, 1.37, 1.45 & 1.50 (4s, 12H, $4CH_3$), 3.96-4.21 (m, 3H), 4.30-4.39 (m, 2H), 4.53-4.55 (d, *J*=3.66 Hz, 1H, H-2), 4.7 (bs, 1H), 5.94-5.96 (d, $J_{1,2}$ =3.66 Hz, 1H, H-1)
^{13}C NMR (50MHz, $CDCl_3$)	**:**	δ_C (ppm) 25.2, 26.2, 26.8, 26.9, 67.7, 73.5, 75.2, 81.1, 85.1, 105.3, 109.7, 111.9
^{13}C-DEPT (50MHz, $CDCl_3$)	**:**	δ_C (ppm) Positive peaks: 25.2, 26.2, 26.8, 26.9, 73.5, 75.2, 81.1, 85.1, 105.3 Negative peaks: 67.7

1,2:5,6-Di-*O*-isopropylidene-*α*-D-ribohexofuranose-3-ulose (3)

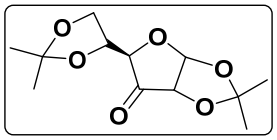

Pyridinium chlorochromate (15g, 69.78mmol) and powdered molecular sieves (30g) were added to compound **2** (5g, 19.35mmol) in dry DCM (50mL) and the mixture was stirred at rt for 12h. The

resulting suspension was diluted with diethylether (50mL), triturated and filtered through a silica gel bed (eluted with diethylether). The solvent was removed from filtrate to give the crude compound **3** as white solid which was unstable and used as such for next reaction. Yield 4.5g, 90 %.

1,2:5,6-Di-*O*-isopropylidene-*α*-D-allofuranose (4)

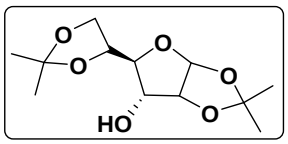

The compound **3** (5g, 19.35mmol) dissolved in mixture of MeOH (160mL) and H_2O (40mL) and cooled to 0°C. $NaBH_4$ (2g, 52.59mmol) was added and solution stirred for 2h. The resulting solution was concentrated, and the crude material was dissolved in EtOAc (200mL), and washed with H_2O (2 X 100mL), dried over anhydrous Na_2SO_4 and concentrated to give crude compound **4** as white solid, which was used for the next reaction without any further purification. Yield 4g, 80%.

Mol. Formula	**:**	$C_{12}H_{20}O_6$
Mol. Weight	**:**	260.29
ESI-Ms m/z	**:**	283.2916 ($M+Na^+$)
^{1}H NMR (200MHz, $CDCl_3$)	**:**	**δ_H** (ppm) 1.38, 1.47, 1.59, 1.65 (4s, 12H, $4CH_3$), 2.55-2.59 (m, 1H), 3.79-3.85 (m, 1H), 4.02-4.13 (m, 3H), 4.30-4.33 (m, 1H), 4.60-4.65 (m, 1H), 5.81-5.83 (d, $J_{1,2}$=3.6 Hz, 1H, H-1)
^{13}C NMR (50MHz, $CDCl_3$)	**:**	**δ_C** (ppm) 25.2, 26.2, 26.4, 26.5, 65.8, 72.3, 75.4, 78.9, 79.5, 103.8, 109.7, 112.7
^{13}C-DEPT (50MHz, $CDCl_3$)	**:**	**δ_C** (ppm) Positive peaks: 25.2, 26.2, 26.4, 26.5, 72.3, 75.4, 78.9, 79.5, 103.8 Negative peaks: 65.7

1, 2:5,6-di-*O*-isopropylidene-3-*O*-*p*-toluenesulphonyl-*α*-D-allofuranose (5)

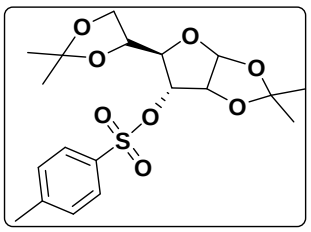

The crude compound **4** (3.5g, 13.44mmol) dissolved in dry pyridine (15mL) and cooled to 0^{o}C. *P*-toluene sulphonyl chloride (5.3g, 27.89mmol) was added in portion and the reaction mixture was stirred for 4h. The mixture was concentrated under reduced pressure and redissolved in EtOAc (200mL), washed with saturated Na_2HCO_3 (2 X 100mL), H_2O (2 X 100mL), and finally

with saturated aqueous NaCl (1 X 20mL). Then EtOAc layer dried over Na_2SO_4, filtered, and evaporated to dryness. The crude was purified by silica gel (60-120mesh) column chromatography using EtOAc / Pet ether (2:8) to offer the title compound **5** as white solid. Yield 3.6g, 65%.

Mol. Formula : $C_{19}H_{26}O_8S$

Mol. Weight : 414.47

ESI-Ms m/z : 437.3269 ($M+Na^+$)

^{1}H NMR (200MHz, $CDCl_3$) : **δ_H** (ppm) 1.29, 1.30, 1.53, 1.60, (4s, 12H, $4CH_3$), 2.46 (s, 3H), 3.74-3.94 (m, 2H), 4.14-4.22 (m, 2H), 4.54-4.79 (m, 2H), 5.76-5.78 (d, $J_{1,2}$ =3.15 Hz, 1H, H-1), 7.33-7.37 (d, 2H, J = 8Hz), 7.86-7.90 (d, 2H, J = 8 Hz)

^{13}C NMR (50MHz, $CDCl_3$) : **δ_C** (ppm) 21.6, 25.0, 26.0, 26.5, 26.6, 65.1, 74.6, 76.5, 79.9, 77.9, 103.8, 109.9, 113.6, 128.3, 129.6, 133.0, 145.2

^{13}C-DEPT (50MHz, $CDCl_3$) : **δ_C** (ppm) Positive peaks: 21.6, 25.0, 26.0, 26.5, 26.6, 74.5, 76.4, 76.8, 77.9, 103.7, 128.3, 129.6 Negative peaks: 65.1

3-deoxy-3-fluoro-1,2:5,6-di-*O*-isopropylidene-*α*-D-glucofuranose (6)

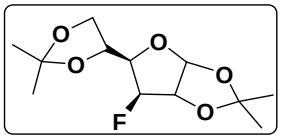

A mixture of compound **5** (2g, 48.25mmol), KF (3.5g, 60.24 mmol), and acetamide (17.5g, 29.62mmoL) was heated to 210^{o}C (internal), the reaction was monitored by TLC until all the starting material disappeared (~15min). After 45min, the dark reaction mixture was cooled to 90^{o}C and poured into a saturated solution of $NaHCO_3$ (50mL). The mixture was filtered from insoluble tar. Both the tar and filterate were extracted with diethyl ether (2 X 50mL and 4 X 40mL, respectively). The combined ether extract were washed with water (2 X 30mL) dried with Na_2SO_4 and evaporated to a yellow syrup which was purified by column chromatography using EtOAC/Pet ether (2:8). Pure compound **6** was obtained as pale-yellow syrup. Yield 0.76g, 60%.

Mol. Formula : $C_{12}H_{19}FO_5$

Mol. Weight : 262.28

ESI-Ms m/z : 285.2435 ($M+Na^+$)

^{1}H NMR : **δ_H** (ppm) 1.33, 1.37, 1.45, 1.51 (4s, 12H, $4CH_3$), 4.0-4.32 (m,

(200MHz, $CDCl_3$) 4H), 4.67-4.74 (m, 1H), 4.89-5.14 (m, 1H), 5.95-5.97 (d, $J_{1,2}$ = 4Hz, 1H, H-1)

^{13}C NMR (50MHz, $CDCl_3$) : δ_C (ppm) 25.1, 26.1, 26.6, 26.8, 67.1, 71.8-71.9 (d), 80.4-80.8 (d), 82.1-82.8 (d), 91.9-95.6 (d), 105.1, 109.4, 112.3

^{13}C-DEPT (50MHz, $CDCl_3$) : δ_C (ppm) Positive peaks: 25.1, 26.1, 26.7, 26.8, 71.8-71.9 (d), 80.4-80.8 (d), 82.2-82.8 (d), 91.9-95.6 (d), 105.1 Negative peaks: 67.1

3-deoxy-3-fluoro-1,2-*O*-isopropylidene-*α*-D-glucofuranose (7)

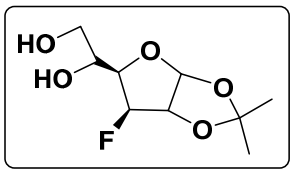

A solution of compound **6** (2g, 76.25mmol) in 6:4 AcOH:H_2O mixture (20mL) was heated at 50°C for 1h. After the starting material disappeared the mixture was concentrated under reduced pressure and co-evaporated with toluene to remove traces of AcOH. The yellow syrup was obtained which is further purified by column chromatography using EtOAc /Pet ether (7:4) solvent system. Yield 1.6g, 95%.

Mol. Formula : $C_9H_{15}FO_5$

Mol. Weight : 222.21

ESI-Ms m/z : 245.2291 ($M+Na^+$)

^{1}H NMR (200MHz, $CDCl_3$) : δ_C (ppm) 1.33, 1.50 (2s, 6H, $2CH_3$), 3.73-3.99 (m, 3H), 4.07-4.26 (m, 1H), 4.67-4.75 (m,1H), 4.97-5.23 (m, 1H), 5.96-5.98 (d, $J_{1,2}$ =3.77 Hz,1H, H-1)

^{13}C NMR (50MHz, $CDCl_3$) : δ_C (ppm) 26.1, 26.5, 64.0, 68.1-68.3 (d), 79.3-79.7 (d), 81.9-82.6 (d), 92.1-95.8 (d), 105.0, 112.3

^{13}C-DEPT (50MHz, $CDCl_3$) : δ_C (ppm) positive peaks: 26.1, 26.5, 68.2-68.3(d), 79.3-79.7 (d), 82.0-82.6 (d), 92.1-95.8 (d), 105.07 Negative peaks: 64.07

3-deoxy-3-fluoro-1,2-*O*-isopropylidene-*α*-D-xylofuranose (8)

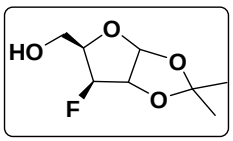

The diol **7** (2.5g, 88.88mmol) was added to a stirred solution of $NaIO_4$ (2.5g, 85.55mmol) in H_2O (37mL) and MeOH (37mL) leading to immediate precipitation of $NaIO_3$. After 1h at room temperature, any residual periodate was destroyed with a drop of ethylene glycol. The reaction mixture was

stirred for 1 h at room temperature with $NaBH_4$ (1g, 26.43mmol), concentrated, and then extracted with EtOAc (2 X 200mL). The organic layer was washed with brine solution, dried over Na_2SO_4, evaporated to dryness, and purified by column chromatography with EtOAc / Pet-ether (4:6) to give compound **8** as yellow syrup. Yield 1.8g, 85%.

Mol. Formula : $C_8H_{13}FO_4$

Mol. Weight : 192.08

ESI-Ms m/z : 225.1245 ($M+Na^+$)

^{1}H NMR (200MHz, $CDCl_3$) : **δ_H** (ppm) 1.34 & 1.50 (2s, 6H, $2CH_3$). 3.83-3.99 (m, 2H, H-5a and H-5b), 4.24-4.46 (m, 1H, H-4), 4.68-4.75 (dd, $J_{2,F}$ = 11.1 Hz, $J_{2,1}$ = 3.8 Hz, 1H, H-2), 4.86-5.12 (dd, $J_{3,F}$ = 50.4 Hz, $J_{3,4}$ = 2.3 Hz, 1H, H-3), 6-6.01 (d, $J_{1,2}$ = 3.8 Hz, 1H, H-1)

^{13}C NMR (50MHz, $CDCl_3$) : **δ_C** (ppm) 26.2, 26.6, 59.5-59.7 (d), 80.1-80.5 (d), 82.4-83.1 (d), 92.2-95.8 (d), 104.8, 112.3

^{13}C-DEPT (50MHz, $CDCl_3$) : **δ_C** (ppm) Positive peaks: 26.2, 26.6, 80.1-80.5 (d), 82.4-83.1 (d), 92.2-95.9 (d), 104.8 Negative peaks: 59.5-59.7 (d)

3-deoxy-3-fluoro-1,2,5-tri-*O*-acetyl-D-xylofuranose (9)

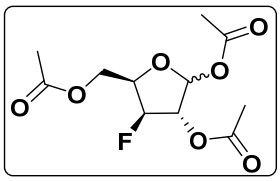

The 1,2 acetonide of compound **8** (2g, 10.41 mmol) was deprotected and then acetylated with 20mL mixture of Ac_2O:AcOH:H_2SO_4 (50:50:2, v/v). After 3h, anhydrous diethylether was added, followed by sodium acetate (10g, 12.19mmol). The mixture was filtered and the residue was washed with diethylether (2 X 50mL). The combined solutions were co-evaporated with toluene and the residue was purified by column chromatography using EtOAc/Pet-ether (2:8) as eluent. Pure compound **9** was collected as thick yellow syrup. Yield 1.6g, 55%.

Mol. Formula : $C_{11}H_{15}FO_7$

Mol. Weight : 278.23

ESI-Ms m/z : 301.0851($M+Na^+$)

^{1}H NMR (α+β) (200MHz, $CDCl_3$) : **δ_H** (ppm) 1.99-2.08 (m, 9H, OAC) 4.05-4.59 (m, 3H, H-4, H-5a, H-5b), 4.90-5.18 (dd, $J_{3,F}$ = 50.4 Hz, $J_{3,4}$ = 4.16 Hz, 1H, H-

3), 5.08-5.38 (m, 1H, H-2), 6.11-6.12 and 6.43-6.45 (α: d $J_{1,2}$ = 4.3 Hz, 0.3H, H-1 β: S, $J_{1,2}$ = 0.7 Hz, 0.7H, H-1)

^{13}C NMR (α+β) (50MHz, $CDCl_3$) : **δ_C** (ppm) 20.0, 20.2, 20.5, 20.7, 60.8, 61.1, 61.6, 61.9, 76.0, 76.2, 76.6, 78.4, 79.0, 80.2, 80.6, 90.2, 91.5, 93.0, 93.1, 94.0, 95.3, 98.4, 168.8, 169.1, 170.3

^{13}C-DEPT (α+β) (50MHz, $CDCl_3$) : **δ_C** (ppm) Positive peak: 20.2, 20.5, 20.7, 20.9, 76.2, 76.4, 76.8, 78.6, 79.2, 80.4, 80.8, 90.4, 91.7, 93.3, 94.2, 95.5, 98.6 Negative peak: 61.0, 61.2, 61.7, 62.0

2′, 5′-di-*O*-acetyl-3′-deoxy-3′-fluoro-xylouridine (10)

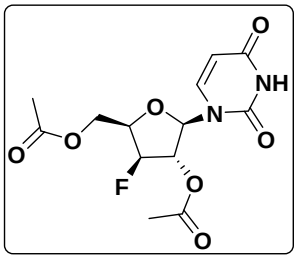

Under N_2 atmosohere *N, O*-bis (trimethylsily acetamide) (0.63mL, 0.52g, 2.54mmol) was added to a stirred solution of compound **9** (0.5g, 1.79mmol) and uracil (0.3g, 2.67mmol) in dry acetonitrile (6mL). The reaction mixture was refluxed for 1h to give a clear solution and then cooled to rt. TMS-triflate (0.78mL, 0.95g, 4.27mmol) was added to the reaction mixture and the resulting mixture was again refluxed for 3h. The reaction mixture was cooled and then concentrated to dryness under reduced pressure and redissolved in DCM (100mL), washed successively with saturated aq. $NaHCO_3$ (3 X 100mL) and H_2O (100mL), dried over Na_2SO_4 and concentrated to dryness *in vacuo*. The residue obtained was purified by column chromatography using EtOAc/Pet ether (6:4) as solvent system. The pure compound was collected as white foam. Yield 0.45g, 75%

Mol. Formula : $C_{13}H_{15}FN_2O_7$

Mol. Weight : 330.27

ESI-Ms m/z : 353.2080 ($M+Na^+$)

^{1}H NMR (200MHz, $CDCl_3$) : **δ_H** (ppm) 2.08-2.15 (m, 6H, OAc), 4.25-4.58 (m, 3H, H-4′, H-5′a, H-5′b), 4.93-5.30 (m, 2H, H-2′, H-3′), 5.79-5.83 (d, $J_{5H\text{-}6H}$ = 8 Hz, 1H, H5), 6.09 (d, $J_{1',2'}$ = 1.77 Hz, 1H, H-1′), 7.36-7.40 (d, $J_{6H\text{-}5H}$ = 8 Hz, 1H, H6)

3′-deoxy-3′-fluoro-xylouridine (11)

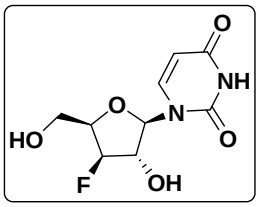

The aqueous ammonia (5mL) was added to a solution of compound **10** (0.5g) in MeOH (10mL). The reaction mixture was stirred at rt for 3h. The solvent was removed under reduced pressure. The crude product purified by column chromatography using DCM/MeOH (9:1) and the pure compound **11** was collected as a white solid. The obtained compound **11** recrystallizes using MeOH as solvent. Yield 0.33g, 90%.

Mol. Formula : $C_9H_{11}FN_2O_5$

Mol. Weight : 246.19

ESI-Ms m/z : 269.1324 ($M+Na^+$)

^{1}H NMR (200MHz, CD_3OD) : **δ_H** (ppm) 3.85-4.01 (m, 2H, H-5′a, H-5′b), 4.26-4.49 (ddd, 1H, H-4′, $J_{4'F}$ = 36.5 Hz, $J_{4'3'}$ = 2.5Hz, $J_{4'5a}$ = 5.9 Hz, $J_{4'5b}$ = 6.1Hz), 4.33-4.40 (ddd, 1H, H-2′, $J_{2'F}$ = 13.5 Hz, $J_{2'3'}$ = 0.9Hz, $J_{2'1'}$ = 1.01 Hz) 4.83-5.10 (ddd, 1H, H-3′, $J_{3'2'}$ = 0.89 Hz, $J_{3'4'}$ = 2.6 Hz, $J_{3'F}$ = 51.6 Hz), 5.68-5.72 (d, $J_{5H\text{-}6H}$ = 8Hz, 1H, H5), 5.83-5.84 (d, $J_{1'2'}$ = 1.01 Hz, 1H, H-1), 7.63-7.67 (d, $J_{6H\text{-}5H}$ = 8 Hz, 1H, H6)

^{13}C NMR (50MHz, CD_3OD) : **δ_C** (ppm) 59.5-59.7 (d), 79.5-80.1 (d), 84.0-84.4 (d), 92.9-94.6 (d), 98.2, 102.3, 141.7-141.8 (d), 152.2, 166.2

^{13}C-DEPT (50MHz, CD_3OD) : **δ_C** (ppm) Positive peaks: 79.5-80.1 (d), 84.0-84.4 (d), 92.9-94.9 (d), 98.2, 102.3, 141.8-141.8 (d) Negative peaks: 59.5-59.7 (d)

^{19}F NMR (100MHz, $(CD_3)_2SO$) : **δ_F** (ppm) -200.53 (dddd, $J_{F\ 3'}$ = 51.20Hz, $J_{F\ 4'}$ = 30.13 Hz, $J_{F\ 2'}$ = 15.05Hz, $J_{F\ 5'5''}$ = 1.9 Hz)

5′-*O*-dimethoxytrityl-3′-deoxy-3′-fluoro-xylouridine (12)

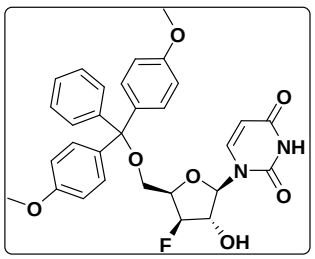

A mixture of compound **11** (0.5g, 2.03mmol) and 4, 4'-dimethoxytrityl chloride (0.67g, 2.03mmol) with Cat. amount of DMAP were dissolved in pyridine (3.0mL). The reaction mixture was stirred at rt for 2h. The pyridine was removed

under vacuum. The residue was dissolved in EtOAc (100mL), washed with saturated $NaHCO_3$ (2 x 50mL) and saturated aqueous NaCl (2 x 30mL). The EtOAc layer was dried over Na_2SO_4, filtered and evaporated to dryness. The crude was purified by silica gel (neutralized with TEA) column chromatography using DCM/MeOH (9.7:0.3) to offer the title compound **12** as a white solid. Yield 0.66g, 60%.

Mol. Formula : $C_{30}H_{29}FN_2O_6$

Mol. Weight : 548.57

HRMS(ESI) : 571.1852 ($M+Na^+$)

^{1}H NMR (200MHz, $CDCl_3$) : δ_H (ppm) 3.42-3.62 (m, 2H, H-5′a, H-5′b). 3.80 (s, 6H, OCH_3), 4.40-4.47 (m, 1H, H-2′), 4.51-4.73 (m, 1H, H-4′), 4.86-5.11 (dd, 1H, $J_{3',F}$ = 50.7 and $J_{3',4'}$ = 3.1Hz), 5.63 (d, 1H, H5, $J_{H5\text{-}H6}$ = 8.2 Hz), 6.87 (m, 4H) 5.81(d, 1H, H-1′, $J_{1',2'}$ = 1Hz), 7.26-7.35 (m, 9H), 7.46 (d, 1H, H6 $J_{6H,5H}$ = 8.2Hz).

^{13}C NMR (50MHz, $CDCl_3$) : δ_C (ppm) 55.2, 60.3-60.5 (d), 78.4-79.0 (d), 82.5-82.9 (d), 92.8-92.8 (d), 93.0, 96.5, 101.7, 113.1, 126.9, 127.9, 128.1, 130.0, 135.4-135.5 (d), 139.9, 144.4, 150.9, 158.5, 164.1.

^{13}C-DEPT (50MHz, $CDCl_3$) : δ_C (ppm) Positive peaks: 55.2, 78.5-79.0 (d), 82.6-82.9 (d), 92.8-92.9 (d), 93.1, 101.8, 113.2, 127.0, 127.9, 128.1, 130.1, 140.0 Negative peaks: 60.4-60.6 (d)

5′-*O*-dimethoxytrityl-3′-deoxy-3′-fluoro-xylouridinyl-2′-*O*-phosphoramidite (13)

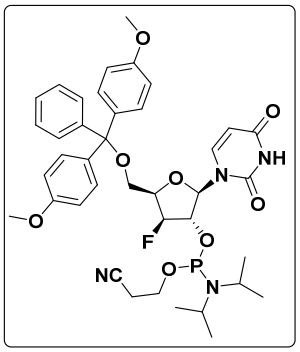

Compound **10a** (0.2g, 0.36mmol) was co-evaporated with dry DCM, and then dissolved in dry DCM (3mL). Diisopropylethylamine (DIPEA) (0.19mL, 1.09mmol) was added, followed by 2-Cyanoethyl *N,N*-diisopropylchlorophosphoramidite (0.16mL, 0.73mmol) at 0^{o}C. The reaction mixture was stirred under argon atmosphere at rt for 3h, when TLC indicated the absence of starting material. The reaction mass was diluted with DCM, washed with $NaHCO_3$ and H_2O, dried over Na_2SO_4, followed by solvent removal. The crude product was purified on a silica gel column (neutralized with TEA) using 1:1 mixture of DCM/EtOAc and 1% TEA. Yield 0.14g, 50%

Mol. Formula : $C_{39}H_{46}FN_4O_8P$

Mol. Weight : 748.79

HRMS(ESI) : 771.2935 ($M+Na^+$)

^{31}P NMR (161MHz, $CDCl_3$) : **δ_P** (ppm) 151.46, 153.51

1,2-*O*-isopropylidene-*α*-D-xylofuranose (15)

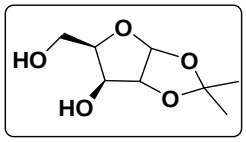

Finely powdered D-xylose compound **1** (10.0g, 67.1mmol) was dissolved in acetone (260mL) containing H_2SO_4 (10.0mL, 96%, 66.0 mmol) and stirred for 30min. A solution of Na_2CO_3 (13.0g, 122.65mmol) in H_2O (112mL) was carefully added under external cooling so as to keep the temperature of the mixture at 20°C, and the mixture was stirred for a further 2.5h. Then, solid Na_2CO_3 (7g, 66.0 mmol) was added till the pH = 7.0, Na_2SO_4 was filtered off and washed with acetone, and the combined filtrates were evaporated to yield 13.8g of crude **15** contaminated with 5% of 1,2:3,5-di-*O*-isopropylidene-α-D-xylofuranose, and 5% of starting D-xylose. The crude **15** was purified by silica gel filtration using 30:1 DCM/MeOH and pure **15** was obtained as syrup, which crystallized on standing. Yield 11g, 90%.

Mol. Formula : $C_8H_{14}O_5$

Mol. Weight : 190.19

ESI-Ms m/z : 213.0823 ($M+Na^+$)

^{1}H NMR (200MHz, $CDCl_3$) : **δ_H** (ppm) 1.33, 1.49 (2s, 6H, CH_3), 4.02-4.18 (m, 3H, H-4, H-5a, H-5b), 4.29-4.33 (m, 1H, H-3), 4.52-4.54 (d, 1H, H-2, $J_{2',1'}$ = 3.5Hz), 5.98-6.00 (d, 1H, H-1, $J_{1',2'}$ = 3.5Hz)

^{13}C NMR (50MHz, $CDCl_3$) : **δ_C** (ppm) 25.9, 26.4, 60.2, 75.5, 79.4, 85.1, 104.5, 111.5

^{13}C-DEPT (50MHz, $CDCl_3$) : **δ_C** (ppm) Positive peaks: 26.0, 26.6, 75.6, 79.6, 85.3, 104.6 negative peaks: 60.3

5-*O*-benzoyl-1,2-*O*-isopropylidene-*α*-D-xylofuranose (16)

Under N_2 atmosphere compound **15** (1g, 5.6mmol) and dry TEA (1.8g, 2.5mL, 18mmol) was added to dry DCM (15mL) and cooled it to 0°C. A solution of benzoyl chloride (0.81g,

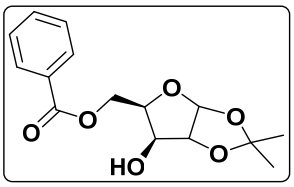

5.78mmol) in dry DCM (2mL) was carefully added to reaction mixture and the mixture was stirred for 5h. The reaction mass was diluted with DCM, washed with $NaHCO_3$ and H_2O, dried over Na_2SO_4, followed by solvent removal. The crude product was purified on a silica gel column using EtOAc/petether (1:9) Yield, 1.4g, 80%

Mol. Formula : $C_{15}H_{18}O_6$

Mol. Weight : 294.30

ESI-Ms m/z : 317.1283 ($M+Na^+$)

^{1}H NMR (200MHz, $CDCl_3$) : **δ_H** (ppm) 1.33, 1.52 (2s, 6H, CH_3), 3.34-3.36 (d, 1H), 4.17-4.18 (m, 1H), 4.35-4.44(m, 2H), 4.60-4.62 (d, 1H, H-2, $J_{2',1'}$ = 3.5Hz), 4.76-4.87 (m, 1H), 5.96-5.98 (d, 1H, H-1, $J_{1',2'}$ = 3.5Hz), 7.43-7.65 (m, 3H, C_6H_6), 8.04-8.08 (m, 2H, C_6H_6)

^{13}C NMR (50MHz, $CDCl_3$) : **δ_C** (ppm) 26.0, 26.7, 61.4, 74.4, 78.5, 85.0, 104.7, 111.8, 128.5, 129.19, 129.8, 133.5, 167.3

^{13}C-DEPT (50MHz, $CDCl_3$) : **δ_C** (ppm) Positive peaks: 26.1, 26.8, 74.4, 78.6, 85.0, 104.8, 128.5, 129.9, 133.6 Negative peaks: 61.4

Methyl 5-*O*-benzoyl-D-xylofuranoside (17)

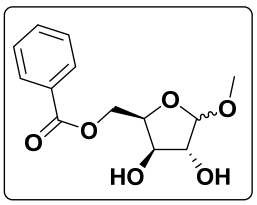

To a solution of compound **16** (4.95g, 16.82mmol) in dry MeOH (95mL), crystalline I_2 (0.95g) was added, and the mixture was refluxed for 4 h. After cooling, the mixture was poured into saturated aqueous $Na_2S_2O_3$ solution (150mL) and extracted with $CHCl_3$ (3 X 200mL), the combined organic extract washed with saturated aqueous NaCl solution (100mL), dried over anhydrous Na_2SO_4, and concentrated to give oily residue (4.92g). This was purified on a silica gel column using pet-ether / EtOAc 6:4 as solvent system to get α/β mix of compound **17**. Yield, 3.6g, 80%

Mol. Formula : $C_{13}H_{16}O_6$

Mol. Weight : 268.26

ESI-Ms m/z : 268.1256 (M+Na+)

^{1}H NMR (α+β) (200MHz, $CDCl_3$) : **δ_H** (ppm) 3.42 & 3.52 (β: s, 2.25H, OCH_3, α: s, 0.75H, OCH_3), 4.16-4.31 (m, 2H), 4.36-4.74 (m, 3H), 4.91 & 5.06-5.07 (β: s,

0.3H, H-1, α: d, 0.7H, $J_{1',2'}$ = 4.27Hz, H-1), 7.43-7.46 (m, 2H, C_6H_6), 7.57-7.58(m, 1H, C_6H_6), 8.04-8.08 (m, 1H, C_6H_6)

^{13}C NMR (α+β) (50MHz, $CDCl_3$) : **δ_C** (ppm) 53.3, 56.1, 62.6, 64.3, 76.3, 76.5, 76.9, 77.9, 79.5, 80.8, 102.0, 108.6, 128.4, 128.5, 129.1, 129.8, 129.9, 129.9, 133.1, 133.3, 166.6, 166.9

^{13}C-DEPT (α+β) (50MHz, $CDCl_3$) : **δ_C** (ppm) Positive peaks: 55.3, 56.1, 76.3, 76.5, 77.9, 77.9, 79.5, 80.8, 102.0, 108.6, 128.4, 128.5, 129.7, 129.7, 133.1, 133.3 Negative peaks: 62.6, 64.3

Methyl 5-*O*-benzoyl-3-deoxy-3-fluoro-D-ribofuranoside (18)

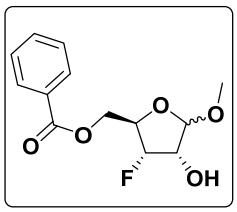

To a solution of compound **17** (0.24g, 0.89mmol) in dry DCM (5mL), DAST (0.71mL, 5.36mmol) was added and the mixture stirred at rt for 19 h. After cooling to 0 °C, the mixture was poured into saturated cold aqueous $NaHCO_3$ solution (60mL), the aqueous phase extracted with DCM (3 X 80 mL), the combined organic extract dried over Na_2SO_4 and evaporated and obtained residue was purified by using 7:3 pet-ether/EtOAc solvent system to get pure compound **18**. Yield, 0.13g, 55%

Mol. Formula : $C_{13}H_{15}FO_5$

Mol. Weight : 270.26

ESI-Ms m/z : 293.3980 ($M+Na^+$)

^{1}H NMR (α+β) (200MHz, $CDCl_3$) : **δ_H** (ppm) 3.34-3.50 (m, 3H, OCH_3), 4.06-4.65 (m, 4H), 4.76-5.35 (m, 2H), 7.41-7.62 (m, 3H, C_6H_6), 7.97-8.09 (m, 2H, C_6H_6)

^{13}C NMR (α+β) (50MHz, $CDCl_3$) : **δ_C** (ppm) 55.4, 55.6, 63.6, 63.8, 64.0, 64.1, 72.0, 72.4, 74.0, 74.3, 78.0, 78.5, 80.1, 80.6, 88.5, 90.3, 92.2, 93.9, 102.2, 107.8, 107.9, 128.3, 128.5, 129.2, 129.5, 129.5, 129.6, 133.2, 133.3, 165.9, 166.2

^{13}C-DEPT (α+β) (50MHz, $CDCl_3$) : **δ_C** (ppm) Positive peaks: 55.5, 55.7, 72.1, 72.5, 74.1, 74.4, 78.1, 78.6, 80.2, 80.7, 88.6, 90.4, 92.3, 94.1, 102.3, 107.9, 108.0, 128.4, 128.6, 129.6, 129.7, 133.3, 133.4 Negative peaks: 63.7, 63.9, 64.1, 64.2

Methyl 5-*O*-benzoyl-2-*O*-acetyl-3-deoxy-3-fluoro-D-ribofuranoside (19)

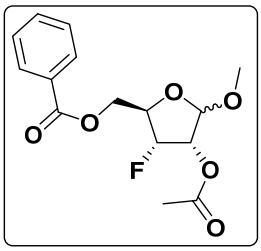

To a solution of compound **18** (0.15g, 0.55mmol) in dry pyridine (5mL), Ac_2O (0.22g, 0.2mL, 2.22mmol) was added and the mixture was stirred at rt for 3h. The pyridine was removed under vacuum. The residue was dissolved in EtOAc (100mL), washed with saturated $NaHCO_3$ (2 x 50mL) and saturated aqueous NaCl (2 x 30mL). The EtOAc layer was dried over Na_2SO_4, filtered and evaporated to dryness. The crude was purified by silica gel column chromatography using EtOAc/pet- ether (1:9) to get compound **19** as yellow syrup. Yield 0.12g, 70%

Mol. Formula : $C_{15}H_{17}FO_6$

Mol. Weight : 312.29

ESI-Ms m/z : 335.2245 ($M+Na^+$)

^{1}H NMR (α-ma) (200MHz, $CDCl_3$) : **δ_H** (ppm) 2.17 (s, OAc), 3.36 (2s, OCH_3), 4.42-4.61 (m, 3H), 5.0-5.39 (m, 3H), 7.44-7.61 (m, 3H, C_6H_6), 8.06-8.09 (m, 2H, C_6H_6)

^{13}C NMR (α-ma) (50MHz, $CDCl_3$) : **δ_C** (ppm) 20.6, 55.7, 63.9-63.9 (d, C5), 74.9-75.1 (d), 79.1-79.3 (d), 89.0-90.9 (d), 106.0-106.0 (d, C1), 128.5, 129.6, 129.7, 133.3, 166.2, 169.8

^{13}C-DEPT (α-ma) (50MHz, $CDCl_3$) : **δ_C** (ppm) Positive peaks: 20.6, 55.7, 74.9-75.1 (d) 79.2-79.3 (d), 89.0-90.9 (d), 106.0-106.02 (d), 128.5, 129.7, 133.3 Negative peaks: 63.9-63.9 (d, $J_{5',F}$ = 4.63Hz)

2′-*O*-acetyl-5'-*O*-benzoyl-3'-deoxy-3'-fluoro uridine (20)

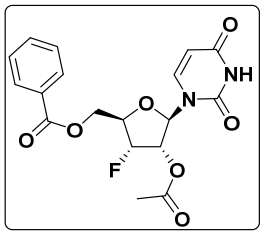

Compound **20** (0.45g) was synthesized by using same Vorbrüggen glycosylation reaction using silylated uracil (0.3g, 2.67mmol) from compound **19** (0.5g, 1.79mmol) accordingly as mentioned earlier for compound **10**. Yield 0.45g, 75%

Mol. Formula : $C_{18}H_{17}FN_2O_7$

Mol. Weight : 392.34

ESI-Ms m/z	**:**	415.16 ($M+Na^+$)
^{1}H NMR (200MHz, $CDCl_3$)	**:**	**δ_H** (ppm) 2.18 (s, 3H, OAc), 4.54-4.71(m, 3H), 5.25-5.52(m, 2H), 5.58-5.62 (d, 1H, H5, $J_{H5,H6}$ = 8Hz), 6.14-6.17 (d, 1H, H-1′, $J_{1'2'}$ = 6.9Hz), 7.25-7.29 (d, 1H, H6, $J_{H5,H6}$ = 8Hz), 7.46-7.67 (m, 3H, C_6H_6), 8.02-8.06 (m, 2H, C_6H_6)
^{13}C NMR (50MHz, $CDCl_3$)	**:**	**δ_C** (ppm) 20.2, 63.2-63.3 (d), 72.7-72.9 (d), 77.4, 80.1-80.6 (d), 86.8-90.6(d), 103.2, 128.3, 128.8, 129.4, 133.5, 139.6, 150.2, 163.3, 165.7, 169.9
^{13}C-DEPT (50MHz, $CDCl_3$)	**:**	**δ_C** (ppm) Positive peaks: 20.4, 72.9-73.2 (d), 80.3-80.8 (d), 87.0-90.8 (d), 103.5, 128.5, 128.8, 129.6, 133.7, 139.8 Negative peaks: 63.4-63.1 (d)

3'-deoxy-3'-fluorouridine (21)

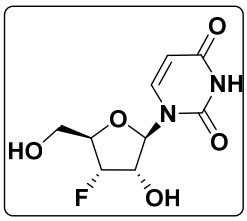

The 5′-*O*-benzoyl and 2′-*O*-acetyl group of compound **20** (0.5g) was deprotected using aqueous ammonia (5mL) in MeOH (10mL) to get compound **21** following previously mentioned procedure for compound **11**. Yield, 0.28g, 90%.

Mol. Formula	**:**	$C_9H_{11}FN_2O_5$
Mol. Weight	**:**	246.19
ESI-Ms m/z	**:**	269.09 ($M+Na^+$)
^{1}H NMR (200MHz, CD_3OD)	**:**	**δ_H** (ppm) 3.75-3.37 (m, 2H, H-5′a, H-5′b), 4.21-4.37 (dtd, 1H, H-4′, $J_{4'F}$ = 28.1Hz, $J_{4'3'}$ = 0.7Hz, $J_{4'5a}$ = 2.6Hz, $J_{4'5b}$ = 3Hz), 4.28-4.46 (ddd, 1H, H-2′, $J_{2'F}$ = 23.5Hz, $J_{2'1'}$ = 7.7Hz, $J_{2'3'}$ = 4.5Hz), 4.84-5.15 (ddd, 1H, H-3′, $J_{3'F}$ = 54.44Hz, $J_{3'2'}$ = 4.5Hz, $J_{3'4'}$ = 0.7Hz), 5.73-5.77 (d, 1H, H5, J_{H5-H6} = 8Hz), 6.04-6.08 (d, 1H, H-1′, $J_{1'2'}$ = 7.7Hz), 7.94-7.98 (d, 1H, H6, J_{H5-H6} = 8Hz)
^{13}C NMR (50MHz, CD_3OD)	**:**	**δ_C** (ppm) 62.2-62.4 (d), 74.5-74.8 (d), 84.8-85.2 (d), 88.5, 92.1-95.7 (d), 103.4, 142.3, 152.6, 165.9
^{13}C-DEPT (50MHz, CD_3OD)	**:**	**δ_C** (ppm) Positive peaks: 74.5-74.9 (d),84.8-85.2 (d), 88.5, 92.1-95.7 (d), 103.4, 142.4 Negative peaks: 62.2-62.5 (d)

^{19}F NMR (376MHz, $(CD_3)_2SO$) : δ_F (ppm) -196.74 (ddd, $J_{F\ 3'}$ = 54.4Hz, $J_{F\ 4'}$ = 28.1Hz, $J_{F\ 2'}$ = 23.5Hz)

5′-*O*-dimethoxytrityl-3′-deoxy-3′-fluoro-uridine (22)

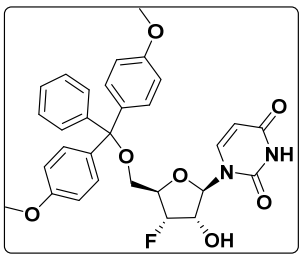

The 5′-hydroxy group of compound **21** (0.5g, 2.0mmol) was protected by 4, 4′-dimethoxy trityl chloride (0.67g, 2.03mmol) to get compound **22** by following the same synthetic procedure mentioned for compound **12**. Yield, 0.66g, 60%

Mol. Formula : $C_9H_{11}FN_2O_5$

Mol. Weight : 548.19

HRMS(ESI) : 571.1848($M+Na^+$)

^{1}H NMR (200MHz, $CDCl_3$) : δ_H (ppm) 3.39-3.54 (m, 2H). 3.78 (s, 6H), 4.36-4.45 (m, 2H), 4.94-5.23 (dd, 1H, $J_{3',F}$ = 54.3 and $J_{3',4'}$ = 2.0Hz), 5.45 (d,1H, $J_{6,5}$ = 8.0Hz), 6.15 (d,1H, $J_{1,2}$=6.5Hz), 6.84 (m, 4H), 7.22-7.33 (m, 9H),7.71 (d, 1H, $J_{5,6}$= 8.0Hz)

^{13}C NMR (50MHz, $CDCl_3$) : δ_C (ppm) 55.2, 62.5-62.7(d), 74.8-75.1 (d), 81.8-82.3 (d), 87.4, 90.0-93.7 (d), 103.1, 113.4, 127.3, 127.9, 128.1, 129.9-130.0 (d), 134.8, 134.9, 139.7, 143.9, 151.3, 158.7, 163.5

^{13}C-DEPT (50MHz, $CDCl_3$) : δ_C (ppm) Positive peaks: 55.2, 74.8-75.2(d), 81.8-82.3 (d), 87.5, 90.1-93.7 (d), 103.1, 113.4, 127.3, 128.0, 128.1, 130.0, 139.8 Negative peaks: 62.6-62.7 (d)

5′-*O*-dimethoxytrityl-3′-deoxy-3′-fluoro-uridinyl-2′-*O*-phosphoramidite (23)

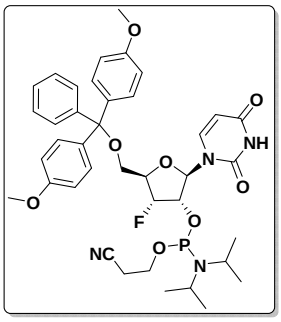

Phosphoramidite derivative of Compound **22** (0.2g, 0.36mmol) was synthesized by using DIPEA and 2-Cyanoethyl *N, N*-diisopropylchlorophosphoramidite (0.15mL, 0.72mmol) accordingly as mentioned earlier for compound **13**. Yield 0.15g, 55%

Mol. Formula- $C_{39}H_{46}FN_4O_8P$; **Mol. Weight**-748.79; **HRMS(ESI)**-771.2929 ($M+Na^+$); **^{31}P NMR (**161MHz, $CDCl_3$): δ_P (ppm) 151.41, 152.51

2.5.2 Synthesis of buffers

Phosphate buffer (pH = 7.4, 150mM NaCl)

Na_2HPO_4 (110mg), $NaH_2PO_4 \cdot H_2O$ (35.3mg), NaCl (877.5mg) was dissolved in minimum quantity of water and the total volume was made 100mL. The pH of the solution was adjusted 7.4 with aq. NaOH solution in DI water, and stored at 4°C.

Triethyl ammonium acetate buffer (TEAA)

TEA (101.19g ≈ 139.38mL, 1M) was diluted up to 500mL DI water and kept aside, then in another container AcOH (60.05g ≈57.24mL, 1M) was diluted up to again with 500 mL DI water. Then slowly AcOH solution was added to the TEA in ice bath with vigoures stirring to make total volume 1L, the pH of the solution was adjusted to 7 using either AcOH or TEA, and stored at room temperature.

2.5.3 Synthesis of oligonucleotides

Control DNA and modified oligomers were synthesized on a CPG solid support using Bioautomation Mer-Made 4 synthesizer using standard β-cyanoethyl phosphoramidite chemistry. The 2′-5′-linked oligomers were synthesized in 2′-5′ direction using universal columns as solid support. For the ONs synthesis, each unmodified (50µL) and modified (100µL) monomer used with 0.06M and 0.1M concentration in ACN respectively. For the modified units, double coupling (300s x 2) was performed. After synthesis, the sequences were cleaved from the support by ammonia treatment for 6h at 55°C to cleave the ester functionality that joins support to the 2′- terminus of the oligomers and deprotects the exocyclic amino protecting groups used during the synthesis. The oligonucleotides purity was ascertained by RP-HPLC on a C18 column, which was more than 98% pure and they were used without further purification in biophysical studies.

2.5.4 Purification and characterization

High performance liquid chromatography

The purity of synthesized oligonucleotides were ascertained using RP-HPLC on a C18 column with either a Varian system (Analytical semi-preparative system consisting of Varian Prostar 210 binary solvent delivery system and Dynamax UV-D2 variable wavelength detector and Star chromatography software) or a Waters system (Waters Delta 600e quaternary solvent delivery system and 2998 photodiode array detector and Empower 2 chromatography software). A gradient elution method 0% A to 100%B in 15min was used with flow rate 1.5mL/min and the eluent was monitored at 260nm. [A = 5% ACN in TEAA (0.1M, pH 7); B = 30% ACN in TEAA (0.1M, pH 7)].

MALDI-TOF characterization

The MALDI-TOF spectra were recorded on either Voyager-De-STR (Applied Biosystems) MALDI-TOF instrument or a AB Sciex TOF/TOF™ Series Explorer™ 72085 instrument. A nitrogen laser (337nm) was used for desorption and ionization. The matrix used for analysis was THAP (2', 4', 6'-trihydroxyacetophenone), and diammonium citrate used as additive. The sample was prepared by mixing 1µL oligomer (10-50µM in DI H_2O) with 10µL of THAP (0.55M in EtOH) mixed well followed by 5µL diammonium citrate (0.1M in DI H_2O) again mixed well and then 1µL of the mixture was spotted on metal plate. The metal plate was loaded to the instrument and the analyte ion were then accelerated by an applied high voltage in linear mode and detected as an electrical signal.

HPLC purified oligonucleotides were characterized through this method and were observed to give good signal to noise ratio, mostly producing higher molecular ion signals. The purity was re-checked and found to be >95%.

2.5.5 Biophysical techniques

UV-T_m Experiment

UV experiments were performed on a Varian Cary 300 UV-VIS spectrophotometer fitted with a Peltier-controlled temperature programmer. The concentration of DNA ONs were calculated on the basis of absorbance from molar extinction coefficients of the corresponding nucleobases (A = 15400, T = 8800, C = 7300 and G = 11700 U = 9900 L/(mol.cm) of DNA/RNA. The experiments were performed at 1μM concentrations. The complexes were prepared by mixing calculated amount of stock ONs and complementary strand together (1:1) in 1.1mL of 10mM sodium phosphate buffer, pH 7.4 containing NaCl (150mM) and were annealed by keeping the samples at 90℃ for 2min followed by slow cooling to room temperature and refrigeration for at least 3h prior to running the experiments. The sample vials then transfer to ice bath and degases with N_2-gas for 10min, which is then transferred to rectangular quartz cell (1cc, 10mm), sealed with teflon stopper for experiment. The sample were equilibriated at starting temperature 10°C for at least 15min, and N_2-gas was purged through the cuvette chamber below 20°C to prevent condensation of moisture on cuvette walls. Absorbance *versus* temperature profiles were obtained by monitoring the absorbance at 260nm from 10–85°C at a ramp rate of 0.5℃ per minute. The data were processed using Microcal Origin 6.1 and T_m (℃) values were derived from the maxima of the first derivative plots. All values are an average of at least 3 experiments and accurate to within ± 0.5℃.

CD experiments

The samples for CD experiments were prepared as for the UV-T_m experiments. Thus, 1μM concentration of each strand was used. The complexes were prepared in 10mM sodium phosphate bufferof pH 7.4 containing NaCl (150mM) and were annealed by keeping the samples at 90℃ for 2min followed by slow cooling to rt and refrigeration for at least 2h prior to running the experiments. CD spectra were recorded in a 1cm pathlength cuvette at 10°C, as an accumulation of 3scans, and using a resolution of 1nm, bandwidth of 1nm, sensitivity of 20mdeg, response of 1s and a scan speed of 200nm/min.

2.6 Appendix A

Compounds	Page Number
Compound 2: ^{1}H, ^{13}C, DEPT NMR	85
Compound 4: ^{1}H, ^{13}C, DEPT NMR	86
Compound 5: ^{1}H, ^{13}C, DEPT NMR	87
Compound 6: ^{1}H, ^{13}C, DEPT NMR	88
Compound 7: ^{1}H, ^{13}C, DEPT NMR	89
Compound 8: ^{1}H, ^{13}C, DEPT NMR	90
Compound 9: ^{1}H, ^{13}C, DEPT NMR	91
Compound 10: ^{1}H NMR and LCMS	92
Compound 11: ^{1}H, ^{13}C, DEPT ^{19}F NMR and LCMS	93-94
Compound 12: ^{1}H, ^{13}C, DEPT NMR and HRMS	95-96
Compound 13: ^{31}P NMR and HRMS	96
Compound 15: ^{1}H, ^{13}C, DEPT NMR	97
Compound 16: ^{1}H, ^{13}C, DEPT NMR	98
Compound 17: ^{1}H, ^{13}C, DEPT NMR	99
Compound 18: ^{1}H, ^{13}C, DEPT NMR	100
Compound 19: ^{1}H, ^{13}C, DEPT NMR	101
Compound 20: ^{1}H, ^{13}C, DEPT NMR and LCMS	102-103
Compound 21: ^{1}H, ^{13}C, DEPT ^{19}F NMR and LCMS	103-104
Compound 22: ^{1}H, ^{13}C DEPT NMR and HRMS	105-106
Compound 23: ^{31}P NMR and HRMS	106
ngDNA HPLC chromatogram	107-108
DNA and ngDNA MALDI-TOF spectra	109-112

^{1}H NMR of compound 2

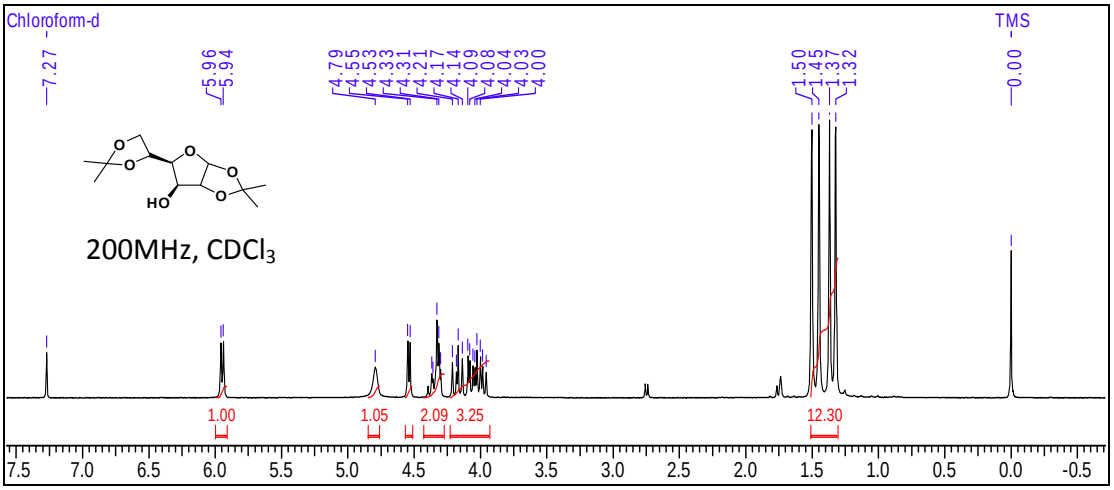

^{13}C NMR of compound 2

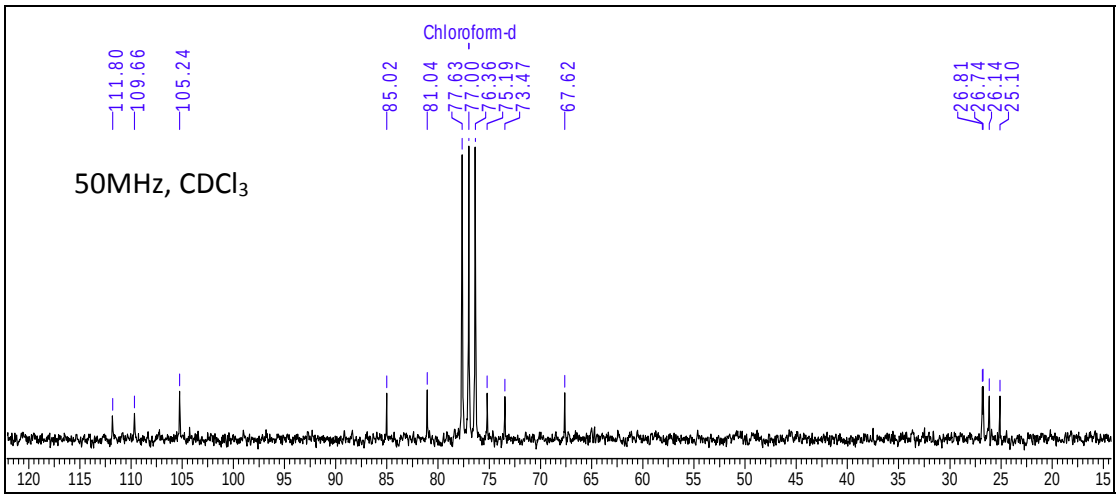

^{13}C-DEPT of compound 2

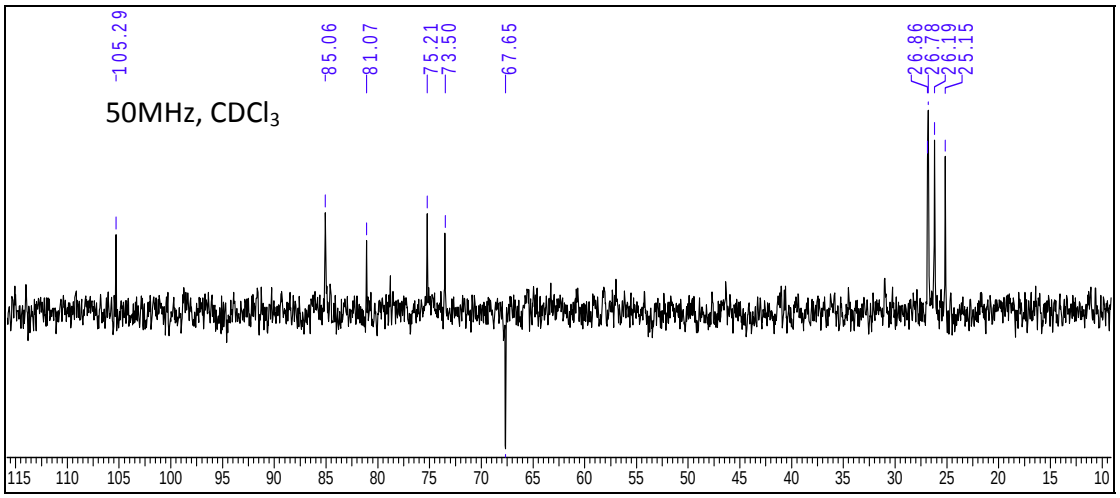

^{1}H NMR of compound 4

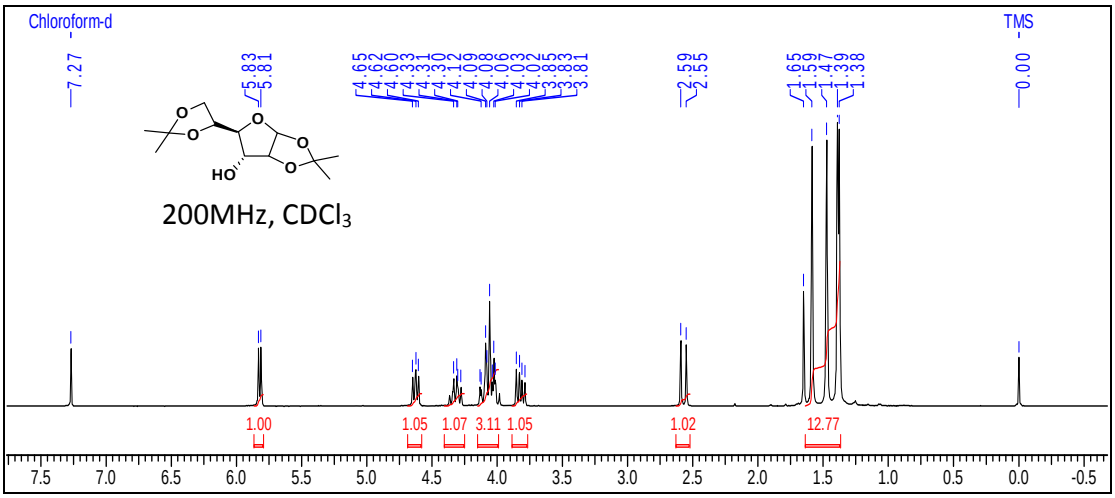

^{13}C NMR of compound 4

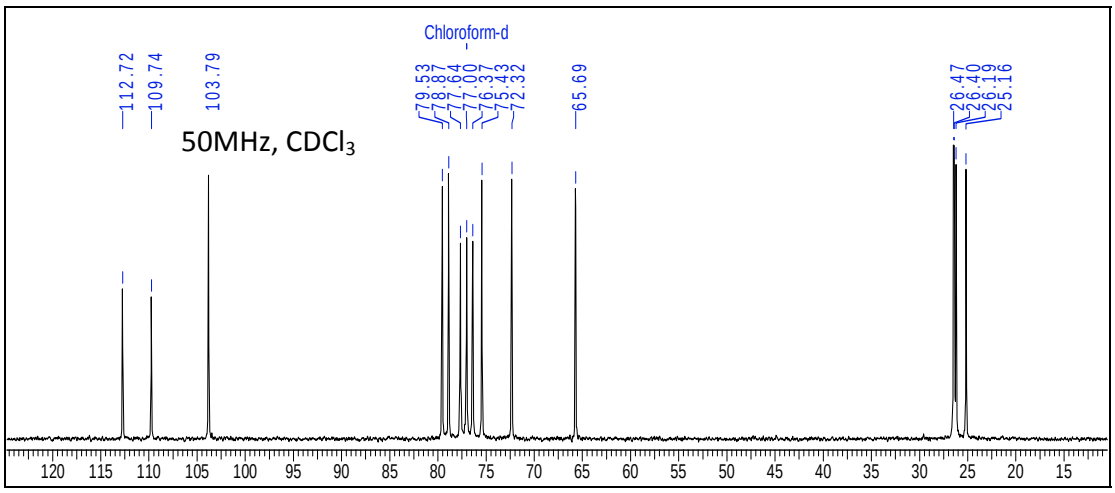

^{13}C-DEPT of compound 4

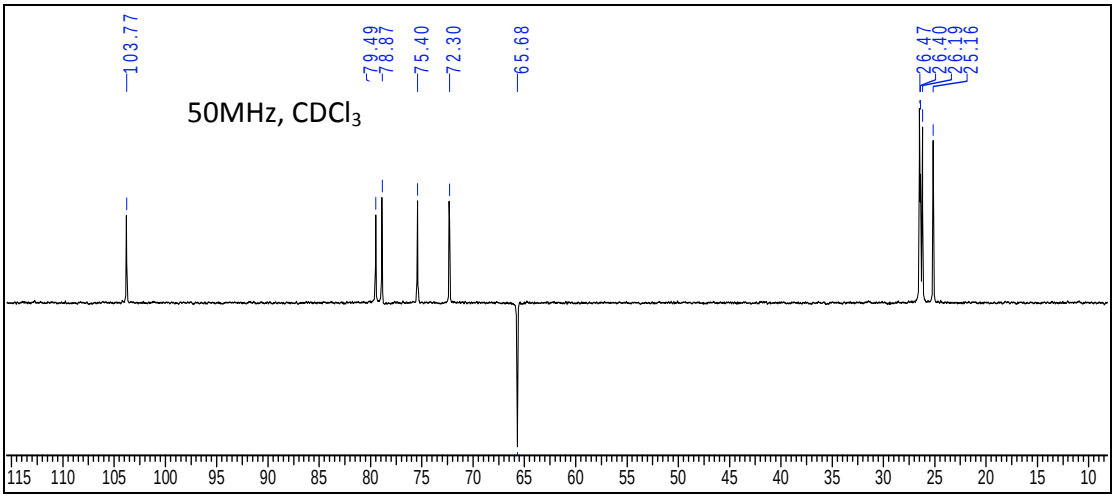

^{1}H NMR of compound 5

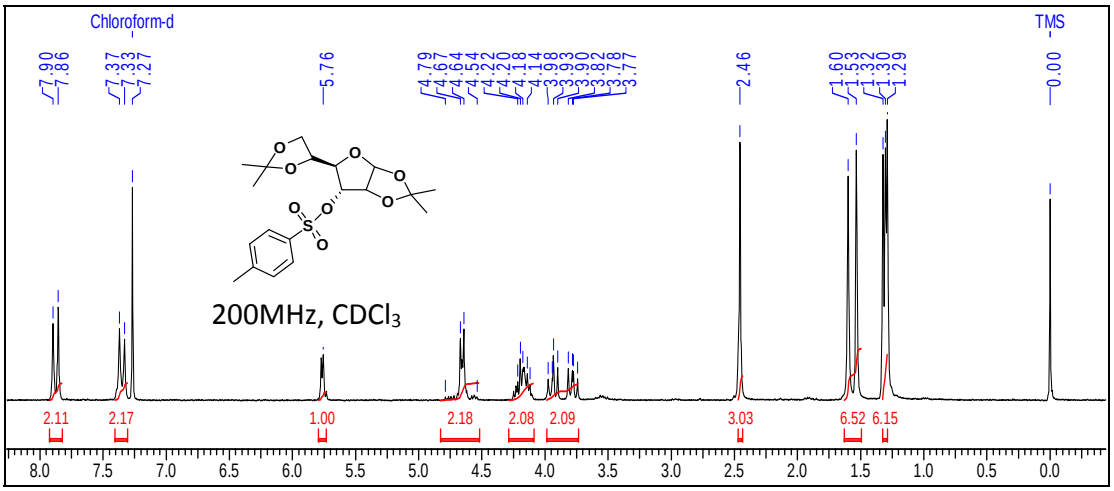

^{13}C NMR of compound 5

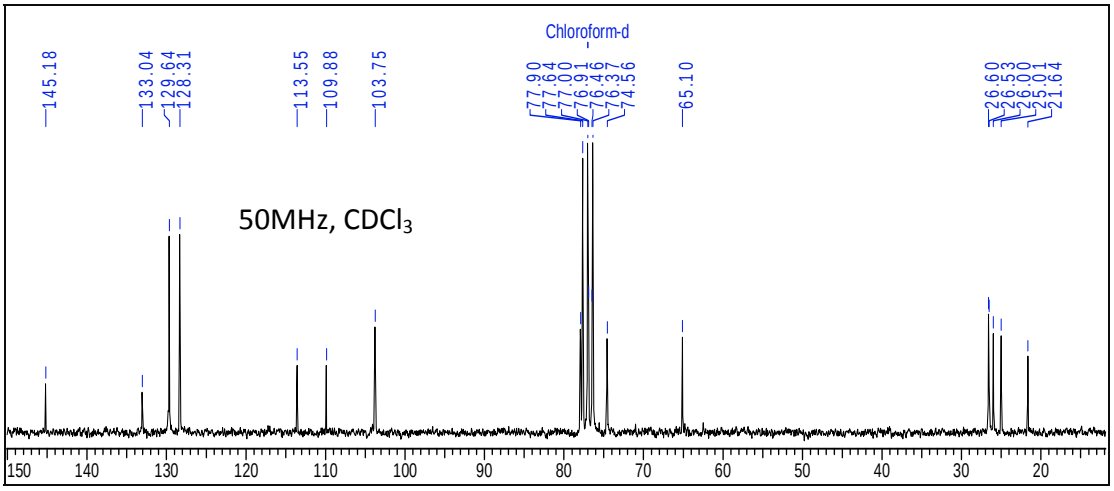

^{13}C-DEPT of compound 5

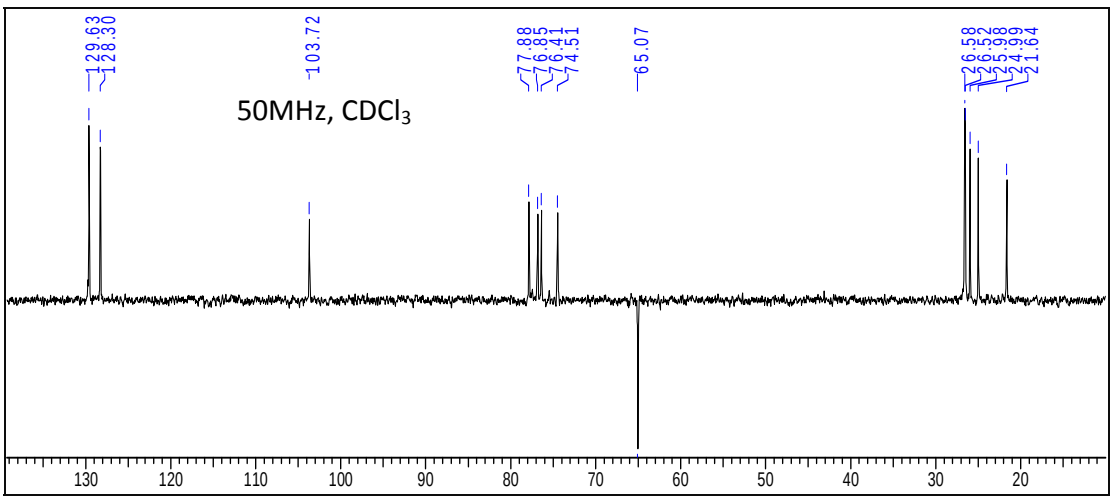

^{1}H NMR of compound 6

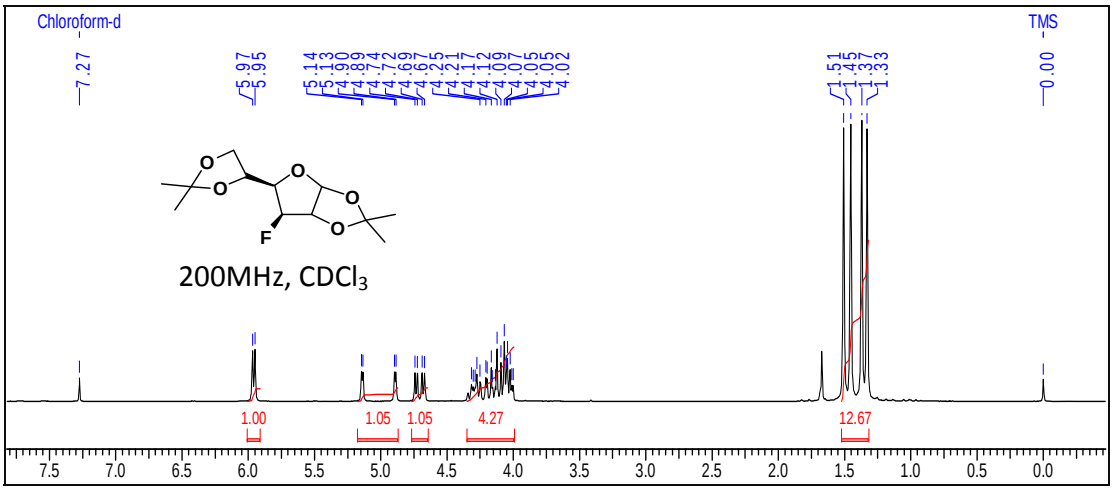

^{13}C NMR of compound 6

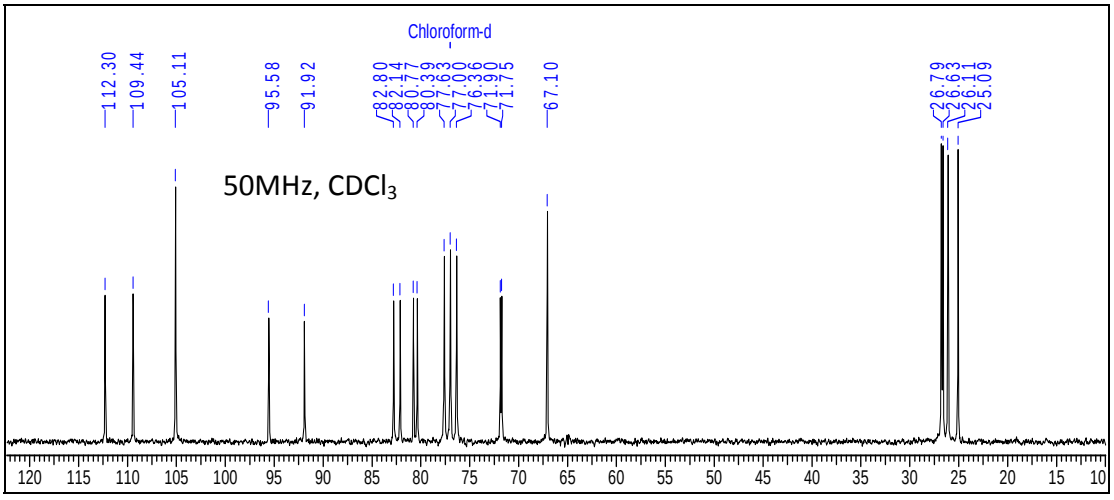

^{13}C-DEPT of compound 6

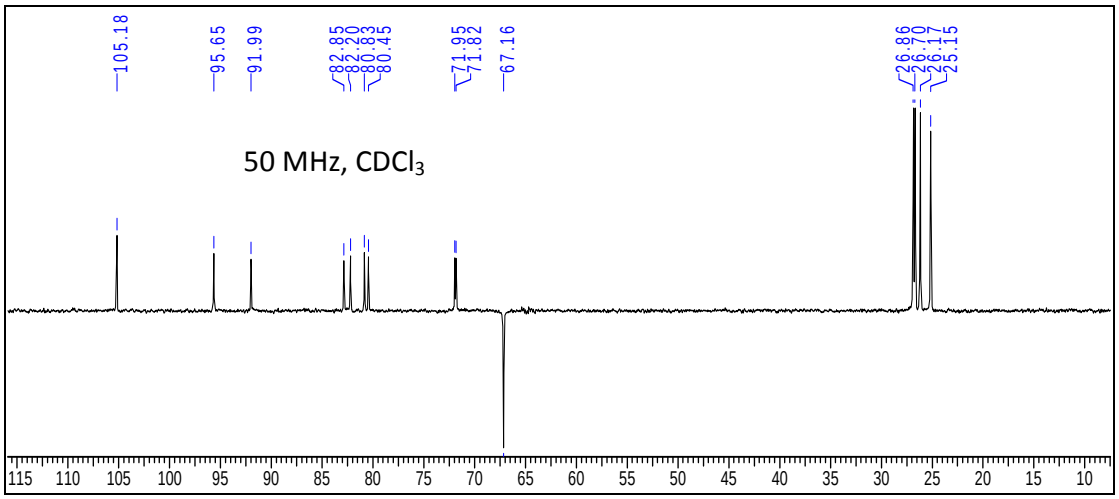

^{1}H NMR of compound 7

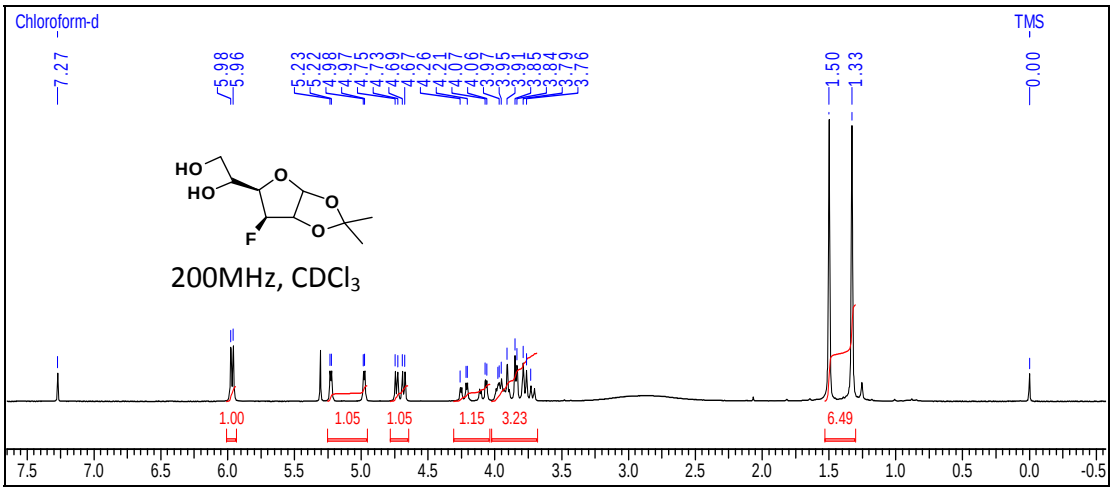

^{13}C NMR of compound 7

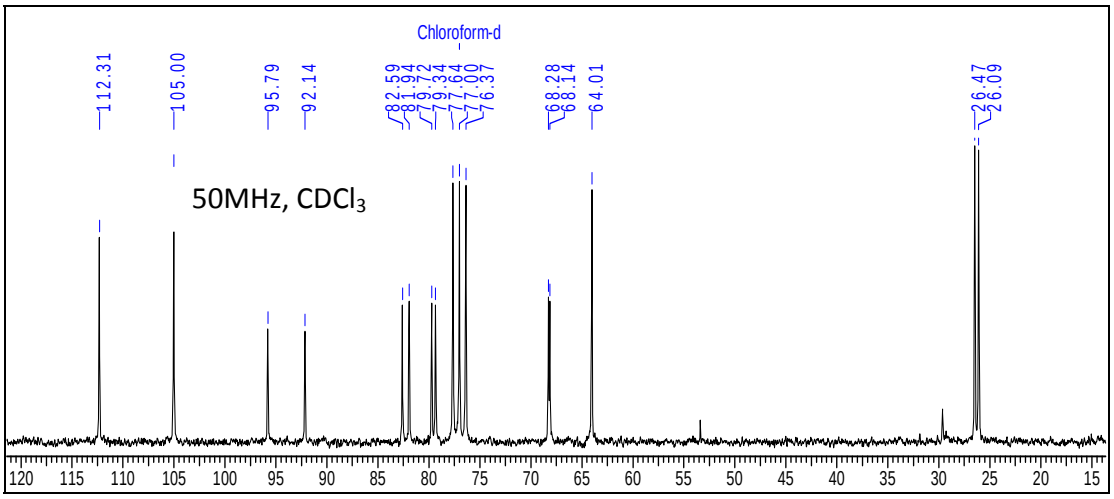

^{13}C-DEPT of compound 7

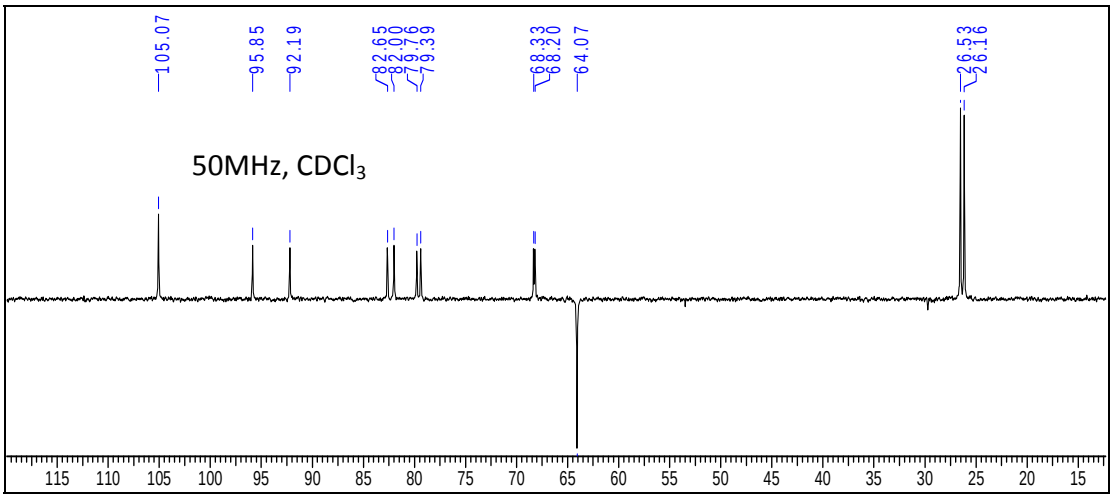

^{1}H NMR of compound 8

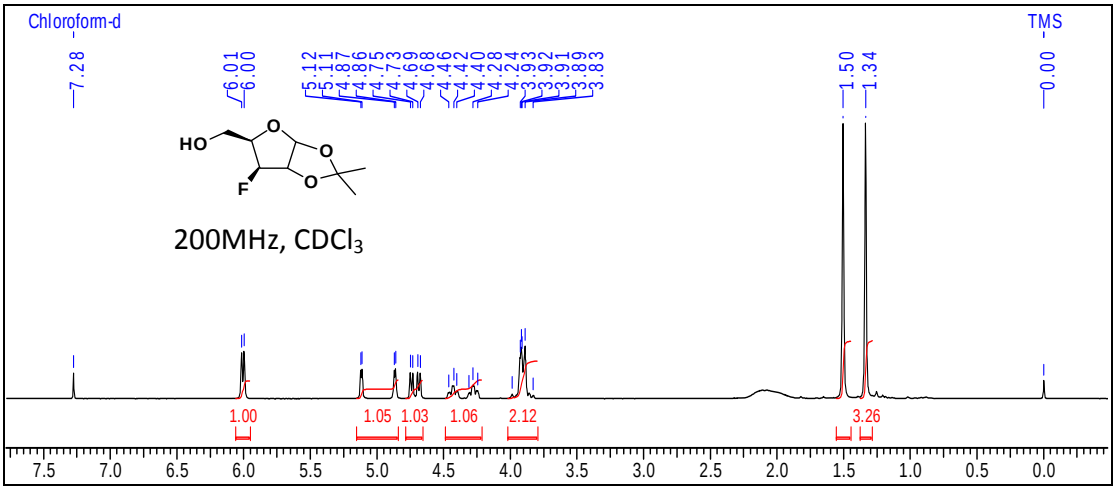

^{13}C NMR of compound 8

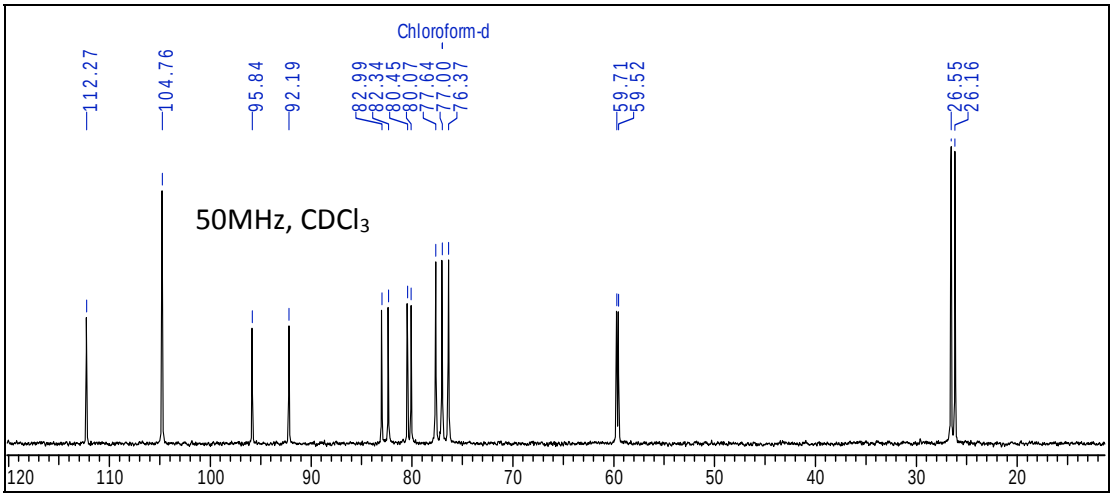

^{13}C-DEPT of compound 8

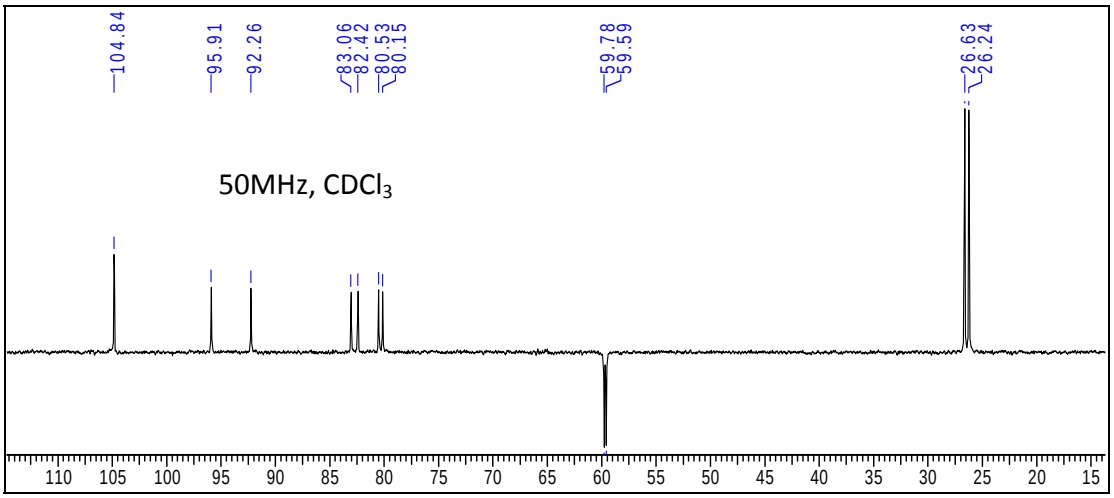

^{1}H NMR of compound 9

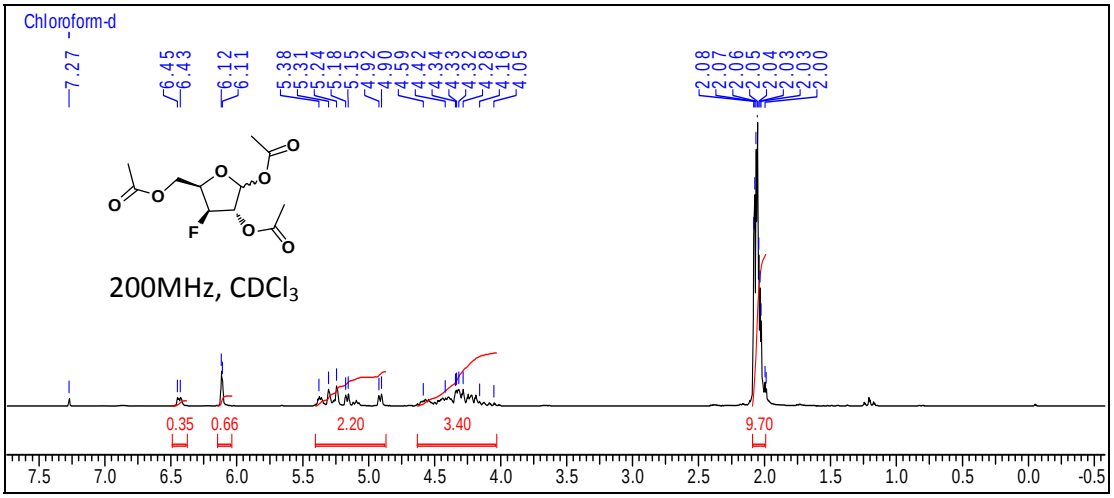

^{13}C NMR of compound 9

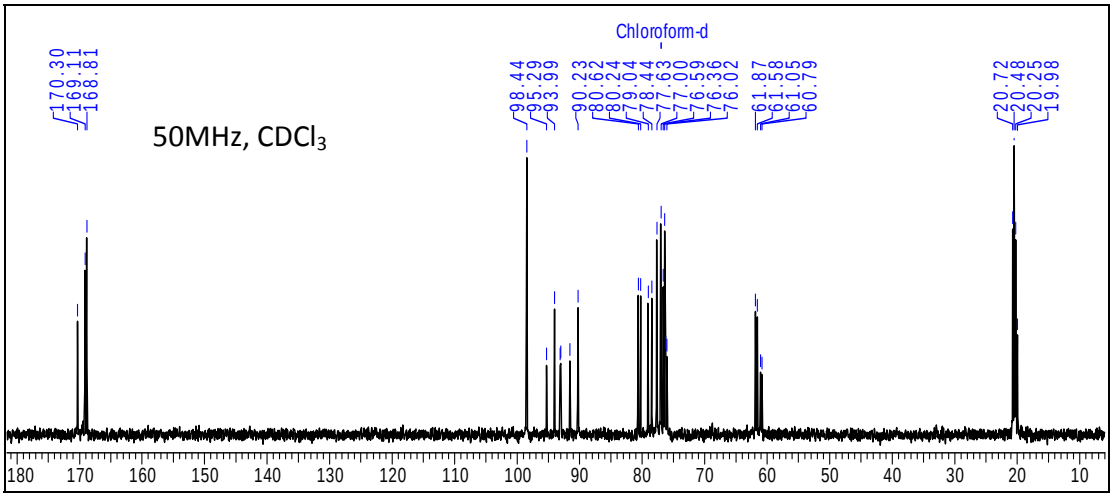

^{13}C-DEPT of compound 9

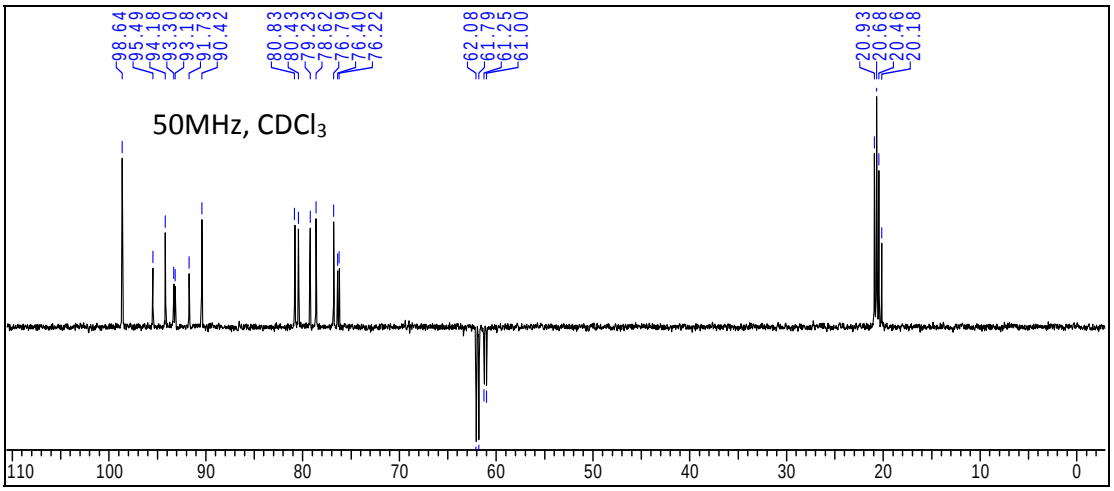

^{1}H NMR of compound 10

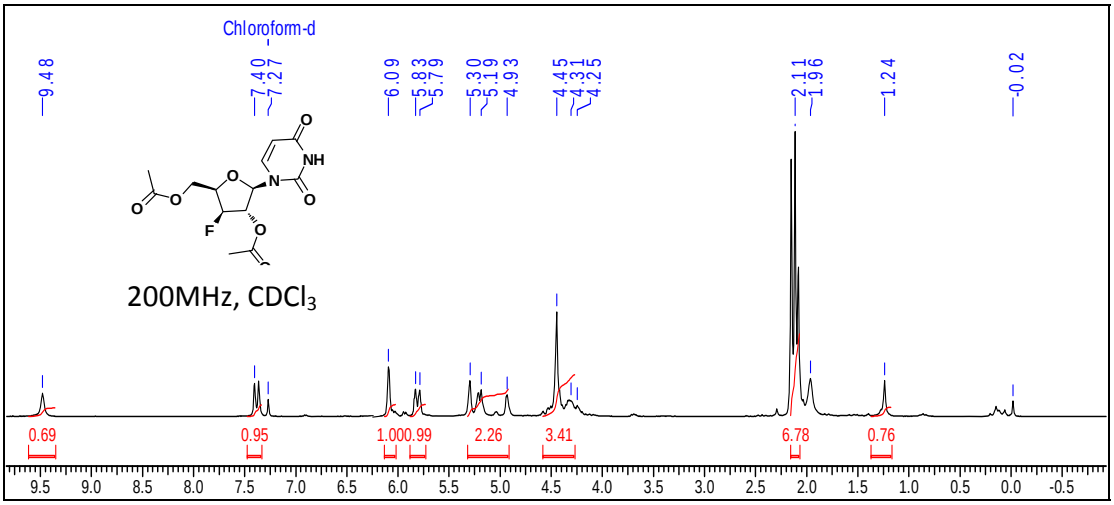

LCMS of compound 10

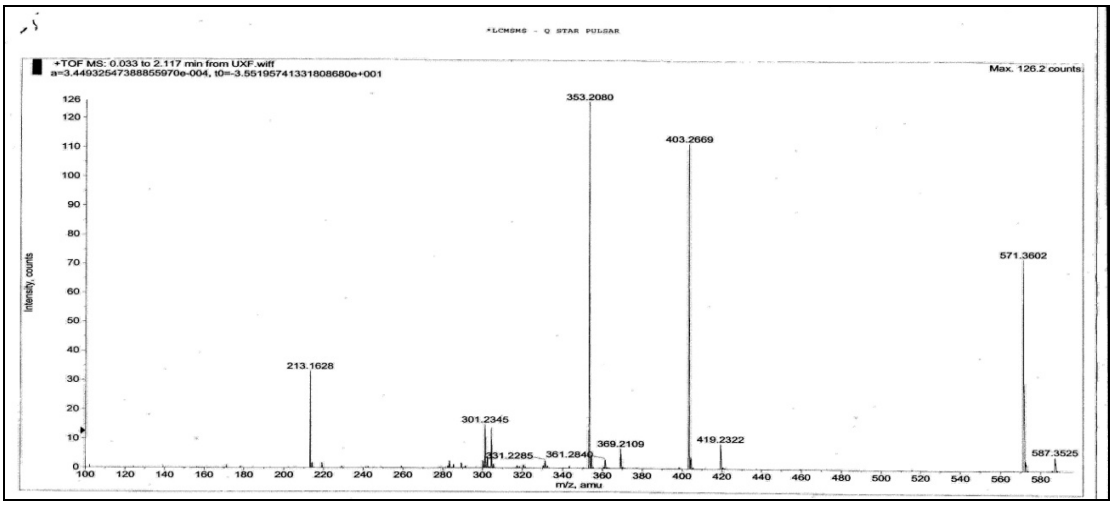

^{1}H NMR of compound 11

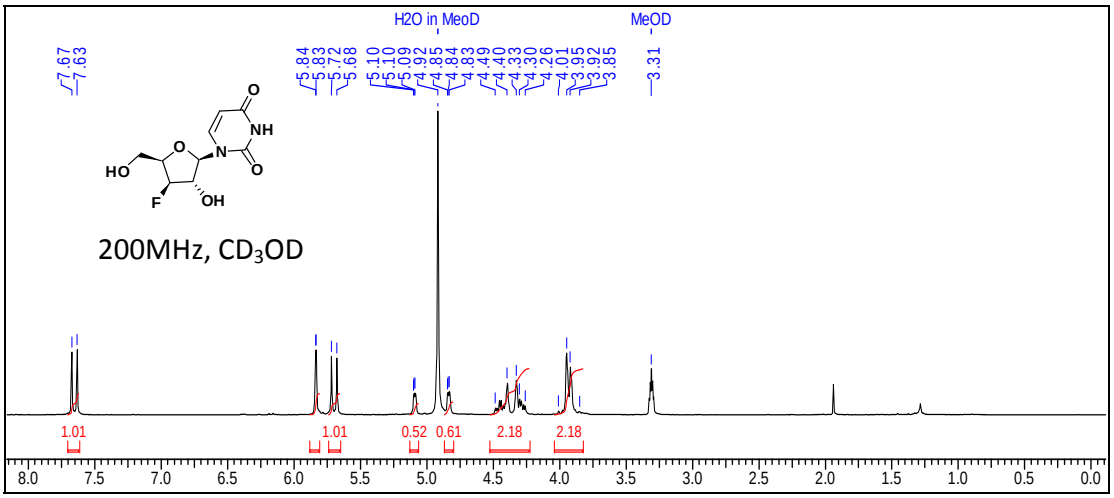

^{13}C NMR of compound 11

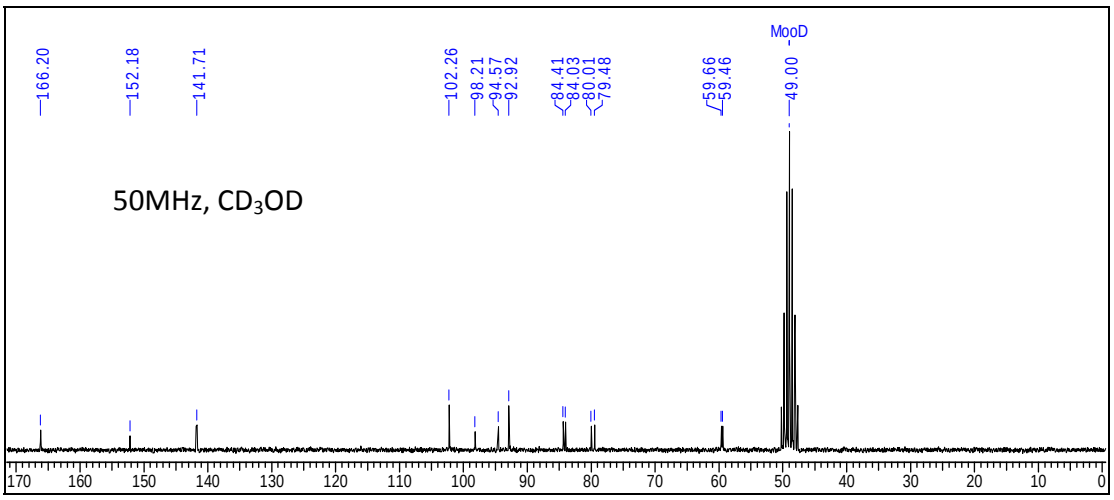

^{13}C-DEPT of compound 11

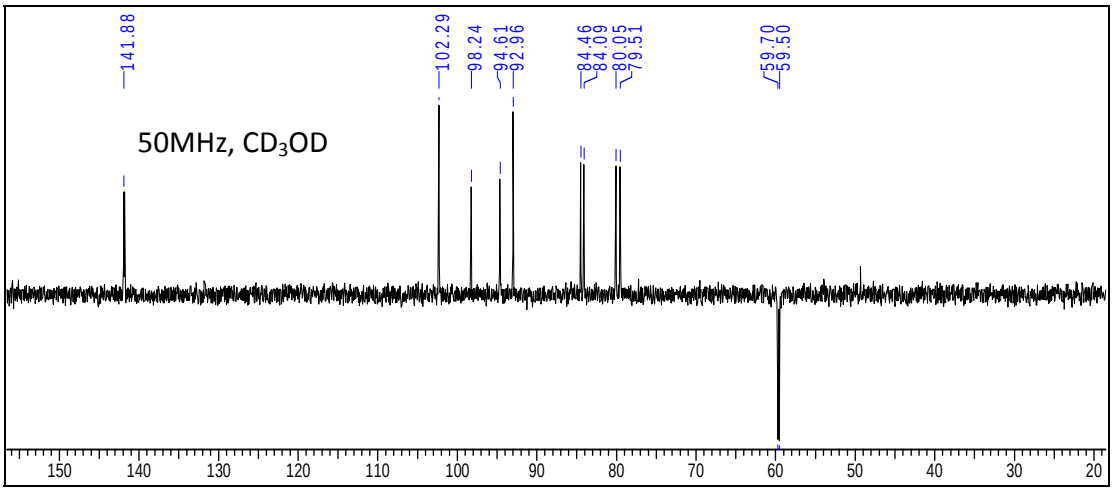

^{19}F NMR of compound 11

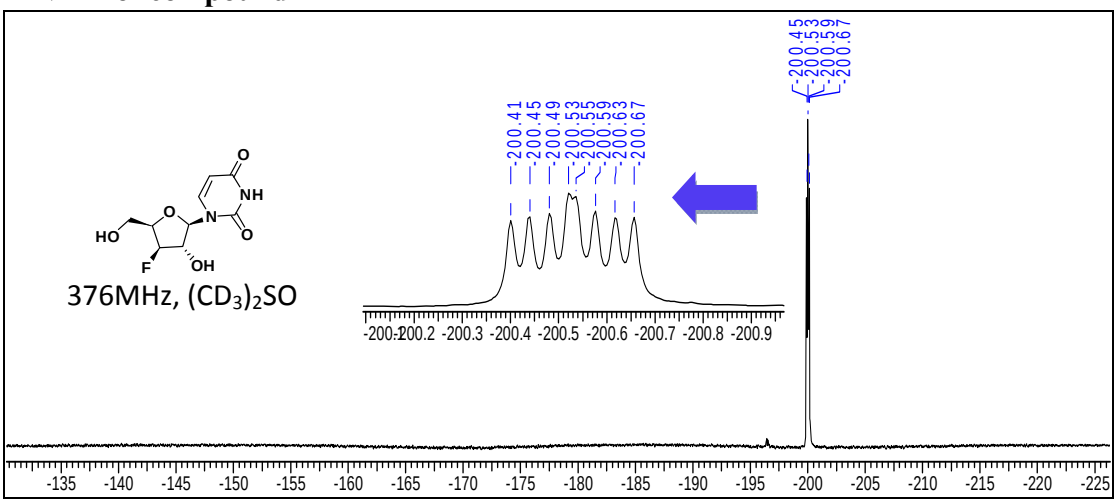

LCMS of compound 11

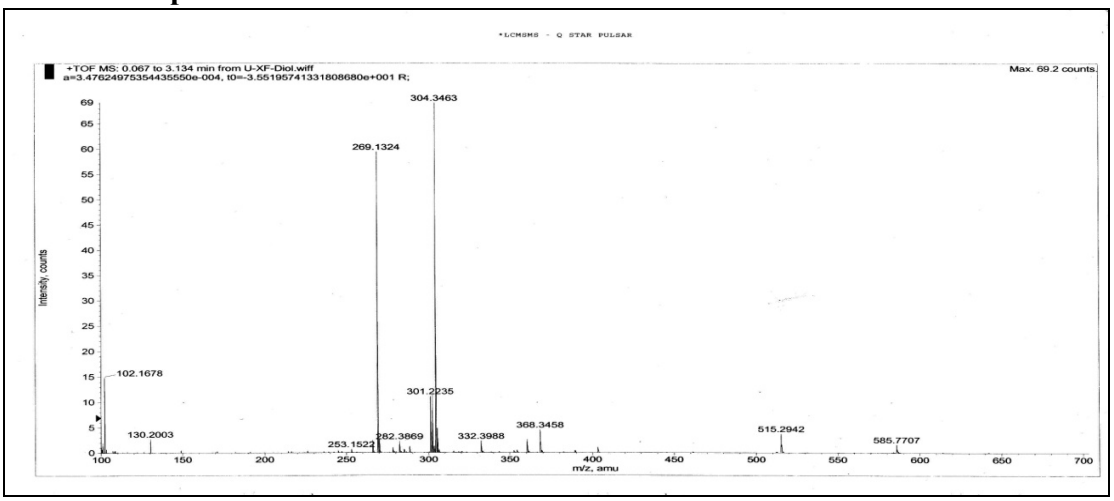

^{1}H NMR of compound 12

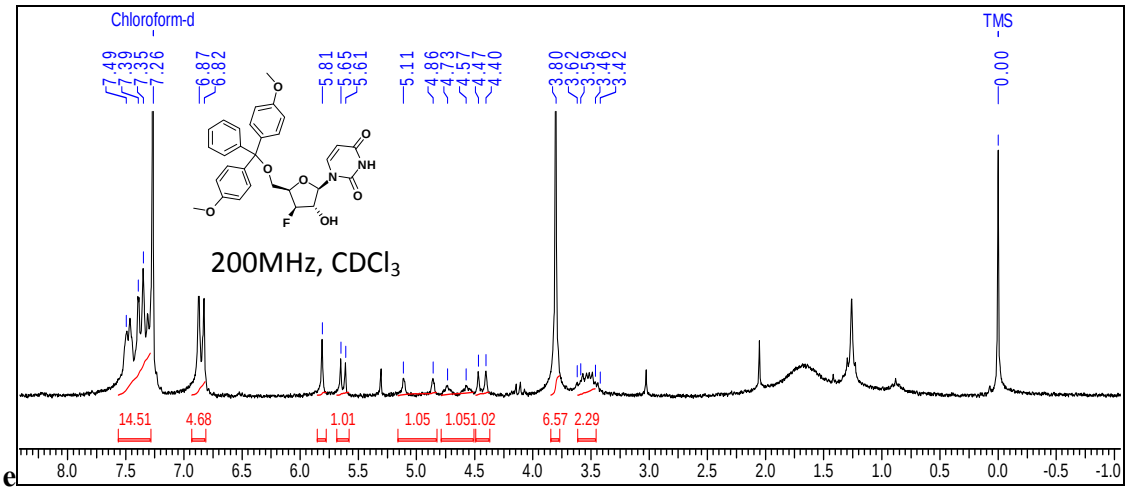

e

^{13}C NMR of compound 12

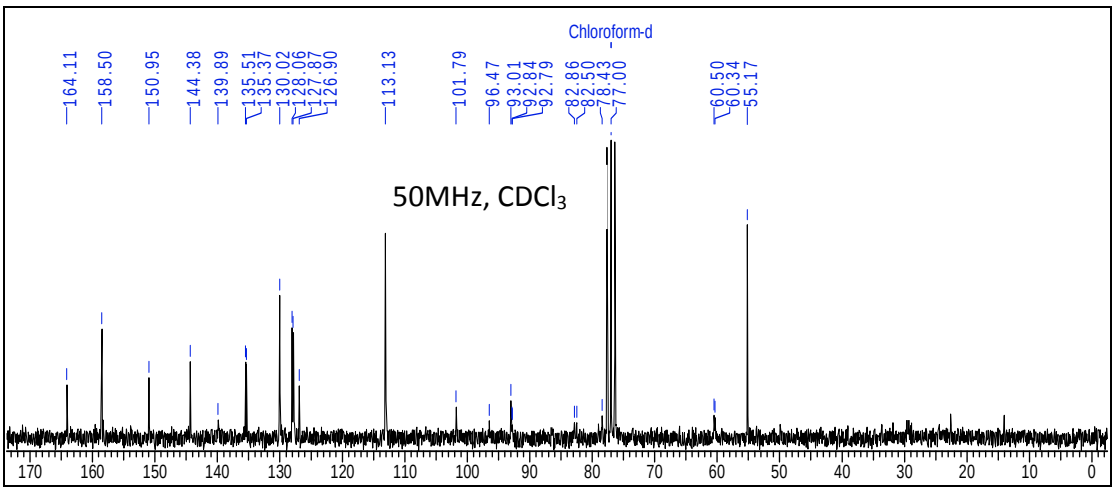

^{13}C-DEPT of compound 12

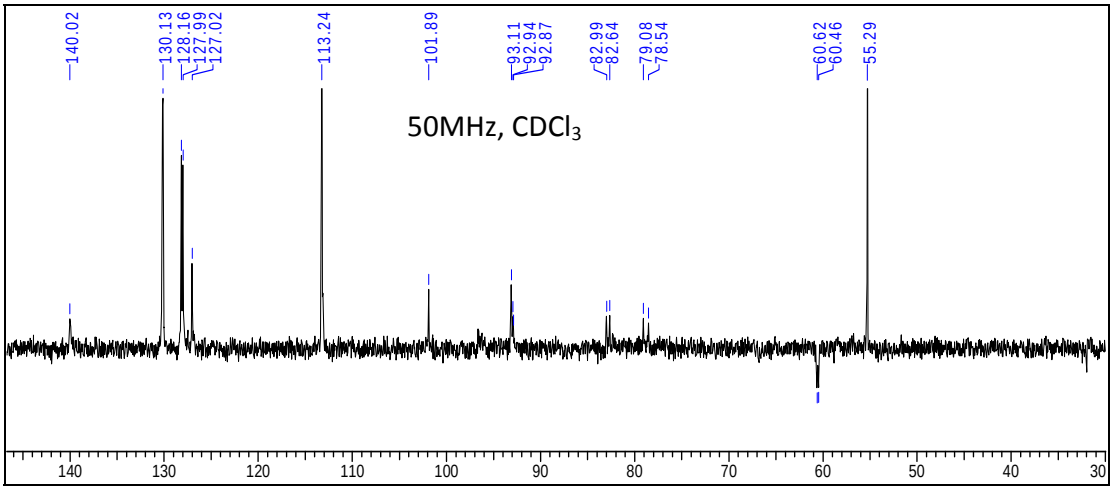

HRMS spectrum of Compound 12

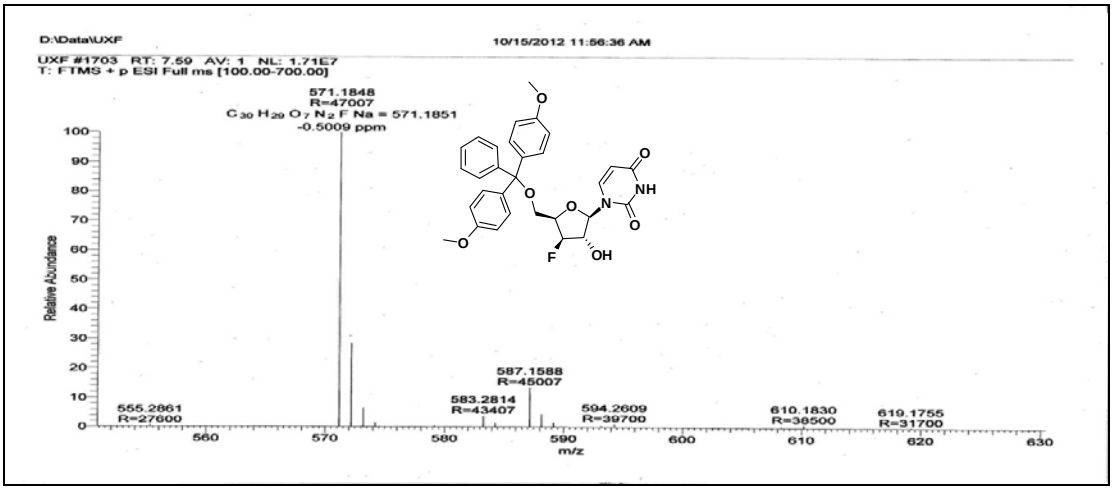

^{31}P NMR of compound 13

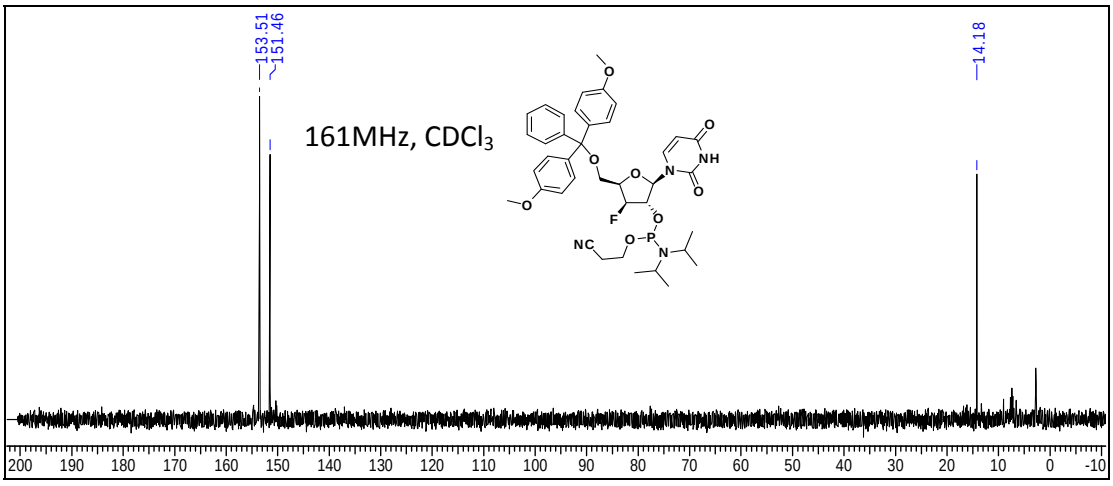

HRMS spectrum of Compound 13

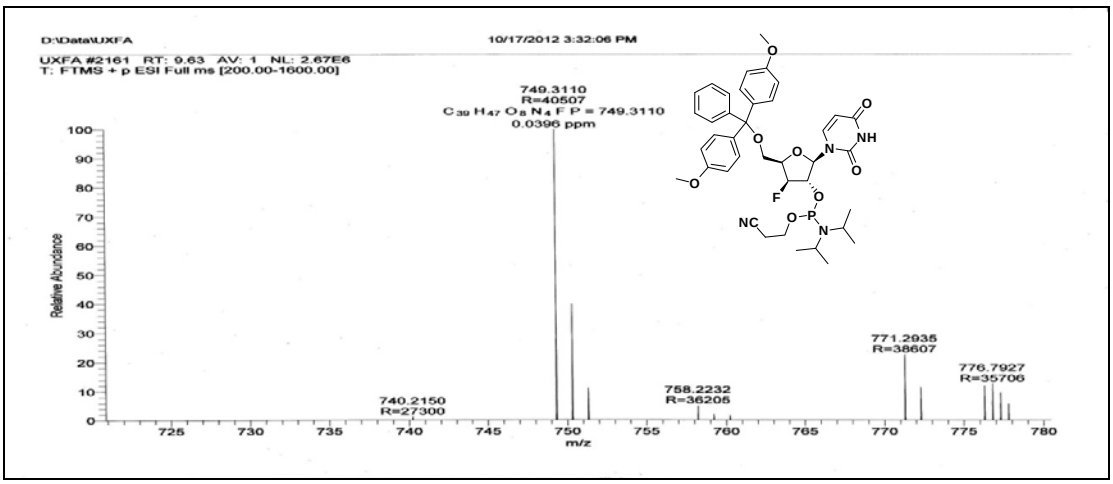

^{1}H NMR of compound 15

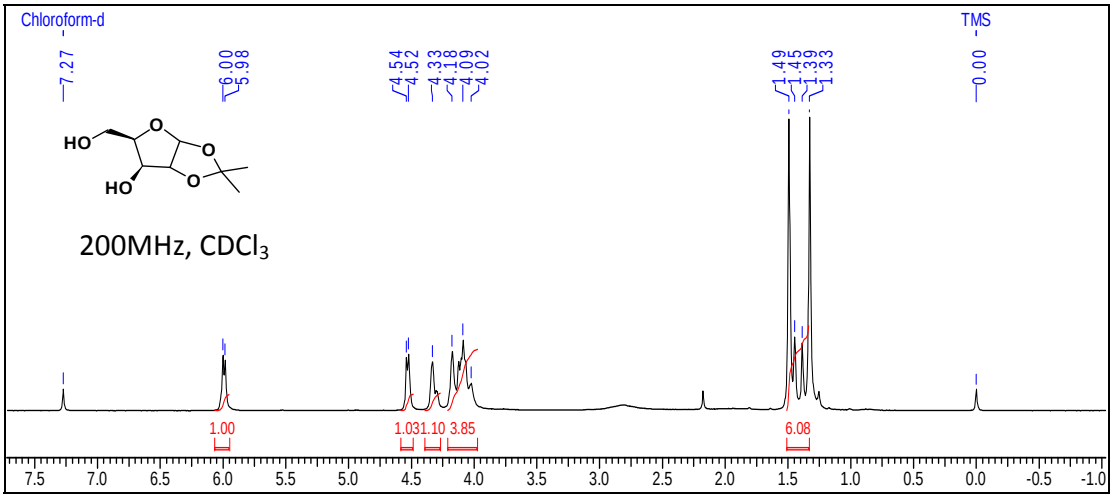

^{13}C NMR of compound 15

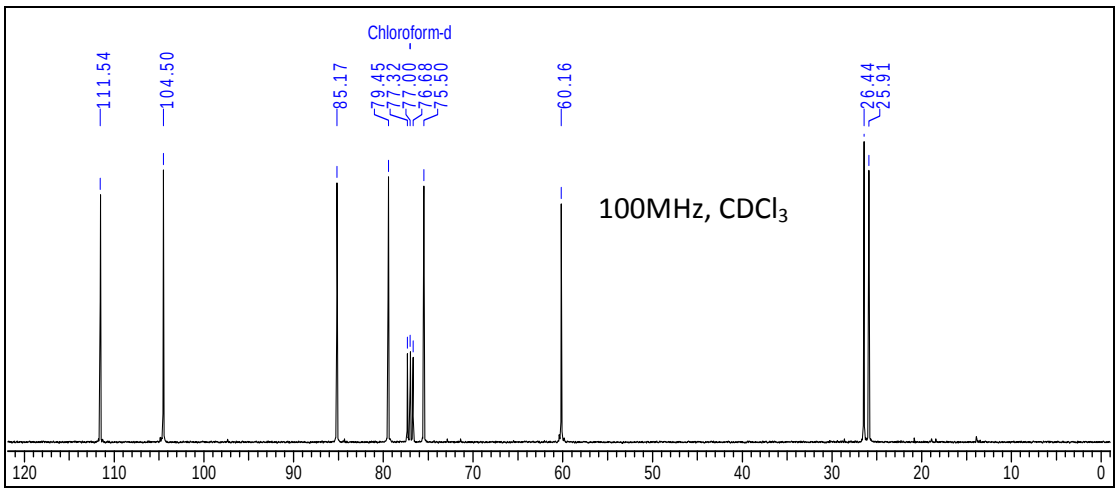

^{13}C-DEPT of compound 15

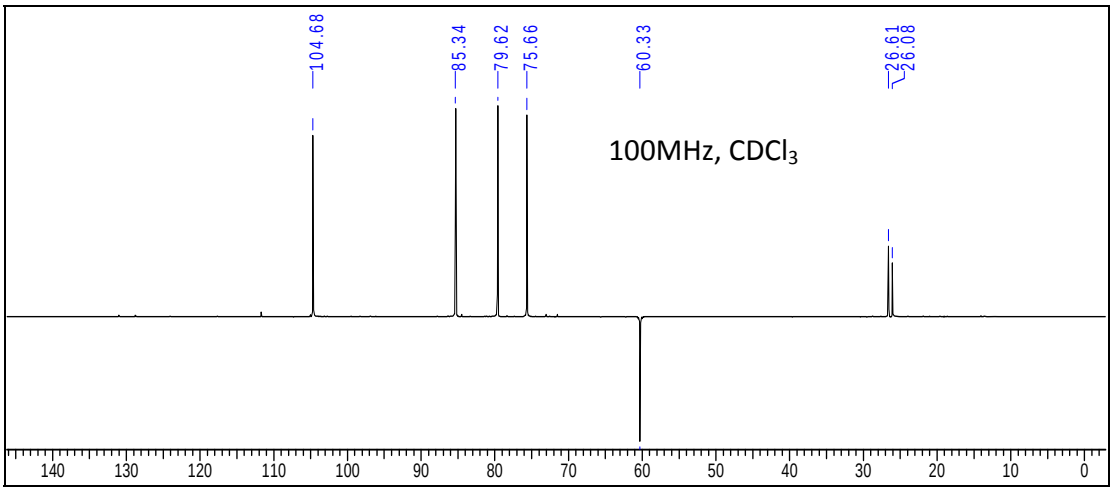

^{1}H NMR of compound 16

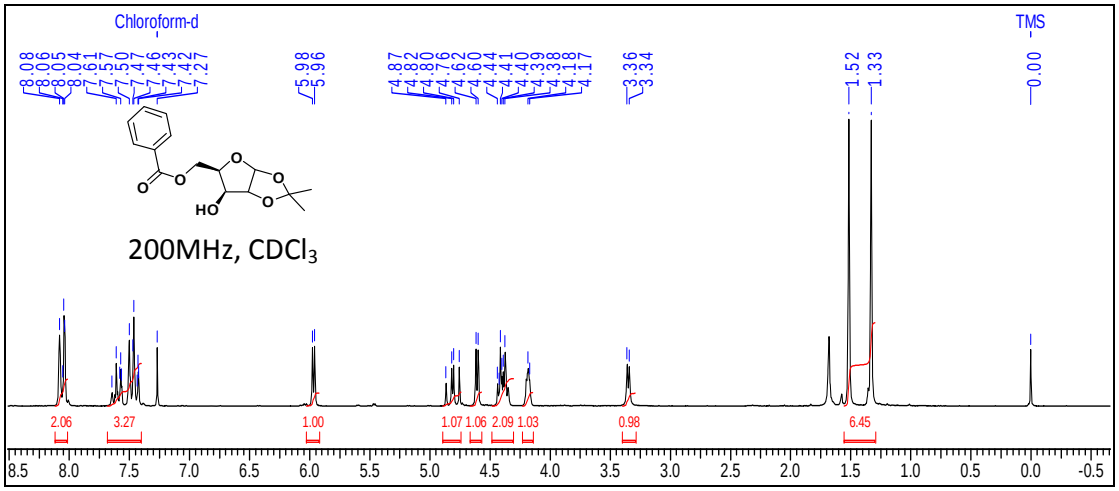

^{13}C NMR of compound 16

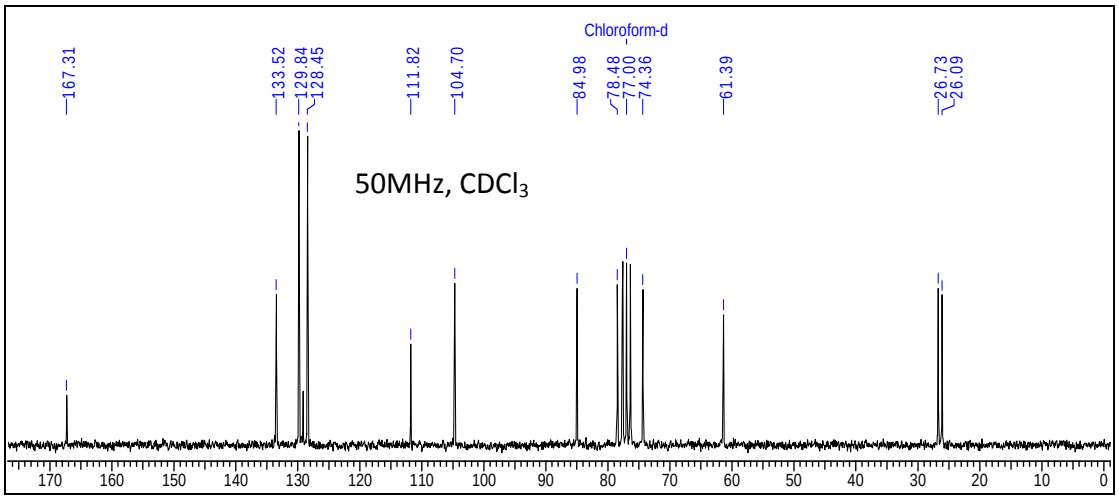

^{13}C-DEPT of compound 16

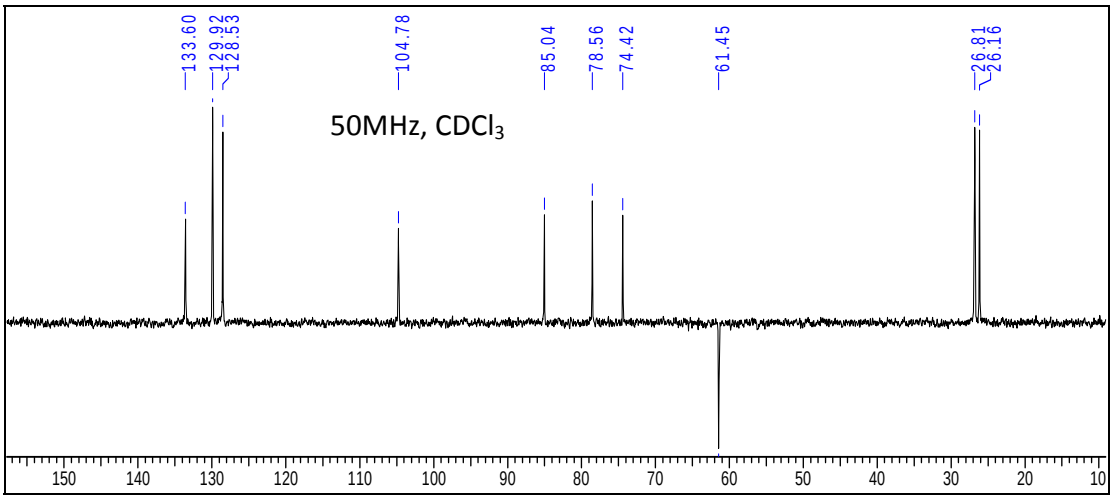

^{1}H NMR of compound 17

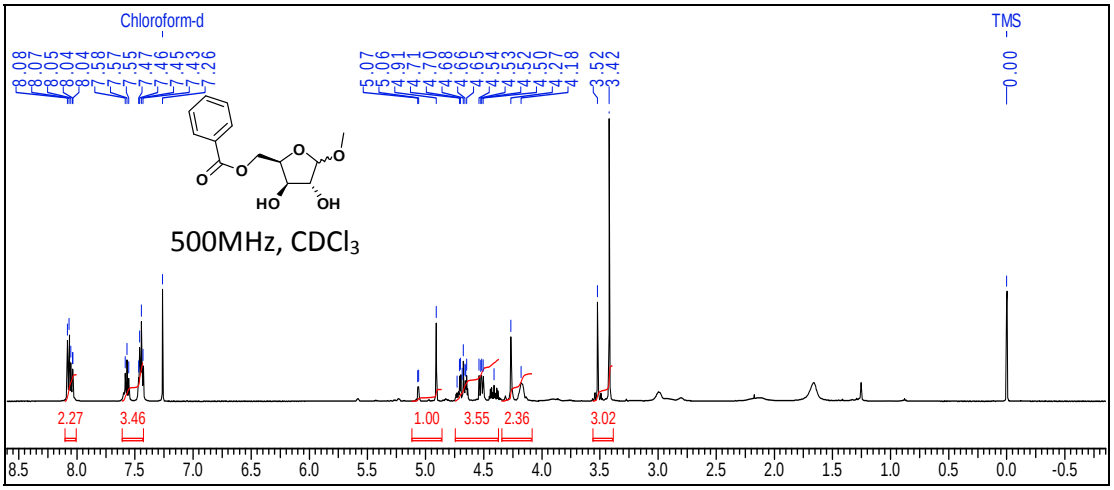

^{13}C NMR of compound 17

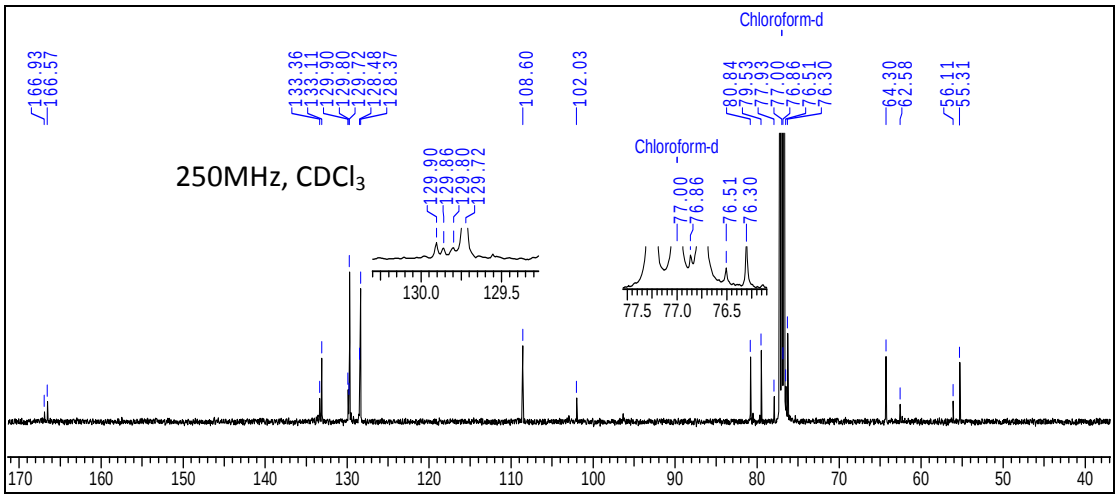

^{13}C-DEPT of compound 17

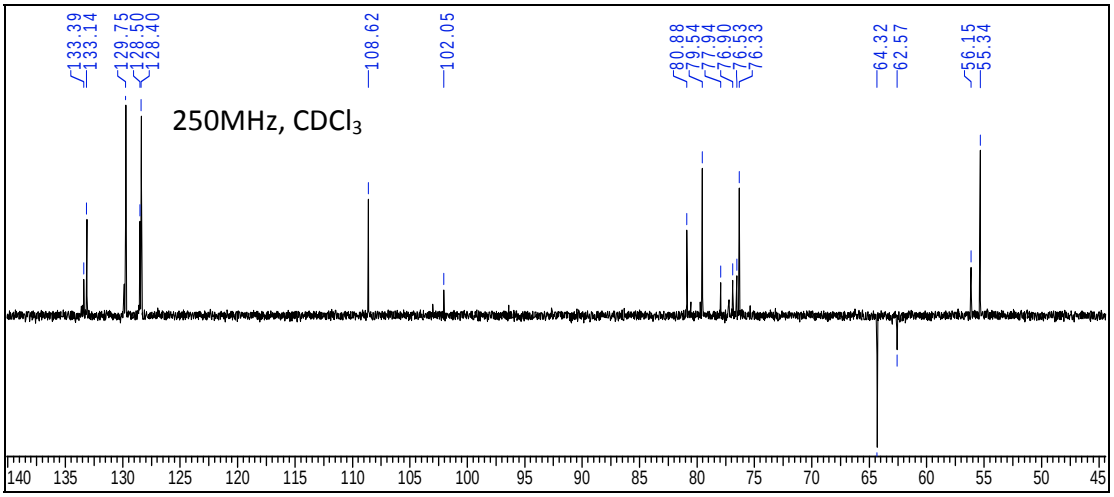

^{1}H NMR of compound 18

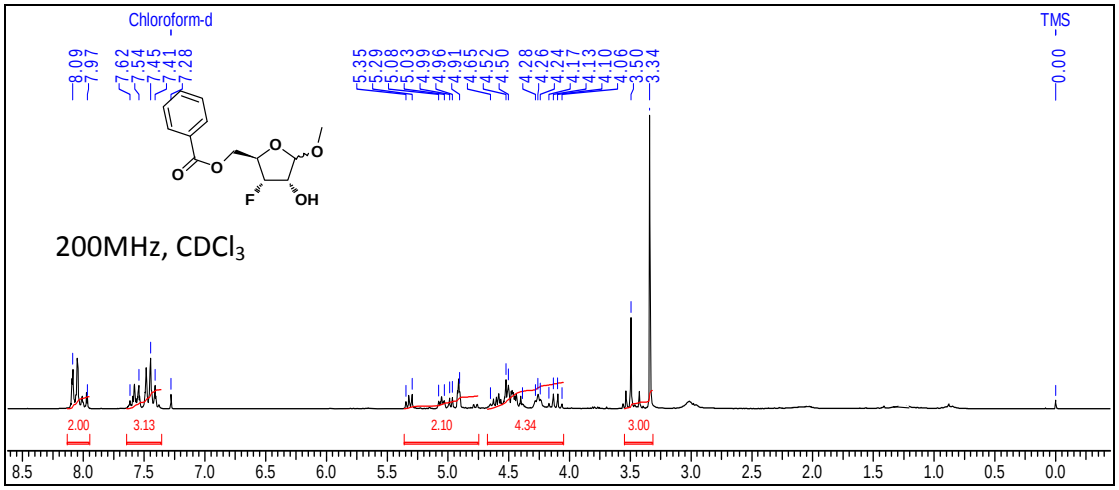

^{13}C NMR of compound 18

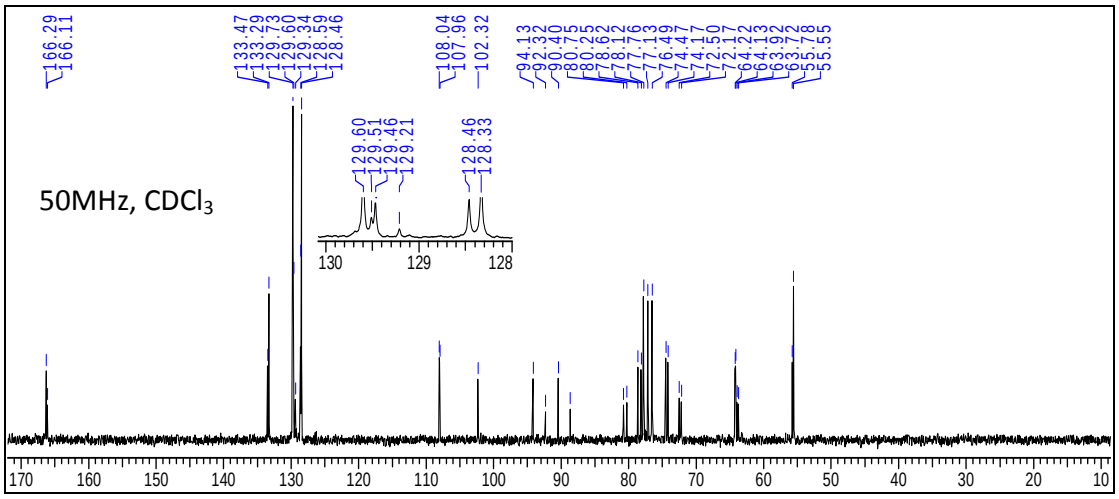

^{13}C-DEPT of compound 18

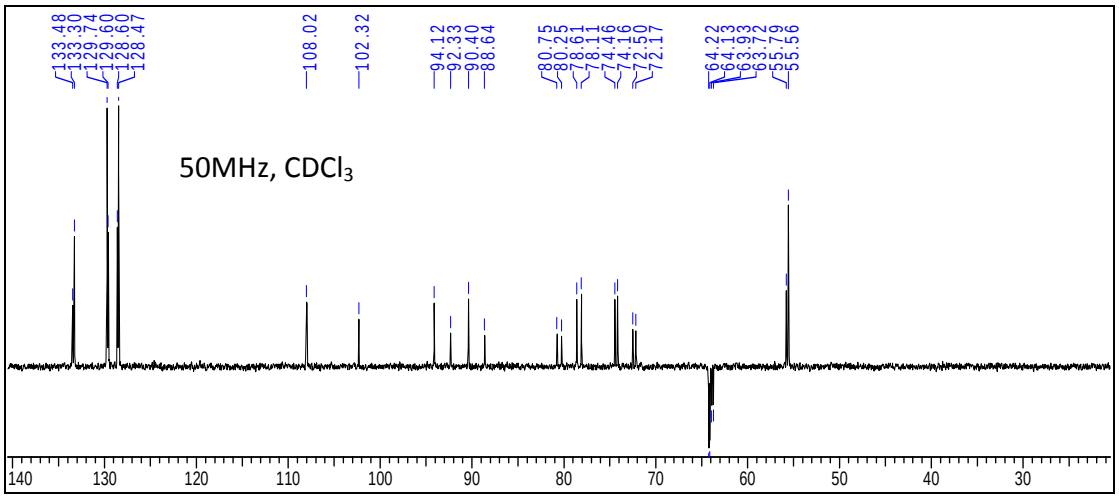

^{1}H NMR of compound 19

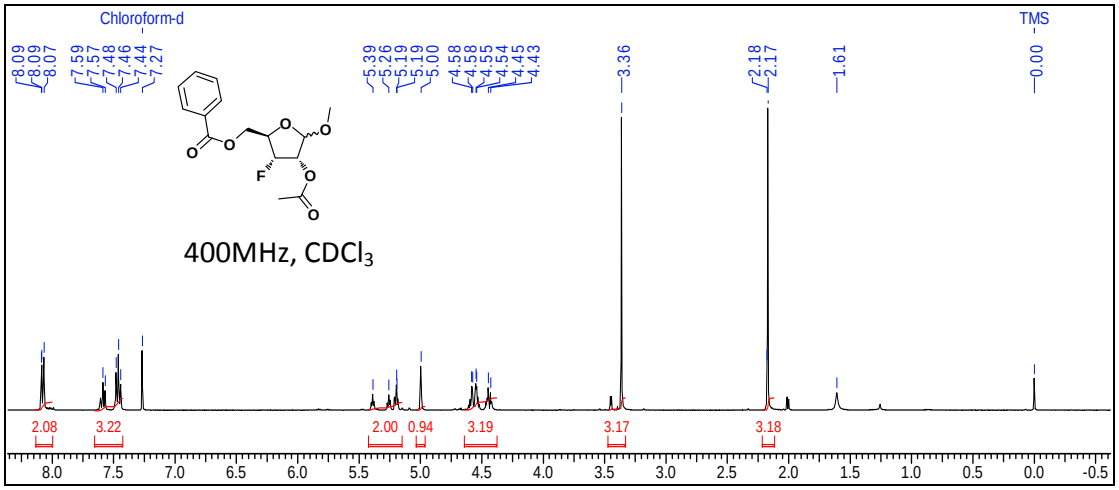

^{13}C NMR of compound 19

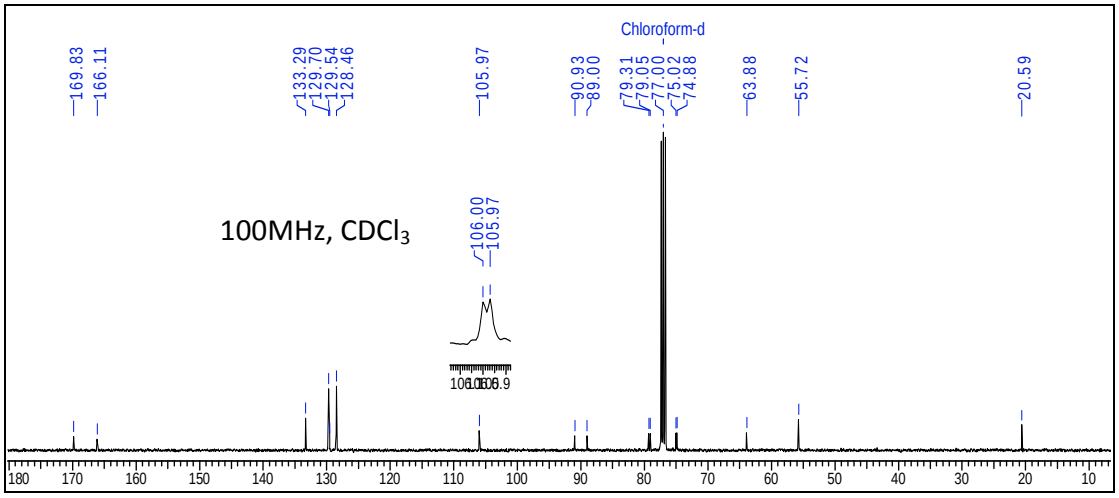

^{13}C-DEPT of compound 19

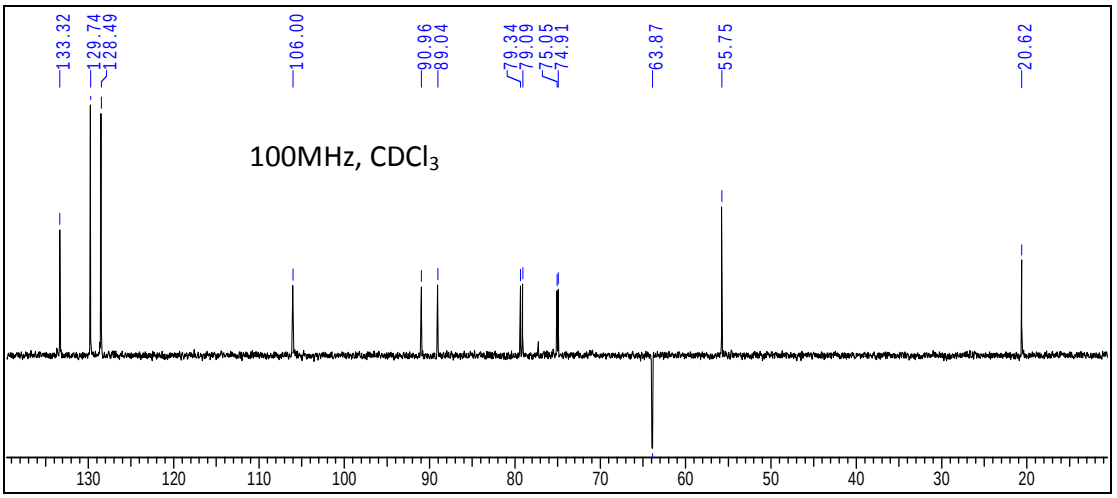

^{1}H NMR of compound 20

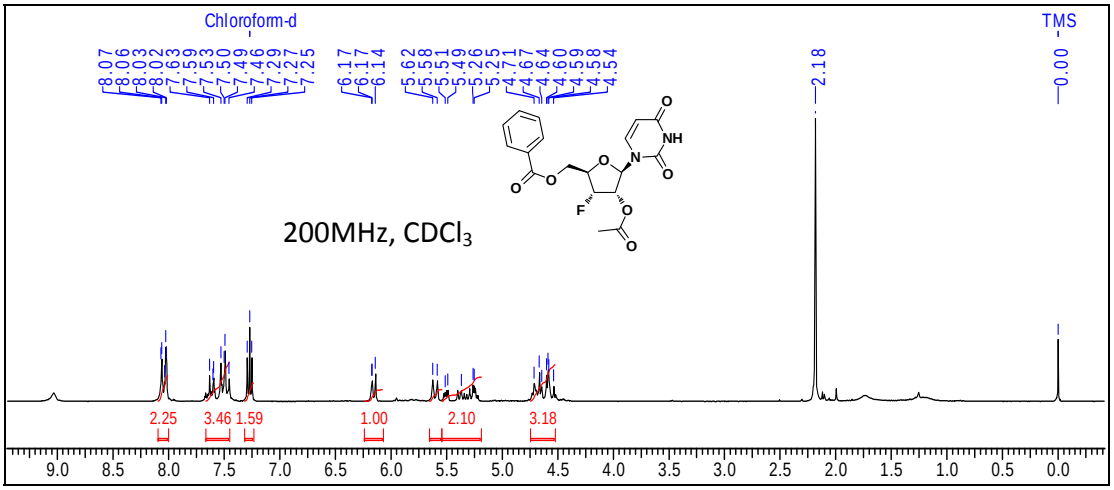

^{13}C NMR of compound 20

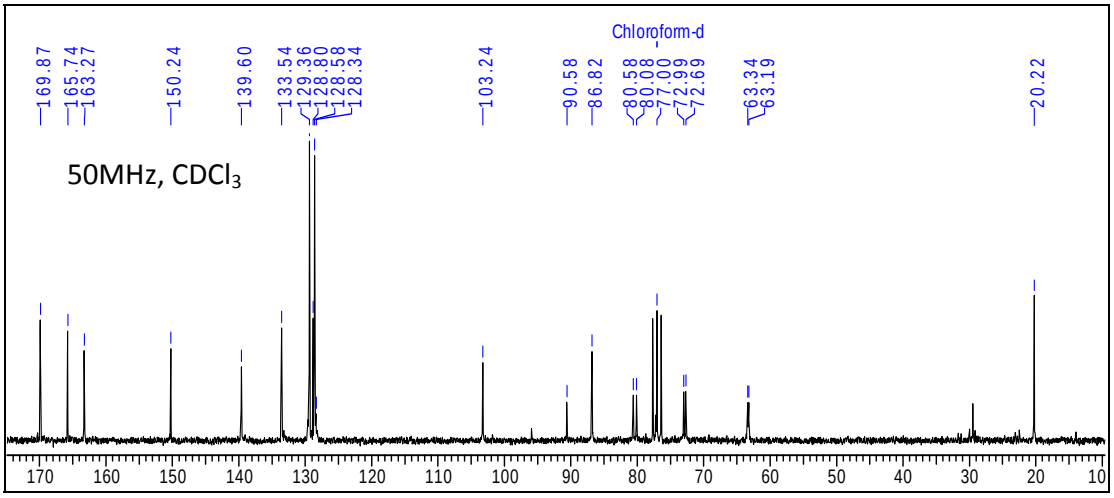

^{13}C-DEPT of compound 20

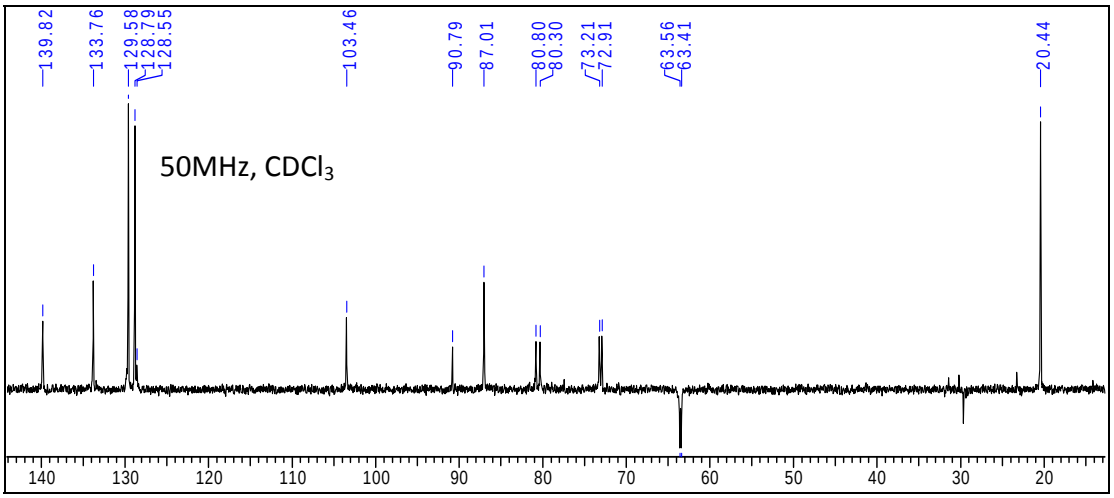

Mass of compound 20

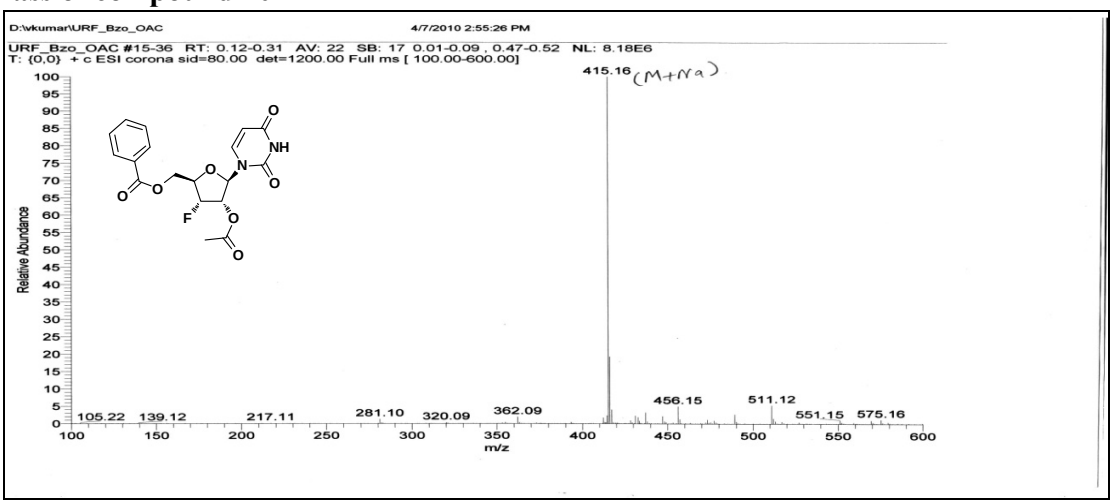

^{1}H NMR of compound 21

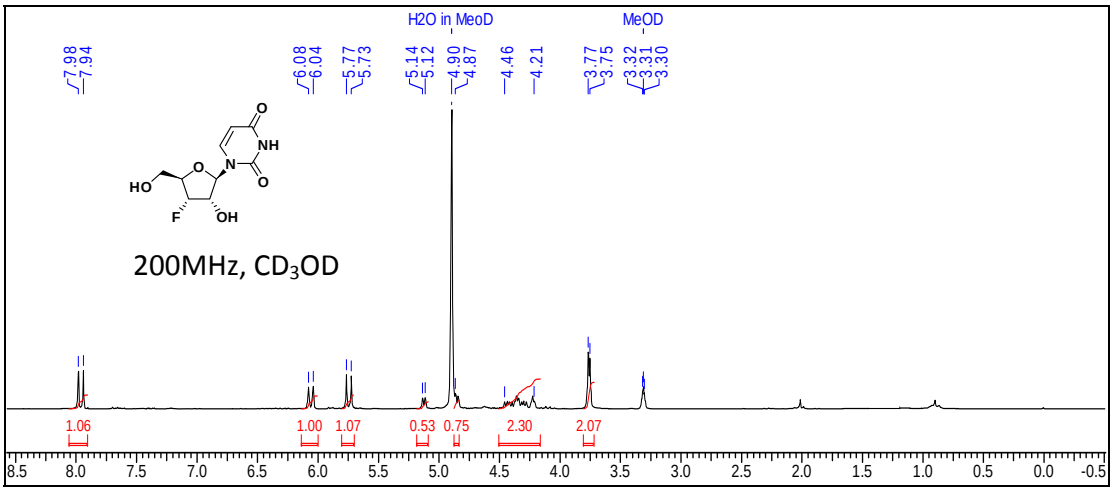

^{13}C NMR of compound 21

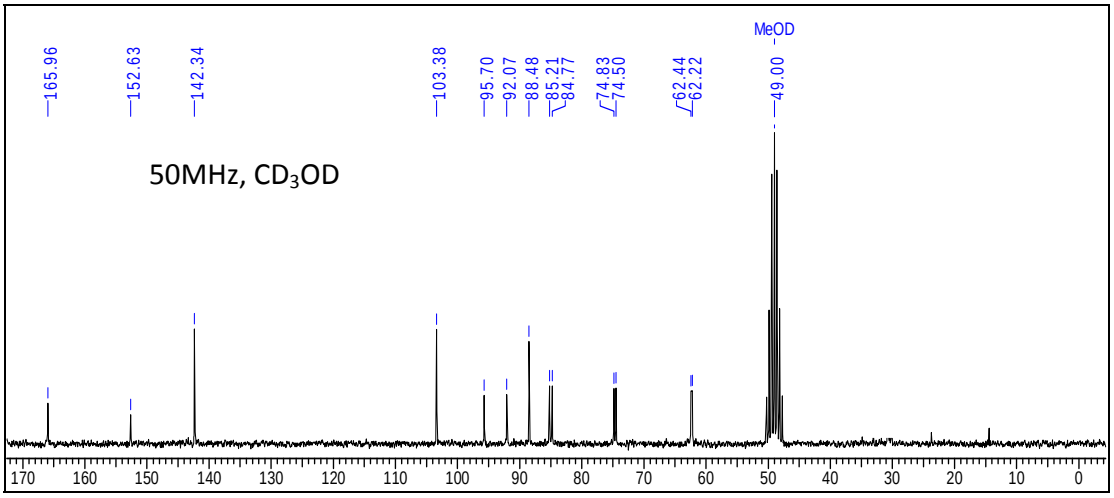

^{13}C-DEPT of compound 21

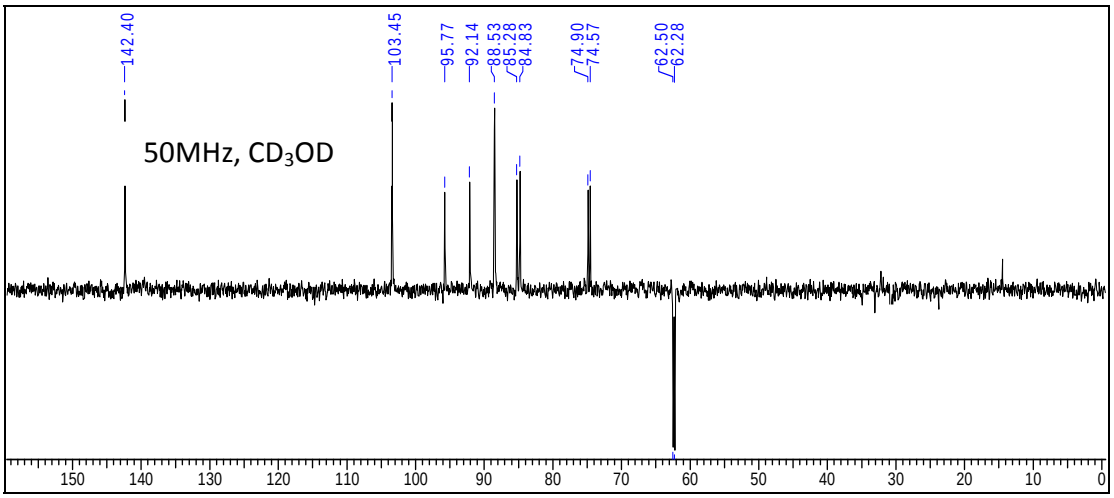

^{19}F NMR of compound 21

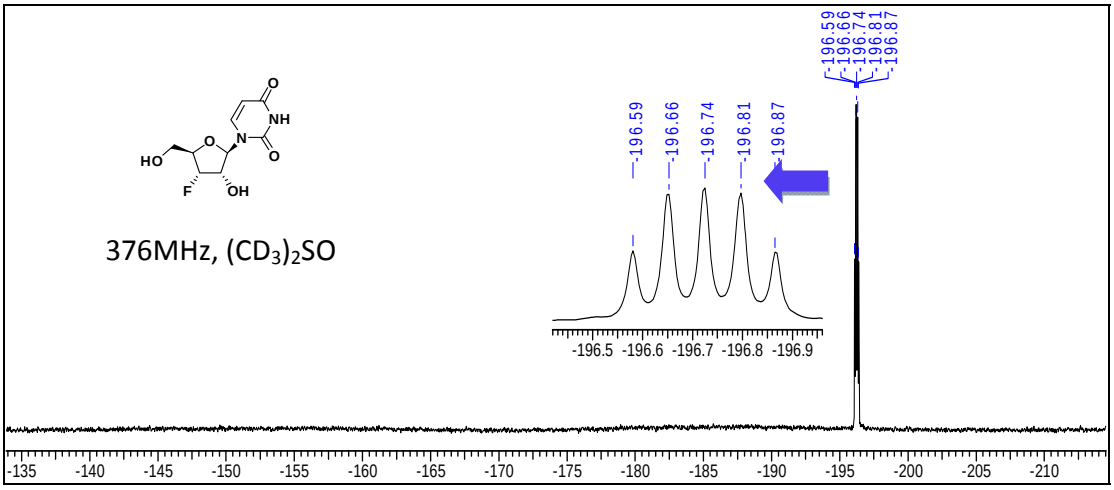

Mass of compound 21

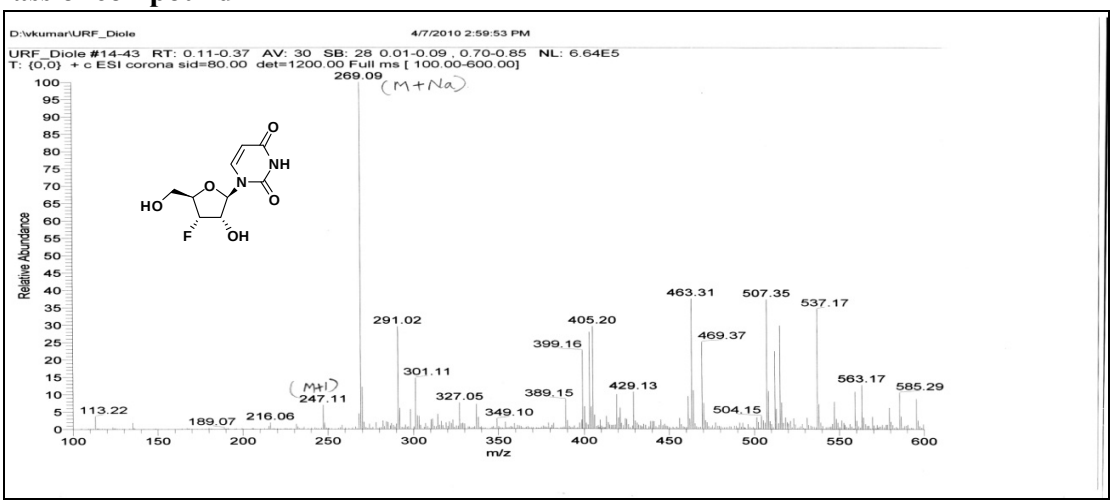

^{1}H NMR of compound 22

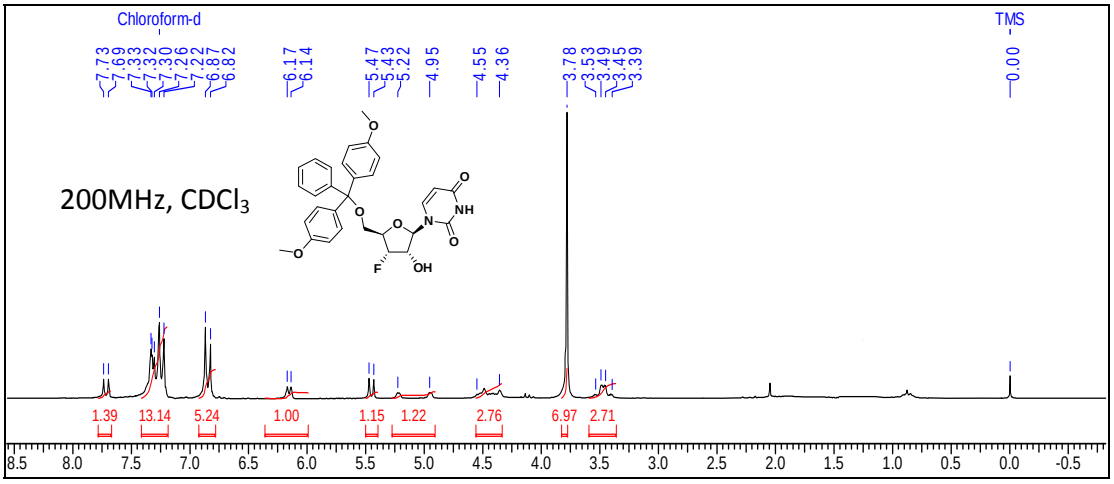

^{13}C NMR of compound 22

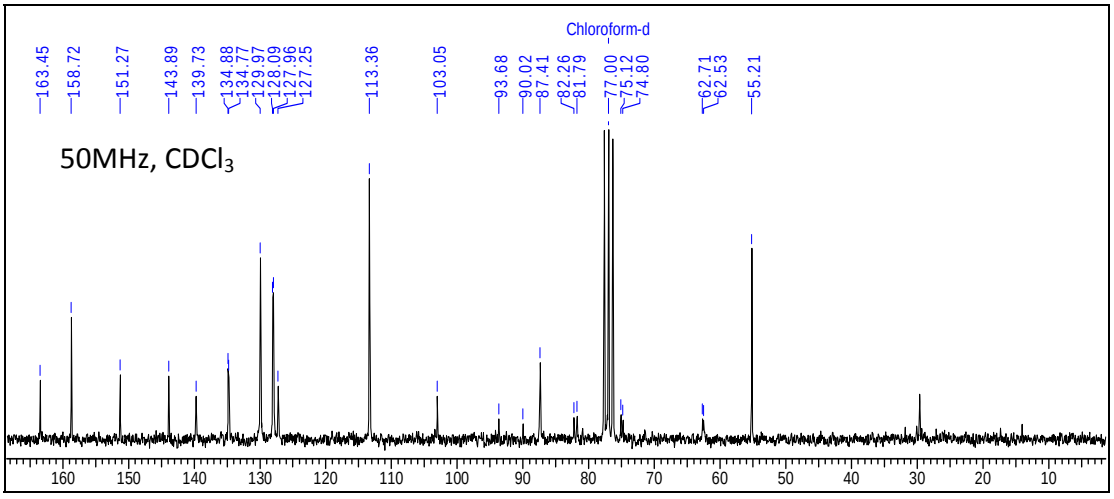

^{13}C-DEPT of compound 22

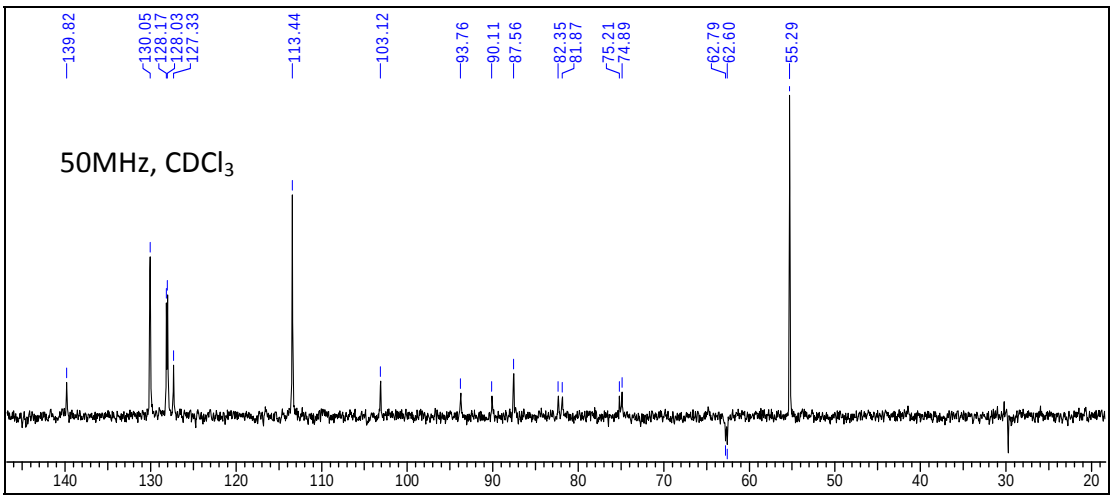

HRMS spectrum of Compound 22

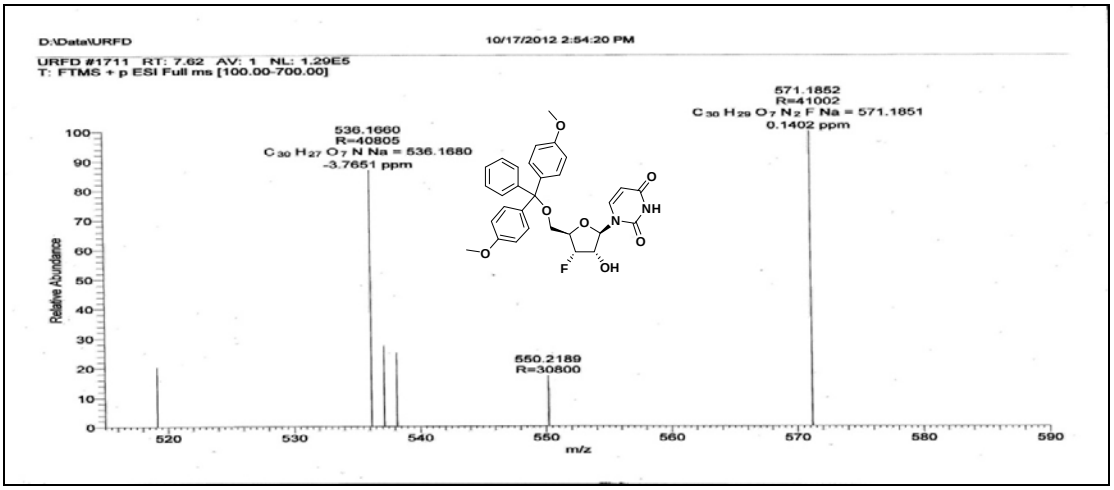

^{31}P NMR of compound 23

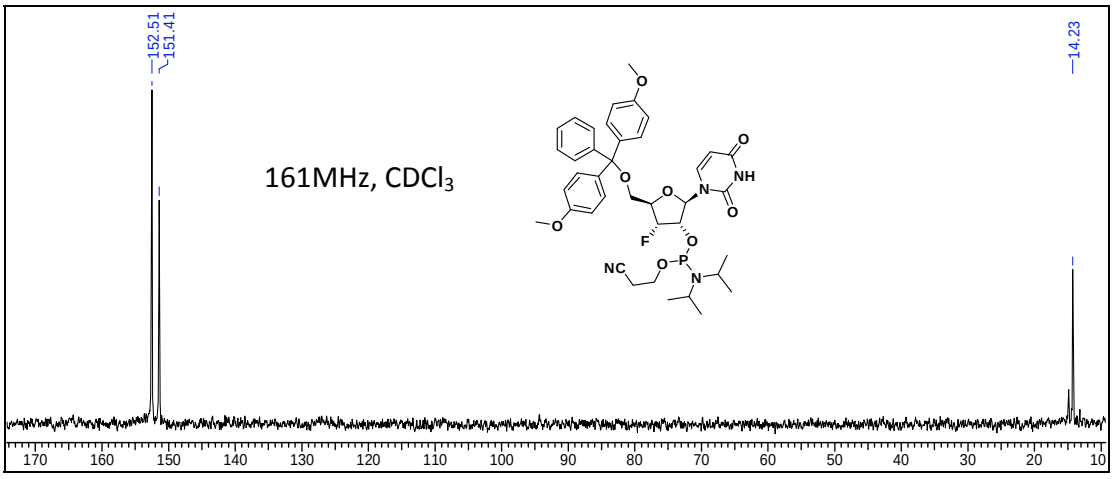

HRMS spectrum of Compound 23

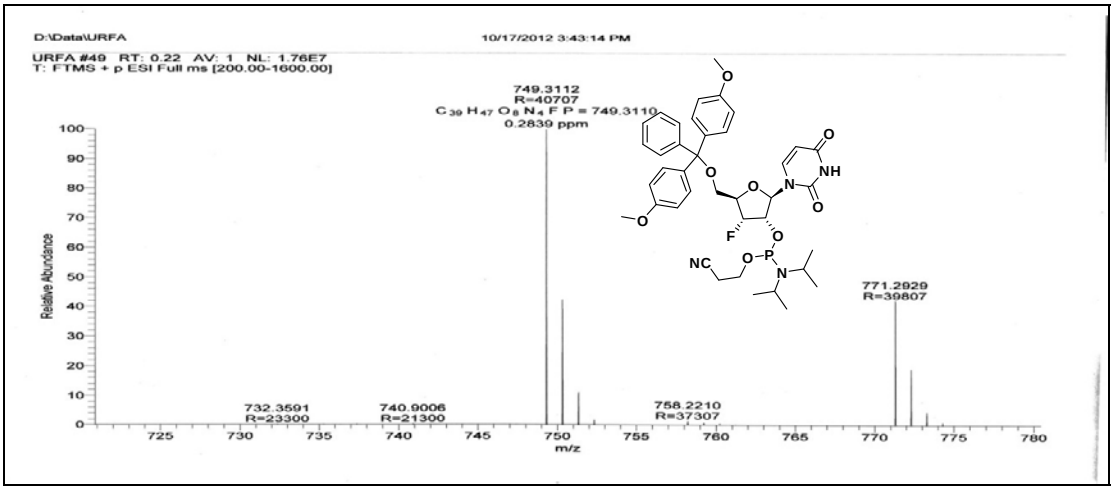

HPLC chromatograms of purified synthesized ngDNA

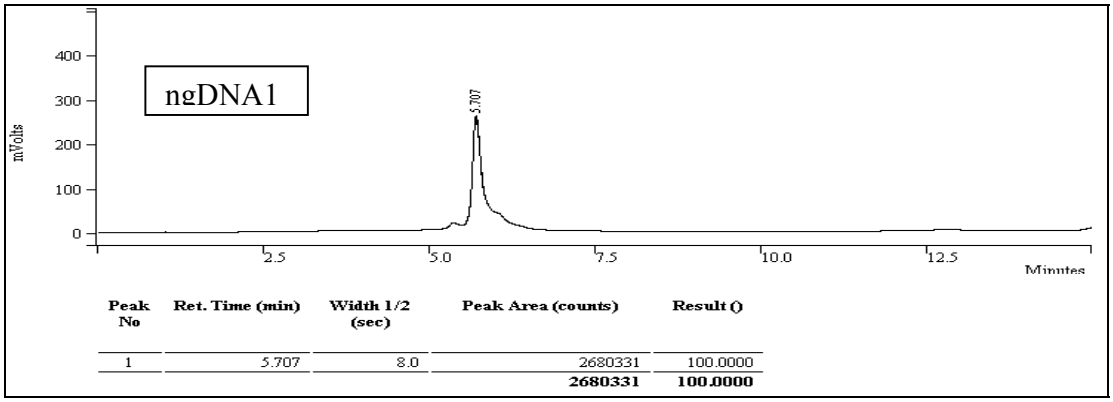

Peak No	Ret. Time (min)	Width 1/2 (sec)	Peak Area (counts)	Result ()
1	5.707	8.0	2680331	100.0000
			2680331	**100.0000**

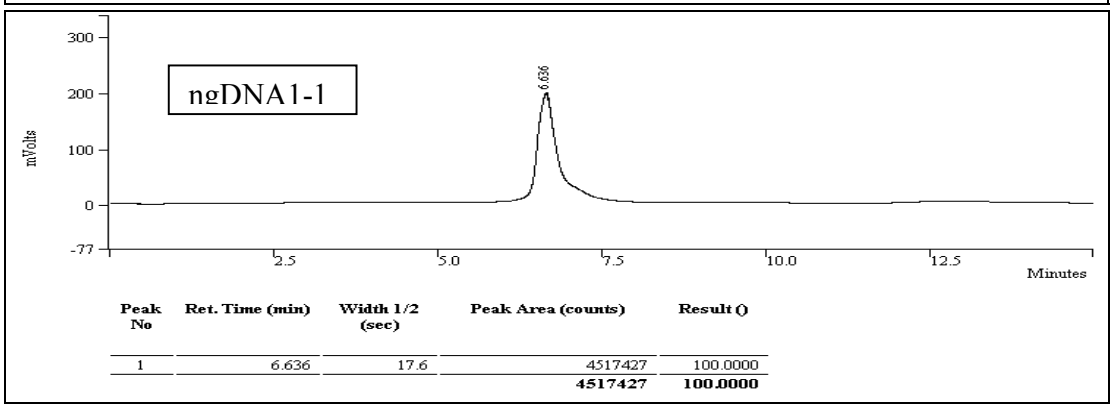

Peak No	Ret. Time (min)	Width 1/2 (sec)	Peak Area (counts)	Result ()
1	6.636	17.6	4517427	100.0000
			4517427	**100.0000**

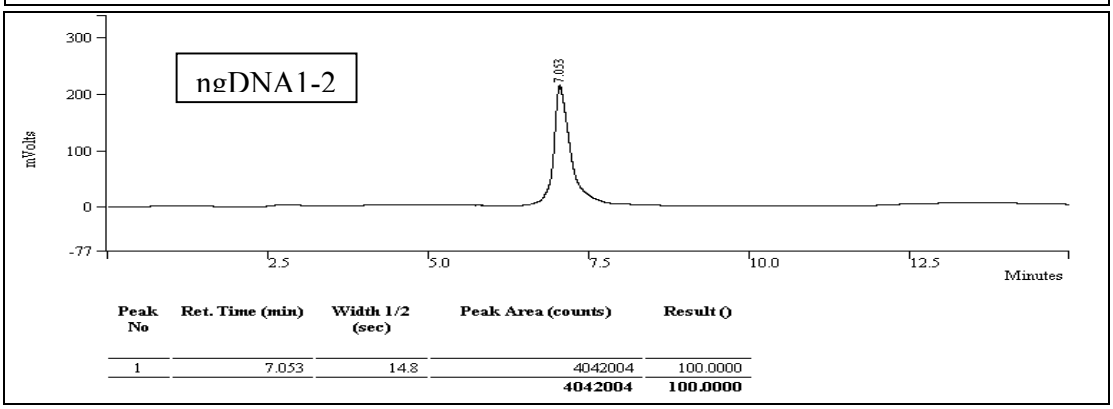

Peak No	Ret. Time (min)	Width 1/2 (sec)	Peak Area (counts)	Result ()
1	7.053	14.8	4042004	100.0000
			4042004	**100.0000**

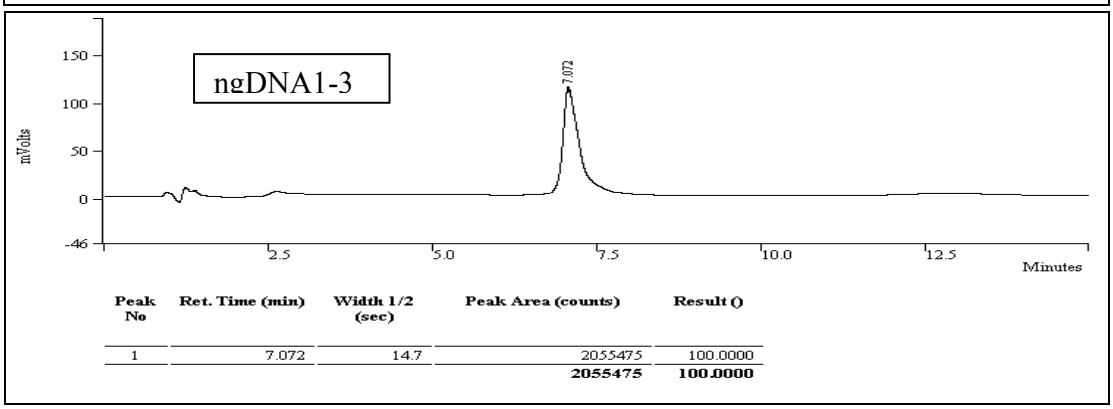

Peak No	Ret. Time (min)	Width 1/2 (sec)	Peak Area (counts)	Result ()
1	7.072	14.7	2055475	100.0000
			2055475	**100.0000**

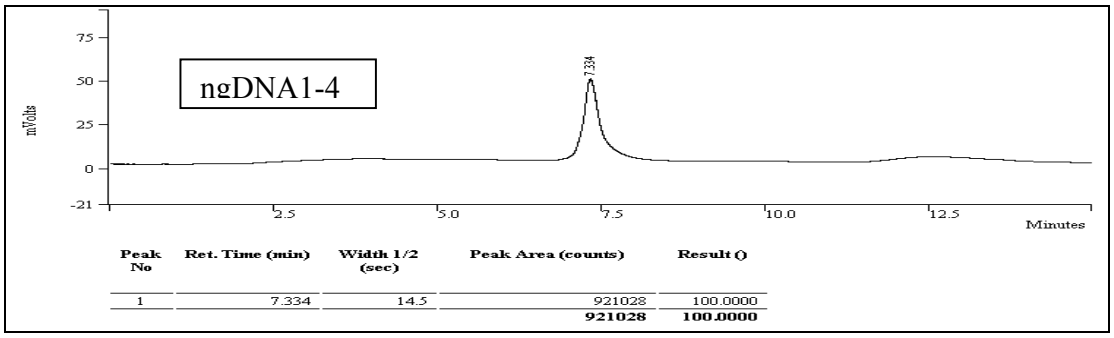

Peak No	Ret. Time (min)	Width 1/2 (sec)	Peak Area (counts)	Result ()
1	7.334	14.5	921028	100.0000
			921028	**100.0000**

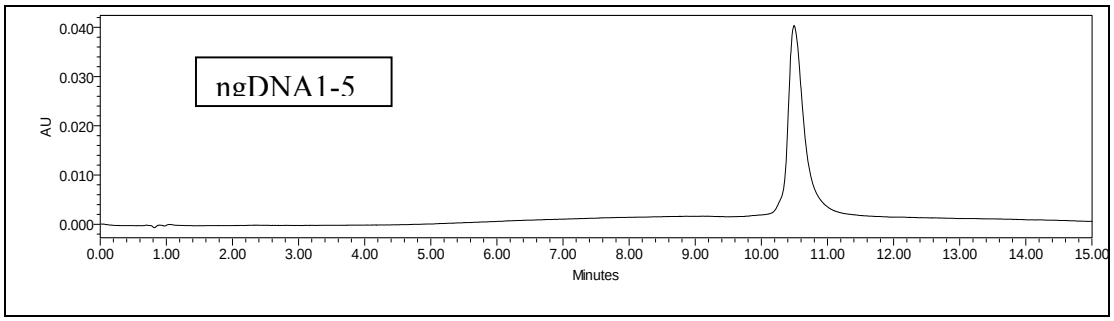

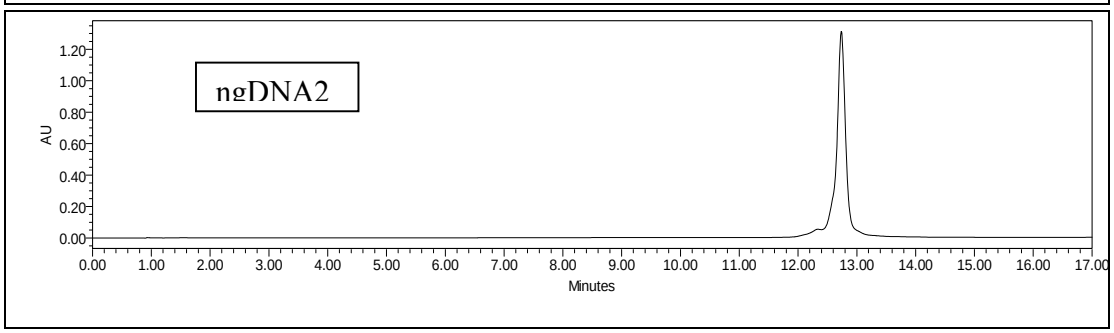

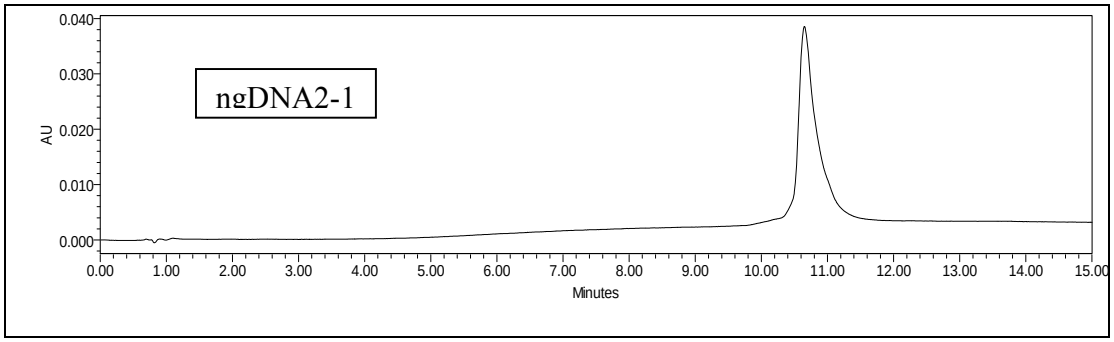

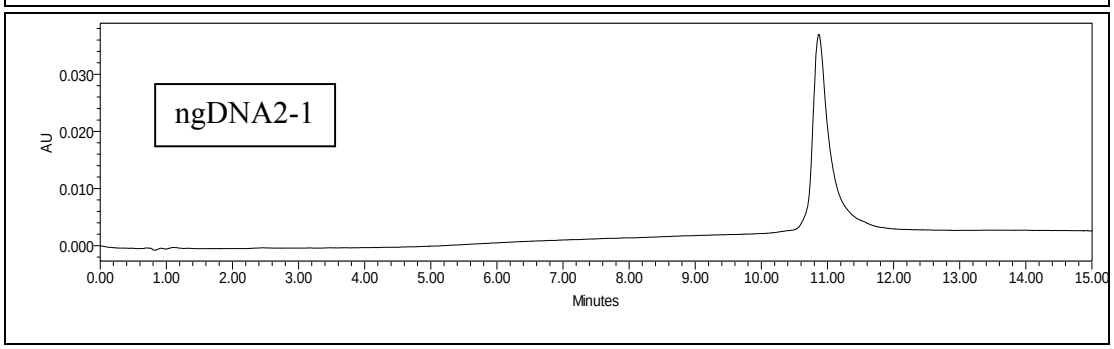

MALDI-TOF mass spectrum of ngDNA

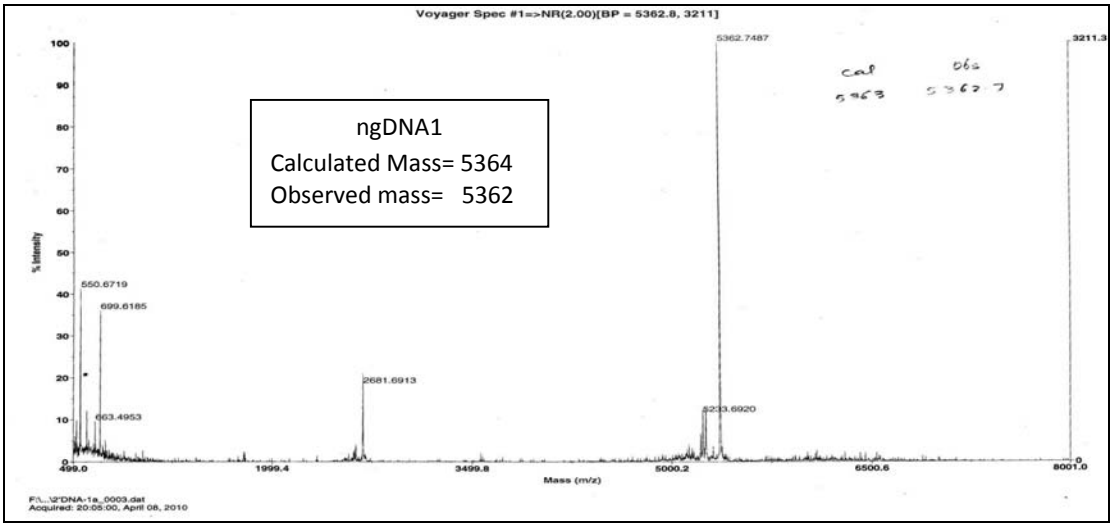

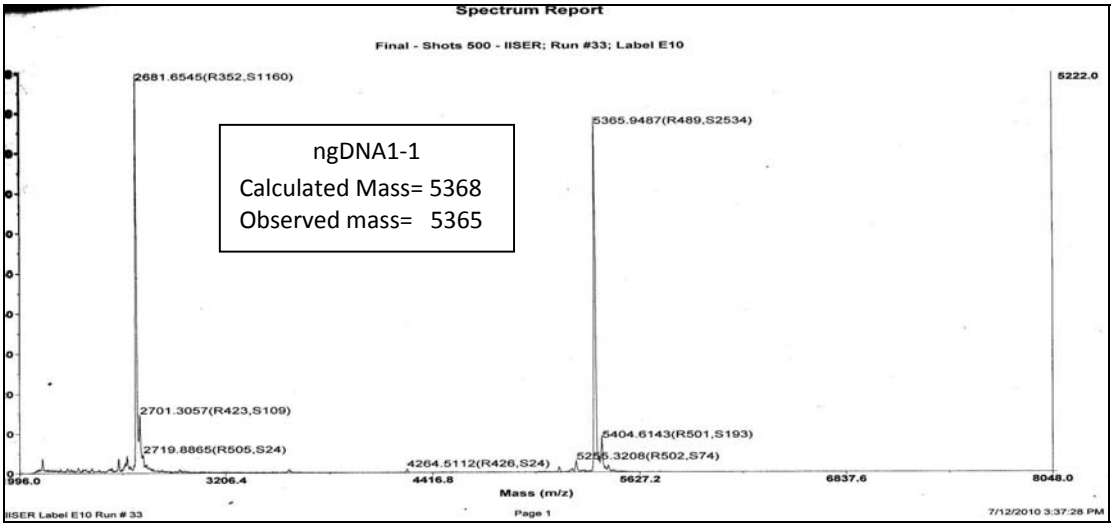

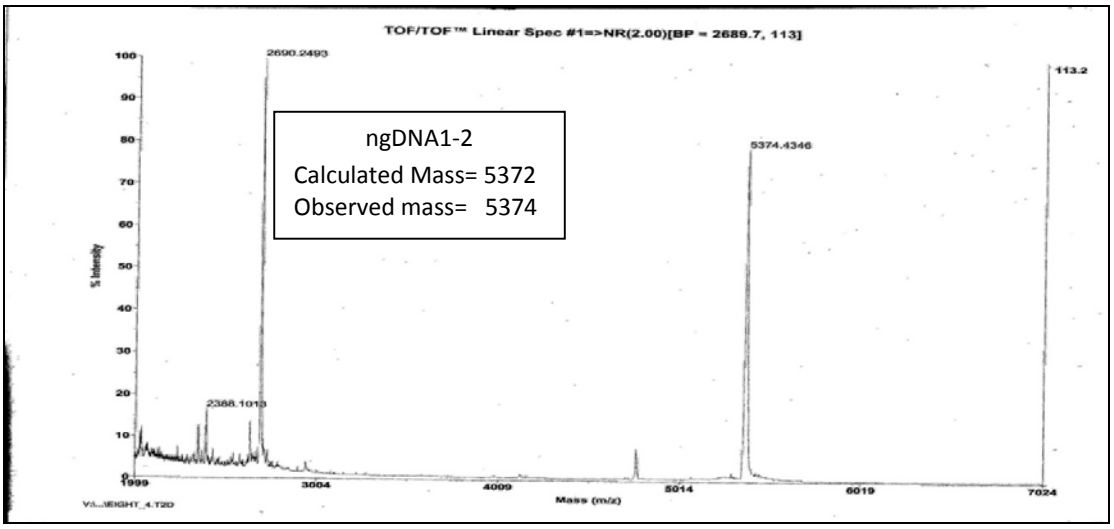

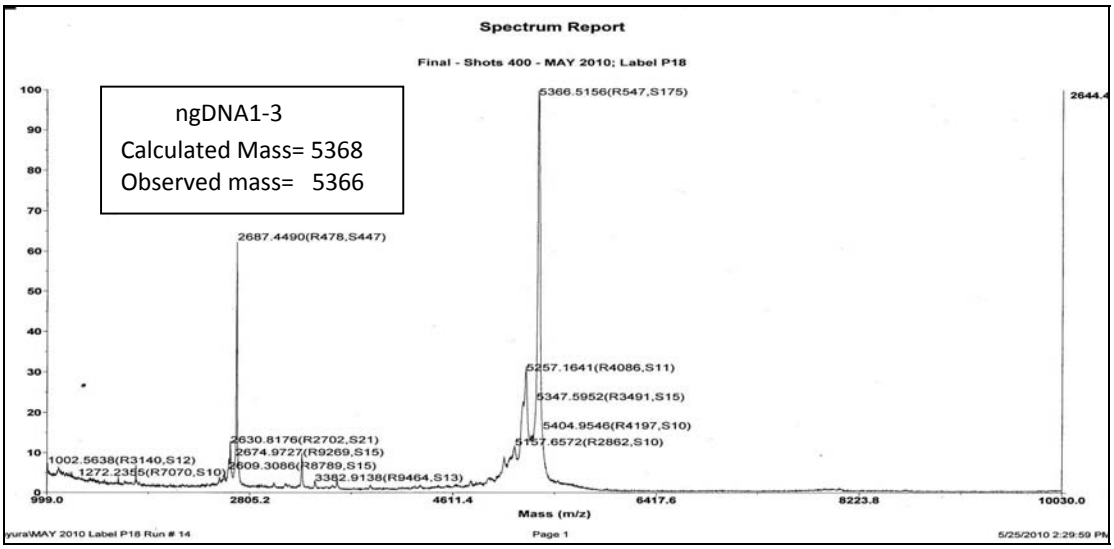
Spectrum Report
Final - Shots 400 - MAY 2010; Label P18
ngDNA1-3
Calculated Mass= 5368
Observed mass= 5366
5366.5156(R547,S175)
2687.4490(R478,S447)
5257.1641(R4086,S11)
5347.5952(R3491,S15)
5404.9546(R4197,S10)
5157.6572(R2862,S10)
2630.8176(R2702,S21)
2674.9727(R9269,S15)
2609.3086(R8789,S15)
3362.9138(R9464,S13)
1002.5638(R3140,S12)
1272.2355(R7070,S10)
Mass (m/z)

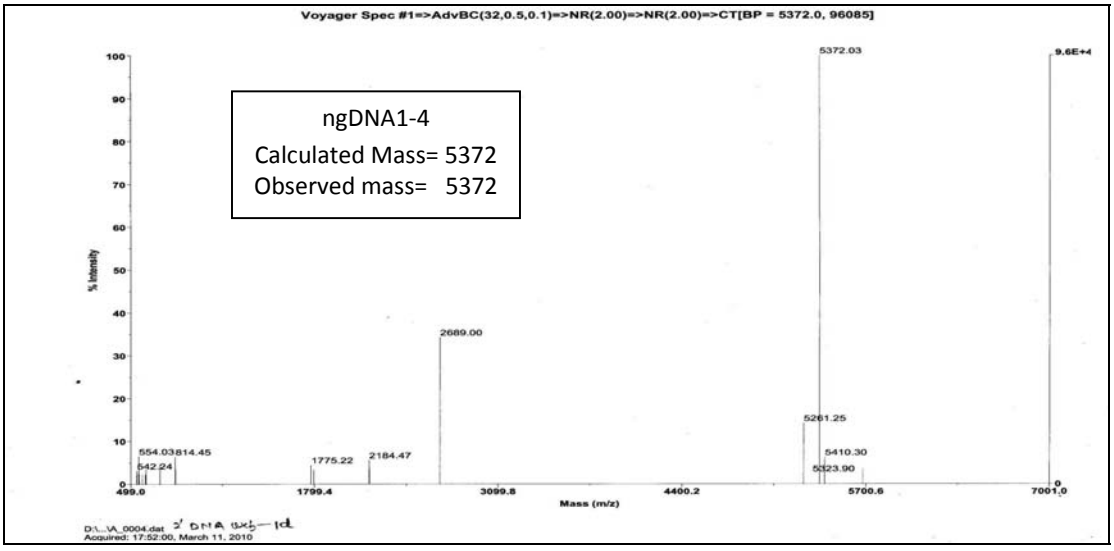
Voyager Spec #1=>AdvBC(32,0.5,0.1)=>NR(2.00)=>NR(2.00)=>CT[BP = 5372.0, 96085]
ngDNA1-4
Calculated Mass= 5372
Observed mass= 5372
5372.03
2689.00
5261.25
554.03814.45
542.24
1775.22
2184.47
5410.30
5323.90
% Intensity
Mass (m/z)

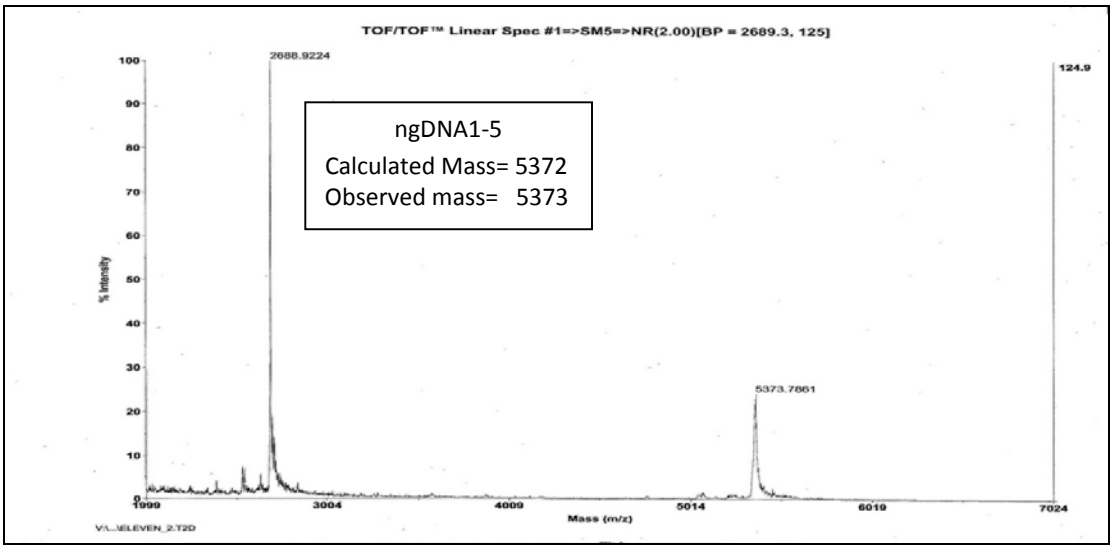
TOF/TOF™ Linear Spec #1=>SM5=>NR(2.00)[BP = 2689.3, 125]
ngDNA1-5
Calculated Mass= 5372
Observed mass= 5373
2688.9224
5373.7861
% Intensity
Mass (m/z)

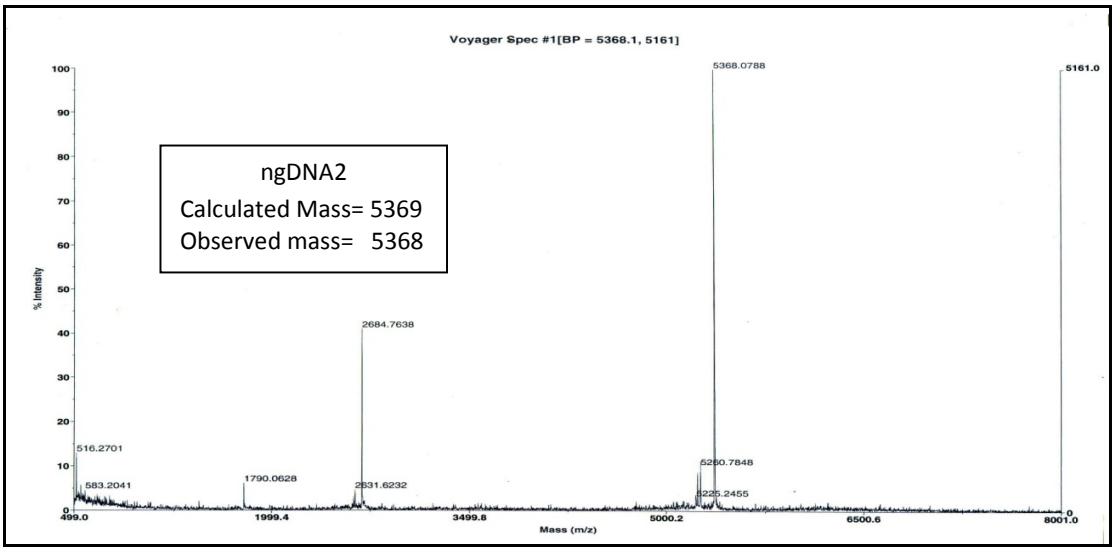
Voyager Spec #1[BP = 5368.1, 5161]
ngDNA2
Calculated Mass= 5369
Observed mass= 5368
5368.0788
5161.0
2684.7638
516.2701
583.2041
1790.0628
2931.6232
5260.7848
5225.2455
% Intensity
Mass (m/z)

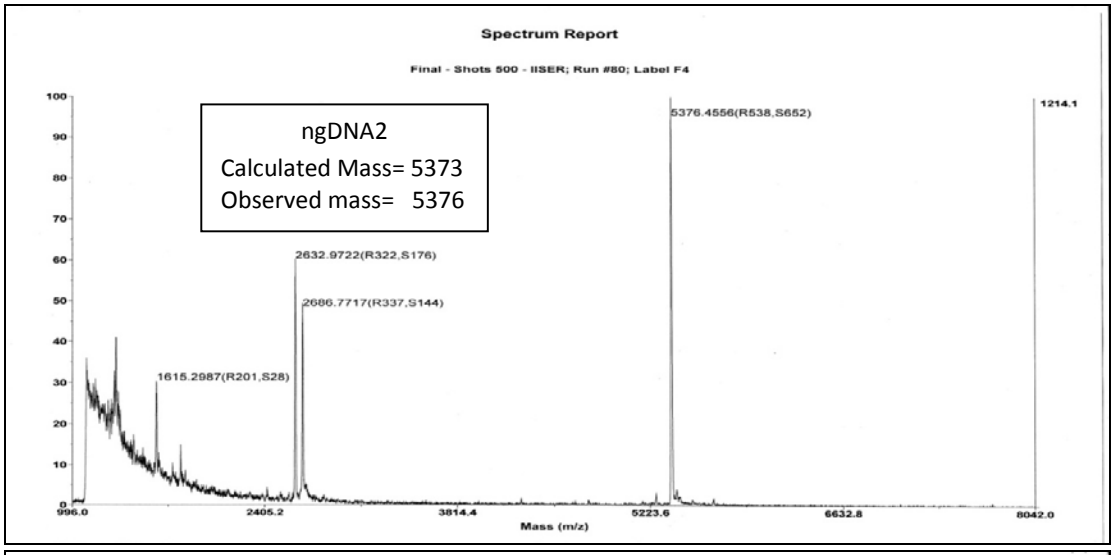
Spectrum Report
Final - Shots 500 - IISER; Run #80; Label F4
ngDNA2
Calculated Mass= 5373
Observed mass= 5376
5376.4556(R538,S652)
1214.1
2632.9722(R322,S176)
2686.7717(R337,S144)
1615.2987(R201,S28)
Mass (m/z)

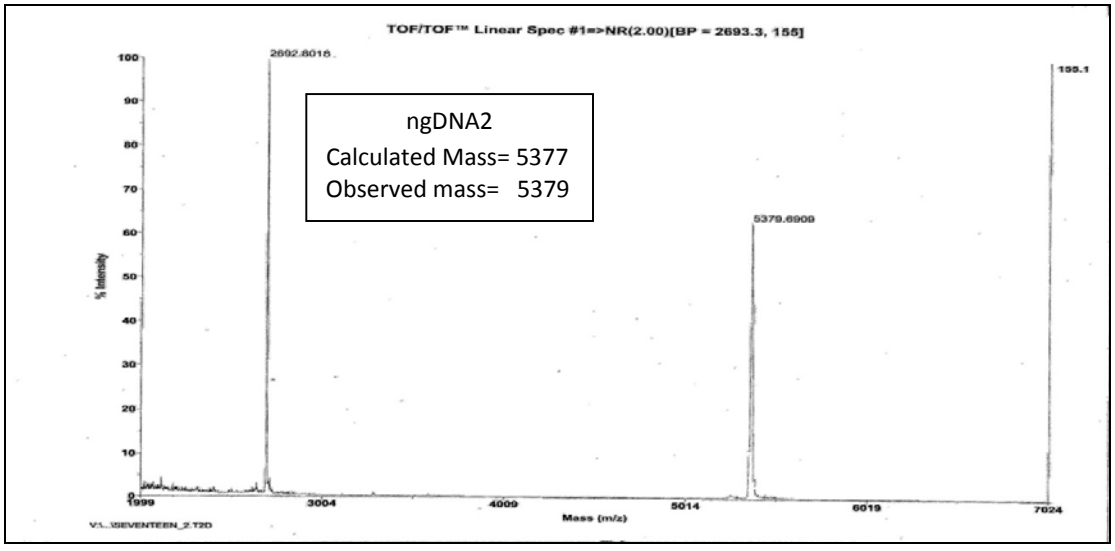
TOF/TOF™ Linear Spec #1=>NR(2.00)[BP = 2693.3, 155]
ngDNA2
Calculated Mass= 5377
Observed mass= 5379
2692.8018
155.1
5379.6909
% Intensity
Mass (m/z)

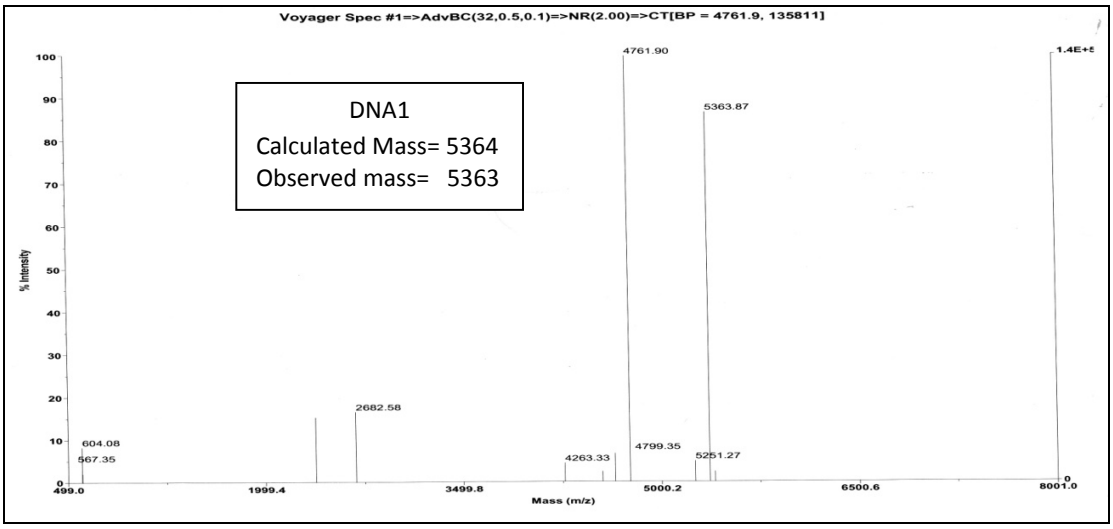
Voyager Spec #1=>AdvBC(32,0.5,0.1)=>NR(2.00)=>CT[BP = 4761.9, 135811]
DNA1
Calculated Mass= 5364
Observed mass= 5363
% Intensity
Mass (m/z)
4761.90
5363.87
2682.58
604.08
567.35
4263.33
4799.35
5251.27

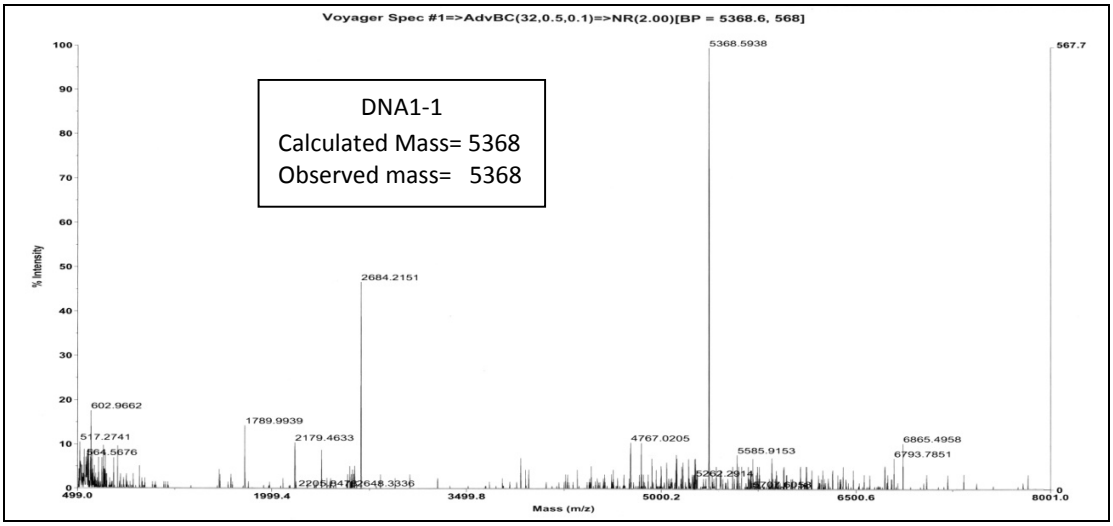
Voyager Spec #1=>AdvBC(32,0.5,0.1)=>NR(2.00)[BP = 5368.6, 568]
DNA1-1
Calculated Mass= 5368
Observed mass= 5368
% Intensity
Mass (m/z)
5368.5938
567.7
2684.2151
602.9662
1789.9939
517.2741
2179.4633
4767.0205
5585.9153
6865.4958
6793.7851

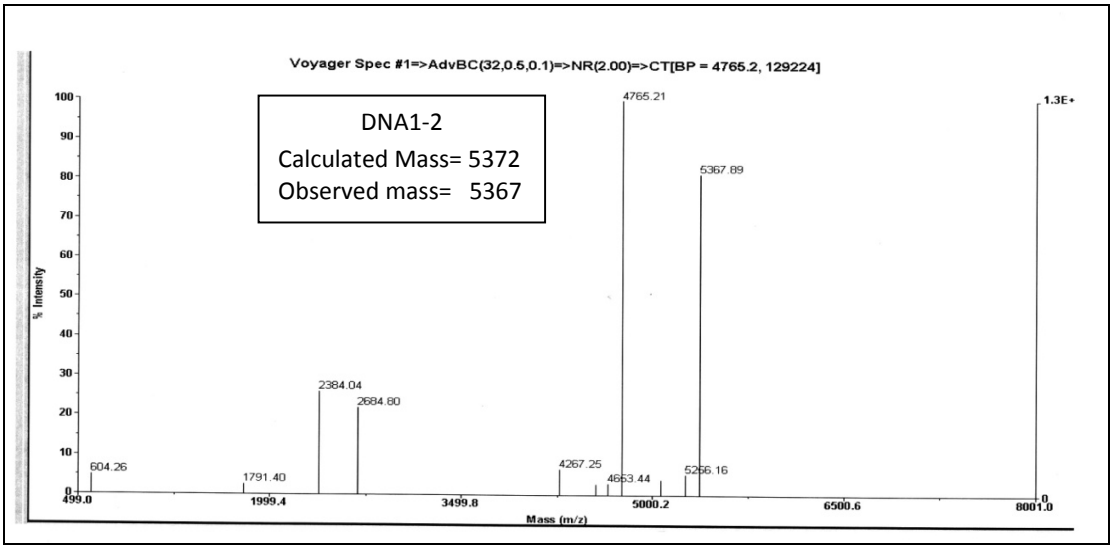
Voyager Spec #1=>AdvBC(32,0.5,0.1)=>NR(2.00)=>CT[BP = 4765.2, 129224]
DNA1-2
Calculated Mass= 5372
Observed mass= 5367
% Intensity
Mass (m/z)
4765.21
5367.89
2384.04
2684.80
604.26
1791.40
4267.25
4663.44
5266.16

2.7 References

1. (a) Obika, S.; Nanbu, D.; Hari, Y.; Morio, K.; In, Y.; Ishida, T.; Imanishi, T., Synthesis of 2'-*O*,4'-C-methyleneuridine and -cytidine. Novel bicyclic nucleosides having a fixed C-3′-*endo* sugar puckering. *Tetrahedron Letters* **1997,** 38, (50), 8735-8738. (b) Obika, S.; Nanbu, D.; Hari, Y.; Andoh, J.; Morio, K.; Doi, T.; Imanishi, T., Stability and structural features of the duplexes containing nucleoside analogues with a fixed N-type conformation, 2'-*O*,4'-C-methyleneribonucleosides. *Tetrahedron Letters* **1998,** 39, (30), 5401-5404.
2. (a) Koshkin, A. A.; Singh, S. K.; Nielsen, P.; Rajwanshi, V. K.; Kumar, R.; Meldgaard, M.; Olsen, C. E.; Wengel, J., LNA (Locked Nucleic Acids): Synthesis of the adenine, cytosine, guanine, 5-methylcytosine, thymine and uracil bicyclonucleoside monomers, oligomerisation, and unprecedented nucleic acid recognition. *Tetrahedron* **1998,** 54, (14), 3607-3630. (b) Singh, S. K.; Nielsen, P.; Koshkin, A. A.; Wengel, J., LNA (locked nucleic acids): synthesis and high-affinity nucleic acid recognition. *Chemical Communications* **1998**, (4), 455-456. (c) Wengel, J., Synthesis of 3'-C- and 4'-C-branched oligodeoxynucleotides and the development of locked nucleic acid (LNA). *Accounts of Chemical Research* **1999,** 32, (4), 301-310.
3. Damha, M. J.; Wilds, C. J.; Noronha, A.; Brukner, I.; Borkow, G.; Arion, D.; Parniak, M. A., Hybrids of RNA and arabinonucleic acids (ANA and 2'F-ANA) are substrates of ribonuclease H. *Journal of the American Chemical Society* **1998,** 120, (49), 12976-12977.
4. Watts, J. K.; Martin-Pintado, N.; Gomez-Pinto, I.; Schwartzentruber, J.; Portella, G.; Orozco, M.; Gonzalez, C.; Damha, M. J., Differential stability of 2'F-ANA.RNA and ANA.RNA hybrid duplexes: roles of structure, pseudohydrogen bonding, hydration, ion uptake and flexibility. *Nucleic Acids Research* **2010** 38, (7), 2498-2511.
5. Viazovkina, E.; Mangos, M. M.; Elzagheid, M. I.; and Damha, M. J. Synthesis of 2′-fluoroarabinonucleoside phosphoramidites and their use in the synthesis of 2′F-ANA. *Current Protocols in Nucleic Acid Chemistry*. **2002**. 4, (15), 1-22.

6. Martin-Pintado, N.; Yahyaee-Anzahaee, M.; Campos-Olivas, R.; Noronha, A. M.; Wilds, C. J.; Damha, M. J.; Gonzalez, C., The solution structure of double helical arabino nucleic acids (ANA and 2'F-ANA): effect of arabinoses in duplex-hairpin interconversion. *Nucleic Acids Research* **2012** 40, (18), 9329-9339.
7. Egli, M.; Pallan, P. S.; Allerson, C. R.; Prakash, T. P.; Berdeja, A.; Yu, J. H.; Lee, S.; Watt, A.; Gaus, H.; Bhat, B.; Swayze, E. E.; Seth, P. P., Synthesis, improved antisense activity and structural rationale for the divergent RNA affinities of 3'-fluoro hexitol nucleic acid (FHNA and Ara-FHNA) modified oligonucleotides. *Journal of the American Chemical Society* **2011,** 133, (41), 16642-16649.
8. Seth, P. P.; Yu, J. H.; Jazayeri, A.; Pallan, P. S.; Allerson, C. R.; Ostergaard, M. E.; Liu, F. W.; Herdewijn, P.; Egli, M.; Swayze, E. E., Synthesis and antisense properties of fluoro cyclohexenyl nucleic acid (F-CeNA), a nuclease stable mimic of 2'-fluoro RNA. *Journal of Organic Chemistry* **2012,** 77, (11), 5074-5085.
9. Pallan, P. S.; Yu, J. H.; Allerson, C. R.; Swayze, E. E.; Seth, P.; Egli, M., Insights from crystal structures into the opposite effects on RNA affinity caused by the S- and R-6'-methyl backbone modifications of 3'-fluoro hexitol nucleic acid. *Biochemistry* **2012,** 51, (1), 7-9.
10. Kandimalla, E. R.; Manning, A.; Zhao, Q. Y.; Shaw, D. R.; Byrn, R. A.; Sasisekharan, V.; Agrawal, S., Mixed backbone antisense oligonucleotides: Design, biochemical and biological properties of oligonucleotides containing 2'-5'-ribo- and 3'-5'-deoxyribonucleotide segments. *Nucleic Acids Research* **1997,** 25, (2), 370-378.
11. Kumar, P.; Takaku, H., Properties of mixed backbone oligonucleotides containing 3'-*O*-methyl ribonucleosides. *Bioorganic & Medicinal Chemistry Letters* **1999,** 9, (17), 2515-2520.
12. (a) Obika, S.; Morio, K.; Hari, Y.; Imanishi, T., Preparation and properties of 2',5'-linked oligonucleotide analogues containing 3'-*O*,4'-C-methyleneribonucleosides. *Bioorganic & Medicinal Chemistry Letters* **1999,** 9, (4), 515-518. (b) Obika, S.; Andoh, J.; Onoda, M.; Nakagawa, O.; Hiroto, A.; Sugimoto, T.; Imanishi, T., Synthesis of a novel bridged nucleoside bearing a fused-azetidine ring, 3'-amino-3',4'-BNA monomer. *Tetrahedron Letters* **2003,** 44, (28), 5267-5270.

13. Zou, R. M.; Matteucci, M. D., Synthesis and hybridization properties of an oligonucleotide analog containing a glucose-derived conformation-restricted ribose moiety and 2', 5' formacetal linkages. *Tetrahedron Letters* **1996,** 37, (7), 941-944.
14. Bhan, P.; Bhan, A.; Hong, M. K.; Hartwell, J. G.; Saunders, J. M.; Hoke, G. D., 2',5'-linked oligo-3'-deoxyribonucleoside phosphorothioate chimeras: thermal stability and antisense inhibition of gene expression. *Nucleic Acids Research* **1997,** 25, (16), 3310-3317.
15. Peng, C. G.; Damha, M. J., Synthesis and hybridization studies of oligonucleotides containing 1-(2-deoxy-2-α-C-hydroxymethyl-β-D-ribofuranosyl) thymine (2'-α-hm-dT). *Nucleic Acids Research* **2005,** 33, (22), 7019-7028.
16. Agha, K. A.; Damha, M. J., Synthesis and binding properties of a homopyrimidine 2',5'-linked xylose nucleic acid (2',5'-XNA). *Nucleosides Nucleotides & Nucleic Acids* **2003,** 22, (5-8), 1175-1178.
17. (a) Premraj, B. J.; Patel, P. K.; Kandimalla, E. R.; Agrawal, S.; Hosur, R. V.; Yathindra, N., NMR structure of a 2',5' RNA favors A type duplex with compact C2'-endo nucleotide repeat. *Biochemical and Biophysical Research Communications* **2001,** 283, (3), 537-543. (b) Lalitha, V.; Yathindra, N., Even nucleic-acids with 2',5'-linkages facilitate duplexes and structural polymorphism-prospects of 2',5'-oligonucleotides as antigene antisense tool in gene-regulation. *Current Science* **1995,** 68, (1), 68-75.
18. Tsoukala, E.; Agelis, G.; Dolinsek, J.; Botic, T.; Cencic, A.; Komiotis, D., An efficient synthesis of 3-fluoro-5-thio-xylofuranosyl nucleosides of thymine, uracil, and 5-fluorouracil as potential antitumor or/and antiviral agents. *Bioorganic & Medicinal Chemistry* **2007,** 15, (9), 3241-3247.
19. Mikhailopulo, I. A.; Sivets, G. G., A novel route for the synthesis of deoxy fluoro sugars and nucleosides. *Helvetica Chimica Acta* **1999,** 82, (11), 2052-2065.
20. Niedballa, U.; and Vorbrüggen, H., A General Synthesis of Pyrimidine Nucleosides. *Angewandte. Chemie. International. Edition (English)* **1970,** 9, 461–462.
21. Robins, M. J.; Fouron, Y.; Mengel, R., Nucleic-acid related compounds .2. Adenosine 2',3'-ribo-epoxide-synthesis, intramolecular degradation, and

transformation into 3'-substituted xylofuranosyl nucleosides and lyxo-epoxide. *Journal of Organic Chemistry* **1974,** 39, (11), 1564-1570.

22. Foster, A. B.; Hems, R.; and Webber, J. M., Fluorinated carbohydrates PART I. 3-deoxy-3-fluoro-D-glucose. *Carbohydrate Research* **1967,** 5. 292.
23. Reichman, U.; Watanabe, K. A.; Fox, J. J., Practical synthesis of 2-deoxy-2-fluoro-D-arabinofuranose derivatives. *Carbohydrate Research* **1975,** 42, (2), 233-240.
24. Tewson, T. J.; Welch, M. J., New approaches to synthesis of 3-deoxy-3-fluoro-D-glucose. *Journal of Organic Chemistry* **1978,** 43, (6), 1090-1092.
25. Wright, J. A.; Taylor, N. F., Fluorocarbohydrates. Part XVI. The synthes is of 3-deoxy-3-fluoro-D-xylose and 3-deoxy-3-fluoro-β-D-arabinose. *Carbohydrate Research* **1967,** 3, 333-339.
26. Mikhailopulo, I. A.; Poopeiko, N. E.; Pricota, T. I.; Sivets, G. G.; Kvasyuk, E. I.; Balzarini, J.; Declercq, E., Synthesis and antiviral and cytostatic properties of 3'-deoxy-3'-fluoro-2',3'-dideoxy-D-ribofuranosides and 2'-azido-3'-fluoro-2',3'-dideoxy-D-ribofuranosides of natural heterocyclic bases. *Journal of Medicinal Chemistry* **1991,** 34, (7), 2195-2202.
27. (a) Obika, S.; Morio, K.; Nanbu, D.; Hari, Y.; Itoh, H.; Imanishi, T., Synthesis and conformation of 3',4'-BNA monomers, 3'-*O*,4'-C-methyleneribonucleosides. *Tetrahedron* **2002,** 58, (15), 3039-3049. (b) Obika, S.; Morio, K.; Nanbu, D.; Imanishi, T., Synthesis and conformation of 3'-*O*,4'-C-methyleneribonucleosides, novel bicyclic nucleoside analogues for 2',5'-linked oligonucleotide modification. *Chemical Communications* **1997**, (17), 1643-1644.
28. Krutzfeldt, J.; Rajewsky, N.; Braich, R.; Rajeev, K. G.; Tuschl, T.; Manoharan, M.; Stoffel, M., Silencing of microRNAs in vivo with 'antagomirs'. *Nature* **2005,** 438, (7068), 685-689.
29. Kang, S. H.; Cho, M. J.; Kole, R., Up-regulation of luciferase gene expression with antisense oligonucleotides: Implications and applications in functional assay developments. *Biochemistry* **1998,** 37, (18), 6235-6239.
30. (a) Gait, M. J. Oligonucleotide synthesis: A practical approach. IRL Press Oxford, UK 217 (b) Agrawal, S. Protocols for oligonucleotides and analogs synthesis and

properties: Methods in Molecular Biology. Totowa, N J,. Humana Press, Inc **1983**, 20.

31. [31]Giannaris, P. A.; Damha, M. J., Oligoribonucleotides containing 2′,5′-phosphodiester linkages exhibit binding selectivity for 3′,5′-RNA over 3′,5′-ssDNA. *Nucleic Acids Research* **1993,** 21, (20), 4742-4749.

Chapter 3

Synthesis of 3′-deoxy-3′-fluoro ribo/xylo thyminyl nucleosides ($^{R}T^{F}$, $^{X}T^{F}$), 3′-deoxy-3′-fluoro ribo/xylo and S-type locked adenine-containing nucleosides ($^{R}A^{F}$, $^{X}A^{F}$ and $^{L}A^{S}$) and arabino-uridine (^{ara}U), their incorporation into ngDNA, and effect on binding properties to target sequences and nuclease resistance property

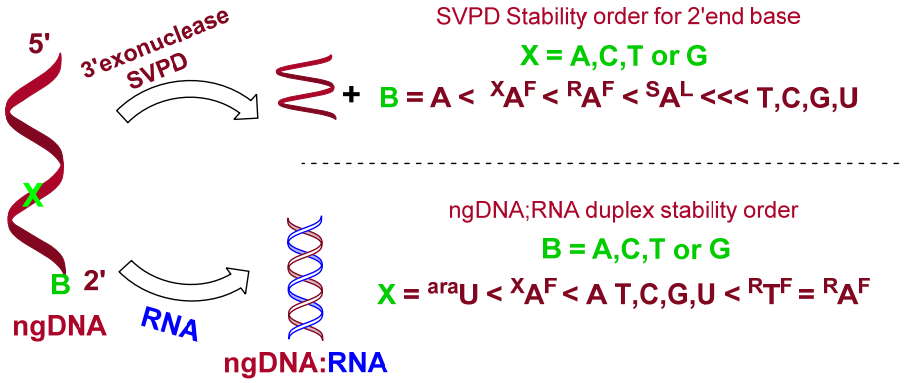

The uracil containing 3′-deoxy-3′-fluoro ribo/xylo nucleoside ($^{R}U^{F}$ and $^{X}U^{F}$) frozen in S and N-type conformation when incorporated in ngDNA exhibited increase or decrease in binding strength while binding with complementary RNA as compared with the unmodified ngDNA (Chapter 2). As it is known that C-5 substitution (methyl, propynyl) of pyrimidines generally results in an improvement in duplex stability due to increase in the hydrogen bonding and base stacking interactions, we synthesized 3′-deoxy-3′-fluoro ribo/xylo thyminyl nucleosides ($^{R}T^{F}$ and $^{X}T^{F}$), and studied their effect on the binding properties of ONs. In addition, the stability of the ONs to 3′-exonucleases (SVPD) was also investigated, where we found that the stability of 2′ end adenosine was very low compared to other nucleosides. We again synthesized the modified 3′-deoxy-3′-fluoro ribo/xylo adenine-containing nucleoside ($^{R}A^{F}$, $^{X}A^{F}$) and S-type locked adenine ($^{L}A^{S}$) monomer and incorporated them at the 2′ end of the ngDNA to study their effect on enzymatic stability. In this chapter, we further discuss the synthesis and effect on binding properties of compact arabino-uridine (^{ara}U).

This chapter is divided into three sections

3.1: Section A: Synthesis and biophysical study of $^{X}T^{F}$, $^{X}A^{F}$, $^{R}T^{F}$, $^{R}A^{F}$, and $^{L}A^{S}$ monomers.

3.2: Section B: Synthesis and rationale for designing arabino-uridine (^{ara}U) monomer, its incorporation into ngDNA and binding study.

3.3: Section C: Stability of oligonucleotides to SVPD

Section A

3.1. Synthesis and biophysical study of $^{X}T^{F}$, $^{X}A^{F}$, $^{R}T^{F}$, $^{R}A^{F}$, and $^{L}A^{S}$ monomers

3.1.1 Introduction

The use of thymine instead of uracil in DNA may probably have arisen due to the possibility of formation of uracil by slow deamination of cytosine as a mutation. The distinction from the mutated U from the correct U by DNA repair enzymes was made possible due to the presence of methyl group on uracil. The other reason could be that the thymine causes significant increase in the thermal stability of DNA duplex.[1,2] There is general agreement in the literature about the existence of a stabilizing effect on both RNA and DNA by the pyrimidine 5-methyl group (Figure 1).[3,4] The substitution of T for U in RNA $(rA)_n.(rU)_n$, increases the transition temperature (T_m) by 12.28°C at 0.03M Na^+.[5,6] which is even larger for DNA $(dA)_n.(dT)_n$ over $(dA)_n.(dU)_n$ (ΔT_m = 17.48°C at 0.03M Na^+).[7]

Several possible intermolecular forces are considered to account for this increased duplex stability. Escudé *et al*.[8] proposed that the favorable contacts between adjacent methyl groups on T may contribute to favorable hydrophobic interactions. In contrast, Sowers *et al*.[9] have suggested that hydrophobic interactions do not satisfactorily account for the methyl effect and instead proposed that the increased polarizability, which occurs upon substitution with a methyl group, is responsible for the enhanced stacking energy. An increase in polarizability will increase both dipole-induced dipole and dispersion energies.[10] To understand the origin of the methyl effect, Wang and Kool[11] measured the melting behavior of duplexes formed between $(dA)_{12}$ and four complementary dodecamers: $(dU)_{12}$,

$(dT)_{12}$, $(dU–dT)_6$ and $(dU_6–dT_6)$. They found that T_m is elevated significantly with the pyrimidine strand containing alternating U and T but elevated even more with the oligomer of the same composition but containing adjacent T's. It was suggested that the increased stabilization could be due to the increase in polarizability on methyl substitution, allowing more favorable van der Waals contacts between neighboring bases. Frank B. Howard[12] reported the stabilizing contribution of thymine in duplex of $(dA)_{24}$ with $(dU)_{24}$, $(dT)_{24}$, $(dU_{12}–dT_{12})$, $(dU–dT)_{12}$, $(dU_2–dT_2)_6$ and $(dU_3–dT_3)_4$. He explained the increase in stability by substitution of a T for a U due to an increase in strength of dipole-induced dipole and dispersion (van der Waals) interactions between neighboring bases.

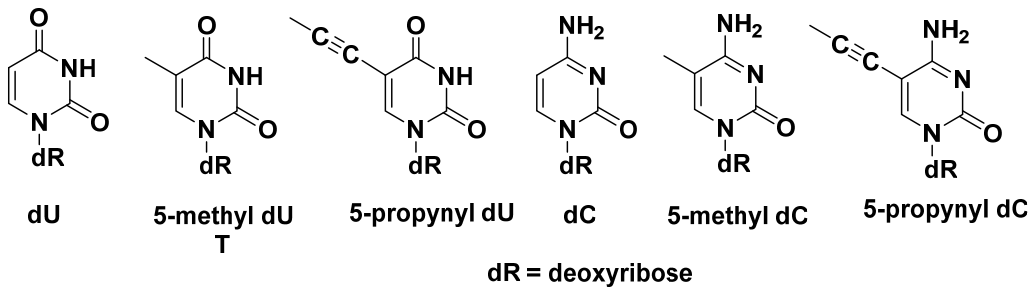

Figure 1. Pyrimidine bases with substitution at 5 positions

Favorable stacking of the heterocyclic bases contributes towards the favorable enthalpy of duplex formation for nucleic acid duplexes.[13,14] This favorable stacking is due primarily to the favorable interactions between dipoles and induced dipoles in adjacent residues. Thus modifications to the heterocycle that improve these interactions are likely to stabilize the duplex. Some more examples include substitution of 5-methyl cytosine (5-methyl dC) for cytosine (dC) which resulted in an average increase of about +0.5°C per substitution.[15] Substitution at the 5-position of pyrimidine with propyne in 5-propynyl dU and 5-propynyl dC also stood out as most stabilizing (Figure 1).[16]

3.1.2 Rationale, design and objectives of the present work

In Chapter 1, we have discussed how chemical modification having preference for N-type sugar conformation improves binding affinity of natural DNA:RNA duplexes. In Chapter 2, our study on conformationally frozen uracil containing 3′-deoxy-3′-fluoro ribo/xylo nucleoside ($^{R}U^{F}$ and $^{X}U^{F}$)-modified ngDNA strongly suggested that the sugar

conformations play a crucial role in stabilizing 2′-5′-linked ngDNA:RNA duplex. The ngDNA:RNA duplexes were stabilized by S-type frozen monomer units ($^{R}U^{F}$) and destabilized by N-type frozen monomers ($^{X}U^{F}$) providing proof, for the first time, for the prediction that in stable ngDNA:RNA duplexes, the DNA strand would prefer to assume S-type geometry. Natural DNA exhibits higher binding affinities to complementary RNA compared to $^{R}U^{F}$-modified ngDNA:RNA, which indicates the need of further improvement in the latter. The substitution of thymine for uracil would generally result in an improvement in duplex stability for natural nucleic acids as discussed above. To determine the influence of thymine over uracil nucleobase on the duplex stability of 2′-5′-linked nongenetic nucleic acid, synthesis of thymine-containing S-type and N-type frozen nucleoside analogues was undertaken. To investigate the effect of 3′-fluorine substitution in purine nucleoside, we also synthesized N-type and S-type frozen adenine nucleosides.

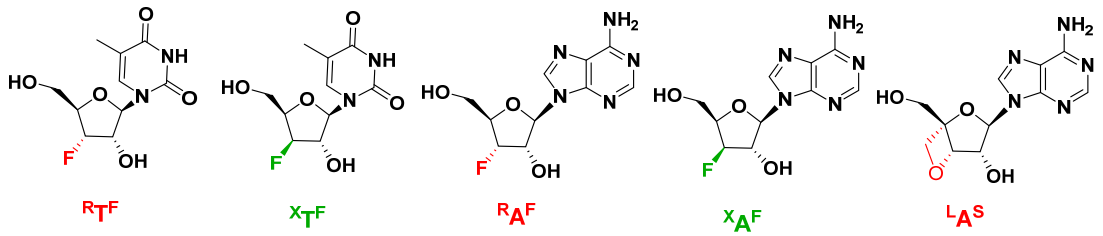

Figure 2. Proposed monomers

Nuclease resistance of ONs is an important factor that determines effectiveness of antisense oligonucleotides *in vivo*. We examined the 3′-exonuclease sensitivity of the ONs using snake venom phosphodiesterase (SVPD). We found that the stability of 2′ end adenosine is very low compared to other bases containing nucleosides in 2′-5′-linked oligomers. In addition to S-type and N-type frozen adenine nucleosides ($^{R}A^{F}$, $^{X}A^{F}$), we further synthesized S-type locked $^{L}A^{S}$ monomer. These monomers were incorporated at 2′-end of oligomers and their nuclease resistance to SVPD was examined.

In section A, we present the synthesis of thymine- and adenine-containing 3′-deoxy-3′-fluoro ribo/xylonucleoside analogues and synthesis of S-type locked $^{L}A^{S}$ monomer. We synthesized the modified ngDNA oligomer with each of these monomers and studied the effect of individual $^{R}T^{F}$, $^{R}A^{F}$ and combination of $^{R}A^{F}$ and $^{R}T^{F}$ on duplex stability with RNA. The ngDNA was modified at the 2′ end by $^{R}A^{F}$, $^{X}A^{F}$ or $^{L}A^{S}$ unit and the comparative

stability to SVPD was also studied; the results are presented in section C. A preliminary study of sugar puckering using ^{1}H NMR $J_{1'2'}$ coupling constants for all the monomers was carried out, which shows that in the $^{X}T^{F}$ monomer, the sugar is in N-type geometry. As the N-type geometry was shown to destabilize the resulting duplex, as discussed in Chapter 2 for $^{X}U^{F}$ monomer, further study for $^{X}T^{F}$ was not carried out.

Objectives of the present work

1. Synthesis of 3′-deoxy-3′-fluoro ribo/xylothymidine ($^{R}T^{F}$, $^{X}T^{F}$), 3′-deoxy-3′-fluoro ribo/xyloadenosine ($^{R}A^{F}$, $^{X}A^{F}$) and S-type locked adenosine ($^{L}A^{F}$) phosphoramidite monomers.
2. Preliminary study of sugar pucker using ^{1}H NMR $J_{1'2'}$ coupling constant.
3. Synthesis of ngDNA oligonucleotides containing these modified units, their purification and characterization.
4. The CD and UV melting studies of the derived oligomers.

3.1.3 Present work, result and discussion

3.1.3.1 Synthesis of $^{R}T^{F}$, $^{X}T^{F}$, $^{R}A^{F}$, $^{X}A^{F}$ and $^{L}A^{F}$ phosphoramidite monomers

3'-Ribofluoroadenosine and 3'-xylofluoroadenosine ($^{R}A^{F}$, $^{X}A^{F}$) have been synthesized,[17] and studied from a structural perspective and for biological activity by Altona *et al.*[18] Obika *et al.*[19] in 2002 reported the synthesis and conformational study for the 3′, 4′-BNA adenosine (S-type locked adenosine ($^{L}A^{F}$)) nucleoside.

Syntheses of all the fluorine-containing monomers were accomplished using synthetic strategies used for 3′-deoxy-3′-fluoro-ribo/xylouridine ($^{R}U^{F}$, $^{X}U^{F}$) discussed in Chapter 2, While the S-type locked adenosine ($^{L}A^{F}$) nucleoside was synthesized following the reported procedure using D-Glucose as starting material.[19] In case of adenine-containing monomer synthesis, *N*6-benzoyl adenine was used.

3.1.3.1a Synthesis of $^{X}T^{F}$ nucleoside and $^{X}A^{F}$ phosphoramidite monomer

Synthesis of the $^{X}T^{F}$, $^{X}A^{F}$ nucleoside and their conversion to the respective phosphoramidite derivatives was achieved as described in Scheme 1. The synthesis of 3-deoxy-3-fluoro-1, 2, 5-tri-*O*-acetyl-xylofuranose **9** was accomplished as described in

Scheme 1 of Chapter 2. The Vorbrüggen glycosylation of an anomeric mixture of compound **9** independently with a silylated base (a) thymine and (b) *N*6-benzoyladenine in presence of TMS-triflate afforded the β-nucleoside as the only isomer **24** (75%), and **25** (70%) respectively (Scheme 1), where neighboring group participation of the 2-*O*-acetyl group allowed exclusive formation of β-nucleoside. Compounds **24** and **25** were then subjected to ammonolysis to give 3′-deoxy-3′-xylofluoro-thymidine **26** (90%) and 3′-deoxy-3′-xylofluoro adenosine **27** (80%) respectively. The free primary hydroxyl group in **26** and **27** was protected as its 4, 4′-dimethoxytrityl (DMTr) group using DMTr-chloride and a catalytic amount of 4-dimethylaminopyridine (DMAP) in dry pyridine to get **28** (60%) and **29** (60%) respectively. Compounds **29** was phosphitylated at the 2′-hydroxy group with 2-cyanoethyl- *N, N*-diisopropylchlorophosphoramidite in dry DCM using *N, N*-diisopropylethylamine (DIPEA) as a base to get the desired phosphoramidite building blocks **31** (43%) as 3′-deoxy-3′-xylofluoro-adenosine ($^{X}A^{F}$) monomer.

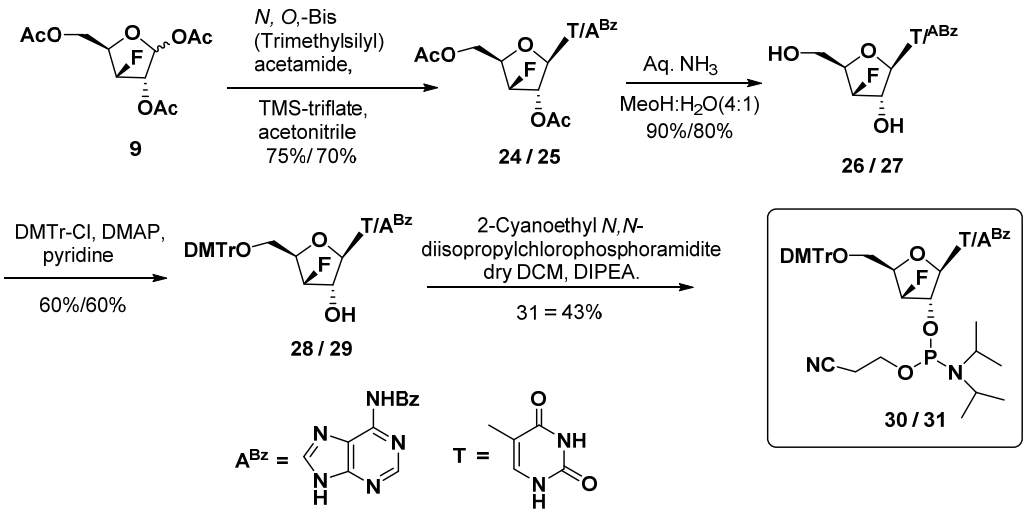

Scheme1: Synthesis of $^{X}T^{F}$ nucleoside and $^{X}A^{F}$ phosphoramidite monomer

3.1.3.1b Synthesis of $^{R}T^{F}$ and $^{R}A^{F}$ phosphoramidite monomers

Synthesis of the $^{R}T^{F}$ and $^{R}A^{F}$ nucleosides and their conversion to the corresponding phosphoramidite derivatives was achieved as described in Scheme 2. The synthesis of 3-deoxy-3-fluoro-1-*O*-methyl-5-*O*-benzoyl-2-*O*-acetyl-D-ribofuranose **19** was accomplished as described in Scheme 3 of Chapter 2. Coupling of **19**, individually with silylated base (a)

thymine, and (b) *N*6-benzoyladenine by Vorbrüggen glycosylation in the presence of TMS-triflate, gave selectively β-nucleoside derivatives **32** (75%) and **33** (70%) respectively (Scheme 2). Here the neighboring group participation of 2-*O*-acetyl group helped for β-selectivity of nucleobase. Compounds **32** and **33** were then subjected to ammonolysis to give 3′-deoxy-3′-fluoro ribothymidine **34** (90%) and 3′-deoxy-3′-fluoro riboadenosine **35** (90%) respectively. The free primary hydroxyl group in **34** and **35** was protected as 4, 4′-dimethoxytrityl (DMTr) group using DMTr-chloride and a catalytic amount of DMAP in dry pyridine to get **36** (60%) and **37** (60%) respectively. Compounds **36** and **37** were phosphitylated at the 2′-hydroxy group using 2-cyanoethyl- *N, N*-diisopropylchlorophosphoramidite to afford the desired phosphoramidite building block **38** (55%) and **39** (53%) as 3′-deoxy-3′-ribofluoro-thymidine and ($^{R}T^{F}$) 3′-deoxy-3′-fluoro riboadenosine ($^{R}A^{F}$) monomers.

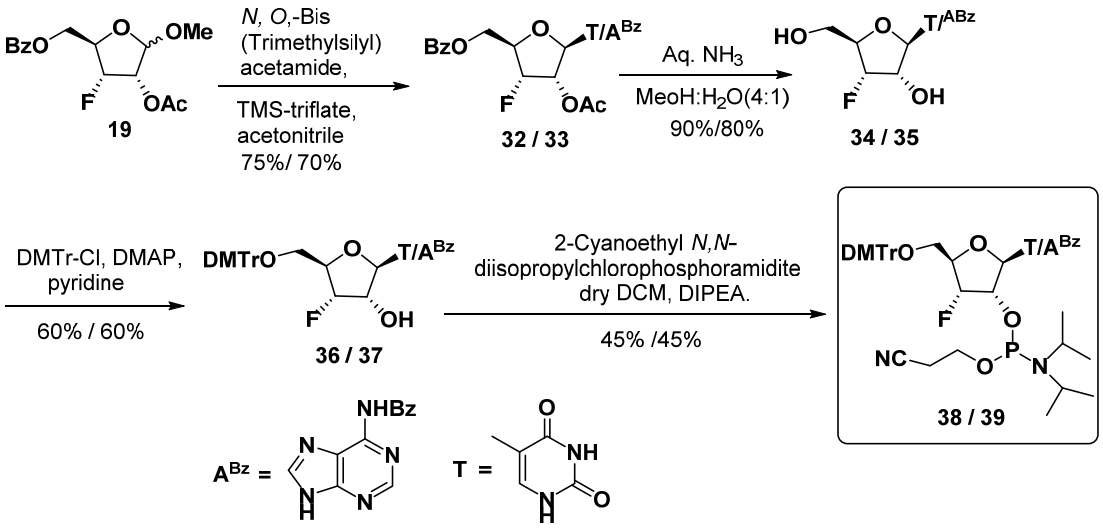

Scheme 2: Synthesis of $^{R}T^{F}$ and $^{R}A^{F}$ phosphoramidite monomers

3.1.3.1c Synthesis of S-type locked adenosine ($^{L}A^{F}$) phosphoramidite monomer

Synthesis of the $^{L}A^{F}$ nucleoside and its conversion to phosphoramidite derivative was achieved as described in Scheme 3. The synthesis of allose diacetonide (ADA) **4** was accomplished as described in Scheme1 of Chapter 2. The free hydroxyl group of **4** was protected as its benzyl ether using benzyl bromide (BnBr) in DMF and sodium hydride as base to get **40** (75%). Selective removal of the 5,6-*O*-isopropylidene group using 1:1 acetic

acid:water mixture at 50°C for 1h, to get **41** (95%). Periodate oxidation, followed by aldol condensation between the intermediate aldehyde and formaldehyde in the presence of aqueous sodium hydroxide gave compound **42** (70%). Selective desymmetrization of **42** was performed by *tert*-butyldiphenylchlorosilane and triethylamine in DCM to give the desired compound **43** (65%) along with small amount of the other regioisomer. *p*-toluenesulfonylation of **43** gave **44** in 80% yield. 1,2 Acetonide deprotection and simultaneous acylation of **44** in the presence of acetic acid, acetic anhydride and sulfuric acid afforded diacetate **45** (70%) as an anomeric mixture. Palladium-catalyzed hydrogenolysis of **45** gave the debenzylated product which was then treated with acetic anhydride in pyridine to give triacetate **46** in 72% overall yield.

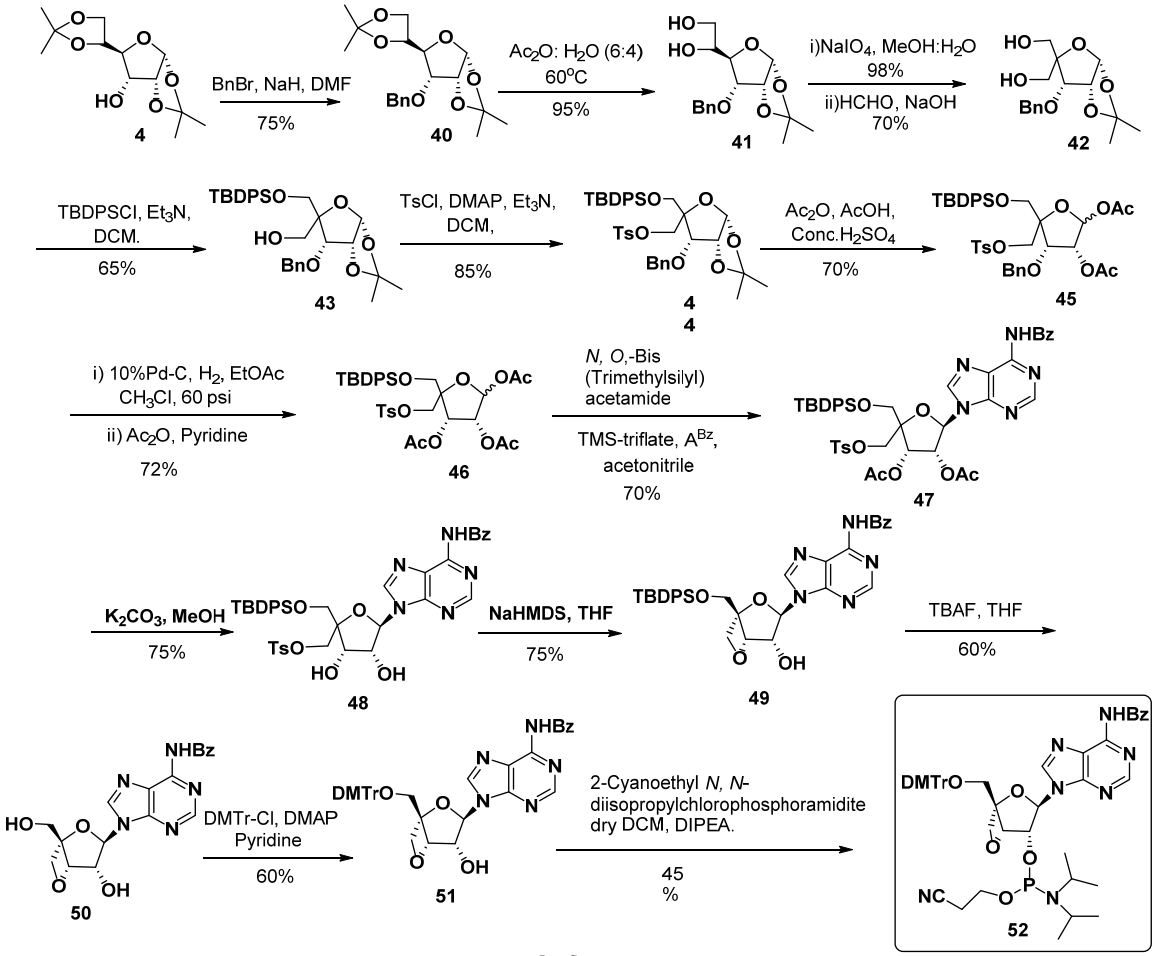

Scheme 3: Synthesis of $^{L}A^{S}$ phosphoramidite monomer

Vorbrüggen glycosylation reaction condition was used for nucleobase attachment. Silylated benzoyl-protected adenine was reacted with triacetate **46** in dichloroethane in the presence of TMS-triflate, which gave selectively β-nucleoside derivative **47** in 70% yield**.** Acetyl group of **47** was deprotected using potassium carbonate in methanol which gave diol **48** in 75% yield. Compound **48** was then treated with sodium hexamethyldisilazide to obtain oxetane derivative **49** (75%). The *tert*-butyldiphenylsilyl group of **49** was deprotected using *tert*-butylammonium fluoride (TBAF) to get **50** (60%). The free primary hydroxyl group of **50** was protected as its 4, 4′-dimethoxytrityl (DMTr) derivative using DMTr-chloride and a catalytic amount of DMAP in dry pyridine to get **51** (60%). Finally the 2′-hydroxy group was phosphitylated by using 2-cyanoethyl *N, N*-diisopropylchlorophosphoramidite to afford the desired phosphoramidite **52** (45%) as S-type locked adenosine ($^{L}A^{F}$) monomer.

3.1.3.2 Preliminary study of sugar pucker using ^{1}H NMR $J_{1',2'}$ coupling constant

Altona *et al.*[18] carried out the conformational analysis by NMR using Pseudorot program for fluorine-containing adenosine monomer, which indicated that the sugar units existed exclusively in the *C2′-endo* (Southe) and *C2′-exo* (Northe) form for $^{R}A^{F}$ and $^{X}A^{F}$ nucleoside respectively, While Obika *et al.*[19] studied the sugar puckering of the $^{L}A^{S}$ by means of ^{1}H NMR, which was found to be restricted in S-conformation (*C2′-endo*).

We calculated the %S for $^{R}A^{F}$ and $^{X}A^{F}$ nucleoside units from the H1′-H2′ NMR coupling constants using the formula **%S = 100 X ($J_{1'2'}$-1)/6.9** as earlier reported.[20] The %S for $^{X}T^{F}$ nucleoside **26,** $^{X}A^{F}$ nucleoside **27**, $^{R}T^{F}$ nucleoside **34,** $^{R}A^{F}$ nucleoside **35**, and S-type locked $^{L}A^{S}$ nucleoside **50** were found to be 2.17%, 3.76%, 97.23%, 100% and 79.71% respectively. This indicates that **34**, **35** and **50** are almost frozen in S-type, while **26** and **27** are frozen in N-type conformations. We have systematically analyzed the conformation of **27, 35** and **50** using NMR, X-ray crystal structure and Matlab pseudorotation GUI program which we discuss in Chapter 4. In these studies we calculated all the four structural parameters i.e., glycosidic torsion angle χ, torsion angle γ, phase angle of pseudorotation *P* and the puckering amplitude ν_{max}, which ultimately gives S-type and N-type population for each monomer in solid state as well as in solution state. In Chapter 4 we discuss the NOESY NMR study for all the units to analyze the *syn/anti* conformation of nucleobase.

3.1.3.3 Synthesis of oligonucleotides containing modified units, their purification and characterization

The control 18mer ON sequence **DNA1** chosen in this study is used for miRNA down-regulation[21] and **DNA2** is specific for the splice correction of an aberrant *β*-globin intron (705 site).[22,23] The oligomers were synthesized using an automated Bioautomation MM4 DNA synthesizer and commercially available 5′-*O*-DMT-3′-deoxy-2′-phosphoramidite building blocks using β–cyanoethyl phosphoramidite method.[24] The modified monomer units were incorporated at pre-determined positions using an extended coupling time to yield the modified oligomers efficiently. A series of **ngDNA2** ONs (Table 1) containing one to three modified building blocks, (**38** and **39)** abbreviated as $^{R}A^{F}$ and $^{R}T^{F}$ were synthesized. To test the SVPD stability, three **ngDNA1** oligomers with modified monomer **31**, **39** and **53** ($^{R}A^{F}$, $^{X}A^{F}$ and $^{L}A^{S}$) at their 2′ ends were also synthesized.

3.1.3.3a Purification and MALDI-TOF characterization of ngDNA oligomers

The synthesized ONs were cleaved from the solid support with concentrated NH_4OH and lyophilized to get the crude deprotected ONs. The purity of the oligomers listed in Table 1 was checked by analytical RP-HPLC (C18 column, 0.1N TEAA buffer, pH 7.0-acetonitrile) which showed more than 75-80% purity. These oligomers were subsequently purified by reverse phase HPLC on a C18 column. The purity of the oligomers was again ascertained by analytical RP-HPLC and found to be >95%. Their integrity was confirmed by MALDI-TOF mass spectrometric analysis. THAP (2,4,6-trihydroxy acetophenone) matrix with diammonium citrate as additive was used for MALDI-TOF mass analysis of oligomers. HPLC retention time and observed values of mass in MALDI-TOF spectrometry for all the ONs are listed in Table 1.

Table 1: Synthesized ngDNA oligomers, their HPLC retention times and characterization using MALDI -TOF mass analysis

Entry No	Sequence code	Sequence (5' → 2')	HPLC t_R (min)	Mass	
				Expected	Observed
1	ngDNA2	CCTCTTACCTCAGTTACA	12.7	5369	5368
2	ngDNA2-3	CCTCTTACCTCAGT^{R}T^{F}ACA	10.5	5387	5385
3	ngDNA2-4	CCTCTTACC^{R}T^{F}CAGT^{R}T^{F}ACA	10.4	5405	5410
4	ngDNA2-5	CCTCTTACCTCAGTT^{R}A^{F}CA	10.5	5387	5388
5	ngDNA2-6	CCTCTTACCTC^{R}A^{F}GTT^{R}A^{F}CA	10.6	5405	5410
6	ngDNA2-7	CCTCTTACCTC^{R}A^{F}G^{R}T^{F}TACA	10.6	5405	5409
7	ngDNA2-8	CCTCTT^{R}A^{F}CCTC^{R}A^{F}GT^{R}T^{F}ACA	10.7	5423	5426
8	ngDNA1	CACCATTGTCACACTCCA	7.2	5364	5362
9	ngDNA1-6	CACCATTGTCACACTCC^{X}A^{F}	7.5	5382	5381
10	ngDNA1-7	CACCATTGTCACACTCC^{R}A^{F}	8.2	5382	5383
11	ngDNA1-8	CACCATTGTCACACTCC^{L}A^{S}	8.3	5392	5395
12	ngDNA1-9	CACCATTGTCAC^{X}A^{F}CTCCA	8.1	5382	5381

3.1.3.4 Duplex stability and CD studies of the derived oligomers

UV-T_m studies were carried out to investigate the binding affinity of the modified ngDNA to complementary DNA and RNA. The T_m experiments of duplexes were carried out in 10mM sodium phosphate buffer (pH 7.2) containing 150mM NaCl. The modified ngDNA ONs were individually hybridized with the complementary DNA and RNA strands, to obtain duplexes.

In Chapter 2 we discussed that the ngDNA1:RNA1 and ngDNA2:RNA2 duplexes are stabilized by uracil-containing S-type frozen monomer units $^{R}U^{F}$ and destabilized by N-type frozen monomers $^{X}U^{F}$. We also observed that $^{R}U^{F}$ stabilized the duplex involving the derived sequences, ngDNA2:RNA2 better than ngDNA1:RNA1. In the sequence context, the difference is that in ngDNA2 one of the modified units is flanked by a purine instead of pyrimidine at the 2′-end which could have helped to increase the stability. We decided to

use the same ngDNA2 sequence, and same sites of modifications, to compare the effect of thymine- and adenine-containing S-type frozen monomer units.

3.1.3.4a Thermal stabilities of duplex formed by $^{R}T^{F}$-, $^{R}A^{F}$-, $^{X}A^{F}$- and $^{L}A^{F}$- modified ngDNA

Similar to the ngRNA sequences reported by Damha *et al*[25] and ngDNA sequences studied in Chapter 2, all modified ngDNA sequences studied here (Table 2, 3 and 4) were also found to bind only to complementary RNA and not to complementary DNA. The melting temperatures, T_ms, of the complexes containing the $^{R}T^{F}$ units were determined and compared with the duplexes formed by unmodified ngDNA2, as well as with $^{R}U^{F}$-modified ngDNA2. The results are summarized in Table 2.

Table 2. T_m (°C) values of 18mer ngDNA2-1 to 4: DNA/RNA duplexes

Entry No	Sequence code	Sequence (5' → 2')	T_m °C cDNA2	T_m °C RNA2	ΔT_m (°C)
1	ngDNA2	CCTCTTACCTCAGTTACA	NB	46.0	0.0
2	ngDNA2-3	CCTCTTACCTCAGT^{R}T^{F}ACA	NB	47.3	+1.3
3	ngDNA2-4	CCTCTTACC^{R}T^{F}CAGT^{R}T^{F}ACA	NB	48.8	+2.8
4	ngDNA2-1	CCTCTTACCTCAGT^{R}U^{F}ACA	NB	48.3	+2.3
5	ngDNA2-2	CCTCTTACC^{R}U^{F}CAGT^{R}U^{F}ACA	NB	49.4	+3.4

Melting temperatures (T_ms) were obtained from the maxima of the first derivatives of the melting curves (A_{260nm} versus temperature), measured in buffer containing 10mM sodium phosphate, 150mM sodium chloride, pH 7.4, using 1μM concentration of each of the two complementary strands. Each experiment was repeated at least thrice and the values are accurate to ±0.5°C. RNA2 = 5′-UGUAACUGAGGUAAGAGG-3′; cDNA2 = 5′-TGTAACTGAGGTAAGAGG-3′; T_m of DNA2:cDNA2 = 54.0°C. $\Delta T_m = T_m - T_m$(control).

The complexes formed by oligomers containing increasing number of $^{R}T^{F}$ S-type frozen monomer (Table 2, entry 2 and 3) with complementary RNA were found to stabilize the duplex as compared to the control **ngDNA2:RNA2** sequence. The oligomer **ngDNA2-4** with inclusion of two modified $^{R}T^{F}$ units caused a larger stabilization of the resulting

complexes (Figure 3, ΔT_m = +2.8°C) compared to the oligomer **ngDNA2-3** containing only a single modified unit (Figure 3, ΔT_m = +1.3°C).

The stability of $^{R}T^{F}$-containing complexes (ΔT_m = +1.3°C & +2.8°C, Figure 3) is found to be lower than the $^{R}U^{F}$-containing complexes (Table 2, entry 4 and 5) (ΔT_m = +2.3° & +3.4°C), which is in contrast to the general phenomenon that substitution of T for U increases stability of duplex. This could be because the S-type conformations would bring the nucleobases in pseudoequatorial position. Therefore the stacking and hydrogen bonding interactions in S-type geometry of nucleoside are not as strong as in the N-type sugar geometry, where the nucleobases assume pseudoaxial orientation as in natural DNA:RNA duplexes. These results indicate that in ngDNA:RNA duplex, where the sugar conformation is S-type, the stabilization effect of 5-methyl substitution of pyrimidine does not work.

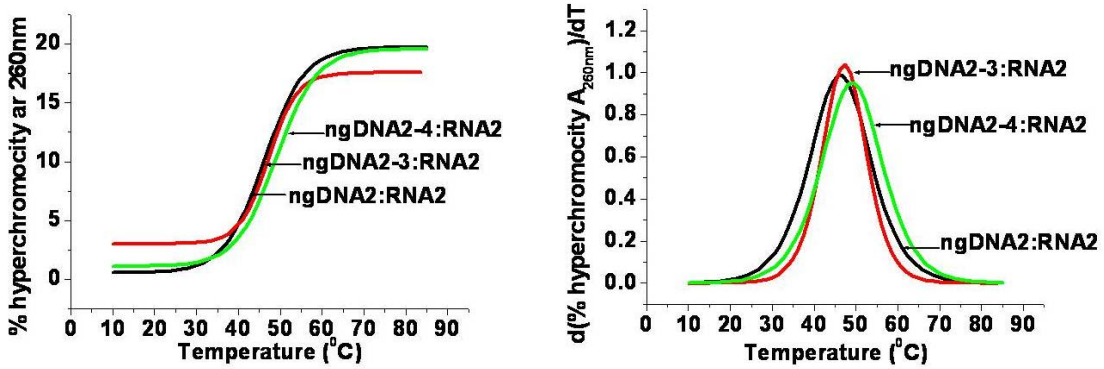

Figure 3. UV-melting plots of complexes of ngDNA2, ngDNA2-3and ngDNA2-4 with complementary RNA2 and corresponding first derivative curves

We have also synthesized the **ngDNA2** sequence with one and two modification of the adenine-containing S-type frozen $^{R}A^{F}$ monomer unit (Table 3, entry 2 and 3). In this case also, the S-type frozen $^{R}A^{F}$ units stabilized the duplex and the stability increased with increase in the number of modified units (Figure 4, ΔT_m = +0.6°C & +3.8°C for single and double modification respectively). In fact, the duplex formed by **ngDNA2-6** containing two $^{R}A^{F}$ units was found to be more stable compared to that by two $^{R}U^{F}$ and $^{R}T^{F}$ units (Table 2). We again modified ngDNA2 with the combination of both $^{R}T^{F}$ and $^{R}A^{F}$ monomers where we avoided the consecutive modifications (Table 3, entry 4 and 5), as the consecutive modified sites were found to marginally destabilize the duplex (Chapter 2). Inclusion of one $^{R}T^{F}$ and one $^{R}A^{F}$ units spaced by two unmodified units in oligomer **ngDNA2-7** lead to

stabilization of the resulting duplex by +3.8°C. The stability further increased in oligomer **ngDNA2-8** (ΔT_m = +4.4°C) with the addition of one more $^{R}A^{F}$ unit (Figure 5).

Table 3. T_m (°C) values of 18mer ngDNA2-5 to 8: DNA/RNA duplexes

Entry No	Sequence code	Sequence (5' → 2')	T_m °C cDNA2	T_m °C RNA2	ΔT_m (°C)
1	ngDNA2	CCTCTTACCTCAGTTACA	NB	46.00	0.0
2	ngDNA2-5	CCTCTTACCTCAGTT$^{R}A^{F}$CA	NB	46.6	+0.6
3	ngDNA2-6	CCTCTTACCTC$^{R}A^{F}$GTT$^{R}A^{F}$CA	NB	49.8	+3.8
4	ngDNA2-7	CCTCTTACCTC$^{R}A^{F}$GT$^{R}T^{F}$ACA	NB	49.8	+3.8
5	ngDNA2-8	CCTCTT$^{R}A^{F}$CCTC$^{R}A^{F}$GT$^{R}T^{F}$ACA	NB	50.4	+4.4

Melting temperatures (T_ms) were obtained from the maxima of the first derivatives of the melting curves (A_{260nm} versus temperature), measured in buffer containing 10mM sodium phosphate, 150mM sodium chloride, pH 7.4, using 1μM concentration of each of the two complementary strands. Each experiment was repeated at least thrice and the values are accurate to ±0.5°C. RNA2 = 5′-UGUAACUGAGGUAAGAGG-3′; cDNA2 = 5′-TGTAACTGAGGTAAGAGG-3′; T_m of DNA2:cDNA2 = 54.0°C. $\Delta T_m = T_m - T_m$(control).

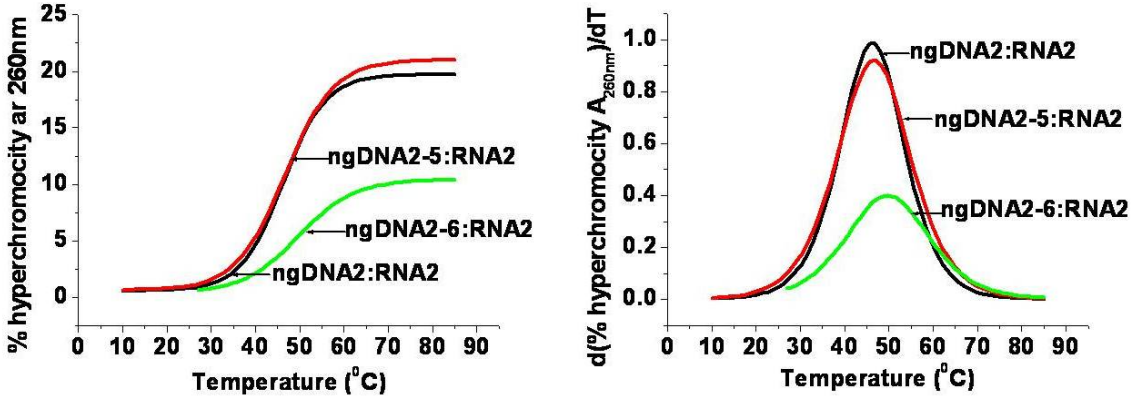

Figure 4. UV-melting plots of complexes of ngDNA2, ngDNA2-5 and ngDNA2-6 with complementary RNA2 and corresponding first derivative curves

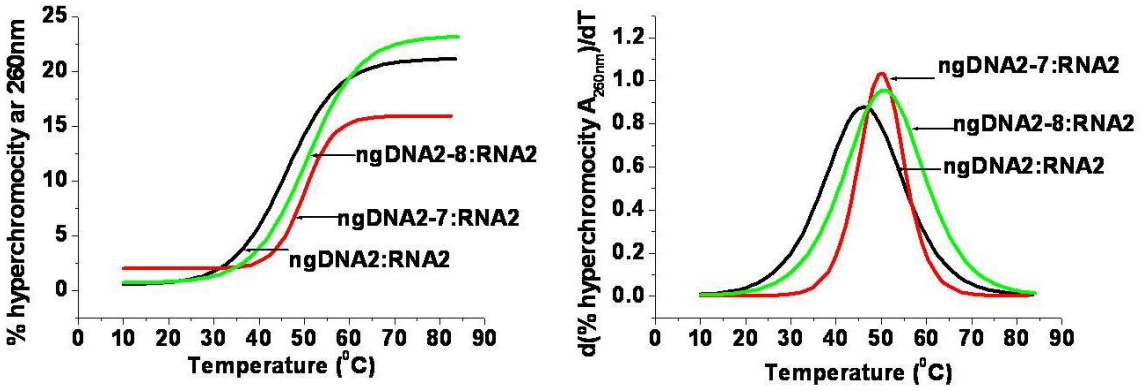

Figure 5. UV-melting plots of complexes of ngDNA2, ngDNA2-7 to ngDNA2-8 with complementary RNA2 and corresponding first derivative curves

Three **ngDNA1-6**, **ngDNA1-7** and **ngDNA1-8** oligomers with $^{R}A^{F}$, $^{X}A^{F}$ or $^{L}A^{S}$ modified monomer at the 2'end and **ngDNA1-9** oligomer with $^{X}A^{F}$ in the middle of the sequence were synthesized (for SVPD study). The end modification either S-type frozen/locked $^{R}A^{F}$, $^{L}A^{S}$ or N-type frozen $^{X}A^{F}$ did not affect the duplex stability and the T_m values were nearly the same as the control (Figure 6). As expected, the sequence **ngDNA1-9** (Table 4, entry 5) with a single N-type frozen $^{X}A^{F}$ unit incorporated in the middle of the sequence destabilized the duplex by -3.4°C (Figure 7).

Table 4. T_m (°C) values of 18mer ngDNA1-6 to 9: DNA/RNA duplexes

Entry No	Sequence code	Sequence (5' → 2')	T_m °C cDNA2	T_m °C RNA2	ΔT_m (°C)
1	ngDNA1	CACCATTGTCACACTCCA	NB	50.5	0.0
2	ngDNA1-6	CACCATTGTCACACTCC^{X}A^{F}	NB	50.4	-0.1
3	ngDNA1-7	CACCATTGTCACACTCC^{R}A^{F}	NB	50.6	+0.1
4	ngDNA1-8	CACCATTGTCACACTCC^{L}A^{S}	NB	50.5	0.0
5	ngDNA1-9	CACCATTGTCAC^{X}A^{F}CTCCA	NB	47.1	-3.4

Melting temperatures (T_ms) were obtained from the maxima of the first derivatives of the melting curves (A_{260nm} versus temperature), measured in buffer containing 10mM sodium phosphate, 150mM sodium chloride, pH 7.4, using 1μM concentration of each of the two complementary strands. Each experiment was repeated at least thrice and the values are accurate to ±0.5°C. RNA1= 5′-UGGAGUGUGACAAUGGUG-3′; cDNA1 = 5′-TGGAGTGTGACAATGGTG-3′; *T*m of DNA1:cDNA1 = 59.0°C. $\Delta T_m = T_m - T_m$(control).

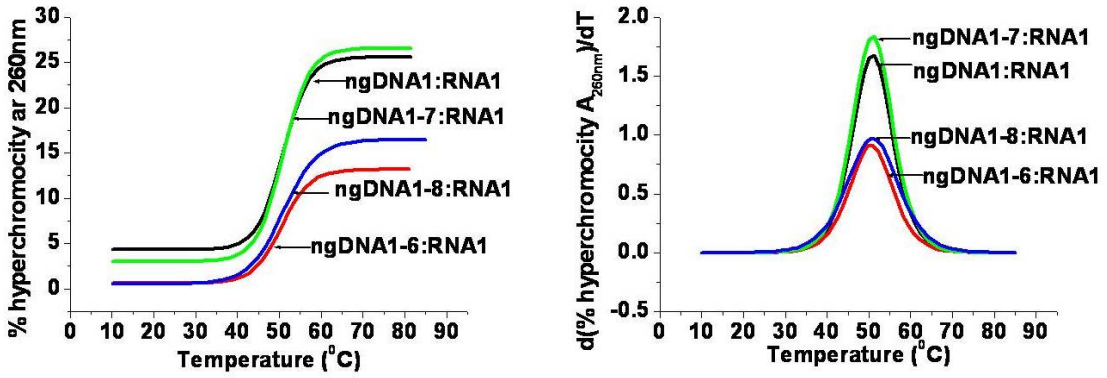

Figure 6. UV-melting plots of complexes of ngDNA1, ngDNA1-6, ngDNA1-7, and ngDNA1-9 with complementary RNA1 and corresponding first derivative curves

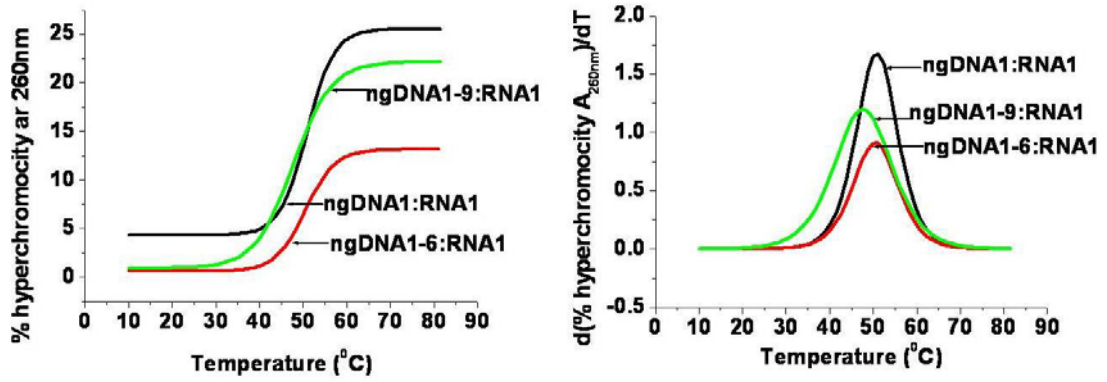

Figure 7. UV-melting plots of complexes of ngDNA1, ngDNA1-6 and ngDNA1-9 with complementary RNA1 and corresponding first derivative curves

3.1.3.4b CD study of $^{R}T^{F}$- and $^{R}A^{F}$-modified ngDNA

The CD spectra of various single stranded ngDNA2 oligomers and duplexes in which the complementary strand is RNA2, are shown in Figure 8. The unmodified and all the modified ngDNA2:RNA2 duplexes are similar and resemble the A-type duplex.

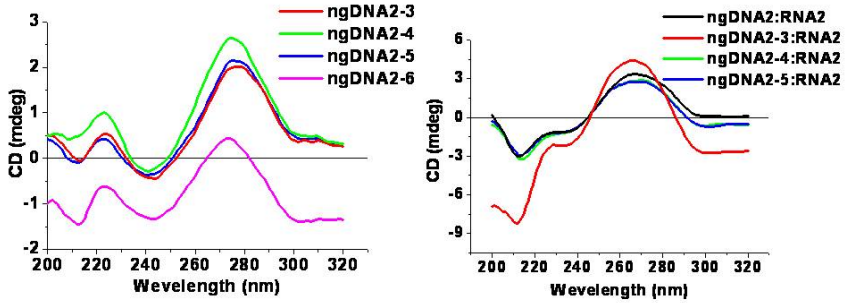

Figure 8. CD spectra of single strand ngDNA2 to ngDNA2-5 and their duplexes with complementary RNA2

Section B

3.2 Synthesis and rationale for designing arabino-uridine (^{ara}U) monomer, its incorporation into ngDNA and binding study

3.2.1 Introduction

Arabinonucleosides are stereoisomers of ribonucleosides, differing only in the configuration at the 2′-position of the sugar ring. Arabinonucleosides[26] and arabinonucleotides[27] have been shown to possess a wide range of biological activities including antiviral and antitumor activity. A number of reports have appeared which describe the synthesis for arabinonucleosides with all natural nucleobases and especially for uracil. The change in configuration at C2' in arabino- against ribonucleosides has only a slight effect on the furanose bond distances and angles[28] and the only noticeable difference is a forbidden high-*anti* orientation of the base in arabinonucleosides, despite the fact that *syn-anti* interconversion can still take place (Figure 9).[29] However, such a small change in configuration of the 2′-hydroxy group from the bottom face in ribonucleosides to the top face in arabinonucleosides produces some admirable properties in 3′-5′-linked arabinonucleic acids (ANA).[30]

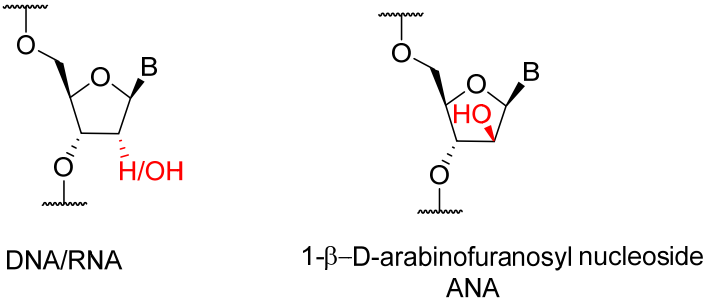

Figure 9: DNA/RNA and arabino nucleic acid (ANA)

3′-5′-linked ANA have the ability to activate RNase H.[31] Most of the modified ONs including 2′-5′-linked nongenetic nucleic acids (ngDNA/ngRNA) do not have the ability to activate RNase H. Acceptance by RNase H of any ON:RNA hybrid as a substrate is one of the very important attributes of antisense oligonucleotides. RNase H binds to double stranded RNA, but does not cleave such duplexes, while a change in stereochemistry of the 2′-hydroxyl group in ANA induces RNase H-mediated degradation of the target RNA. To

study this difference, Damha *et al*. determined the NMR solution structures of ANA:RNA and DNA:RNA, and they demonstrated that the sugar of RNA nucleotides of ANA:RNA duplexes adopt the C3′-*endo* conformation, whereas the ANA strand adopts a 'rigid' *O*4′-*endo* (east) sugar pucker and the duplex is intermediate between that of A- and B-form duplexes that closely mimic the native DNA/RNA structure needed for RNase H cleavage.[32]

3.2.2 Rationale, design and objectives of the present work

As presented in the work so far, improved hybridization results were obtained by S-type frozen nucleosides with compact geometry using uracil, thymine and adenine compared to the control ngDNA:RNA duplex. However, to achieve thermal stabilities comparable to or higher than those of unmodified natural 3′-5′-linked duplexes, a more favourable geometry would be warranted for 2′-5′ -linked oligomers.

Arabinonucleoside with 2′-5′ linkages is proposed in this study. In an arabinonucleoside, the sugar ring is in equilibrium between S- and N-type conformations. In this case, the 2′-hydroxyl group is above the plane, therefore the P-P distance is less and the nucleotide would have a compact geometry (Figure 10) in both S-type and N-type sugar conformations.

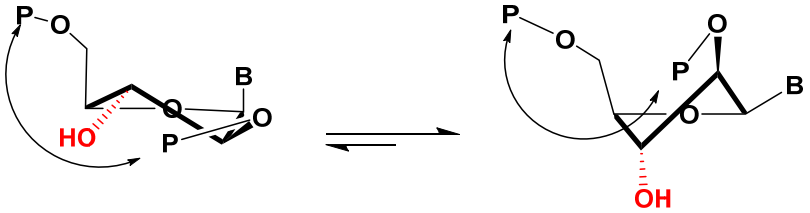

Figure 10: 2'-5'arabino nucleoside showing compact geometry

Objectives of the Section B

1. Synthesis of arabino-uridine (^{ara}U) phosphoramidite monomer.
2. Preliminary study of sugar puckering using ^{1}H NMR $J_{1'2'}$ coupling constant.
3. Synthesis of ngDNA oligonucleotides containing ^{ara}U units, their purification and characterization.
4. UV melting studies of the derived oligomers.

3.2.3 Present work, result and discussion

3.2.3.1 Synthesis of arabino-uridine (^{ara}U) phosphoramidite monomer

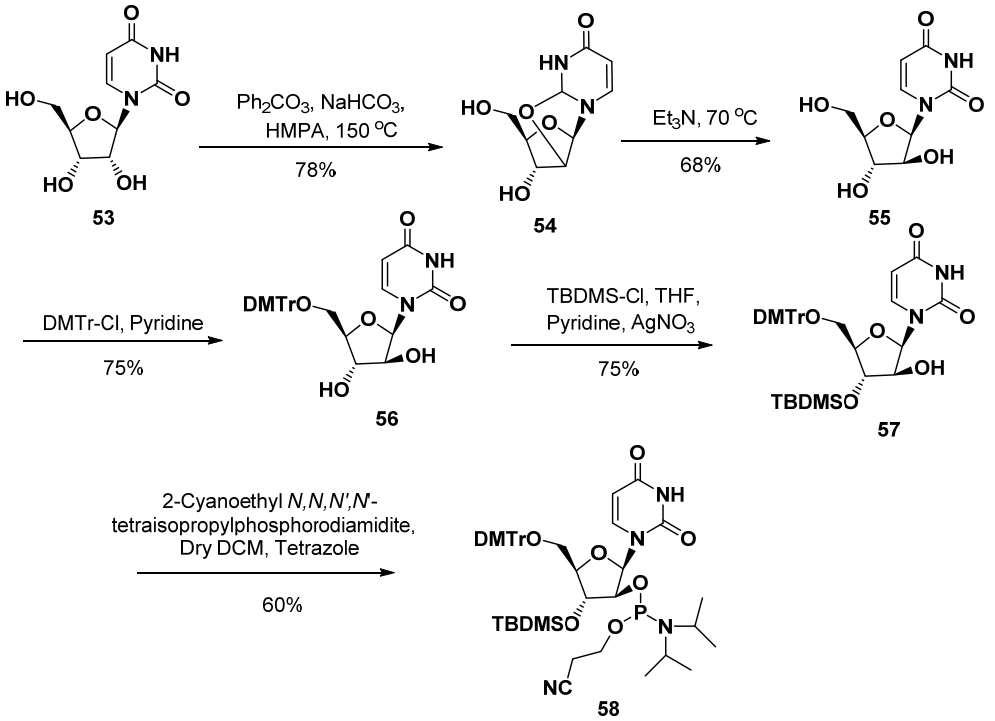

Scheme 4: Synthesis of ^{ara}U phosphoramidite monomer

Arabino uridine **55** was synthesized according to the procedure of Moffatt and co-workers[33] in two steps (Scheme 4). The first step was the formation of the 2, 2′-anhydrouridine. Uridine was heated with diphenyl carbonate in the presence of a small quantity of sodium hydrogen carbonate in hexamethylphosphoric triamide at 150°C, to afford the desired compound **54** in 78% yield. The second step was the opening of the 2, 2′-anhydro bond to generate a β-hydroxyl group at C2′. This was achieved by heating with an excess of triethylamine in aqueous solution at 70°C for 5h, which gave **55** in 68% yield. Reaction of 1-β-D-arabinofuranosyl uracil **55** with DMTr-chloride in pyridine proceeded in a selective manner to give 5'-*O*-DMT derivative **56** (75%), as reported.[34] The standard silylation conditions used in the ribose series was used for silylation (THF, pyridine, $AgNO_3$)[35] of 5'-*O*-DMTr nucleoside **56** which gave 3'-*O*-TBDMS isomer **57** (75%) exclusively and no 2'-*O*-TBDMS product was detected. Finally the 2′-hydroxyl group was phosphitylated by using 2-cyanoethyl *N, N, N', N'*-tetraisopropylphosphorodiamidite in

presence of tetrazole in dry DCM to afford the desired phosphoramidite **58** (60%) as arabino uridine monomer ^{ara}U.

3.2.3.2 Preliminary study of sugar pucker using ^{1}H NMR $J_{1',2'}$ coupling constant

P. Tollin *et al.* reported a crystal structure of arabino uridine **55**, according to which, the sugar pucker in **55** is C2′-*endo* (S-type). We calculated the %S for the same using the formula **%S = 100 x ($J_{1',2'}$-1)/6.9**[20] and H1′-H2′ NMR coupling constants as earlier reported and was found to be 47.8%.[15] We have thoroughly analyzed the conformation of **55** using NMR, X-ray crystal structure and Matlab pseudorotation GUI program which is discussed in Chapter 4. We calculated all the four structural parameters i.e., glycosidic torsion angle χ, torsion angle γ, phase angle of pseudorotation (P) and the puckering amplitude (ν_{max}), which ultimately gives the S-type and N-type population for each monomer in solid state as well as in solution state. In Chapter 4, we also discuss the NOESY NMR study to analyze the *syn/anti* conformation of the nucleobase- uridine.

3.2.3.3 Synthesis of oligonucleotides containing modified units, their purification and characterization

Control 18mer oligonucleotide **DNA2** chosen for the present study is specific for the splice correction of an aberrant β-globin intron (705 site).[22] The oligomers were synthesized using an automated Bioautomation MM4 DNA synthesizer and commercially available 5'-*O*-DMT-3'-deoxy-2'-phosphoramidite building blocks using β–cyanoethyl phosphoramidite method. The modified monomer unit **58** abbreviated as ^{ara}U was incorporated at pre-determined positions using an extended coupling time to yield the modified oligomers efficiently. ONs ngDNA2-9 and ngDNA2-10 (Table 5) were synthesized containing one and two modified building blocks respectively.

3.2.2.3a Purification and MALDI-TOF characterization of modified ngDNA

The synthesized ONs were cleaved from the solid support with conc. NH_4OH, followed by lyophilization. The silyl group was deprotected by adding 0.1mL desilylation solution (1.5mL NMP + 0.75mL TEA + 1.00mL 3HF:TEA) and heated at 65°C for two hours. The reaction mixture was then cooled and neutralized with 0.1mL NH_4HCO_3

(0.5M), lyophilized and desalted to get the crude ONs. The purity of the oligomers listed in Table 5 was checked by analytical RP-HPLC (C18 column, 0.1N TEAA buffer-pH = 7.0 - acetonitrile) which showed more than 75-80% purity. These oligomers were subsequently purified by reverse phase HPLC on a C18 column. The purity of the oligomers was again ascertained by analytical RP-HPLC and found to be >95%. Their integrity was confirmed by MALDI-TOF mass spectrometric analysis. THAP (2,4,6-trihydroxy acetophenone) matrix with diammonium citrate as additive was used for MALDI-TOF mass analysis of oligomers. The HPLC retention times and observed values of mass in MALDI-TOF spectrometry are listed in Table 5.

Table 5. ngDNA oligomers, their HPLC retention times and characterization using MALDI -TOF mass analysis

Entry No	Sequence Code	Sequence (5' → 2')	HPLC t_R (min)	Mass	
				Expected	Observed
1	ngDNA2	CCTCTTACCTCAGTTACA	8.6	5369	5368
2	ngDNA2-9	CCTCTTACCTCAGT^{ara}UACA	7.9	5385	5383
3	ngDNA2-10	CCTCTTACC^{ara}UCAGT^{ara}UACA	8.2	5401	5392

3.2.3.4 Duplex stability studies of arabino-uridine (^{ara}U) modified oligomers

UV-T_m studies were carried out to investigate the binding of the modified oligomers to complementary DNA and RNA. The T_m experiments of duplexes were carried out in 10mM sodium phosphate buffer (pH 7.2) containing 150mM NaCl. Chimeric DNA oligonucleotides were individually hybridized with the complementary DNA and RNA strands, to obtain duplexes. The binding affinity of 18mer chimeric ONs **ngDNA2-9** and **ngDNA2-10** (Table 6, entry 2 and 3) with complementary **DNA2** and **RNA2** was investigated by measuring the melting temperatures (T_ms) of the duplexes and the results are summarized in Table 6**.**

Table 6. T_m (°C) values of 18mer ngDNA2-9 &10: DNA/RNA duplexes

Entry No	Sequence Code	Sequences (5' → 2')	UV-T_m °C		
			cDNA2	RNA2	ΔT_m °C
1	ngDNA2	CCTCTTACCTCAGTTACA	NB	46.0	0.0
2	ngDNA2-9	CCTCTTACCTCAGT^{ara}UACA	NB	45.30	-0.7
3	ngDNA2-10	CCTCTTACC^{ara}UCAGT^{ara}UACA	NB	43.20	-2.3

Similar to the unmodified 18mer ngDNA2 sequence, both the modified ngDNA sequences studied here (Table 6) were found to bind only to complementary RNA and not to complementary DNA. Introduction of a single monomeric unit towards the 2′ end in the 18mer oligomer **ngDNA2-9**, caused a destabilization of 0.7ºC with complementary RNA2. A cumulative effect was observed in destabilization in the **ngDNA2-10** when two ^{ara}U units were incorporated (Figure 11). Thus, intermittent change to arabino 2′-5′ linkage in continuous ribo-2′-5′ backbone at a single or more positions destabilized the duplexes with RNA. It would be perhaps necessary to synthesize a completely modified 2′-5′ phosphodiester-linked DNA oligomer to fully understand the usefulness of this designed oligomer backbone.

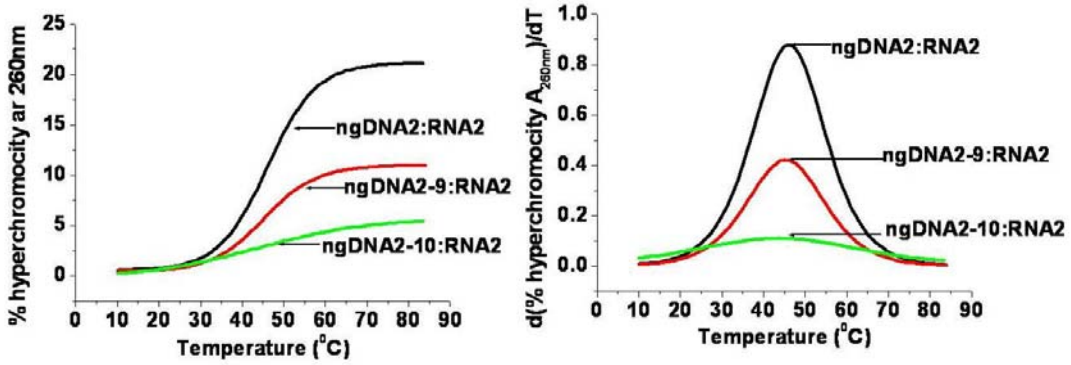

Figure 11: UV-melting plots of complexes of ngDNA2, ngDNA2-9and ngDNA2-410 with complementary RNA2 and corresponding derivative curves

Section C

3.3 Stability of oligonucleotides to SVPD

3.3.1 Introduction

The antisense technology and RNA interference (RNAi) have large potential for human therapeutics and are being explored for some time.[36] In order to be effective and practically useful in the above technologies, AS-ONs must have specific characteristics such as high target-binding affinity, sequence specificity and nuclease resistance. Among all these, nuclease resistance is an important factor, which determines the effectiveness of AS-ONs *in vivo*. The exo- and endo- nucleases cleave the phosphodiester bonds between the nucleotide subunits of AS-ONs *in vivo* and the predominant nuclease activity is of 3′-exonuclease.[37] Exonucleases are enzymes which cleave nucleotides one at a time from the ends (*exo*) (either the 3'- or the 5'-end) of a polynucleotide chain while the endonucleases, cleave phosphodiester bonds in the middle (*endo*) of a polynucleotide chain. A 3'-exonuclease catalyzes the degradation of nucleic acid in 3′→5′ direction with the removal of a nucleoside-5'-phosphate from the 3′-end of DNA (Figure 12).

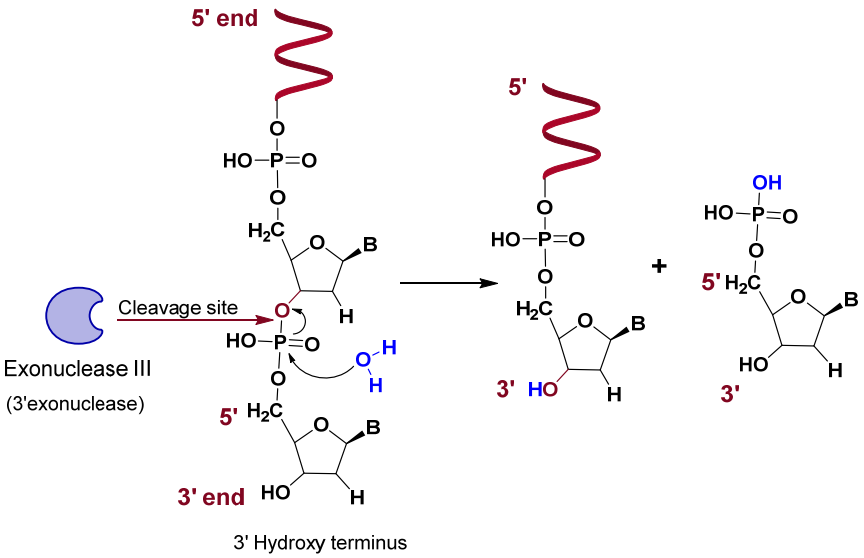

Figure 12: The exonucleolytic cleavage in the 3'- to 5'-direction to yield nucleoside 5'-phosphates

Native ONs do not have acceptable antisense properties mainly because of lack of nuclease resistance. This has stimulated enormous chemical efforts to produce

therapeutically significant modified ONs to provide improved stability, while maintaining high target affinity and specificity. First generation AS-ONs with chemical modification of the phosphodiester linkage to the phosphorothioate have shown improved nuclease resistance but reduced affinity towards a complementary RNA sequence.[38] The second generation of AS-ONs involves various 2′-modifications[39] of the ribose moiety with appropriate electronegative substituents having RNA-like 3′-*endo* sugar puckering. This results in a considerable improvement of binding affinity to the target RNA. In this case, size, electronegativity, and configuration of the 2′-substituents are all very important factors for the target affinity and nuclease resistance.[40] The new third generation of AS-ONs, containing conformationally constrained LNA (also called BNA)[41-42] have rigid bicyclic ring systems that result in typical locked 3′-*endo* conformation of the sugar puckering which shows unusually high affinity toward complementary RNA strand (3-8°C per modification). Unfortunately, though LNA containing AS-ONs are more nucleolytically stable than the native PO AS-ONs, they do not have nuclease resistance as good as that of the PS AS-ONs.[43] The nuclease resistance of 3′-amino-2′, 4′-BNA is excellent, much higher than that of natural and 2′,4′-BNA (LNA) oligonucleotides, and substantially higher even than that of 3′-amino-DNA and phosphorothioate oligonucleotides and these also form highly stable duplexes (Figure 13).[44]

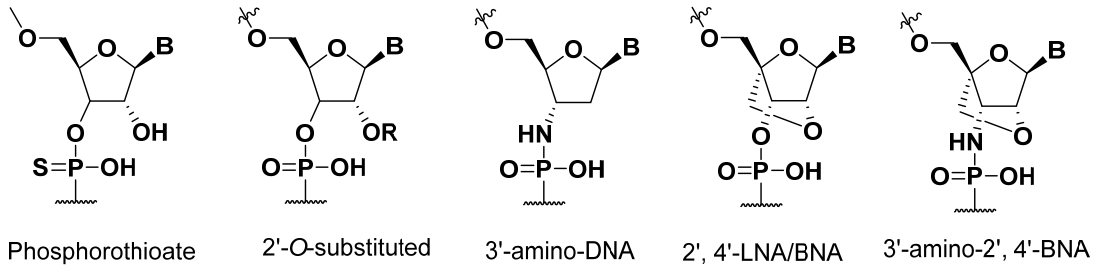

Figure 13: AS-ONs with different chemical modifications

The 2′-5′ linked nongenetic ngDNA and ngRNA show high resistance to nuclease digestion compared with the natural 3′-5′-linked oligomer.[45] However, it is also reported that natural 2′-5′ oligoadenylate $(2'\text{-}5')A_n$ which activates RNase L (which cleave mRNA) has short biological half-life and is rapidly degraded by phosphatases and nucleases (like phosphodiesterases) in cells and in serum.[46] Obika *et al*[46a] reported that the incorporation of a longer alkylene bridging linkage in the third adenosine of $(2'\text{-}5')A_n$ tetramer gave greater

nuclease resistance and high RNase L activity. In this case the 3'-*O*,4'-*C*-propyleneadenosine **P** showed the highest stability among (2′-5′)A_n analogues containing a modified adenosine such as the 3'-*O*-methyladenosine **M**, 3'-*O*,4'-*C*-methyleneadenosine **B** and 3'-*O*,4'-*C*-ethyleneadenosine **E** (Figure 14).

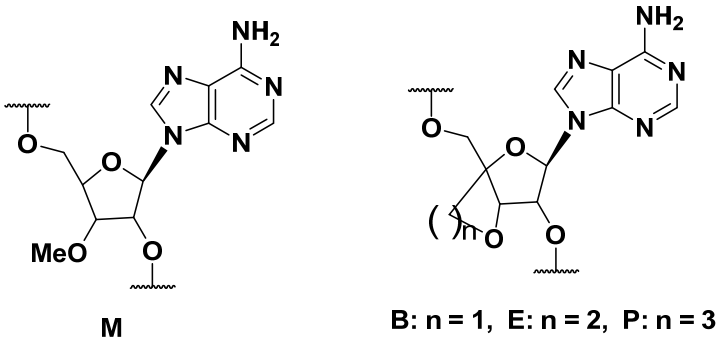

Figure 14: (2′-5′)A_n analogues composed of 3′-*O*,4′-C-alkyleneadenosine

3.3.2 Present work, results and discussion

Considering nuclease resistance as an important factor, we examined the 3′-exonuclease sensitivity of the unmodified and modified ngDNA using phosphodiesterase I from *Crotalus adamanteus* venom [snake venom phosphodiesterase (SVPD)] and compared them with natural DNA. The 18mer unmodified ngDNA1 and modified ngDNA1-2 and ngDNA1-4 containing two $^{R}U^{F}$ and $^{X}U^{F}$ units respectively were chosen for the experiment (Table 7).

Table 7. Oligonucleotides used for 3′-exonuclease degradation study

Entry No.	Scequence code	Sequences	18 mer Mass	17 mer Mass
1	DNA1	**5′** CACCATTGTCACACTCC**A 3′**	5364/5364	not observed
2	ngDNA1	**5′** CACCATTGTCACACTCC**A 2′**	5364/5364	5050/5357
3	ngDNA1-2	**5′** CACCATTG$^{X}U^{F}$CACAC$^{X}U^{F}$CC**A 2′**	5372/5372	5058/5058
4	ngDNA1-4	**5′** CACCATTG$^{R}U^{F}$CACAC$^{R}U^{F}$CC**A 2′**	5372/5372	5058/5057
5	ngDNA3	**5'**GAAGGGCTTCTTCCTTA**T 2'**	5480/5480	not observed

The synthesis, purification and characterization of these sequences are discussed in chapter 1. Literature reports[45] have shown the superior nuclease resistance of the ngDNA/ngRNA oligonucleotides over natural DNA. Therefore, in the present study, in order to understand the relative nuclease resistance of modified and unmodified ngDNA with natural DNA, we conducted nuclease resistance studies at high nuclease concentration [SVPD 20µg/mL, ONs 7.5µM, 50mM Tris-HCl (pH 8.0), 15mM $MgCl_2$, total volume 500μL, and aliquot volume for analysis, 20μL].

The ONs were incubated at 37°C in the presence of SVPD in Tris-HCl. Aliquots were taken out at appropriate time intervals and the percentage of intact ONs at each time point was analyzed by RP-HPLC. The HPLC peaks obtained for each sequence at every time point are overlaid in the plot shown in Figure 14.

The natural 3′-5′ linked single strand DNA1 did not show any 3′-exonuclease resistance and was completely degraded in 20min. In the case of modified and unmodified 2′-5′ linked 3′-deoxy-oligonucleotides (ngDNA), the last nucleotide, A18, was removed quickly within 20min to give 17mer oligonucleotides. Once the A18 nucleotide was cleaved, the obtained 17mer of the unmodified as well as modified ngDNAs were found to be considerably stable under these conditions. This indicates that the stability of the 2′-end adenosine is very less compared to other nucleosides. SVPD is known to cleave the tetrameric 2′-5′ adenine sequences[32] and in this particular study, the sequences used happened to contain an adenine nucleoside at the 2′-end. The HPLC peak arising after the A18 cleavage was identified by MALDI-TOF mass spectrometry as the oligomer in which one adenosine-5′-phosphate unit is deleted (Table 7). To confirm this finding, we further synthesized an unmodified 2′-5′ linked 3′-deoxy oligomer (ngDNA3), that has a thymine nucleotide at the 2′-end. This oligomer was found to be stable towards nucleolytic cleavage and T18 nucleotide cleavage was not observed (Figure 15).

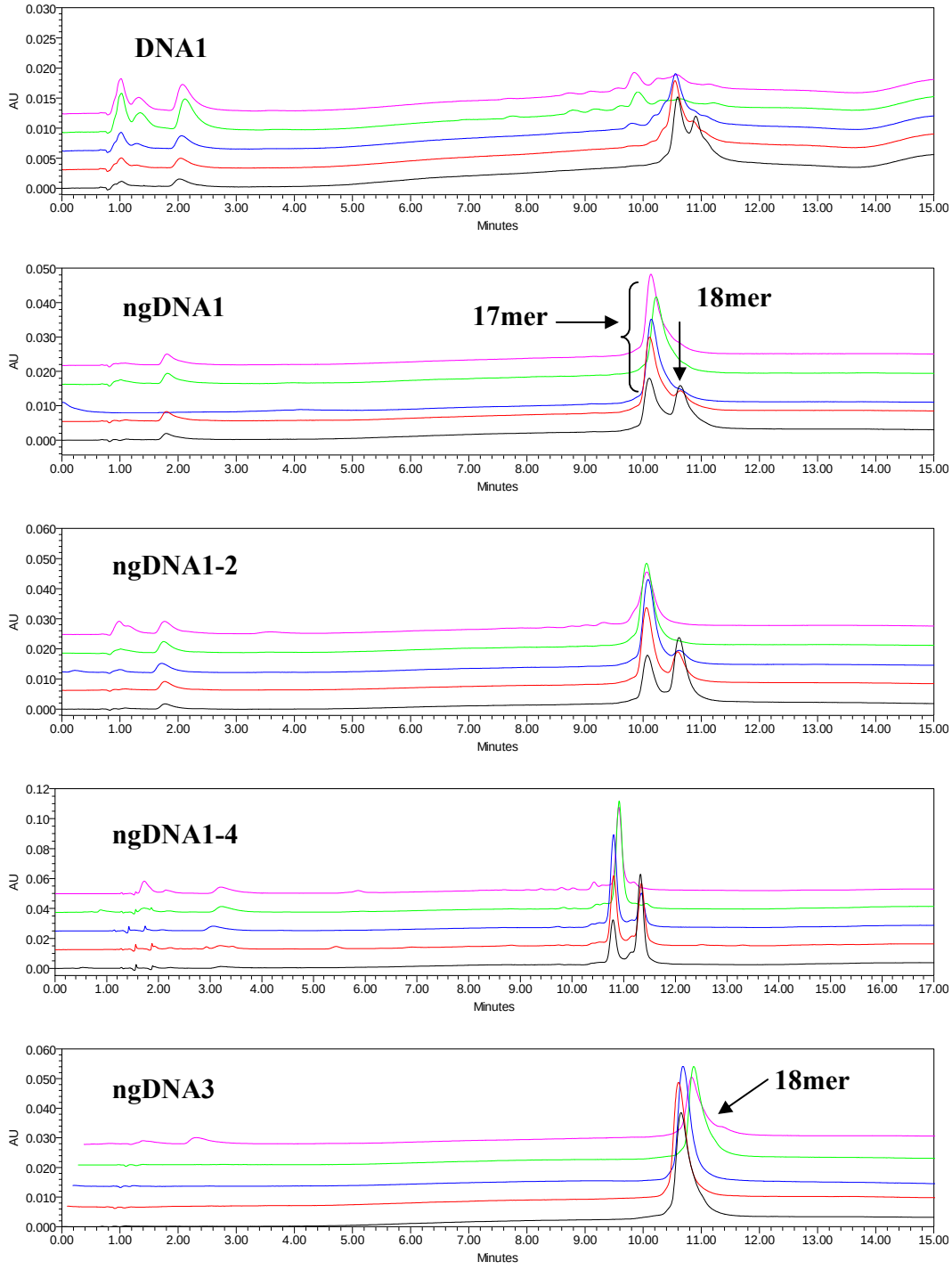

Figure 15: RP-HPLC at several time-points for SVPD study for DNA1, ngDNA1, ngDNA1-2, ngDNA1-4 and ngDNA3
(Black-2min, Red-5min, Blue-10min, Green-30min, Magenta-120min)

In Figure 16, total percentages of intact 17mer ONs were plotted against time points to give SVPD digestion curves for each ONs. Thus, it can be concluded that the 2′-5′ oligonucleotides were found to be resistant to digestion by the 3′-exonuclease except for the hydrolytic cleavage of the 2′-terminal adenosine-5′-phosphate. Thus we decided to study the effect of modified adenosine nucleotide on SVPD digestion by incorporating it at the 2′-end of the sequences.

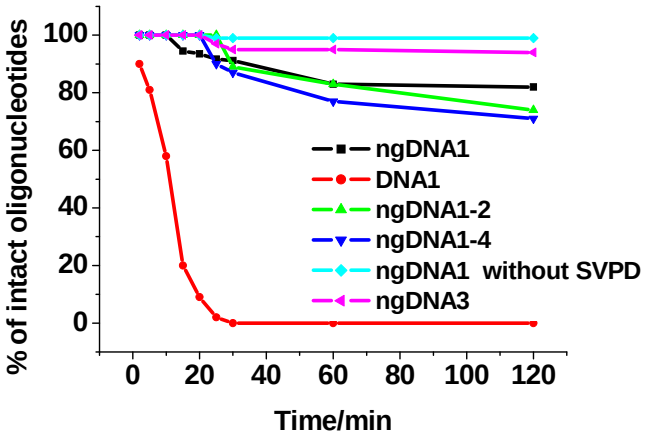

Figure 16: Stability assay of the 17mer (after A18Cleavage) ONs to degradation by SVPD.

3′-deoxy-3′-fluoro ribo/xyloadenosine ($^{R}A^{F}$, $^{X}A^{F}$) are modified nucleosides which have an S- and N-type frozen sugar conformation respectively due to the 3′-fluoro group. The S-type locked adenosine ($^{L}A^{S}$) is locked in S-type sugar due to the bridging methylene linkage in the furanose. To test the 3′-exonuclease stability by the oligomers comprising these modified adenosine nucleotide, three oligomers with $^{R}A^{F}$, $^{X}A^{F}$ or $^{L}A^{S}$ modified monomers at their 2′-ends were synthesized (Table 8). The synthesis, purification and characterization data for the monomers as well as oligomers are given in section A.

In this particular experiment, in order to understand the relative nuclease resistance of $^{R}A^{F}$-, $^{X}A^{F}$- and $^{L}A^{S}$-modified ngDNA in comparison to unmodified ngDNA, we conducted the nuclease resistance experiment at lower nuclease concentration (SVPD 5µg/mL, ONs 7.5µM, 50mM Tris-HCl (pH 8.0), 15mM $MgCl_2$, total volume 500μL, and aliquot volume 20μL). This enabled us to determine the difference in stability of particular 2′-end-modified adenosine units. In this experiment, the stability of oligomers is considered only for 2′-end adenosine deletion.

Table 8. 2′end adenosine-modified ($^{R}A^{F}$, $^{X}A^{F}$ and $^{L}A^{S}$) ONs

Entry No	Sequence code	Sequence
1	ngDNA1	**5**‘CACCATTGTCACACTCC**A 2**’
2	ngDNA1-6	**5**‘CACCATTGTCACACTCC^{X}**A**^{F} **2’**
3	ngDNA1-7	**5**‘CACCATTGTCACACTCC^{R}**A**^{F} **2’**
4	ngDNA1-8	**5**‘CACCATTGTCACACTCC^{L}**A**^{S} **2’**

All the entire 2′-end-modified ngDNAs showed increased stability to SVPD than unmodified ngDNA (Figure 17). The **ngDNA1-8**, which is modified with S-type locked adenosine ($^{L}A^{S}$), had highest stability among all the modified ngDNA. The **ngDNA1-7** with the S-type frozen $^{R}A^{F}$ unit showed more stability than **ngDNA1-6** with N-type frozen unit, $^{X}A^{F}$. These results suggest that the incorporation of S-type frozen/locked adenosine gave greater nuclease resistance. The **ngDNA1-6** with the N-type frozen $^{X}A^{F}$ unit also showed slightly higher stability than the unmodified ngDNA1, probably because of the fluoro group of $^{X}A^{F}$ at 3′ position.

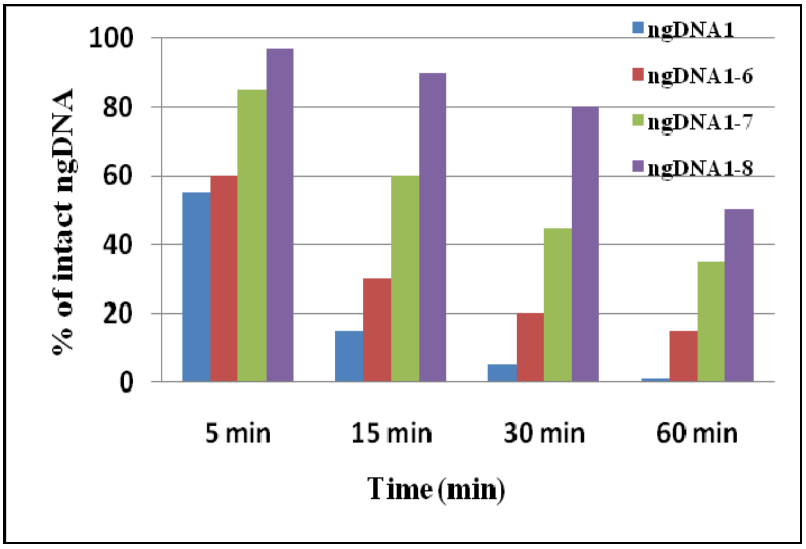

Figure 17: Stability assay of the ngDNA to degradation by SVPD

3.4 Summary and conclusion

1. Synthesis of the 3′-deoxy-3′-fluoro ribo/xylo thyminyl, and adeninyl nucleoside monomers ($^{R}T^{F}$, $^{X}T^{F}$ and $^{R}A^{F}$, $^{X}A^{F}$) was completed and these were successfully incorporated into ngDNA oligomers.

2. Synthesis of S-type locked ($^{L}A^{S}$) monomer was completed and ngDNA oligomer containing $^{L}A^{S}$, $^{R}A^{F}$ and $^{X}A^{F}$ monomer at 2′ end were synthesized to study the nuclease resistance properties.

3. Preliminary NMR study showed that $^{R}T^{F}$, $^{R}A^{F}$ and $^{L}A^{S}$ prefer S-type while $^{X}A^{F}$, $^{X}T^{F}$ prefer N-type sugar conformations.

4. UV-melting experiments showed stabilization of *ng*DNA:RNA by S-type frozen monomer and destabilization of the same by N-type frozen monomers but the substitution of thymine for uracil did not improve T_m.

5. Synthesis of compact arabino uridine (^{ara}U) monomer was completed. Its incorporation in ngDNA caused destabilization of the resulting ngDNA:RNA duplex.

6. Nuclease resistance studies of all the 2′-end modified ngDNAs showed them to be stabler to SVPD digestion than unmodified ngDNA and the stability order was $^{L}A^{S}$ ngDNA>> $^{R}A^{F}$ ngDNA> $^{X}A^{F}$ ngDNA > ngDNA.

Conclusion

The stabilization caused by the S-type frozen monomer ($^{R}T^{F}$ and $^{R}A^{F}$) and destabilization by N-type frozen $^{X}A^{F}$ monomer and by the compact arabino uridine (^{ara}U) is again in accordance with the prediction of S-type conformation for the ngDNA strand in an ngDNA:RNA duplex.[16] Thymine does not improve stability over uracil in 2′-5′ linked ngDNA, which is in contrast to the natural DNA. This could be due to pseudoequatorial base orientation in S-type sugar geometry, where stacking and hydrogen bonding is not strong. S-type frozen/locked $^{R}A^{F}$ and $^{L}A^{S}$ units confer high stability to SVPD, while the N-type frozen $^{X}A^{F}$ leads to successful modulation of the nuclease resistance.

3.5 Experimental

3.5.1 Synthesis of compounds/monomers

General remarks: All the reagents were purchased from Sigma-Aldrich and used without purification. DMF, ACN, were dried over P_2O_5 and CaH_2 respectively and stored by adding 4 Å molecular sieves. Pyridine, TEA were dried over KOH and stored on KOH. THF was passed over basic alumina and dried by distillation over sodium. Reactions were monitored by TLC, which were carried out on pre-coated silica gel GF254 sheets (Merck 5554). TLCs were run either in Pet-ether/EtOAc or DCM/MeOH solvent system for most of the compounds and were visualized with UV light and iodine spray and/or by spraying perchloric acid solution and heating. Usual reaction work up involved sequential washing of the organic extract with water and brine followed by drying over anhydrous sodium sulfate (Na_2SO_4) and evaporation of the solvent under vacuum. Column chromatographic separations were performed using silica gel 60-120 mesh and 200-400 mesh (Merck) and using the solvent systems EtOAc/Pet ether and MeOH/DCM.

^1H and ^{13}C NMR spectra were obtained using Bruker AC-200, AC-400 and AC-500 NMR spectrometers. The chemical shifts (δ/ppm) are referred to internal TMS/DMSO-d_6 for ^1H and chloroform-*d*/DMSO-d_6 for ^{13}C NMR. ^1H NMR data are reported in the order of chemical shift, multiplicity (s, singlet; d, doublet; t, triplet; br, broad; br s, broad singlet; m, multiplet and/ or multiple resonance), number of protons. Mass spectra were recorded on APQSTAR spectrometer, LC-MS on a Finnigan-Matt instrument. DNA oligomers were synthesized on CPG solid support using Bioautomation Mer-Made 4 synthesizer. The RNA oligonucleotides were obtained commercially (Sigma-Aldrich). RP-HPLC was carried out on C18 column using Waters system (Waters Delta 600e quaternary solvent delivery system and 2998 photodiode array detector and Empower2 chromatography software). MALDI-TOF spectra were recorded on a AB Sciex TOF/TOF™ Series Explorer™ 72085 instrument and the matrix used for analysis was THAP. UV experiments were performed on Varian Cary 300 UV-VIS spectrophotometer fitted with Peltier-controlled temperature programmer. CD spectra were recorded on Jasco J-715 Spectropolarimeter, with ThermoHaake K20 programmable water circulator for temperature control of the sample.

Experimental procedures and spectral data

2′,5′-di-*O*-acetyl-3′-deoxy-3′-fluoro-xylothymidine (24)

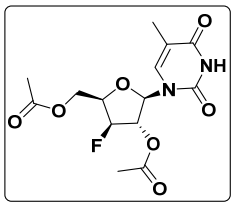

Compound **24** (0.46g) was synthesized by Vorbrüggen glycosylation reaction using silylated thymine (0.34g, 2.67mmol) and compound **9** (0.5g, 1.79mmol) accordingly as mentioned earlier in Chapter 1 for compound **10**. Yield 0.46g, 75%.

Mol. Formula : $C_{14}H_{17}FN_2O_7$

Mol. Weight : 344.30

ESI-Ms m/z : 367.0547($M+Na^+$)

^{1}H NMR (200MHz, $CDCl_3$) : **δ_H** (ppm) 1.95 (s, 3H, CH_3), 2.14 (s, 3H, OAc), 2.16 (s, 3H, OAc), 4.43-4.50 (m, 3H), 4.95-5.31 (m, 2H), 6.13-6.14 (d, 1H, H-1′, $J_{1',2'}$= 2.4Hz), 7.17 (s, 1H, H6)

^{13}C NMR (50MHz, $CDCl_3$) : **δ_C** (ppm) 12.5, 20.3, 20.5, 60.3-60.4 (d), 78.6-78.9 (d), 79.0-79.5 (d), 87.9, 91.3-94.9 (d), 112.1, 134.5, 138.6, 150.3, 163.7, 169.0, 170.4

^{13}C-DEPT (50MHz, $CDCl_3$) : **δ_C** (ppm) Positive peaks: 12.6, 20.5, 20.7, 78.7-79.0 (d), 79.1-79.6 (d), 88.0, 91.4-95.0 (d), 134.6, 134.7 Negative peaks: 60.4-60.6 (d)

***N*^{6}-Benzoyl-2′,5′-di-*O*-acetyl-3′-deoxy-3′-fluoro-xyloadenosine (25)**

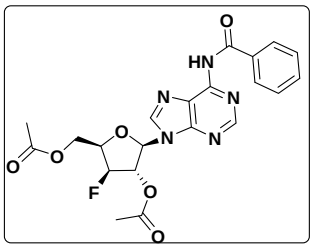

Compound **25** was synthesized by using same Vorbrüggen glycosylation reaction using silylated N^6-benzoyl adenenine (0.47g, 1.97mmol) from compound **9** (0.5g, 1.79mmol) accordingly as mentioned earlier in Chapter **1** for compound **10**. Yield 0.57g, 70%.

Mol. Formula : $C_{21}H_{20}FN_5O_6$

Mol. Weight : 457.42

ESI-Ms m/z : 480.1770 ($M+Na^+$)

^{1}H NMR (200MHz, $CDCl_3$) : **δ_H** (ppm) 2.14, 2.21 (2S, OAc), 4.42-4.65 (m, 3H), 5.10-5.35 (m, 1H), 5.58-5.66 (m, 1H), 6.40 (d, 1H), 7.50-7.63 (m, 3H),

8.02-8.05 (m, 2H), 8.23 (S, 1H), 8.83 (S, 1H), 9.14 (S, 1H)

^{13}C NMR (50MHz, $CDCl_3$) : **δ_C** (ppm) 20.3, 20.4, 60.2-60.4 (d), 78.9-80.0 (d), 79.5-79.6 (d), 87.0, 90.9-94.6 (d), 122.5, 127.8, 128.3, 132.4, 133.3, 140.4, 149.5, 151.2, 152.6, 165.0, 168.7, 170.2.

^{13}C-DEPT (50MHz, $CDCl_3$) : **δ_C** (ppm) Positive peaks: 20.5, 20.6, 79.1-80.2 (d),79.7-79.9 (d), 87.2, 91.1, 94.8, 128.0, 128.6, 132.6, 140.8, 152.82 Negative peaks: 60.4-60.6 (d)

3′-deoxy-3′-fluoro-2′-hydroxy-xylothymidine (26)

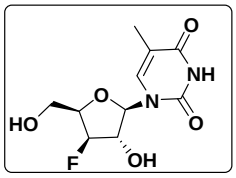

The 5′ and 2′-*O*-acetyl group of compound **24** (0.5g) was deprocted using aqueous ammonia (5mL) in MeOH (10mL) to get diol compound **26** following the same previously mentioned procedure in Chapter 1 for compound **11**. Yield, 0.34g, 90%.

Mol. Formula : $C_{10}H_{13}FN_2O_5$

Mol. Weight : 260.22

ESI-Ms m/z : 283.1902 ($M+Na^+$)

^{1}H NMR (200MHz, CD_3OD) : **δ_H** (ppm) 1.87 (s, 1H, CH_3), 3.80-3.95 (m, 2H), 4.27-4.40 (m, 2H), 4.85-5.10 (m, 1H), 5.85 (s, 1H, H-1), 7.84 (s, 1H, H6)

^{13}C NMR (50MHz, CD_3OD) : **δ_C** (ppm) 12.6, 59.5-59.7 (d), 79.5-80.0 (d), 83.6-83.9 (d), 92.4, 94.7-98.4 (d), 111.2, 137.3, 137.4, 152.3, 166.3

^{13}C-DEPT (50MHz, CD_3OD) : **δ_C** (ppm) Positive peaks: 12.6, 79.5-80.1 (d), 83.6-84.0 (d), 92.5, 94.8-98.4 (d), 137.4, 137.5 Negative peaks: 59.6-59.8

***N*^{6}-Benzoyl-3′-deoxy-3′-fluoro-xyloadenosine (27)**

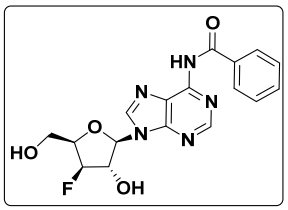

The 5′ and 2′-*O*-acetyl group of compound **25** (0.25g) was deprotected using aqueous ammonia (5mL) in MeOH (10mL) to get diol compound **27** following previously mentioned procedure in Chapter **1** for compound **11**. Yield, 0.16g, 80%.

Mol. Formula : $C_{17}H_{16}FN_5O_4$

Mol. Weight : 373.34

ESI-Ms m/z : 374.2248 ($M+H^+$), 395.9864 ($M+Na^+$)

^{1}H NMR (500MHz, CD_3OD)	**:**	**δ_H** (ppm) 3.94-4.02 (m, 2H, H5′, H-5′′), 4.47-4.54 (m, 1H), 4.78-4.81 (m, 1H), 5.07-5.18 (m, 1H, H3′), 6.25 (s, 1H, H1′), 7.55-7.67 (m, 3H, C_6H_6), 8.07-8.09 (m, 2H, C_6H_6), 8.44 (s, 1H), 8.73 (s, 1H)
^{13}C NMR (250MHz, CD_3OD)	**:**	**δ_C** (ppm) 59.5-59.9 (d), 79.5-79.8 (d), 84.3-84.4 (d), 91.7, 95.9-97.4 (d), 125.0, 129.4, 129.7, 133.9, 134.9, 143.4, 151.0, 153.0, 153.3, 168.1
^{13}C-DEPT (250MHz, CD_3OD)	**:**	**δ_C** (ppm) Positive peaks: 79.5-79.8 (d), 84.3-84.49 (d), 91.7, 95.9-97.4 (d), 129.4, 129.7, 133.9, 143.3, 153.3 Negative peaks: 59.5-59.9 (d)

5′-*O*-dimethoxytrityl-3′-deoxy-3′-fluoro-2′-hydroxy-xylothymidine (28)

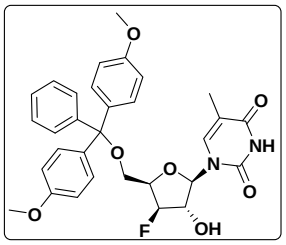

The 5′-hydroxy group of compound **26** (0.53g, 2.03mmol) was protected by 4, 4′-dimethoxytrityl chloride (0.67g, 2.03mmol) to get compound **28** by following the same synthetic procedure mentioned in Chapter **1** for compound **12**. Yield 0.67g, 60%.

Mol. Formula	**:**	$C_{31}H_{31}FN_2O_7$
Mol. Weight	**:**	562.59
HRMS(ESI)	**:**	585.2008 ($M+Na^+$)
^{1}H NMR (400MHz, $CDCl_3$)	**:**	**δ_H** (ppm) 1.75 (s, 3H, CH_3), 3.44-3.59 (m, 2H), 3.77 (s, 6H, OCH_3), 4.47-5.07 (m, 3H), 5.90 (s, 1H), 6.83-6.85 (m, 4H), 7.23-7.51 (m, 10H)
^{13}C NMR (100MHz, $CDCl_3$)	**:**	**δ_C** (ppm) 12.4, 55.0, 60.5-60.6 (d), 78.6-78.9 (d), 82.4-82.5 (d), 86.3, 92.8, 93.8-95.6 (d), 110.2, 113.0, 126.8, 127.8, 128.0, 129.9-130.0 (d), 135.4, 135.5, 144.4, 150.8, 158.4, 164.6
^{13}C-DEPT (100MHz, $CDCl_3$)	**:**	**δ_C** (ppm) Positive peaks: 12.4, 55.0, 78.6-78.8 (d), 82.4-82.5 (d), 92.8, 93.8-95.6 (d), 113.0, 126.8, 127.8, 128.0, 129.9-130.0 (d), 135.4, Negative peaks: 60.6-60.6 (d)

N^6-Benzoyl-5′-*O*-dimethoxytrityl-3′-deoxy-3′-fluoro-xyloadenosine (29)

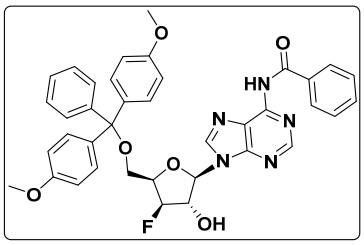

The 5′-hydroxy group of compound **27** (0.75g, 2.03mmol) was protected by 4, 4′-dimethoxy trityl chloride (0.67g, 2.03mmol) to get compound **29** by following the same synthetic procedure mentioned in Chapter 1 for compound **12**. Yield, 0.8g, 60%.

Mol. Formula : $C_{38}H_{34}FN_5O_6$

Mol. Weight : 675.72

ESI-Ms m/z : 698.23 ($M+Na^+$)

^{1}H NMR (400MHz, $CDCl_3$) : **δ_H** (ppm) 3.47-3.59 (m, 2H), 3.74 (s, 6H), 4.62-5.17 (m, 3H), 6.28 (s, 1H), 6.80-6.82 (m, 2H), 7.19-7.47 (m, 14H), 7.91-7.93 (m, 2H), 8.10 (s, 1H), 8.90 (s, 1H)

^{13}C NMR (100MHz, $CDCl_3$) : **δ_C** (ppm) 55.0, 60.4-60.5 (d), 78.7-79.0 (d), 81.9-82.1 (d), 86.4, 90.7, 94.3, 96.0-96.1 (d), 113.0, 122.5, 126.8, 127.7, 128.0, 128.6, 129.9, 132.8, 133.2, 135.4, 135.6, 144.4, 149.0, 150.89, 152.2, 158.4, 164.8

^{13}C-DEPT (100MHz, $CDCl_3$) : **δ_C** (ppm) Positive peaks: 55.0, 78.7-79.0 (d), 81.9-82.1 (d), 90.7, 94.3-96.1 (d), 113.0, 126.8, 127.7, 127.9, 128.6, 129.91, 129.9, 132.8 Negative peaks: 60.4-60.5 (d)

N^6-Benzoyl-5′-*O*-dimethoxytrityl-3′-deoxy-3′-fluoro-xyloadenosinyl-2′-*O*-phosphoramidite (31)

Phosphoramidite derivative of Compound **29** (0.24g, 0.36mmol) was synthesized by using

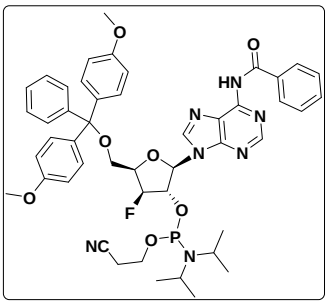

2-Cyanoethyl *N,N*-diisopropylchlorophosphoramidite (0.15ml, 0.72mmol) accordingly as mentioned earlier in Chapter **1** for compound **13**. Yield 0.12g, 43%.

Mol.Formula : $C_{47}H_{51}FN_7O_7P$

Mol.Weight : 875.94

HRMS (ESI) : 876.3644($M+H^+$)

^{31}P NMR (161MHz, $CDCl_3$) : **δ_H** (ppm) 151.34, 152.55

2′-*O*-acetyl-5'-*O*-benzoyl-3'-deoxy-3'-fluoro-thymidine (32)

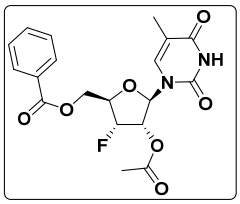

Compound **32** (0.44g) was synthesized by Vorbrüggen glycosylation reaction using silylated thymine (0.35g, 2.67mmol) and compound 1**9** (0.5g, 1.79mmol) accordingly as mentioned earlier in Chapter **1** for compound **10**. Yield 0.44g, 75%.

Mol. Formula : $C_{19}H_{19}FN_2O_7$

Mol. Weight : 406.37

ESI-Ms m/z : 429.56 ($M+Na^+$)

^{1}H NMR (200MHz, $CDCl_3$) : **δ_H** (ppm) 1.57 (s, 3H), 2.18 (s, 1H), 4.48-4.77 (m, 3H), 5.26-5.53 (m, 2H), 6.23-6.27 (d, 1H, $J_{1',2'}$= 7.33), 7.04 (s, 1H), 7.46-7.67 (m, 3H), 8.05-8.09 (m, 2H), 9.30 (s, 1H)

N^6-Benzoyl-2′-*O*-acetyl-5'-*O*-benzoyl-3'-deoxy-3'-fluoro-adenosine (33)

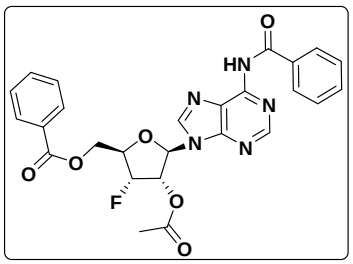

Compound **33** (0.53g) was synthesized by using same Vorbrüggen glycosylation reaction using silylated N^6-benzoyl adenenine (0.47g, 1.97mmol) from compound **19** (0.5g, 1.79mmol) accordingly as mentioned earlier in Chapter **1** for compound **10**. Yield 0.53g, 70%.

Mol. Formula : $C_{26}H_{22}FN_5O_6$

Mol. Weight : 519.49

ESI-Ms m/z : 542.23 ($M+Na^+$)

^{1}H NMR (200MHz, $CDCl_3$) : **δ_H** (ppm) 2.14 (s, 3H), 4.53-4.86 (m, 3H), 5.51-5.81 (m, 1H), 6.13-6.31 (m, 2H), 7.43-7.63 (m, 6H), 8.0-8.11 (m, 5H), 8.54 (s, 1H), 9.05 (s, 1H)

^{13}C NMR (100MHz, $CDCl_3$) : **δ_C** (ppm) 20.3, 62.9-63.0 (d), 72.6-72.7 (d), 81.0-81.2 (d), 85.7, 88.1-90.0 (d), 123.8, 127.8, 128.6, 128.8, 129.1, 129.7, 132.8, 133.3, 133.5, 142.0, 149.7, 151.8, 152.7, 164.5, 165.9, 169.6

^{13}C-DEPT (100MHz, $CDCl_3$) : **δ_C** (ppm) Positive peaks: 20.5, 72.6-72.7 (d), 81.0-81.3 (d), 85.7, 88.1-90.0 (d), 127.9, 128.6, 128.9, 129.7, 132.9, 133.6, 142.0, 152.8 Negative peaks: 62.9-63.0 (d)

3′-deoxy-3′-fluoro-2′-hydroxy-thymidine (34)

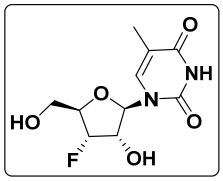

The 5′-*O*-benzoyl and 2′-*O*-acetyl group of compound **32** (0.5g) was deprotected using aqueous ammonia (5mL) in MeOH (10mL) to get compound **34** following the same previously mentioned procedure in Chapter **1** for compound **11**. Yield, 0.29g, 90%.

Mol. Formula : $C_{10}H_{13}FN_2O_5$

Mol. Weight : 260.22

ESI-Ms m/z : 282.97 ($M+Na^+$)

^{1}H NMR (400MHz, CD_3OD) : **δ_H** (ppm) 1.89 (s, 3H, CH_3), 3.77 (m, 2H, H5', H5''), 4.25-4.42 (m, 2H, H2', H4'), 4.91-5.06 (m, 2H, H3'), 6.04-6.06 (d, 1H, H1'), 7.78 (s, 1H, H6')

^{13}C NMR (100MHz, CD_3OD) : **δ_C** (ppm) 12.4, 62.3-62.4 (d), 74.3-74.5 (d), 84.8-85.0 (d), 88.2, 93.0-94.8 (d), 112.1, 137.9, 152.9, 166.2

^{13}C-DEPT (100MHz, CD_3OD) : **δ_C** (ppm) Positive peaks: 12.4, 74.3-74.5 (d), 84.8-85.0 (d), 88.2, 92.9-94.8 (d), 137.9 Negative peaks: 62.3-62.4 (d)

***N*^{6}-Benzoyl-3′-deoxy-3′-fluoro-adenosine (35)**

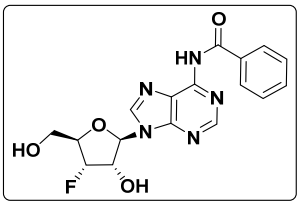

The 5′-*O*-benzoyl and 2′-*O*-acetyl group of compound **33** (0.25g) was deprocted using aqueous ammonia (5mL) in MeOH (10mL) to get diol compound **35** following previously mentioned procedure in chapter 1 for compound **11**. Yield, 0.14g, 80%.

Mol. Formula : $C_{17}H_{16}FN_5O_4$

Mol. Weight : 373.34

ESI-Ms m/z : 396.11 ($M+Na^+$)

^{1}H NMR (200MHz, CD_3OD) : **δ_H** (ppm) 3.69-3.95 (m, 2H), 4.48-4.62 (m,1H), 4.92-5.33 (m, 2H), 6.03-6.07 (d, 1H, $J_{1',2'}$= 7.96), 7.92-7.66 (m, 3H), 8.08-8.12 (m, 2H), 8.33 (s, 1H), 8.76 (s, 1H)

^{13}C NMR (100MHz, CD_3OD) : **δ_C** (ppm) 62.2-62.3 (d), 73.5-73.6 (d), 85.5-85.7 (d), 90.1, 92.5-94.3 (d), 114.1, 128.4, 128.9, 133.1, 133.5, 143.6, 150.7, 151.0, 152.1, 166.2

^{13}C-DEPT : δ_C (ppm) Positive peaks: 73.1-73.3 (d), 85.2-85.4 (d), 89.8, 92.1-94.0 (d), 128.0, 128.5, 132.8, 143.2, 151.7 Negative peaks: 61.9-62.0 (d)
(100MHz, CD_3OD)

5′-*O*-dimethoxytrityl-3′-deoxy-3′-fluoro-2′-hydroxy-thymidine (36)

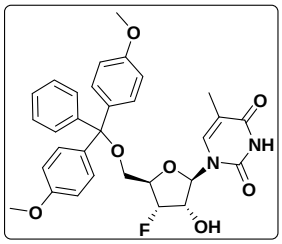

The 5′-hydroxy group of compound **34** (0.53g, 2.03mmol) was protected by 4, 4′-dimethoxytrityl chloride (0.67g, 2.03mmol) to get compound **36** by following the same synthetic procedure mentioned in Chapter **1** for compound **12**. Yield 0.68g, 60%.

Mol. Formula : $C_{31}H_{31}FN_2O_7$

Mol. Weight : 562.59

HRMS(ESI) : 285.4984 ($M+Na^+$)

^{1}H NMR : δ_H (ppm) 1.46 (s, 3H, CH_3), 3.34-3.55 (m, 2H), 3.80 (s, 6H), 4.38-4.57 (m, 2H), 4.99-5.14 (m, 1H), 6.11-6.13 (m, 1H), 6.83-6.86 (m, 4H), 7.22-7.37 (m, 15H), 7.54 (s, 1H)
(400MHz, $CDCl_3$)

^{13}C NMR : δ_C (ppm) 11.7, 55.2, 62.9-63.0 (d), 74.6-74.8 (d), 82.0, 82.3, 87.3-87.5 (d), 91.8-93.6 (d), 111.9, 113.4, 127.3, 127.9, 128.1, 130.0, 134.8, 135.0, 143.8, 150.9, 158.8, 193.1
(100MHz, $CDCl_3$)

^{13}C-DEPT : δ_C (ppm) Positive peaks: 11.7, 55.2, 74.6-74.8 (d), 82.1-82.3 (d), 87.3, 91.8-93.6 (d), 113.4, 127.3, 127.9, 128.1, 130.0, 135.1 Negative peaks: 62.9-63.0 (d)
(100MHz, $CDCl_3$)

N^6-Benzoyl-5′-*O*-dimethoxytrityl-3′-deoxy-3′-fluoro-adenosine (37)

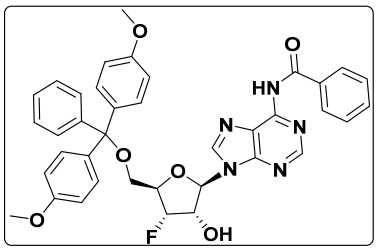

The 5′-hydroxy group of compound **35** (0.75g, 2.03mmol) was protected by 4, 4′-dimethoxytrityl chloride (0.67g, 2.03mmol) to get compound **37** by following the same synthetic procedure mentioned in Chapter **1** for compound **12**. Yield 0.81g, 60%.

Mol. Formula : $C_{38}H_{34}FN_5O_6$

Mol. Weight : 675.72

ESI-Ms m/z : 698.21 ($M+Na^+$)

^{1}H NMR (200MHz, $CDCl_3$) : **δ_H** (ppm) 3.31-3.50 (m, 2H), 3.76 (s, 6H), 4.53-4.58 (m, 1H), 5.11-5.21 (m, 2H), 6.10-6.12 (d, 1H, $J_{1',2'}$= 6.71Hz), 6.75-6.77 (m, 4H), 7.19-7.29 (m, 10H), 7.49-7.62 (m, 3H), 8.00-8.01 (m, 2H), 8.23 (s, 1H), 8.71 (s, 1H)

^{13}C NMR (250MHz, $CDCl_3$) : **δ_C** (ppm) 55.2, 62.7-62.8 (d), 74.8-74.9 (d), 83.7-83.9 (d), 86.8, 88.9, 92.2-93.7 (d), 113.2, 127.0, 127.8, 127.8, 127.9, 128.8, 129.9, 132.8, 133.4, 135.0, 135.2, 141.5, 144.1, 149.6, 151.3, 152.5, 158.6, 164.4

^{13}C-DEPT (250MHz, $CDCl_3$) : **δ_C** (ppm) Positive peaks: 55.2, 74.8-74.9 (d), 83.7-83.9 (d), 88.9, 92.3-93.7 (d), 113.2, 127.0, 127.8, 127.9, 127.9, 128.9, 129.9, 132.9, 141.5, 152.5 Negative peaks: 62.7-62.8(d)

5′-*O*-dimethoxytrityl-3′-deoxy-3′-fluoro-thymidinyl-2′-*O*-phosphoramidite (**38**)

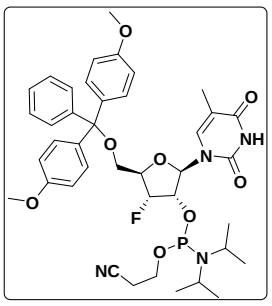

Phosphoramidite derivative of compound **36** (0.24g, 0.36mmol) was synthesized by using 2-Cyanoethyl *N,N*-diisopropylchlorophosphoramidite (0.15mL, 0.72mmol) accordingly as mentioned earlier in Chapter **1** for compound **13**. Yield 0.14g, 45%.

Mol.Formula : $C_{40}H_{48}FN_4O_8P$

^{31}P NMR (161MHz, $CDCl_3$) : **δ_H** (ppm) 151.38, 152.86

N^6-Benzoyl-5′-*O*-dimethoxytrityl-3′-deoxy-3′-fluoro-adenosinyl-2′-*O*-phosphoramidite (**39**)

Phosphoramidite derivative of compound **37** (0.24g, 0.36mmol) was synthesized by using 2-Cyanoethyl *N,N*-diisopropylchlorophosphoramidite (0.15mL, 0.72mmol) accordingly as mentioned earlier in Chapter 1 for compound **13**. Yield 0.14g. 45%.

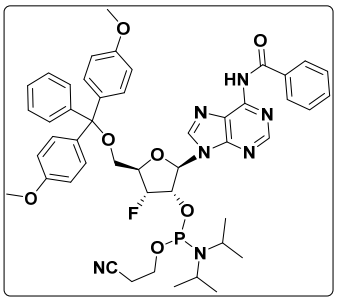

Mol. Formula : $C_{47}H_{51}FN_7O_7P$

Mol. Weight : 875.94

HRMS(ESI) : 876.3643($M+H^+$)

^{31}P NMR (161MHz, $CDCl_3$) : δ_H (ppm) 151.06, 152.01

3-*O*-Benzyl- 1,2:5,6-Di-*O*-isopropylidene-*α*-D-allfuranose (40)

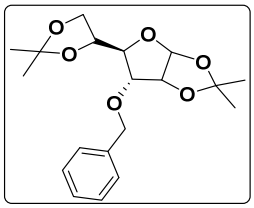

A pouder sodium hydride (0.3g), was added in small portion to a stirred solution of compound **4** (3g, 11.5mmol) in dry DMF (50mL) at 0°C. Then the mixture was stirred for 30min at rt and after 30min benzyl bromide (1.55mL, 13mmol) in dry DMF (1mL) was added. The mixture was stirred for 1h and the excess of reagents was then decomposed by the addition of MeOH (3mL). The solvent was removed and the residue was extracted with $CHCl_3$ (150mL), and the extract was washed with H_2O (3 X 150mL) and dried over Na_2SO_4. Removal of the solvent gave syrup which further purified by silica gel column chromatography using DCM/Pet ether (8:2) to offer the compound **39**. Yield 0.3g, 75%.

Mol. Formula : $C_{19}H_{26}O_6$

Mol. Weight : 350.41

ESI-Ms m/z : 373.21($M+Na^+$)

^{1}H NMR (200MHz, $CDCl_3$) : δ_H (ppm) 1.36, 1.59 (m, 12H, CH_3), 3.85-4.17 (m, 4H), 4.33-4.41 (m, 1H), 4.56-4.62 (m, 2H), 4.75-4.80 (m, 1H), 5.74-5.76 (m, 1H), 7.32-7.42 (m, 5H, C_6H_6)

^{13}C NMR (50MHz, $CDCl_3$) : δ_C (ppm) 25.0, 26.1, 26.5, 26.8, 64.9, 72.2, 74.6, 77.3, 77.7, 77.9, 103.8, 109.6, 112.9, 128.0, 128.2, 128.4, 137.4

^{13}C-DEPT (50MHz, $CDCl_3$) : δ_C (ppm) Positive peaks: 26.1, 26.2, 26.6, 26.8, 72.2, 74.7, 77.3, 77.8, 77.9, 103.8, 128.0, 128.3, 128.5 Negative peaks: 65.0

3-*O*-Benzyl-1,2-*O*-isopropylidene-*α*-D-allfuranose (41)

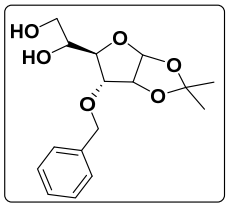

A solution of compound **39** (2g, 76.25mmol) in 6:4 AcOH:H_2O mixture (20mL) heated at 50°C for 1h. After the starting material disappeared the mixture was concentrated under reduced pressure and co-evaporated with toluene to remove traces of AcOH. The obtained yellow syrup was purified by column chromatography using 4:7 EtOAc/Petether solvent systems. Yield 1.6g, 95%.

Mol. Formula	**:**	$C_{16}H_{22}FO_6$
Mol. Weight	**:**	310.34
ESI-Ms m/z	**:**	333.11($M+Na^+$)
^{1}H NMR (200MHz, $CDCl_3$)	**:**	**δ_C** (ppm) 1.36-1.60 (2s, 6H, CH_3), 3.61-3.77 (m, 2H), 3.99-4.15 (m, 1H), 4.53-4.64 (m, 2H), 4.76-4.82 (m,1H), 5.76-5.78 (m, 1H), 7.32 (m, 5H)
^{13}C NMR (50MHz, $CDCl_3$)	**:**	**δ_C** (ppm) 26.1, 26.3, 62.5, 70.6, 71.6, 76.1, 76.8, 77.4, 103.6, 112.5, 127.7, 128.0, 136.6
^{13}C-DEPT (50MHz, $CDCl_3$)	**:**	**δ_C** (ppm) positive peaks: 26.1, 26.3, 70.6, 76.3, 76.9, 78.4, 103.6, 127.6, 127.7 128.0 Negative peaks: 62.5, 71.6

3-*O*-Benzyl-1,2-*O*-isopropylidene-α-D-aldoribofuranose

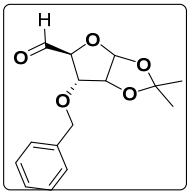

An aqueous solution of **40** (1.85g, 6mmo1) was slowly added with stirring to a solution of sodium periodate (1.5g, 7mmol) in water (5mL) at 0°C. After 30min, ethylene glycol (0.2mL) was added and the mixture was extracted three times with EtOAc (100mL X 3). The dried extracts were evaporated, to obtained compound **41** as syrup. The crude compound **41** is used for next reaction without any purification. Yield of crude 1.66g 100%.

3-*O*-Benzyl-4-*C*-hydroxymethyl-1,2-*O*-isopropylidene-α-D-ribofuranose (42)

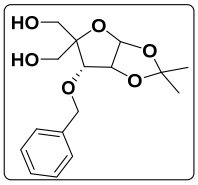

Aqueous 37% formaldehyde (2mL) and then 1N sodium hydroxide (10mL) were added at 0°C to a stirred solution of crude **41** (1.0g, 3.5mmol) in water (9mL). The mixture was then stirred at rt for 12h and evaporated to dryness. The residue was extracted with DCM, and the

dried extracts were purified by silica gel column chromatography using DCM/MeOH (20:1) as solvent system. Yield 0.78, 70%.

Mol. Formula	**:**	$C_{16}H_{22}FO_6$
Mol. Weight	**:**	310.34
ESI-Ms m/z	**:**	333.07 ($M+Na^+$)
^{1}H NMR (200MHz, $CDCl_3$)	**:**	**δ_C** (ppm) 1.34, 1.64 (2s, 6H, CH_3), 3.53-3.92 (m, 4H), 4.21-4.23 (m, 1H), 4.53-4.84 (m, 3H), 5.76-5.78 (m, 1H), 7.36 (m, 5H)
^{13}C NMR (50MHz, $CDCl_3$)	**:**	**δ_C** (ppm) 25.6, 26.3, 62.7, 63.6, 72.3, 78.0, 78.2, 86.4, 104.1, 113.2, 127.5, 127.8, 128.3, 137.1
^{13}C-DEPT (50MHz, $CDCl_3$)	**:**	**δ_C** (ppm) positive peaks: 25.6, 26.3, 78.0, 78.2, 104.1, 127.5, 127.8, 128.3 Negative peaks: 62.7, 63.5, 72.3

3-*O*-Benzyl-5-*O*-*tert*-butyldiphenylsilyl-4-*C*-hydroxymethyl-1,2-*O*-isopropylidene-α-D-ribofuranose (43)

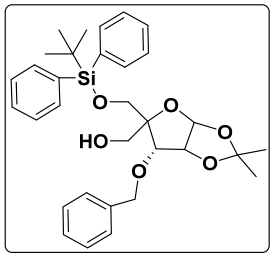

Under N_2 atmosphere, TEA (2.7g, 26.6mmol) and *tert*-butyldiphynylsilyl chloride (7.1g, 25.8mmol) were added to a stirred solution of **42** (2.5g, 8.1mmol), in DCM (50mL) at rt. After having been stirred for 11h at the same temperature, the reaction mixture was partitioned with saturated $NaHCO_3$ and the mixture was extracted with DCM. Usual work-up and purification by silica gel column chromatography (petether/EtOAc, 4:1 to 3:1) afforded **43**. Yield 2.85g, 65 %.

Mol. Formula	**:**	$C_{32}H_{40}O_6Si$
Mol. Weight	**:**	548.74
ESI-Ms m/z	**:**	571.25 ($M+Na^+$)
^{1}H NMR (200MHz, $CDCl_3$)	**:**	**δ_H** (ppm) 0.99 (s, 9H, CH_3), 1.37-1.67 (2s, 6H), 2.40 (t,1H), 3.65-3.84 (m, 4H), 4.42-4.54 (m, 2H), 4.67-4.85 (m, 2H), 5.81-5.83 (m, 1H), 7.34-7.39 (m, 11H), 7.58-7.65 (m, 4H)
^{13}C NMR (50MHz, $CDCl_3$)	**:**	**δ_C** (ppm) 19.2, 26.2, 26.5, 26.8, 63.2, 65.4, 72.5, 77.9, 79.1, 87.4, 104.4, 113.7, 127.6, 127.7, 128.0, 128.5, 129.6, 129.7, 132.9, 133.1, 135.5, 135.5, 137.3

^{13}C-DEPT (50MHz, $CDCl_3$) : **δ_C** (ppm) positive peaks: 26.2, 26.8, 26.8, 77.9, 79.1, 104.4, 127.7, 127.7, 128.0, 128.5, 129.6, 135.5 Negative peaks: 63.2, 65.4, 72.5

3-*O*-Benzyl-5-*O*-*tert*-butyldiphenylsilyl-1,2-*O*-isopropylidene-4-*C*-(*p*-toluenesulfonyl)oxymethyl-α-D-ribofuranose (44)

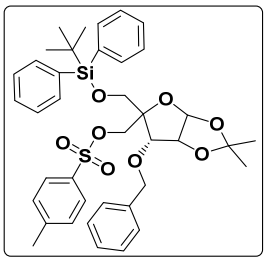

Under N_2 atmosphere, TEA (0.29g, 2.83 mmol), *P*-toluenesulfonyl chloride (0.13g, 0.07mmol) and 4,4'-dimethylaminopyridine (0.56g, 0.05mmol) in dichloromethane (5mL) were added to a stirred solution of **43** (0.25g, 0.46mmol) at rt. After having been stirred for 12h at the same temperature, the reaction mixture was washed with saturated $NaHCO_3$ and extracted with DCM. Usual work-up and purification by silica gel column chromatography using pet-ether/EtOAc, (1:6) as solvent system afforded **44** as colourless oil. Yield 0.27g, 85 %.

Mol. Formula : $C_{39}H_{46}O_8SSi$

Mol. Weight : 702.93

ESI-Ms m/z : 725.38 ($M+Na^+$)

^{1}H NMR ($200MHz$, $CDCl_3$) : **δ_H** (ppm) 0.96 (s, 9H), 1.29 (s, 3H), 1.33 (s,3H), 2.37(s, 3H), 3.52-3.74 (2H, ABq, J=11 Hz), 4.30-4.73 (7H, m), 5.70 (d, 1H, J= 4 Hz), 7.19-7.39 (m, 15H), 7.54-7.60 (m, 5H), 7.69-7.73 (m, 2H)

3-*O*-Benzyl-5-*O*-*tert*-butyldiphenylsilyl-1,2-di-*O*-acetyl-4-C-(*p*- toluenesulfonyl) oxymethyl-D-ribofuranose (45)

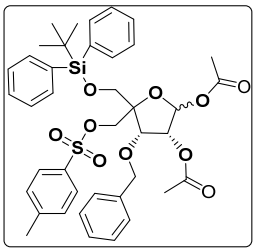

To a stirred solution of **44** (3.7g, 5.3mmol) in AcOH (56mL), Ac_2O (6mL, 64mmol) and concentrated H_2SO_4 (56µL, 1.1µmol) were added. The solution was stirred at rt for 2h. Then the reaction mixture was poured into ice-water (300mL) and stirred for 30 min. Saturated NH_4Cl was added and the mixture was extracted with DCM. Usual work-up and purification by silica gel column chromatography using petether/EtOAc, (1:2) as solvent system afforded **45** as pale yellow oil. Yield 2.75g, 70%.

Mol. Formula : $C_{40}H_{46}O_{10}SSi$

Mol. Weight : 746.94

ESI-Ms m/z : 769.31 ($M+Na^+$)

^{1}H NMR (ma) (200MHz, $CDCl_3$) : **δ_C** (ppm) 1.02 (s ,9H), 1.77 (s, 3H), 1.98 (s, 3H), 2.39 (s, 3H), 3.59-3.79 (2H, ABq, *J*=11 Hz), 4.25-4.49 (m, 5H), 5.26 (1H, d, *J*= 5 Hz), 5.95 (s, 1H), 7.21-7.40 (13H, m), 7.59-7.75 (m, 6H)

5-*O*-*tert*-Butyldiphenylsilyl-4-(*p*-toluenesulfonyl)-oxymethyl-1,2,3-tri-*O*-acetyl-D-ribofuranose (46)

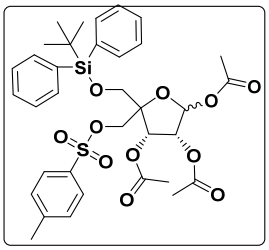

Under H_2 atmosphere, 10% Pd-C (1.0g) was added to a stirred solution of **45** (1.85g, 2.5mmol) in EtOAc:$CHCl_3$ (10:1, v/v, 220mL) at rt. After having been stirred for 12h, the reaction mixture was filtered, and the filtrate was concentrated. The residue was dissolved in pyridine (10mL) and acetic anhydride (0.68g, 6.7mmol) was added at rt. After having been stirred for 5h, the reaction mixture was concentrated under reduced pressure. The residue was purified by silica gel column chromatography using pet-ether/EtOAc, (1:2) as solvent system afforded **46** as pale yellow oil. Yield 1.24g, 72%.

Mol. Formula : $C_{35}H_{42}O_{11}SSi$

Mol. Weight : 698.85

ESI-Ms m/z : 721.34 ($M+Na^+$)

^{1}H NMR (500MHz, $CDCl_3$) : **δ_H** (ppm) 0.98 (s, 9H), 1.80 (s, 3H), 2.08 9s, 6H), 2.41 (s, 3H), 3.54-3.77 (m, 2H), 4.20-4.41 (m, 2H), 5.32 (m, 1H), 5.51 (m, 1H), 6.01 (s, 1H) 7.26-7.44 (m, 10H), 7.59-7.77 (m, 7H)

^{13}C NMR (250MHz, $CDCl_3$) : **δ_C** (ppm) 14.1, 19.0, 20.3, 20.7, 21.5, 26.5, 60.3, 65.3, 67.7, 72.1, 74.3, 84.3, 97.2, 127.7, 128.0, 129.7, 129.9, 132.1, 132.5, 132.5, 135.4, 135.5, 144.8, 168.7, 169.1

^{13}C-DEPT (250MHz, $CDCl_3$) : **δ_C** (ppm) positive peaks: 14.2, 20.3, 20.4, 20.8, 21.8, 21.6, 26.6, 72.1, 74.3, 97.2, 127.8, 128.0, 129.7, 129.9, 135.5, 135.6
Negative peaks: 60.4, 65.4, 67.7

N^6-Benzoyl-5′-*O*-*tert*-butyldiphenylsilyl-2′,3′-di-*O*-acetyl-4′-*C*-(*p*-toluenesulfonyl) oxymethyladenosine (47)

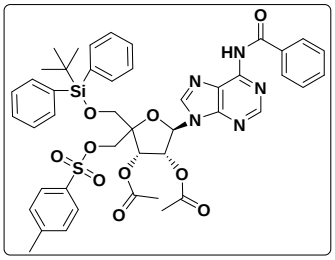

Compound **47** (0.2g) was synthesized by using same Vorbrüggen glycosylation reaction using silylated N^6-benzoyl adenenine (0.47g, 1.97mmol) from compound **46** (0.25g, 0.32 mmol) accordingly as mentioned earlier in Chapter 1 for compound **10**. Yield 0.17g, 70%.

Mol. Formula : $C_{45}H_{47}N_5O_{10}SSi$

Mol. Weight : 878.06

ESI-Ms m/z : 900.40 ($M+Na^+$)

^{1}H NMR (200MHz, $CDCl_3$) : **δ_H** (ppm) 1.02 (s, 9H), 2.04 (s, 3H), 2.16 (s, 3H), 2.40 (s, 3H), 3.79-3.93 (2H, ABq, J= 9Hz), 4.27-4.43 (2H, ABq, J= 10Hz), 5.94 (1H, d, J=8Hz), 6.04-6.15 (m, 2H), 7.24-7.65 (m, 20H), 8.0 (1H, s), 8.57 (s, 1H), 9.05 (s, 1H)

N^6-Benzoyl-5′-*O*-*tert*-butyldiphenylsilyl-4′-C-(*p*-toluenesulfonyl) oxymethyladenosine (48)

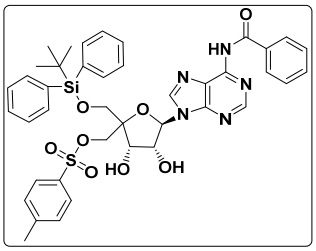

Anhydrous K_2CO_3 (0.3g, 0.19mmol) was added to a stirred solution of compound **47** (0.54g, 0.62mmol) in dry MeOH (30mL). After having been stirred for 15min, the reaction mixture was neutralized with conc. HCl and concentrated under reduced pressure. The remaining residue was purified by silica gel column chromatography DCM/MeOH (15:1) afforded **48** as white solid. Yield 0.36g, 75%

Mol. Formula : $C_{41}H_{43}N_5O_8SSi$

Mol. Weight : 793.96

ESI-Ms m/z : 816.23 ($M+Na^+$)

^{1}H NMR (400MHz, $CDCl_3$) : **δ_H** (ppm) 0.94 (s, 9H), 2.37 (s, 3H), 3.68-3.84 (m, 2H), 4.45-4.53 (m, 3H), 4.82-4.88 (m, 1H), 5.89-5.92 (d, 1H), 7.26-7.60 (m, 17H), 7.73-7.98 (m, 5H), 8.47 (s, 1H), 9.14 (s, 1H)

^{13}C NMR (100MHz, $CDCl_3$) : **δ_C** (ppm) 19.1, 21.5, 26.6, 29.6, 64.2, 68.2, 72.6, 74.4, 87.6, 89.1, 122.5, 127.8, 128.0, 128.8, 129.7, 130.0, 132.1, 132.3,

132.6, 132.9, 133.3, 135.4, 135.4, 141.7, 144.8, 149.2, 150.8, 152.1, 164.7

^{13}C-DEPT (100MHz, $CDCl_3$) : δ_C (ppm) positive peaks: 26.5, 72.7, 74.9, 89.6, 127.7, 129.7, 129.9, 135.3, 135.3, 141.2, 152.1 Negative peaks: 61.8, 66.1

N^6-Benzoyl-5′-*O*-*tert*-butyldiphenylsilyl-3′-*O*,4′-*C*-methyleneadenosine (49)

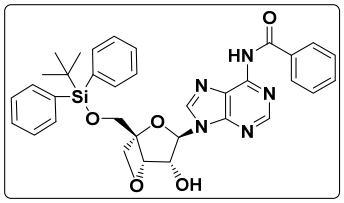

Under N_2 atmosphere, sodium bis(trimethylsilylamide) (0.32g, 0.085mmol), was added to a stirred solution of **48** (0.25g, 0.35 mmol), in THF (1.5mL) at rt. After having been stirred for 3h at the same temperature, the reaction mixture was extracted with DCM and washed with saturated $NaHCO_3$. The obtained organic extract was concentrated and purified by silica gel column chromatography using EtOAc/MeOH (15:1) as solvent system afforded **49** as white solid. Yield 0.19g, 75%.

Mol. Formula : $C_{34}H_{35}N_5O_5Si$

Mol. Weight : 621.76

ESI-Ms m/z : 644.23 ($M+Na^+$)

^{1}H NMR (400MHz, $CDCl_3$) : δ_H (ppm) 1.07 (s, 9H), 3.91 (s, 2H), 4.64, 4.96 (ABq, 2H, J = 8Hz), 4.70 (dd, 1H, J = 7, 5 Hz), 5.30 (d, 1H, J = 5 Hz), 6.46 (d, 1H, J = 7 Hz), 7.33-7.65 (m, 13H), 8.03 (d, 2H, J = 7 Hz), 8.14 (s, 1H), 8.70 (s, 1H)

^{13}C NMR (100MHz, $CDCl_3$) : δ_C (ppm) 19.2, 26.7, 63.0, 76.0, 78.2, 85.2, 86.7, 88.8, 122.5, 127.3, 127.8, 128.5, 128.7, 130.0, 130.0, 132.0, 132.4, 132.8, 133.4, 135.4, 135.5, 141.2, 149.2, 151.6, 152.7, 164.7

^{13}C-DEPT (100MHz, $CDCl_3$) : δ_C (ppm) positive peaks: 26.6, 76.0, 85.3, 88.8, 127.3, 127.9, 128.8, 130.0, 132.0, 132.9, 135.5, 141.3, 152.8 Negative peaks: 63.0, 78.2

N^6-Benzoyl-3′-*O*, 4′-*C*-methyleneadenosine (50)

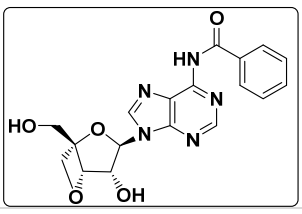

A solution of *tert*-butylammonium fluoride (0.96mL, 0.96mmol 1.0M solution in THF) was added to a stirred solution of **49** (0.5g, 0.7mmol) in THF (2mL), at rt. After having been stirred

for 15min, the reaction mixture was concentrated under reduced pressure. The remaining residue was purified by silica gel column chromatography using EtOAc/MeOH (15:1) as solvent system. Compound **50** was obtained as white solid. Yield 0.18g, 60%.

Mol. Formula : $C_{18}H_{17}N_5O_5$

Mol. Weight : 383.36

ESI-Ms m/z : 406.31 ($M+Na^+$)

^{1}H NMR (500MHz, $CDCl_3$) : **δ_H** (ppm) 3.81, 3.88 (2H, ABq, *J* = 13 Hz), 4.63, 4.93, (2H, ABq, *J* = 8 Hz), 4.80 (1H, dd, *J* = 8, 4 Hz), 5.22 (1H, d, *J* = 4Hz), 6.57 (1H, d, *J* = 8 Hz), 7.56-7.59 (2H, m), 7.64-7.68 (1H, m), 8.08-8.10 (2H, m), 8.67 (1H, s), 8.73 (1H, s)

^{13}C NMR (250MHz, $CDCl_3$) : **δ_C** (ppm) 62.5, 75.9, 79.1, 86.8, 88.1, 89.7, 125.5, 129.4, 129.8, 133.98, 134.9, 144.7, 151.4, 153.4, 153.7

^{13}C-DEPT (250MHz, $CDCl_3$) : **δ_C** (ppm) positive peaks: 74.5, 85.4, 88.3, 128.0, 128.4, 132.5, 143.3, 152.0 Negative peaks: 61.2, 77.7

N^6-Benzoyl-5′-*O*-dimethoxytrityl-3′-*O*,4′-C-methyleneadenosine (51)

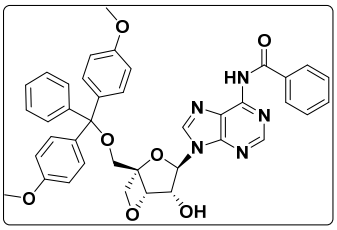

The 5′-hydroxy group of compound **50** (0.5g, 1.3mmol) was protected by 4, 4′-dimethoxytrityl chloride (0.43g, 1.3mmol) to get compound **51** by following the same synthetic procedure mentioned in Chapter **1** for compound **12**. Yield 0.53g, 60%.

Mol. Formula : $C_{39}H_{35}N_5O_7$

Mol. Weight : 685.72

ESI-Ms m/z : 708.25 ($M+Na^+$)

^{1}H NMR (200MHz, $CDCl_3$) : **δ_C** (ppm) 3.37-3.52 (ABq,2H), 3.78 (s, 6H), 4.63-4.91 (3H, m), 5.27 (d, 1H), 6.45 (d, 1H), 6.80 (m, 4H), 7.23-7.40 (m, 12H), 7.55-7.62 (m, 3H), 8.02-8.06 (m, 2H), 8.23 (s, 1H), 8.73 (s, 1H)

N^6-Benzoyl-5′-*O*-dimethoxytrityl-3′-deoxy-3′-fluoro-adenosinyl-2′-*O*-phosphoramidite (52)

Phosphoramidite derivative of compound **51** (0.25g, 0.36mmol) was synthesized by using

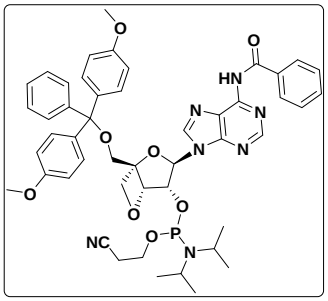

2-Cyanoethyl *N, N*-diisopropylchlorophosphoramidite (0.15ml, 0.72mmol) accordingly as mentioned earlier in Chapter 1 for compound **13**. Yield 0.14g, 45%

Mol. Formula	**:**	$C_{48}H_{52}N_7O_8P$
Mol. Weight	**:**	885.94
^{31}P NMR (161MHz, $CDCl_3$)	**:**	**δ_H**(ppm) 149.86, 150.72

2, 2′-anhydro-arabinouridine (53)

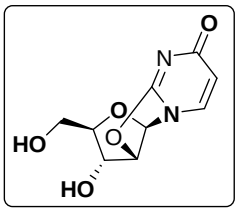

Uridine (5.00g, 20.47mmol) and diphenyl carbonate (4.88g, 22.80 mmol) were suspended in DMF (40mL). The slurry was heated to 100°C and sodium bicarbonate (150mg) was then added and the reaction mixture was again heated up to 137°C for 1.5h. After completion, the reaction was cooled down to rt, filtered and washed with MeOH (60mL). The filtrate was concentrated under vacuum, the compound **53** obtained as a white solid. Yield 3.60g 78%.

Mol. Formula	**:**	$C_9H_{10}N_2O_5$
Mol. Weight	**:**	226.90
ESI-Ms m/z	**:**	249.23($M+Na^+$)
^{1}H NMR (200MHz, $(CD_3)_2SO$)	**:**	**δ_H** (ppm) 3.19-3.29 (m, 2H), 4.08 (m, 1H), 4.38 (m, 1H), 4.96-5.02 (m, 1H), 5.19-5.22 (m, 1H), 5.83-5.91 (m, 2H), 6.30-6.33 (d, 1H), 7.82-7.86 (d, 1H, *J* = 7.45, H-6)
^{13}C NMR (50MHz, $(CD_3)_2SO$)	**:**	**δ_C** (ppm) 61.0, 75.0, 89.1, 89.5, 90.4, 108.9, 137.3, 160.2, 171.8
^{13}C-DEPT (50MHz, $(CD_3)_2SO$)	**:**	**δ_C** (ppm) Positive peaks: 74.6, 88.7, 89.1, 90.0, 108.5, 136.9 Negative peaks: 60.6

Arabinouridine (54)

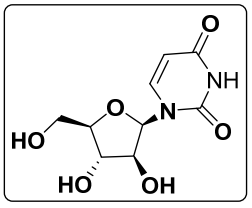

After completion of above reaction, the reaction mixture was cooled and poured into cold water (85mL), the reaction mixture extracted with $CHCl_3$, (3 X 50mL) and the extracts discarded. TEA (5mL,

0.036mmol) was added to the remaining aqueous layer (3.5g, 15.47mmol) which was then heated at 70°C for 5h. The products were then cooled and evaporated to dryness under reduced pressure and was purified by column chromatography using MeOH/DCM (1.5:8.5) as solvent system gives compound **54** as white solid. Yield 2.6g 68%.

Mol. Formula : $C_9H_{10}N_2O_5$

Mol. Weight : 244.20

ESI-Ms m/z : 267.25 ($M+Na^+$)

^{1}H NMR (400MHz, D_2O) : **δ_H** (ppm) 3.74-4.06 (m, 4H), 4.29-4.34 (m, 1H), 5.75-.79 d, 1H), 6.08-6.10 (d, 1H), 7.74-7.78 (d, 1H)

^{13}C NMR (100MHz, D_2O) : **δ_C** (ppm) 60.3, 74.7, 75.4, 82.9, 85.1, 101.0, 142.9, 151.3, 166.2

^{13}C-DEPT (100MHz, D_2O) : **δ_C** (ppm) Positive peaks: 74.6, 75.4, 82.91, 85.1, 101.0, 142.9 Negative peaks: 60.3

5′-*O*-dimethoxytrityl arabinouridine (55)

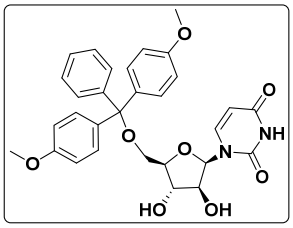

The compound **54** (0.5g 2.04mmol) was dissolved in pyridine. A 4, 4′-dimethoxytrityl chloride (0.83g, 2.4mmol) was added in 3 equal portions (1h between additions) to the solution stirred at 0°C. One hour after the final addition the pyridine was evaporated. The obtained crude resedue was purified by silica gel column chromatography using DCM/MeOH (9.5:0.5) solvent system. Yield 0.83g, 75%

Mol. Formula : $C_{30}H_{30}N_2O_8$

Mol. Weight : 546.58

ESI-Ms m/z : 569.12 ($M+Na^+$)

^{1}H NMR (200MHz, $CDCl_3$) : **δ_H** (ppm) 3.48 (m, 2H), 3.72 (s, 6H), 3.93-3.96 (m, 1H), 4.31-4.42 (m, 2H), 5.33-5.37 (d, 1H), 6.09-6.11 (d, 1H), 6.78-6.83 (m, 4H), 7.16-7.41 (m, 12H), 7.91-7.95 (d, 1H)

5′-*O*-dimethoxytrityl-3-*O*-*tert*-butyldimethylsilyl arabinouraidine (56)

To a solution of **55** (0.1g, 0.18mmol) in THF (5mL), the pyridine (0.073 mL, 0.9mmol) and $AgNO_3$ (0.068g, 0.39mmol) were added. The mixture was stirred for 5min at rt until all silver nitrate had dissolved. After that a *tert*-butyldimethylsilyl chloride (0.061g,

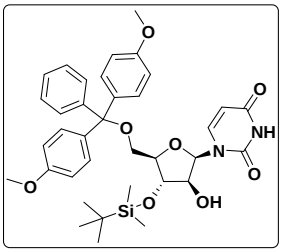

0.39mmol) was added and the reaction mixture was stirred for 1h. The solution was collected by filtration and the solvents concentrated to a small volume. The residual syrup was purified by chromatography on silica gel using ether-Pet-ether (4:1). Compound **56** was obtained as colourless foam. Yield 0.09g, 75%.

Mol. Formula : $C_{36}H_{44}N_2O_8Si$

Mol. Weight : 660.84

ESI-Ms m/z : 683.27 ($M+Na^+$)

^{1}H NMR (200MHz, $CDCl_3$) : **δ_H** (ppm) 0.00, 0.10 (2s, 6H), 0.83 (s, 9H), 3.34-3.36 (m, 1H), 3.64-3.65 (m, 1H), 3.80 (s, 6H), 3.96 (m, 1H), 4.21-4.32 (m,2H), 5.41-5.43 (d, 1H), 6.14-6.15 (d, 1H), 6.85-6.86 (m, 4H), 7.25-7.44 (m, 10H), 7.89-7.91 (d, 1H)

^{13}C NMR (50MHz, $CDCl_3$) : **δ_C** (ppm) -5.17, -4.48, 25.64, 55.21, 61.88, 83.47, 86.08, 87.08, 101.05, 113.21, 116.12, 127.12, 127.96, 128.17, 130.11, 130.16, 135.09, 135.20, 141.94, 144.02, 150.76, 158.65, 164.20

^{13}C-DEPT (50MHz, $CDCl_3$) : **δ_C** (ppm) Positive peaks: -5.11, -4.11, 25.71, 55.27, 76.56, 83.52, 86.13, 101.12, 113.26, 116.18, 127.18, 128.02, 128.23, 130.17, 142.02 Negative peaks: 61.93

5′-*O*-dimethoxytrityl-3-*O*-*tert*-butyldimethylsilyl arabinouraidinyl-2′-*O*-phosphoramidite (57)

Compound **56** (0.13g, 0.19mmol) was co-evaporated with dry DCM, and then dissolved in dry DCM (3.0mL). Tetrazole (0.12 g, 0.18mmol) was added, followed by 2-cyanoethyl *N, N ,N′, N′*-tetraisopropylphosphorodiamidite, (0.069mL, 0.22mmol) at 0^{o}C. The reaction mixture was stirred under argon atmosphere at rt for 3h. The reaction mass was diluted with DCM, washed with $NaHCO_3$ and H_2O, dried over Na_2SO_4, and concentrated. The crude product was purified on a neutralized silica gel column using DCM/EtOAc (1:1) and 1% TEA. Yield: 0.1g, 60%.

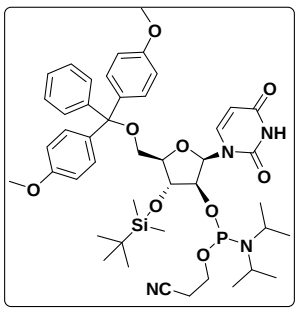

Mol.Formula-$C_{45}H_{61}N_4O_9Psi$; **Mol Weight**-861.06; **ESI-Ms m/z**-883.37;

^{31}P NMR (161MHz, $CDCl_3$): **δ_P** (ppm) 150.34, 151.66

3.4.2 Synthesis of buffer

Phosphate buffer (pH = 7.4, 150mM NaCl) and Triethyl ammonium acetate (TEAA) buffer (1M, pH = 7)

Phosphate buffer and TEAA buffer was prepared accordingly as mentioned earlier in Chapter 1.

Tris-HCL buffer (0.1 M, pH = 8.0)

Tris (1.21g, 100mM), $MgCl_2 \cdot 6H_2O$ (305mg, 15mM)) and NaCl (585mg, 100mM) was dissolve into the 30mL deionized water, and then HCl (e.g., 1M HCl) was added until the pH meter gives desired pH 8 for Tris buffer solution. The buffer was then diluted with water to reach the desired final volume of solution 100mL.

3.4.3 Synthesis of oligonucleotides, Purification and characterization

The regular procedures of oligonucleotide synthesis, their purification and characterization are same as discussed earlier in Chapter 1.

3.4.4 Biophysical techniques

UV-*Tm* experiment and CD experiments

UV-*Tm* experiments and CD experiment were carried out by using standard procedure. All the particulars of experiment are same as discussed previously in chapter 1.

Nuclease resistance study

Enzymatic hydrolysis of the ONs (7.5μM) was carried out at 37℃ in buffer (100μl) containing 100mM Tris-HCl (pH 8), 15mM $MgCl_2$, 100mM NaCl and SVPD (2μg, $1.2x10^{-4}$U or 0.5μg $0.3x10^{-4}$U). Aliquots were removed at several time-points; each aliquots of reaction mixture was heated to 90℃ for 2min to inactivate the nuclease. The amount of intact ONs was analyzed at several time points by RP-HPLC. The percentage of intact ON was then plotted against the exposure time to obtain the ON degradation curve with time.

3.5 Appendix B

Compounds	Page Number
Compound 24: ^{1}H, ^{13}C, DEPT NMR	170
Compound 25: ^{1}H, ^{13}C, DEPT NMR	171
Compound 26: ^{1}H, ^{13}C, DEPT NMR	172
Compound 27: ^{1}H, ^{13}C, DEPT NMR	173
Compound 28: ^{1}H, ^{13}C, DEPT NMR	174
Compound 29: ^{1}H, ^{13}C, DEPT NMR	175
Compound 31: ^{31}P NMR and HRMS	176
Compound 32: ^{1}H NMR	176
Compound 33: ^{1}H, ^{13}C, DEPT NMR	177
Compound 34: ^{1}H, ^{13}C, DEPT NMR	178
Compound 35: ^{1}H, ^{13}C, DEPT NMR	179
Compound 36: ^{1}H, ^{13}C, DEPT NMR	180
Compound 37: ^{1}H, ^{13}C, DEPT NMR	181
Compound 38: ^{31}P NMR	182
Compound 39: ^{31}P NMR and HRMS	182
Compound 40: ^{1}H, ^{13}C, DEPT NMR	183
Compound 41: ^{1}H, ^{13}C, DEPT NMR	184
Compound 42: ^{1}H, ^{13}C, DEPT NMR	185
Compound 43: ^{1}H, ^{13}C, DEPT NMR	186
Compound 44: ^{1}H NMR	187
Compound 45: ^{1}H NMR	187
Compound 46: ^{1}H, ^{13}C, DEPT NMR	187-188
Compound 47: ^{1}H NMR	188
Compound 48: ^{1}H, ^{13}C, DEPT NMR	189
Compound 49: ^{1}H, ^{13}C, DEPT NMR	190
Compound 50: ^{1}H, ^{13}C, DEPT NMR	191

Compound 51: ^{1}H NMR, HRMS 192

Compound 52: ^{31}P NMR 192

Compound 53: ^{1}H, ^{13}C, DEPT NMR 193

Compound 54: ^{1}H, ^{13}C, DEPT NMR 194

Compound 55: ^{1}H NMR 195

Compound 56: ^{1}H, ^{13}C, DEPT NMR 195-196

Compound 56: ^{31}P NMR, LCMS 196

ngDNA MALDI-TOF spectra 197-200

MALDI-TOF mass spectrum of ngDNA1, ngDNA1-2 and ngDNA1-4 with deletion of the 2′terminal Adenosine-5′-phosphate. 201

^{1}H NMR of compound 24

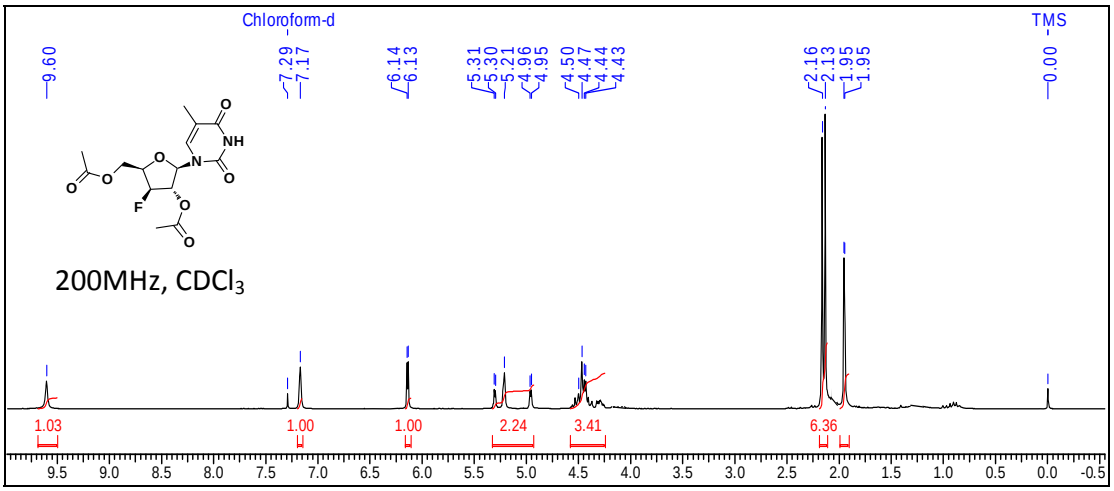

^{13}C NMR of compound 24

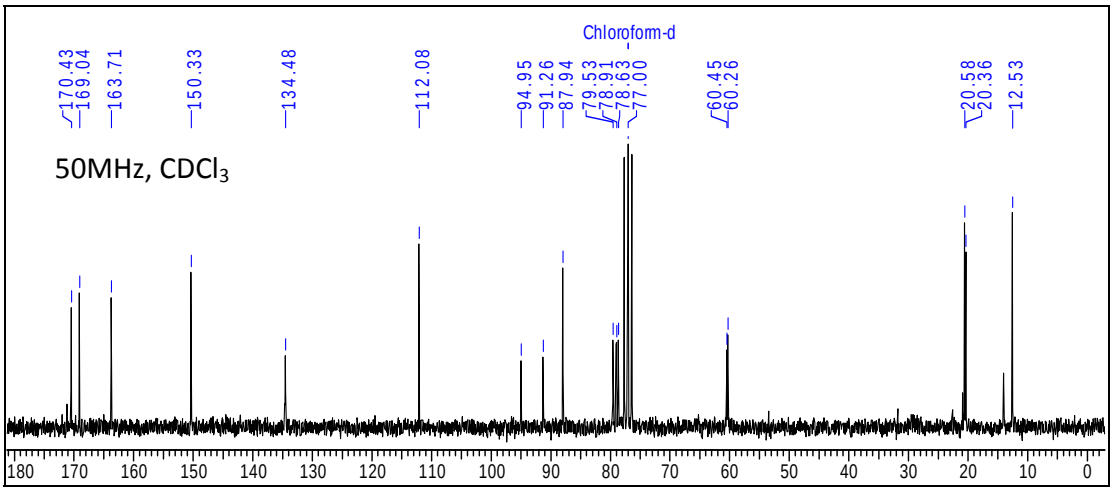

^{13}C-DEPT of compound 24

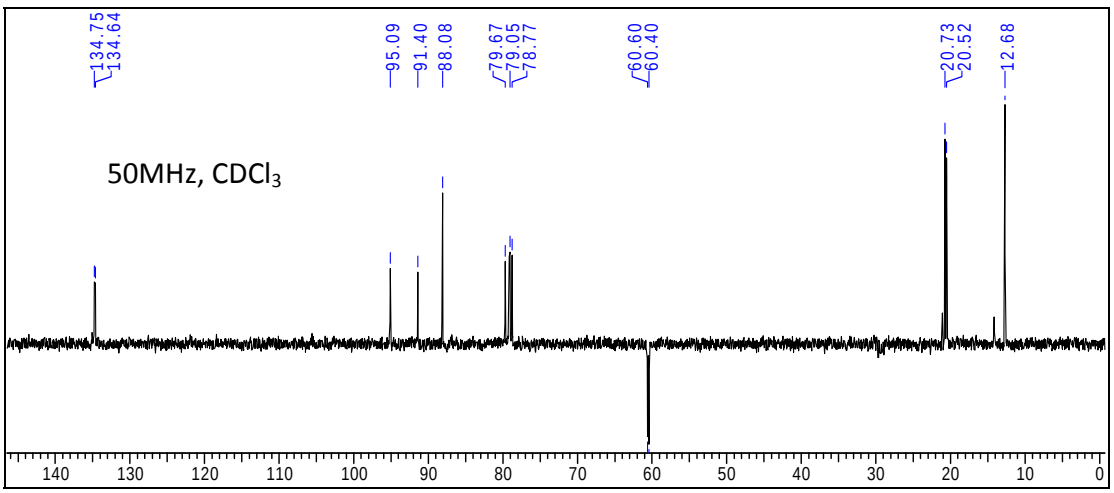

^{1}H NMR of compound 25

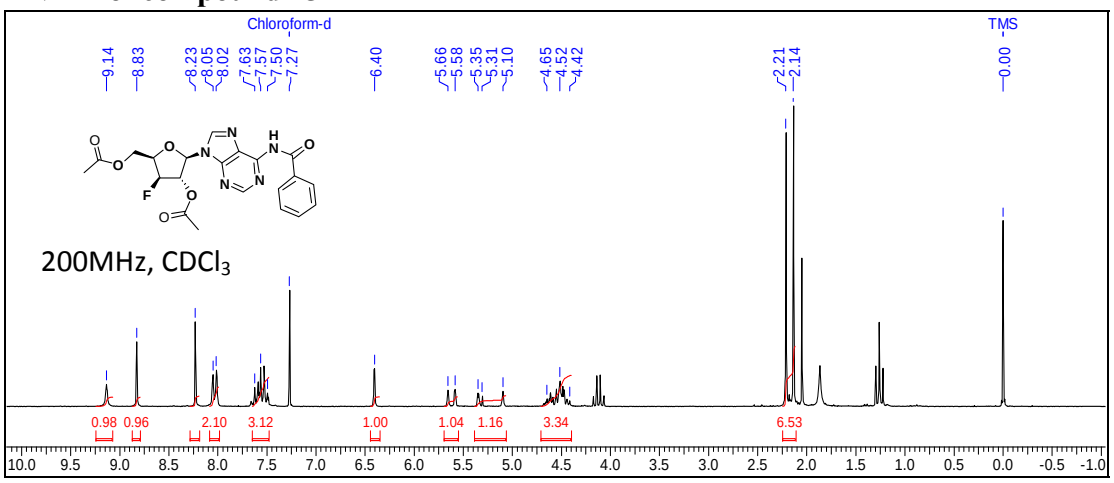

^{13}C NMR of compound 25

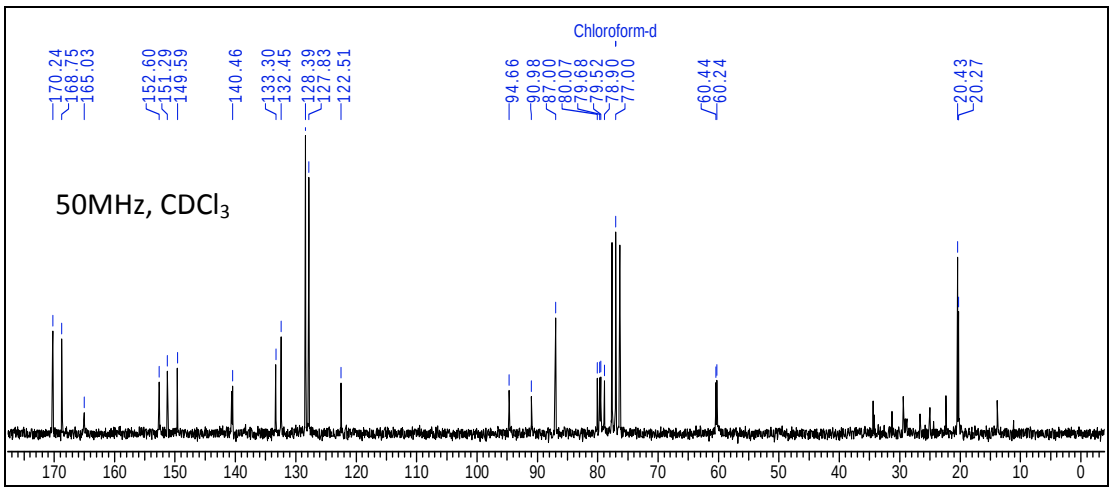

^{13}C-DEPT of compound 25

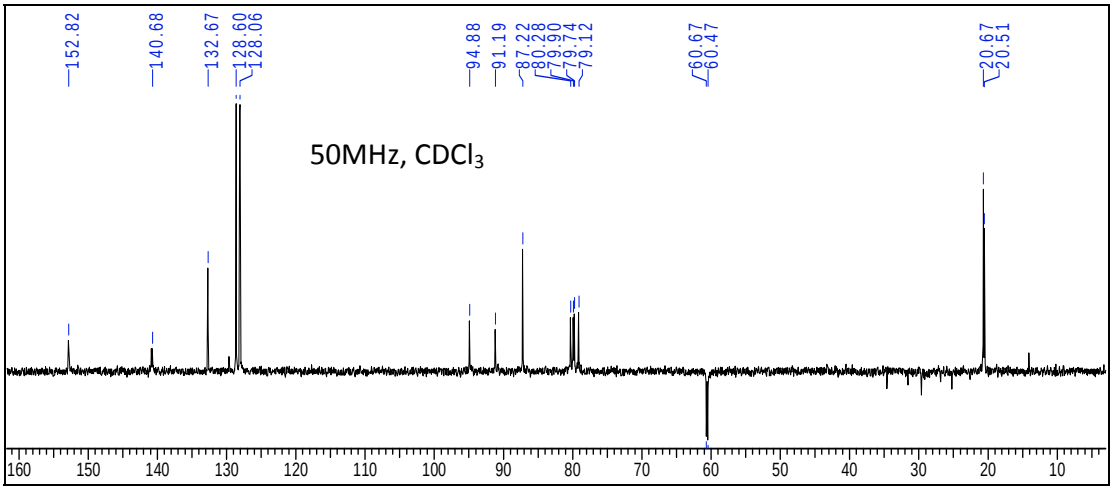

^{1}H NMR of compound 26

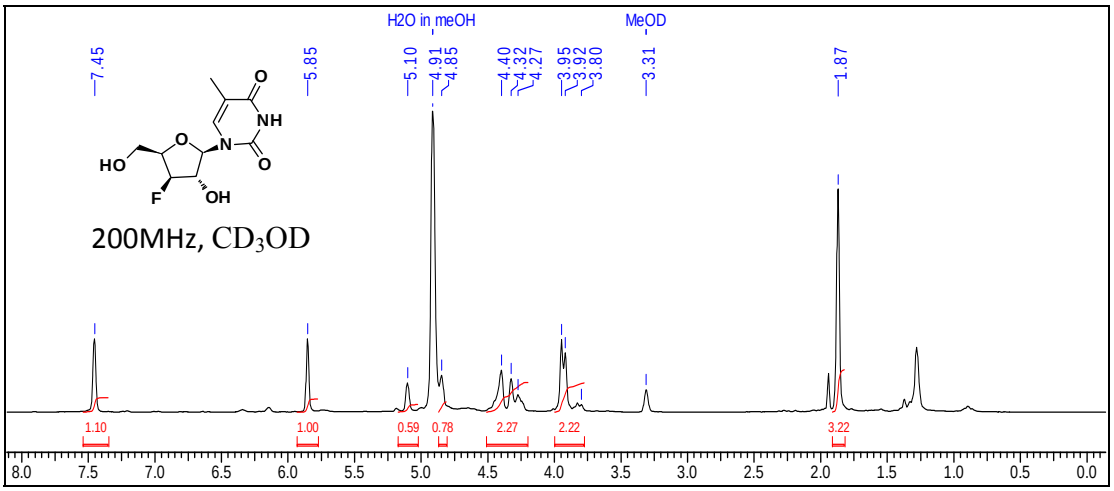

^{13}C NMR of compound 26

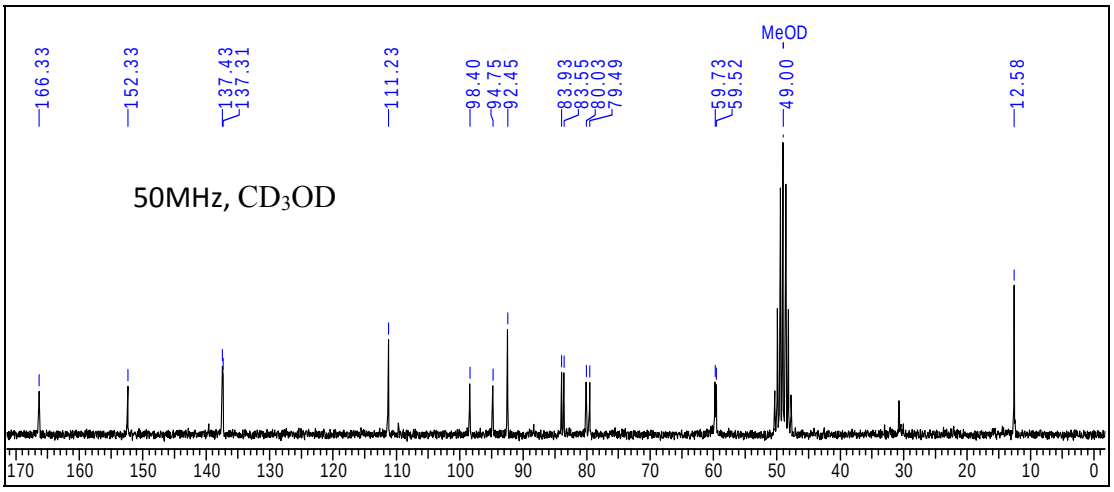

^{13}C-DEPT of compound 26

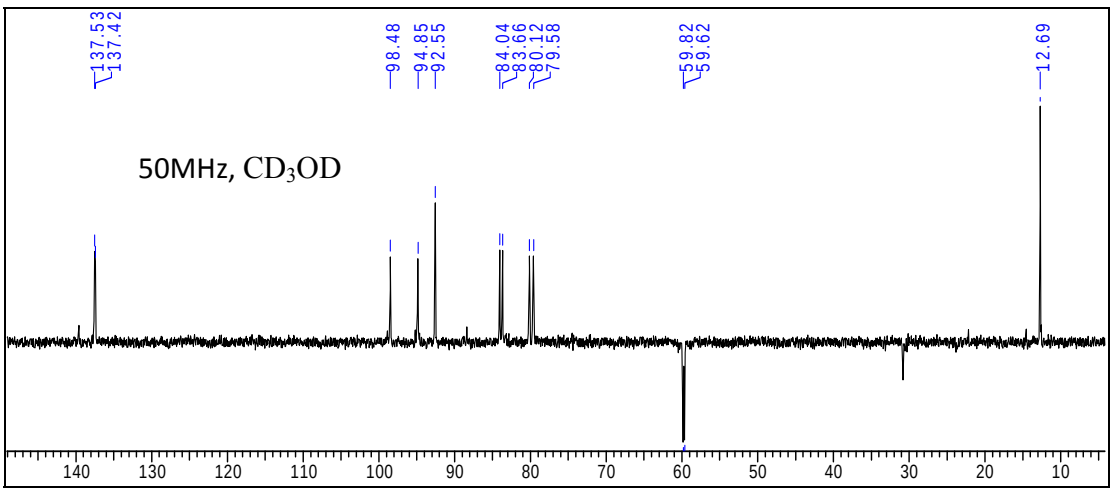

^{1}H NMR of compound 27

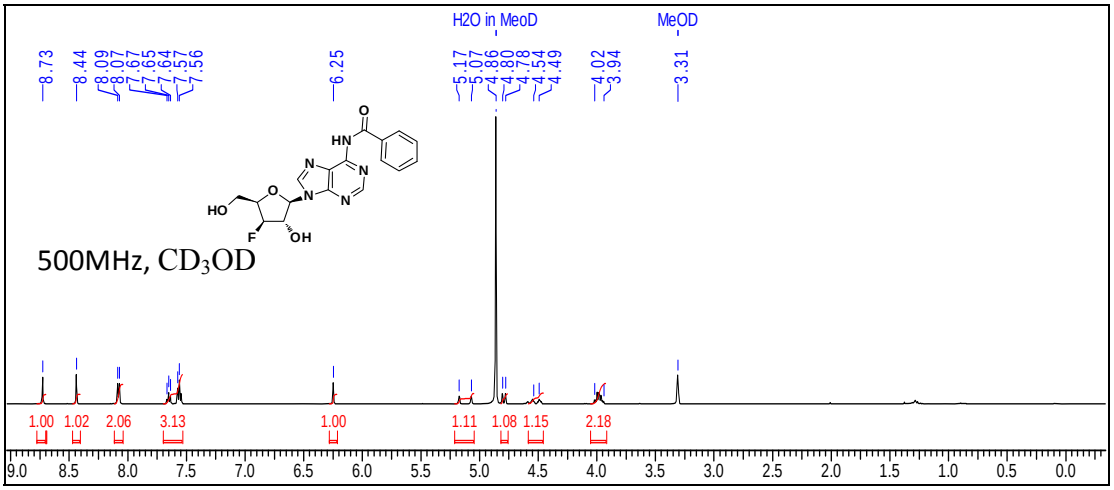

^{13}C NMR of compound 27

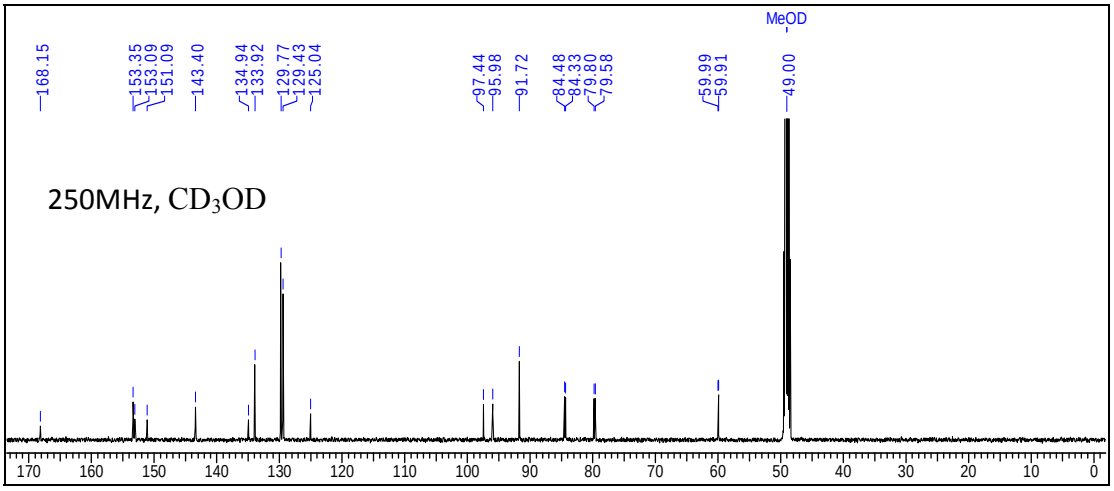

^{13}C-DEPT of compound 27

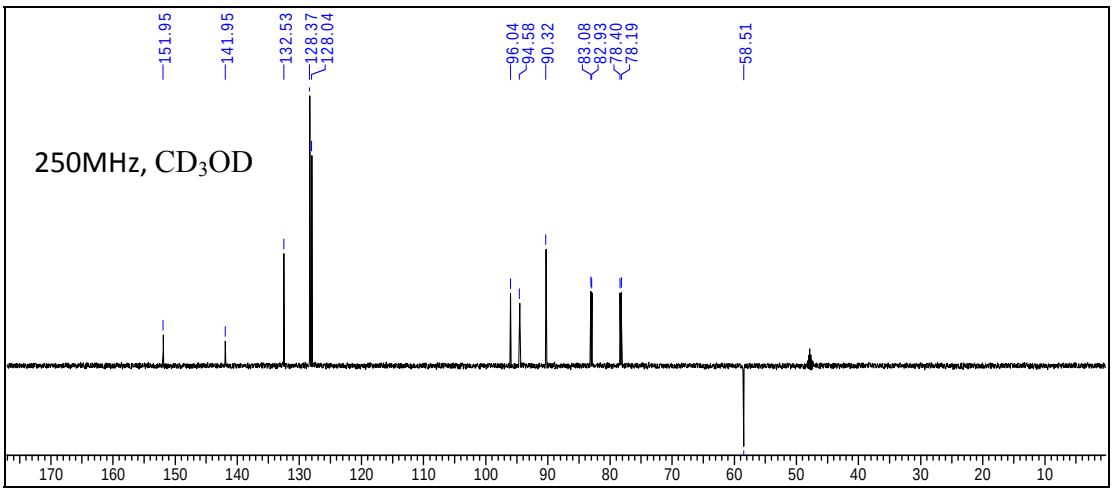

^{1}H NMR of compound 28

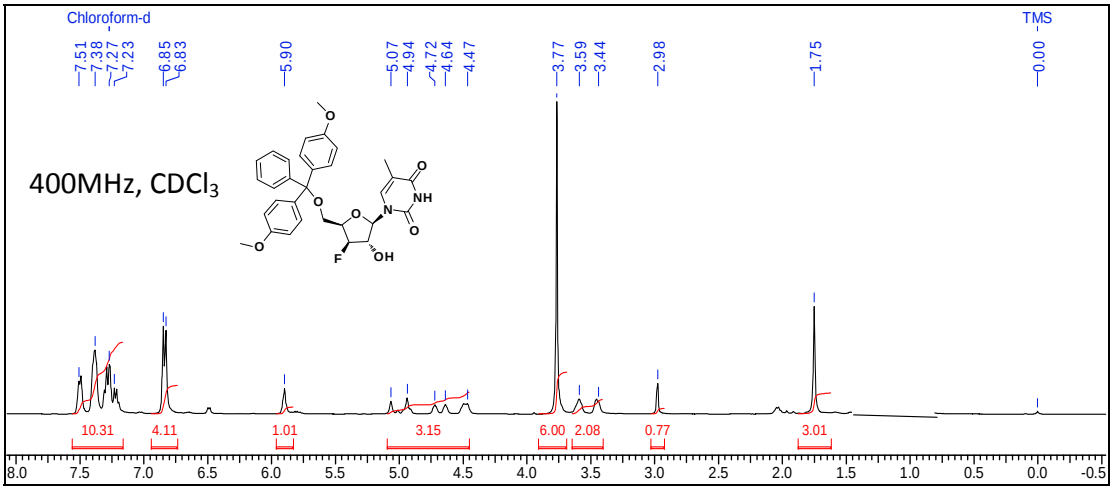

^{13}C NMR of compound 28

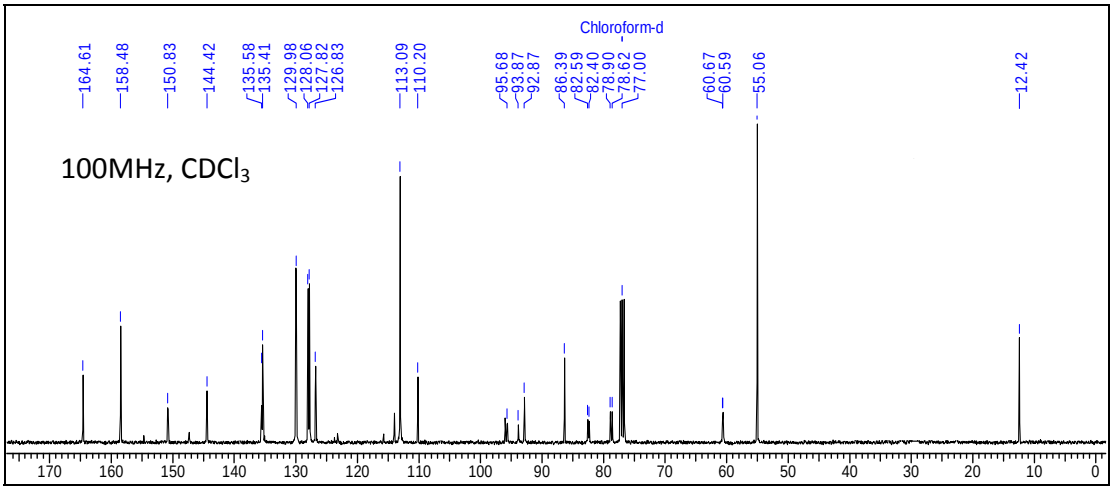

^{13}C-DEPT of compound 28

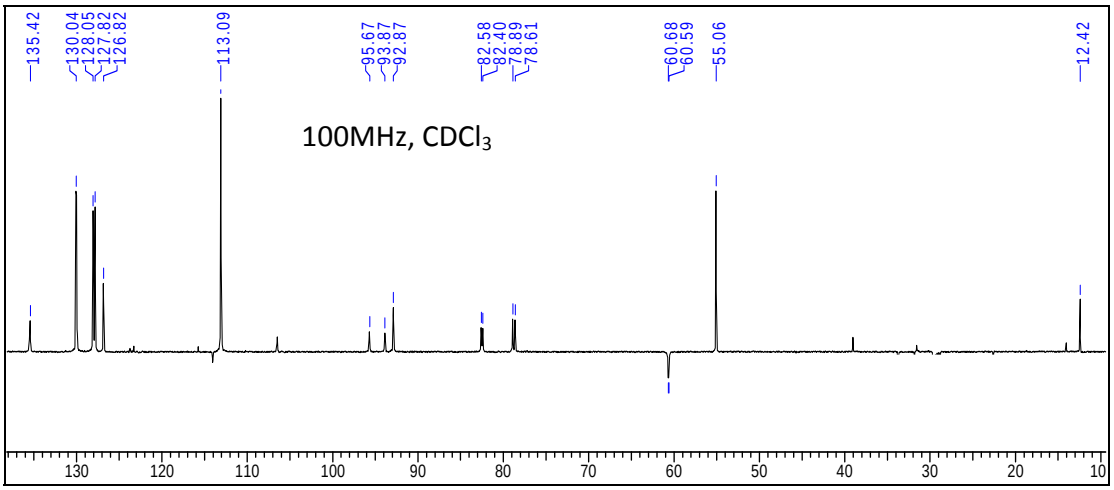

^{1}H NMR of compound 29

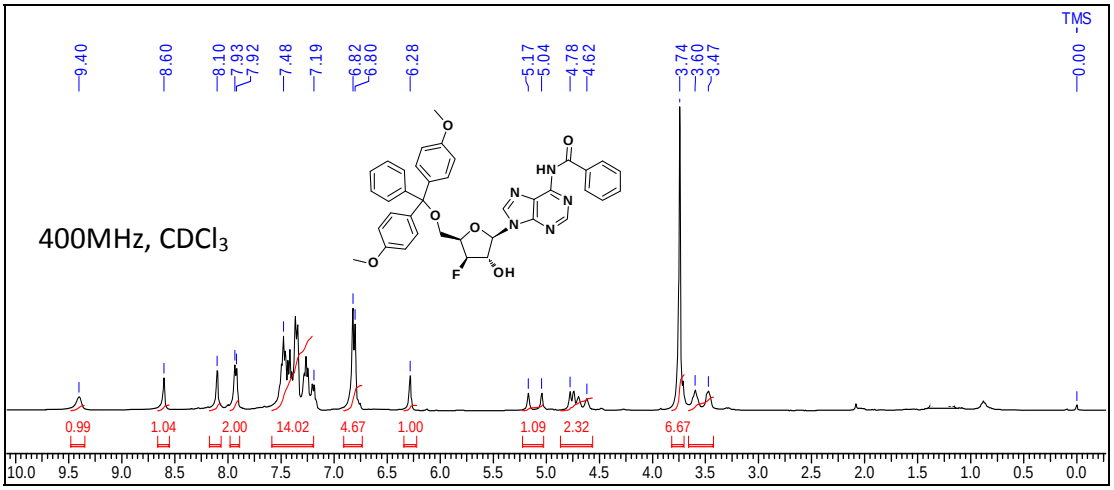

^{13}C NMR of compound 29

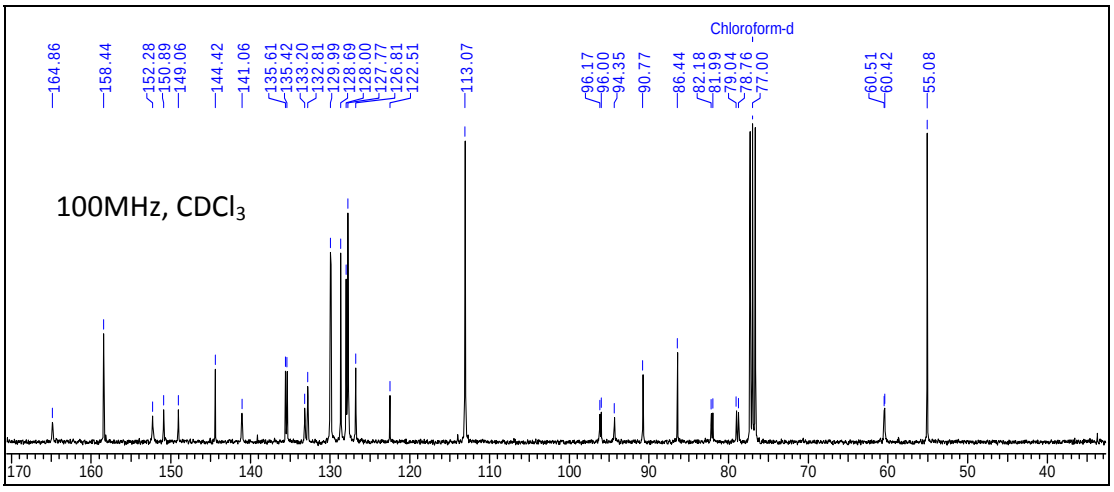

^{13}C-DEPT of compound 29

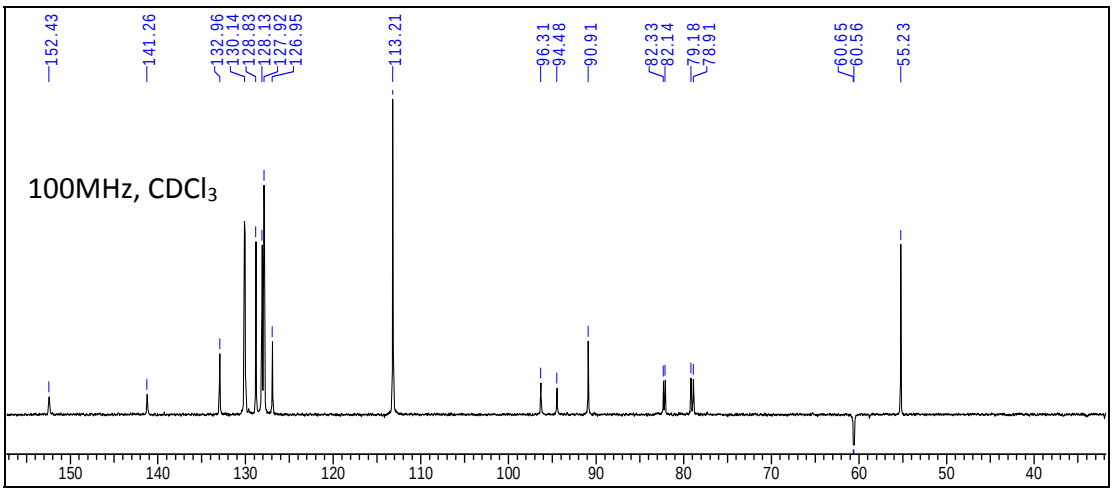

^{31}P NMR of compound 31

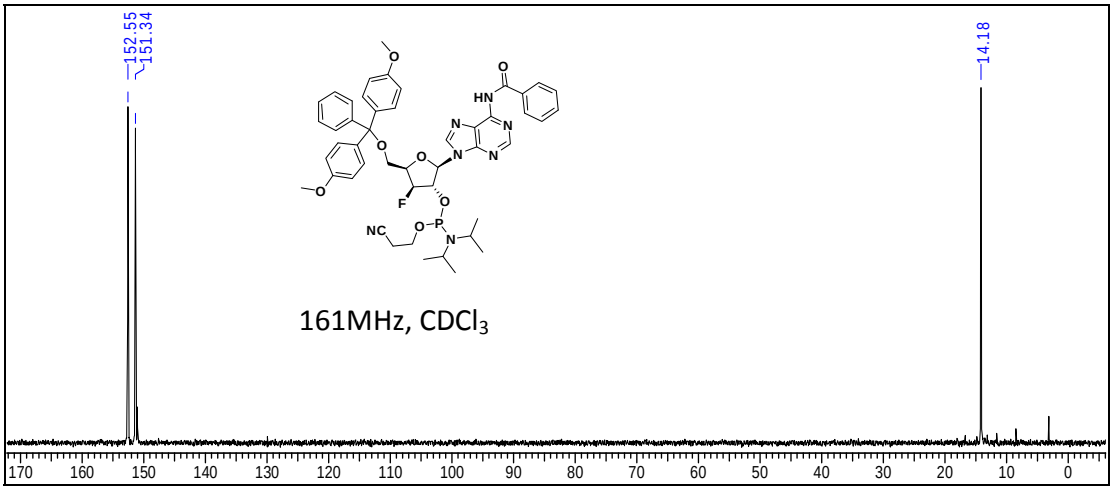

HRMS of compound 31

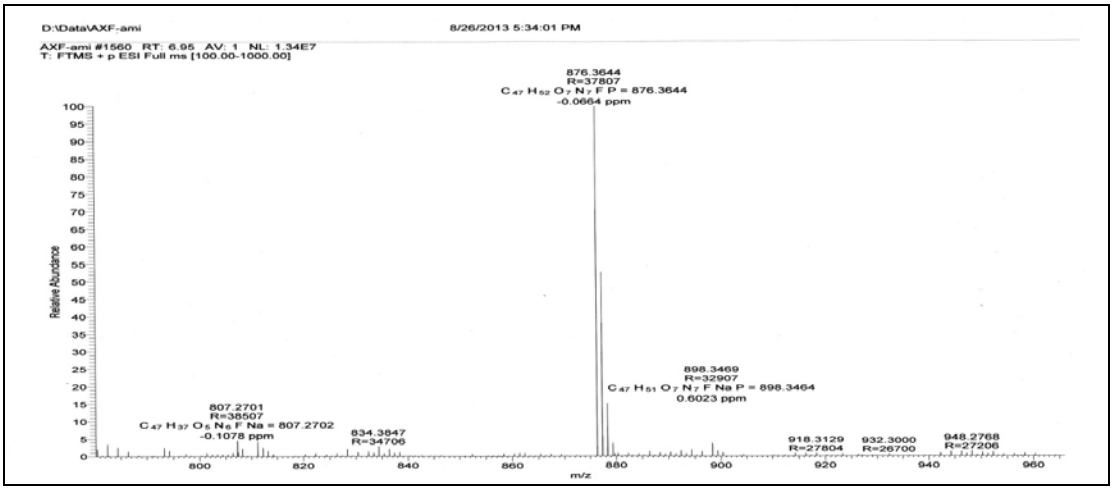

^{1}H NMR of compound 32

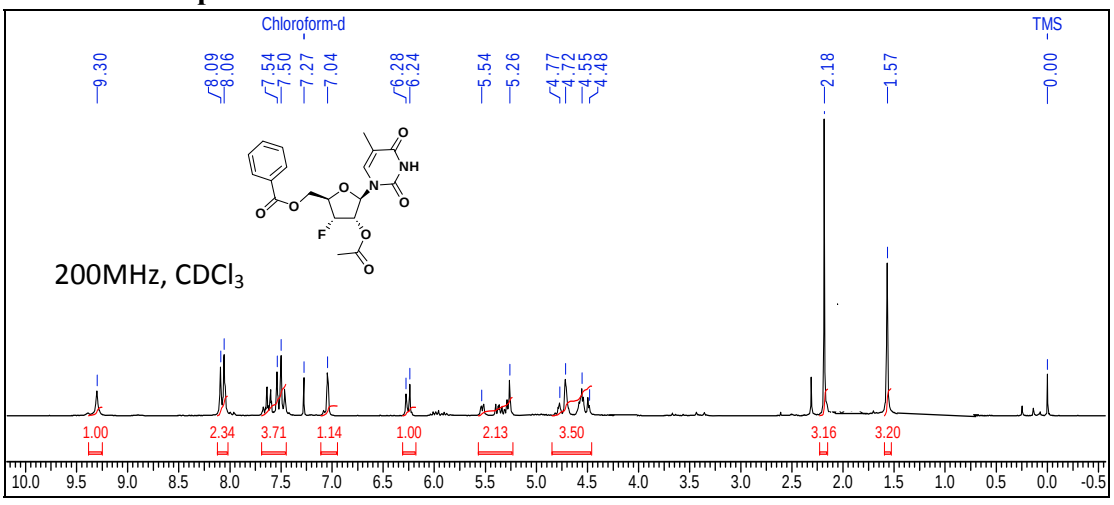

^{1}H NMR of compound 33

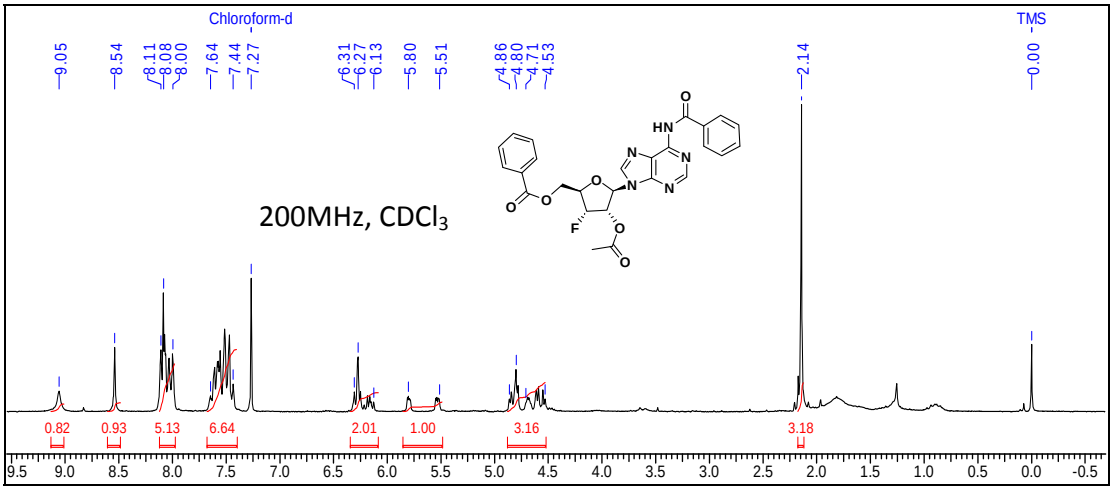

^{13}C NMR of compound 33

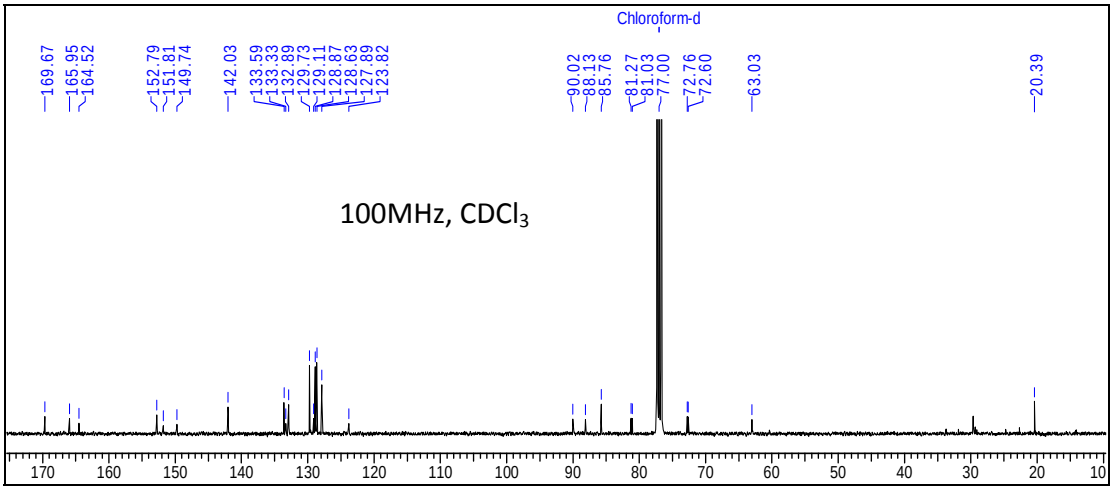

^{13}C-DEPT of compound 33

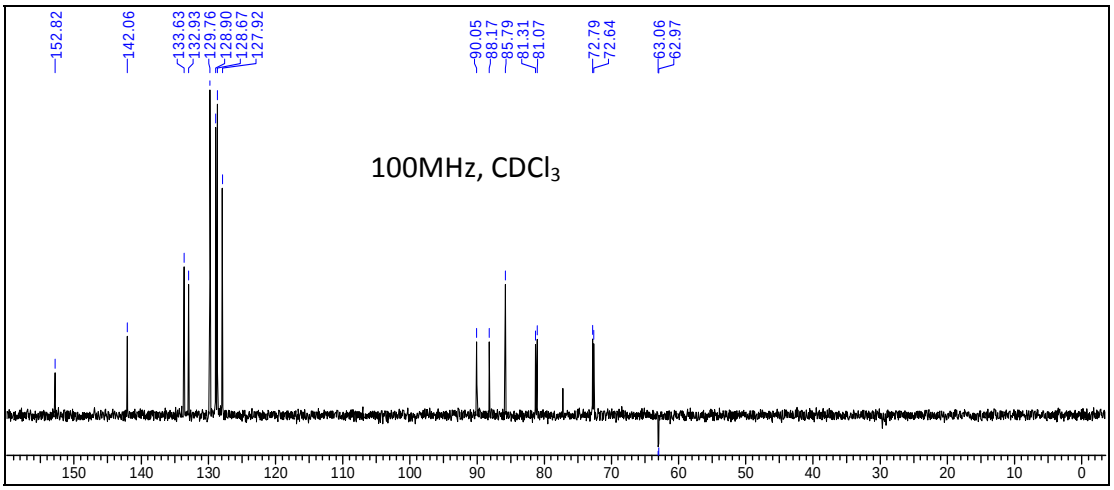

^{1}H NMR of compound 34

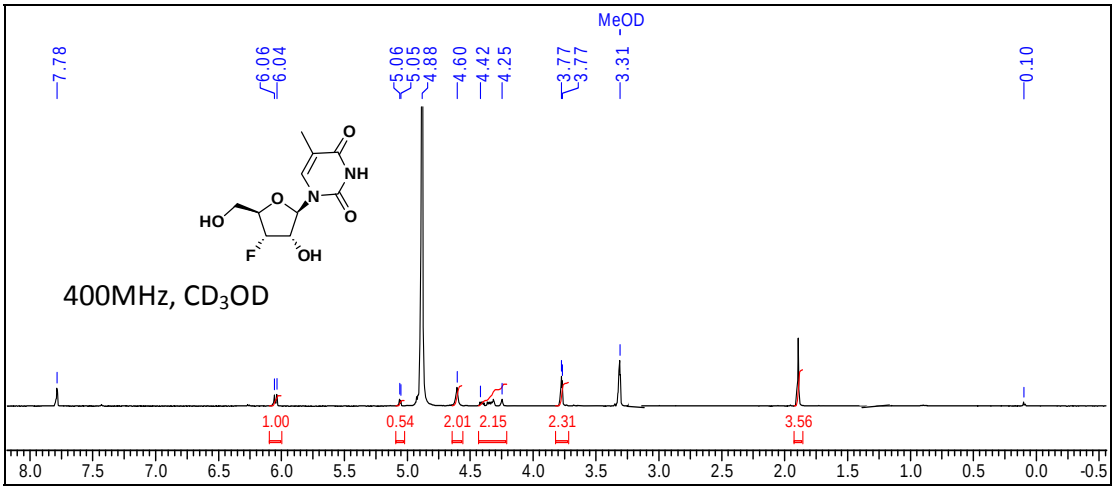

^{13}C NMR of compound 34

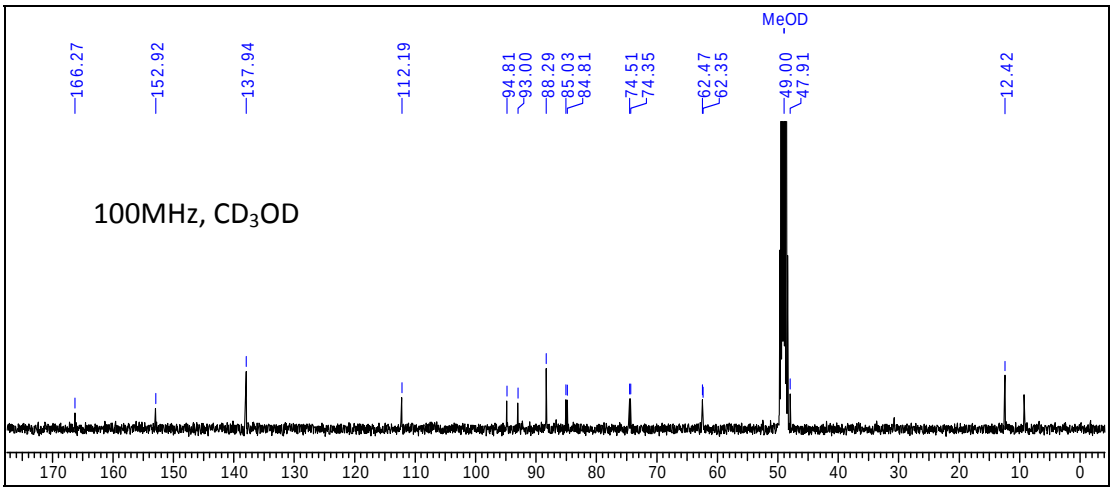

^{13}C-DEPT of compound 34

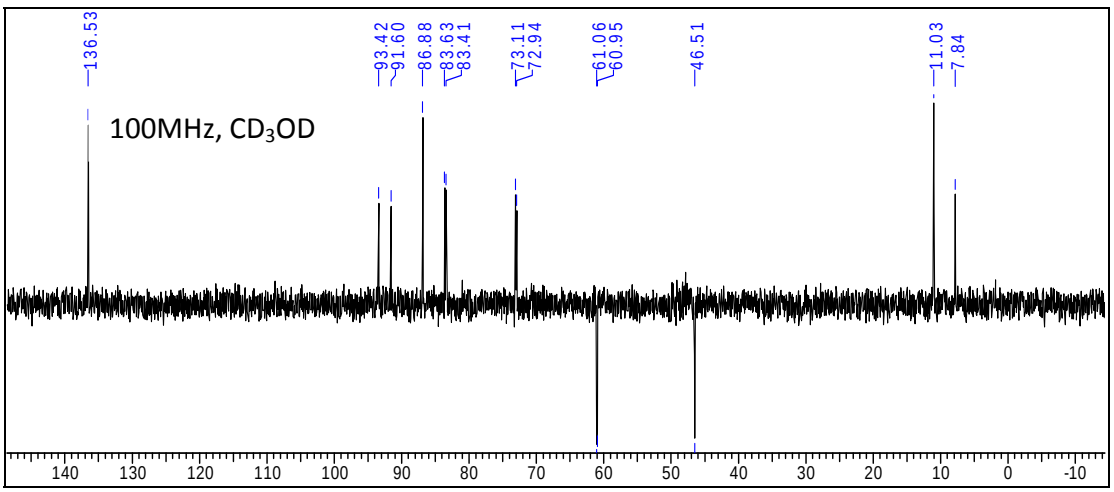

^{1}H NMR of compound 35

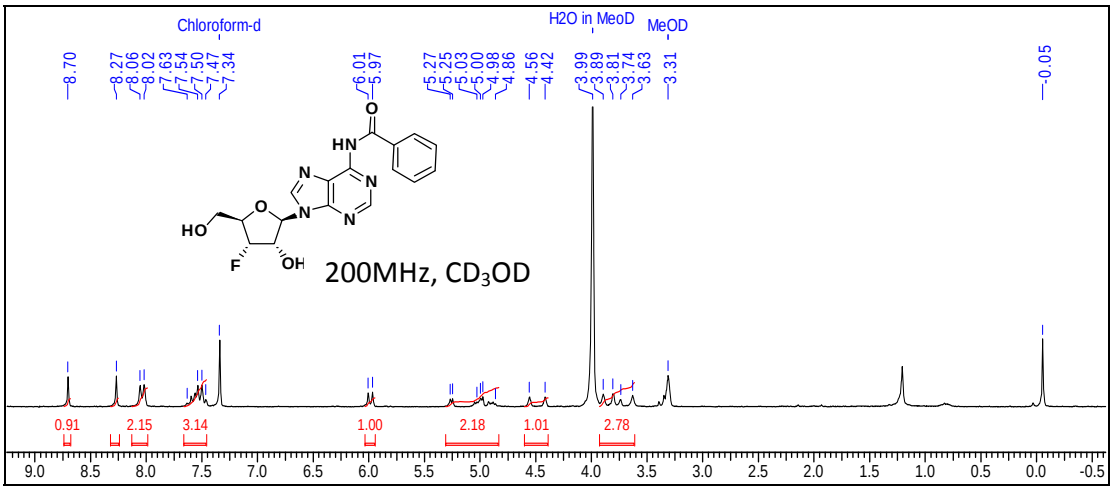

^{13}C NMR of compound 35

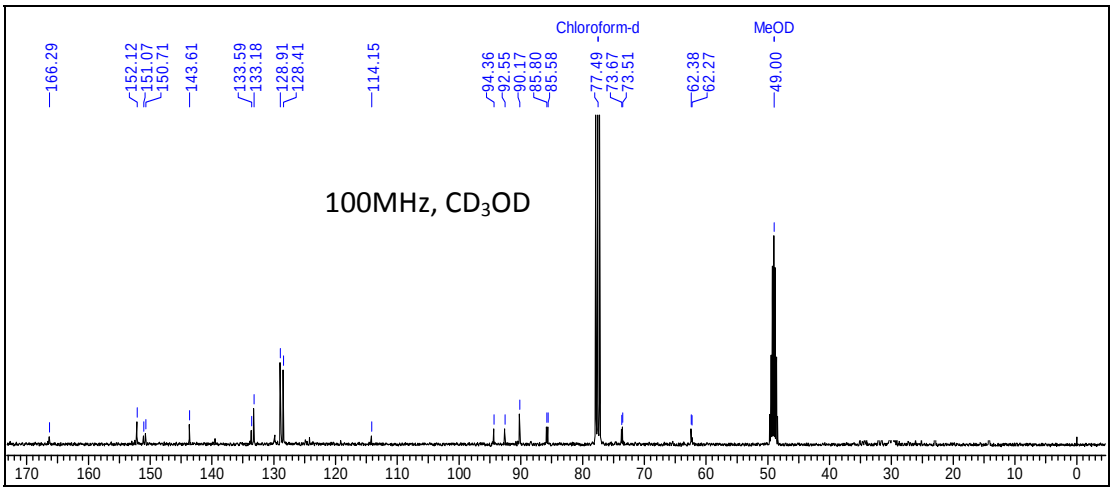

^{13}C-DEPT of compound 35

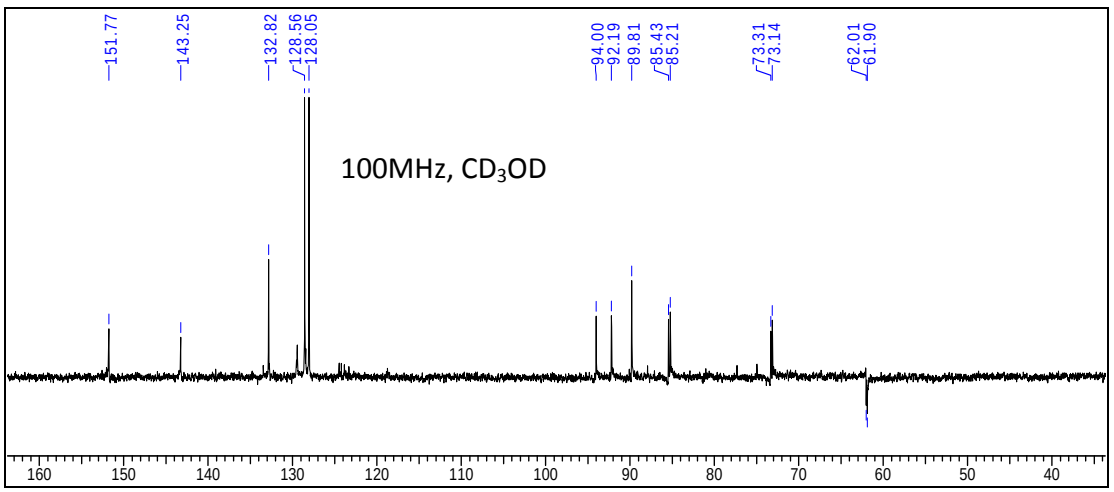

^{1}H NMR of compound 36

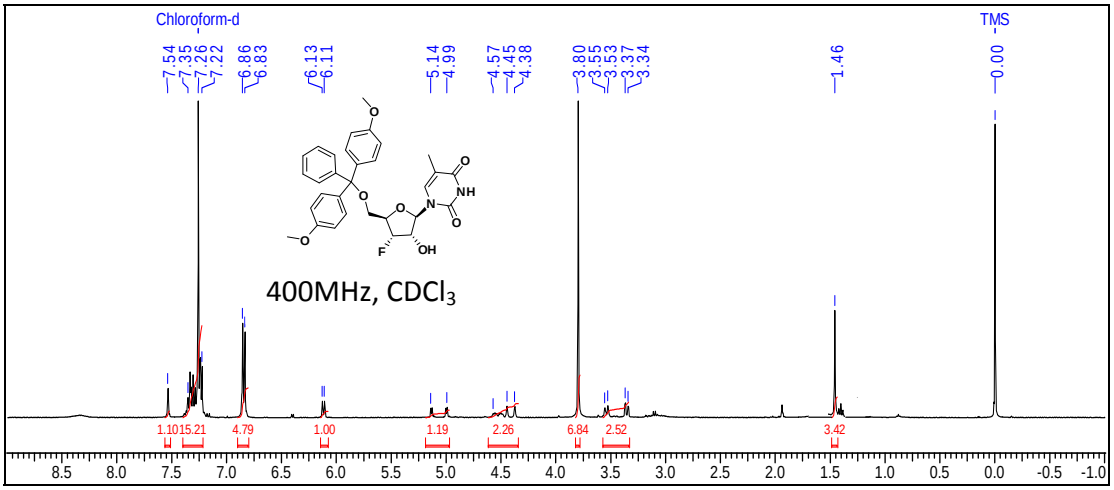

^{13}C NMR of compound 36

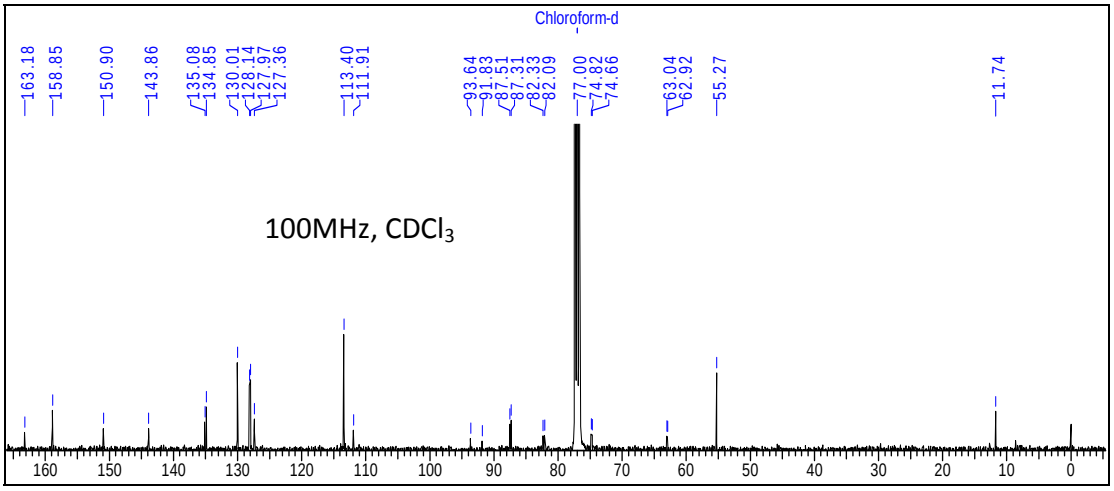

^{13}C-DEPT of compound 36

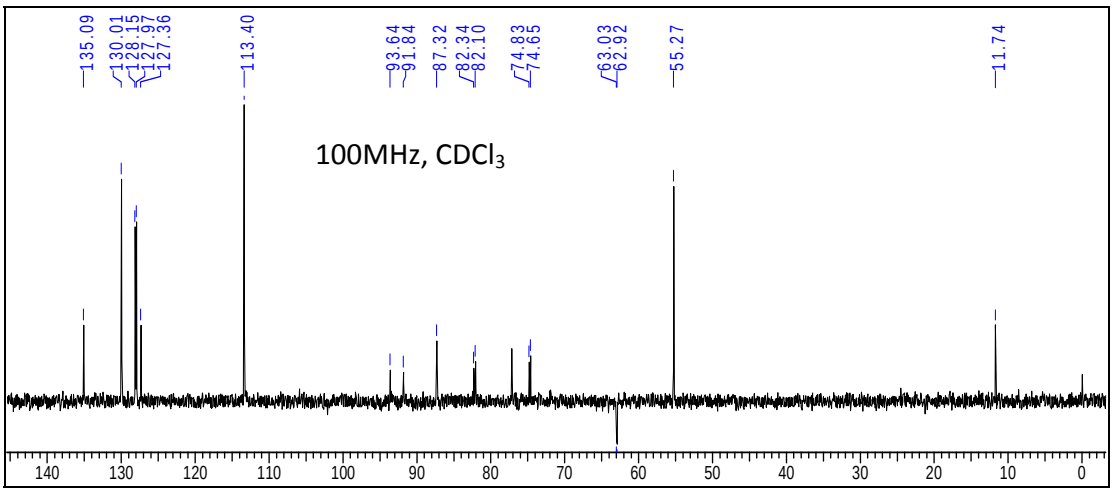

^{1}H NMR of compound 37

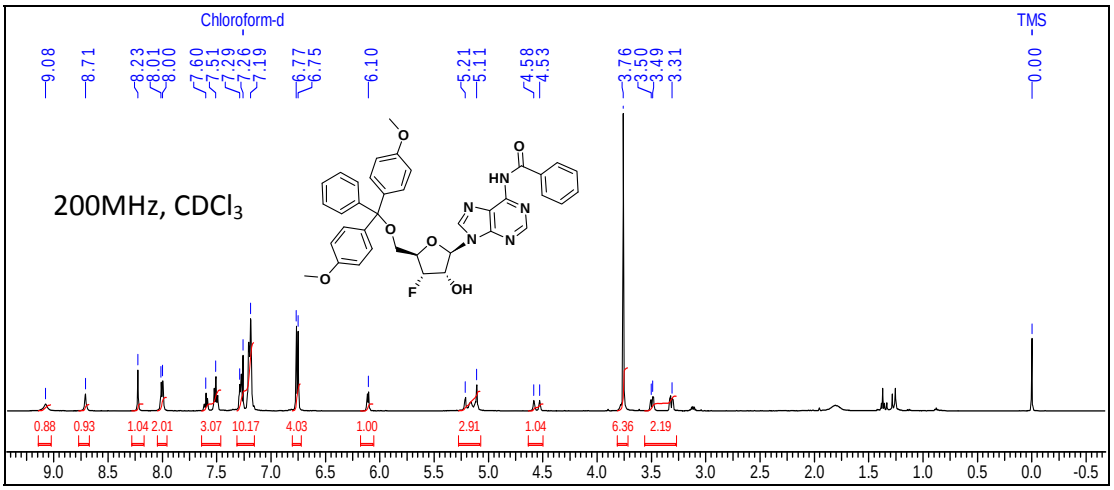

^{13}C NMR of compound 37

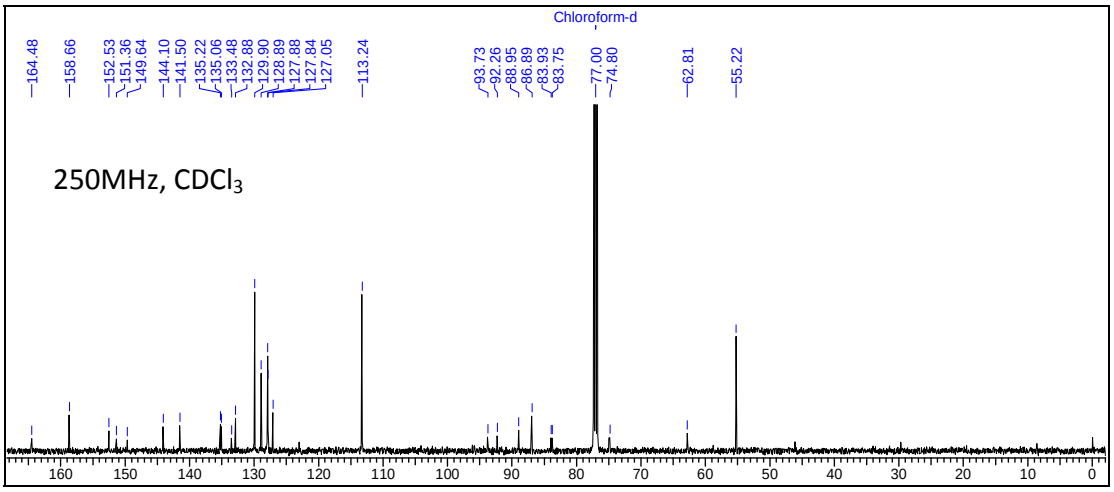

^{13}C-DEPT of compound 37

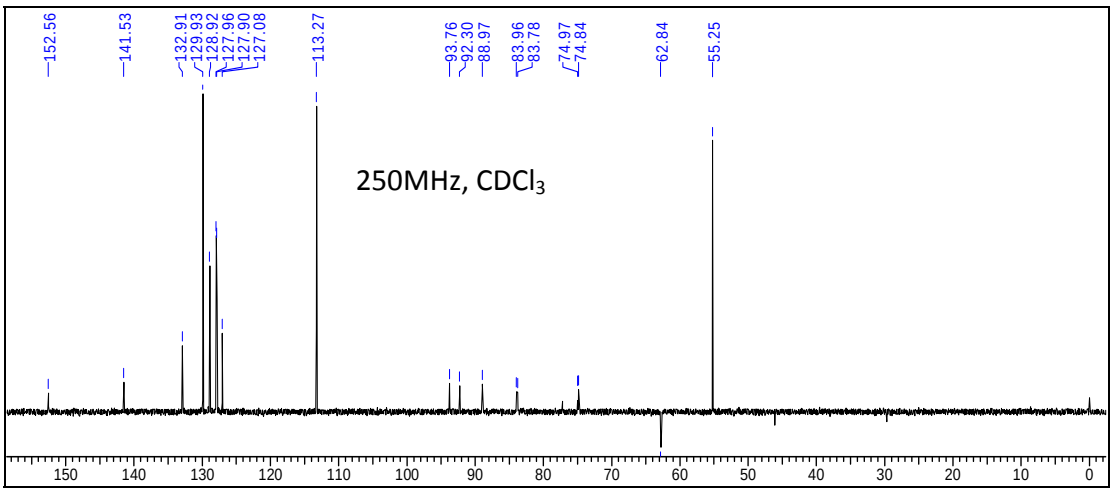

^{31}P NMR of compound 38

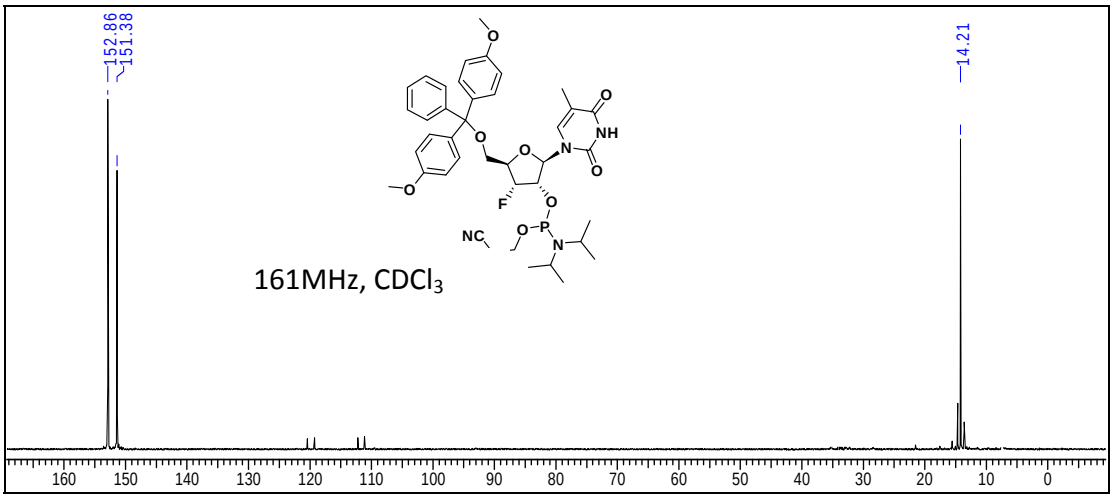

^{31}P NMR of compound 39

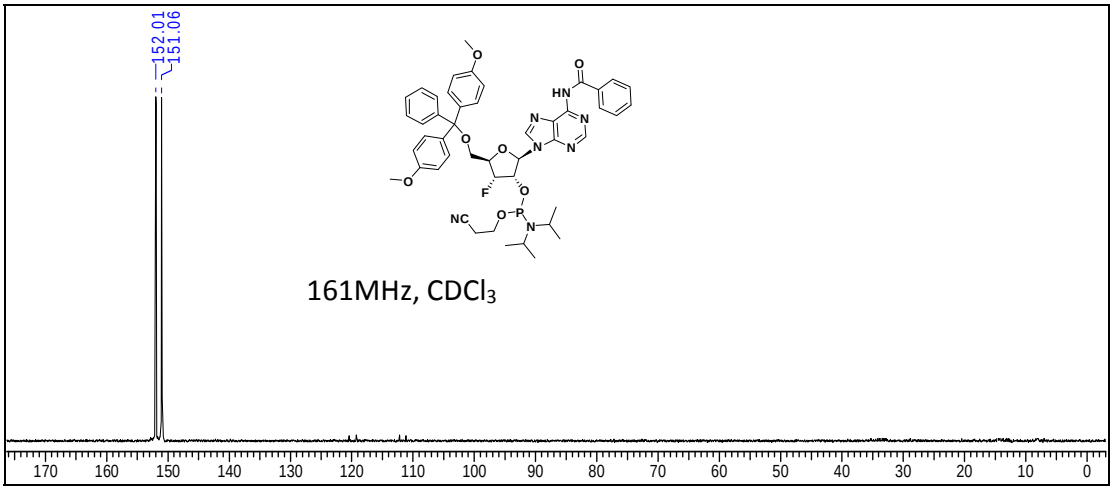

HRMS of compound 39

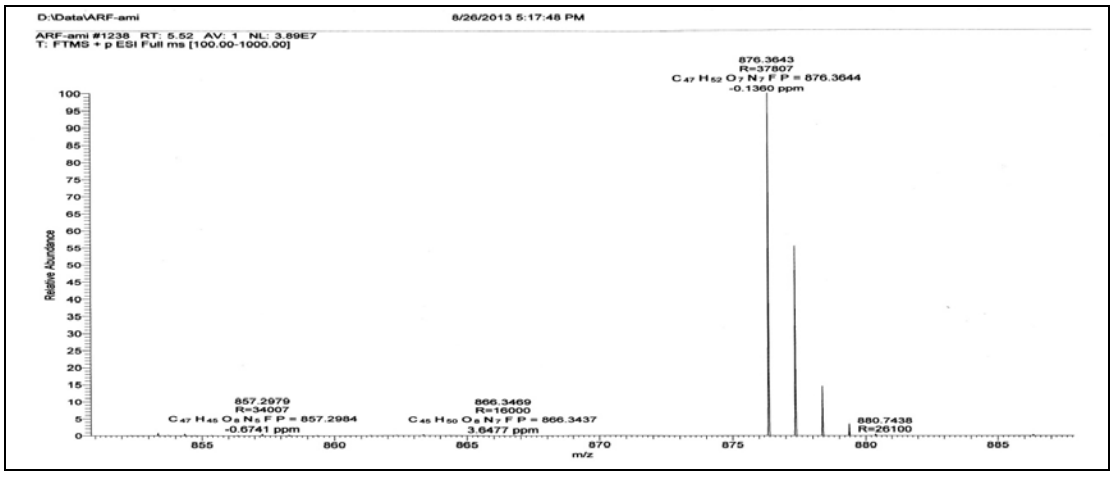

^{1}H NMR of compound 40

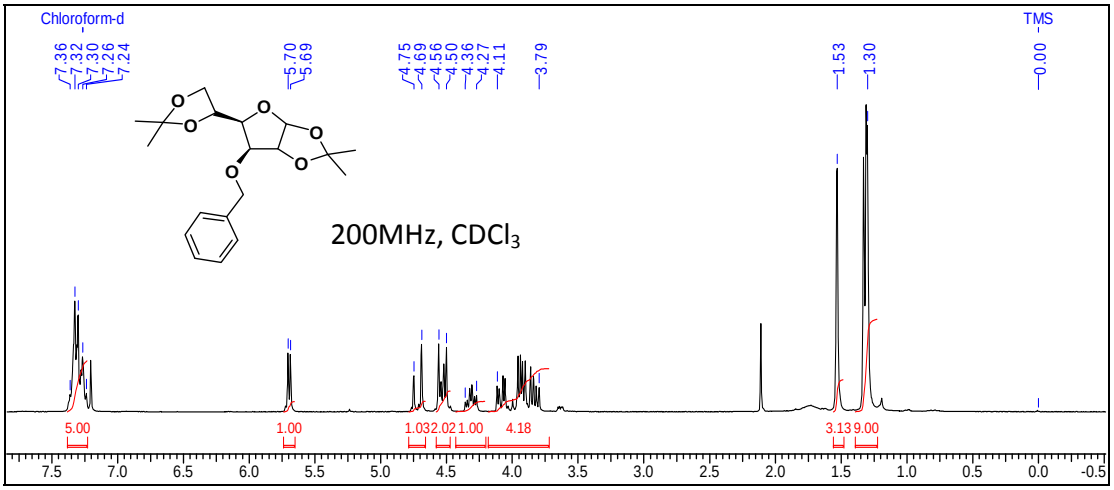

^{13}C NMR of compound 40

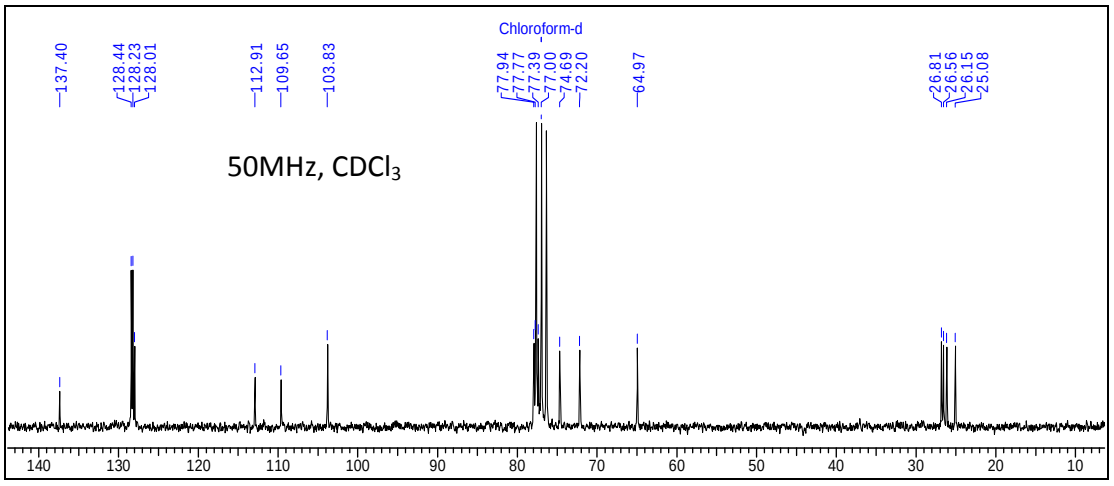

^{13}C-DEPT of compound 40

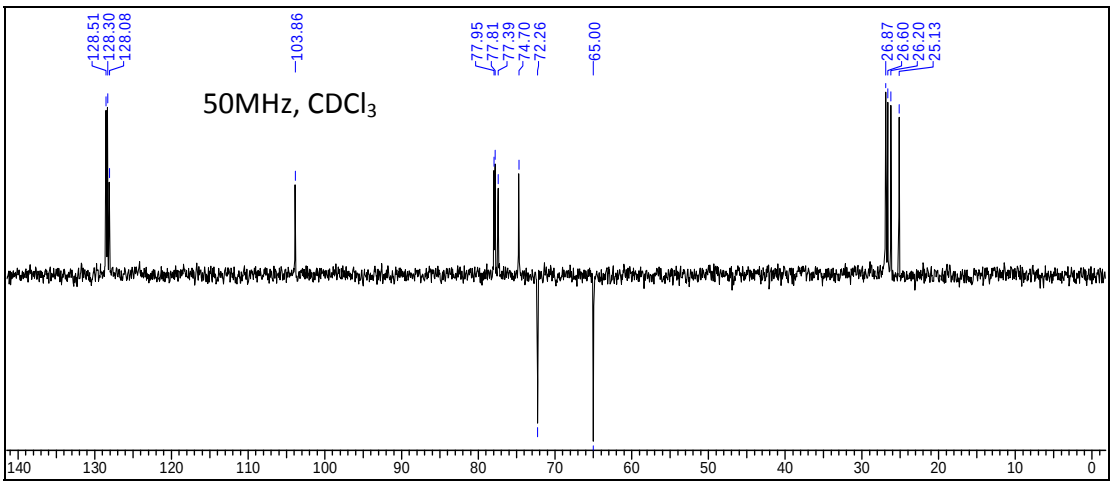

^{1}H NMR of compound 41

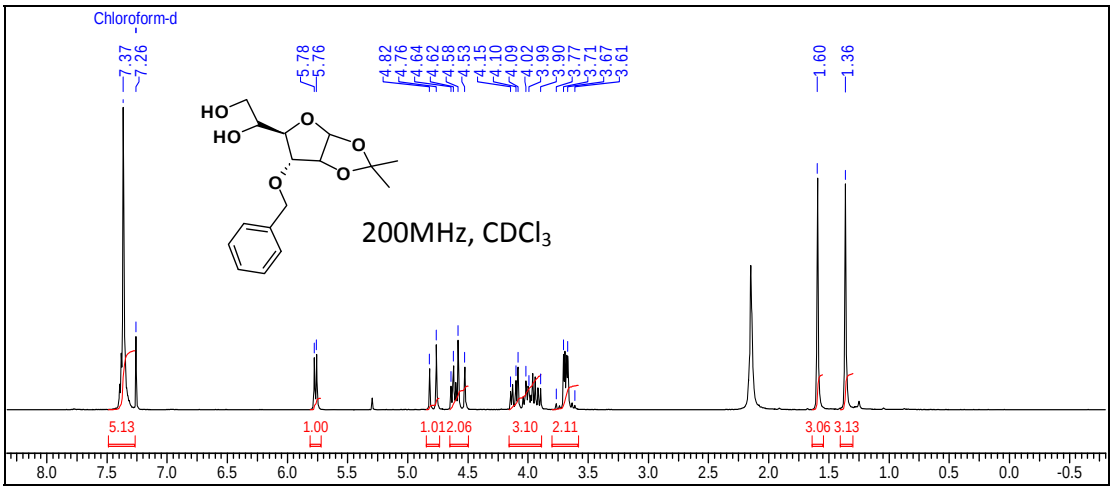

^{13}C NMR of compound 41

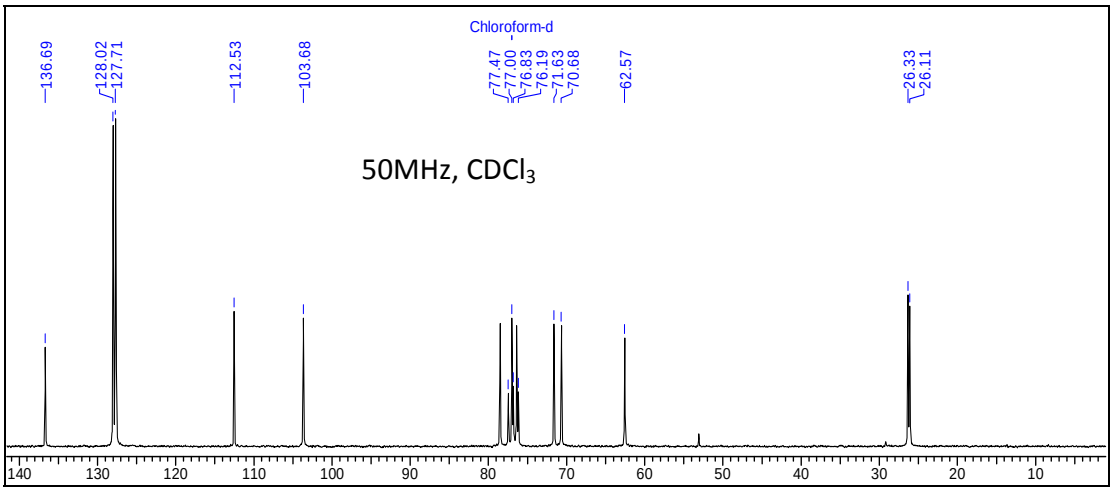

^{13}C-DEPT of compound 41

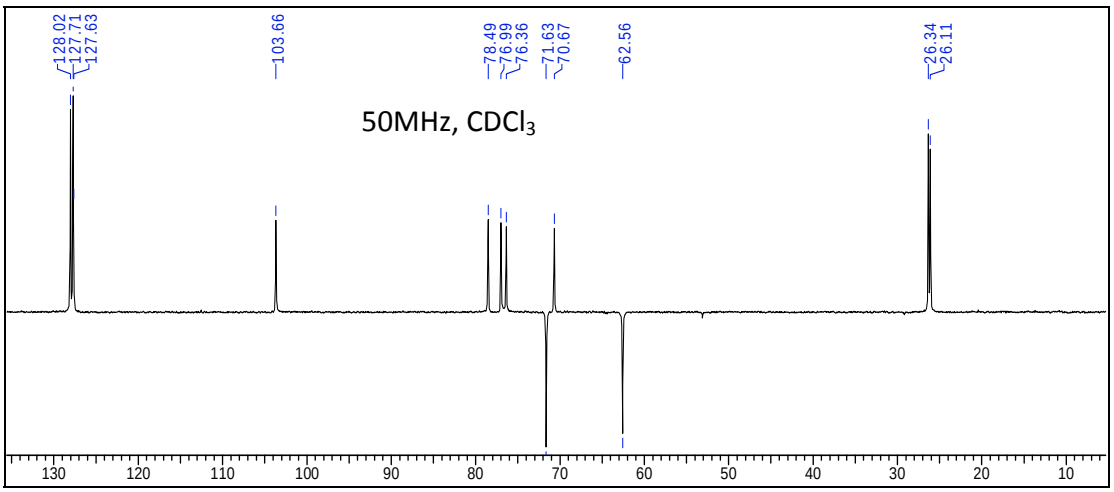

^{1}H NMR of compound 42

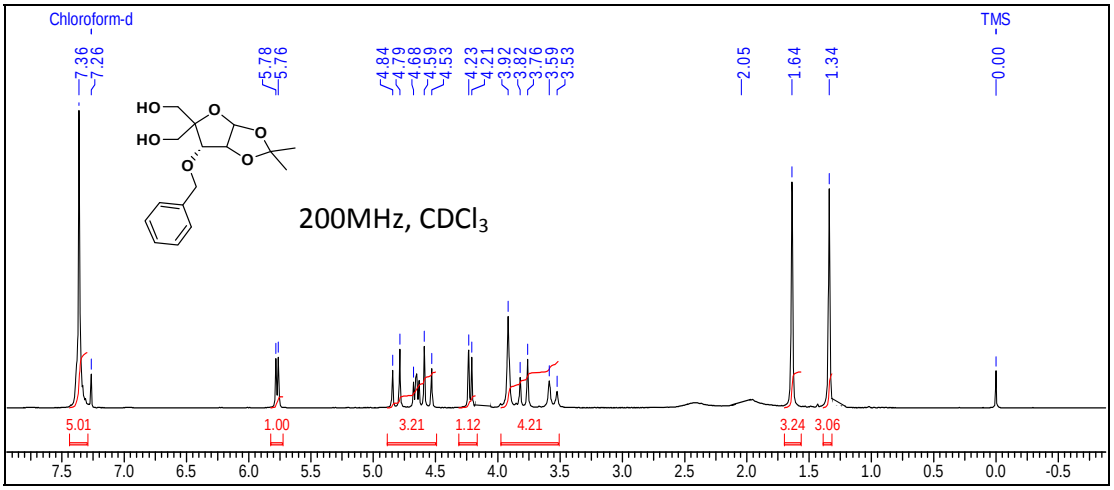

^{13}C NMR of compound 42

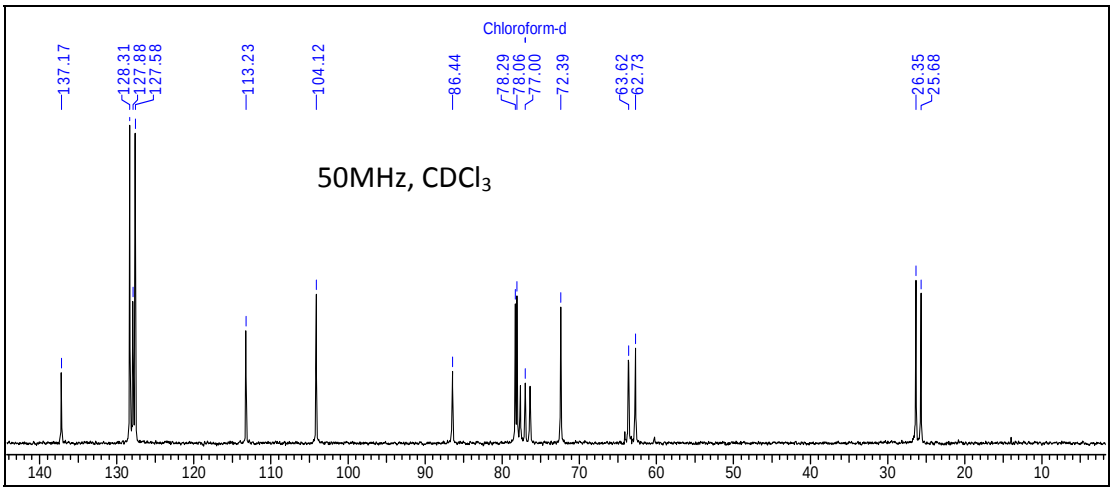

^{13}C-DEPT of compound 42

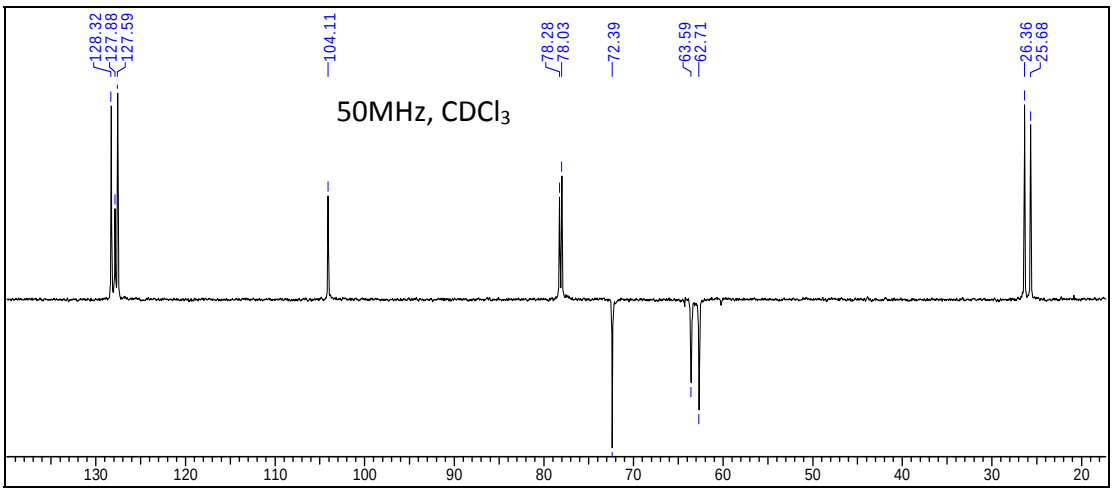

^{1}H NMR of compound 43

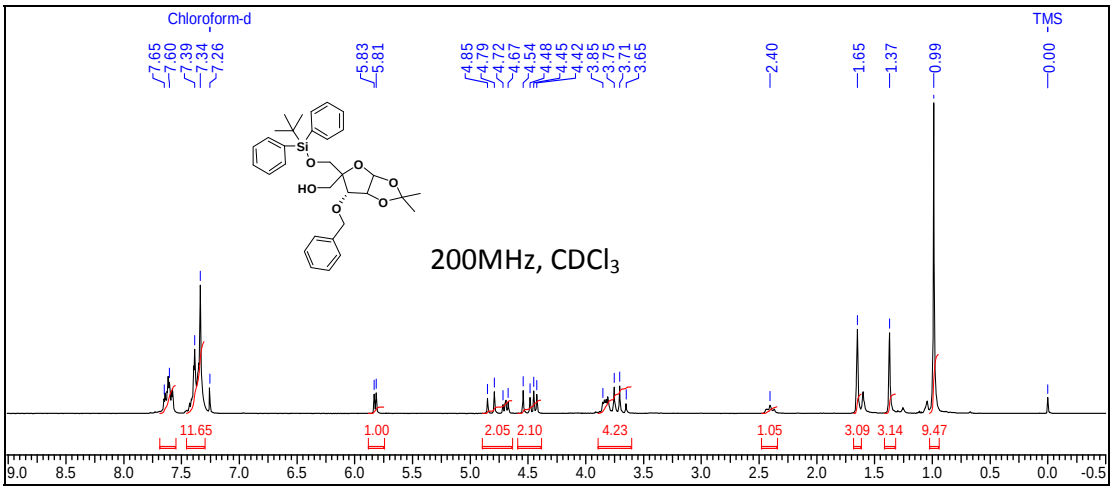

^{13}C NMR of compound 43

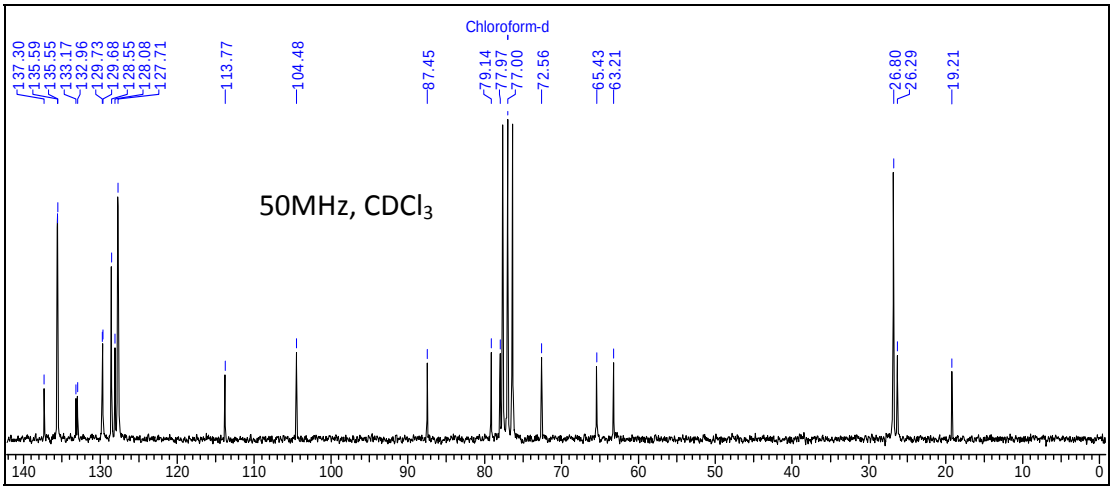

^{13}C-DEPT of compound 43

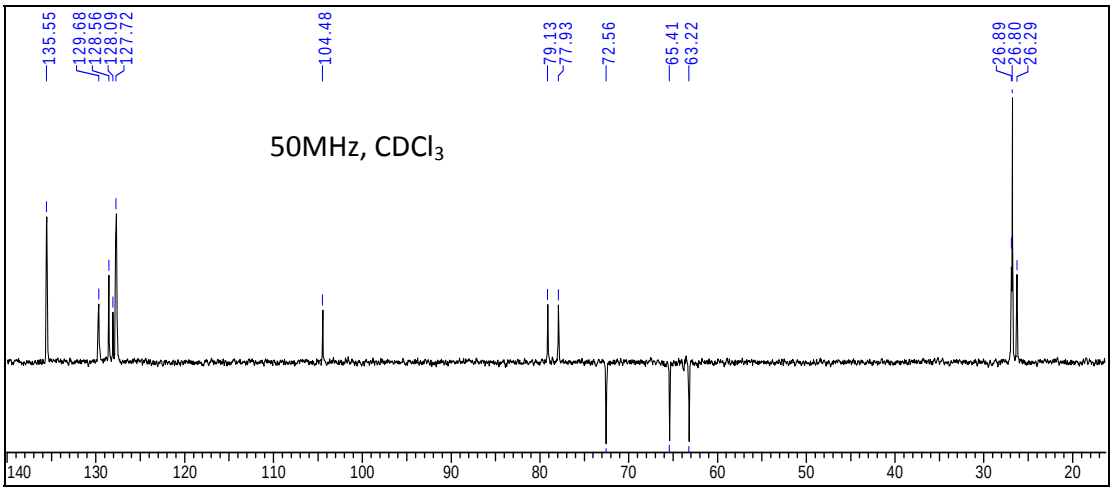

^{1}H NMR of compound 44

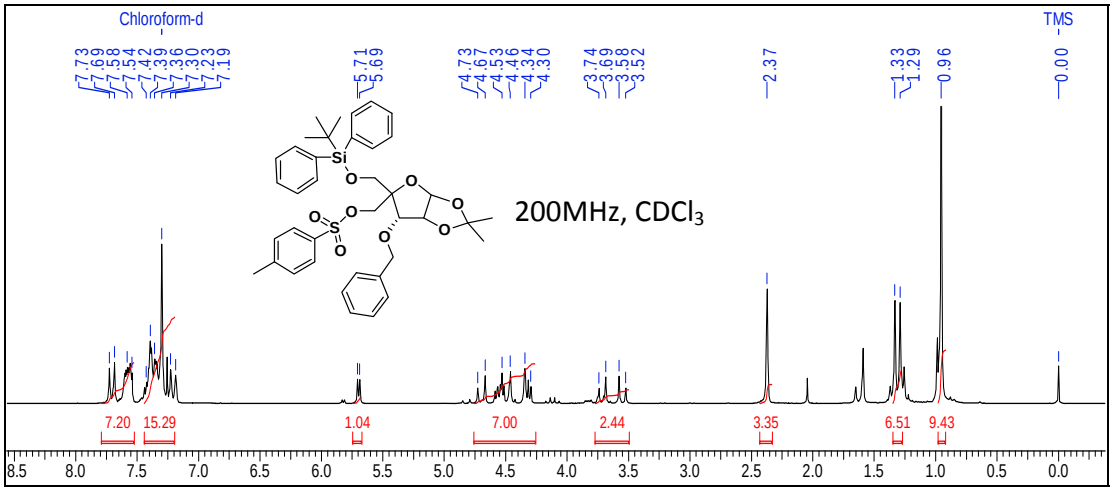

^{1}H NMR of compound 45

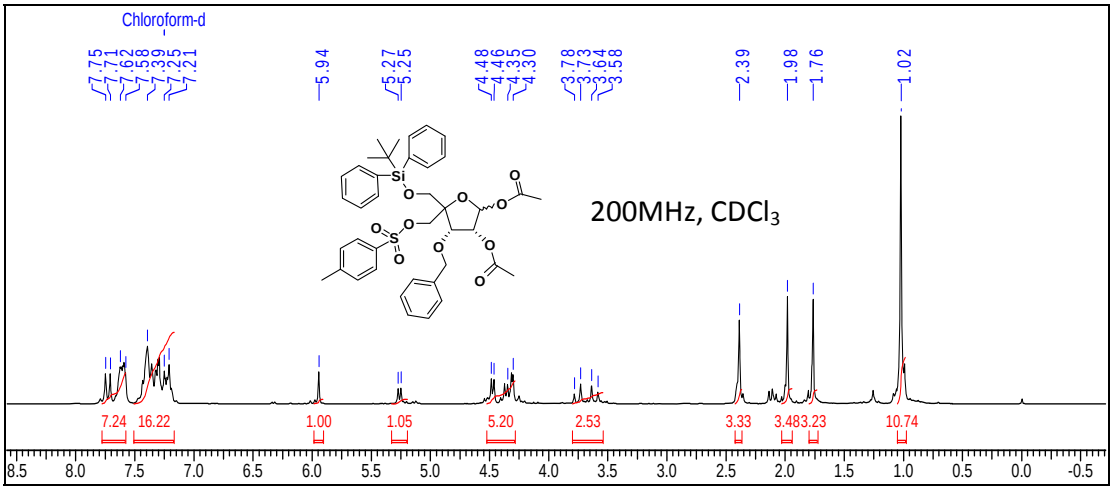

^{1}H NMR of compound 46

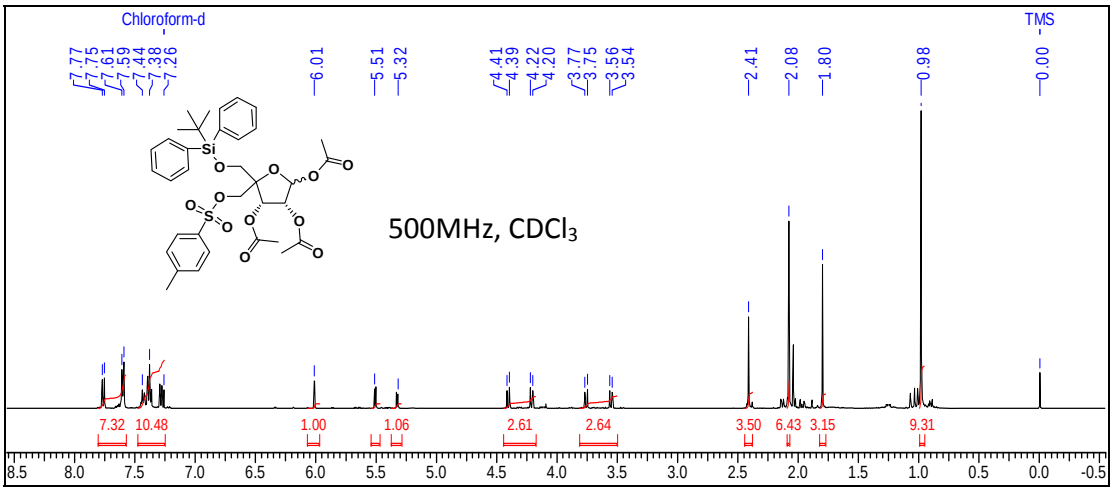

^{13}C NMR of compound 46

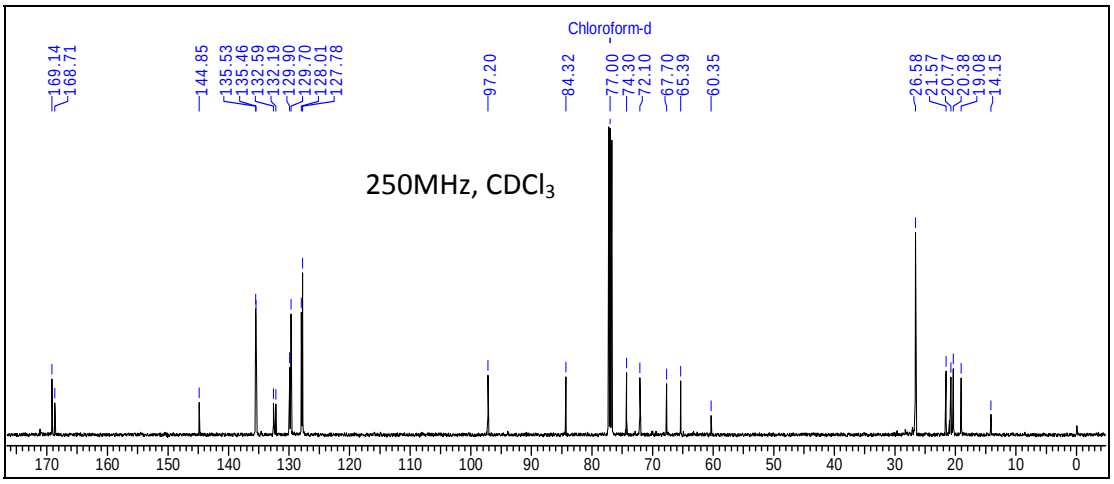

^{13}C-DEPT of compound 46

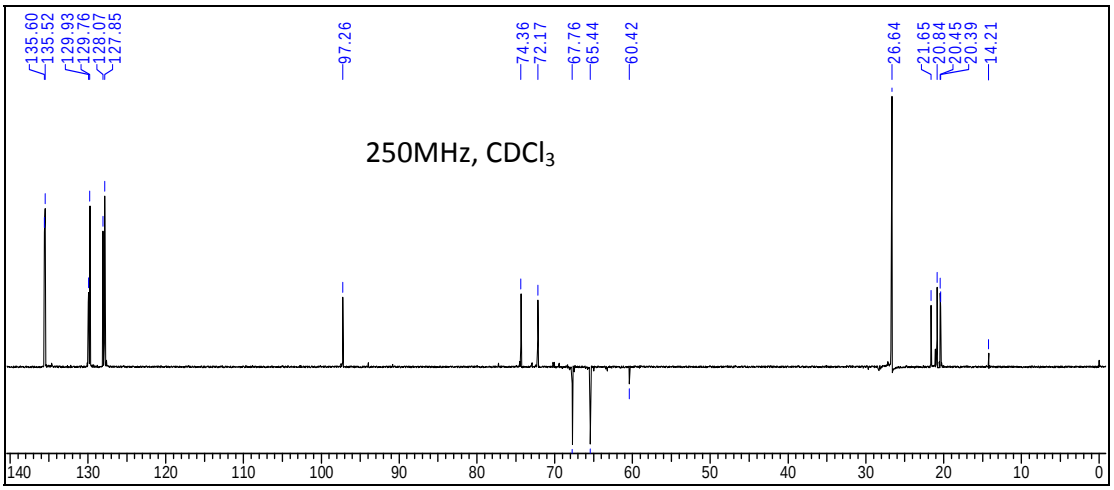

^{1}H NMR of compound 47

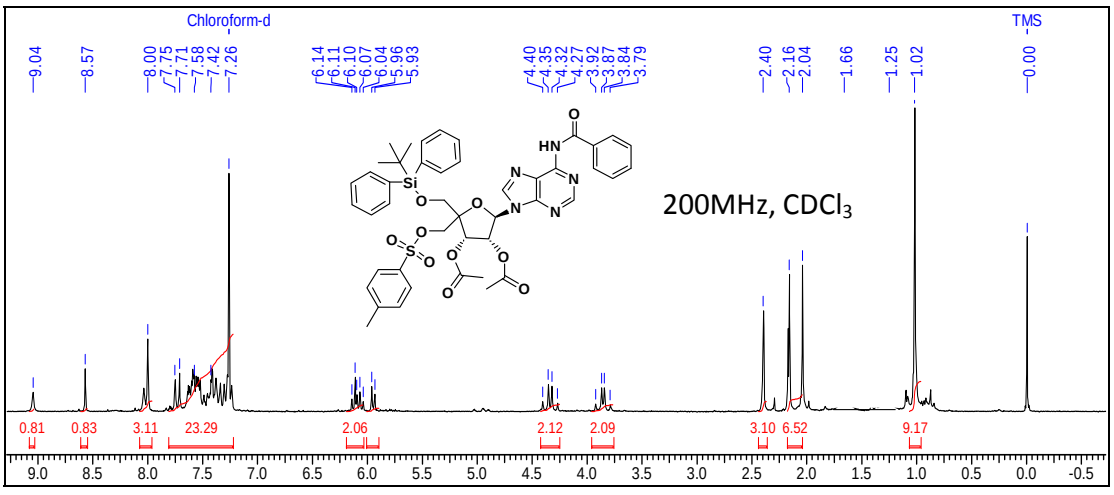

^{1}H NMR of compound 48

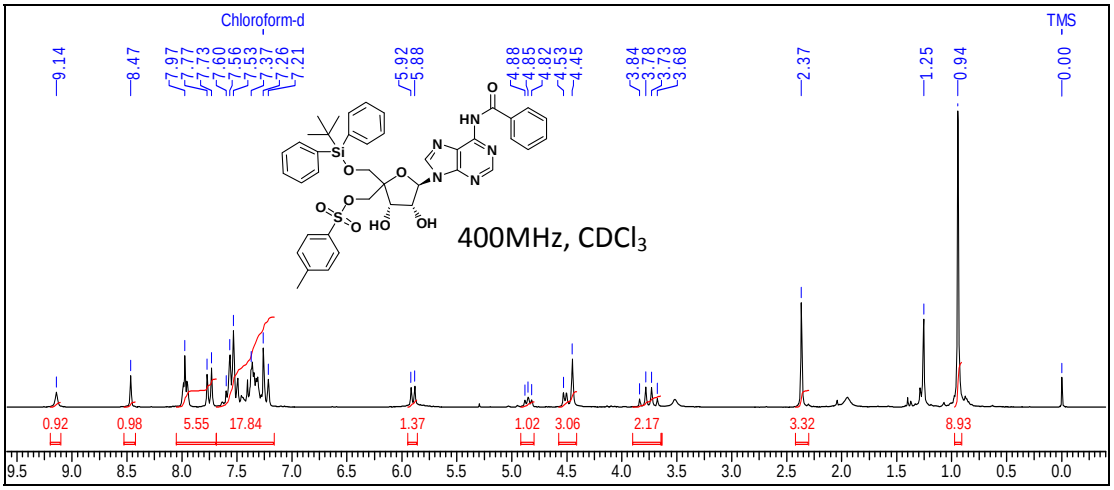

^{13}C NMR of compound 48

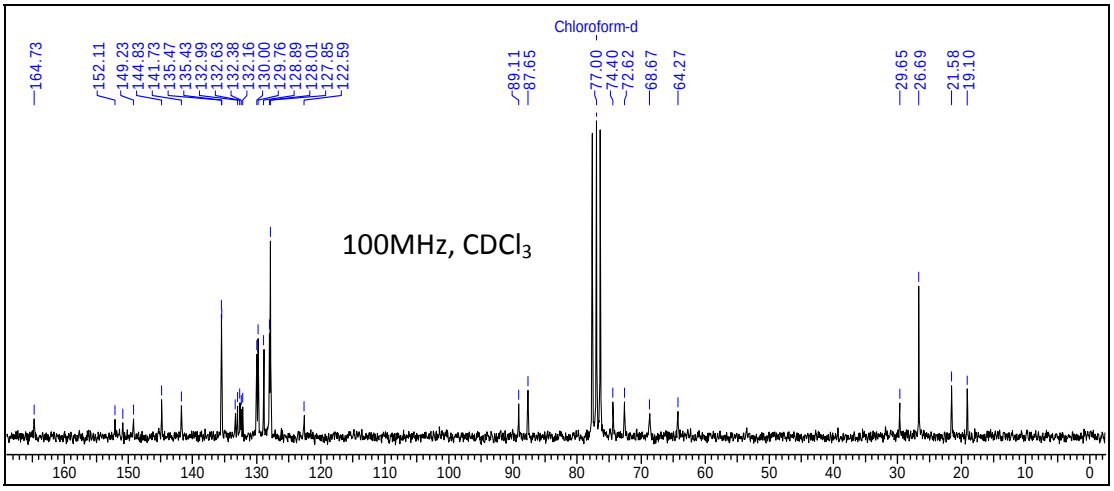

^{13}C-DEPT of compound 48

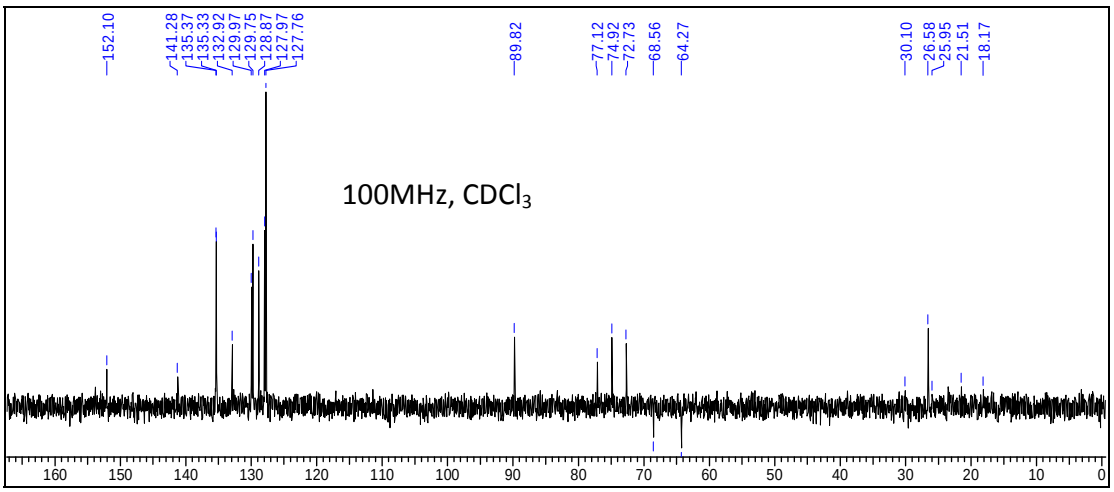

^{1}H NMR of compound 49

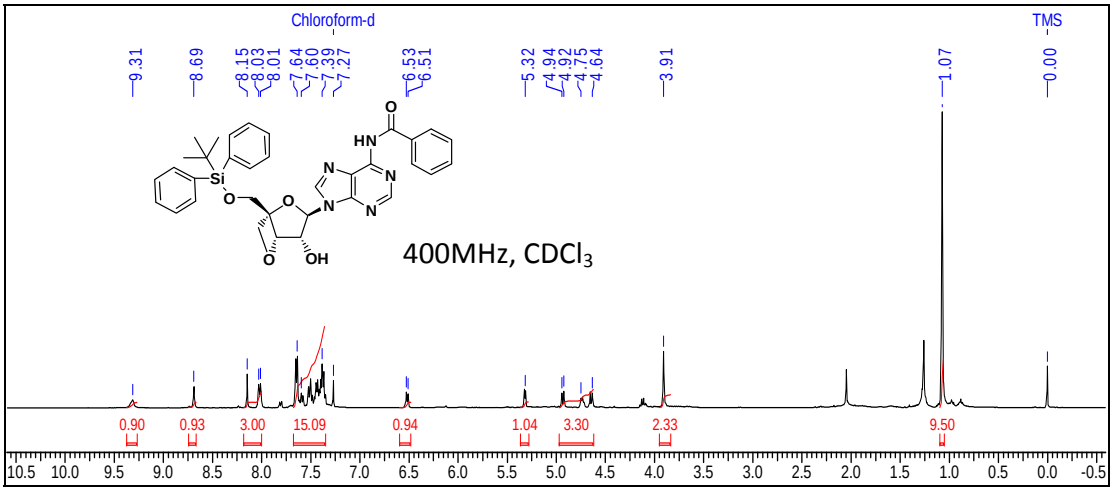

^{13}C NMR of compound 49

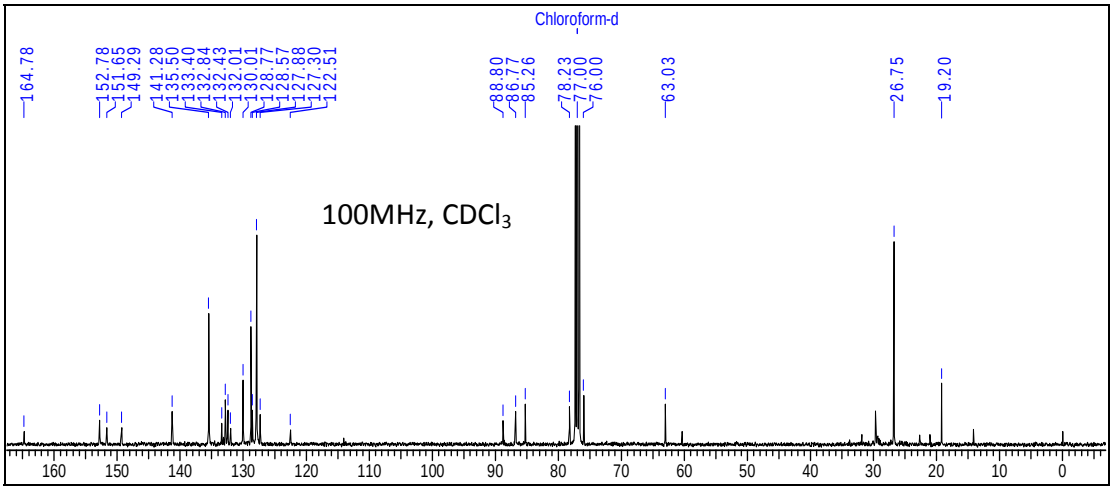

^{13}C-DEPT of compound 49

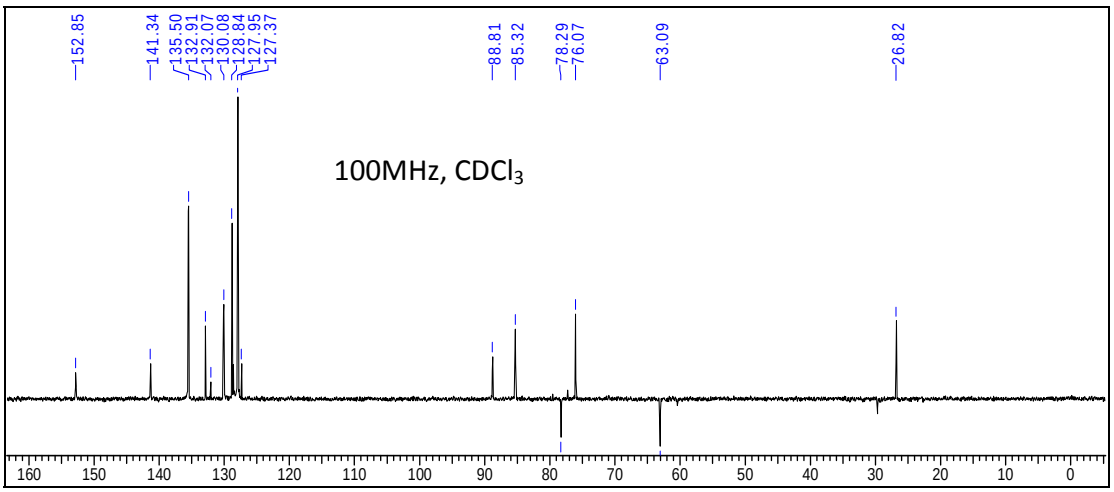

^{1}H NMR of compound 50

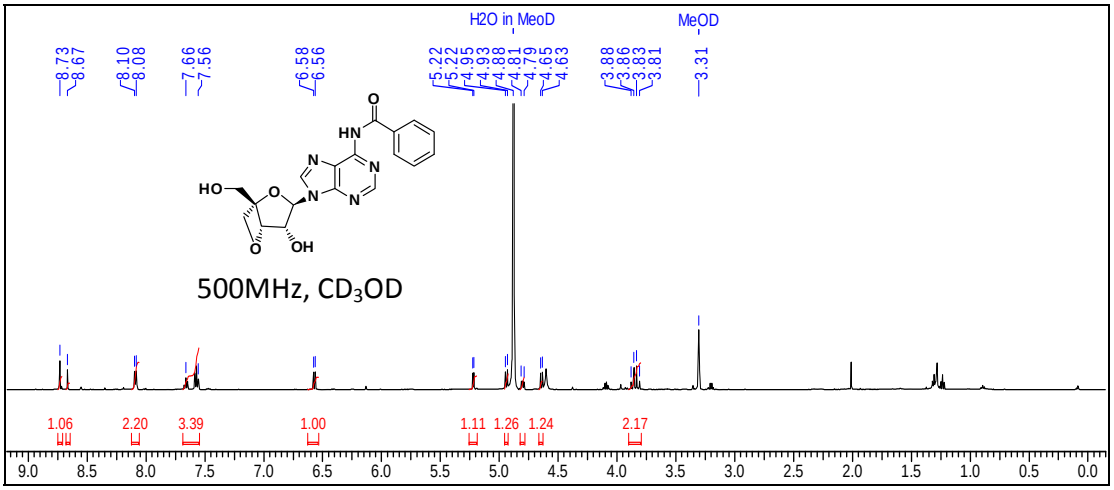

^{13}C NMR of compound 50

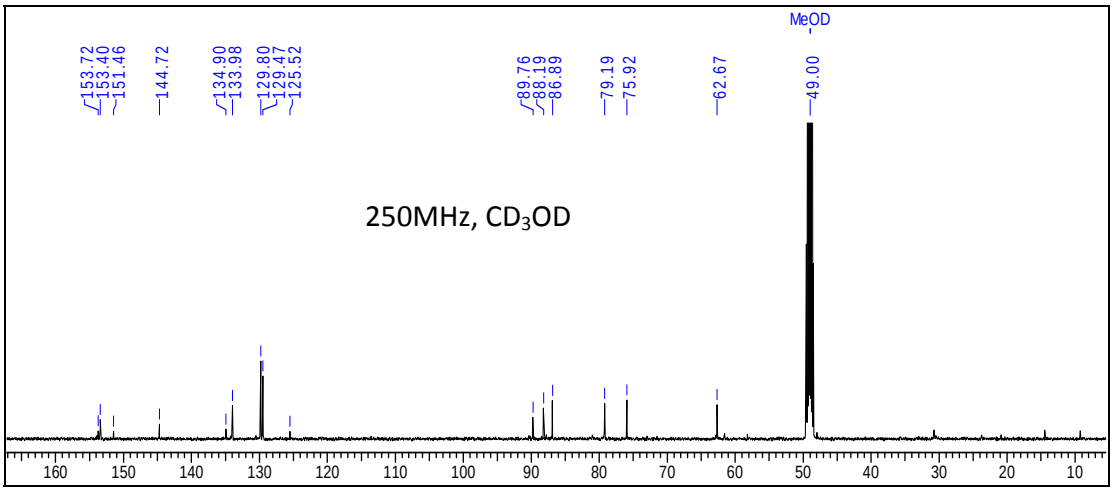

^{13}C-DEPT of compound 50

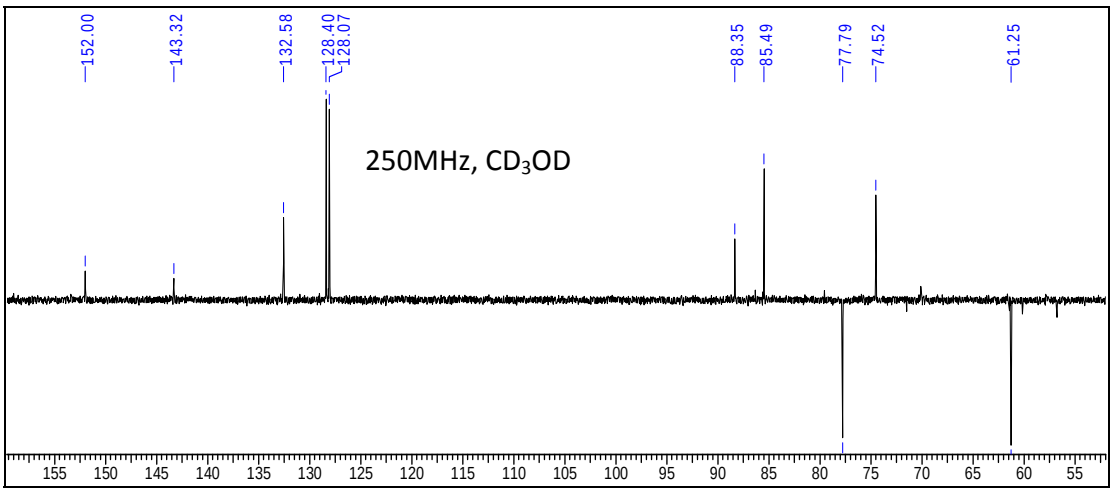

^{1}H NMR of compound 51

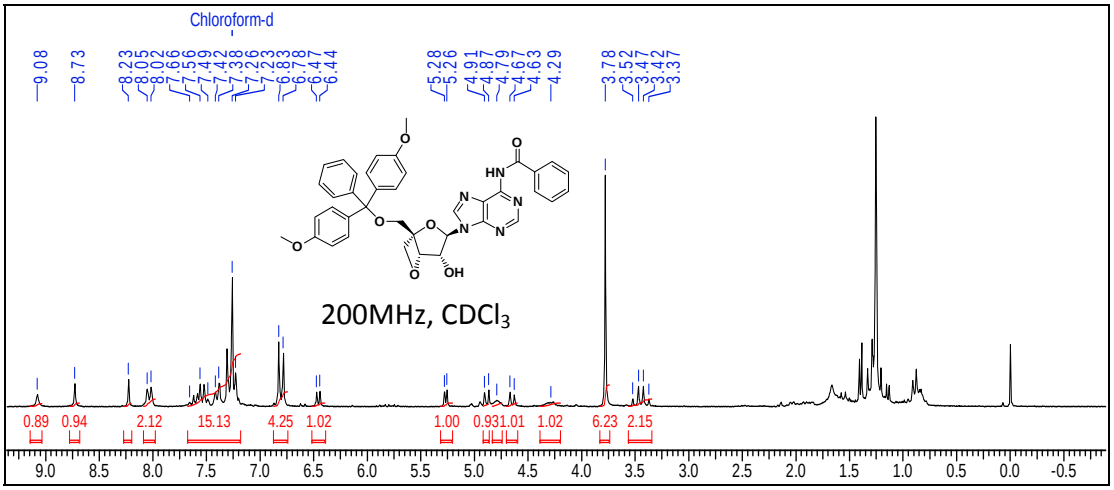

HRMS of compound 51

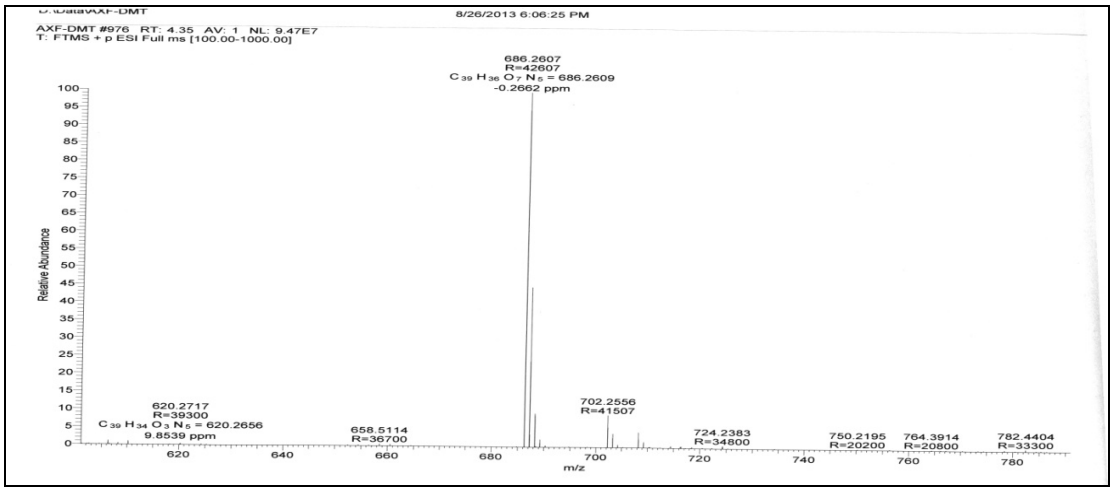

^{31}P NMR of compound 52

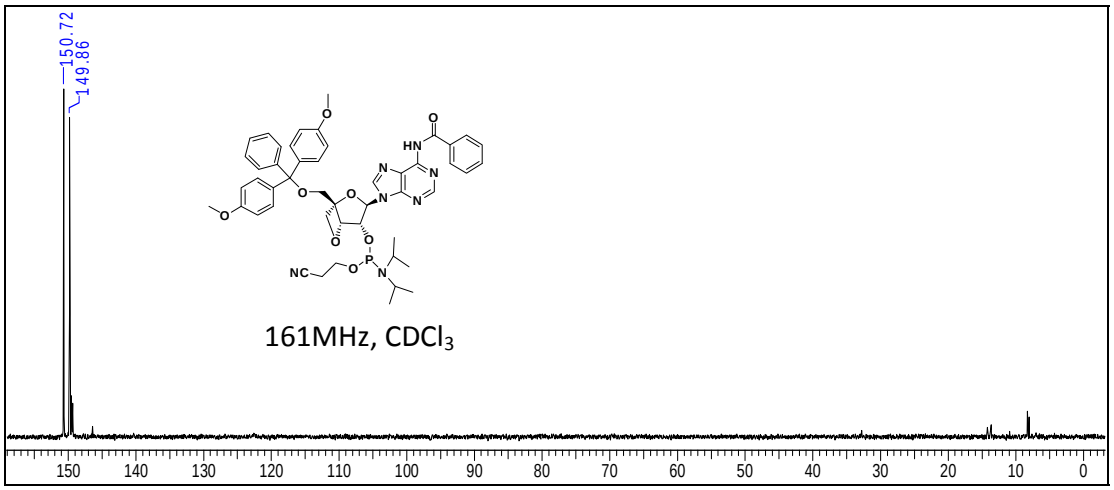

^{1}H NMR of compound 53

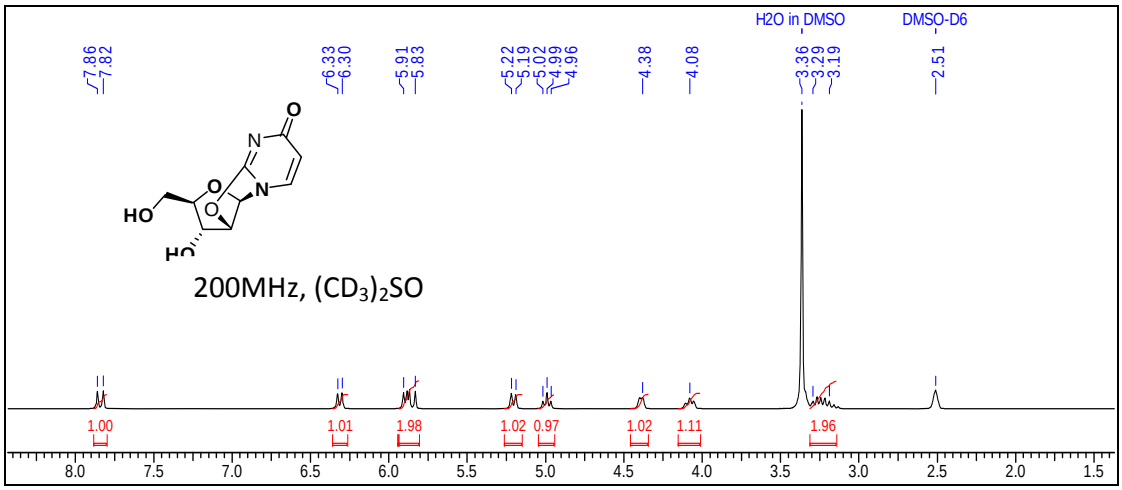

^{13}C NMR of compound 53

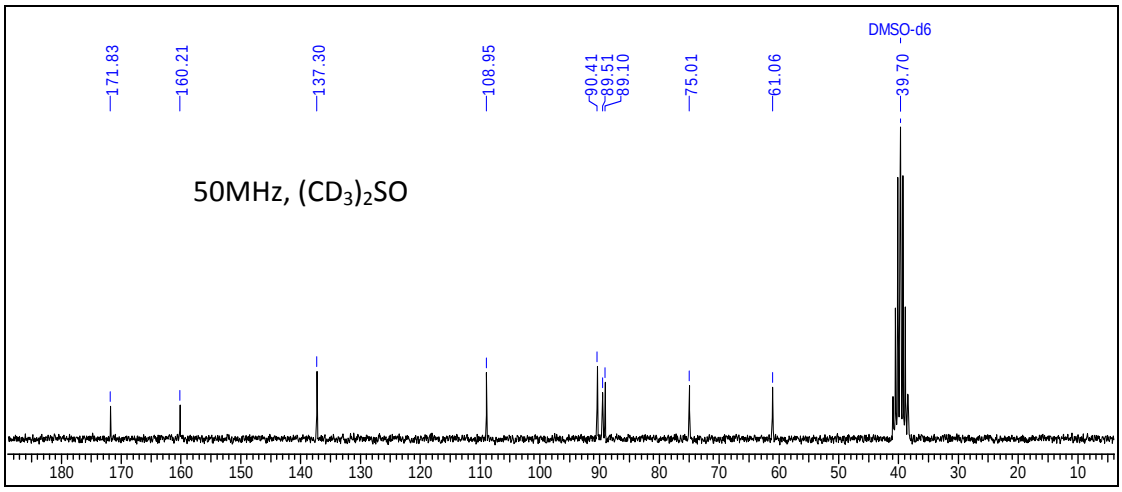

^{13}C-DEPT of compound 53

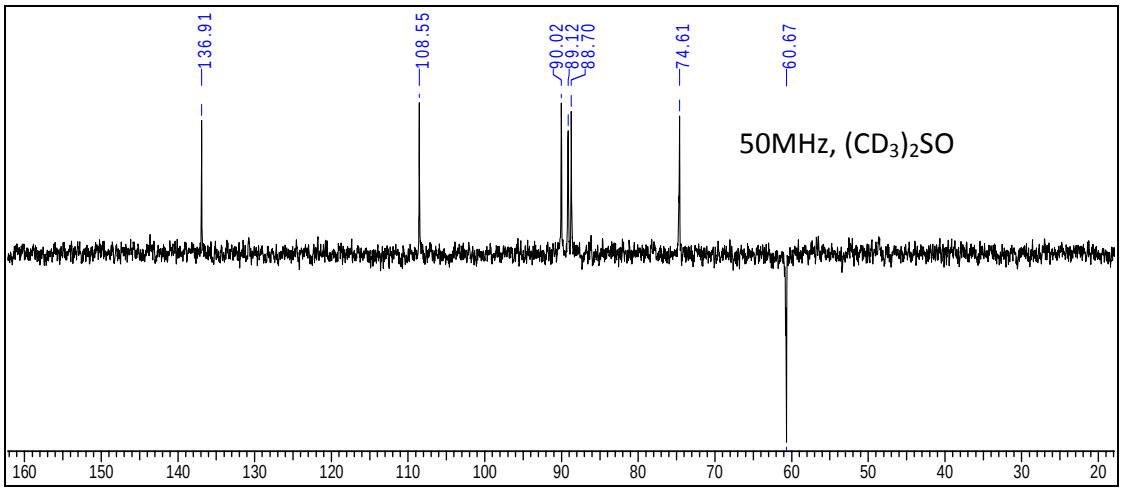

^{1}H NMR of compound 54

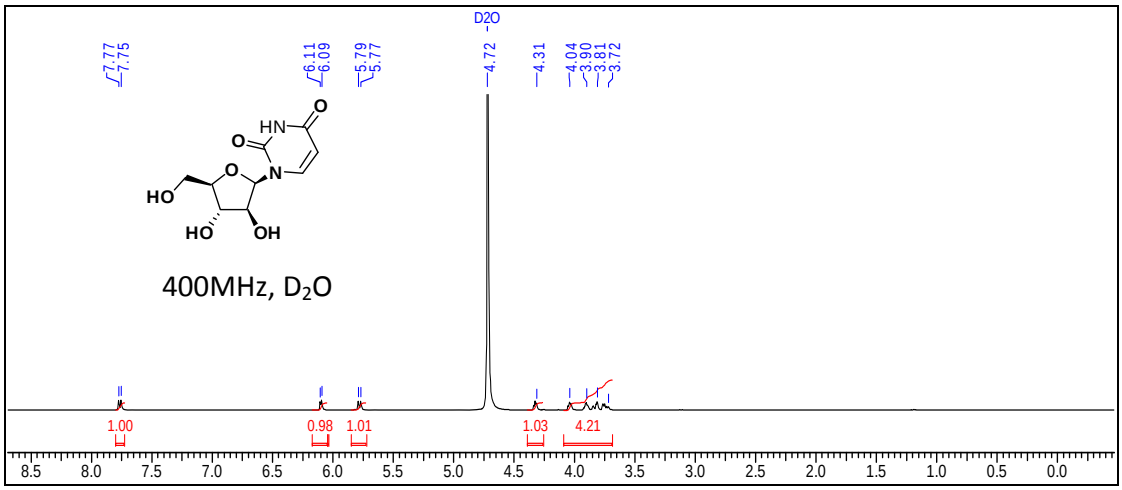

^{13}C NMR of compound 54

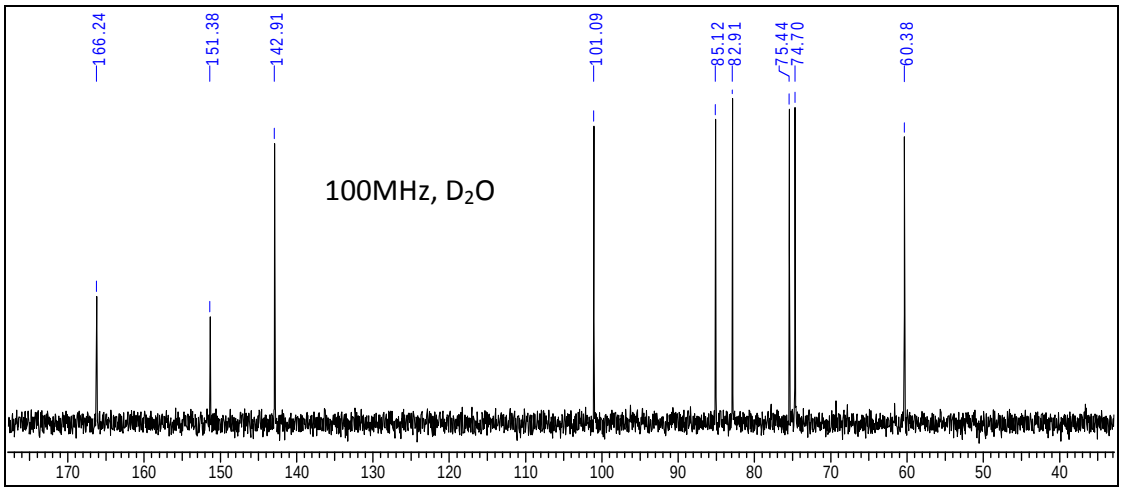

^{13}C-DEPT of compound 54

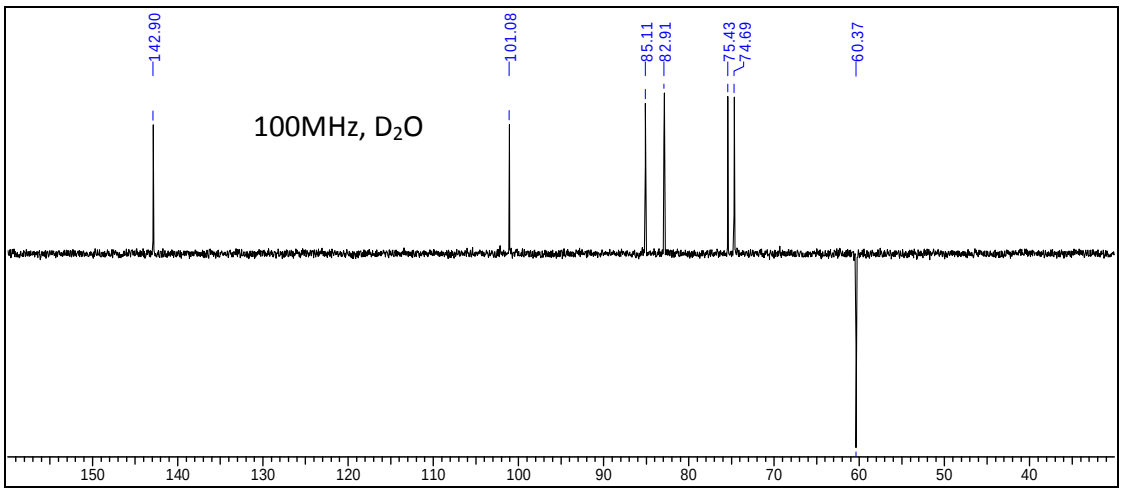

^{1}H NMR of compound 55

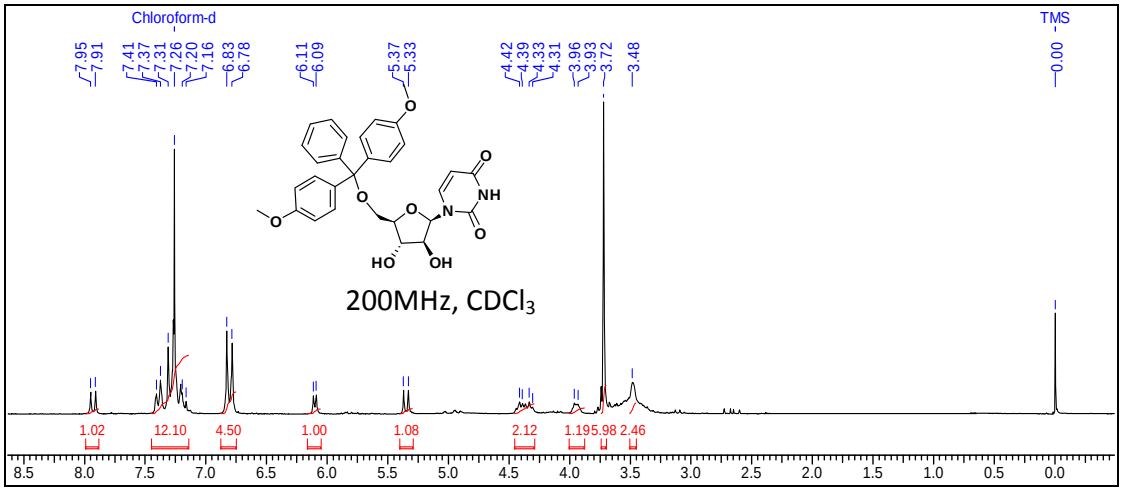

^{1}H NMR of compound 56

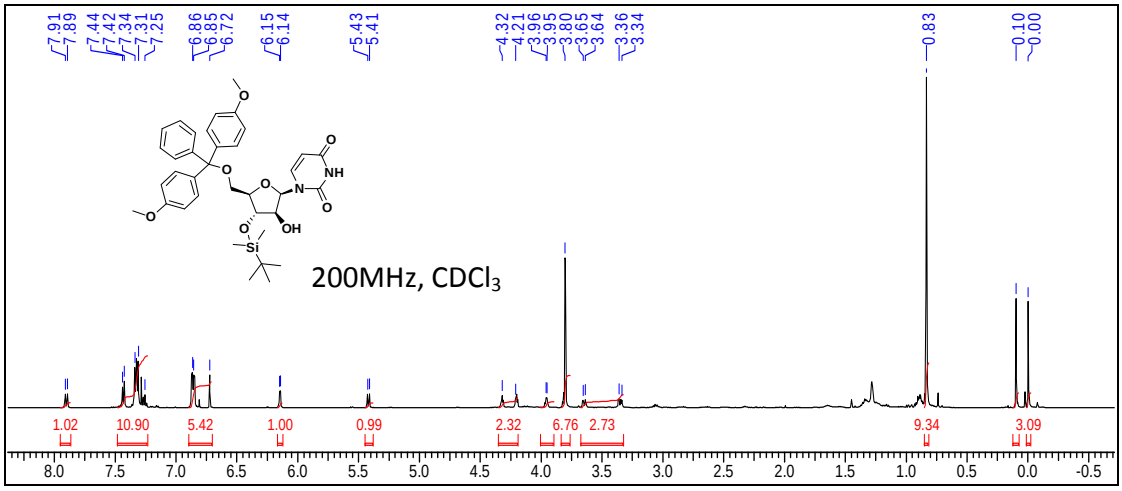

^{13}C NMR of compound 56

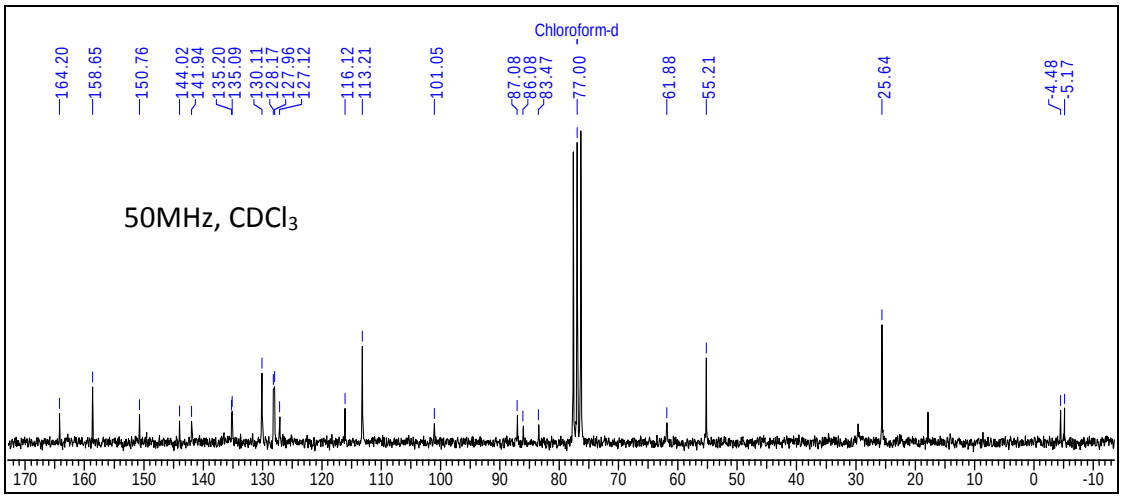

^{13}C-DEPT of compound 56

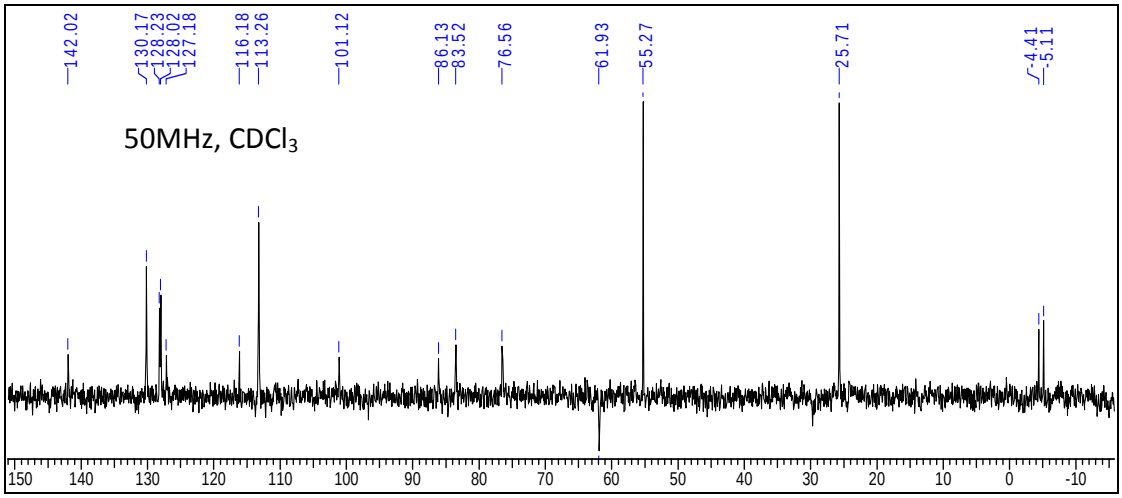

^{31}P NMR of compound 57

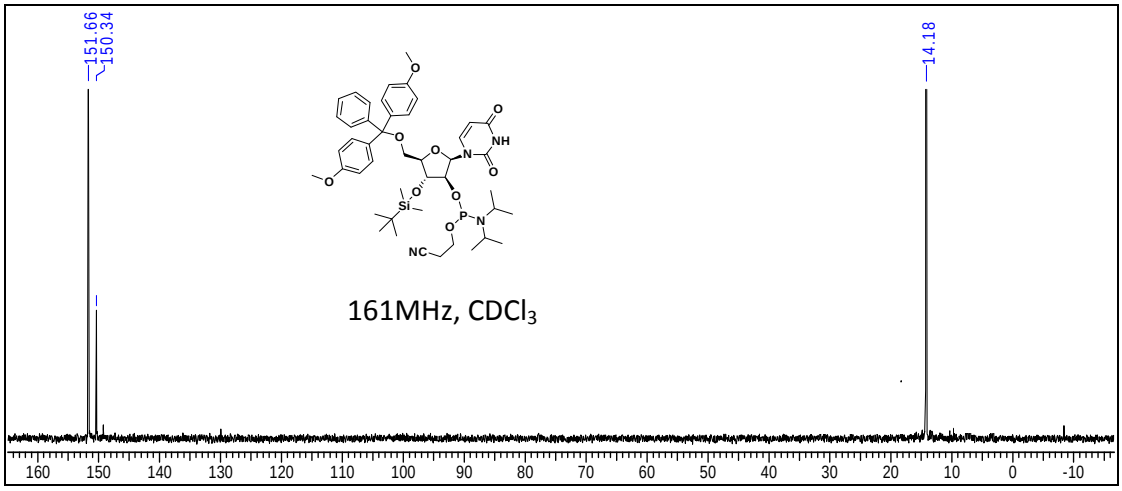

Mass of compound 57

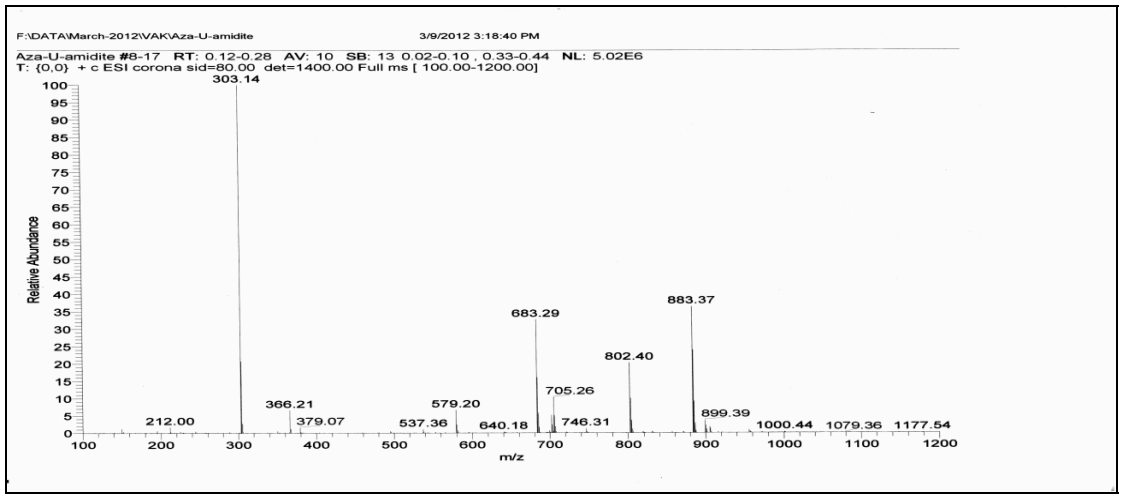

MALDI-TOF mass spectrum of ngDNA

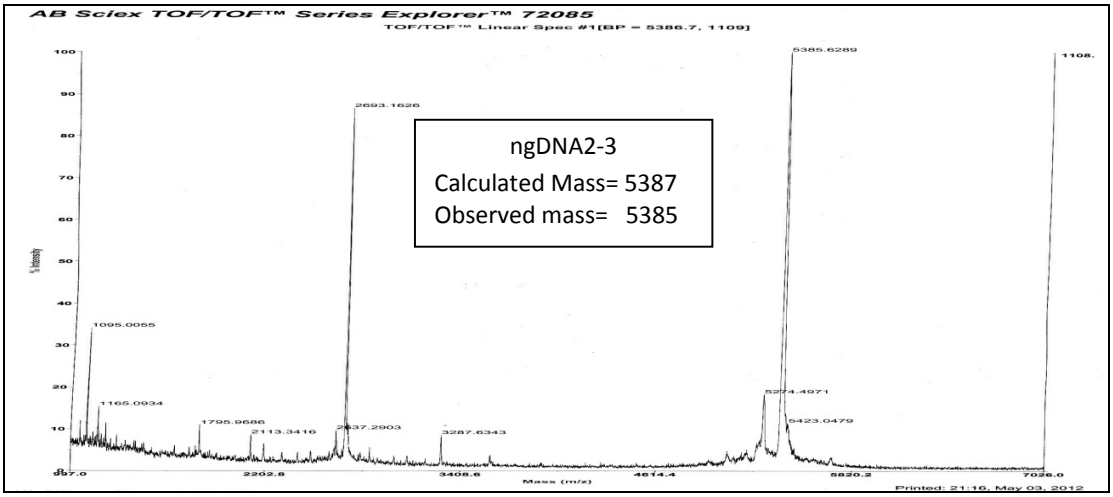

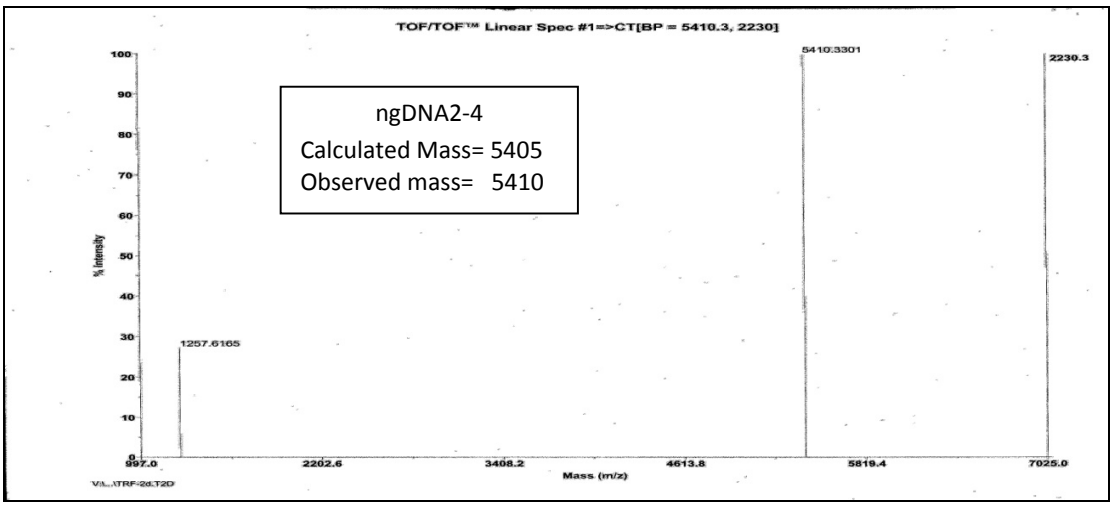

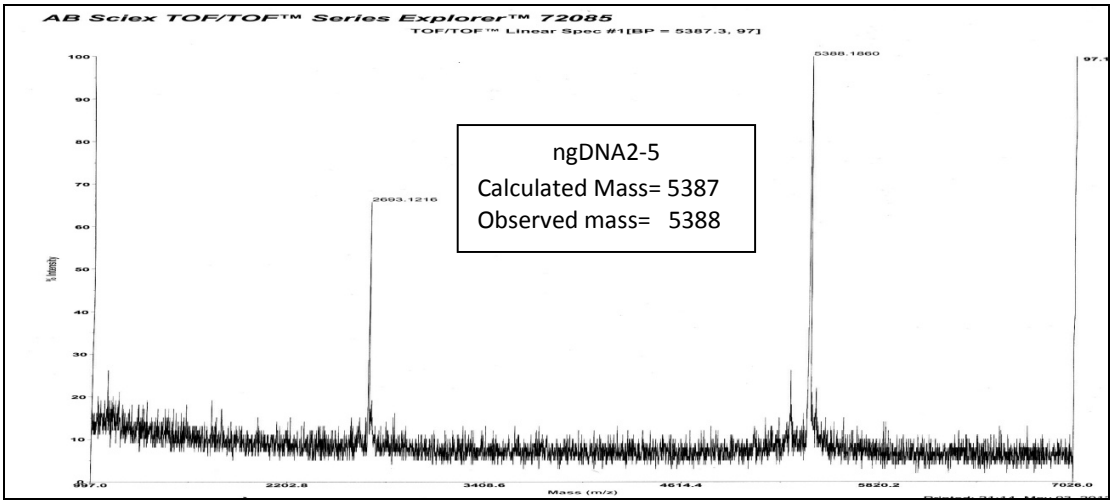

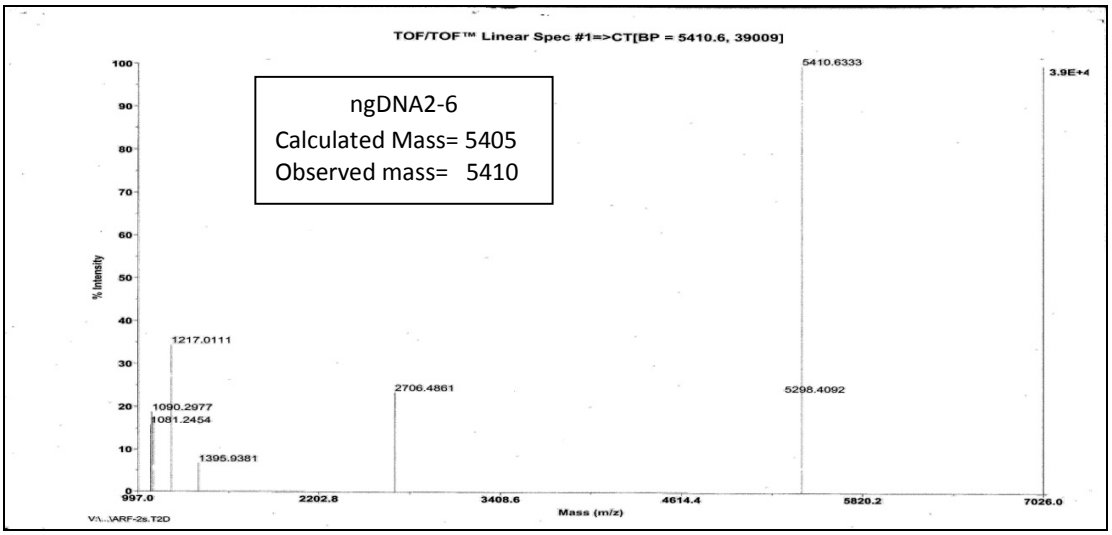
TOF/TOF™ Linear Spec #1=>CT[BP = 5410.6, 39009]
ngDNA2-6
Calculated Mass= 5405
Observed mass= 5410
5410.6333
3.9E+4
1217.0111
2706.4861
5298.4092
1090.2977
1081.2454
1395.9381
% Intensity
Mass (m/z)
997.0
2202.8
3408.6
4614.4
5820.2
7026.0

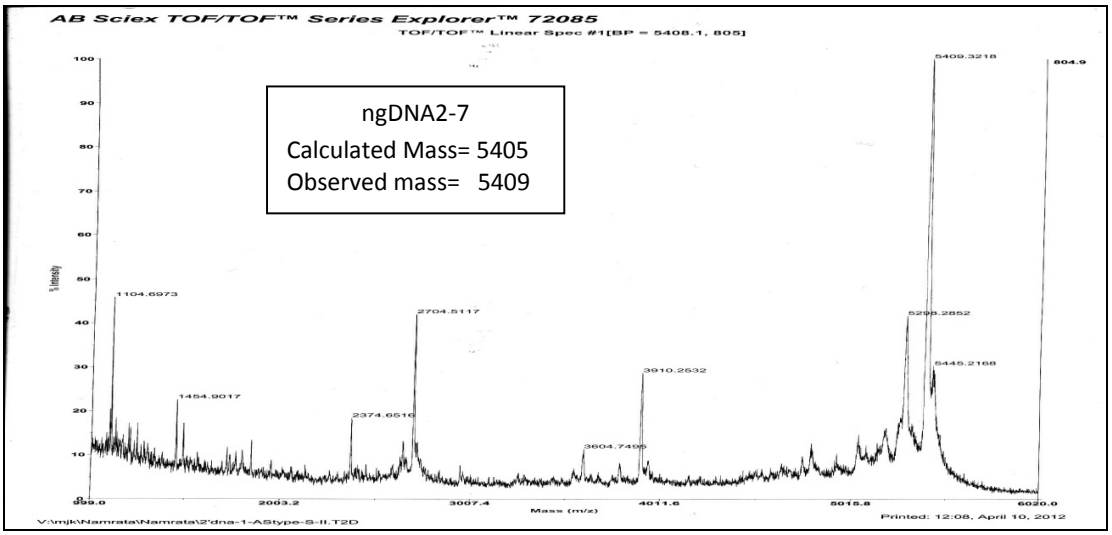
AB Sciex TOF/TOF™ Series Explorer™ 72085
TOF/TOF™ Linear Spec #1[BP = 5408.1, 805]
ngDNA2-7
Calculated Mass= 5405
Observed mass= 5409
5409.3218
804.9
1104.6973
2704.5117
1454.9017
2374.6516
3910.2532
5298.2852
5445.2168
3604.7495
% Intensity
Mass (m/z)
999.0
2003.2
3007.4
4011.6
5015.8
6020.0
Printed: 12:08, April 10, 2012

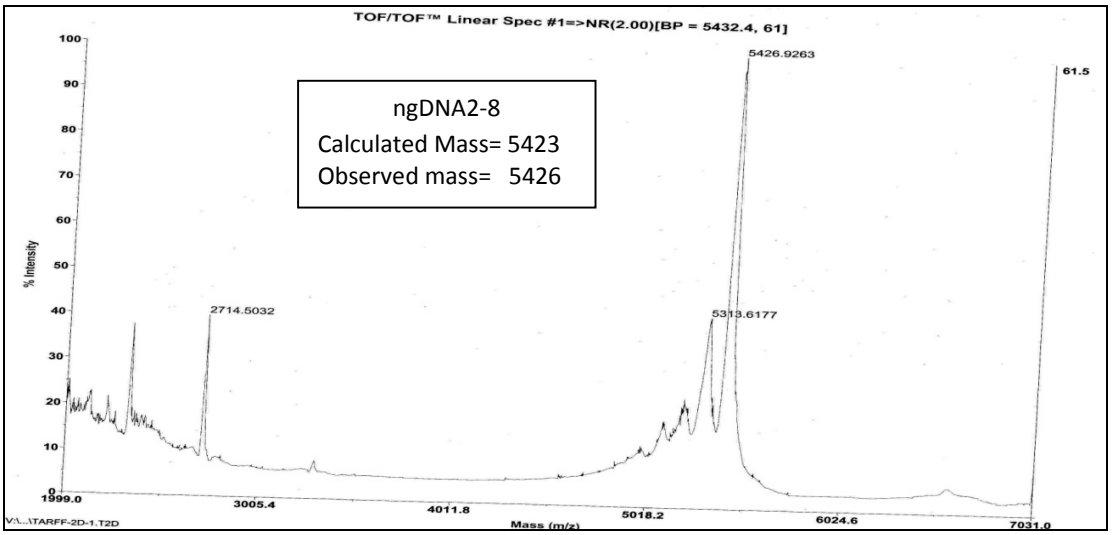
TOF/TOF™ Linear Spec #1=>NR(2.00)[BP = 5432.4, 61]
ngDNA2-8
Calculated Mass= 5423
Observed mass= 5426
5426.9263
61.5
2714.5032
5313.6177
% Intensity
Mass (m/z)
1999.0
3005.4
4011.8
5018.2
6024.6
7031.0

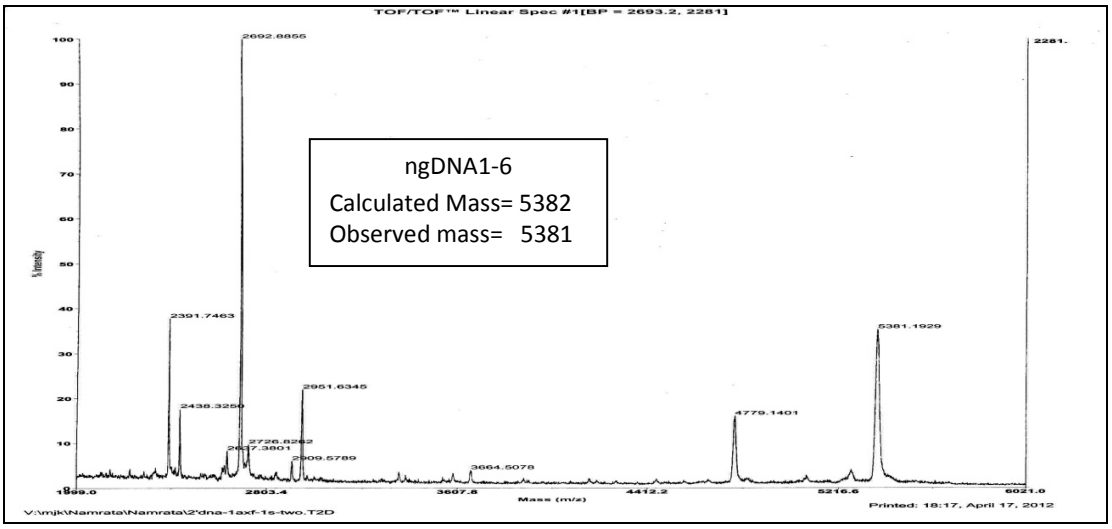
TOF/TOF™ Linear Spec #1[BP = 2693.2, 2281]
ngDNA1-6
Calculated Mass= 5382
Observed mass= 5381
2692.8855
2391.7463
5381.1929
2951.6345
2438.3250
4779.1401
Mass (m/z)
Printed: 18:17, April 17, 2012

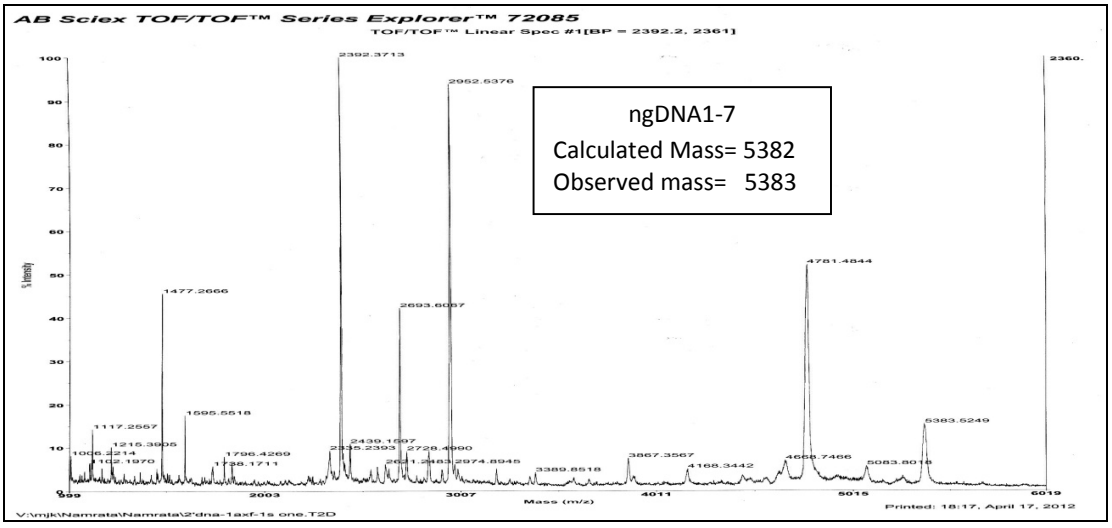
AB Sciex TOF/TOF™ Series Explorer™ 72085
TOF/TOF™ Linear Spec #1[BP = 2392.2, 2361]
ngDNA1-7
Calculated Mass= 5382
Observed mass= 5383
2392.3713
2962.6376
4781.4844
1477.2666
2693.6087
5383.6249
Mass (m/z)
Printed: 18:17, April 17, 2012

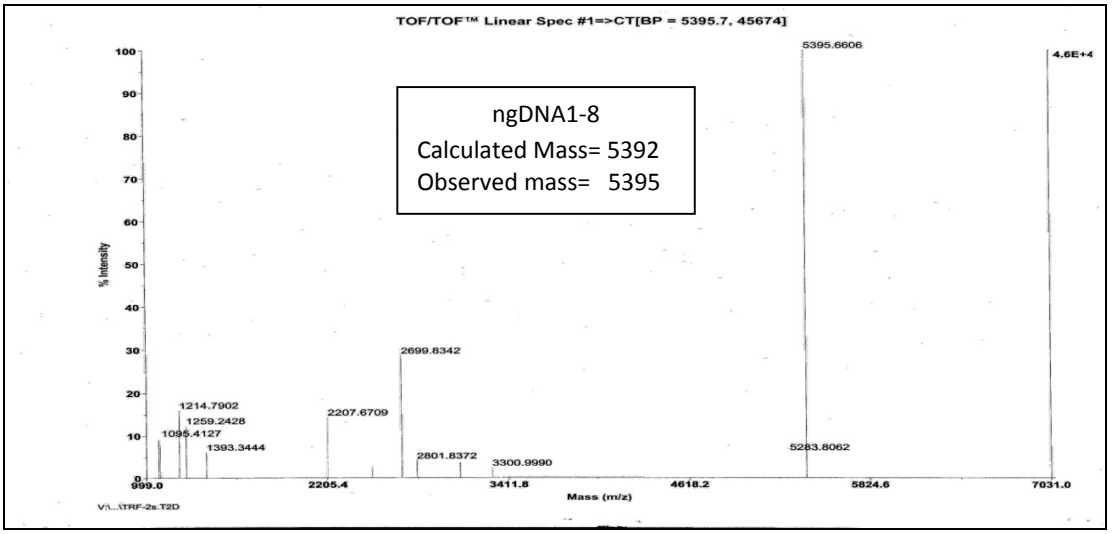
TOF/TOF™ Linear Spec #1=>CT[BP = 5395.7, 45674]
ngDNA1-8
Calculated Mass= 5392
Observed mass= 5395
5395.6606
4.6E+4
2699.8342
1214.7902
1259.2428
1095.4127
1393.3444
2207.6709
2801.8372
3300.9990
5283.8062
% Intensity
Mass (m/z)

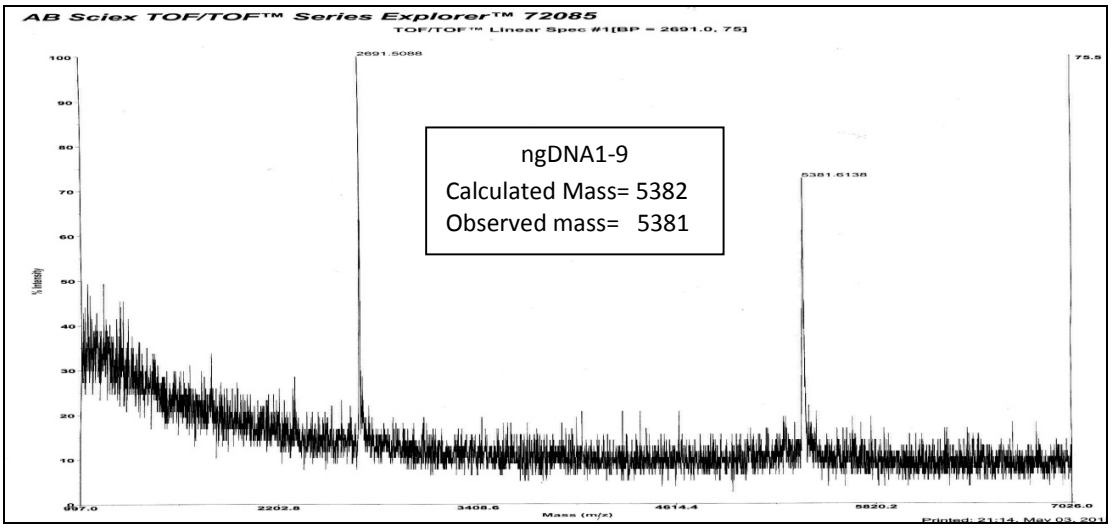
AB Sciex TOF/TOF™ Series Explorer™ 72085
TOF/TOF™ Linear Spec #1[BP = 2691.0, 75]
2691.5088
5381.6138
75.5
ngDNA1-9
Calculated Mass= 5382
Observed mass= 5381
% Intensity
Mass (m/z)
Printed: 21:14, May 03, 201

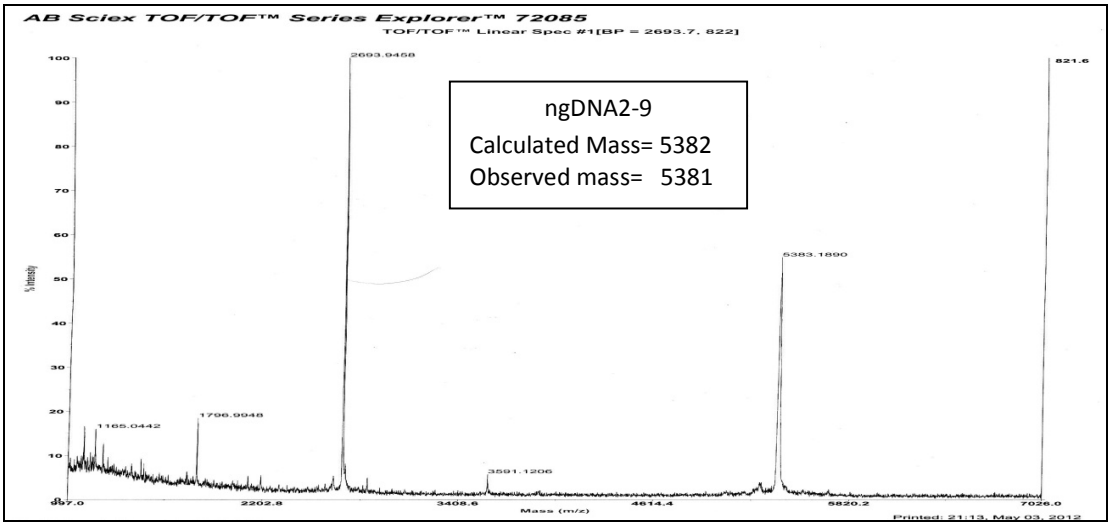
AB Sciex TOF/TOF™ Series Explorer™ 72085
TOF/TOF™ Linear Spec #1[BP = 2693.7, 822]
2693.9458
821.6
ngDNA2-9
Calculated Mass= 5382
Observed mass= 5381
5383.1890
1165.0442
1706.9948
3591.1206
% Intensity
Mass (m/z)
Printed: 21:13, May 03, 2012

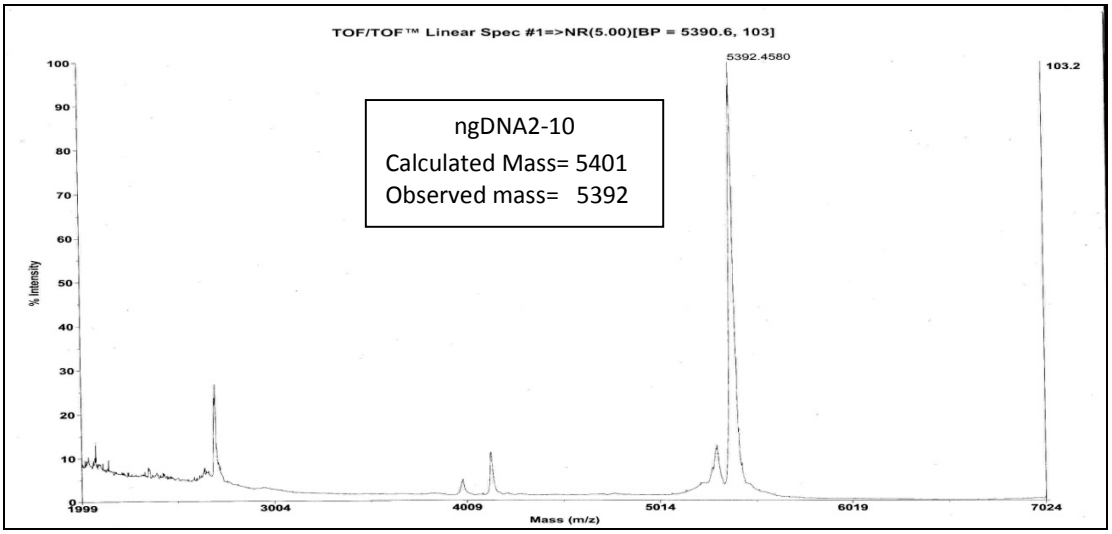
TOF/TOF™ Linear Spec #1=>NR(5.00)[BP = 5390.6, 103]
5392.4580
103.2
ngDNA2-10
Calculated Mass= 5401
Observed mass= 5392
% Intensity
Mass (m/z)

MALDI-TOF mass spectrum of ngDNA1, ngDNA1-2 and ngDNA1-4 with deletion of the 2′terminal Adenosine-5′-phosphate.

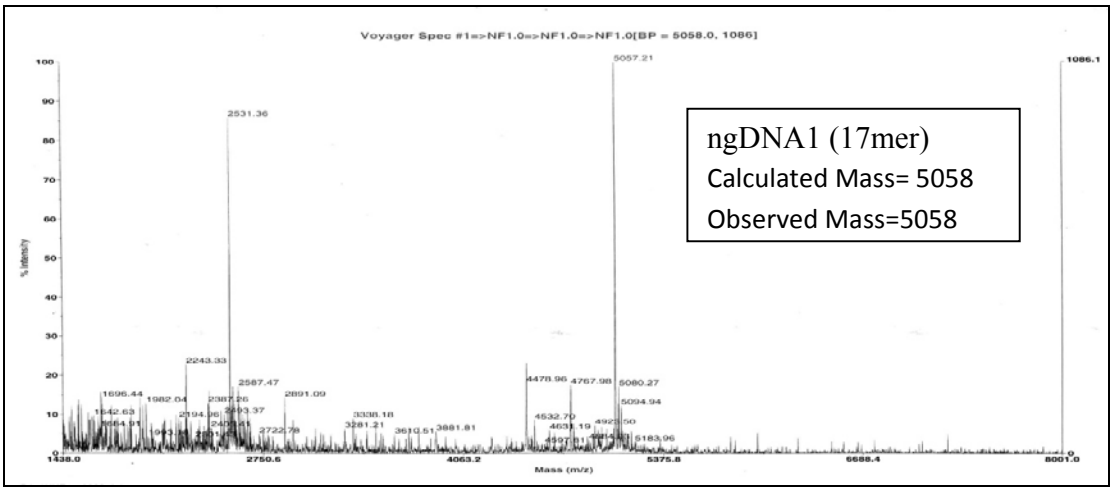

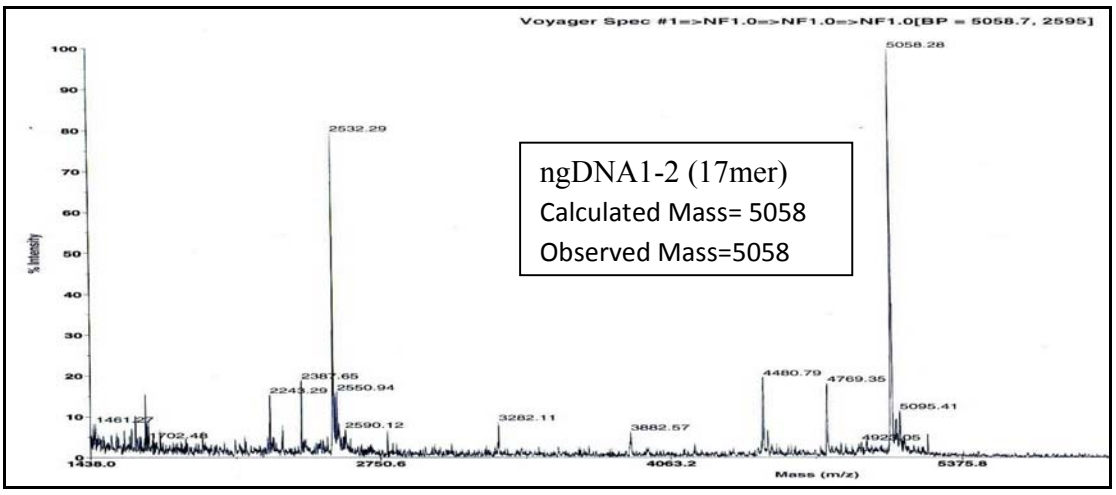

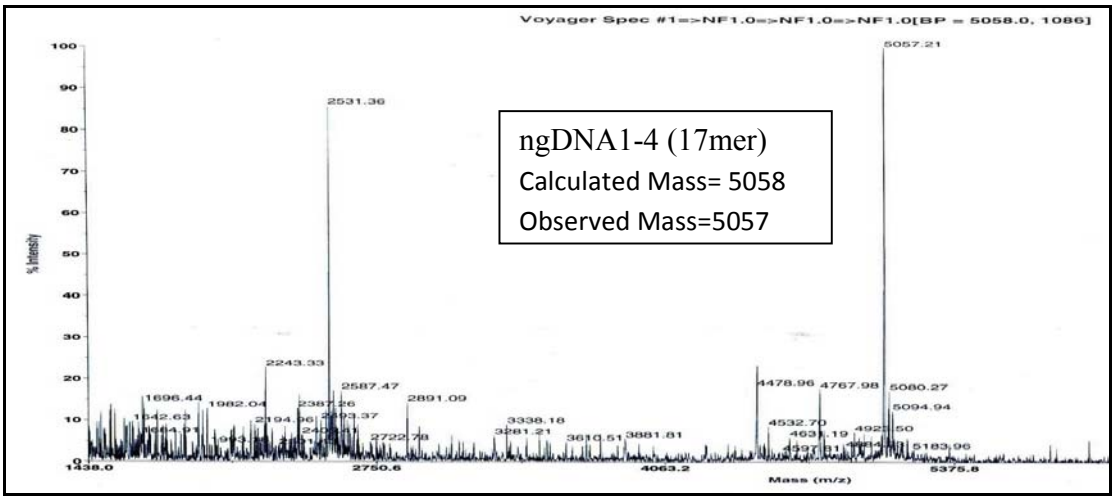

References:

1. Watson, J. D.; Hopkins, N. H.; Roberts, J. W.; Steitz, J. A.; Weiner, A. M., Molecular Biology of the Gene; Benjamin/Cummings: Menlo Park, CA, . **1987**.
2. Freifelder, D., Molecular Biology; Jones and Bartlett: Boston, **1983.**
3. Saenger, W., Principles of Nucleic Acid Structure; Springer-Verlag: New York, **1984**.
4. Felsenfe.G; Miles, H. T., Physical and chemical properties of nucleic acids. *Annual Review of Biochemistry* **1967,** 36, 407.
5. Stevens, C. L.; Felsenfeld, G., The conversion of 2-stranded poly (A+U) to 3-strand poly (A+2U) and poly-A by heat. *Biopolymers* **1964,** 2, (4), 293-314.
6. Howard, F. B.; Frazier, J.; Miles, H. T., Interaction of polyribothymidylic acid with polyadenylic acid. *Journal of Biological Chemistry* **1971,** 246, (23), 7073-7086.
7. Riley, M.; Maling, B.; Chamberl.M. J., Physical and chemical characterization of 2- and 3-stranded adenine-thymine and adenine-uracil homopolymer complexes. *Journal of Molecular Biology* **1966,** 20, (2), 359-389.
8. Escudé C, François JC, Sun JS, Ott G, Sprinzl M, Garestier T, Hélène C. Stability of triple helices containing RNA and DNA strands: experimental and molecular modeling studies. *Nucleic Acids Res*earch. **1993,** 21, (24), 5547–5553.
9. Sowers, L. C.; Shaw, B. R.; Sedwick, W. D., Base stacking and molecular polarizability-effect of a methyl-group in the 5-position of pyrimidines. *Biochemical and Biophysical Research Communications* **1987,** 148, (2), 790-794.
10. Hill, T. L., Lectures on Matter & Equilibrium; Chap 3. W. A. Benjamin: New York, **1966**.
11. Wang, S. H.; Kool, E. T., Origins of the large differences in stability of DNA and RNA helices-C-5 methyl and 2'-hydroxyl effects. *Biochemistry* **1995,** 34, (12), 4125-4132.
12. Howard, F. B., The stabilizing contribution of thymine in duplexes of (dA)(24) with (dU)(24), (dT)(24), (dU(12)-dT(12)), (dU-dT)(12), (dU(2)-dT(2))(6),or (dU(3)dT(3))(4): Nearest neighbor and next-nearest neighbor effects. *Biopolymers* **2005,** 78, (4), 221-229.

13. Petersheim, M.; Turner, D. H., Base-stacking and base-pairing contributions to helix stability-thermodynamics of double-helix formation with CCGG, CCGGP, CCGGAP, ACCGGP, CCGGUP, and ACCGGUP. *Biochemistry* **1983,** 22, (2), 256-263.
14. Dewey, T. G.; Turner, D. H., Laser temperature jump study of solvent effects on poly(adenylic acid) stacking. *Biochemistry* **1980,** 19, (8), 1681-1685.
15. Sanghvi, Y. S.; Hoke, G. D.; Freier, S. M.; Zounes, M. C.; Gonzalez, C.; Cummins, L.; Sasmor, H.; Cook, P. D., Antisense oligodeoxynucleotides-synthesis, biophysical and biological evaluation of oligodeoxynucleotides containing modified pyrimidines. *Nucleic Acids Research* **1993,** 21, (14), 3197-3203.
16. Froehler, B. C.; Wadwani, S.; Terhorst, T. J.; Gerrard, S. R., Oligodeoxynucleotides containing C-5 propyne analogs of 2'-deoxyuridine and 2'-deoxycytidine. *Tetrahedron Letters* **1992,** 33, (37), 5307-5310.
17. Kovacs, T.; Pabuccuoglu, A.; Lesiak, K.; Torrence, P. F., Fluorodeoxy sugar analogs of 2',5'-oligoadenylates as probes of hydrogen-bonding in enzymes of the 2-5A system. *Bioorganic Chemistry* **1993,** 21, (2), 192-208.
18. Vandenboogaart, J. E.; Kalinichenko, E. N.; Podkopaeva, T. L.; Mikhailopulo, I. A.; Altona, C., Conformational-analysis of 3'-fluorinated A(2'-5')A(2'-5')A fragments - relation between conformation and biological-activity. *European Journal of Biochemistry* **1994,** 221, (2), 759-768.
19. Obika, S.; Morio, K.; Nanbu, D.; Hari, Y.; Itoh, H.; Imanishi, T., Synthesis and conformation of 3',4'-BNA monomers, 3'-*O*,4'-C-methyleneribonucleosides. *Tetrahedron* **2002,** 58, (15), 3039-3049.

1. (a) Obika, S.; Morio, K.; Nanbu, D.; Hari, Y.; Itoh, H.; Imanishi, T., Synthesis and conformation of 3',4'-BNA monomers, 3'-*O*,4'-C-methyleneribonucleosides. *Tetrahedron* **2002,** 58, (15), 3039-3049. (b) Obika, S.; Morio, K.; Nanbu, D.; Imanishi, T., Synthesis and conformation of 3'-*O*,4'-C-methyleneribonucleosides, novel bicyclic nucleoside analogues for 2',5'-linked oligonucleotide modification. *Chemical Communications* **1997**, (17), 1643-1644.

20. Krutzfeldt, J.; Rajewsky, N.; Braich, R.; Rajeev, K. G.; Tuschl, T.; Manoharan, M.; Stoffel, M., Silencing of microRNAs in vivo with 'antagomirs'. *Nature* **2005,** 438, (7068), 685-689.
21. Abes, S.; Turner, J. J.; Ivanova, G. D.; Owen, D.; Williams, D.; Arzumanov, A.; Clair, P.; Gait, M. J.; Lebleu, B. Efficient splicing correction by PNA conjugation to an R6-Penetratin delivery peptide, *Nucleic Acids Research.* **2007**, 13, 4495.
22. (a) Nowell, P.; Hungerford, D., A minute chromosome in human chronic granulo cytic leukemia. *Science*, **1960**, 132, 1497; (b) Deininger, M. W. N., Goldman J. M. Melo J. V., The molecular biology of chronic myeloid leukemia. *Blood*, **2000**, 96, 3343.
23. (a) Gait, M. J., Oligonucleotide synthesis: A practical approach. IRL Press Oxford, UK 217; (b) Agrawal, S., Protocols for oligonucleotides and analogs Synthesis and Properties :Methods in Molecular Biology. Totowa, NJ,. Humana Press, Inc. **1993**, 20.
24. Giannaris, P. A.; Damha, M. J., Oligoribonucleotides containing 2′,5′-phosphodiester linkages exhibit binding selectivity for 3′,5′-RNA over 3′,5′-ssDNA. *Nucleic Acids Research* **1993**, 21, (20), 4742-4749.
25. Farmer, P. B.; Suhadoln. R. J., Nucleoside antibiotics-biosynthesis of arabinofuranosyladenine by streptomyces-antibioticus .10. *Biochemistry* **1972**, 11, (5), 911.
26. Gephart, J. F.; Lerner, A. M., Comparison of the effects of arabinosyladenine, arabinosylhypoxanthine, and arabinosyladenine 5'-monophosphate against herpes-simplex virus, varicella-zoster virus, and cytomegalo-virus with their effects on cellular deoxyribonucleic-acid synthesis. *Antimicrobial Agents and Chemotherapy* **1981,** 19, (1), 170-178.
27. Sundaralingam, M. J., *Annals of the New York Academy of Science* **1976**, 255, 3-42.
28. Miles, D. L.; Miles, D. W.; Redington, P.; Eyring, H., Conformational basis for selective action of ara-adenine. *Journal of Theoretical Biology* **1977**, 67, (3), 499-514.

29. Noronha, A.M.; Wilds, C.J.; Lok, C.N.; Viazovkina K.; Arion D.; Parniak M.A.; Damha M.J., Synthesis and biophysical properties of arabinonucleic acids (ANA): circular dichroic spectra, melting temperatures, and ribonuclease H susceptibility of ANA.RNA hybrid duplexes. *Biochemistry*, **2000**, 39, 7050–7062
30. Damha, M. J.; Wilds, C. J.; Noronha, A.; Brukner, I.; Borkow, G.; Arion, D.; Parniak, M. A., Hybrids of RNA and arabinonucleic acids (ANA and 2' F-ANA) are substrates of ribonuclease H. *Journal of the American Chemical Society* **1998,** 120, (49), 12976-12977.
31. Denisov, A. Y.; Noronha, A. M.; Wilds, C. J.; Trempe, J. F.; Pon, R. T.; Gehring, K.; Damha, M. J., Solution structure of an arabinonucleic acid (ANA)/RNA duplex in a chimeric hairpin: comparison with 2'-fluoro-ANA/RNA and DNA/RNA hybrids. *Nucleic Acids Research* **2001**, 29, (21), 4284-4293.
32. Verheyde.J. P.; Wagner, D.; Moffatt, J. G., Synthesis of some pyrimidine 2'-amino-2'-deoxynucleosides. *Journal of Organic Chemistry* **1971,** 36, (2), 250.
33. Ogilvie, K. K.; McGee, D. P. C.; Boisvert, S. M.; Hakimelahi, G. H.; Proba, Z. A., Silyl protecting groups in nucleoside and nucleotide chemistry .21. The preparation of protected arabinonucleosides. *Canadian Journal of Chemistry-Revue Canadienne De Chimie* **1983,** 61, (6), 1204-1212.
34. Hakimelahi, G. H.; Proba, Z. A.; Ogilvie, K. K., New catalysts and procedures for the dimethoxytritylation and selective silylation of ribonucleosides. *Canadian Journal of Chemistry-Revue Canadienne De Chimie* **1982,** 60, (9), 1106-1113.
35. (a) Bennet, C. F.; Swayze, E. E., RNA targeting therapeutics: molecular mechanisms of antisense oligonucleotides as a therapeutic platform. *Annual Review of Pharmacology and Toxicology* **2010**, 50, 259; (b) Kole, R.; Krainer, A. R.; Altman, S., RNA therapeutics: beyond RNA interference and antisense oligonucleotides *Nature Reviews Drug Discovery.* **2012**, 11, 125.
36. Shaw, J. P.; Kent, K.; Bird, J.; Fishback, J.; Froehler, B., Modified deoxyoligonucleotides stable to exonuclease degradation in serum. *Nucleic Acids Research* **1991**, 19, (4), 747-750.

37. Campbell, J. M.; Bacon, T. A.; Wickstrom, E., Oligodeoxynucleoside phosphorothioate stability in subcellular extracts, culture media, sera and cerebrospinal-fluid. *Journal of Biochemical and Biophysical Methods* **1990,** 20, (3), 259-267.
38. Freier, S. M.; Altmann, K. H., The ups and downs of nucleic acid duplex stability: structure-stability studies on chemically-modified DNA:RNA duplexes. *Nucleic Acids Research* **1997**, 25, (22), 4429-4443.
39. Lesnik, E. A.; Guinosso, C. J.; Kawasaki, A. M.; Sasmor, H.; Zounes, M.; Cummins, L. L.; Ecker, D. J.; Cook, P. D.; Freier, S. M., Oligodeoxynucleotides containing 2'-*O*-modified adenosine - synthesis and effects on stability of DNA-RNA duplexes. *Biochemistry* **1993**, 32, (30), 7832-7838.
40. (a) Obika, S.; Nanbu, D.; Hari, Y.; Morio, K.; In, Y.; Ishida, T.; Imanishi, T., Synthesis of 2'-*O*,4'-C-methyleneuridine and -cytidine. Novel bicyclic nucleosides having a fixed C3-*endo* sugar puckering. *Tetrahedron Letters* **1997**, 38, (50), 8735-8738. (b) Obika, S.; Nanbu, D.; Hari, Y.; Andoh, J.; Morio, K.; Doi, T.; Imanishi, T., Stability and structural features of the duplexes containing nucleoside analogues with a fixed N-type conformation, 2'-*O*,4'-C-methyleneribonucleosides. *Tetrahedron Letters* **1998,** 39, (30), 5401-5404.
41. (a) Koshkin, A. A.; Singh, S. K.; Nielsen, P.; Rajwanshi, V. K.; Kumar, R.; Meldgaard, M.; Olsen, C. E.; Wengel, J., LNA (Locked Nucleic Acids): Synthesis of the adenine, cytosine, guanine, 5-methylcytosine, thymine and uracil bicyclonucleoside monomers, oligomerisation, and unprecedented nucleic acid recognition. *Tetrahedron* **1998,** 54, (14), 3607-3630.(b) Singh, S. K.; Nielsen, P.; Koshkin, A. A.; Wengel, J., LNA (locked nucleic acids): synthesis and high-affinity nucleic acid recognition. *Chemical Communications* **1998**, (4), 455-456. (c) Wengel, J., Synthesis of 3'-C- and 4'-C-branched oligodeoxynucleotides and the development of locked nucleic acid (LNA). *Accounts of Chemical Research* **1999,** 32, (4), 301-310.
42. Morita, K.; Takagi, M.; Hasegawa, C.; Kaneko, M.; Tsutsumi, S.; Sone, J.; Ishikawa, T.; Imanishi, T.; Koizumi, M., Synthesis and properties of 2'-*O*,4'-*C*-

ethylene-bridged nucleic acids (ENA) as effective antisense oligonucleotides. *Bioorganic & Medicinal Chemistry* **2003**, 11, (10), 2211-2226.

43. Obika, S.; Rahman, S. M. A.; Song, B.; Onoda, M.; Koizumi, M.; Morita, K.; Imanishi, T., Synthesis and properties of 3'-amino-2', 4'-BNA, a bridged nucleic acid with a N3'→P5' phosphoramidate linkage. *Bioorganic & Medicinal Chemistry* **2008**, 16, (20), 9230-9237.
44. Kandimalla, E. R.; Manning, A.; Zhao, Q. Y.; Shaw, D. R.; Byrn, R. A.; Sasisekharan, V.; Agrawal, S., Mixed backbone antisense oligonucleotides: Design, biochemical and biological properties of oligonucleotides containing 2'-5'-ribo- and 3'-5'-deoxyribonucleotide segments. *Nucleic Acids Research* **1997**, 25, (2), 370-378
45. (a) Morita, K.; Obika, S.; Imanishi, T.; Kitade, Y.; and Koizumi, M. *Nucleic Acids Symposium Series* **2008**, 52, 637-638.(b) Nagaoka, K.; Kito, S.; Kitamura, Y.; Ueno, Y.; and Kitade, Y., *Nucleic Acids Symposium Series* **2009**, 53, 123.(c) Nagaoka, K.; Kitamura, Y.; Ueno, Y.; and Kitade, Y. *Bioorganic and Medicinal Chemistry Letters* **2010**, 20, 1186.

Chapter 4

Conformational studies of $^{R}U^{F}$, $^{R}A^{F}$, $^{X}U^{F}$, $^{X}A^{F}$, $^{L}A^{S}$, and ^{ara}U nucleosides using NMR, X-ray crystal structure and Matlab Pseudorotation GUI program.

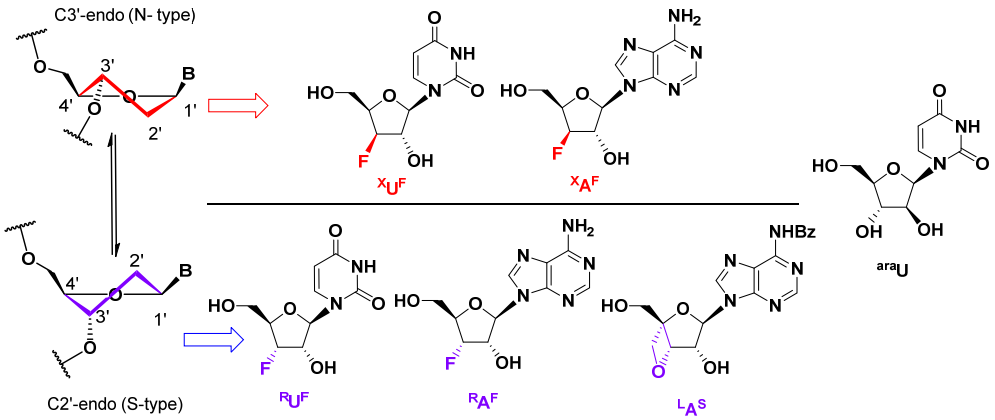

In this chapter we present the results of our studies to understand the furanose ring conformation of $^{R}U^{F}$, $^{R}A^{F}$, $^{X}U^{F}$, $^{X}A^{F}$, $^{L}A^{S}$, and ^{ara}U nucleosides, in solution as well as solid state. We used the recently-developed Matlab GUI pseudorot software for the calculation of population of N/S-conformer and structural parameters (*P* and ν_{max}) for all the six nucleoside in solution state. We also used X-ray crystallographic studies to compare the structural parameters (*P* and ν_{max}) of nucleosides in the solid state.

4.1 Introduction

We have discussed in chapter 1 that the sugar puckering of natural ribo- and deoxyribonucleosides are known to exist in dynamic equilibrium between two major conformers: the North (N) and the South (S) types.[1,2] In the solid state, one conformation is prevalent in relation to the other. In solution, the North/South interconversion is rapid, depending upon the energy barrier (Figure 1). However when a nucleotide polymerizes to form a single strand oligomer or binds to complementary strand forming a duplex, only one conformer is chosen preferentially. We have also discussed in chapter 1 that the conformational restriction of the furanose ring is influenced by the stereoelectronic *gauche* and *anomeric* effects, which are modulated by the electronegativity, steric hindrance and stereochemistry of the substituents on the furanose ring.[3,4] For example, the amounts of N conformers increase linearly with the electronegativities of the substituents in the 2′-positions in 2′-deoxyribonucleoside derivatives, owing to their preferential axial orientations due to the *gauche* effect.

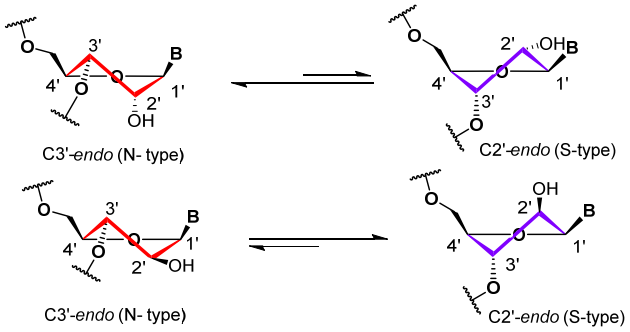

Figure 1. Sugar conformations in two-state *North*↔*South* equilibrium

The conformational behavior of natural or modified nucleosides is defined by the four structural parameters shown in Figure 2[5] and detailed below.

1. The glycosidic torsion angle χ determines the *syn* or *anti* disposition of the base relative to the sugar moiety. The *anti* conformation has the N1, C2 face of purines and the C2, N3 face of pyrimidines directed away from the sugar ring so that the hydrogen atoms attached to C8 of purines and C6 of pyrimidines, are lying over the sugar ring. Thus, the Watson–Crick hydrogen-bonding groups of the bases are directed away from the sugar ring. These orientations are reversed for the *syn* conformation, with these hydrogen-bonding groups now oriented toward the sugar.

2. The torsion angle γ determines the position of the 5′-OH with respect to C-3′ as represented by the three main rotamers γ+, γ^t and γ–.
3. The pseudorotational phase angle *P* determines the conformation of the furanose ring. *P* is calculated from the endocyclic torsion angles (ν_0–ν_4) as shown in equation (1). In cases where ν_2 is negative, one should add 180° to the calculated value of *P*, while when *P* is negative 360° should be added.

$$\tan P = \frac{(\nu_4 + \nu_1) - (\nu_3 + \nu_0)}{2\,\nu_2\,(\mathrm{Sin}\,36° + \mathrm{Sin}\,72°)} \qquad (1)$$

4. The maximal puckering amplitude ν_{max} determines the furanose ring deviation from planarity, calculated by P and ν_2 as shown in equation (2).

$$\nu_{max} = \frac{\nu_2}{\mathrm{Cos}\,P} \qquad (2)$$

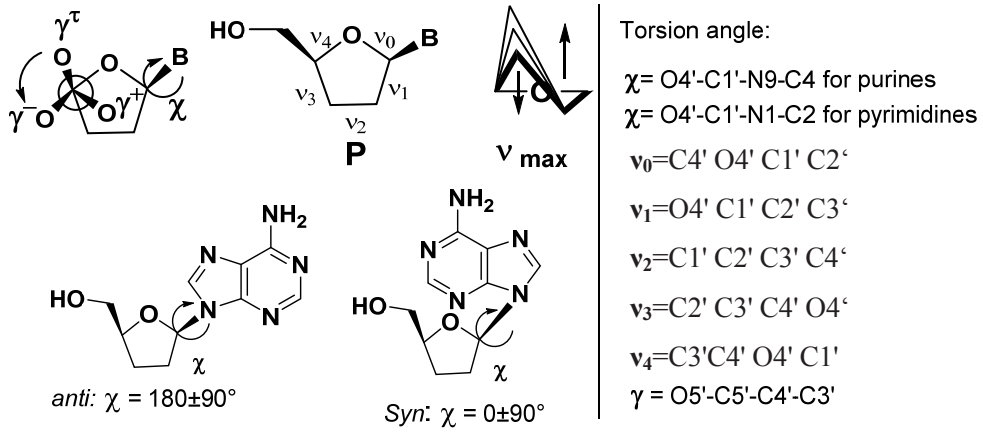

Figure 2: Torsion angles present in nucleosides (ν_0–ν_4, γ and χ)

The pseudorotation concept has been introduced by Kilpatrick *et al.*[6] to describe the continuous interconversions between the infinite numbers of indefinite puckered forms of the cyclopentane ring. The concept of pseudorotation was applied for the first time to furanose by Hall *et al.*,[7] in their conformational analyses of pentofuranosyl fluorides. The conformation of the furanose ring can be described easily when values of *P* in combination with ν_{max} are plotted in the pseudorational cycle (Figure 3).[1,5] Values of phase angles are given in multiples of 36° and vary from 0° to 360°. Twenty distinct twist (T) and envelope (E) conformations alternate every 18°. The T conformation is observed at even multiples of 18°, and E is found at odd multiples. By convention, a phase angle of P = 0° is defined such

that the torsion angle ν_2 is maximally positive and corresponds to an absolute north conformation possessing a symmetrical C2′-*exo*–C3′-*endo* twist form ($^{3}_{2}T$). The mirror image is represented by P = 180° and corresponds to an absolute south conformation with a symmetrical C2′-*endo*–C3′-*exo* twist form ($^{2}_{3}T$). For the great majority of natural nucleosides, the values of *P* are either of a North-type (N) conformation (*P* = 18°, ^{3}E, C3′-*endo*) or a South-type (S) conformation (*P* = 162°, ^{2}E, C2′-*endo*). In both regions, the values of ν_{max} are found in a range from 30° to 46°, and most of them fall around 38°.[8]

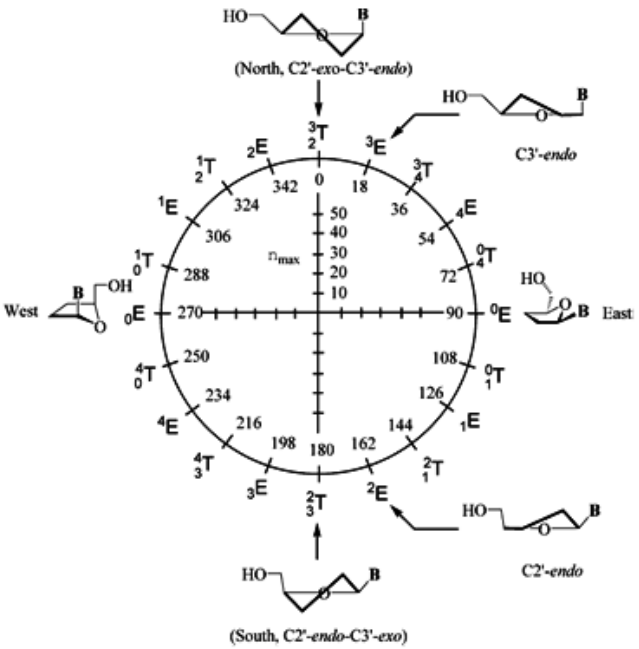

Figure 3. Pseudorotational cycle for nucleosides showing the characterisic North, South, East and West conformations. The radius of the cycle corresponds to ν_{max}. The units of *P* and ν_{max} values are degrees. Envelope (E) and twist (T) forms alternate ever 18°

4.1.1 Conformational analysis of the furanose ring

The origin for all studies of nucleoside and nucleotide conformation is provided by the X-ray analysis of their structures, which provides accurate bond angles, bond lengths, and the torsional angles and thus accurately determines the conformations present in the solid state. However, most modified nucleosides show conformational equilibrium in aqueous solution. It is for this reason that NMR spectroscopy can be a valuable complement to X-ray crystallographic studies. The vicinal proton-proton ($^{3}J_{HH}$) coupling constants $J_{1'2'}$, $J_{1'2''}$, $J_{2'3'}$ and $J_{3'4'}$,[9] can be related to the corresponding proton–proton torsion

angle Hi–Ci–Cj–Hj using the Diez-Donders equation [eq.(3)].[10] This is a generalized Karplus-type equation which depends on electronic effects of substituents, therefore uses the group-electronegativities.[8,11] The exocyclic torsion angles thus obtained can then be related to the corresponding endocyclic Xh–Ci–Cj–Xk angles [eq. (4)]. The parameters A and B[11,12] and the αi and εi were determined to provide an optimal representation of the ring conformation *via* two pseudorotation parameters- *P* and ν_{max}.

$$\nu i = \alpha i * \nu_{max} * \cos(P + \varepsilon i + 4\pi i/5) \quad \text{.....(3)}$$

$$\nu_{exo} = A*\nu_{endo} + B \quad \text{.....(4)}$$

Where,

ν_{exo} = torsional angle between two adjacent hydrogens, ν_{endo} = endocyclic torsional angle

P = pseudorotation angle,

ν_{max} = puckering amplitude and A, B and Diez-parameters αi, εi are constants.

As mentioned previously, the furanose ring of a nucleoside may be in equilibrium between two conformations. Using the above equations, $^3J_{HH}$ couplings can be used to calculate the mole fraction of N and S conformers as well as their geometry expressed by their phase angle of pseudorotation P_N and P_S and puckering amplitude ν_N and ν_S. Two different softwares are available for such analysis- one is the PSEUROT program developed by Altona *et al.*[13] and the other is the Matlab Pseudorotation GUI (Graphical User Interface) program developed by Pieter *et al*.[14] The program, PSEUROT, has purely text-based interface as well as output. On the other hand the Matlab Pseudorotation GUI program is a user-friendly Matlab program, including a self-explanatory graphical user interface (GUI). Alternatively, a semi-empirical method termed as "Sum rule"[15,16] based on NMR coupling constants can also be employed to have some preliminary idea about N↔S equilibrium in case of sugar conformations.

4.1.2 Matlab Pseudorotation GUI program[14]

Matlab Pseudorotation GUI program consists of a computational core which is accessed and controlled through a GUI, both written in Matlab. This program helps to search pseudorotation parameters (*P*, ν_{max}) for two conformations as well as their relative population at *n* temperatures that fit a series of experimental NMR scalar coupling

constants. Generally two sets of pseudorotation parameters (*P* and ν_{max}) and the relative population (%1, i.e., the percentage of the first conformation present with %2 = 1 - %1) need to be fitted to the experimental NMR data. Therefore to avoid an under-determined model, experimental data measured at different temperatures are generally used. In such cases, the model assumes that only the relative population of the two conformations varies when changing the temperature. The role of electronegativities of substituents in 5-membered rings is in addition very important in determining the pucker of rings. Therefore the group electronegativity values of different substituents in ribose ring also have to be given as inputs. The correct order of the electronegativities of the four substituents (S1, S2, S3, S4) for each possible coupling to be used in the MATLAB GUI is given in Figure 4 and Table 1. A secondary GUI (the electronegativity editor) is also integrated in the program. Table 2 and 3 show the electronegativity of the most common substituents.

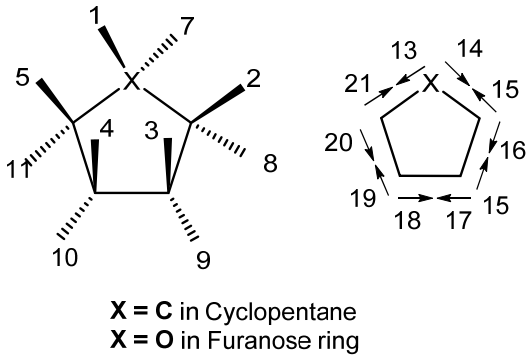

Figure 4. Substituent numbering used in five-membered ring within the GUI

Table 1: Substituent numbers for each possible coupling

No.	Coupling	S_1	S_2	S_3	S_4	No.	Coupling	S_1	S_2	S_3	S_4
1	1 - 2	8	16	13	7	11	9 - 10	20	4	17	3
2	1 - 8	16	2	13	7	12	4 - 9	10	20	3	17
3	7 - 8	16	2	13	1	13	4 - 5	11	22	19	10
4	2 - 7	8	16	1	13	14	4 - 11	22	5	19	10
5	2 - 3	9	18	15	8	15	10 - 11	22	5	19	4
6	2 - 9	18	3	15	8	16	5 - 10	11	22	4	19
7	8 - 9	18	3	15	2	17	5 - 6	12	24	21	11
8	3 - 8	9	18	2	15	18	5 - 12	24	6	21	11
9	3 - 4	10	20	17	9	19	11 - 12	24	6	21	5
10	3 -10	20	4	17	9	20	6 - 11	12	24	5	21

Table 2: Solvent-dependent electronegativities

Group	λ (D_2O)	λ($CDCl_3$)	λ(DMSO)
OH	1.25	1.34	1.39
OR	1.26	1.40	1.40
$OPO(OEt_2)$	1.27	1.27	1.29
$OPO_2(OEt)$	1.25	-	-
OAc	1.17	1.17	1.22
NH_2	1.10	1.19	1.24
NH_3^+	0.82	-	-
NR_2	1.01	1.12	1.20
NHR	1.02	1.16	1.22
NHAr	1.12	1.19	1.20

Table 3: Solvent-independent electronegativities in deuteroform. Values indicated between brackets are extrapolations

Group	λ	Group	λ	Group	λ
H	0.00	Adenine	0.56	CH_2OR	0.68
CH_3	0.80	Guanine	0.56	$CH(OR)_2$	(0.50)
CH_2Me	0.74	Cytosine	0.56	CHMe(OR)	0.62
$CHMe_2$	0.60	Thymine	0.56	$CHMe(OR)_2$	(0.40)
CMe_3	0.48	Uracil	0.56	CHF(OR)	(0.50)
CHMeF	(0.65)	F	1.37	CN	0.33
CHMeBr	0.92	Cl	0.94	SR	(0.70)
Ph	0.45	Br	0.80	NO_2	0.77
COOMe	0.42	I	0.63		

Input for Matlab GUI program

When the graphical user interface is started, the main window (Figure 5) containing four subpanels and several drop-down menus appears. The top-left panel 'Couplings' contains a list box in which the measured couplings can be defined. The top-right panel is 'Constant / Electronegativities' contains three listboxes, all strongly linked to the first panel. The first listbox (Constant) is used to assign coupling constants at five different temperatures. A second listbox (Electronegativity) used to input electronegativities for each

substituent of the furanose ring. A third listbox named 'Other' contains four parameters which are related to the conversion of puckering parameters into exocyclic torsion angles. The first two values are respectively the parameters A and B relating exocyclic and endocyclic torsion angles [eq. (4)]. The next two values are respectively the Diez-parameters αi and εi [eq. (3)]. As these last two values are actually not specific for a single coupling, but for all couplings involving the same endocyclic bond, a change of one of these values will automatically be propagated to all couplings involving the same endocyclic bond. These four values are automatically set to reasonable values by default.

The bottom left panel is 'Load/Save' which is used to save and retrieve all parameters of pseudorotation calculation. Finally, the bottom right panel 'Start parameters' is used to set up the starting conditions of the calculations. The initial pseudorotation parameters are set by the user at the start of the computational procedure and next the pseudorotation parameters are adapted so as to minimize the root-mean-square-deviation (RMSD) with respect to experimental NMR coupling constants.

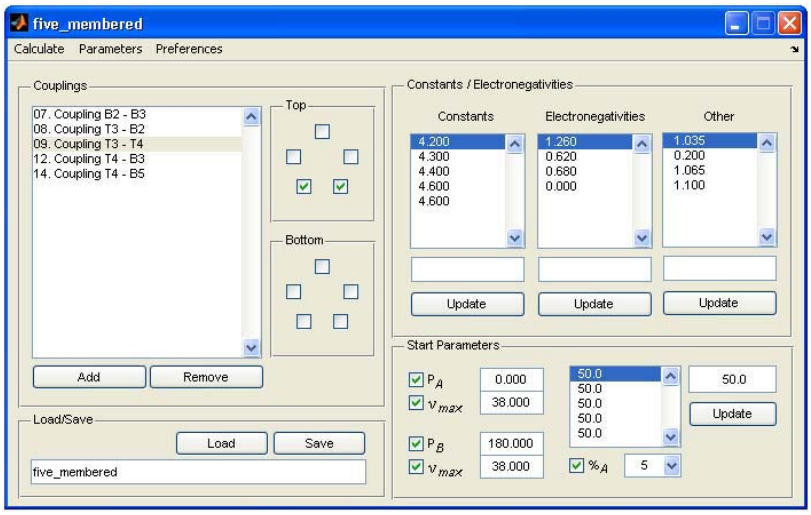

Figure 5: The MATLAB graphical user interface

Calculation of the pseudorotational parameter

Two modes of calculation are present in the program (a) Finding the optimal fit and (b) scanning the pseudorotational space, both are accessible from the 'Calculation' menu. In the first mode, a simple optimization of the 'checked' starting parameters is performed which yield the pseudorotation parameters that best fit the experimental data. The output generated in this operation mode is purely text-based and contains the optimized variables, their corresponding *endo*-cyclic torsion angles and a tabular comparison between experimental and fitted NMR data.

In the second mode of the program, the complete pseudorotation space of the cycle of interest is explored *via* 3600 combinations of pseudorotation parameters (P, ν_{max}). The second mode of calculation has some advantages over the first mode. In this case a better appreciation of the conformational space of the cycle is obtained which is in agreement with the experimental data. Furthermore, the extent of the contour levels holds direct information that allows to establish whether the model is under-determined or not. Even when under-determined, such calculation can already indicate those conformations that can be excluded from further investigation.

Typical textual output of the fitting protocol:

```
----------------------------------------
Conformation 1
P : 3.855`1ax`1axio
Phi_m : 41.663
Conformation 2
P : 184.315
Phi_m : 41.928
Temperature Coefficients
%Conformation1 :  28.883
%Conformation1 :  31.143
%Conformation1 :  32.386
%Conformation1 :  34.831
%Conformation1 :  36.657
----------------------------------------
Endocyclic torsion angles
----------------------------------------
        Conf.1        Conf.2
Phi0:  40.650       -40.879
Phi1: -34.916        35.307
Phi2:  15.845       -16.249
Phi3:  9.278        -9.015
Phi4: -30.857        30.836
----------------------------------------
```

```
Final couplings
----------------------------------------
Temperature 1:
----------------------------------
Conf1  Conf2  Avg.  Exp.  Diff.
----------------------------------
7.87   6.28   6.74  6.70  0.04
0.94   10.92  8.04  8.00  0.04
5.93   3.69   4.34  4.20  0.14
10.52  1.66   4.22  4.20  0.02
8.55   0.86   3.08  3.10 -0.02
----------------------------------
RMSD : 0.07 Hz
Temperature 2:
----------------------------------
Conf1   Conf2   Avg.   Exp.  Diff.
----------------------------------
7.87    6.28    6.77   6.70  0.07
0.94    10.92   7.82   7.80  0.02
5.93    3.69    4.39   4.30  0.09
10.52   1.66    4.42   4.40  0.02
8.55    0.86    3.26   3.30 -0.04
----------------------------------
RMSD : 0.06 Hz
```

4.2 Rationale and objectives of the present work

The study of the furanose ring conformation for the synthesized modified 2'-5' nucleosides described in chapter 2 and 3 is presented in this chapter. Small variations in the structure of a nucleoside analogue can produce drastic changes in its biological properties. This indicates that conformational features of a particular nucleoside analogue are very important with respect to its biological activity. In our discussion about the RNA-binding selectivity of modified ngDNA, we observed that the nucleosides with differing stereochemistry of the fluorine substituent at 3′ position showed contrasting results. The nucleoside having 3′-fluorine below the plane of furanose ring [(*S*), 3′-deoxy-3′-fluoro xylofuranosyl nucleoside] favours stable complex formation with complementary RNA, while the nucleoside with the opposite stereochemistry at C3′ with the fluorine atom above the plane of the sugar ring [(*R*) 3′-deoxy-3′-fluoro ribofuranosyl nucleoside] caused a destabilization. We discussed how the *gauche* effect of fluorine affects the sugar puckering and freezes it in either S- or N-type conformation. In previous chapters, we used the semi-empirical method termed as the "Sum rule" to get a preliminary idea about the N↔S equilibrium in sugar conformations of the modified nucleosides. The "Sum rule" depends on the $J_{1'2'}$ coupling constant and %S can be calculated using the following equation.[16]

%S = 100 X ($J_{1'2'}$-1)/6.9)

The Sum rule gives only a rough idea about the sugar conformation, but it is necessary to evaluate the conformations of nucleosides systematically.

In this Chapter, we present the results of our studies to understand the furanose ring conformation of $^{R}U^{F}$, $^{R}A^{F}$, $^{X}U^{F}$, $^{X}A^{F}$, $^{L}A^{S}$, and ^{ara}U nucleoside, in solution as well as solid state. We report an integrated high field (400MHz) ^{1}H NMR and X-ray crystallographic study on the conformation of the sugar rings of these modified nucleoside analogues. We analyzed vicinal scalar *J*-coupling constants and nuclear Overhauser effects to reveal important information about the dynamic conformation in solution, e.g., to derive characteristics of the individual conformers. The vicinal proton-proton ($^{3}J_{HH}$) coupling constants $J_{1'2'}$, $J_{1'2''}$, $J_{2'3'}$ and $J_{3'4'}$ at different temperatures were used as inputs for the pseudorotation analysis of the sugar using the MATLAB GUI PSEUDOROTATION program.

The objectives of the work are:

1. NMR assignment of furanose ring protons of $^{R}U^{F}$, $^{R}A^{F}$, $^{X}U^{F}$, $^{X}A^{F}$, $^{L}A^{S}$ and ^{ara}U nucleoside by a combination of 1D proton and 2D- COSY NMR experiments.
2. Determination of $^{3}J_{HH}$ coupling constants by using ^{1}H NMR at five different temperatures.
3. Determination of *syn*/*anti* conformation of nucleobase in $^{R}U^{F}$, $^{R}A^{F}$, $^{X}U^{F}$, $^{X}A^{F}$, and ^{ara}U nucleoside with the help of NOESY NMR experiments and X-ray crystallography studies.
4. Determination of the conformation of the furanose ring of $^{R}U^{F}$, $^{R}A^{F}$, $^{X}U^{F}$, $^{X}A^{F}$, $^{L}A^{S}$ and ^{ara}U nucleoside by comparative *P* and ν_{max} values obtained from Matlab Pseudorotation GUI program as well as by X-ray crystallography study.

4.3 Present work, result and discussion

To determine the conformational preferences of the deoxyribose ring in ngDNA nucleoside analogues it is essential to obtain the corresponding $^{3}J_{HH}$ scalar coupling constants required for the calculations using Matlab Pseudorotation GUI program as well as "Sum rule". The modified nucleosides $^{R}U^{F}$, $^{R}A^{F}$, $^{X}U^{F}$, $^{X}A^{F}$, and ^{ara}U chosen for the conformational analysis are shown in Figure 6. Synthesis of all the compounds is discussed in Chapters 2 and 3. In the case of $^{X}A^{F}$ and $^{R}A^{F}$ nucleosides, N^{6}-benzoyl group of adenine was deprotected to increase the D_2O-solubility. The nucleoside $^{L}A^{S}$ has N^{6}-benzoyladenine, where we used CD_3OD as solvent.

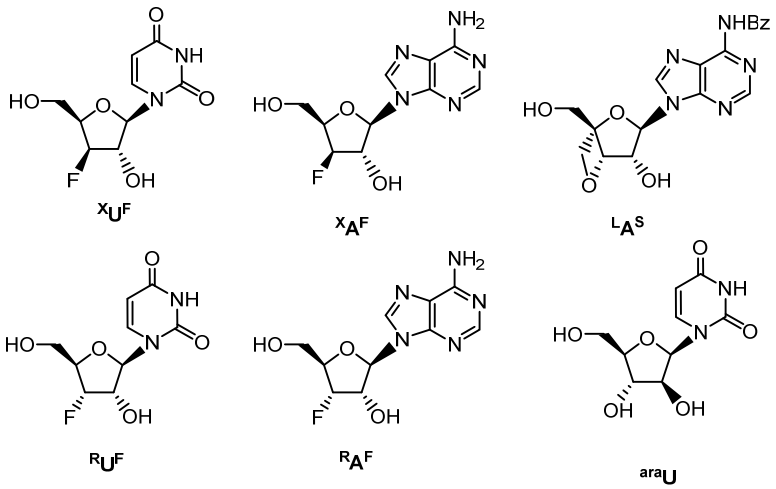

Figure 6. Chemical structure of the all the modified analogues used for conformational analysis

4.3.1 Assignments and coupling constants from ^{1}H NMR spectra of modified nucleoside analogues

Conformational analysis was undertaken for the six modified monomers shown in Figure 6. The assignment of the non-exchangeable proton resonances was achieved by using 2D COSY experiments (Table 4, Figure 7-11) while the coupling constants were determined from 1D ^{1}H NMR spectra (Table 5). The H5′/H5″ protons were assigned according to rule of thumb also called as the Remin and Shugar rule[17] where downfield proton of C5′ was assigned as H5′ while the upfield proton is assigned as H5″. One-dimensional ^{1}H NMR spectra were recorded at 400MHz at the sample temperatures 285, 300, 313, 333 and 353K. Chemical shifts and coupling constants for all the compounds were determined relative to D_2O, where the change in chemical shift at different temperatures for D_2O was considered. The ^{1}H NMR spectra for compound $^{L}A^{S}$ was recorded at 500MHz, and at only one temperature, viz., 296K in CD_3OD solvent.

Table 4. Chemical shift value of modified nucleoside analogues at different sample temperatures (solvent D_2O)

Comp	Temp K	δ (ppm)							
		H1′	H2′	H3′	H4′	H5′	H5″	H5/H2	H6/H8
$^{X}U^{F}$	285	5.89	4.57	5.11	4.48	4.05	4.01	5.84	7.76
	300	5.88	4.55	5.12	4.49	4.04	3.98	5.84	7.74
	313	5.89	a	5.14	4.51	4.04	4.00	5.86	7.74
	333	5.87	4.55	5.13	a	4.02	3.98	5.86	7.72
	353	5.89	5.56	5.15	4.49	4.01	3.98	5.87	7.71
$^{R}U^{F}$	285	6.09	4.49	5.10	4.45	3.84	3.80	5.92	7.86
	300	6.06	4.49	5.10	4.44	3.84	3.80	5.92	7.83
	313	6.06	4.51	5.12	4.45	3.86	3.82	5.94	7.84
	333	6.03	4.51	5.12	4.48	3.83	3.82	5.94	7.81
	353	6.01	4.52	5.12	4.44	3.84	3.82	5.94	7.79
$^{X}A^{F}$	285	6.07	4.83	5.24	4.58	4.03	3.99	8.10	8.15
	300	6.10	4.85	5.25	4.58	4.03	3.97	8.16	8.18
	313	6.12	4.87	5.27	a	4.03	3.97	8.21	8.21
	333	6.13	4.88	5.27	4.58	4.03	3.97	8.24	8.22
	353	6.14	4.90	5.28	4.59	4.04	3.97	8.27	8.23
$^{R}A^{F}$	285	6.80	a	5.25	4.61	3.89	3.88	8.13	8.28
	300	6.90	4.96	5.25	4.59	3.88	3.87	8.18	8.29
	313	6.11	4.98	5.26	a	3.89	3.89	8.22	8.31
	333	6.11	4.98	5.26	4.58	3.89	3.88	8.25	8.31
	353	6.11	4.99	5.26	4.58	3.89	3.88	8.27	8.31
^{ara}U	285	6.19	4.41	4.12	3.99	3.92	3.83	5.86	7.86
	300	6.18	4.41	4.12	3.98	3.91	3.82	5.86	7.84
	313	6.18	4.42	4.14	4.00	3.92	3.83	5.87	7.84
	333	6.17	a	4.13	3.99	3.91	3.83	5.87	7.82
	353	6.16	4.42	4.14	3.99	3.92	3.83	5.87	7.81
$^{cL}A^{S}$	296	6.57	4.81	5.22	b H5b′ 4.64, H5b″ 4.94	H5a′ 3.82	H5a″ 3.86	8.67	8.74

chemical shift of Solvent D_2O at different temperatures: 285K = 4.93δ; 300K = 4.74δ; 313K = 4.61δ; 333K = 4.40δ; 353K = 4.22δ; a = Peaks merge with D_2O; b = In $^{L}A^{S}$ H4′ proton is absent while additional H5b′, H5b″ proton are present; c = Nucleoside $^{L}A^{S}$ has N^6-benzoyladenine. For $^{L}A^{S}$ we used CD_3OD solvent.

Table 5. $^{3}J_{HH}$ ^{1}H NMR coupling constant of modified nucleoside analogues at different sample temperatures

Comp	Temp K	*J* (Hz)										
		1′2′	2′3′	2′F	3′4′	3′F	4′5′	4′5″	4′F	5′5″	5′F/ 5″F	H5 ,H 6
$^{X}U^{F}$	285	0.77	0.97	13.80	2.76	51.95	5.02	6.78	31.87	12.30	0.5	8.03
	300	0.87	1.02	14.05	2.76	50.19	5.27	6.78	31.62	12.30	0.6	8.28
	313	1.00	1.10	a	2.76	50.44	5.02	6.78	39.40	12.30	0.7	8.28
	333	1.51	1.25	15.31	1.25	50.44	5.02	6.78	a	12.30	0.7	8.03
	353	2.25	1.51	16.06	1.25	50.44	5.02	6.27	33.00	12.30	0.5	8.03
$^{R}U^{F}$	285	7.78	4.64	22.84	0.80	53.96	3.51	3.26	26.35	13.05	b	8.03
	300	7.65	4.67	22.52	0.80	53.96	3.70	3.70	28.36	13.36	b	8.09
	313	7.53	4.77	23.34	0.80	53.96	4.02	3.26	27.10	13.50	b	8.03
	333	7.53	4.77	21.69	1.75	53.96	a	a	a	b	b	8.03
	353	7.28	4.77	21.33	2.01	53.96	4.00	4.00	28.86	b	b	8.28
$^{X}A^{F}$	285	1.47	1.71	14.18	3.18	50.86	4.89	6.60	28.61	12.23	0.88	c
	300	1.96	1.71	14.43	3.18	50.86	4.89	6.36	28.61	12.23	0.98	c
	313	2.20	1.71	14.43	3.18	51.11	5.14	6.36	a	12.23	0.96	c
	333	2.20	1.71	14.92	3.18	51.11	5.14	6.36	28.37	12.23	b	c
	353	2.20	1.71	15.41	3.18	51.11	4.89	6.11	28.37	12.23	b	c
$^{R}A^{F}$	285	8.28	4.27	a	0.50	53.96	1.80	1.80	28.11	b	b	c
	300	8.03	4.27	24.85	0.50	53.96	2.76	2.76	28.11	b	b	c
	313	8.03	4.52	24.59	0.50	53.96	2.94	2.94	a	b	b	c
	333	7.78	4.52	24.09	0.50	53.96	3.27	3.27	27.86	b	b	c
	353	7.78	4.77	23.84	0.50	53.96	3.00	3.00	27.61	b	b	c
^{ara}U	285	5.02	4.77	c	5.52	c	3.01	5.52	c	12.55	c	8.03
	300	5.02	4.77	c	5.52	c	3.26	5.52	c	12.55	c	8.03
	313	5.27	5.27	c	5.27	c	3.26	5.52	c	12.55	c	8.03
	333	5.02	5.02	c	5.02	c	3.26	5.52	c	12.55	c	8.03
	353	5.02	5.27	c	5.02	c	3.26	5.52	c	12.55		8.03
$^{dL}A^{S}$	296	7.63	4.27	c	c	c	c	c	c	5a′5a″ 12.4 5b′5b″ 7.93	c	c

a = Peaks merge with D_2O; b = Not determined, due to overlap (ABX pattern where $\nu_{AB} = 1$); c = not applicable for the given compound; d = Coupling constant for additional H5b′, H5b″ proton of $^{L}A^{S}$ are given.

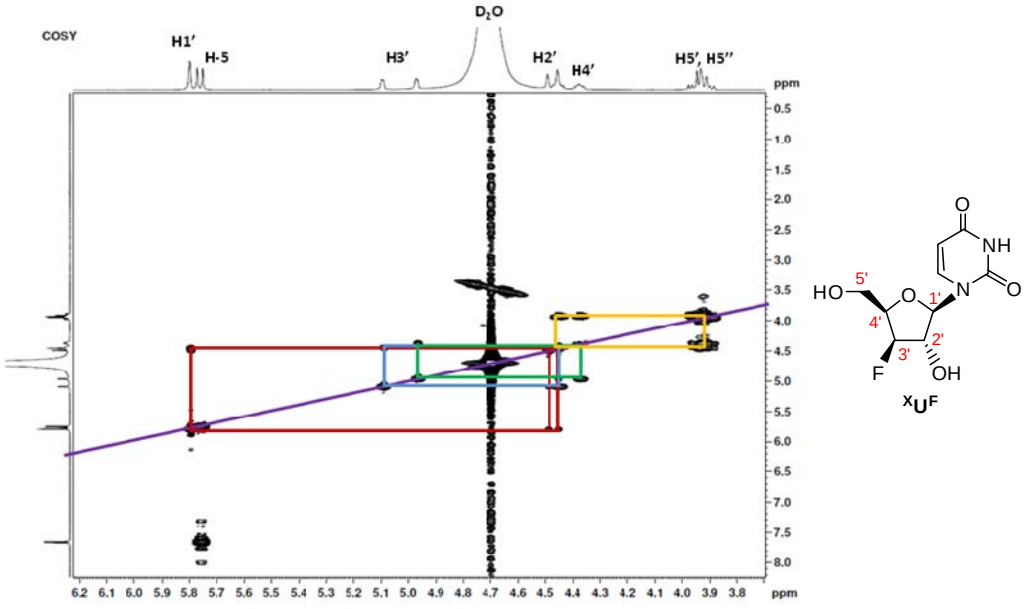

Figure 7. COSY spectrum of $^{X}U^{F}$ nucleoside

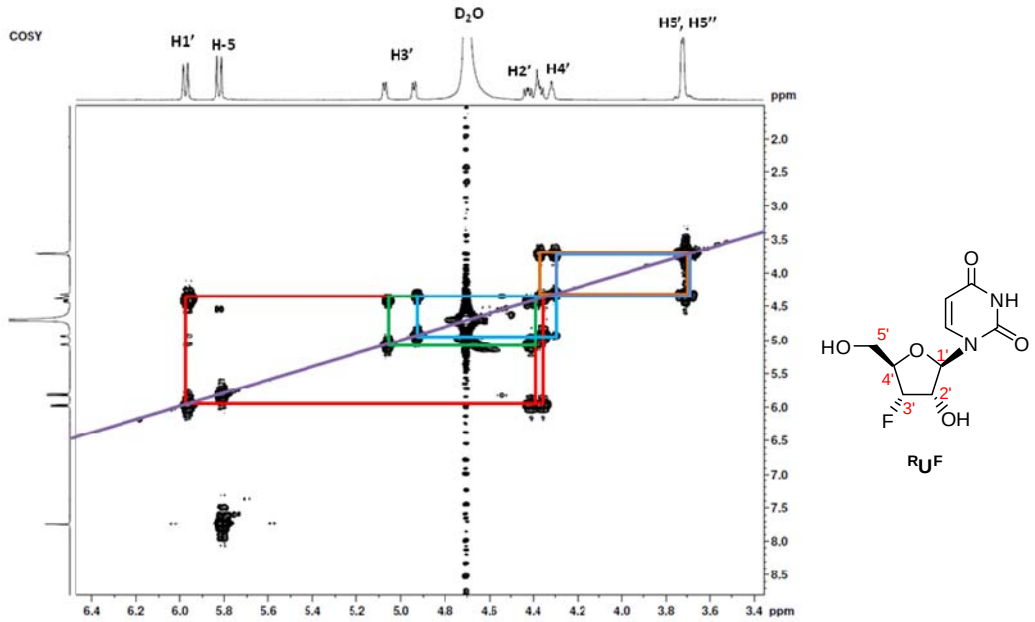

Figure 8. COSY spectrum of $^{R}U^{F}$ nucleoside

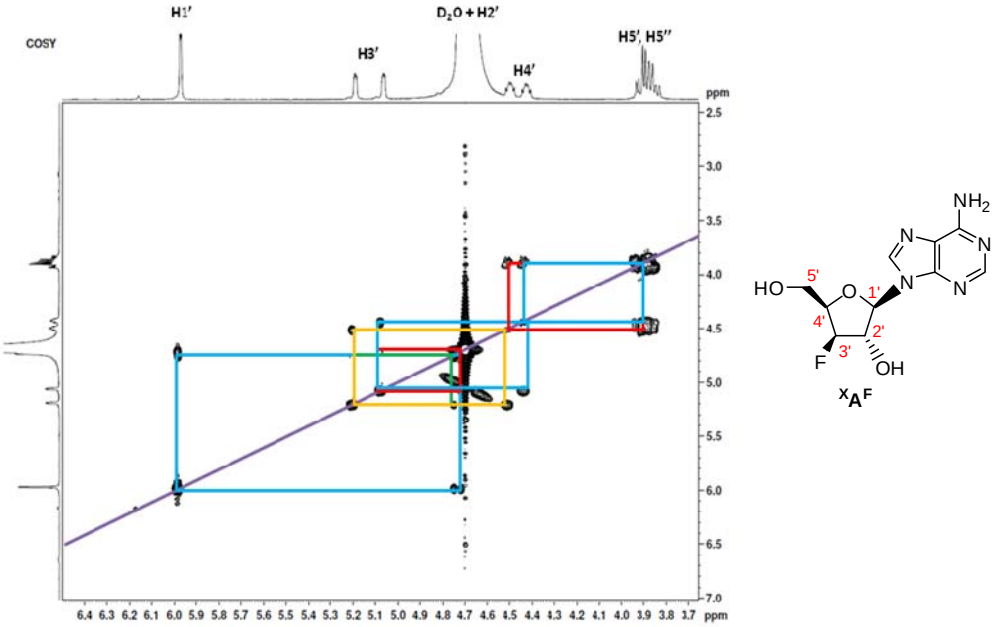

Figure 9. COSY spectrum of $^{X}A^{F}$ nucleoside

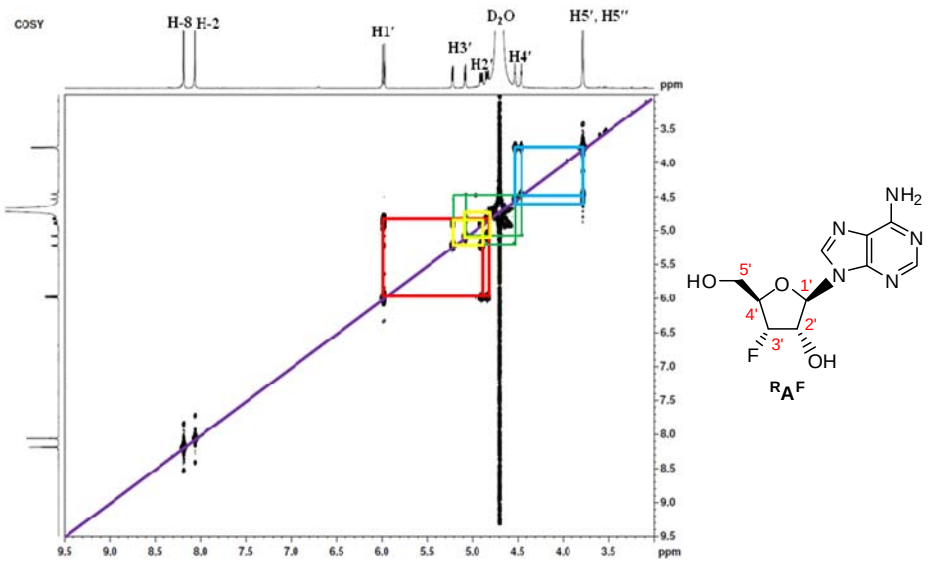

Figure 10. COSY spectrum of $^{R}A^{F}$ nucleoside

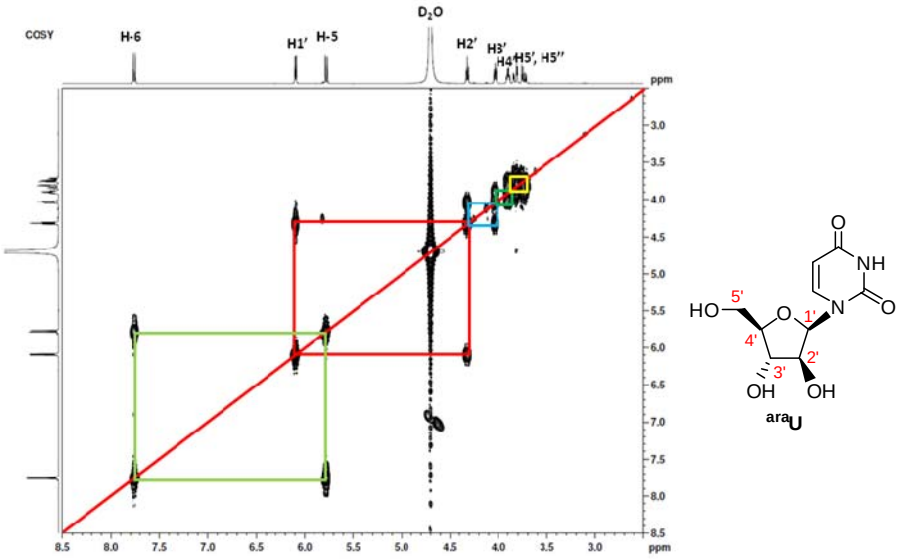

Figure 11. COSY spectrum of ^{ara}U nucleoside

4.3.2 Matlab Pseudorotation GUI results

The pseudorotation analysis of $^{X}U^{F}$-, $^{R}U^{F}$-, $^{X}A^{F}$-, $^{R}A^{F}$-, ^{ara}U- and $^{L}A^{S}$-nucleoside was executed using the Matlab GUI pseudorotation program. All $^{3}J_{HH}$ coupling constants in D_2O at five temperatures (Table 5) and electronegativity of the four substituents for each coupling were used as input parameters. First, the five unknown parameters (P_1, $\nu_{max,1}$, P_2, $\nu_{max,2}$, % conformer 1) were determined. The five values were adjusted or sometimes one of the ν_{max} value was kept constant so as to get the least RMSD and ultimately to get the best fit. The obtained textual results are presented in Table 6. This table includes the optimized pseudorotation parameters for the North and South conformations (P_N, ν_N, P_S, ν_S) in degrees and the population of the North and South conformer for two extreme temperatures (285K and 353K). The table also includes the maximal deviation and RMSD between the fitted couplings and the experimental values. The results presented in Table 6 clearly show that the nucleosides $^{R}U^{F}$, $^{R}A^{F}$ and $^{L}A^{S}$ are found in more than 70% S-type conformation while $^{X}U^{F}$, $^{X}A^{F}$ are more than 70% in N-type conformation. ^{ara}U is 60% in N-type conformation at 285K while its percentage increases up to 70% at 353K. This first mode of calculation gives only a couple of conformations, but actually the number of conformations populated by a five-membered ring needs not be limited to two.

In order to get a better appreciation of these optimal values we also used the second mode of calculation. The full pseudorotation wheel of all the six nucleosides ($^{R}U^{F}$, $^{R}A^{F}$, $^{X}U^{F}$, $^{X}A^{F}$, $^{L}A^{S}$ and ^{ara}U) were scanned by Matlab Pseudorot GUI.[14] The obtained plots are shown in Figures 12, 13 and 14. In Figure 12, the contour plots indicate the root-mean-square-deviation between the fitted and the experimental scalar couplings for all the nucleosides. In this mode of calculation, the regions that have an RMSD lower than a certain threshold (e.g. 0.2Hz), as representative of the cycle's conformation is interpreted, which actually seems more reasonable than taking the optimal fit for granted.

As can be seen in Figure 12, nucleosides $^{R}U^{F}$ and $^{R}A^{F}$, which have the 3′-fluorine in ribo configuration, exhibit similar results. Looking at the extent of the contour lines, it is clear that for these nucleosides the major South-conformation is better defined and shows a narrow solution space. The other minor N-conformer (±20%) for $^{R}U^{F}$ and $^{R}A^{F}$ is amiss, and showed the physically unrealistic conformation values of *P* and ν_{max}. The RMSD is small for both nucleosides.

Compounds $^{X}U^{F}$ and $^{X}A^{F}$, where 3′-fluorine has xylo conformation, show a reverse influence on the conformation of the furanose moiety. In both these nucleosides, the major North-conformation is better defined, showing a narrow solution space. In this case also the minor S-conformer (±25%) again goes amiss and shows physically unrealistic values for *P* and $\nu_{max.}$

The very narrow solution space observed for the major conformation and the faulty minor conformation for $^{R}U^{F}$, $^{R}A^{F}$ and $^{X}U^{F}$, $^{X}A^{F}$ are possibly because of the 3′-fluorine substituent. The 3'-fluorine in ribo and xylo configuration freeze the sugar conformation in S- and N-type respectively due to its O_4'-C4'-C3'-F_3' *gauche* effect. Thus the furanose ring is not able to change its conformation much in solution and therefore shows a very narrow solution space. The energy barrier of the frozen furanose ring is probably very high to change its conformation from S to N or N to S, and this could be the reason that it shows unrealistic physical values for the minor conformation.

For $^{L}A^{S}$ the major South-conformation is found be defined, but in this case it is clear that the fitting procedure has problems finding the optimal pseudorotation parameters for the minor conformation, resulting in a highly discontinuous contour surface. In $^{L}A^{S}$ the

sugar ring is locked in S-type, by 3′-*O*,4′-C-methylene bridge this may be the result for the fitting problem observed for the minor conformation.

For ^{ara}U nucleoside the result obtained seems to be faulty showing again, a physically unrealistic value P =84.29, for the minor S conformer (±40%) and P = -44 for the major N conformer. For higher RMSD (0.2 to 0.24 Hz), this compound shows some valid values of P and ν_{max} (Figure 12) for both N and S conformer.

In addition to Figure 12, the Figures 13 and 14 can be used to interpret the allowed population-range for each conformation. These graphs represent the population of two extreme conformations of all six nucleosides. Contour lines indicate the percentage of conformation present in the best fit. The thick black contour is the highest contour level of Figure 12. Within this black contour level a variety of populations can be seen ranging from 75 to 95 percent of South-conformation for $^{R}U^{F}$, $^{R}A^{F}$ and $^{L}A^{S}$ and 75 to 95 percent of North-conformation for $^{X}U^{F}$ and $^{X}A^{F}$ at both 285K and 353K. In all the cases the the percentage of the minor conformation was only 10 to 20. For ^{ara}U nucleoside both the south and north conformation show population in the range of 50 percent.

Table 6: Conformational parameters obtained from Matlab pseudorotation GUI calculations for $^{R}U^{F}$, $^{R}A^{F}$, $^{X}U^{F}$, $^{X}A^{F}$, $^{L}A^{S}$ and ^{ara}U.

Comp	Torsion angle $(\nu_0\text{-}\nu_4)^a$	$P_N{}^b$	$\nu_N{}^c$	$P_S{}^d$	$\nu_S{}^e$	ΔJ^{maxf}	RMSD[g]	%N[h] 285K	%S[i] 285K	%N[j] 353K	%S[k] 353K
$^{X}U^{F}$	-25.083 -8.498 38.833 -54.335 49.083	45.11	55.03	288.55	41.00*	-0.58	0.22	72.4	38.6	100	0.0
$^{R}U^{F}$	-15.832 32.155 -36.195 26.410 -6.538	69.27	60.00	172.31	36.52	0.14	0.07	2.6	97.4	16.8	83.2
$^{X}A^{F}$	6.433 -30.313 42.614 -38.638 19.904	9.43	43.19	92.38	39.0 *	-0.14	0.05	84.6	15.4	73.5	26.5
$^{R}A^{F}$	-19.767 36.153 -38.730 26.513 -4.169	-91.08	42.00*	168.04	39.58	-0.23	0.09	0.0	100	7.8	92.2
^{ara}U	36.702 -40.313 28.525 -5.841 -19.073	-44.99	40.81	84.29	38.50*	-0.23	0.11	59.8	40.2	71.2	28.8
$^{L}A^{S}$	24.459 -46.711 51.122 -36.006 7.136	-10.10	51.92	146.54	48.00	0.00	0.00	296K 23.2	296K 76.8	-	-

[P_N, ν_N, P_S, ν_S and torsion angle ($\boldsymbol{\nu_0\text{-}\nu_4}$) are in degrees, temperature is in K, RMSD error and ΔJ^{max} are in Hz. The calculation was done using *J* values at five temperatures, but here the population at only lower and upper temperature is mentioned (285K & 353K); For $^{L}\mathbf{A}^{S}$ the calculation was done at only one temperature, 296K]

[a] torsion angle ($\boldsymbol{\nu_0\text{-}\nu_4}$) given for major conformer; [b]P_N pseudorotation angle for N-conformer; [c]ν_N Puckering amplitude for N conformer; [d]P_S pseudorotation angle for S-conformer; [e]ν_S Puckering amplitude for S conformer; [f]ΔJ^{max} the maximum value of the difference between the experimental $^3J_{HH}$ coupling constants and their calculated values; [g]RMSD root-mean-square-deviation; [h]%N 285K percentage of N-conformer at 285K temperature; [i]%S 285K percentage of S-conformer at 285K temperature; [j]%N 353K percentage of N-conformer at 353K temperature,[k]%S 353K percentage of S-conformer at 353K temperature. Constrained values are indicated with an asterisk

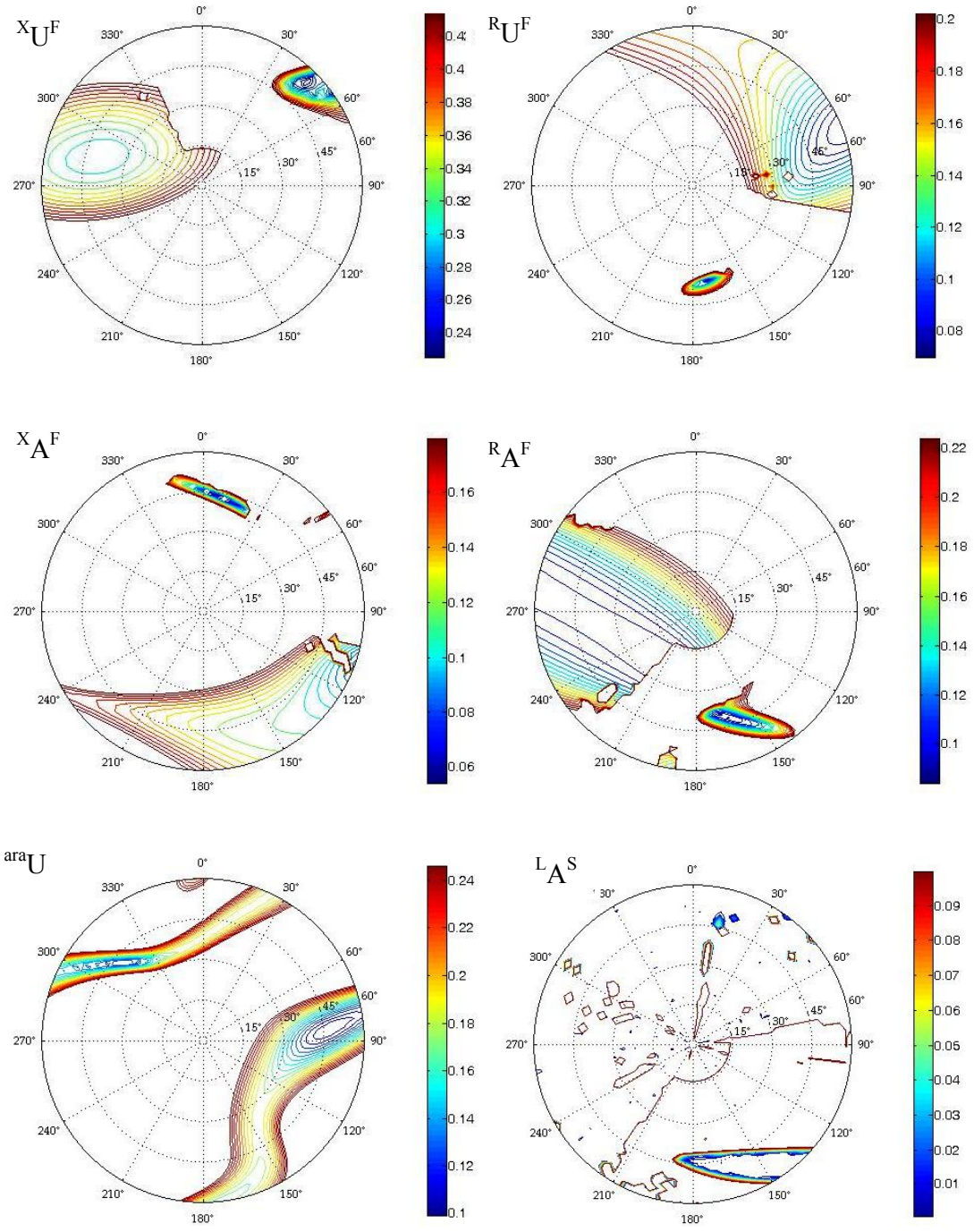

Figure 12. Pseudorotation wheel for $^{R}U^{F}$, $^{R}A^{F}$, $^{X}U^{F}$, $^{X}A^{F}$, $^{L}A^{S}$ and ^{ara}U nucleosides. Contour levels show the RMSD (Hz) between the experimental and fitted scalar coupling constants for each combination of P and ν_{max}. These graphs were created by plotting the RMSD between the experimental values and their best fitting scalar coupling constants

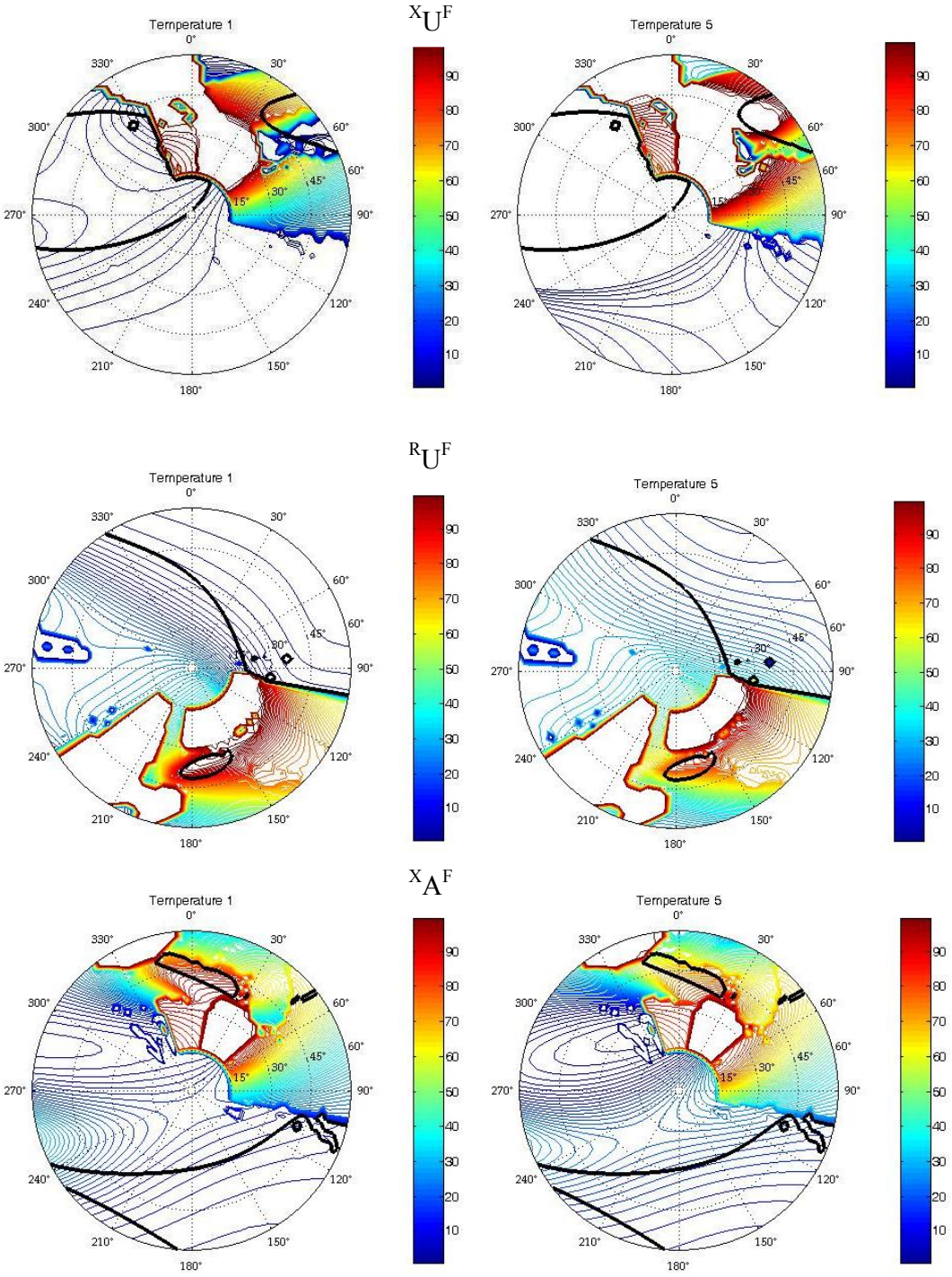

Figure 13. Pseudorotation wheel of partition coefficients of $^{X}U^{F}$, $^{R}U^{F}$and $^{X}A^{F}$nucleosides for the two extreme temperatures 1 and 5 (285K and 353K). Contour lines indicate the percentage of conformation present in the best fit. The thicker black contour line is the outer contour line of Figure 12.

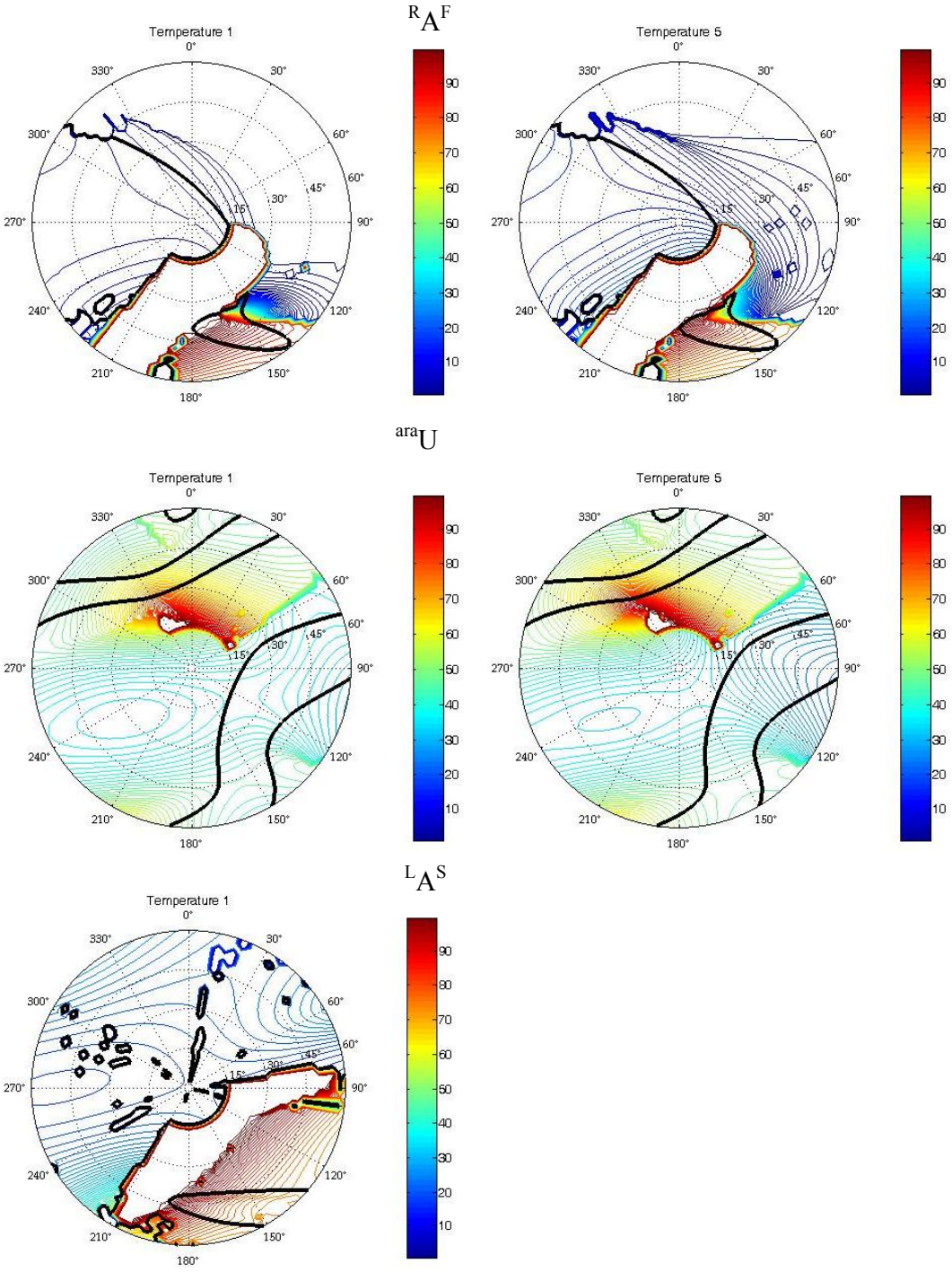

Figure 14. Pseudorotation wheel of partition coefficients of $^{X}U^{F}$, $^{R}U^{F}$and $^{X}A^{F}$nucleosides for the two extreme temperatures 1 and 5 (285K and 353K). Contour lines indicate the percentage of conformation present in the best fit. The thicker black contour line is the outer contour line of Figure 12.

4.3.3 NOE experiments for modified nucleoside analogues

We performed the NOE NMR experiments to determine the preferred conformation around the glycosidic (Cl'-Nl/N9) bond, i.e. *anti* or *syn* orientation of the base (Figure 16-20). Figure 15 shows the percentage of observed NOE enhancement of H6 and H8 protons of uracil and adenine respectively. The NOE cross peaks between H2′–H6 protons in compounds $^{X}U^{F}$, $^{R}U^{F}$ and ^{ara}U, as well as H5'-H6 in $^{X}U^{F}$ and ^{ara}U suggest the *anti* conformation of uracil base. The $^{X}A^{F}$ and $^{R}A^{F}$ nucleosides show the H5′–H8 and H2′–H8 NOE enhancement respectively which again confirms the *anti* conformation of adenine base.

The proof for the S/N conformation in solution further comes from the observed strong NOE cross peaks as shown in Figure 14. The NOE cross peak between the *beta*-oriented H2′ and nucleobase H6 is 13.6% in $^{R}U^{F}$ **(**the S-type sugar), whereas in compound $^{X}U^{F}$ where the N-type geometry is preferred, the observed NOE (2%) is relatively weaker (due to increased distance between the two interacting protons).[18] Further, the preferred O5′-C5′-C4′-C3′ geometry in solution would be γ+ for the $^{R}U^{F}$ nucleoside and is in equilibrium with γ– and γt for the $^{X}U^{F}$ derivatives based on the $^{3}J_{H4'\text{-}H5'}$ and $^{3}J_{H4'\text{-}H5''}$ coupling constants[19] (Table 5).

Similarly, in $^{X}A^{F}$ and $^{R}A^{F}$ nucleosides the S-type sugar conformation of $^{R}A^{F}$ was confirmed by the presence of an NOE cross peak between H2′ and nucleobase H8 (3.6%) which is not observed in $^{X}A^{F}$ due to its N-type sugar conformation.

In ^{ara}U nucleoside the H2′ orientation is *alpha*, therefore the H6-H2′ NOE is not useful in this case. However, the NOE cross peak between H6 and *beta*-oriented H3′ is 3.8%, and with H5′ H5″ is 2%, indicating the presence of N-type sugar conformation in solution.

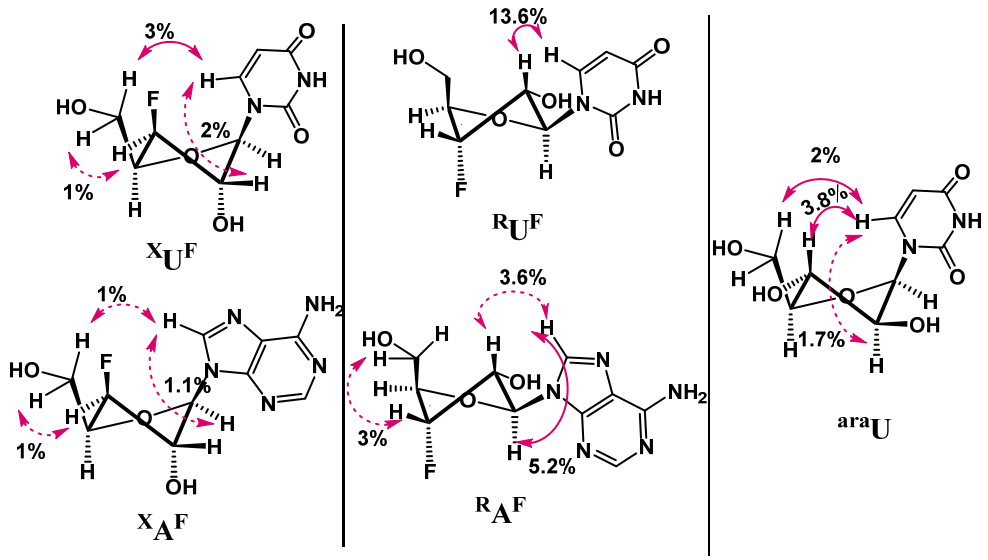

Figure 15. Percent NOE cross peaks and possible conformers for the five nucleosides of the study

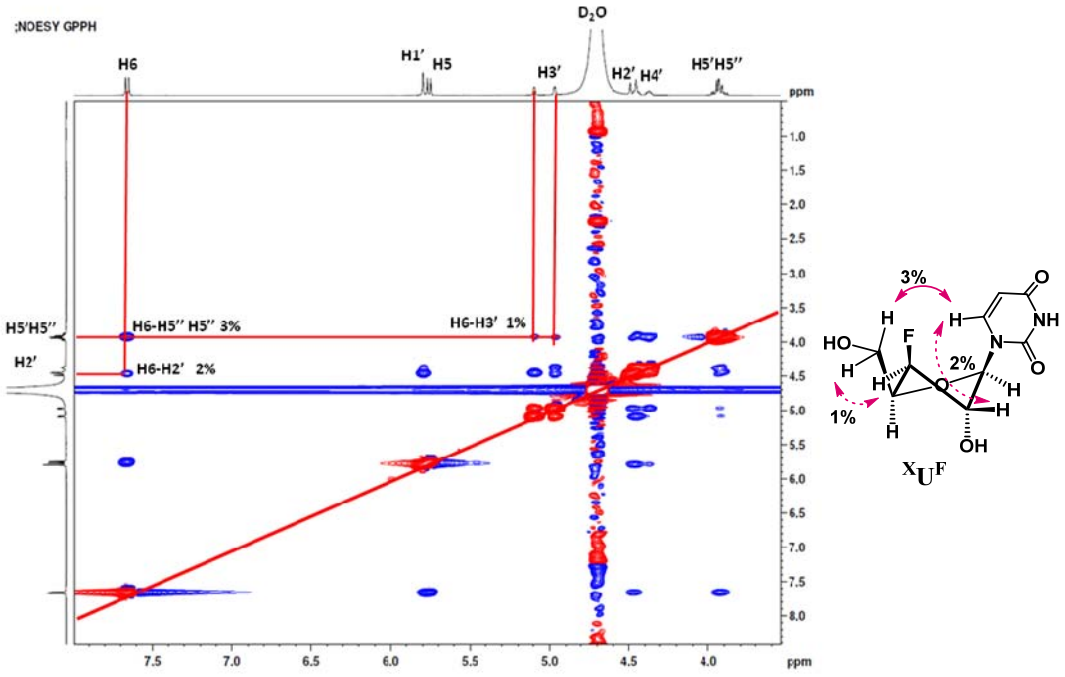

Figure 16. NOESY spectrum of $^{X}U^{F}$ nucleoside

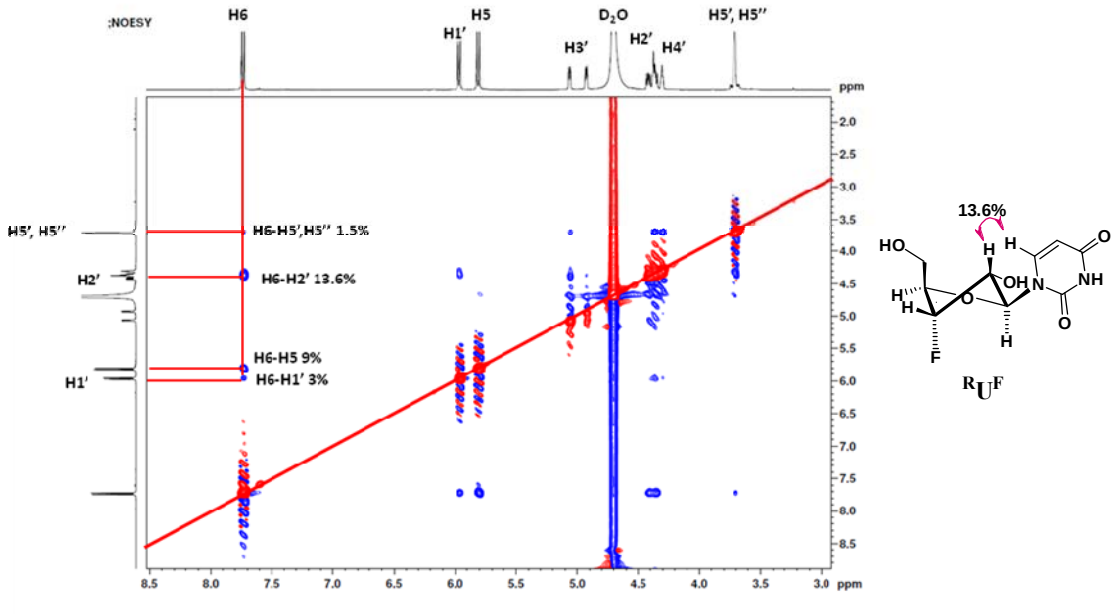

Figure 17. NOESY spectrum of $^{R}U^{F}$ nucleoside

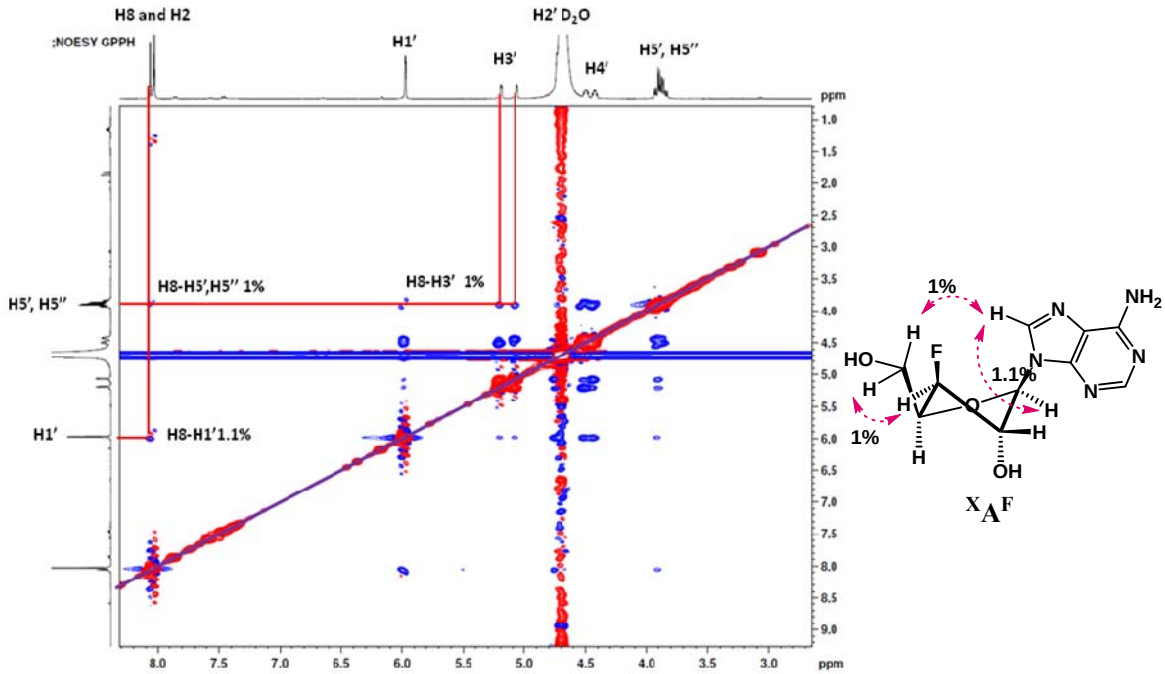

Figure 18. NOESY spectrum of $^{X}A^{F}$ nucleoside

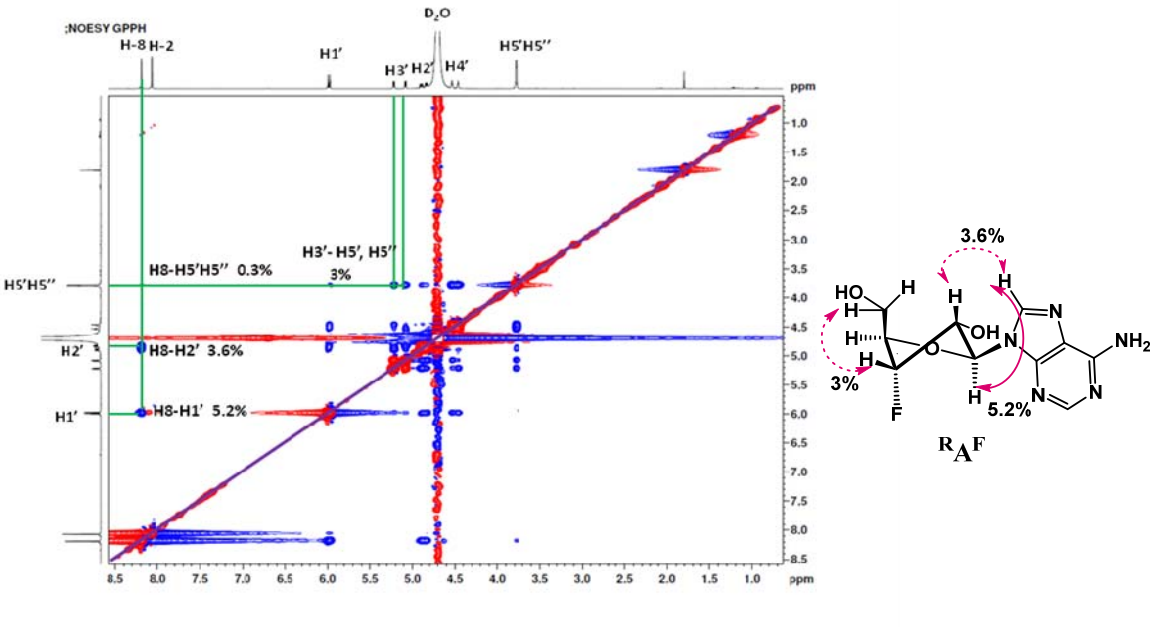

Figure 19. NOESY spectrum of $^{R}A^{F}$ nucleoside

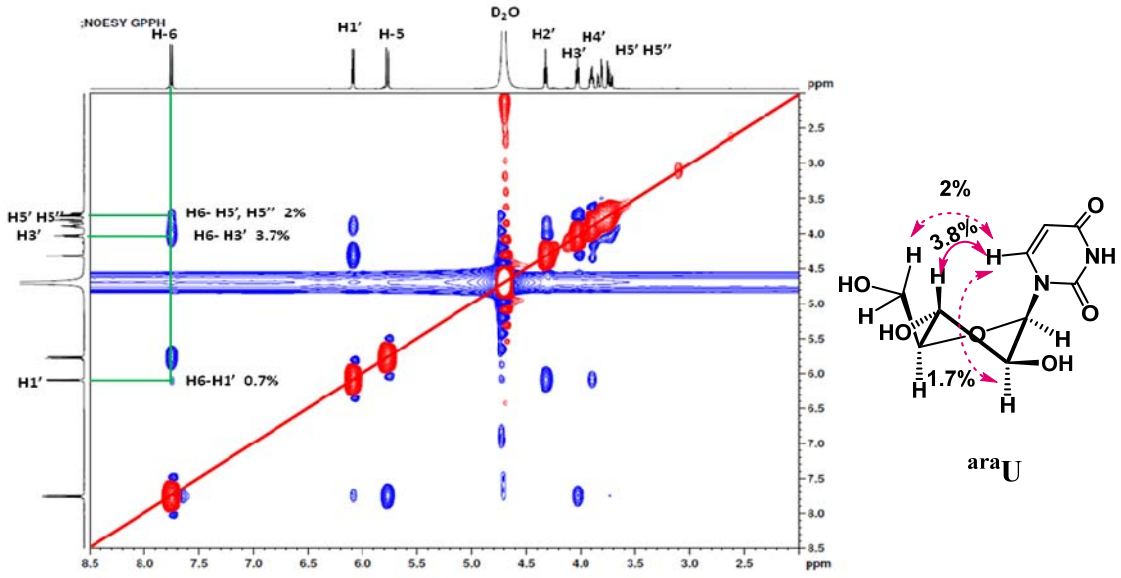

Figure 20. NOESY spectrum of ^{ara}U nucleoside

4.3.4 X-ray crystal structure of modified nucleoside analogues

Among the six modified analogues which we have chosen for conformational analysis, here we discuss the crystal structure of four nucleosides ($^{X}U^{F}$, $^{R}U^{F}$, $^{X}A^{F}$ and ^{ara}U). The X-ray crystallographic data for two of these nucleosides, ^{ara}U[20] and $^{X}U^{F21}$, were also reported earlier. The data for compounds $^{R}U^{F}$ and $^{X}A^{F}$ have not been reported before. In this study, the $^{X}A^{F}$ nucleoside is with *N*6-benzoylated adenine. The compounds $^{X}U^{F}$, $^{R}U^{F}$ and $^{X}A^{F}$ were crystallized from MeOH/DCM. The ORTEP diagrams for crystal structures of compounds $^{X}U^{F}$ and $^{X}A^{F}$ and ^{ara}U are shown in Figures 21 and 22 respectively. Three crystal forms were observed for $^{R}U^{F}$, the ORTEP diagram for Form A and the superimposition of the three forms are shown in Figure 23. Table 7 summarizes the most important conformational characteristics for the four nucleosides- $^{R}U^{F}$, $^{X}U^{F}$, $^{X}A^{F}$ and ^{ara}U.

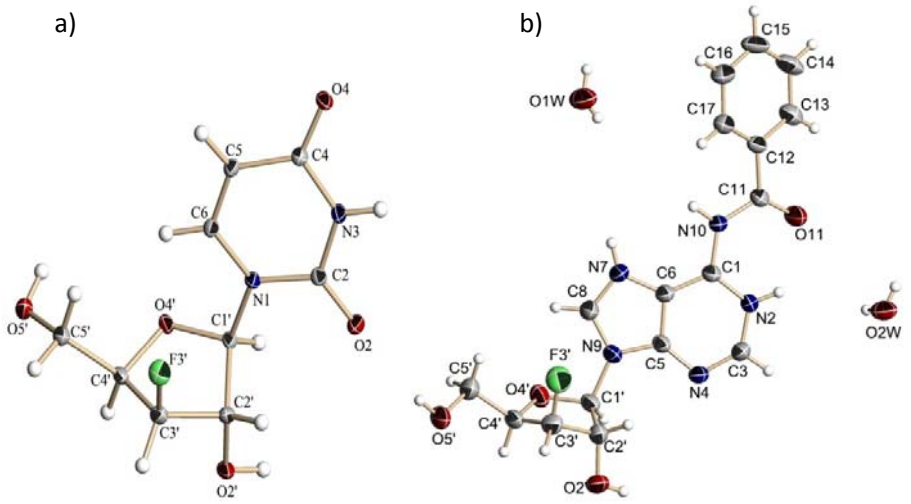

Figure 21. ORTEP drawing for nucleosides (a) 3′-deoxy-3′-fluoro-xylouridine ($^{X}U^{F}$) and (b) 3′-deoxy-3′-fluoro-xylo(N6-benzoyl)adenosine ($^{X}A^{F}$)

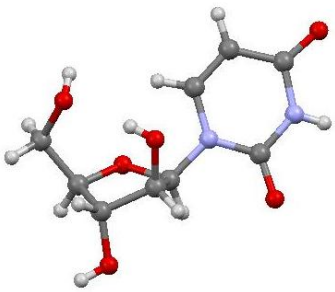

Figure 22. X-ray crystal structure of arabino-uridine ^{ara}U (Ball-and-stick model)[20]

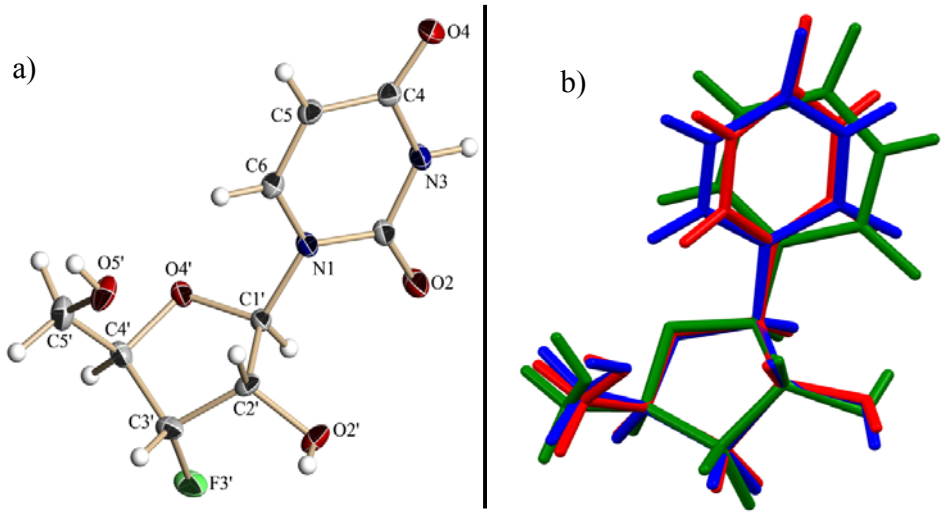

Figure 23. (a) ORTEP drawing for 3'-deoxy-3'-fluoro-ribouridine ($^{R}U^{F}$) Form A **(b)** X-Ray Crystal Structure Overlay of three forms of $^{R}U^{F}$ (Red = FormA, Blue = FormB, Green = FormC)

All the three forms of $^{R}U^{F}$ nucleoside are found in the South-type puckered sugar conformation with pseudorotation phase angle *P* = 171.2°, 185.7° and 126.8° and maximum puckering amplitude ν_{max} = 38.60°, 34.16° and 36.62°. The C4'-C5' (γ) bond in all three forms of $^{R}U^{F}$ nucleoside is found in the γ+ conformation with γ [O5'-C5'-C4'-C3'] = 50.5°, 42.0° and 49.9°. The uracil base is in *anti* conformation in all three forms of $^{R}U^{F}$ with glycosidic torsion angle [O4'-C1'-N1-C2] = -128.73°, -149.70° and -178.67°.

The nucleosides $^{X}U^{F}$ and $^{X}A^{F}$ are both found in North-type puckered sugar geometry. The pseudorotation phase angle (*P*) equals 0.88° and 14.64°, while maximum puckering amplitude ν_{max} is 37.59°, 36.69° respectively. The C4'-C5' bond in the $^{X}U^{F}$ nucleoside is found in the γt conformation while in the $^{X}A^{F}$ nucleoside, it is in γ- with γ [O5'-C5'-C4'-C3'] = -172.13° and -74.03° respectively. The uracil base in $^{X}U^{F}$ and *N*6-benzoyladenine base in $^{X}A^{F}$ nucleoside is in *anti* conformation. The glycosidic torsion angle for $^{X}U^{F}$ nucleoside (pyrimidine base) is [O4'-C1'-N1-C2] = -164.34° and for $^{X}A^{F}$ (purine base) is [O4'-C1'-N9-C4] = -168.56°.

The ^{ara}U nucleoside has the sugar puckered in S-type conformation with pseudorotation phase angle (*P*) equal to 153.93° and maximum puckering amplitude (ν_{max}) is 37.85°. In ^{ara}U nucleoside, the torsion angle γ [O5'-C5'-C4'-C3'] is 55.8° which indicates the γ+ conformation of C4'-C5' bond. The glycosidic torsion angle [O4'-C1'-N1-C2] = -148.39° indicates the *anti* orientation of uracil.

Table 7: Geometrical parameters obtained from X-ray crystal structure for modified nucleoside analogues

	3′-deoxy-3′-fluoro-ribouridine ($^{R}U^{F}$)			3′-deoxy-3′-fluoro-xylofuridine ($^{X}U^{F}$)	3′-deoxy-3′-fluoro- xylo-*N6*-benzoyl adenosine ($^{X}A^{F}$)^{Bz}	Arabino uridine (^{ara}U)
	FormA	**FormB**	**FormC**			
Torsion Angles (deg)						
ν_0 = [C4'-O4'-C1'-C2']	-18.12	-7.84	-35.54	11.58	2.72	-27.5
ν_1 = [O4'-C1'-C2'-C3']	34.95	26.27	35.24	-30.98	-24.27	38.1
ν_2 = [C1'-C2'-C3'-C4']	-38.14	-34.03	-21.94	37.52	35.50	-34.0
ν_3 = [C2'-C3'-C4'-O4']	28.46	30.32	2.00	-31.59	-34.96	19.4
ν_4 = [C3'-C4'-O4'-C1']	-6.57	-14.32	21.35	12.76	20.58	5.0
χ = **[O4'-C1'-N1-C2]**or χ = **[O4'-C1'-N9-C4]**	-128.73	-149.70	-178.67	-164.34	-168.56	-148.39
anti, χ = 180±90°. *Syn,* χ = 0±90°	*anti*	*anti*	*anti*	*anti*	*anti*	*anti*
γ = [O5'-C5'-C4'-C3']	50.5	42.0	49.9	-172.13	-74.03	55.8
γ+/ γt/ γ- =180°/60°/-60°	γ+	γ+	γ+	γt	γ-	γ+
Pseudorotation Parameters (deg)						
phase angle *(P)*	171.2	185.7	126.8	0.88	14.64	153.93
puckering amplitude(ν_{max})	38.60	34.16	36.62	37.59	36.69	37.85
S (P =180±90); N (P= 0±90)	S-type	S-type	S-type	N-type	N-type	S-type

4.4 Comparative results

Comparative results obtained from the Sum rule, X-ray crystallography and Matlab Pseudorotation GUI calculation are shown in Table 8. The conformational properties of the nucleoside $^{X}U^{F}$, $^{R}U^{F}$ and $^{X}A^{F}$ in solution and in the crystalline state show quite a consistent picture. However, in the ^{ara}U nucleoside, the X-ray crystallography results indicate S-type conformation of sugar ring in solid state while both Sum rule calculation as well as Matlab Pseudorotation calculations show that it is in ~ 60% N-type conformation in solution state. The N-type conformation of ^{ara}U was also indicated by the NOE study. $^{R}A^{F}$ and $^{L}A^{S}$ show S-type conformation in solution.

Table 8: Comparative result from Sum rule, X-ray crystallography and Matlab GUI Pseurot

Constrained values are indicated with an asterisk

Nucleoside analogue	%S= 100X($J_{1'2'}$-1)/6.9[15,16]	Matlab Pseudorotation GUI (285K)		X-ray crystal structure
$^{X}U^{F}$	% N=99.71 % S= 0.29	Conformer 1 P = 45.11 ν_{max} = 55.03 %N= 72.4	Conformer 2 P = 288.5 ν_{max} = 41* %S= 38.6	P = 0.88 ν_{max} =37.59 N-Type
$^{R}U^{F}$	% N=02.76 % S= 97.24	Conformer 1 P = 69.27 ν_{max} = 60 %N= 2.6	Conformer 2 P = 172.31 ν_{max} = 36.52 %S= 97.4	P = 171.2 ν_{max} =38.60 S-Type
$^{X}A^{F}$	% N=96.24 % S= 3.76	Conformer 1 P = 9.43 ν_{max} = 43.29 %N= 84.6	Conformer 2 P = 92.38 ν_{max} = 39.0* %S= 15.4	P = 14.64 ν_{m} =36.69 N-Type
$^{R}A^{F}$	% N=0 % S= 100	Conformer 1 P = -91.08 ν_{max} = 42.0* %N= 0.0	Conformer 2 P = 168.04 ν_{max} = 39.58 %S= 100	-----
^{ara}U	% N=52.2 % S= 47.8	Conformer 1 P = -44.9 ν_{max} = 40.8 %N= 59.8	Conformer 2 P = 84.29 ν_{max} = 38.5* %S= 40.2	P = 153.93 ν_{max} =37.85 S-Type
$^{L}A^{S}$	% N=20.29 % S= 79.71	Conformer 1 P = -10.10 ν_{max} = 51.92 %N= 23.2	Conformer 2 P = 146.54 ν_{max} = 48.0 %S= 76.8	-----

4.5 Summary and conclusion

1. NMR experiments were carried out at five different temperatures and the chemical shifts of the furanose ring protons of $^{R}U^{F}$-, $^{R}A^{F}$-, $^{X}U^{F}$-, $^{X}A^{F}$-, $^{L}A^{S}$- and ^{ara}U-nucleosides were assigned and $^{3}J_{HH}$ scalar coupling constants were determined by a combination of 1D proton and 2D COSY NMR experiments.
2. *Anti* conformation of nucleobases and S/N-type of furanose ring conformation in $^{X}U^{F}$, $^{R}U^{F}$, $^{X}A^{F}$, $^{R}A^{F}$ and ^{ara}U nucleosides was confirmed by NOESY NMR experiments as well as X-ray crystallography study.
3. The possible conformation of the furanose ring of $^{R}U^{F}$, $^{R}A^{F}$, $^{X}U^{F}$, $^{X}A^{F}$, $^{L}A^{S}$ and ^{ara}U nucleosides was determined by comparative *P* and ν_{max} values obtained from Matlab Pseudorotation GUI program as well as by X-ray crystallography study.
4. All the experimental results show that the sugar rings of $^{R}U^{F}$ and $^{R}A^{F}$ nucleosides are frozen in S-type conformation while the sugar rings of $^{X}U^{F}$ and $^{X}A^{F}$ nucleosides are frozen in N-type conformation.
5. In $^{L}A^{S}$ nucleoside, the conformation of the sugar ring is locked in S-type.
6. In case of ^{ara}U, the sugar ring is in S-type conformation in solid state while it is 60% N-type conformation in solution state.

Conclusion

The configuration of fluorine at 3′ position in the nucleoside affects the furanose ring conformation. The 3′ ribofluoro and 3'xylofluoro substituents are responsible for frozen S-type and frozen N-type conformations of furanose ring respectively in solid as well as solution state.

4.6 Supporting information

4.6.1 Matlab Pseudorotation textual output

Compound $^{X}U^{F}$

```
//////////////////////////////////////////////////////////////
  START Pseudorotational calculation
//////////////////////////////////////////////////////////////
Optimization terminated: Magnitude of directional derivative in search
 direction less than 2*options.TolFun and maximum constraint violation
  is less than options.TolCon.
Active inequalities (to within options.TolCon = 1e-006):
  lower      upper     ineqlin   ineqnonlin
                15
```

```
------------------------------------------------------------
 Optimized parameters
------------------------------------------------------------
  Conformation 1
   P     :  45.117
   Phi_m :  55.030

  Conformation 2
   P     : 288.555
   Phi_m :  41.000

  Temperature Coefficients
   %Conformation1  :  72.442
   %Conformation1  :  72.806
   %Conformation1  :  73.390
   %Conformation1  :  99.606
   %Conformation1  : 100.000
 ------------------------------------------------------------
  Endocyclic torsion angles
------------------------------------------------------------
          Conf.1       Conf.2
  Phi0:    38.833       13.047
  Phi1:   -54.335       12.292
  Phi2:    49.083      -32.935
  Phi3:   -25.083       40.998
  Phi4:    -8.498      -33.401
------------------------------------------------------------
  Final couplings
------------------------------------------------------------
  Temperature 1:
   ------------------------------------
   Conf1  Conf2   Avg.   Exp.  Diff.
   ------------------------------------
    1.67   0.65   1.39   1.00   0.39
    1.46   0.23   1.12   1.00   0.12
    1.30   6.94   2.86   2.76   0.10
   ------------------------------------
   RMSD :     0.24 Hz
```

```
Temperature 2:
   ------------------------------------
   Conf1  Conf2   Avg.   Exp.  Diff.
   ------------------------------------
    1.67   0.65   1.39   1.10   0.29
    1.46   0.23   1.13   1.02   0.11
    1.30   6.94   2.84   2.76   0.08
   ------------------------------------
   RMSD :     0.18 Hz

  Temperature 3:
   ------------------------------------
   Conf1  Conf2   Avg.   Exp.  Diff.
   ------------------------------------
    1.67   0.65   1.40   1.20   0.20
    1.46   0.23   1.13   1.10   0.03
    1.30   6.94   2.80   2.76   0.04
   ------------------------------------
   RMSD :     0.12 Hz

  Temperature 4:
   ------------------------------------
   Conf1  Conf2   Avg.   Exp.  Diff.
   ------------------------------------
    1.67   0.65   1.66   1.50   0.16
    1.46   0.23   1.46   1.25   0.21
    1.30   6.94   1.32   1.25   0.07
   ------------------------------------
   RMSD :     0.16 Hz
  Temperature 5:
   ------------------------------------
   Conf1  Conf2   Avg.   Exp.  Diff.
   ------------------------------------
    1.67   0.65   1.67   2.25  -0.58
    1.46   0.23   1.46   1.51  -0.05
    1.30   6.94   1.30   1.25   0.05
   ------------------------------------
   RMSD :     0.34 Hz
```

ERROR ANALYSIS
---

i	P1/dPi	dP2/dPi	dP3/dPi	dP4/dPi	dP5/dPi	dP6/dPi	dP7/dPi	dP8/dPi	dRMSD/dPi
1	1.000	1.435	-0.123	-0.775	-0.765	-0.759	-1.027	-0.461	0.031
2	0.454	1.000	0.701	-0.591	-0.589	-0.586	-0.766	-0.231	0.012
3	-0.010	0.014	1.000	-0.051	-0.052	-0.057	-0.017	0.000	0.000
4	-0.167	-0.349	-0.723	1.000	0.237	0.234	0.079	0.000	0.009
5	-0.164	-0.348	-0.722	0.235	1.000	0.234	0.079	0.000	0.009
6	-0.164	-0.348	-0.682	0.235	0.235	1.000	0.079	0.000	0.009
7	0.000	0.000	0.000	0.000	0.000	0.000	0.539	0.000	0.004
8	0.000	0.000	0.000	0.000	0.000	0.000	0.000	0.500	-0.004

i	dP1/dCi	dP2/dCi	dP3/dCi	dP4/dCi	dP5/dCi	dP6/dCi	dP7/dCi	dP8/dCi	dRMSD/dCi
1	11.274	9.939	-7.773	-5.504	-5.300	-5.212	-8.516	-1.719	-0.045
2	0.217	9.939	-30.716	-6.565	-6.683	-6.919	-9.615	-5.233	-0.009
3	1.224	0.760	-10.761	-16.647	-16.615	-16.669	-17.114	-11.563	-0.021

RMSD : 0.22 Hz
Total time : 2.46 s

Compound $^{R}U^{F}$

//
START Pseudorotational calculation
//
Optimization terminated: Magnitude of directional derivative in search
direction less than 2*options.TolFun and maximum constraint violation
is less than options.TolCon.
Active inequalities (to within options.TolCon = 1e-006):
lower upper ineqlin ineqnonlin
7

Optimized parameters

Conformation 1
P : 172.311
Phi_m : 36.523

Conformation 2
P : 69.272
Phi_m : 60.000

Temperature Coefficients
%Conformation1 : 97.433
%Conformation1 : 96.978
%Conformation1 : 96.432
%Conformation1 : 86.697
%Conformation1 : 83.258

Endocyclic torsion angles

	Conf.1	Conf.2
Phi0:	-36.195	21.236
Phi1:	26.410	-50.165
Phi2:	-6.538	59.932
Phi3:	-15.832	-46.807
Phi4:	32.155	15.804

Final couplings

Temperature 1:

Conf1	Conf2	Avg.	Exp.	Diff.
7.76	5.13	7.69	7.78	-0.09
4.61	6.10	4.65	4.64	0.01
0.55	9.26	0.77	0.80	-0.03

RMSD : 0.05 Hz

Temperature 2:

Conf1	Conf2	Avg.	Exp.	Diff.
7.76	5.13	7.68	7.65	0.03
4.61	6.10	4.66	4.67	-0.01
0.55	9.26	0.81	0.80	0.01

RMSD : 0.02 Hz

Temperature 3:

Conf1	Conf2	Avg.	Exp.	Diff.
7.76	5.13	7.67	7.53	0.14
4.61	6.10	4.66	4.77	-0.11
0.55	9.26	0.86	0.80	0.06

RMSD : 0.11 Hz

Temperature 4:

Conf1	Conf2	Avg.	Exp.	Diff.
7.76	5.13	7.41	7.53	-0.12
4.61	6.10	4.81	4.77	0.04
0.55	9.26	1.71	1.75	-0.04

RMSD : 0.08 Hz

Temperature 5:

Conf1	Conf2	Avg.	Exp.	Diff.
7.76	5.13	7.32	7.28	0.04
4.61	6.10	4.86	4.77	0.09
0.55	9.26	2.01	2.01	-0.00

RMSD : 0.06 Hz

ERROR ANALYSIS

---

i	dP1/dPi	dP2/dPi	dP3/dPi	dP4/dPi	dP5/dPi	dP6/dPi	dP7/dPi	dP8/dPi	dP9/dPi	dRMSD/dPi
1	1.000	-0.142	1.434	0.000	-0.011	0.006	0.015	-0.086	-0.076	0.009
2	-2.335	1.000	-0.374	0.000	0.307	0.307	0.313	0.291	0.280	0.126
3	0.346	-0.021	1.000	0.000	-0.009	0.002	0.008	-0.062	-0.057	0.002
4	0.000	0.000	0.000	0.500	0.000	0.000	0.000	0.000	0.000	-0.001
5	0.000	0.000	0.000	0.000	0.757	0.000	0.000	0.000	0.000	0.045
6	0.000	0.000	0.000	0.000	0.000	0.802	0.000	0.000	0.000	0.049
7	0.000	0.000	0.000	0.000	0.000	0.000	0.857	0.000	0.000	0.054
8	-0.772	0.135	-2.145	0.000	0.035	0.020	0.008	1.000	0.157	0.064
9	-0.819	0.136	-2.311	0.000	0.036	0.016	0.008	0.168	1.000	0.064

i	dP1/dCi	dP2/dCi	dP3/dCi	dP4/dCi	dP5/dCi	dP6/dCi	dP7/dCi	dP8/dCi	dP9/dCi	dRMSD/dCi
1	-200.460	-46.953	188.050	-44.278	-190.390	-188.522	-186.275	-147.188	-133.349	0.003
2	-30.242	8.203	3.135	0.000	5.135	5.640	5.762	4.456	4.171	-0.006
3	-204.912	-46.953	205.347	-44.665	-178.181	-176.336	-174.106	-135.291	-121.542	0.003

RMSD : 0.07 Hz
Total time : 2.75 s

Compound $^{X}A^{F}$

//
START Pseudorotational calculation
//
Optimization terminated: Magnitude of directional derivative in search
direction less than 2*options.TolFun and maximum constraint violation
is less than options.TolCon.
No active inequalities

Optimized parameters

Conformation 1
P : 9.436
Phi_m : 43.198

Conformation 2
P : 92.382
Phi_m : 39.000

Temperature Coefficients
%Conformation1 : 84.662
%Conformation1 : 77.173
%Conformation1 : 73.503
%Conformation1 : 73.500
%Conformation1 : 73.510

Endocyclic torsion angles

	Conf.1	Conf.2
Phi0:	42.614	-1.621
Phi1:	-38.638	-21.593
Phi2:	19.904	36.558
Phi3:	6.433	-37.560
Phi4:	-30.313	24.215

Final couplings

Temperature 1:

Conf1	Conf2	Avg.	Exp.	Diff.
0.61	6.53	1.52	1.47	0.05
1.87	1.17	1.77	1.71	0.06
2.76	4.56	3.04	3.18	-0.14

RMSD : 0.09 Hz

Temperature 2:

Conf1	Conf2	Avg.	Exp.	Diff.
0.61	6.53	1.96	1.96	0.00
1.87	1.17	1.71	1.71	0.00
2.76	4.56	3.17	3.18	-0.01

RMSD : 0.01 Hz

Temperature 3:

Conf1	Conf2	Avg.	Exp.	Diff.
0.61	6.53	2.18	2.20	-0.02
1.87	1.17	1.69	1.71	-0.02
2.76	4.56	3.24	3.18	0.06

RMSD : 0.04 Hz

Temperature 4:

Conf1	Conf2	Avg.	Exp.	Diff.
0.61	6.53	2.18	2.20	-0.02
1.87	1.17	1.69	1.71	-0.02
2.76	4.56	3.24	3.18	0.06

RMSD : 0.04 Hz

Temperature 5:

Conf1	Conf2	Avg.	Exp.	Diff.
0.61	6.53	2.18	2.20	-0.02
1.87	1.17	1.69	1.71	-0.02
2.76	4.56	3.24	3.18	0.06

RMSD : 0.04 Hz

ERROR ANALYSIS
---

i	dP1/dPi	dP2/dPi	dP3/dPi	dP4/dPi	dP5/dPi	dP6/dPi	dP7/dPi	dP8/dPi	dRMSD/dPi
1	1.000	-0.182	1.437	0.152	0.243	0.289	0.289	0.287	0.001
2	-3.602	1.000	-5.338	-0.715	-1.078	-1.256	-1.256	-1.258	0.023
3	0.650	-0.128	1.000	0.108	0.172	0.204	0.205	0.203	0.001
4	3.724	-0.630	6.348	1.000	1.011	1.188	1.188	1.187	0.026
5	3.030	-0.526	5.000	0.523	1.000	0.958	0.958	0.957	0.015
6	2.718	-0.479	4.423	0.466	0.727	1.000	0.859	0.855	0.011
7	2.716	-0.478	4.420	0.466	0.727	0.857	1.000	0.854	0.011
8	2.715	-0.478	4.420	0.465	0.726	0.855	0.856	1.000	0.012

i	dP1/dCi	dP2/dCi	dP3/dCi	dP4/dCi	dP5/dCi	dP6/dCi	dP7/dCi	dP8/dCi	dRMSD/dCi
1	7.715	2.271	1.334	-16.896	-16.368	-16.115	-16.098	-16.125	0.006
2	-15.144	7.106	11.117	5.466	6.578	7.123	7.127	7.110	0.005
3	-27.490	-1.536	1.918	4.311	3.473	3.065	3.070	3.054	-0.015

RMSD : 0.05 Hz
Total time : 2.70 s

Compound $^{R}A^{F}$

//
START Pseudorotational calculation
//
Optimization terminated: Magnitude of directional derivative in search
direction less than 2*options.TolFun and maximum constraint violation
is less than options.TolCon.
Active inequalities (to within options.TolCon = 1e-006):
lower upper ineqlin ineqnonlin
7

Optimized parameters

Conformation 1
P : 168.045
Phi_m : 39.589
Conformation 2
P : -91.082
Phi_m : 42.000

Temperature Coefficients
%Conformation1 : 100.000
%Conformation1 : 96.996
%Conformation1 : 96.115
%Conformation1 : 93.094
%Conformation1 : 92.217

Endocyclic torsion angles

	Conf.1	Conf.2
Phi0:	-38.730	-0.793
Phi1:	26.513	25.324
Phi2:	-4.169	-40.182
Phi3:	-19.767	39.692
Phi4:	36.153	-24.041

Final couplings

Temperature 1:

Conf1	Conf2	Avg.	Exp.	Diff.
8.31	0.67	8.31	8.28	0.03
4.37	6.60	4.37	4.27	0.10
0.55	0.55	0.55	0.50	0.05

RMSD : 0.07 Hz

Temperature 2:

Conf1	Conf2	Avg.	Exp.	Diff.
8.31	0.67	8.08	8.03	0.05
4.37	6.60	4.44	4.27	0.17
0.55	0.55	0.55	0.50	0.05

RMSD : 0.10 Hz

Temperature 3:

Conf1	Conf2	Avg.	Exp.	Diff.
8.31	0.67	8.01	8.03	-0.02
4.37	6.60	4.46	4.52	-0.06
0.55	0.55	0.55	0.50	0.05

RMSD : 0.05 Hz

Temperature 4:

Conf1	Conf2	Avg.	Exp.	Diff.
8.31	0.67	7.78	7.78	0.00
4.37	6.60	4.52	4.52	0.00
0.55	0.55	0.55	0.50	0.05

RMSD : 0.03 Hz

Temperature 5:

Conf1	Conf2	Avg.	Exp.	Diff.
8.31	0.67	7.71	7.78	-0.07
4.37	6.60	4.54	4.77	-0.23
0.55	0.55	0.55	0.50	0.05

RMSD : 0.14 Hz

ERROR ANALYSIS

---

i	dP1/dPi	dP2/dPi	dP3/dPi	dP4/dPi	dP5/dPi	dP6/dPi	dP7/dPi	dP8/dPi	dRMSD/dPi
1	1.000	-0.045	0.003	0.000	0.291	0.283	0.276	0.268	0.012
2	-2.107	1.000	-0.298	-1.251	-1.216	-1.206	-1.168	-1.159	0.002
3	0.006	-0.000	1.000	-0.001	0.005	0.006	0.009	0.009	0.000
4	0.000	0.000	0.000	0.500	0.000	0.000	0.000	0.000	0.014
5	0.000	0.000	0.000	0.000	0.800	0.000	0.000	0.000	0.033
6	0.000	0.000	0.000	0.000	0.000	0.888	0.000	0.000	0.039
7	0.746	-0.312	0.964	0.000	0.496	0.492	1.000	0.476	0.027
8	0.732	-0.315	1.213	0.000	0.496	0.492	0.481	1.000	0.027

i	dP1/dCi	dP2/dCi	dP3/dCi	dP4/dCi	dP5/dCi	dP6/dCi	dP7/dCi	dP8/dCi	dRMSD/dCi
1	-17.068	3.815	-0.176	0.000	0.929	1.104	1.411	1.581	0.011
2	-18.777	-5.973	0.116	0.000	1.613	1.857	1.614	1.902	0.057
3	-61.508	39.365	8.951	-34.933	-33.862	-33.545	-32.436	-32.125	-0.004

RMSD : 0.09 Hz
Total time : 2.51 s

Compound ^{ara}U

//
START Pseudorotational calculation
//
Optimization terminated: Magnitude of directional derivative in search
direction less than 2*options.TolFun and maximum constraint violation
is less than options.TolCon.
No active inequalities

Optimized parameters

Conformation 1
P : -44.999
Phi_m : 40.810

Conformation 2
P : 84.291
Phi_m : 38.500

Temperature Coefficients
%Conformation1 : 59.897
%Conformation1 : 59.897
%Conformation1 : 67.467
%Conformation1 : 68.060
%Conformation1 : 71.207

Endocyclic torsion angles

	Conf.1	Conf.2
Phi0:	28.525	4.369
Phi1:	-5.841	-26.073
Phi2:	-19.073	37.818
Phi3:	36.702	-35.117
Phi4:	-40.313	19.003

Final couplings

Temperature 1:

Conf1	Conf2	Avg.	Exp.	Diff.
4.47	6.21	5.17	5.02	0.15
6.56	2.12	4.78	4.77	0.01
4.04	7.58	5.46	5.52	-0.06

RMSD : 0.09 Hz

Temperature 2:

Conf1	Conf2	Avg.	Exp.	Diff.
4.47	6.21	5.17	5.02	0.15
6.56	2.12	4.78	4.77	0.01
4.04	7.58	5.46	5.52	-0.06

RMSD : 0.09 Hz

Temperature 3:

Conf1	Conf2	Avg.	Exp.	Diff.
4.47	6.21	5.04	5.27	-0.23
6.56	2.12	5.12	5.27	-0.15
4.04	7.58	5.19	5.27	-0.08

RMSD : 0.17 Hz

Temperature 4:

Conf1	Conf2	Avg.	Exp.	Diff.
4.47	6.21	5.03	5.02	0.01
6.56	2.12	5.14	5.02	0.12
4.04	7.58	5.17	5.02	0.15

RMSD : 0.11 Hz

Temperature 5:

Conf1	Conf2	Avg.	Exp.	Diff.
4.47	6.21	4.97	5.02	-0.05
6.56	2.12	5.28	5.27	0.01
4.04	7.58	5.06	5.02	0.04

RMSD : 0.03 Hz

ERROR ANALYSIS
---

i	dP1/dPi	dP2/dPi	dP3/dPi	dP4/dPi	dP5/dPi	dP6/dPi	dP7/dPi	dP8/dPi	dRMSD/dPi
1	1.000	-0.579	1.487	0.473	0.473	0.596	0.396	0.480	0.002
2	-1.382	1.000	-1.705	-0.708	-0.708	-0.932	-0.716	-0.839	0.003
3	0.654	-0.376	1.000	0.307	0.307	0.393	0.260	0.317	0.001
4	1.469	-0.894	2.199	1.000	0.731	0.906	0.612	0.730	0.006
5	1.469	-0.894	2.199	0.731	1.000	0.906	0.612	0.730	0.006
6	1.298	-0.798	1.921	0.648	0.648	1.000	0.550	0.656	0.004
7	1.386	-0.911	1.970	0.729	0.729	0.905	1.000	0.750	0.008
8	1.355	-0.869	1.954	0.698	0.698	0.869	0.605	1.000	0.006

i	dP1/dCi	dP2/dCi	dP3/dCi	dP4/dCi	dP5/dCi	dP6/dCi	dP7/dCi	dP8/dCi	dRMSD/dCi
1	119.276	-8.186	167.818	-4.187	-4.165	-16.563	-24.927	-28.242	0.069
2	97.533	5.623	165.830	-8.646	-8.657	-20.992	-28.501	-31.815	0.071
3	1.889	6.060	-4.982	-16.319	-16.352	-17.708	-17.574	-17.908	0.006

RMSD : 0.11 Hz
Total time : 1.16 s

Compound $^{L}A^{S}$

//
START Pseudorotational calculation
//
Optimization terminated: Magnitude of directional derivative in search
direction less than 2*options.TolFun and maximum constraint violation
is less than options.TolCon.
No active inequalities

Optimized parameters

Conformation 1
P : -10.101
Phi_m : 51.927
Conformation 2
P : 146.543
Phi_m : 48.000
Temperature Coefficients
%Conformation1 : 23.263

Endocyclic torsion angles

	Conf.1	Conf.2
Phi0:	51.122	-40.046
Phi1:	-36.006	16.844
Phi2:	7.136	12.793
Phi3:	24.459	-37.543
Phi4:	-46.711	47.953

Final couplings

Temperature 1:

Conf1	Conf2	Avg.	Exp.	Diff.
1.29	9.55	7.63	7.63	-0.00
3.42	4.53	4.27	4.27	0.00

RMSD : 0.00 Hz

ERROR ANALYSIS
---

i	dP1/dPi	dP2/dPi	dP3/dPi	dP4/dPi	dRMSD/dPi
1	1.000	-0.007	-0.063	-0.046	0.000
2	-0.214	1.000	-0.748	0.130	0.000
3	-0.383	-1.288	1.000	-0.130	0.000
4	-8.462	2.818	-0.132	1.000	0.059

i	dP1/dCi	dP2/dCi	dP3/dCi	dP4/dCi	dRMSD/dCi
1	5.912	-20.891	13.922	-15.134	0.000
2	9.506	-46.957	-0.555	-3.261	0.000

RMSD : 0.00 Hz
Total time : 0.51 s

4.6.2 Crystal data:

Crystal data of $^{R}U^{F}$

X-ray intensity data measurements of compound $^{R}U^{F}$ were carried out on a Bruker SMART APEX II CCD diffractometer with graphite-monochromatized (MoK_{α}= 0.71073Å) radiation at 100 (2) K. The X-ray generator was operated at 50 kV and 30 mA. A preliminary set of cell constants and an orientation matrix were calculated from 694 reflection harvested from three sets of 90 frames. Data were collected with ω scan width of 0.5° at different settings of φ and 2θ with a frame time of 10 sec keeping the sample-to-detector distance fixed at 5.00 cm. The X-ray data collection was monitored by APEX2 program (Bruker, 2006).[22]

$C_9H_{11}FN_2O_5$, M = 246.20, colorless plate, 0.59 x 0.17 x 0.10 mm^3, monoclinic, space group $P2_1$, a = 15.4056(4), b = 6.8529(2), c = 15.8005(4) Å, β = 116.0190(10)°, V = 1499.04(7) $Å^3$, Z = 6, T = 100(2) K, $2\theta_{max}$=56.00°, D_{calc} (g cm^{-3}) = 1.636, $F(000)$ = 768, μ (mm^{-1}) = 0.146, 24993 reflections collected, 7180 unique reflections (R_{int}=0.0295), 6731 observed ($I > 2\sigma(I)$) reflections, multi-scan absorption correction, T_{min} = 0.919, T_{max} = 0.986, 484 refined parameters, S = 1.067, $R1$=0.0342, $wR2$=0.0861 (all data R = 0.0376, $wR2$ = 0.0882), maximum and minimum residual electron densities; $\Delta\rho_{max}$ = 0.30, $\Delta\rho_{min}$= -0.22 ($eÅ^{-3}$). The asymmetric unit contains three sysmmetry independent molecules. Structure overlay of all the three symmetry independent molecules shows major conformational difference at the orientation of uracil moiety. The OH group at C2′ and CH_2OH group at C4′ also showed noticable difference. All the data were corrected for Lorentzian, polarization and absorption effects using SAINT and SADABS programs (Bruker, 2006). SHELX-97 was used for structure solution and full matrix least-squares refinement on F^2.[23] Hydroxyl H-atoms in compounds $^{X}U^{F}$ were located in difference Fourier map and refined isotropically. Other H-atoms were placed in geometrically idealized position and constrained to ride on their parent atoms.

Crystal data of $^{X}U^{F}$

X-ray intensity data measurements of compound $^{X}U^{F}$ were carried out on a Bruker SMART APEX II CCD diffractometer with graphite-monochromatized (MoK_{α}=

0.71073Å) radiation at 100 (2) K. The X-ray generator was operated at 50 kV and 30 mA. A preliminary set of cell constants and an orientation matrix were calculated from 155 reflections harvested from three sets of 36 frames. Data were collected with ω scan width of 0.5° at different settings of φ and 2θ with a frame time of 5 sec keeping the sample-to-detector distance fixed at 5.00 cm. The X-ray data collection was monitored by APEX2 program (Bruker, 2006).

$C_9H_{11}FN_2O_5$, M = 246.20, colorless plate, 0.58 x 0.30 x 0.22 mm^3, monoclinic, space group $P2_1$, a = 6.3007(3), b = 7.3372(3), c = 10.8989(4) Å, β = 92.277(2)°, V = 503.45(4) $Å^3$, Z = 2, T = 100(2) K, $2\theta_{max}$=56.00°, D_{calc} (g cm^{-3}) = 1.624, $F(000)$ = 256, μ (mm^{-1}) = 0.144, 10593 reflections collected, 2440 unique reflections (R_{int}=0.0175), 2398 observed ($I > 2\sigma(I)$) reflections, multi-scan absorption correction, T_{min} = 0.921, T_{max} = 0.969, 162 refined parameters, S = 1.054, $R1$=0.0239, $wR2$=0.0643 (all data R = 0.0242, $wR2$ = 0.0645), maximum and minimum residual electron densities; $\Delta\rho_{max}$ = 0.27, $\Delta\rho_{min}$= -0.17 ($eÅ^{-3}$). All the data were corrected for Lorentzian, polarization and absorption effects using SAINT and SADABS programs (Bruker, 2006). SHELX-97 was used for structure solution and full matrix least-squares refinement on F^2. Hydroxyl H-atoms in compounds $^{X}U^{F}$ were located in difference Fourier map and refined isotropically. Other H-atoms were placed in geometrically idealized position and constrained to ride on their parent atoms.

Crystal data of $^{X}A^{F}$

X-ray intensity data measurements of compound was carried out on a Bruker SMART APEX II CCD diffractometer with graphite-monochromatized (MoK_α= 0.71073Å) radiation at 297 (2) K. The X-ray generator was operated at 50 kV and 30 mA. A preliminary set of cell constants and an orientation matrix were calculated from the reflections harvested from three sets of 36 frames. Data were collected with ω scan width of 0.5° at different settings of φ and 2θ with a frame time of 10 sec keeping the sample-to-detector distance fixed at 5.00 cm. A total of 1323 frames were collected in ~ 5hrs. The X-ray data collection was monitored by APEX2 program (Bruker, 2006).

C_{17} H18 F N5 O4, 2(H2O), M = 411.40, colorless plate, 0.78 x 0.20 x 0.06 mm^3, monoclinic, space group $P2_1$, a = 11.1031(13), b = 7.0529(10), c = 12.0406(15) Å, β =

92.635(7)°, V = 941.9(2) Å^3, Z = 2, T = 297(2) K, $2\theta_{max}$ = 56.00°, D_{calc} (g cm^{-3}) = 1.451, $F(000)$ = 432, μ (mm^{-1}) = 0.118, 8785 reflections collected, 4201 unique reflections (R_{int}=0.0389), 3612 observed ($I > 2\sigma(I)$) reflections, multi-scan absorption correction, T_{min} = 0.914, T_{max} = 0.993, 280 refined parameters, S = 1.048, $R1$=0.0422, $wR2$=0.1083 (all data R = 0.0508, $wR2$ = 0.1147), maximum and minimum residual electron densities; $\Delta\rho_{max}$ = 0.23, $\Delta\rho_{min}$= -0.37 (eÅ^{-3}). The asymmetric unit contains two molecules of water having full occuancy along with the host molecule.

All the data were corrected for Lorentzian, polarization and absorption effects using SAINT and SADABS programs (Bruker, 2006). SHELX-97 was used for structure solution and full matrix least-squares refinement on F^2. All H-atoms of the host molecule were placed in geometrically idealized position and constrained to ride on their parent atoms except the H-atoms bonded to water molecules which were located in difference Fourier map and refined isotropically.

4.7 Appendix C

Overlay of ^{1}H NMR Spectrum for $^{X}U^{F}$, $^{R}U^{F}$, $^{X}A^{F}$, $^{R}A^{F}$ and ^{ara}U nucleosides for five different temperatures (400MHz ; solvent- D_2O)

Compounds	**Page Number**
$^{X}U^{F}$ nucleoside:	250
$^{R}U^{F}$ nucleoside:	250
$^{X}A^{F}$ nucleoside:	251
$^{R}A^{F}$ nucleoside:	251
^{ara}U nucleoside:	252
$^{L}A^{S}$ nucleoside: ^{1}H NMR (296K; 500MHz ; CD_3OD)	252

$^{X}U^{F}$ nucleoside

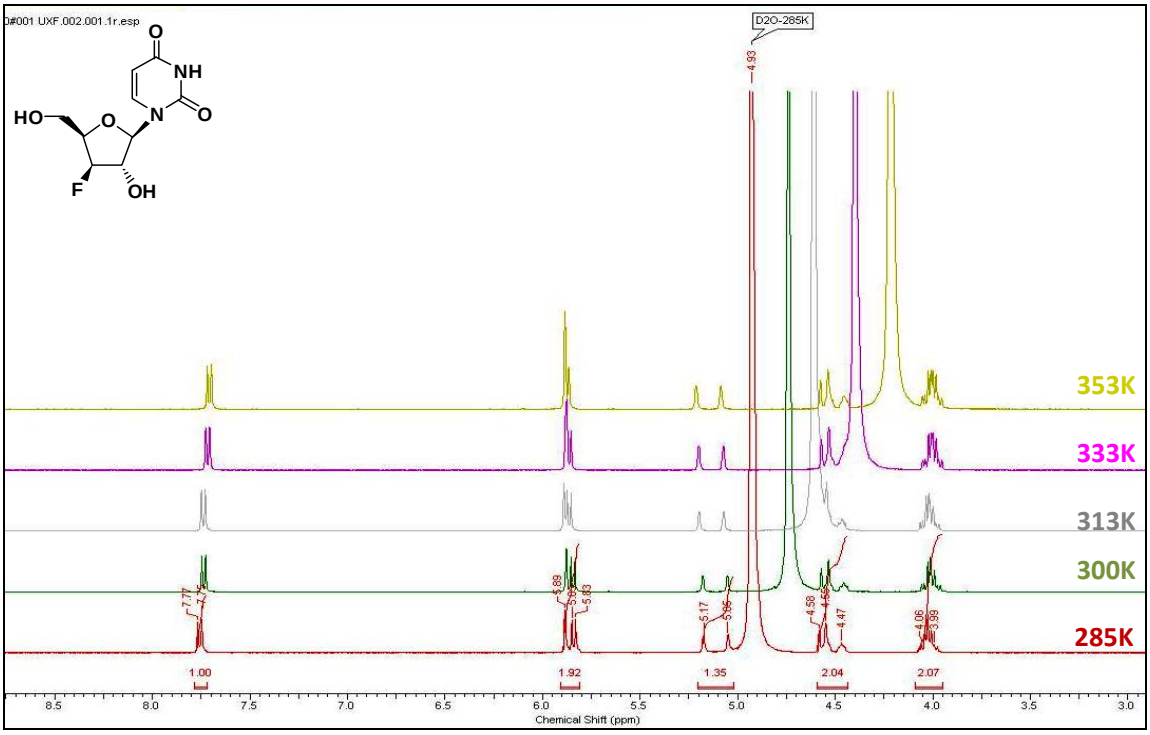

$^{R}U^{F}$ nucleoside

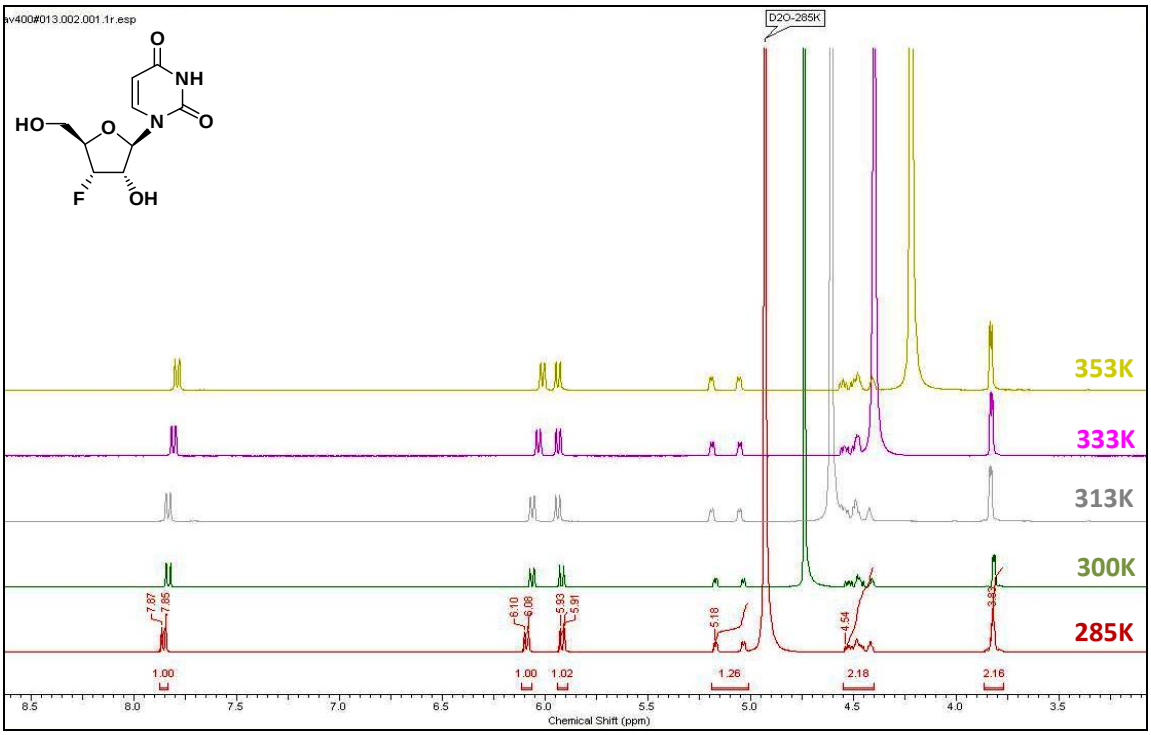

$^{X}A^{F}$ nucleoside

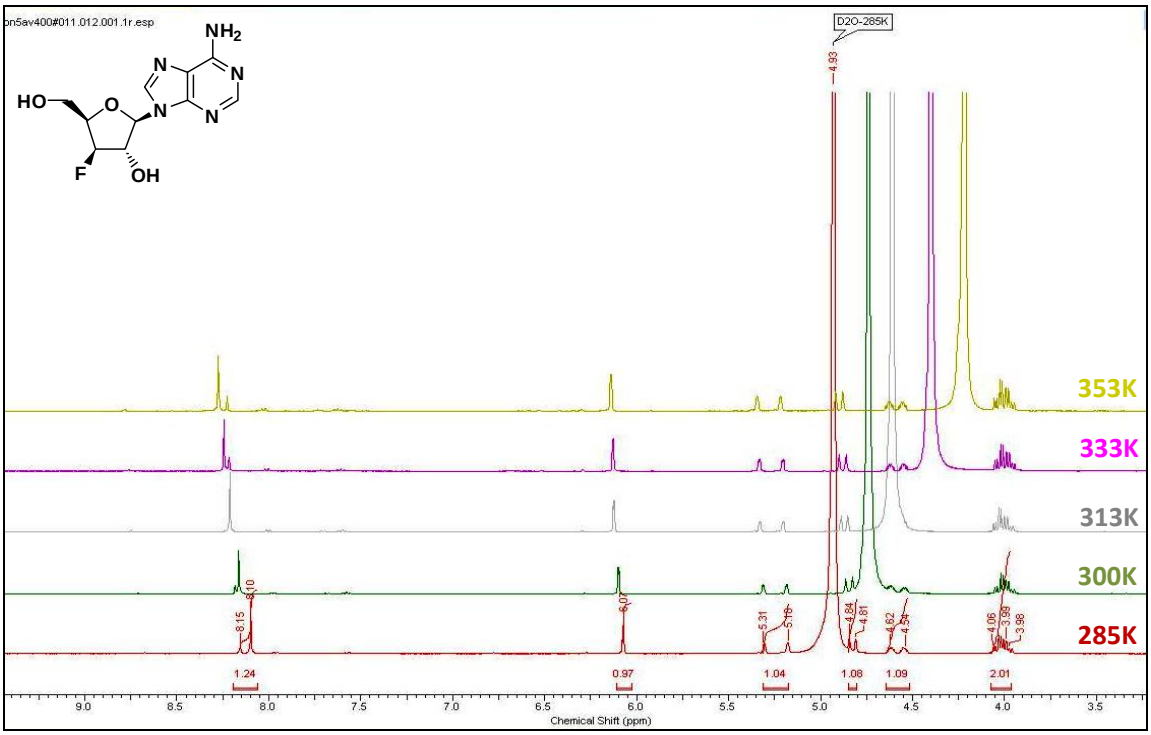

$^{R}A^{F}$ nucleoside

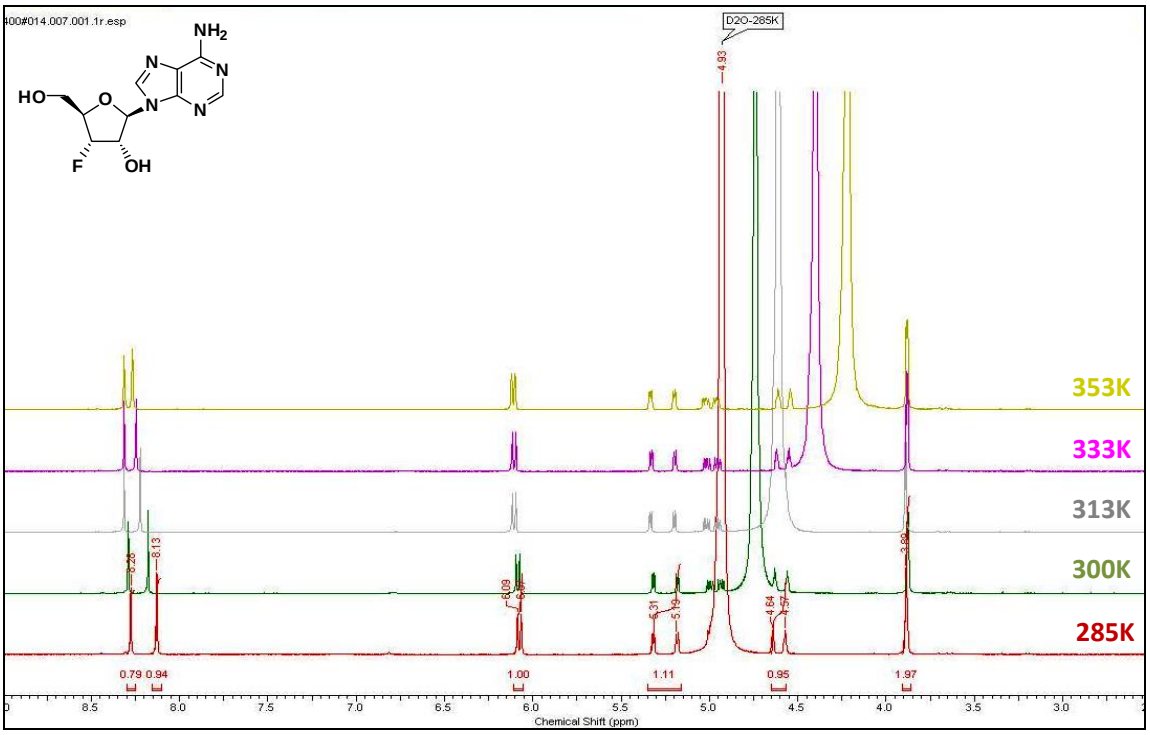

^{ara}U nucleoside

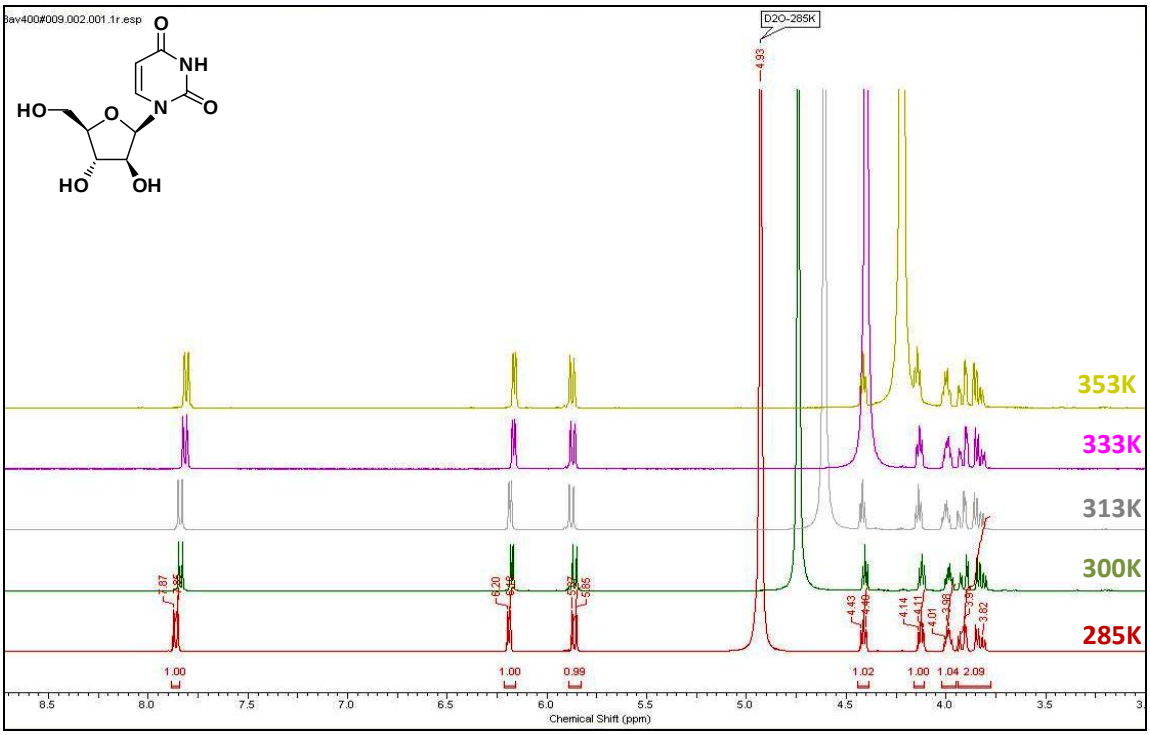

$^{L}A^{S}$ nucleoside

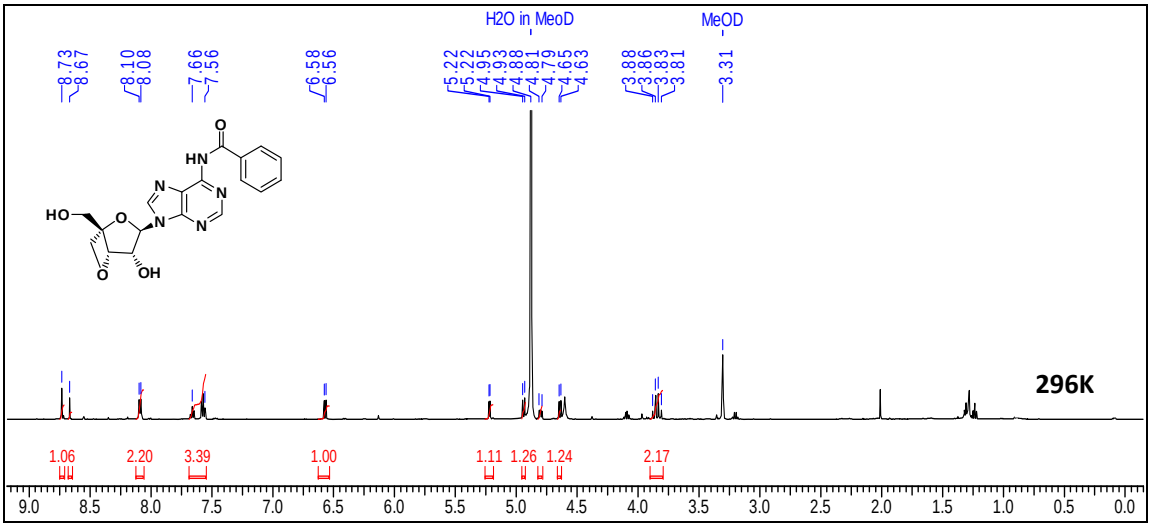

4.8 Reference:

1. (a) Saenger W.; Principles of Nucleic Acid Structure, Springer- Verlag; New York,. **1984**. (b) Lescrinier, E.; Froeyen, M.; Herdewijn, P., Difference in conformational diversity between nucleic acids with a six-membered 'sugar' unit and natural 'furanose' nucleic acids. *Nucleic Acids Research* **2003,** 31, (12), 2975-2989.
2. Sundaralingam, M. J., Stereochemistry of nucleic acids and their constituents. IV. Allowed and preferred conformations of nucleosides, nucleoside mono-, di-, tri-, tetraphosphates, nucleic acids and polynucleotides. *Biopolymers* **1969**, *7*, 821-860.
3. Plavec, J.; Thibaudeau, C.; Chattopadhyaya, J., How does the 2'-hydroxy group drive the pseudorotational equilibrium in nucleoside and nucleotide by the tuning of the 3'-gauche effect. *Journal of the American Chemical Society* **1994,** 116, (15), 6558-6560.
4. Plavec, J.; Tong, W. M.; Chattopadhyaya, J., How do the gauche and anomeric effects drive the pseudorotational equilibrium of the pentofuranose moiety of nucleosides. *Journal of the American Chemical Society* **1993,** 115, (21), 9734-9746.
5. Altona, C.; Sundaralingam, M. J., Conformational Analysis of the Sugar Ring in Nucleosides and Nucleotides. A New Description Using the Concept of Pseudorotation' *Journal of the American chemical Society* **1972,** 94, 8205-1822.
6. Kilpatrick, J. E.; Pitzer, K. S.; Spitzer, R., The thermodynamics and molecular structure of cyclopentane. *Journal of the American Chemical Society* **1947,** 69, (10), 2483-2488.
7. Hall, L. D.; Steiner, P. R.; Pedersen, C., Studies of specifically fluorinated carbohydrates .6. Some pentofuranosyl fluorides. *Canadian Journal of Chemistry* **1970,** 48, (7), 1155.
8. Deleeuw, H. P. M.; Haasnoot, C. A. G.; Altona, C., Nucleic-acid constituents .13. Empirical correlations between conformational parameters in beta-d-furanoside fragments derived from a statistical-survey of crystal-structures of nucleic-acid constituents - full description of nucleoside molecular geometries in terms of 4 parameters. *Israel Journal of Chemistry* **1980,** 20, (1-2), 108-126.

9. Altona, C.; Sundaral.M, Conformational-analysis of sugar ring in nucleosides and nucleotides - improved method for interpretation of proton magnetic-resonance coupling-constants. *Journal of the American Chemical Society* **1973,** 95, (7), 2333-2344.
10. (a) Donders, L. A.; Deleeuw, F. A. A. M.; Altona, C., Relationship between proton proton nmr coupling-constants and substituent electronegativities .4. An extended karplus equation accounting for interactions between substituents and its application to coupling-constant data calculated by the extended huckel-method. *Magnetic Resonance in Chemistry* **1989,** 27, (6), 556-563.(b) Altona, C.; Ippel, J. H.; Hoekzema, A. J. A. W.; Erkelens, C.; Groesbeek, M.; Donders, L. A., Relationship between proton proton nmr coupling-constants and substituent electronegativities .5. Empirical substituent constants deduced from ethanes and propanes. *Magnetic Resonance in Chemistry* **1989,** 27, (6), 564-576.
11. Altona, C.; Francke, R.; Dehaan, R.; Ippel, J. H.; Daalmans, G. J.; Hoekzema, A. J. A. W.; Vanwijk, J., Empirical group electronegativities for vicinal nmr proton-proton couplings along a c-c bond - solvent effects and reparameterization of the haasnoot equation. *Magnetic Resonance in Chemistry* **1994,** 32, (11), 670-678.
12. Deleeuw, F.; Altona, C., Conformational-analysis of beta-d-ribo-nucleosides, Beta-D-deoxyribo-nucleosides, Beta-D-arabino-nucleosides, Beta-D-xylo-nucleosides, and beta-D-lyxo-nucleosides from proton-proton coupling-constants. *Journal of the Chemical Society-Perkin Transactions 2* **1982**, (3), 375-384.
13. (a) Vanwijk, J., Haasnoot, C. A. G., de Leeuw, F. A. A. M., Huckriede, B. D., Westra Hoekzema, A. and Altona, C. *PSEUROT 6.2 1993*, *PSEUROT 6.3 1999*; Leiden Institute of Chemistry, Leiden University. (b)Deleeuw, F.; Altona, C., Computer-assisted pseudorotation analysis of 5-membered rings by means of proton spin spin coupling-constants-program PSEUROT. *Journal of Computational Chemistry* **1983,** 4, (3), 428-437. (c) Altona, C., Conformational-analysis of nucleic-acids - determination of backbone geometry of single-helical rna and dna in aqueous-solution. *Recueil Des Travaux Chimiques Des Pays-Bas-Journal of the Royal Netherlands Chemical Society* **1982,** 101, (12), 413-433.

14. Software : A user-friendly Matlab program and GUI for the pseudorotation analysis of saturated five-membered ring systems based on scalar coupling constants Pieter MS Hendrickx and José C Martins Ghent University, Belgium, Chemistry Central Journal **2008**.
15. Rinkel, L. J.; Altona, C., Conformational-analysis of the deoxyribofuranose ring in dna by means of sums of proton-proton coupling-constants - a graphical-method. *Journal of Biomolecular Structure & Dynamics* **1987,** 4, (4), 621-649.
16. Obika, S.; Morio, K.; Nanbu, D.; Imanishi, T., Synthesis and conformation of 3'-O,4'-C-methyleneribonucleosides, novel bicyclic nucleoside analogues for 2',5'-linked oligonucleotide modification. *Chemical Communications* **1997**, (17), 1643-1644.
17. Remin, M.; Shugar, D., Conformation of exocyclic 5'-CH_2OH in nucleosides and nucleotides in aqueous solution from specific assignments of H5' and H5" signals in. *Biochemical and Biophysical Research Communications* **1972,** 48, (3), 636.
18. Zhang, N.; Zhang, S. L.; Szostak, J. W., Activated Ribonucleotides Undergo a Sugar Pucker Switch upon Binding to a Single-Stranded RNA Template. *Journal of the American Chemical Society* **2012** 134, (8), 3691-3694.
19. Plavec, J.; Koole, L. H.; Sandstrom, A.; Chattopadhyaya, J., Structural studies of anti-HIV 3'-Alpha-fluorothymidine and 3'-alpha-azidothymidine by 500 MHZ H-1-NMR spectroscopy and molecular mechanics (MM2) calculations. *Tetrahedron* **1991,** 47, (35), 7363-7376.
20. (a) Sherfinski J.; Marsh R. E., The crystal structure of 1-β-D-arabinofuranosyluracil. *Acta Crysallographica*. **1974,** B30, 868-872. (b) Tollin P.; Wilson H. R.; Young D. W.; The crystal and molecular structure of uracil-β-D-arabinofuranoside. *Acta Crysallographica* **1973,** B29, 1641-1647
21. Hayakawa, H.; Takai, F.; Tanaka, H.; Miyasaka, T.; Yamaguchi, K., Diethylaminosulfur trifluoride (DAST) as a fluorinating agent of pyrimidine nucleosides having a 2',3'-vicinal diol system. *Chemical & Pharmaceutical Bulletin* **1990,** 38, (5), 1136-1139.

22. Bruker, *APEX2*, *SAINT* and *SADABS*. Bruker AXS Inc., Madison, Wisconsin, USA **2006**.

23. Sheldrick G. M., A short history of *SHELX*. *Acta Crysallographica*., **2008**, A64, 112-122.